

Fossil

---

Record

---

27 (1) 2024

# **Fossil Record**

## An International Journal of Palaeontology

### Editor-in-Chief

#### **Florian Witzmann**

Museum für Naturkunde Berlin  
Invalidenstraße 43  
10115 Berlin  
E-Mail: [florian.witzmann@mfn-berlin.de](mailto:florian.witzmann@mfn-berlin.de)  
Tel: +49 30 889140 · 8820  
Fax: +49 30 889140 · 8565

### Editorial Secretary

#### **Boryana Ovcharova**

Pensoft Publishers,  
Prof. Georgi Zlatarski Street 12  
1700 Sofia, Bulgaria  
Tel: +359-2-8704281  
Fax: +359-2-8704282  
E-Mail: [journals@pensoft.net](mailto:journals@pensoft.net)

### Editorial Board

**Christian Klug**, Zürich, Switzerland  
**Johannes Müller**, Berlin, Germany  
**Torsten Scheyer**, Zurich, Switzerland  
**Alexander Schmidt**, Göttingen, Germany  
**Florian Witzmann**, Berlin, Germany  
**Hui-ting Wu**, Beijing, China

### **Fossil Record**

#### **2024. Volume 27. Issue 1**

ISSN: 2193-0066 (print), 2193-0074 (online)

### **In Focus**

The cover picture shows UCMP 36834, a complete right dentary of the novel brachyopoid photographed in lingual, ventral and dorsal view.

See the paper by **So C, Mann A** "A large brachyopoid from the Middle Triassic of northern Arizona and the diversity of brachyopoid temnospondyls from the Moenkopi Formation".

### **Cover design**



# Fossil Record

An International Journal of Palaeontology

Content of volume **27 (1)** 2024

<b>Beurel S, Bachelier JB, Munzinger J, Shao F, Hammel JU, Shi G, Sadowski E-M</b> First flower inclusion and fossil evidence of <i>Cryptocarya</i> (Laurales, Lauraceae) from Miocene amber of Zhangpu (China)	1
<b>Rollot Y, Evers SW, Joyce WG</b> A digital redescription of the Middle Miocene (Langhian) carettochelyid turtle <i>Allaeochelys libyca</i>	13
<b>Arratia G, Schultze H-P</b> The oldest teleosts (Teleostomorpha): their early taxonomic, phenotypic, and ecological diversification during the Triassic	29
<b>Marjanović D, Maddin HC, Olori JC, Laurin M</b> The new problem of <i>Chinlestegophis</i> and the origin of caecilians (Amphibia, Gymnophionomorpha) is highly sensitive to old problems of sampling and character construction	55
<b>Tsai C-H, Kimura T, Hasegawa Y</b> Coexistence of Oligocene toothed and baleen-assisted mysticetes in the northwestern Pacific	95
<b>Ferreira J, Josse H, Denadai de Campos L, Nel A, Desutter-Grandcolas L</b> First 3D reconstruction of a forewing of a fossil Orthoptera: Interpreting the venation pattern in the smallest known cricket with a stridulatory apparatus, † <i>Picogryllus carentonensis</i> (Orthoptera, Grylloidea, Oecanthidae)	101
<b>Ebersole JA, Cicimurri DJ, Harrell Jr. TL</b> A new species of <i>Palaeohypotodus</i> Glückman, 1964 (Chondrichthyes, Lamniformes) from the lower Paleocene (Danian) Porters Creek Formation, Wilcox County, Alabama, USA	111
<b>Viertler A</b> Another one bites the dust: A new <i>Lithoserix</i> species (Hymenoptera, Ichneumonidae, Pimplinae) from the early Oligocene in France, with an evaluation of wing morphometrics	135
<b>Sander PM, Wellnitz PW</b> A phytosaur osteoderm from a late middle Rhaetian bone bed of Bonenburg (North Rhine-Westphalia, Germany): Implications for phytosaur extinction	147
<b>Čerňanský A, Vasilyan D</b> Roots of the European Cenozoic ecosystems: lizards from the Paleocene (~MP 5) of Walbeck in Germany	159

---

## Abstract & Indexing Information

Biological Abstracts® (Thompson ISI)  
BIOSIS Previews® (Thompson ISI)  
Cambridge Scientific Abstracts (CSA/CIG)  
Web of Science® (Thompson ISI)  
Zoological Record™ (Thompson ISI)

# Fossil Record

An International Journal of Palaeontology

Content of volume **27 (1)** 2024

**Carrillo-Briceño JD, Ruiz-Ramoni D, Sánchez R, Jaimes A, Chávez-Aponte E, Prevosti FJ, Segura V, Carlini AA, Garbé L, Tombret O, Zazzo A, Sánchez-Villagra MR**

Cauca: megafaunal and felid fossils (Mammalia) from a Pleistocene site in northwest Venezuela

187

**Pang L-bo, Chen S-kun, Hu X, Wu Y, Wei G-biao**

Fossil flying squirrels (Petauristinae, Sciuridae, Rodentia) from the Yumidong Cave in Wushan County, Chongqing, China

209

**Farida M, Jaya A, Ahmad A, Nugraha J**

The Eocene to Oligocene boundary and paleoclimatic indications based on calcareous nannofossils of Tonasa Formation, South Sulawesi, Indonesia

221

**So C, Mann A**

A large brachyopoid from the Middle Triassic of northern Arizona and the diversity of brachyopoid temnospondyls from the Moenkopi Formation

233

# First flower inclusion and fossil evidence of *Cryptocarya* (Laurales, Lauraceae) from Miocene amber of Zhangpu (China)

Simon Beurel<sup>1</sup>, Julien B. Bachelier<sup>2</sup>, Jérôme Munzinger<sup>3</sup>, Fuchen Shao<sup>2</sup>, Jörg U. Hammel<sup>4</sup>, Gongle Shi<sup>5</sup>, Eva-Maria Sadowski<sup>1</sup>

<sup>1</sup> Museum für Naturkunde, Leibniz Institute for Evolution and Biodiversity Science, Invalidenstraße 43, 10115 Berlin, Germany

<sup>2</sup> Freie Universität Berlin, Institute of Biology/Dahlem Centre of Plant Sciences, Altensteinstraße 6, 14195 Berlin, Germany

<sup>3</sup> AMAP, Université Montpellier, IRD, CIRAD, CNRS, INRAE, 34000 Montpellier, France

<sup>4</sup> Institute of Materials Physics, Helmholtz-Zentrum Hereon, Max-Planck-Straße 1, 21502 Geesthacht, Germany

<sup>5</sup> State Key Laboratory of Palaeobiology and Stratigraphy, Nanjing Institute of Geology and Palaeontology and Center for Excellence in Life and Palaeoenvironment, Chinese Academy of Sciences, Nanjing 210008, China

<https://zoobank.org/145575FB-0BE7-4916-88D0-2CA73D69B62C>

Corresponding author: Simon Beurel ([Simon.Beurel@mfn.berlin](mailto:Simon.Beurel@mfn.berlin))

Academic editor: Florian Witzmann ♦ Received 17 July 2023 ♦ Accepted 16 November 2023 ♦ Published 4 January 2024

## Abstract

Lauraceae have one of the oldest fossil records of angiosperms with the earliest known evidence from the mid-Cretaceous. However, most of these records are based on leaves, especially from the Cenozoic of Asia, which are often challenging to assign to extinct or extant genera or species. In contrast, fossils of reproductive organs are more informative, but remain scarce. We here described the first Cenozoic Lauraceae flower of Asia and confirmed the presence of *Cryptocarya* in the Miocene Zhangpu flora (Fujian Province, south-eastern China) based on an amber inclusion. We scanned the specimen using synchrotron radiation-based micro-computed tomography (SR $\mu$ CT) and then compared the fossil with extant flowers of the genus. The present fossil flower is small, bisexual, and polysymmetric, with a whorled and trimerous perianth and androecium along with a hypanthium around the gynoecium. The perianth comprises six undifferentiated tepals, the androecium consists of nine stamens and three innermost staminodes, and the gynoecium of a single carpel with a superior, unilocular (and uniovulate) ovary. Our study also shows that the fossil shares an unusual position of the typical staminal glands and a short androecial tube on the rim of the hypanthium with at least one extant Australian species of *Cryptocarya*, which have not been reported before. Nowadays, Lauraceae are still present in tropical to subtropical regions, mostly in American and Asian rainforests. The discovery of many Lauraceae leaf fossils in Zhangpu, as well as the amber flower of this study, is consistent with the current reconstruction of the amber source environment as a megathermal seasonal rainforest during the Mid-Miocene.

## Key Words

Angiosperm, Cenozoic, palaeobotany, synchrotron X-ray tomography, 3D reconstruction

## Introduction

The Lauraceae are one of the most species rich families of Magnoliidae, with worldwide ecological and economic importance. Some taxa are key ecosystem components, especially in Asian and American tropical lowland and montane forests. Lauraceae also

comprise crops and spices, such as avocado, cloves and cinnamon (Rohwer 1993). This family has a vast meso- to megafossil record, mostly consisting of leaves from all over the world (Friis et al. 2011). Lauraceous leaves are notoriously difficult to assign to species but also to generic level, as key features are widespread across extinct and extant taxa and geographical areas

(Hill 1986; Christophel et al. 1996). In contrast, fossil fruits and flowers show more diagnostic features than leaves and are particularly valuable for generic or even species level identification (Rohwer 1993). Such reproductive structures are nevertheless rare, as they are not often preserved in the sedimentary fossil record (Friis et al. 2011).

The oldest currently known lauraceous fossil flower stems are from the Early Cretaceous Puddledock locality (von Balthazar et al. 2007). Additionally, fossils of lauraceous origin from North America (Drinnan et al. 1990; Friis et al. 2011), Europe (Kvaček 1992; Eklund and Kvaček 1998; Kvaček and Eklund 2003; Viehofen et al. 2008; Coiffard et al. 2009; Moreau et al. 2016) and South Asia (Poinar 2017) show that early members of the family were already widely distributed and diverse by the mid-Cretaceous. In Asia, the earliest Lauraceae fossil records date back to the Cenomanian with a flower inclusion of *Cascolaurus burmitis* Poinar in Burmese amber (Poinar 2017) and inflorescences and flowers of *Mauldinia hirsuta* Frumin, Eklund and Friis from Kazakhstan (Frumin et al. 2004). Additional Cretaceous fossils include flowers from the Coniacian of Japan (Takahashi et al. 1999, 2001, 2014). However, molecular clock study infers that diversification of modern Lauraceae in Asia is more recent, and probably took place during the early Cenozoic (Chanderbali et al. 2001). This is supported by the large fossil leaves record, mostly from China (e.g. Hu et al. 2007; Jacques et al. 2011; Sun et al. 2011; Shi et al. 2014c; Huang et al. 2016; Wang et al. 2019; Wang et al. 2021), but fossil flowers from this time period remain scarce. Therefore, the discovery of additional Cenozoic lauraceous reproductive organs is particularly interesting to gain more insight into the evolution and diversification of Lauraceae.

In this paper, we aim to describe a new fossil flower of Lauraceae from Chinese Miocene Zhangpu amber by using non-destructive X-ray imaging techniques. We noticed similarities, such as an the unusual position of the staminal glands and an androecial tube, with an extant member of *Cryptocarya* R. Br. from Australia, and discuss the significance of the oldest unambiguous fossil of the genus in the Miocene Zhangpu flora.

## Material and methods

The amber specimen derives from the Zhangpu amber deposit of the Fotan Group, in Zhangpu County (Fujian province, SE China; see detailed map in Wang et al. 2021: fig. 1). The group is formed by sedimentary layers of conglomerates, sandstone and mudstone alternating with layers of basaltic rocks (Zheng and Wang 1994; Wang et al. 2021). Plant macro-remains are commonly found co-occurring with the amber in the same layers of blue-grey mudstone with lignite and diatomite (Wang et al.

2021). Based on the  $^{40}\text{Ar}/^{39}\text{Ar}$  dating of the basaltic units associated the fossil layers, the age of the amber has been well constrained at  $14.8 \pm 0.6$  Ma to  $14.7 \pm 0.4$  Ma, corresponding to the Langhian stage of the Middle Miocene (Ho et al. 2003; Zheng et al. 2019; Wang et al. 2021). This is consistent with the previous palynological studies of the Fotan Group (Zheng and Wang 1994). The terpenoid composition of Zhangpu amber indicates that it derived from the tropical Dipterocarpaceae. Additionally, fossilized winged fruits with affinities to this angiosperm family were found in the same deposit (Shi and Li 2010; Shi et al. 2014a, b). The amber piece was deposited in the palaeobotanical collections of the Nanjing Institute of Geology and Palaeontology, Chinese Academy of Sciences in China (NIGPAS) under the collection number PB21525.

Separation of the fossil flower from other syninclusions in the same amber piece was achieved by using the sawing machine ALGE. Then, the piece containing the fossil was ground and polished with a LaboPol-25 machine (Struers, Sarasota, Florida, USA) using wet silicon polishing papers with successively finer grit sizes (250 to 4000 nm, Struers) to create even surfaces parallel to the inclusion (see Sadowski et al. 2021 for details).

The amber specimen was studied under a Carl Zeiss AxioScope A1 compound microscope (Carl Zeiss, Oberkochen, Germany), using incident and transmitted light simultaneously. Images were taken with a Canon EOS 80D digital camera (Canon, Tokyo, Japan) that was mounted on the microscope. To accommodate the three-dimensionality of the inclusion, 65 single photographs were taken and then digitally stacked to a composite image, by applying the HeliconFocus 7.7 software.

Imaging of the flower inclusion was performed using synchrotron-radiation based X-ray microtomography (SR $\mu$ CT) at beamline P05 of the storage ring PETRA III (Deutsches Elektronen-Synchrotron, DESY, Hamburg, Germany) that is operated by Helmholtz-Zentrum Hereon (Haibel et al. 2010; Greving et al. 2014; Wilde et al. 2016). The amber piece was mounted on a sample-stub with beeswax and imaged using an attenuation contrast setup (Greving et al. 2014). The specimen was scanned using a commercial CMOS camera system with an effective pixel size of  $0.45 \mu\text{m}$ , a sample to detector distance of 75 mm and a photon energy of 18 keV. A total of 3501 projections were recorded for the tomographic scan, at equal intervals between 0 and  $\pi$ . A transport of intensity phase retrieval approach and a filtered back projection was used to perform the tomographic reconstruction implemented with the Astra Toolbox (Palenstijn et al. 2011; van Aarle et al. 2015, 2016) and Matlab (MathWorks), integrated in a bespoke reconstruction pipeline (Moosmann et al. 2014). Raw projections were binned twice during processing, resulting in an effective voxel size of  $0.91 \mu\text{m}$  for the reconstructed volume.

The size of the resulting tomographic images was decreased from 32-bit floating point data to 16-bit, by applying ImageJ 1.52 (Wayne Rasband, National Institutes of Health, Bethesda, Maryland, USA). The software Volume Graphics Studio Max, version 3.4 (Volume Graphics, Heidelberg, Germany) was used to complete the segmentation, 3D reconstructions, and length measurements.

We additionally examined flowers of some extant species of *Cryptocarya* from the Oceanic region, including one from Australia (originally *C. hypotephra* F. Muell., now *C. vulgaris* B. Hyland; MB.Pb.HB.00569 [Schrader Herbarium (BHUPM), Museum für Naturkunde Berlin (MfN)]), and four from New Caledonia (*C. adpressa* Munzinger & McPherson [Munzinger *et al.* 5832, P, Type specimen], *C. aristata* Kosterm. [Munzinger *et al.* 5866, P], *C. cf. odorata* Guillaumin [Munzinger (*leg. Waikedre*) 6716, MPU], and Vanuatu (*C. wilsonii* Guillaumin [Munzinger & Bruy 8232], NOU). Each flower sample was mounted on a specimen holder to facilitate microCT scanning with a Phoenix X-ray Nanotom at the MfN. The scans comprised 1440 to 2000 projections and were conducted using the following settings: voltage = 80 to 100 kV, current = 75 to 100  $\mu$ A, exposure time = 0.75 to 1 s, average = 3 to 6, skip = 1 and isotropic resolution = 1.64 to 3.6  $\mu$ m.

## Data resources

Supplementary data including SR $\mu$ CT videos, 3D models of the *Cryptocarya* flower inclusion and of extant flowers of the genus are available here: <https://doi.org/10.7479/pzxcg-2x16>.

## Results

### Systematic palaeontology

**Order Laurales Juss. ex Burch. & J. Presl, 1820**

**Family Lauraceae Juss. 1789**

**Genus *Cryptocarya* R. Br., 1810**

***Cryptocarya* sp.**

Figs 1, 2

**Specimen studied.** PB21525. Nanjing Institute of Geology and Palaeontology, Chinese Academy of Sciences in China (NIGPAS).

**Locality.** Zhangpu County, Fujian Province, China.

**Horizon and age.** Middle part of the Fotan Group, Langhian (ca. 14.7–14.8 Ma), Middle Miocene.

**Description.** The flower is 3.11 mm long and 1.66 mm wide (without the pedicel, not preserved) (Fig. 1A, B). It is perfect, polysymmetric, and comprises six tepals, nine stamens, and three staminodes, which are arranged in six

trimerous and alternate whorls around the gynoecium (Fig. 1C–G). It is also perigynous with a hypanthium (1.71 mm long and 0.60 mm wide) that encloses the superior ovary and lowest third of the style entirely (Fig. 1D). The position of perianth organs forming a narrow opening and of the apical flaps still covering the pollen sacs suggest a late pre-anthetic stage or early (female) anthetic phase.

The tepal lobes (1.72–2.04 mm long and 0.66–1.05 mm wide) are free and arranged in an outer and inner whorl, and share a similar narrowly ovate to elliptical shape and an acute tip (Fig. 1A, B).

All stamens are shorter than the tepals in length and have basifixed anthers with unilocular thecae opening by two slightly lobed to flattened apically attached or hinged flaps (Figs 1C–E, 2A, C). Stamens of the first and second whorls have introrse, ovate and incurved anthers (ca. 0.57–0.68 mm long and 0.40–0.50 mm wide). Their filaments are adnate to a tepal lobe (Fig. 1F) and distinctly shorter than their anthers (ca. 0.25–0.48 mm long and 0.08–0.11 mm wide). Three pairs of large glands are inserted on the hypanthium rim, between the united bases of the tepals and filaments (Fig. 1D). These glands are formed by a subglobose distal part (ca. 0.34–0.56 mm long and 0.29–0.38 mm wide) and a long stalk (ca. 0.31–0.40 mm long and 0.09–0.12 mm wide; Figs 1D, F, 2B). Stamens of the third whorl have latero-extrorse, erect and narrow anthers (ca. 0.68–0.75 mm long and 0.37–0.39 mm wide). The filaments are just about as long as their anthers (ca. 0.64–0.74 mm long and 0.09–0.14 mm wide) and their bases form, together with those of the staminodes, a short staminal tube projecting beyond the rim of the hypanthium (ca. 0.13 mm long and 0.45 mm wide; Figs 1D, G, 2C). The staminodes have a sagittate (triangular-ovate and acuminate) sterile anther and a short and stout filament (ca. 0.60–0.65 mm long and 0.38–0.40 mm wide and 0.31–0.41 mm long and 0.15 mm wide respectively; Figs 1D, F–G, 2C).

The gynoecium consists of a single carpel (ca. 2.03 mm long). The slender superior ovary (1.22 mm long and 0.18 mm wide) is entirely enclosed in the hypanthium. The style (ca. 0.81 mm long and 0.14 mm wide) ends in an inconspicuous stigma (Fig. 1D). The ovary has a single locule and an apical pendulous ovule (ca. 0.71 mm long and 0.16 mm wide).

The flower is densely pubescent with appressed simple acute trichomes covering all organs, except for the inner surface of the distal part of the hypanthium, the fertile and sterile anthers and the gynoecium (Fig. 1).

### Syninclusions

The specimen contains inclusions of two *Tetramorium* and five *Carebara* ants (Formicidae), one Collembola, two Chironomidae, and wood fragments.

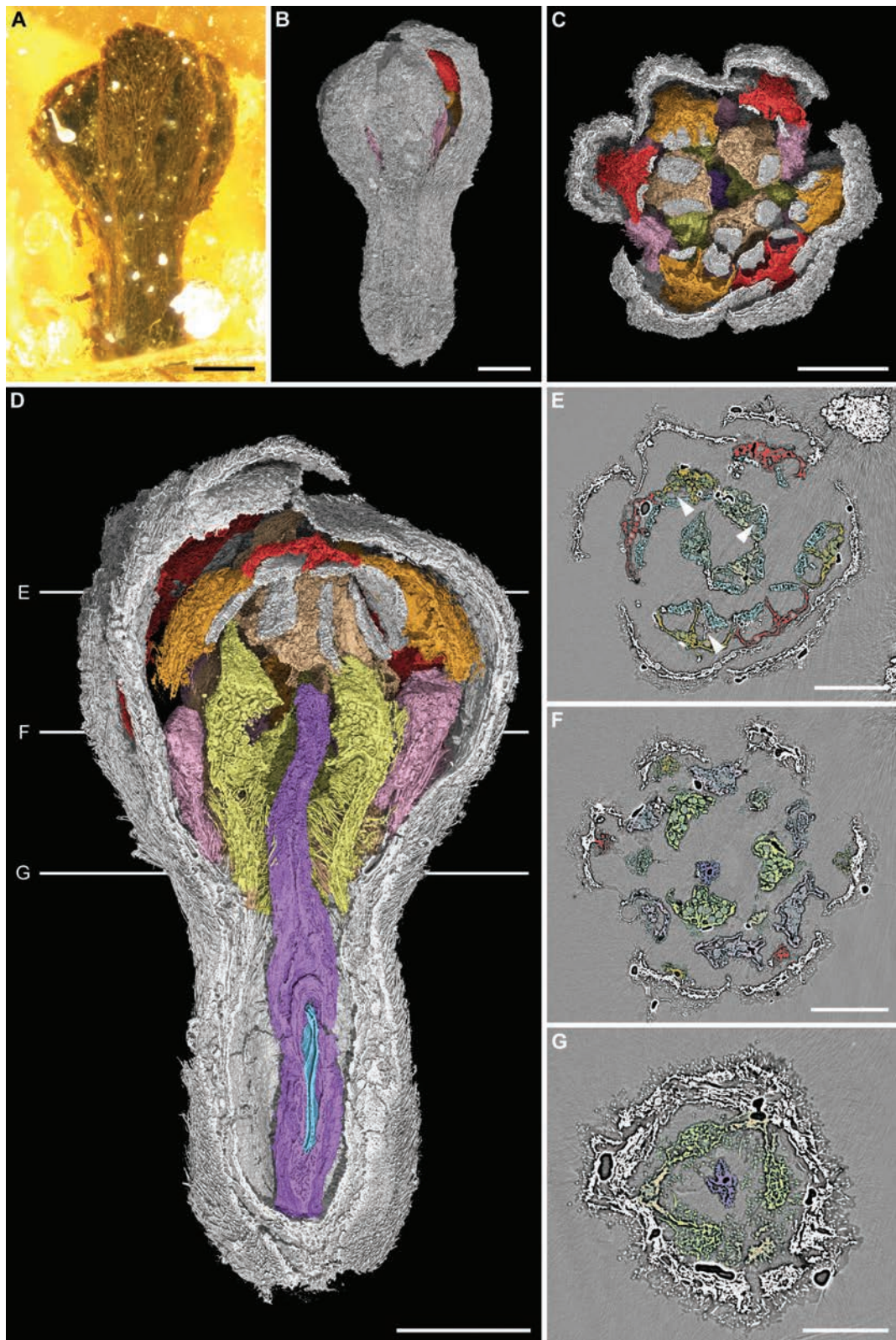


**Figure 1.** *Cryptocarya* fossil flower from Miocene Zhangpu amber, PB21525. **A.** Overview of the flower inclusion, taken under the light microscope; **B–D.** Virtual 3D reconstruction from segmented SR $\mu$ CT data; **B.** Overall flower; **C.** Cross section; **D.** Longitudinal section; **E–G** SR $\mu$ CT cross-sections, indicated in **D** and arranged from top to bottom; **E.** Bilocular anthers with two valves and laterally fused pollen sacs (septa indicated by white arrowheads); **F.** Style, staminodes, glands, and the filaments of the fertile stamens adnate to a tepal lobe; **G.** Short staminal tube resulting from the fusion of the third whorl of stamens with the whorl of staminodes. Perianth – grey; Stamens of the first whorl – red; Stamens of the second whorl – orange; Stamens of the third whorl – beige; Anther valves – white; Staminal glands – pink; Stamminodes – yellow; Gynoecium – purple; Ovule – blue. Scale bars: 0.5 mm (**A–D**); 0.4 mm (**E–F**); 0.3 mm (**G**).

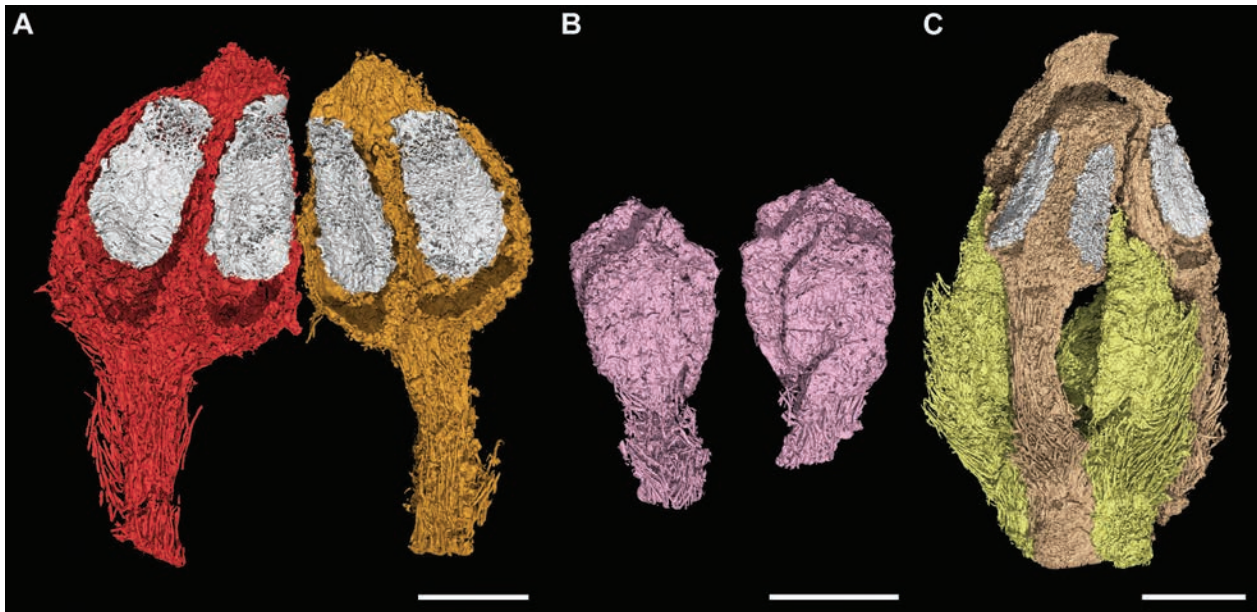


**Figure 2.** Androecium of the *Cryptocarya* flower from Miocene Zhangpu amber, PB21525. **A.** Stamens of the first and second whorl; **B.** Staminal glands; **C.** Stamens of the third whorl fused with the staminodes at the base of the filaments, forming a short staminal tube. Stamen of the first whorl – red; Stamen of the second whorl – orange; Stamens of the third whorl – beige; Anther valves – white; Staminal glands – pink; Staminodes – yellow. Scale bars: 0.2 mm (**A**); 0.3 mm (**B–C**).

## Discussion

### Systematic affinity

Our non-invasive and non-destructive approach shows that our fossil flower exhibits essentially the same Bauplan as most extant Lauraceae, with two trimerous whorls of tepals, followed by three trimerous whorls of fertile stamens and an innermost trimerous whorl of staminodes, and a unicarpellate gynoecium. In addition, like in all Lauraceae, the anthers are unmistakably valvate with apical flaps, and the single ovary is superior and unilocular with one apical ovule (Rohwer 1993; van der Werff 2001; Li et al. 2008a; Simpson 2010). The bithecal anthers also exhibit a bilocular structure with septal remains in some thecae. However, whether lateral fusion of the two pollen sacs happened before anthesis or earlier is unclear, but such anthers may have evolved multiple times in Lauraceae, with intermediate forms observed in several genera (Rohwer 1994). According to Rohwer (1993), bilocular anthers most likely originated in Lauraceae from the reduction of the upper or lower pollen sac(s) but may also have been formed by the lateral fusion of the pair of pollen sacs, which is a synapomorphy of the “larger part of the *Cryptocarya* group” that contains at least the genera *Cryptocarya*, *Beilschmiedia* Nees, *Endiandra* R. Br., *Aspidostemon* Rohwer & H.G. Richt., *Potameia* Thouars, *Eusideroxylon* Teijsm. & Binn., *Potoxylon* Kosterm., *Dahlgrenodendron* J.J.M. van der Merwe & A. E. van Wyk, *Sinopora* J. Li, N.H. Xia & H.W. Li, *Triadodaphne* Kosterm. and *Yasunia* van der Werff (Rohwer et al. 2014).

Within this group, the fossil flower exhibits a combination of distinctive features with members of the extant genus *Cryptocarya*, including six tepals, nine stamens that are all fertile and a deep hypanthium entirely encompassing the ovary (Fig. 3; van der Werff 1991, 2001; Rohwer 1993; Moraes 2007; Li et al. 2008b).

Extant *Cryptocarya* flowers are small (about 3–5 mm, Fig. 3), actinomorphic, bisexual and perigynous. The perianth also consists of six tepals arranged in an outer and inner whorl usually of similar size and shape. The androecium comprises three whorls with three fertile stamens and an innermost whorl of staminodes. The first and second whorl of stamens have introrse anthers, while the ones of the third whorl can be extrorse, lateral or rarely introrse (Kostermans 1937; Moraes 2007). The stamen filaments are inserted on the rim of the hypanthium, each close or connected to the base of a tepal. In addition, stamens of the first/second or third whorl bear a pair of glands, distant or adnate to the base of their filament (Fig. 3G; Hyland 1989; Moraes 2007). A fourth whorl of conspicuous, sagittate staminodes also occurs in the flowers. The style is long and the stigma is small or inconspicuous (Kostermans 1937; Moraes 2007).

### Position of glands and staminal tube in *Cryptocarya*

Androecial characters are highly variable among extant Lauraceae and may also vary within genera. In most cases, the pairs of staminal glands are connected to or born on the filament bases of the third whorl of stamens (Rohwer 1993). However, they can also occur on the outermost

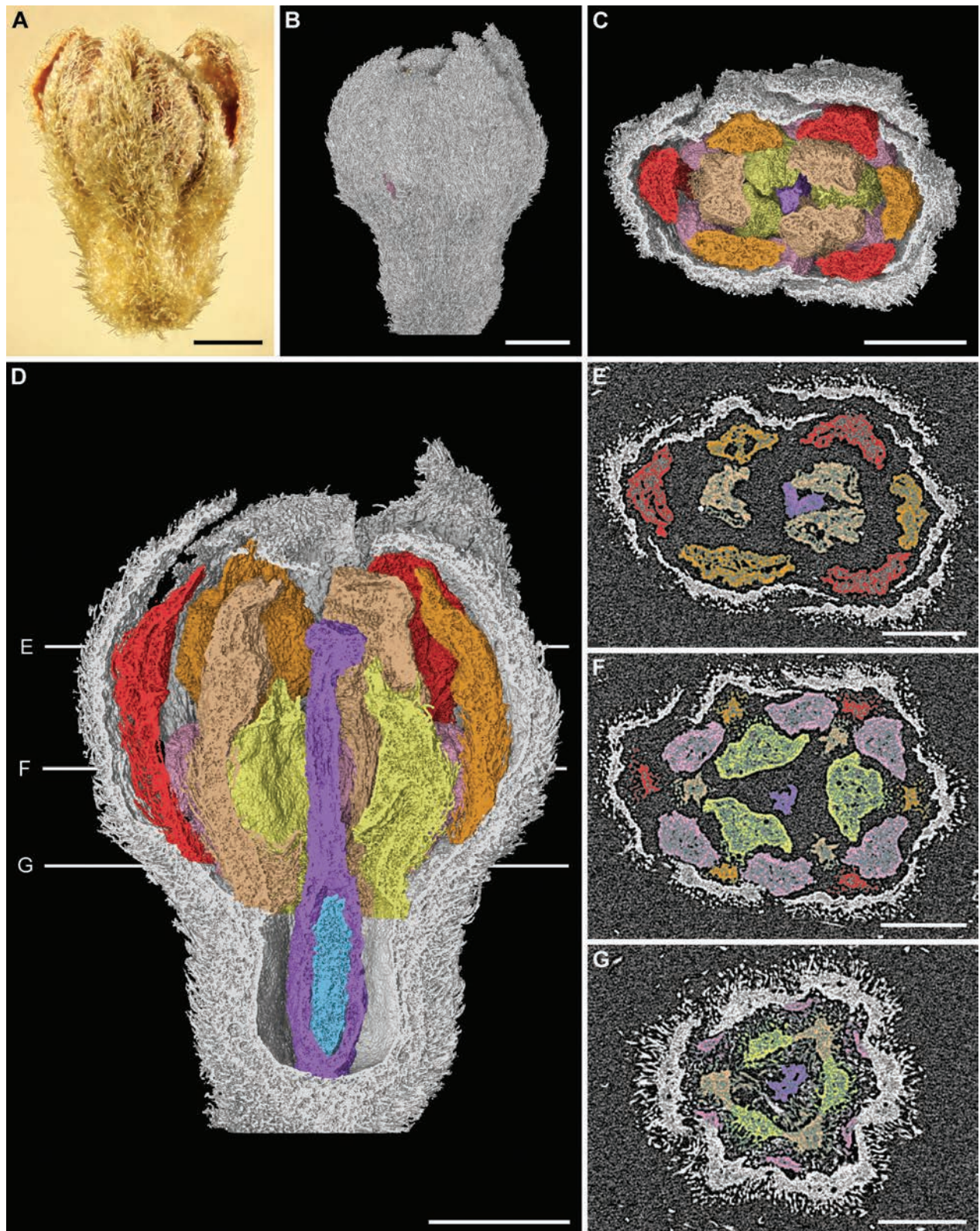


**Figure 3.** Extant *Cryptocarya vulgaris* flower from Australia, MB.Pb.HB.00569. **A.** Overview of a flower, taken under the light microscope; **B–D.** Virtual 3D reconstruction from segmented microCT data; **B.** Overall flower; **C.** Cross section; **D.** Longitudinal section; **E–G.** microCT cross-sections, indicated in **D** and arranged from top to bottom; **E.** Immature bilocular anthers of the androecium and the bilobed stigma; **F.** Style, staminodes, glands, and filaments of the fertile stamens; **G.** Staminal tube resulting from the fusion of the third whorl of stamens with the whorl of staminodes; note the glands inserted at the division point of the tepal lobes. Perianth – grey; Stamens of the first whorl – red; Stamens of the second whorl – orange; Stamens of the third whorl – beige; Staminal glands – pink; Staminodes – yellow; Gynoecium – purple; Ovule – blue. Scale bars: 0.4 mm (**A–D**); 0.3 mm (**E–G**).

androecial whorl such as in *Rhodostemonodaphne* Rohwer and Kubitzki, *Urbanodendron* Mez, *Chlorocardium* Rohwer, Richter and van der Werff, and *Brassiendendron* C.K. Allen (Rohwer 1993). Also, in some extant representatives of *Cryptocarya* from Australia and South America, the paired staminal glands are associated with the two outer whorls of stamens or rather distant from the filaments (in *C. brassii* C.K. Allen, *C. grandis* B. Hyland, *C. pleurosperma* C.T. White and W.D. Francis, *C. putida* B. Hyland, *C. vulgaris* in Hyland 1989; *C. moschata* Nees and Martius, *C. guianensis* Meisner, *C. riedeliana* P.L.R. Moraes in Moraes 2007). As in some of these extant species, the staminal glands of our *Cryptocarya* fossil flower are free from the filament and inserted towards the distal end of the floral cup (Fig. 1D). However, it is often unclear in the literature and in our material which whorl the glands are associated with. For instance, we observed in the herbarium specimen *C. vulgaris* (MB.Pb.HB.00569) that they are inserted at the division point of the tepal lobes (Fig. 3G) whereas Hyland (1989) associates the glands with the first whorl of stamens (fig. 37G).

In the fossil flower from Zhangpu, as well as in the herbarium flowers of *Cryptocarya vulgaris* (MB.Pb.HB.00569), the filaments of the third stamen whorl are similarly fused with those of the staminodes whorl (Figs 1G, 2C, 3G), forming a short staminal tube extending beyond the rim of the hypanthium. Judging from flowering stage, the staminal tube in the fossil is less prominent than in the extant specimen. In addition, the tube observed in extant *Cryptocarya* flowers is more defined when the flower is less mature, suggesting that, depending on the developmental stage of the specimen, a staminal tube is only temporarily present in the early development of some *Cryptocarya* flowers. They can thus be superficially different in older stages and prevent a detailed comparison with classic descriptions of fully developed flowers in the literature. These morphological variations should be considered in future morphological studies of the genus.

The glands and the staminal tube are distinctive in the herbarium flower (MB.Pb.HB.00569) and in the fossil. However, such a staminal tube elaborated only by the third and fourth androecium whorls has, to our knowledge, never been pictured or mentioned before in Lauraceae. Similarly, pairs of staminal glands on different whorls were also only occasionally depicted (Hyland 1989, figs 13G, 21G, 31I, 32G, 37G; Moraes 2007, figs 33D, 52D). Therefore, future morphological and anatomical studies are needed to gain more insight into the variation of the gland position and staminal tube development in *Cryptocarya*. Additionally, our results show that X-ray based methods, like micro-CT scanning, is a valuable tool for analysing extant plant specimens, as they allow detailed observations of reproductive plant organs non-invasively, compared to standard methods like microtome sections, which are usually applied in botany.

Due to the morphological variations in *Cryptocarya* flowers and the lack of distinctive characters in the fossil, it does not seem reasonable to assign the flower inclusion to any extant species of *Cryptocarya*. Furthermore, additional plants organs, such as leaves or fruits would be necessary to clarify the affiliation of the fossil to the species level. For all these reasons, we refrain from describing the amber inclusion as a new fossil species.

## Fossil records and challenges in assigning *Cryptocarya* and Lauraceae fossils

According to molecular data, *Cryptocarya* diverged around about  $90 \pm 20$  million years ago and is probably of Gondwanan origin (Chanderbali 2001). Nevertheless, fossils with affinities to the *Cryptocarya* group, and more specifically to *Cryptocarya*, are only known since the Cenozoic. The oldest representatives are possibly fossil leaves from the Eocene of Australia (Hill 1986, 1988; Conran and Christophel 1998; Carpenter et al. 2004) and North America (MacGinitie 1941). In addition, numerous putative leaves and fruit fossils were discovered in the Miocene and Pleistocene of New Zealand (Holden 1982; Pole 1993, 2007, 2019; Bannister et al. 2012), the Miocene of New Caledonia (Garrouste et al. 2021), as well as in the Oligocene, Miocene and Pleistocene of China (Liu 1993; Shi et al. 2014c; Wang et al. 2019), while fewer were discovered in the New World (i.e. in the Paleogene of Patagonia; Carpenter et al. 2018). It is only recently that a fossil has been reliably assigned to the genus in Asia, based on Pleistocene wood (Huang et al. 2023).

However, most of those fossils are leaf impressions and compressions or cuticle fragments. Moreover, the fossil pollen record of Lauraceae is scarce, as their pollen has a low fossilisation potential (Herendeen et al. 1994; Friis et al. 2011) and thus the pollen record for *Cryptocarya* is inexistent. Although placement of fossil leaves in Lauraceae is unequivocal, the assignment to genera or even species is more complex with vegetative organs alone, as leaf morphology varies greatly. This is also the case in extant and fossil *Cryptocarya* (Hill 1986; Christophel et al. 1996; van der Werff 1991, 2001; Bannister et al. 2012). For instance, Christophel et al. (1996) observed that the presumed diagnostic cuticular “butterfly-shaped” ledges of Australian *Cryptocarya* also occur in other extant Lauraceae genera of South America.

Additionally, van der Werff (1991, 2001) noted that the majority of extant genera are defined by floral characters; however, extant flower and fruit samples are difficult to obtain or even unavailable for study (Rohwer 1993; Li et al. 2008a). This makes the identification of fossil Lauraceae even more challenging. Moreover, small delicate reproductive organs are often not preserved as fossils. It should be noted that the presence of *Cryptocarya* in the Miocene of China was previously suggested by fossil fruits found in Zhangpu county which showed similarities

to extant *Cryptocarya bhutanica* Long (Wang et al. 2019), but could not be unambiguously assigned to the genus. Therefore, the fossil flower of this study confirms the occurrence of *Cryptocarya* in the Miocene of Zhangpu and gives new insight into its flower morphology in the geological past.

## Extant biodiversity and palaeoecological implications

Lauraceae are pantropical with about 50 genera and probably 2500 to 3500 species that are mostly evergreen trees and shrubs (Rohwer 1993). While they are mainly distributed in tropical to subtropical regions of Central and South America as well as Southeast Asia, the family is particularly diverse and sometimes dominant in rainforests (Rohwer 1993; Li et al. 2008a; Simpson 2010). About 25 genera and 445 species occur in China and mainly inhabit the southern provinces (Li et al. 2008a, Tan et al. 2023). In the family, *Cryptocarya* is one of the most widespread genera throughout the tropics, with between 200 and 350 species growing in South America, South Africa, Madagascar, Asia, Australia and Oceania, and a centre of diversity in Malaysia (Hyland 1989; van der Werff 1992, 2001; Rohwer 1993; Moraes 2007; Li et al. 2008b; Rohwer et al. 2014). It has been noted that the disjunct distribution of some *Cryptocarya* species was probably caused by fruits dispersion of birds from Gondwana across the Pacific, but that the genus was nonetheless, explicitly monophyletic (Rohwer et al. 2014). Although *Cryptocarya* as a whole still requires a global extensive revision (Rohwer 1993; Rohwer et al. 2014), some studies have recently improved our knowledge of the taxonomy of this genus in South Asia (de Kok 2015, 2016; Nishida et al. 2016).

The Zhangpu amber deposit, where the fossil flower was collected, is a highly diverse megathermal rainforest biome. Amber inclusions of arthropods include more than 250 families, with at least 200 being insects. Bryophytes are represented by about seven liverworts genera, as well as five extant moss taxa (Wang et al. 2021). In contrast, seed plant inclusions from Zhangpu amber are rare and up to date; only three species were described (*Canarium wangboi* Beurel et al. and *Canarium leenhoutsii* Beurel et al. (Burseraceae); Beurel et al. 2023; *Parrotia zhiyanii* Wu et al. (Hamamelidaceae); Wu et al. 2023). Nevertheless, plant megafossils from the amber-bearing sedimentary rocks are extremely rich, including about 24 families. Most of them are megathermal pantropical plant families, such as Annonaceae, Melastomataceae and Moraceae. Among these taxa, Dipterocarpaceae, Leguminosae, Lauraceae and Clusiaceae are the most abundant and diverse ones, with only slight morphological variations compared to their modern members, indicating a possible morphological stasis in the plant community (Wang et al. 2019, 2022; Wang et al. 2021). Within Lauraceae, fossils leaves with probable affinities to *Alseodaphne* Nees, *Cinnamomum* Schaeff. and *Lindera* Thunb. were recently discovered

(Wang et al. 2021, supplementary material, table S1). The palaeoclimate of Zhangpu, as well as the fossil plant taxa are similar to tropical rainforests of Southeast Asia today, suggesting that the Zhangpu amber forest was a megathermal seasonal rainforest during the Mid-Miocene Climatic Optimum (Jacques et al. 2015; Zheng et al. 2019; Wang et al. 2021). Nowadays, *Cryptocarya* is still an important element of evergreen broad-leaved forests in South China, where it is part of the canopy and subcanopy (Wang et al. 2003; Li et al. 2008b). For instance, *C. chinensis* Hemsl. can be found in lower subtropical monsoon evergreen broad-leaved forests (Wang et al. 2003). Thus, the presence of *Cryptocarya* in the Zhangpu amber forest is consistent with the current palaeoclimatic and palaeoenvironmental interpretations (Jacques et al. 2015; Wang et al. 2021).

## Conclusion

In our study, we present the first Cenozoic Lauraceae flower of Asia, based on an amber inclusion from Zhangpu. The application of non-invasive X-ray computed tomography techniques facilitated a detailed morphological examination of the amber inclusion and an in-depth comparison of the fossil flower with extant *Cryptocarya* flowers, revealing their remarkable resemblances. The fossil and extant flowers both have a perianth with six tepals, an androecium comprising nine fertile stamens with bilocular anthers and three staminodes, and a gynoecium with a unicarpellate carpel forming a superior ovary with one apical ovule surrounded by a hypanthium. The distinct presence of a similar staminal tube and position of staminal gland pairs are reported for the first time in *Cryptocarya*, in both the examined extant *C. vulgaris* from Australia and our fossil. This highlights the need to re-evaluate the occurrence (and potential significance) of those characters in other species.

In addition, the amber fossil supports the morphological stasis of Zhangpu plant communities alongside insects in tropical rainforests of Asia since at least the Middle Miocene (Wang et al. 2019, 2022; Wang et al. 2021; Beurel et al. 2023). However, it should be noted that previous affinities of Lauraceae fossil leaves to *Cryptocarya* are still debatable, as the family exhibits a wide range of leaf characters and morphological convergence between genera (Christophel et al. 1996). Nevertheless, the inclusion of this study represents the first fossil record of a flower of *Cryptocarya* and confirms the presence of this genus in the Miocene Zhangpu flora, which was only previously assumed from putative fossil fruits (Wang et al. 2019).

## Acknowledgements

We would like to thank Bo Wang (NIGPAS) and Vincent Perrichot (Univ. Rennes) for the fossil specimen acquisition. We recognise the provision of beamtime, related

to the proposal BAG-20210019 at beamline P05 at PETRA III at DESY, a member of the Helmholtz Association (HGF). This research was supported in part through the Maxwell computational resources operated at Deutsches Elektronen-Synchrotron DESY, Hamburg, Germany.

We are grateful to Kristin Mahlow (MfN) for the scanning of the extant *Cryptocarya* flowers and to David Bruy (NOU, IRD), Pete Lowry (Missouri Botanical Garden), Chrissen Gemmill (Univ. Waikato), Sven Buerki (Univ. Boise), Martin Callmänder (Conservatoire et Jardin Botaniques de Genève), and Jean Waikedre (IRD, Nouméa) for help in the field. *Cryptocarya wilsonii* was collected thanks to the Plants mo Pipol blong Vanuatu project (National Science Foundation grant 1555657 to the New York Botanical Garden). Angelika Haufe (MfN) provided access to extant specimens of Australian *Cryptocarya* from the Schrader herbarium (MfN, Berlin). We also thank Raymond J. Carpenter (Univ. Adelaide) for literature discussion and Corentin Jouault (MNHN) for insect identification. Conservation authorities of the North and South Provinces of New Caledonia (DDEE and DDDT) provided JM with collecting permits. This study was supported by the German Research Foundation [DFG, grant no. 423862824]. We would like to thank Yong Yang and Maria von Balthazar for their comments, which have improved the manuscript.

## References

- Bannister JM, Conran JG, Lee DE (2012) Lauraceae from rainforest surrounding an early Miocene maar lake, Otago, southern New Zealand. *Review of Palaeobotany and Palynology* 178: 13–34. <https://doi.org/10.1016/j.revpalbo.2012.03.015>
- Beurel S, Bachelier JB, Hammel JU, Shi GL, Wu XT, Rühr PT, Sadowski EM (2023) Flower inclusions of *Canarium* (Burseraceae) from Miocene Zhangpu amber (China). *Palaeoworld* 32(4): 592–606. <https://doi.org/10.1016/j.palwor.2023.02.006>
- Carpenter RJ, Iglesias A, Wilf P (2018) Early Cenozoic vegetation in Patagonia: new insights from organically preserved plant fossils (Ligorio Márquez Formation, Argentina). *International Journal of Plant Sciences* 179(2): 115–135. <https://doi.org/10.1086/695488>
- Carpenter RJ, Hill RS, Greenwood DR, Partridge AD, Banks MA (2004) No snow in the mountains: Early Eocene plant fossils from Hotham Heights, Victoria, Australia. *Australian Journal of Botany* 52(6): 685–718. <https://doi.org/10.1071/BT04032>
- Chanderbali AS, van der Werff H, Renner SS (2001) Phylogeny and historical biogeography of Lauraceae: evidence from the chloroplast and nuclear genomes. *Annals of the Missouri Botanical Garden* 88: 104–134. <https://doi.org/10.2307/2666133>
- Christophel DC, Kerrigan R, Rowett AI (1996) The use of cuticular features in the taxonomy of the Lauraceae. *Annals of the Missouri Botanical Garden* 83: 419–432. <https://doi.org/10.2307/2399871>
- Coiffard C, Gomez B, Thiébaud M, Kvaček J, Thévenard F, Néraudeau D (2009) Intramarginal veined Lauraceae leaves from the Albian-Cenomanian of Charente-Maritime (Western France). *Palaeontology* 52(2): 323–336. <https://doi.org/10.1111/j.1475-4983.2009.00845.x>
- Conran JG, Christophel DC (1998) A new species of triplinerved *Laurophyllum* from the Eocene of Nerriga, New South Wales. *Alcheringa* 22(4): 343–348. <https://doi.org/10.1080/03115519808619332>
- De Kok RPJ (2015) A revision of *Cryptocarya* (Lauraceae) from Thailand and Indochina. *Gardens' Bulletin Singapore* 67(2): 309–350. <https://doi.org/10.3850/S2382581215000277>
- De Kok RPJ (2016) A revision of *Cryptocarya* R. Br. (Lauraceae) of peninsular Malaysia. *Kew Bulletin* 71(1): 1–26. <https://doi.org/10.1007/s12225-016-9613-1>
- Drinnan AN, Crane PR, Friis EM, Pedersen KR (1990) Lauraceous flowers from the Potomac Group (mid-Cretaceous) of eastern North America. *Botanical Gazette* 151(3): 370–384. <https://doi.org/10.1086/337838>
- Eklund H, Kvaček J (1998) Lauraceous inflorescences and flowers from the Cenomanian of Bohemia (Czech Republic, central Europe). *International Journal of Plant Sciences* 159(4): 668–686. <https://doi.org/10.1086/297585>
- Friis EM, Crane PR, Pedersen KR (2011) Early flowers and angiosperm evolution. Cambridge University Press, 585 pp. <https://doi.org/10.1017/CBO9780511980206>
- Frumin S, Eklund H, Friis EM (2004) *Mauldinia hirsuta* sp. nov., a new member of the extinct genus *Mauldinia* (Lauraceae) from the Late Cretaceous (Cenomanian-Turonian) of Kazakhstan. *International Journal of Plant Sciences* 165(5): 883–895. <https://doi.org/10.1086/421479>
- Garrouste R, Munzinger J, Leslie A, Fisher J, Folcher N, Locatelli E, Foy W, Chaillon T, Cantrill DJ, Maurizot P, Cluzel D, Lowry II PP, Crane P, Bahain JJ, Voinchet P, Jourdan H, Grandcolas P, Nel A (2021) New fossil discoveries illustrate the diversity of past terrestrial ecosystems in New Caledonia. *Scientific reports* 11(1): 1–10. <https://doi.org/10.1038/s41598-021-97938-5>
- Greving I, Wilde F, Ogurreck M, Herzen J, Hammel JU, Hipp A, Friedrich F, Lottermoser L, Dose T, Burmester H, Müller M, Beckmann F (2014) P05 imaging beamline at PETRA III: first results. In: Stock SR (Eds) *Developments in X-ray Tomography IX, Proceedings of SPIE 9212*, 166–173. <https://doi.org/10.1117/12.2061768>
- Haibel A, Beckmann F, Dose T, Herzen J, Ogurreck M, Müller M, Schreyer A (2010) Latest developments in microtomography and nanotomography at PETRA III. *Powder Diffraction* 25(2): 161–164. <https://doi.org/10.1154/1.3428364>
- Herendeen PS, Crepet WL, Nixon KC (1994) Fossil flowers and pollen of Lauraceae from the Upper Cretaceous of New Jersey. *Plant Systematics and Evolution* 189(1): 29–40. <https://doi.org/10.1007/BF00937576>
- Hill RS (1986) Lauraceous leaves from the Eocene of Nerriga, New South Wales. *Alcheringa* 10(4): 327–351. <https://doi.org/10.1080/03115518608619144>
- Hill RS (1988) Australian Tertiary angiosperm and gymnosperm leaf remains – an updated catalogue. *Alcheringa* 12(3): 207–219. <https://doi.org/10.1080/03115518808619133>
- Ho KS, Chen JC, Lo CH, Zhao HL (2003) <sup>40</sup>Ar–<sup>39</sup>Ar dating and geochemical characteristics of late Cenozoic basaltic rocks from the Zhejiang-Fujian region, SE China: eruption ages, magma evolution and petrogenesis. *Chemical Geology* 197(1–4): 287–318. [https://doi.org/10.1016/S0009-2541\(02\)00399-6](https://doi.org/10.1016/S0009-2541(02)00399-6)
- Holden AM (1982) Fossil Lauraceae and Proteaceae from the Longford Formation, Murchison, New Zealand. *Journal of the Royal Society of New Zealand* 12(1): 79–90. <https://doi.org/10.1080/03036758.1982.10427169>

- Hu YQ, Ferguson DK, Li CS, Xiao YP, Wang YF (2007) *Alseodaphne* (Lauraceae) from the Pliocene of China and its paleoclimatic significance. *Review of Palaeobotany and Palynology* 146(1–4): 277–285. <https://doi.org/10.1016/j.revpalbo.2007.06.002>
- Huang LL, Li SF, Huang WY, Jin JH, Oskolski AA (2023) *Cryptocarya chinensis* from the Upper Pleistocene of South China and its biogeographic and paleoecological implications. *Iscience* 26(8): 107313. <https://doi.org/10.1016/j.isci.2023.107313>
- Huang Y, Jia L, Wang Q, Mosbrugger V, Utescher T, Su T, Zhou Z (2016) Cenozoic plant diversity of Yunnan: a review. *Plant Diversity* 38(6): 271–282. <https://doi.org/10.1016/j.pld.2016.11.004>
- Hyland BPM (1989) A revision of Lauraceae in Australia (excluding *Cassytha*). *Australian Systematic Botany* 2(2): 135–367. <https://doi.org/10.1071/SB9890135>
- Jacques FM, Guo SX, Su T, Xing YW, Huang YJ, Liu YSC, Ferguson DK, Zhou ZK (2011) Quantitative reconstruction of the Late Miocene monsoon climates of southwest China: a case study of the Lincang flora from Yunnan Province. *Palaeogeography, Palaeoclimatology, Palaeoecology* 304(3–4): 318–327. <https://doi.org/10.1016/j.palaeo.2010.04.014>
- Jacques FM, Shi G, Su T, Zhou Z (2015) A tropical forest of the middle Miocene of Fujian (SE China) reveals Sino-Indian biogeographic affinities. *Review of Palaeobotany and Palynology* 216: 76–91. <https://doi.org/10.1016/j.revpalbo.2015.02.001>
- Kostermans AJGH (1937) Revision of the Lauraceae II. The genera *Endlicheria*, *Cryptocarya* (American species) and *Licaria*. *Recueil des Travaux Botaniques Néerlandais* 34(2): 500–609. <https://naturtijdschriften.nl/pub/552261>
- Kvaček Z (1992) Lauralean angiosperms in the Cretaceous. *Courier Forschungsinstitut Senckenberg* 147: 345–367.
- Kvaček J, Eklund H (2003) A report on newly recovered reproductive structures from the Cenomanian of Bohemia (Central Europe). *International Journal of Plant Sciences* 164(6): 1021–1039. <https://doi.org/10.1086/378824>
- Li XW, Li J, Huang PH, Wei FN, Cui HB, van der Werff H (2008a) Lauraceae. In: Wu ZY, Raven PH, Hong DY (Eds) *Flora of China*, Vol. 7. Science Press, Beijing, and Missouri Botanical Garden Press, St. Louis, 102–254. [http://www.efloras.org/florataxon.aspx?flora\\_id=2&taxon\\_id=10479](http://www.efloras.org/florataxon.aspx?flora_id=2&taxon_id=10479)
- Li XW, Li J, van der Werff H (2008b) *Cryptocarya*. In: Wu ZY, Raven PH, Hong DY (Eds) *Flora of China*, Vol. 7. Science Press, Beijing, and Missouri Botanical Garden Press, St. Louis, 247–254. [http://www.efloras.org/florataxon.aspx?flora\\_id=2&taxon\\_id=108511](http://www.efloras.org/florataxon.aspx?flora_id=2&taxon_id=108511)
- Liu YS (1993) A palaeoclimatic analysis on early Pleistocene flora of Changsheling Formation, Baise Basin, Guangxi. *Acta Palaeontologica Sinica* 32(2): 151–169. [in Chinese, with English abstract]
- MacGinitie HD (1941) A Middle Eocene flora from the central Sierra Nevada. *Carnegie Institute Washington Publication* 534: 1–169. <http://sierrageology.org/documents/references/a-middle-eocene-flora-from-the-central-sierra-nevada/>
- Moosmann J, Ershov A, Weinhardt V, Baumbach T, Prasad MS, LaBonne C, Xiao X, Kashef J, Hofmann R (2014) Time-lapse X-ray phase-contrast microtomography for in vivo imaging and analysis of morphogenesis. *Nature Protocols* 9(2): 294–304. <https://doi.org/10.1038/nprot.2014.033>
- Moraes PLR de (2007) Taxonomy of *Cryptocarya* species of Brazil. *ABC Taxa* 3: 1–191.
- Moreau JD, Gomez B, Daviero-Gomez V, Néraudeau D, Tafforeau P (2016) Inflorescences of *Mauldinia* sp. (Lauraceae) and associated fruits from the Cenomanian of Languedoc Roussillon, France. *Cretaceous Research* 59: 18–29. <https://doi.org/10.1016/j.cretres.2015.10.018>
- Nishida S, De Kok R, Yang Y (2016) Cuticular features of *Cryptocarya* (Lauraceae) from Peninsular Malaysia, Thailand and Indo-China and its taxonomic implications. *Phytotaxa* 244(1): 26–44. <https://doi.org/10.11646/phytotaxa.244.1.2>
- Palenstijn WJ, Batenburg KJ, Sijbers J (2011) Performance improvements for iterative electron tomography reconstruction using graphics processing units (GPUs). *Journal of Structural Biology* 176(2): 250–253. <https://doi.org/10.1016/j.jsb.2011.07.017>
- Poinar Jr G (2017) A mid-Cretaceous Lauraceae flower, *Cascolaurus burmitis* gen. et sp. nov., in Myanmar amber. *Cretaceous Research* 71: 96–101. <https://doi.org/10.1016/j.cretres.2016.11.015>
- Pole M (1993) Early Miocene flora of the Manuhierikia Group, New Zealand. 6. Lauraceae. *Journal of the Royal Society of New Zealand* 23(4): 303–312. <https://doi.org/10.1080/03036758.1993.10721228>
- Pole M (2007) Lauraceae macrofossils and dispersed cuticle from the Miocene of southern New Zealand. *Palaeontologia Electronica* 10(1): 1–38.
- Pole M (2019) A Survey of Pliocene to Mid Quaternary leaf cuticle from the North Island, New Zealand. *Palaeontologia Electronica* 22(1): 1–32. <https://doi.org/10.26879/862>
- Rohwer JG (1993) Lauraceae. In: Kubitzki K, Rohwer JG, Bittrich V (Eds) *The families and genera of vascular plants*, vol 2. Springer, Berlin, 366–391. [https://doi.org/10.1007/978-3-662-02899-5\\_46](https://doi.org/10.1007/978-3-662-02899-5_46)
- Rohwer JG (1994) A note on the evolution of the stamens in the Laurales, with emphasis on the Lauraceae. *Botanica Acta* 107: 103–110. <https://doi.org/10.1111/j.1438-8677.1994.tb00415.x>
- Rohwer JG, Moraes PLR de, Rudolph B, Van der Werff H (2014) A phylogenetic analysis of the *Cryptocarya* group (Lauraceae), and relationships of *Dahlgrenodendron*, *Sinopora*, *Triadodaphne*, and *Yasunia*. *Phytotaxa* 158(2): 111–132. <https://doi.org/10.11646/phytotaxa.158.2.1>
- Sadowski EM, Schmidt AR, Seyfullah LJ, Solórzano-Kraemer MM, Neumann C, Perrichot V, Hamann C, Milke R, Nascimbene PC (2021) Conservation, preparation and imaging of diverse ambers and their inclusions. *Earth-Science Reviews* 220: 103653. <https://doi.org/10.1016/j.earscirev.2021.103653>
- Shi G, Li H (2010) A fossil fruit wing of *Dipterocarpus* from the middle Miocene of Fujian, China and its palaeoclimatic significance. *Review of Palaeobotany and Palynology* 162(4): 599–606. <https://doi.org/10.1016/j.revpalbo.2010.08.001>
- Shi G, Jacques FM, Li H (2014a) Winged fruits of *Shorea* (Dipterocarpaceae) from the Miocene of Southeast China: Evidence for the northward extension of dipterocarps during the Mid-Miocene Climatic Optimum. *Review of Palaeobotany and Palynology* 200: 97–107. <https://doi.org/10.1016/j.revpalbo.2013.09.003>
- Shi G, Dutta S, Paul S, Wang B, Jacques FM (2014b) Terpenoid compositions and botanical origins of Late Cretaceous and Miocene amber from China. *PLoS ONE* 9(10): e111303. <https://doi.org/10.1371/journal.pone.0111303>
- Shi GL, Xie ZM, Li HM (2014c) High diversity of Lauraceae from the Oligocene of Ningming, South China. *Palaeoworld* 23(3–4): 336–356. <https://doi.org/10.1016/j.palwor.2014.08.001>

- Simpson MG (2010) Laurales. In: Simpson MG (Ed.) Plant Systematics. Academic Press, Amsterdam, 190–192. <https://doi.org/10.1016/B978-0-12-374380-0.50001-4>
- Sun BN, Wu JY, Liu YSC, Ding ST, Li XC, Xie SP, Yan DF, Lin ZC (2011) Reconstructing Neogene vegetation and climates to infer tectonic uplift in western Yunnan, China. *Palaeogeography, Palaeoclimatology, Palaeoecology* 304(3–4): 328–336. <https://doi.org/10.1016/j.palaeo.2010.09.023>
- Takahashi M, Crane PR, Ando H (1999) Fossil flowers and associated plant fossils from the Kamikitaba locality (Ashizawa Formation, Futaba Group, lower Coniacian, upper Cretaceous) of Northeast Japan. *Journal of Plant Research* 112(2): 187–206. <https://doi.org/10.1007/PL00013872>
- Takahashi M, Herendeen PS, Crane PR (2001) Lauraceous fossil flower from the Kamikitaba locality (Lower Coniacian; Upper Cretaceous) in northeastern Japan. *Journal of Plant Research* 114(4): 429–434. <https://doi.org/10.1007/PL00014008>
- Takahashi M, Herendeen PS, Xiao X, Crane PR (2014) Lauraceous fossil flowers from the Kamikitaba assemblage (Coniacian, Late Cretaceous) of northeastern Japan (Lauraceae). *Systematic Botany* 39(3): 715–724. <https://doi.org/10.1600/036364414X681464>
- Tan C, Ferguson DK, Tang ZY, Yang Y (2023) Distribution and conservation of Lauraceae in China. *Global Ecology and Conservation* 46: e02566. <https://doi.org/10.1016/j.gecco.2023.e02566>
- van Aarle W, Palenstijn WJ, De Beenhouwer J, Altantzis T, Bals S, Batenburg KJ, Sijbers J (2015) The ASTRA Toolbox: A platform for advanced algorithm development in electron tomography. *Ultramicroscopy* 157: 35–47. <https://doi.org/10.1016/j.ultramicro.2015.05.002>
- van Aarle W, Palenstijn WJ, Cant J, Janssens E, Bleichrodt F, Dabrovolski A, De Beenhouwer J, Batenburg KJ, Sijbers J (2016) Fast and flexible X-ray tomography using the ASTRA toolbox. *Optics Express* 24(22): 25129–25147. <https://doi.org/10.1364/OE.24.025129>
- van der Werff H (1991) A key to the genera of Lauraceae in the New World. *Annals of the Missouri Botanical Garden* 78(2): 377–387. <https://doi.org/10.2307/2399567>
- van der Werff H (1992) Proposal to conserve 2813 *Cryptocarya* against *Ravensara* (Lauraceae). *Taxon* 41: 129. <https://doi.org/10.2307/1222506>
- van der Werff H (2001) An annotated key to the genera of Lauraceae in the Flora Malesiana region. *Blumea* 46(1): 125–140. <https://repository.naturalis.nl/pub/525118>
- Viehofen A, Hartkopf-Fröder C, Friis EM (2008) Inflorescences and flowers of *Mauldinia angustiloba* sp. nov. (Lauraceae) from middle Cretaceous karst infillings in the Rhenish Massif, Germany. *International Journal of Plant Sciences* 169(7): 871–889. <https://doi.org/10.1086/589975>
- von Balthazar M, Pedersen KR, Crane PR, Stambanoni M, Friis EM (2007) *Potomacanthus lobatus* gen. et sp. nov., a new flower of probable Lauraceae from the Early Cretaceous (Early to Middle Albian) of Eastern North America. *American Journal of Botany* 94(12): 2041–2053. <https://doi.org/10.3732/ajb.94.12.2041>
- Wang B, Shi G, Xu C, Spicer RA, Perrichot V, Schmidt AR, Feldberg K, Heinrichs J, Chény C, Pang H, Liu X, Gao T, Wang Z, Ślipiński A, Solórzano-Kraemer MM, Heads SW, Thomas MJ, Sadowski E-M, Szwedo J, Azar D, Nel A, Liu Y, Chen J, Zhang Q, Zhang Q, Luo C, Yu T, Zheng D, Zhang H, Engel MS (2021) The mid-Miocene Zhangpu biota reveals an outstandingly rich rainforest biome in East Asia. *Science Advances* 7(18): eabg0625. <https://doi.org/10.1126/sciadv.abg0625>
- Wang Z, Shi G, Sun B, Jia H, Dong C, Yin S, Wu X (2022) A new *Cercis* (Leguminosae) from the middle Miocene of Fujian, China. *Historical Biology* 34(1): 94–101. <https://doi.org/10.1080/08912963.2021.1900170>
- Wang Z, Sun F, Wang J, Yan D, Dong J, Sun M, Sun B (2019) New fossil leaves and fruits of Lauraceae from the Middle Miocene of Fujian, southeastern China differentiated using a cluster analysis. *Historical Biology* 31(5): 581–599. <https://doi.org/10.1080/08912963.2017.1379517>
- Wu XT, Shu JW, Yin SX, Sadowski EM, Shi GL (2023) *Parrotia* flower blooming in Miocene rainforest. *Journal of Systematics and Evolution*. <https://doi.org/10.1111/jse.13001>
- Wang ZF, Peng SL, Liu SZ, Li Z (2003) Spatial pattern of *Cryptocarya chinensis* life stages in lower subtropical forest, China. *Botanical Bulletin of Academia Sinica* 44: 159–166.
- Wilde F, Ogurreck M, Greving I, Hammel JU, Beckmann F, Hipp A, Lottermoser L, Khokhriakov I, Lytaev P, Dose T, Burmester H, Müller M, Schreyer A (2016) Micro-CT at the imaging beamline P05 at PETRA III. In: Shen Q, Nelson C (Eds) Proceedings of the 12<sup>th</sup> International Conference on Synchrotron Radiation Instrumentation, New York (USA), 2015. American Institute of Physics Conference Proceedings 1741(1): 030035. <https://doi.org/10.1063/1.4952858>
- Zheng D, Shi G, Hemming SR, Zhang H, Wang W, Wang B, Chang SC (2019) Age constraints on a Neogene tropical rainforest in China and its relation to the Middle Miocene Climatic Optimum. *Palaeogeography, Palaeoclimatology, Palaeoecology* 518: 82–88. <https://doi.org/10.1016/j.palaeo.2019.01.019>
- Zheng Y, Wang W (1994) Sequence of Miocene Fotan Group in SE Fujian and its palyno-assemblages. *Acta Palaeontologica Sinica* 33(2): 200–216. [in Chinese, with English abstract]



# A digital redescription of the Middle Miocene (Langhian) carettochelyid turtle *Allaeochelys libyca*

Yann Rollot<sup>1</sup>, Serjoscha W. Evers<sup>1</sup>, Walter G. Joyce<sup>1</sup>

<sup>1</sup> Chemin du Musée 6, Department of Geosciences, University of Fribourg, Fribourg, Switzerland

<https://zoobank.org/EB036D6D-C69E-4741-845B-748FD9C47065>

Corresponding author: Yann Rollot ([yann.rollot@gmail.com](mailto:yann.rollot@gmail.com))

Academic editor: Torsten Scheyer ♦ Received 1 November 2023 ♦ Accepted 11 December 2023 ♦ Published 4 January 2024

## Abstract

*Allaeochelys libyca* is a carettochelyid turtle from the Middle Miocene of Libya. The species is the only valid carettochelyid taxon recovered from Africa and was named based on fragmentary material that includes a partial cranium and isolated shell remains. The description of the holotype cranium was limited to external aspects, and micro-computed tomography was only performed later on that material. Here, we use these micro-computed tomography scans to reinvestigate the external and internal anatomy of the holotype cranium to document several erroneous anatomical interpretations and provide new insights into the morphology of the trigeminal foramen area, the endosseous labyrinth, and circulatory system of *Allaeochelys libyca*. The anatomical insights provided herein have the potential to be translated into new phylogenetic characters that are expected to improve the resolution among the *Anosteira* and *Allaeochelys* lineages, which are still poorly resolved.

## Key Words

anatomy, Carettochelyidae, micro-computed tomography, Miocene

## Introduction

Carettochelyidae is a clade of aquatic, hidden neck turtles (Cryptodira), of which the only extant representative, the pig-nosed turtle *Carettochelys insculpta*, lives as a relict species in New Guinea and Australia (Ramsay 1887; Joyce 2014; TTWG 2021). The clade used to have a wider geographic distribution and higher diversity. The oldest occurrences in the fossil record are fragmentary remains from the mid Cretaceous. Two taxa are currently recognized from that time period, *Kizylkumemys khoratensis* from the Aptian of Thailand and *Kizylkumemys schultzi* from the Cenomanian of Uzbekistan (Nessov 1976, 1977; Tong et al. 2005, 2006). More abundant remains are known from the Cenozoic with a dozen valid species having been described from deposits across Asia, North America, Europe, and Africa (Joyce 2014 and references therein; Carbot-Chanona et al. 2020; White et al. 2023). The available fossil material mostly consists of shell material, but skull remains are known for about half of the

valid carettochelyid taxa, in particular *Anosteira pulchra* (Joyce et al. 2018), *Anosteira maomingensis* (Tong et al. 2010; Danilov et al. 2017), *Allaeochelys crassesculpta* (Harrassowitz 1922), *Allaeochelys libyca* (Havlik et al. 2014), and *Carettochelys niahensis* (White et al. 2023). Several studies documented the cranial anatomy of the extant *Carettochelys insculpta* (Ramsay 1887; Baur 1889; Waite 1905; Walther 1922; Joyce 2014).

*Allaeochelys libyca* from the Middle Miocene (Langhian) of Libya was described based on a partial cranium and several, isolated shell fragments (Havlik et al. 2014). Although other carettochelyid remains have been reported from Egypt (Dacqué 1912; Lapparent de Broin 2000), the Democratic Republic of the Congo (Hirayama 1992), and perhaps Saudi Arabia (Thomas et al. 1982), these consist of rare, isolated shell elements that are currently not diagnostic enough to identify additional species. *Allaeochelys libyca*, therefore, is the only valid African taxon to date. The study of Havlik et al. (2014) documented all externally available aspects

of the anatomy of the cranium, but as tomographic scans were not performed at that time, internal structures and cavities, such as the inner ear, the cavum acustico-jugulare, and canals for arteries and nerves, were not described. In the meantime, this cranium was scanned using micro-computed tomography ( $\mu$ CT) and the slice data alongside the 3D models of the inner ear and cranium were made publicly available on the online repository MorphoSource (Evers 2021) as part of a study on turtle inner ears (Evers et al. 2022). As part of an ongoing project that aims to document unpublished and historical carettochelyid material, we downloaded the  $\mu$ CT scans of the cranium of *Allaeochelys libyca*, but noticed differences in the interpretation of some anatomical features between our three-dimensional reconstructions and the original description provided by Havlik et al. (2014). We, therefore, here present the results of the bone-by-bone segmentation of this skull, which allows us to correct said erroneous anatomical interpretations and to document additional features that could not be documented originally, such as the anatomy of the cavum acustico-jugulare or the circulatory system. The new anatomical information highlighted in the present contribution does not challenge the validity of the species *Allaeochelys libyca*, but is expected to have an impact on phylogenetic matrices, which will be explored elsewhere.

## Institutional abbreviations

**BSPG**, Bayerische Staatssammlung für Paläontologie und Geologie, München, Germany; **FMNH**, Field Museum of Natural History, Chicago, USA; **NHMUK**, Natural History Museum London, London, England.

## Material and methods

The material of *Allaeochelys libyca* is housed at the Bayerische Staatssammlung für Paläontologie und Geologie, Munich, Germany. BSPG 1991 II 130 was scanned at the School of Earth Sciences X-ray Tomography Facility of the University of Bristol using a Nikon Metrology XT H 225 ST scanner, with a voltage of 125 kV, a current of 265  $\mu$ A, 1601 projections, and no filter. The scanning resulted in 1813 coronal slices and a voxel size of 37.8  $\mu$ m. Scans are available at MorphoSource (<https://www.morphosource.org/concern/media/000350560>; Evers 2021). BSPG 1991 II 130 was segmented in Mimics Innovation Suite 25 (<https://www.materialise.com/en/healthcare/mimics-innovation-suite>) using the lasso and interpolation tools. The segmented objects were exported as .ply files and visualized in Blender 2.79b (<https://www.blender.org>) to create high-quality illustrations and figures. 3D models were deposited at MorphoSource (<https://www.morphosource.org/projects/000570948>).

We frequently cite for comparison the cranial anatomy of *Carettochelys insculpta*. Although this species has seen several cranial descriptions (Ramsay 1887; Baur 1889; Waite 1905; Walther 1922; Joyce 2014), many of our observations are not based on these descriptions, but on a fully segmented specimen (NHMUK 1903.7.10.1), which will be described in detail elsewhere. The CT scans of that specimen as well as 3D models of its cranium and endosseous labyrinth have already been published (CT scans: <https://www.morphosource.org/concern/media/000077378>; 3D models: cranium, <https://www.morphosource.org/concern/media/000373013>; endosseous labyrinth, <https://www.morphosource.org/concern/media/000373016>), whereas the bone-by-bone segmentations will be released with the aforementioned description.

## Systematic palaeontology

**Testudines Batsch, 1788**

**Cryptodira Cope, 1868**

**Trionychia Baur, 1891**

**Carettochelyidae Gill, 1889**

***Allaeochelys* Noulet, 1867**

***Allaeochelys libyca* Havlik et al., 2014**

**Holotype.** BSPG 1991 II 130, an incomplete cranium.

**Referred material.** BSPG 1991 II 96, a left hypoplastron; BSPG 1991 II 97, a left hypoplastron; BSPG 1991 II 110, a bridge peripheral; BSPG 1991 II 113, an anterior peripheral; BSPG 1991 II 114, a peripheral I; BSPG 1991 II 131, an incomplete supraoccipital.

**Type locality and horizon.** Gebel Zelten (Jabal Zaltan), southwestern slopes, localities “MS 2” or “Wadi Shatirat,” Al Wahat District, Libya (Wessels et al. 2003). Lower Maradah Formation, Middle Miocene, Langhian (Desio 1935; Wessels et al. 2003).

**Revised diagnosis.** *Allaeochelys libyca* can be diagnosed as a representative of Carettochelyidae based on its dermal ornamentation made of thick ridges separated by equally sized grooves, presence of a deep fossa on the posterior surface of the quadrate, and a reduced antrum postoticum and a member of Carettochelyinae based on the absence of carapacial and plastral scutes and the presence of a broad plastron. *Allaeochelys libyca* can be differentiated from *Carettochelys insculpta* by having a broader and shorter cranium, a secondary contact between the prefrontal and frontal within the orbit, a more posteriorly located foramen posterius canalis carotici interni close to the fenestra postotica, a larger contribution of the opisthotic to the tubercula basioccipitale, a deeper pterygoid fossa, a larger quadrate fossa, a deeper sulcus between the mandibular condyles, a reduced canalis cavernosus, and absence of the sulcus cavernosus. *Allaeochelys libyca* resembles *Carettochelys niahensis* by having a secondary contact between the prefrontal and frontal, but appears to have an even broader skull.

## Description and comparisons of the cranium of *Allaeochelys libyca*

**General comments.** The cranium of BSPG 1991 II 130, the holotype of *Allaeochelys libyca*, lacks most of its anteroventral and ventrolateral portions (Fig. 1). The premaxillae, maxillae, jugals, vomer, epipterygoids, and squamosals are not preserved. The palatines and postorbitals are almost completely lacking as well, and only small pieces of bone belonging to the most posterior and most medial portions of the right palatine and left postorbital, respectively, remain attached to the cranium. The prefrontals, frontals, parietals, pterygoids, parabasisphenoid, supraoccipital, and opisthotics lack substantial amounts of their original anatomy, whereas the prootics, quadrates, and basioccipital suffer from minor signs of damage. The exoccipitals are the only bones that are fully preserved.

The preserved portions of the skull roof highlight the presence of the characteristic carettochelyid skull sculpturing, made of thick ridges separated by equally sized grooves (Fig. 1). As in all carettochelyids (see Baur 1889; Harrassowitz 1922; Walther 1922; Joyce 2014; Danilov et al. 2017; Joyce et al. 2018; White et al. 2023), the upper temporal emargination is deep, the supraoccipital is posteriorly expanded by means of a well-developed crista supraoccipitalis and horizontal plate, the incisura columella auris is fully enclosed by the quadrate, the mandibular condyle is low, the palatines posteriorly contact the parabasisphenoid and fully separate the pterygoids, and the quadrate is posteriorly excavated by a fossa. The cranium is more robust and less gracile than that of *Anosteira pulchra* (Joyce et al. 2018), but broader than *Carettochelys insculpta* (Walther 1922). Although comparisons are difficult, proportions seem to be similar to *Carettochelys niahensis* (White et al. 2023). A unique feature exhibited by the cranium of *Allaeochelys libyca* is the complete reduction of the sulcus cavernosus, which is accompanied by a particular morphology of the trigeminal nerve foramen area.

The “trigeminal foramen” of turtles is somewhat of a misnomer, as only two of three of the trigeminal nerve rami exit this passage (Evers et al. 2019). The foramen instead is a lateral window from the outside into the region of the sulcus cavernosus, through which said nerve rami pass in addition to the mandibular artery of some groups of turtles (Albrecht 1967, 1976; Rollot et al. 2021a). When viewed from the side, the trigeminal foramen of *Carettochelys insculpta* is a large, diagonally arranged, oval opening. Superficially, the anterodorsal third of this opening corresponds to the trigeminal passage per se, while the posteroventral third corresponds to the passage of the mandibular artery into the lower temporal fossa. In BSPG 1991 II 130, the descending branch of the prootic is laterally displaced, perhaps obliterating the passage of the lateral head vein and visually separating passage of the trigeminal nerve rami and the mandibular artery. As preserved, only portions of the trigeminal foramen system can be observed, making it necessary to communicate

about its subparts. We here explicitly refer to the anterior foramen of BSPG 1991 II 130 as the trigeminal foramen *sensu stricto*, but the posterior foramen as the mandibular artery foramen, while recognizing that the two combined, if separated, are homologous with the trigeminal foramen *sensu lato* of *Carettochelys insculpta* (see Prootic below).

**Nasal.** The nasals are absent in BSPG 1991 II 130 (Fig. 1A–D), as in all carettochelyids (Waite 1905; Harrassowitz 1922; Walther 1922; Danilov et al. 2017; Joyce et al. 2018; White et al. 2023).

**Prefrontal.** The two prefrontals are heavily damaged. While most of the right element is missing, with only the most dorsomedial part being apparent, its left counterpart preserves the dorsal plate, but the descending process is completely missing (Fig. 1A–D). The anterior surface of the left prefrontal is smooth and an articulation facet is missing, showing that the nasal is absent (Fig. 1E). The prefrontal, therefore, forms the dorsal margin of the apertura narium externa and the dorsal roof of the fossa nasalis. The prefrontal also forms the dorsal margin of the orbit. The ventrolateral portion of the prefrontal forms the dorsal base of the descending process. The lateral half of that base forms an articulation facet, which corresponds to the ventrolateral contact of the prefrontal with the ascending process of the maxilla (Fig. 1C), while the medial half ventrally highlights a broken surface, i.e., the area where the descending process of the prefrontal is broken off. The prefrontal otherwise contacts the frontal posteriorly along a convex suture. The left prefrontal additionally exhibits a small, asymmetric, posteromedial contact with the right frontal (Fig. 1A, B).

**Frontal.** The two frontals are nearly complete. The right element lacks its most anterolateral portion. Additional, minor damage can be seen along the crista cranii of both bones (Fig. 1A, B). The frontal contacts the prefrontal anteriorly along a slightly concave suture, the parietal posteriorly, and the postorbital posterolaterally (Fig. 1A, B). The frontal is wider than long and anterolaterally forms a short process that forms the posterodorsal margin of the orbit (Fig. 1A). The extent of this contribution to the orbit margin is similar to that of most carettochelyids (Waite 1905; Harrassowitz 1922; Walther 1922; White et al. 2023) but not *Anosteira pulchra* and *Anosteira maomingensis*, in which this contribution is slightly broader (Danilov et al. 2017; Joyce et al. 2018). Ventrally, the frontals form low crista cranii, which jointly delimit a moderately broad sulcus olfactorius (Fig. 1B). The posterior half of the two cristae collectively encapsulate an area that is enlarged relative to the sulcus olfactorius and that contained the olfactory bulbs (Evers et al. 2019). The anteromedial part of the crista cranii is mediolaterally broadened and forms an oval articulation facet (Fig. 1B). This facet, previously not reported by Havlik et al. (2014), likely corresponds to a secondary contact between the crista cranii of the frontal and the descending process of the prefrontal. A similar arrangement is present in *Carettochelys niahensis*, where a secondary contact

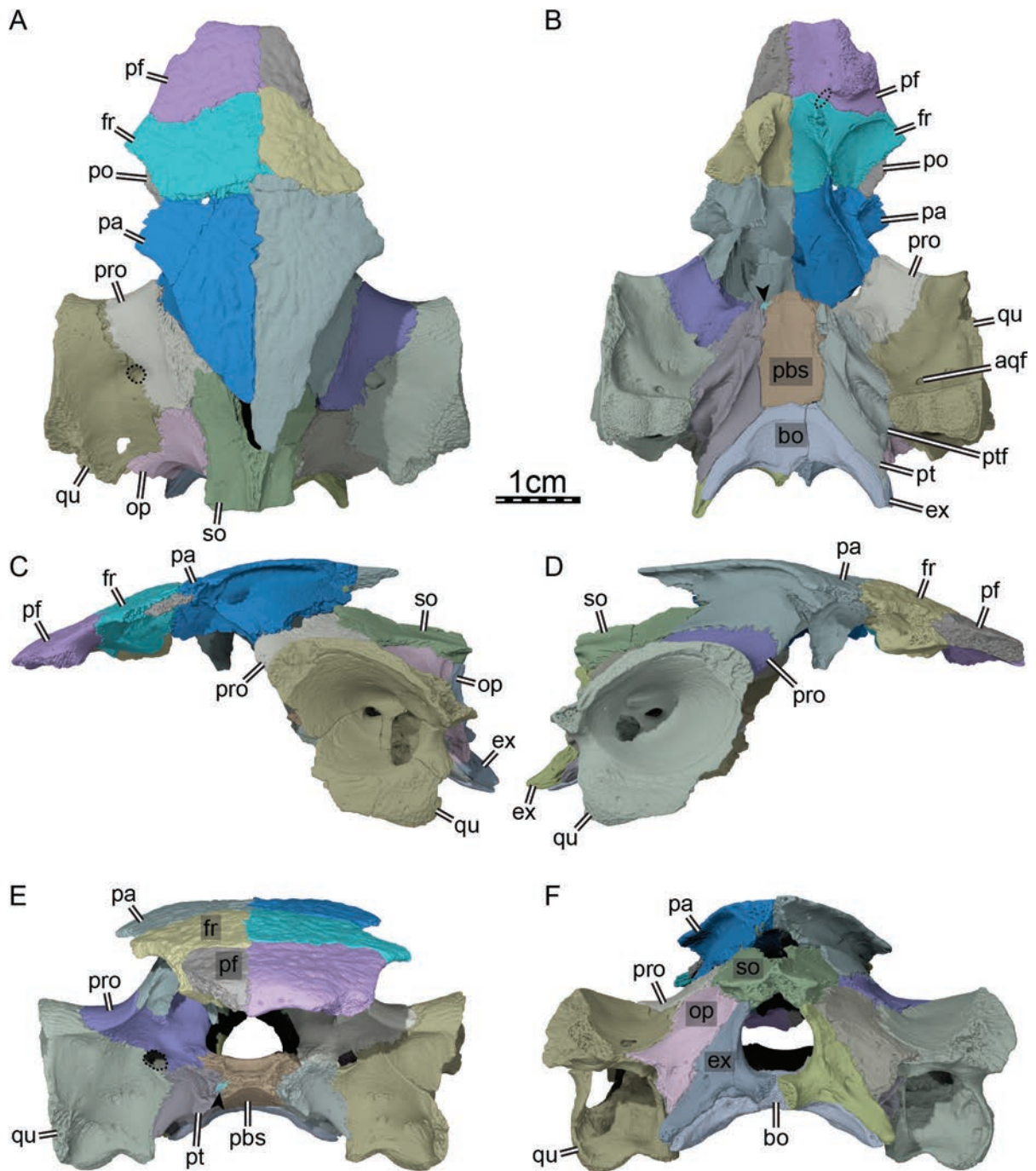


**Figure 1.** Three-dimensional renderings of the segmented cranium of BSPG 1991 II 113. **A.** Dorsal view; **B.** Ventral view; **C.** Left lateral view; **D.** Right lateral view; **E.** Anterior view; **F.** Posterior view. Abbreviations: aqf, anterior quadrate foramen; bo, basioccipital; ex, exoccipital; fr, frontal; op, opisthotic; pa, parietal; pbs, parabasisphenoid; pf, prefrontal; po, postorbital; pro, prootic; pt, pterygoid; ptf, pterygoid fossa; qu, quadrate; so, supraoccipital. Black arrowhead indicates the small, preserved portion of the right palatine. Dashed lines indicate the foramen stapedio-temporale in **A**, the passage between the orbit and nasal cavity in **B**, and the mandibular artery foramen in **E**.

between the frontal and prefrontal anteriorly delimits a foramen that forms a passage between the orbit and the nasal cavity (White et al. 2023). In the extant turtle *Carettochelys insculpta*, such a contact is not present, but the crista cranii closely approaches the descending process of the prefrontal, forming a slit-like passage between the orbital and nasal cavities along the most anterior portion of the foramen interorbitale (Walther

1922; Joyce 2014). The condition described for *Carettochelys niahensis* and *Allaeochelys libyca* likely highlights an extended degree of ossification of the interorbital area compared to *Carettochelys insculpta*.

**Parietal.** The parietal forms the posterior half of the skull roof, the lateral half of the upper temporal emargination, and roofs the braincase. The dorsal plate of the parietal is nearly complete, only missing its most distal

part, and contacts the frontal anteriorly, the postorbital anterolaterally, and the supraoccipital posteroventrally (Fig. 1). Within the upper temporal fossa, the parietal contacts the prootic laterally and the supraoccipital posteriorly (Fig. 1A). The descending process of each parietal is severely damaged and only preserves its most dorsal portions (Fig. 1C, D). Nevertheless, the bony contacts of the parietal around the foramen nervi trigemini *sensu stricto* can be inferred based on comparisons with the extant *Carettochelys insculpta*. In both the extant form and BSPG 1991 II 130, the posterior margin of the foramen nervi trigemini *sensu stricto* is imprinted onto the anterior surface of the prootic. The dorsal end of this imprint is formed by a small, anteroventral bump-like process of the prootic, which is well visible in the fossil on both sides. As preserved, this bump prohibits the posterior end of the descending process of the parietal to enter the dorsal margin of the foramen nervi trigemini *sensu stricto* on the right side of the fossil. This can also be appreciated on the left side, where the process is broken, but where the prootic bump and sutural contact for the descending process indicate a symmetrical morphology with the right side. In *Carettochelys insculpta*, the prootic bump serves as an articulation site for a posterodorsal process of the epipterygoid, which prohibits the descending parietal process from entering the trigeminal foramen *sensu stricto* margin at a more anterior position. The morphology of BSPG 1991 II 130 is fully consistent with that of *Carettochelys insculpta*, and thus it is reasonable to infer that an epipterygoid–prootic contact in the anterodorsal margin of the foramen nervi trigemini *sensu stricto* precluded a parietal contribution to this opening. The preserved portion of the descending process shows that it is continuous with the crista cranii of the frontal and also forms a prominent ridge along its lateral surface that extends posteroventrolaterally from the base of the process within the upper temporal fossa (Fig. 1B, E). This ridge is continuous with the processus trochlearis oticum, and forms parts of its anteriorly overhanging margin, as in *Carettochelys insculpta* and *Anosteira maomingensis* (Walther 1922; Joyce 2014; Danilov et al. 2017). Within the braincase, the descending process of the parietal is deeply recessed and, jointly with the prootic, forms a broad cavity that housed large cerebral hemispheres, as in trionychians more generally (Fig. 1B; Ferreira et al. 2023). In the median contact of both parietals, there is an additional constriction of the brain cavity toward the supraoccipital contact, which corresponds to a median, bulge-like cartilaginous rider (Werneburg et al. 2021).

**Postorbital.** The postorbitals are almost completely missing. Only the most medial portion of the left element is preserved, which contacts the frontal anteromedially and the parietal posteromedially (Fig. 1A, B). The fully preserved left frontal and parietal and comparisons with *Carettochelys insculpta* also allow to infer that the postorbital contributed to the orbital margin and the upper temporal emargination.

**Jugal.** The jugals are not preserved in BSPG 1991 II 130.

**Quadratojugal.** A small part of the right quadratojugal was described by Havlik et al. (2014) as preserved in articulation with the remainder of the fossil, in a position anteroventral to the cavum tympani. This portion of the quadratojugal disarticulated along its suture with the quadrate in the specimen prior to CT scanning but was scanned alongside the rest of the fossil. The ventral margin of the quadratojugal fragment was formerly aligned with the ventral margin of the quadrate's articular process and showed no indication of a dorsal upcurving that is generally present in taxa with moderate or deep cheek emarginations. Instead, the fragment is fully consistent with the morphology of *Carettochelys insculpta*, in which the cheek emargination is minimal and limited to a more anterior portion of the quadratojugal (Waite 1905; Walther 1922; Joyce 2014). In addition, the preserved quadrates on both sides of BSPG 1991 II 130 show that the posterodorsal articulation of the quadratojugal with the quadrate was limited to the anterodorsal margin of the cavum tympani and did not extend posteriorly further along the dorsal margin. A quadratojugal–squamosal contact was certainly absent in BSPG 1991 II 130 as the articular facets of the quadratojugal and squamosal on the quadrates are widely spaced from one another, much as in *Carettochelys insculpta*.

**Squamosal.** The squamosals are not preserved in BSPG 1991 II 130. Nevertheless, the quadrates on both sides show well-developed articular facets for the squamosals. These facets are triangular and somewhat broader than in *Carettochelys insculpta*. However, as in the extant taxon, the facets are anteriorly clearly separated from those of the quadratojugal, showing that no contact with the quadratojugal was present. The quadrate bone surrounding the squamosal facet furthermore shows that, again as in *Carettochelys insculpta*, the squamosal of BSPG 1991 II 130 was excluded from the posterodorsal margin of the cavum tympani.

**Premaxilla.** The premaxillae are not preserved in BSPG 1991 II 130.

**Maxilla.** The maxillae are not preserved in BSPG 1991 II 130.

**Palatine.** The  $\mu$ CT scans of BSPG 1991 II 130 reveal that a very small portion of the right palatine is preserved just anterior to the suture between the parabasisphenoid and pterygoid (Fig. 1B, E). Although this piece is so small that it barely allows making statements about the anatomy of the palatine, it nevertheless shows that a contact between the palatine and pterygoid, and palatine and parabasisphenoid was present, as in all carettochelyids (Waite 1905; Harrassowitz 1922; Walther 1922; Danilov et al. 2017; Joyce et al. 2018). The location of this fragment at the level of the sella turcica between the pterygoid and parabasisphenoid also suggests that a contact of the pterygoid with its counterpart was likely absent, again, as in all carettochelyids (Waite 1905; Harrassowitz 1922; Walther 1922; Danilov et al. 2017; Joyce et al. 2018).

**Vomer.** The vomer is not preserved in BSPG 1991 II 130.

**Pterygoid.** Only the posterior half of the pterygoids are preserved in BSPG 1991 II 130, which contact the

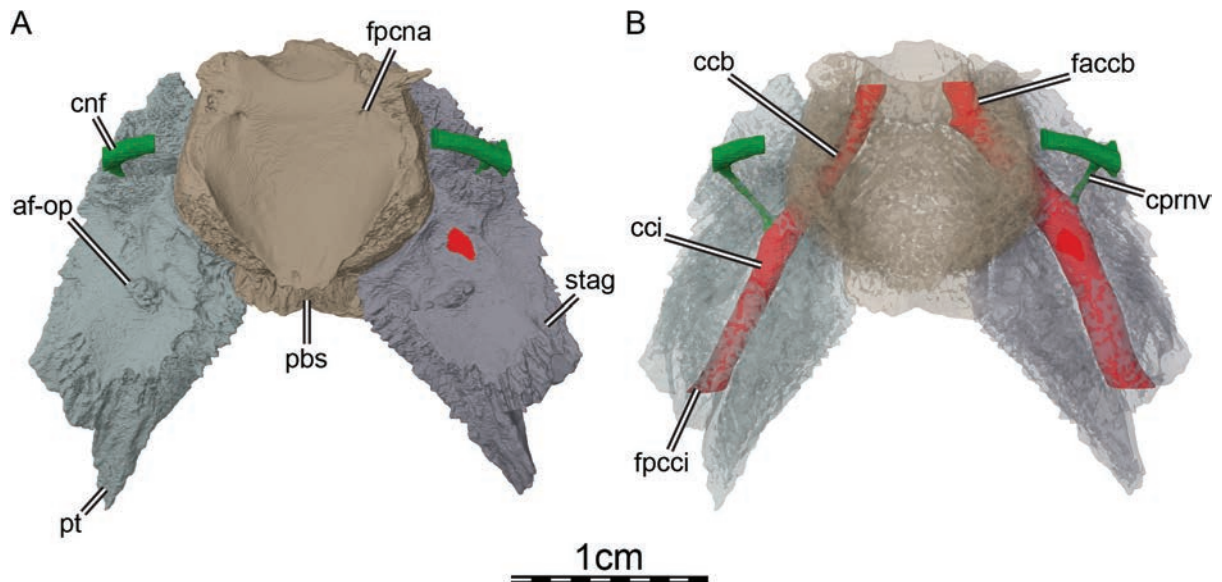


**Figure 2.** Three-dimensional renderings of the circulatory system of BSPG 1991 II 113. **A.** Dorsal view; **B.** Dorsal view with bones rendered transparent. Abbreviations: af-op, articulation facet for the opisthotic; ccb, canalis caroticus basisphenoidalis; cci, canalis caroticus internus; cnf, canalis nervus facialis; cprnv, canalis pro ramo nervi vidiani; faccb, foramen anterius canalis carotici basisphenoidalis; fpcbi, foramen posterius canalis carotici interni; fpcna, foramen posterius canalis nervi abducentis; pbs, parabasisphenoid; pt, pterygoid; stag, stapedia artery groove.

parabasisphenoid medially, the palatine anteriorly, the prootic anterodorsolaterally, the quadrate laterally, the basioccipital posteromedially, the opisthotic posterodorsally, and the exoccipital posterodorsomedially (Figs 1B, E, 2). Additionally, there was likely a contact with the epipterygoid. Ventrally, the pterygoid forms a deep pterygoid fossa and contributes to the elongate tubercula basioccipitale anterolaterally (Fig. 1B). At about mid-length between the parabasisphenoid and quadrate, the pterygoid forms a low ridge that delineates the pterygoid fossa medially (Fig. 1B). The ridge is ventrally broken, and it likely formed an enfolded structure that partially covered the pterygoid fossa ventrally, as in *Carettochelys insculpta* (Walther 1922; Joyce 2014), but likely not *Anosteira maomingensis*, in which this ridge seems to be absent (Danilov et al. 2017), and definitely not *Anosteira pulchra*, in which the ridge is clearly absent (Joyce et al. 2018). The pterygoid of BSPG 1991 II 130 ventromedially minorly enters the margin of the mandibular artery foramen (Figs 1E, 3). The ventral half of the canalis pro ramo nervi vidiani, which transmits the vidian nerve from the geniculate ganglion to the canalis caroticus internus (Gaffney 1979; Rollot et al. 2021a), is also formed by the pterygoid (Fig. 2A). The pterygoid floors the endosseous labyrinth and cavum acustico-jugulare and forms the ventral margin of the fenestra ovalis and ventromedial margin of the small fenestra postotica. Dorsally, at about mid-length, the pterygoid forms a low bulging articulation facet for contact with the processus interfenestralis of the opisthotic (Fig. 2A). This dorsal articular boss is unusual among turtles, but certainly present in *Carettochelys insculpta*. Within the cavum acustico-jugulare, the posterodorsal surface of the pterygoid forms a narrow groove, as in *Carettochelys insculpta*,

and that is interpreted as having housed the stapedia artery and/or the lateral head vein (Fig. 2A). Posteriorly, the pterygoid entirely forms the foramen posterius canalis carotici interni, the position of which differs from the early branching carettochelyids *Anosteira pulchra* (Joyce et al. 2018) and *Anosteira maomingensis* (Danilov et al. 2017), in which the foramen is located more anteroventrally and between the parabasisphenoid and pterygoid, similar to the generalized position of paracryptodires (Gaffney 1975). The foramen posterius canalis carotici interni of BSPG 1991 II 130 leads into the canalis caroticus internus, which extends anteromedially through the pterygoid (Fig. 2B) before entering the parabasisphenoid as the canalis caroticus basisphenoidalis. A canalis caroticus lateralis is absent, as in *Carettochelys insculpta* (Rollot et al. 2021a). At about mid-length, the canalis caroticus internus is slightly exposed dorsally within the floor of the endosseous labyrinth (Fig. 2). Dorsal to the foramen posterius canalis carotici interni, the pterygoid forms a bony platform that contacts the opisthotic dorsally, forming a secondary wall posterior to the processus interfenestralis, as in *Carettochelys insculpta* (Walther 1922).

**Epipterygoid.** A large epipterygoid was described on the left side of BSPG 1991 II 130 by Havlik et al. (2014), but the  $\mu$ CT scans of that specimen show that this piece of bone anteroventral to the mandibular artery foramen actually belongs to the pterygoid (Fig. 3). The epipterygoid usually lies along the anterior and ventral margins of the foramen nervi trigemini *sensu lato* in other carettochelyids (Walther 1922; Joyce et al. 2018) and overlies the pterygoid in about the area where Havlik et al. (2014) drew their epipterygoid. In BSPG 1991 II 130, the area that was indicated as being the epipterygoid by Havlik et al. (2014) has a slightly different, somewhat rougher surface texture than

the surrounding bone surfaces exposed along the lower temporal fossa. We consider it likely, based on comparisons of a completely segmented specimen of *Carettochelys insculpta* (NHMUK 1903.7.10.1), that this area represents an articulation area for a formerly present but not preserved epipterygoid of BSPG 1991 II 130. Details of this are further given below in the context of descriptions and discussions surrounding the foramen for the mandibular artery.

**Quadrate.** The quadrates are nearly complete, with only minor damage along the anterior and posterior margins of the cavum tympani (Figs 1C, D, 4). The quadrate contacts the quadratojugal anteriorly, the prootic anteromedially, the opisthotic posteromedially, and the pterygoid ventromedially (Fig. 1A, B, E, F). Posterodorsolaterally, the quadrate forms a mediolaterally expanded articular facet for articulation with the

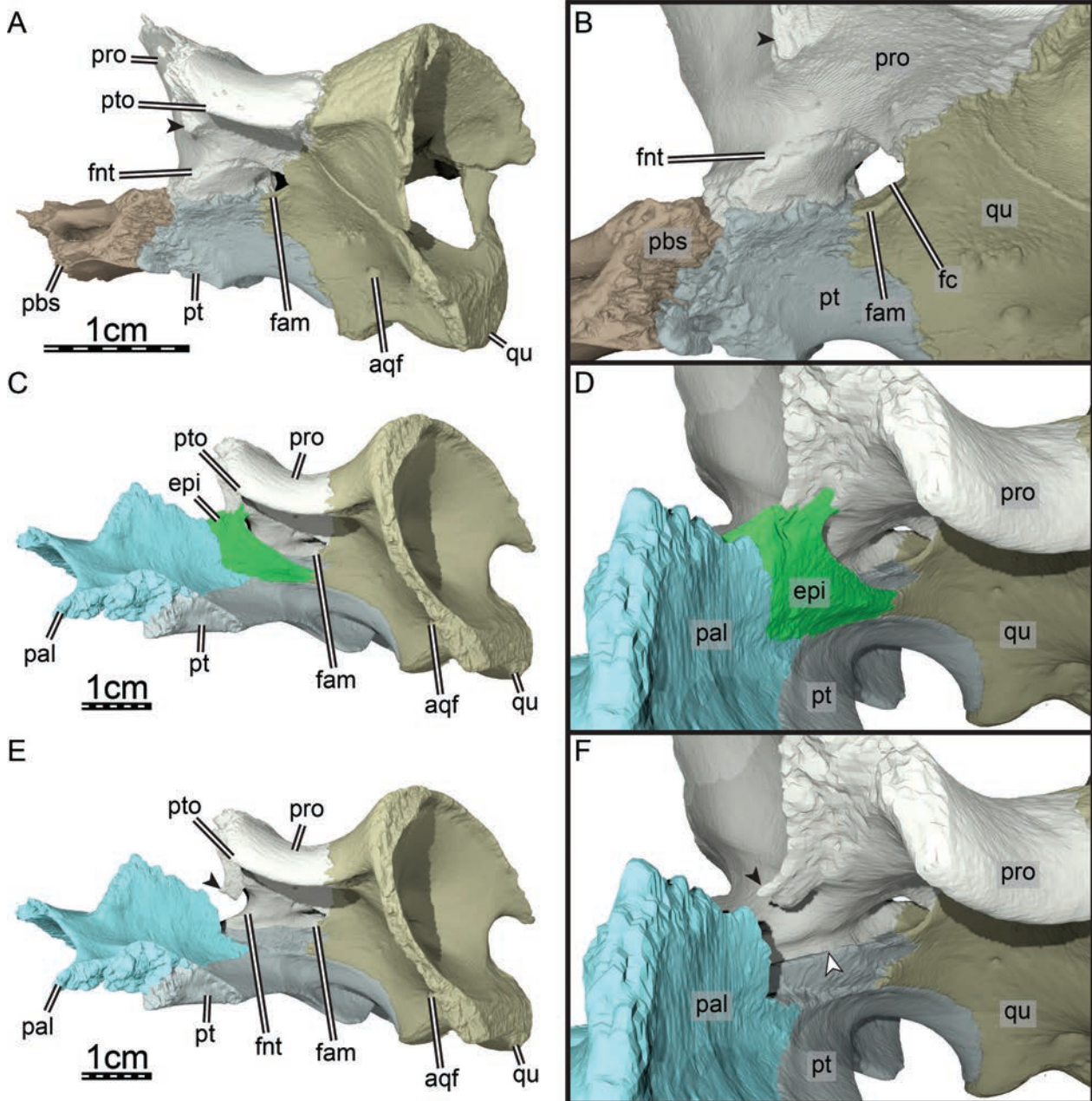


**Figure 3.** Three-dimensional renderings of the left trigeminal area of *Allaeochelys libyca* (BSPG 1991 II 113) and *Carettochelys insculpta* (NHMUK 1903.7.10.1). **A.** Left trigeminal area of *Allaeochelys libyca* in anterolateral view; **B.** Close-up on the left trigeminal area of *Allaeochelys libyca*; **C.** Left trigeminal area of *Carettochelys insculpta* in anterolateral view; **D.** Close-up on the left trigeminal area of *Carettochelys insculpta*; **E.** Left trigeminal area of *Carettochelys insculpta* in anterolateral view with the epipterygoid removed; **F.** Close-up on the left trigeminal area of *Carettochelys insculpta* with the epipterygoid removed. Abbreviations: aqf, anterior quadrate foramen; epi, epipterygoid; fam, foramen arteriomandibulare; fc, foramen cavernosum; fnt, foramen nervi trigemini; pal, palatine; pbs, parabasisphenoid; pro, prootic; pt, pterygoid; pto, processus trochlearis oticum; qu, quadrate. Black arrowheads indicate the anteroventral bump on the prootic that is interpreted as serving for the contact with the epipterygoid, and the white arrowhead indicates the lateral margin of the sulcus cavernosus formed by the pterygoid in *Carettochelys insculpta*.

squamosal (Figs 1A, 4). A contact with the supraoccipital is absent, as in other carettochelyids (Walther 1922; Danilov et al. 2017; Joyce et al. 2018). As the quadrate only forms a short epipterygoid process anteriorly, a contact between the epipterygoid and quadrate was likely absent in BSPG 1991 II 130 or minimal (Fig. 3), as in some *Carettochelys insculpta* specimens. The quadrate of BSPG 1991 II 130 forms the lateral and ventrolateral margin of the mandibular artery foramen, and less than half of the processus trochlearis oticum (Figs 1E, 3). Along its ventral surface, anterior to the condylus mandibularis, the quadrate forms a conspicuous foramen of several millimeter width, which leads into a canal that extends dorsally within the quadrate and joins the most anterior aspect of the quadrate fossa (Fig. 1B). We herein refer to this foramen as the anterior quadrate foramen. The path and location of its canal somewhat resembles that of the canalis chorda tympani quadrati (sensu Gaffney 1972), which transmits the chorda tympani branch of the facial nerve (CN VII). However, the chorda tympani canal generally opens along the posterior surface of the quadrate and connects dorsally to the incisura columella auris, which has a direct connection to the facial nerve path via the cavum acustico-jugulare. Here, we are not able to identify any connection between the quadrate canal in BSPG 1991 II 130 and the incisura columella auris or otherwise the cavum acustico-jugulare, and therefore cannot know its precise identity. However, as the foramen is also evident in the extant *Carettochelys insculpta*, but absent in the early branching carettochelyid *Anosteira pulchra* for which we have CT scans to ascertain this statement, we provide a new name for the structure as a potential shared character of derived carettochelyids. The quadrate forms a low, ventrally oriented mandibular condyle, of which the lateral articular surface is about twice the size of the medial one (Figs 1B, 4). The two articular facets are separated by a deep and relatively wide sulcus (Fig. 4B). Anterolateral to the articular process, the quadrate extends with a vertical, sheeted process that is ventrally projecting from the margin of the cavum tympani, and which effectively forms a lateral wall to the most posterior portion of the lower temporal fossa. This sheeted process anteriorly contacted the quadratojugal (Havlik et al. 2014), but the respective quadratojugal piece is now disarticulated. Within the upper temporal fossa, the quadrate forms the lateral margin of the foramen stapedio-temporale (Fig. 1A). The foramen leads into the canalis stapedio-temporalis, which is notably short, mostly oriented mediolaterally, and laterally bordered by the quadrate. The canalis stapedio-temporalis leads into the cavum acustico-jugulare, of which the quadrate forms the lateral wall. The medial surface of the quadrate forms an imprint that allows to determine the path of the stapedia artery. A large groove extends anteriorly and slightly dorsally from the fenestra postotica and, anterodorsal to the incisura columella auris, abruptly curves to extend ventrally and join the mandibular artery foramen. Dorsally and at about mid-length between the incisura columella auris and mandibular

artery foramen, the quadrate forms a low ridge, which with the prootic collectively defines a passage for the stapedia artery from the cavum acustico-jugulare to the canalis stapedio-temporalis. It is likely that the split between the stapedia and mandibular artery occurred at that level, with the stapedia artery extending laterally through the canalis stapedio-temporalis and the mandibular artery curving ventrally to exit the skull by means of the foramen cavernosum. Laterally, the quadrate forms most of the cavum tympani, to the exception of the most anterior margin that is formed by the quadratojugal (Figs 1C, D, 4A), as in other carettochelyids (Walther 1922; Danilov et al. 2017; Joyce et al. 2018). The quadrate also completely encloses the incisura columella auris and forms a small antrum postoticum (Figs 3A, 4A), which extends posterodorsolaterally through the quadrate and squamosal, as in *Anosteira pulchra* (Joyce et al. 2018) and *Anosteira maomingensis* (Danilov et al. 2017). Along its posterior surface, the quadrate forms the quadrate fossa (Fig. 4B), as in other carettochelyids (Harrassowitz 1922; Walther 1922; Danilov et al. 2017; Joyce et al. 2018). The quadrate fossa is broad and deep, as in more derived members of the clade (Joyce 2014).

**Prootic.** The prootics are intact in BSPG 1991 II 130. Within the upper temporal fossa, the prootic contacts the parietal anteromedially, the supraoccipital posteromedially, the quadrate laterally, and the opisthotic posteriorly, and forms the medial margin of the foramen stapedio-temporale (Fig. 1A). Ventrally, the prootic contacts the parabasisphenoid medially, the pterygoid ventrally, the quadrate laterally, and, likely, the epipterygoid anteroventrolaterally (Figs 1B, E, 3). The prootic forms the greater half of the processus trochlearis oticum, which is medially continuous with a prominent ridge formed by the descending process of the parietal (Figs 1B, E, 3). The anterior margin of the process overhangs the lower temporal fossa and forms a broadly concave surface for the adductor musculature and associated tendons. Within the lower temporal fossa, the prootic forms the posterior margin of the foramen nervi trigemini *sensu stricto*, i.e., the opening through which the maxillary and mandibular nerve rami of the trigeminal nerve system pass (“external trigeminal foramen” of Evers et al. 2019), and the medial margin of the mandibular artery foramen, which was labelled as the “posterior” foramen nervi trigemini by Havlik et al. (2014) (Figs 1E, 3). These foramina and the associated canalis cavernosus are described in conjunction further below, as the morphology seen in *Allaeochelys libyca* is quite unusual. Within the braincase, the prootic anteriorly forms the posterior portion of a deep cavity, which collectively with the parietal encapsulates the cerebral hemisphere, which appears to be notably large, as has also been reported for extant trionychids (Ferreira et al. 2023). Posterior to the foramen nervi trigemini *sensu stricto* of BSPG 1991 II 130, and ventral to the cerebral hemisphere imprints, the course of the trigeminal nerve tissue can be inferred to pass along the anteromedial surface of the prootic, which walls a broad cavum epiptericum. On its medial surface, the prootic forms the fenestra acustico-facialis, but the latter is

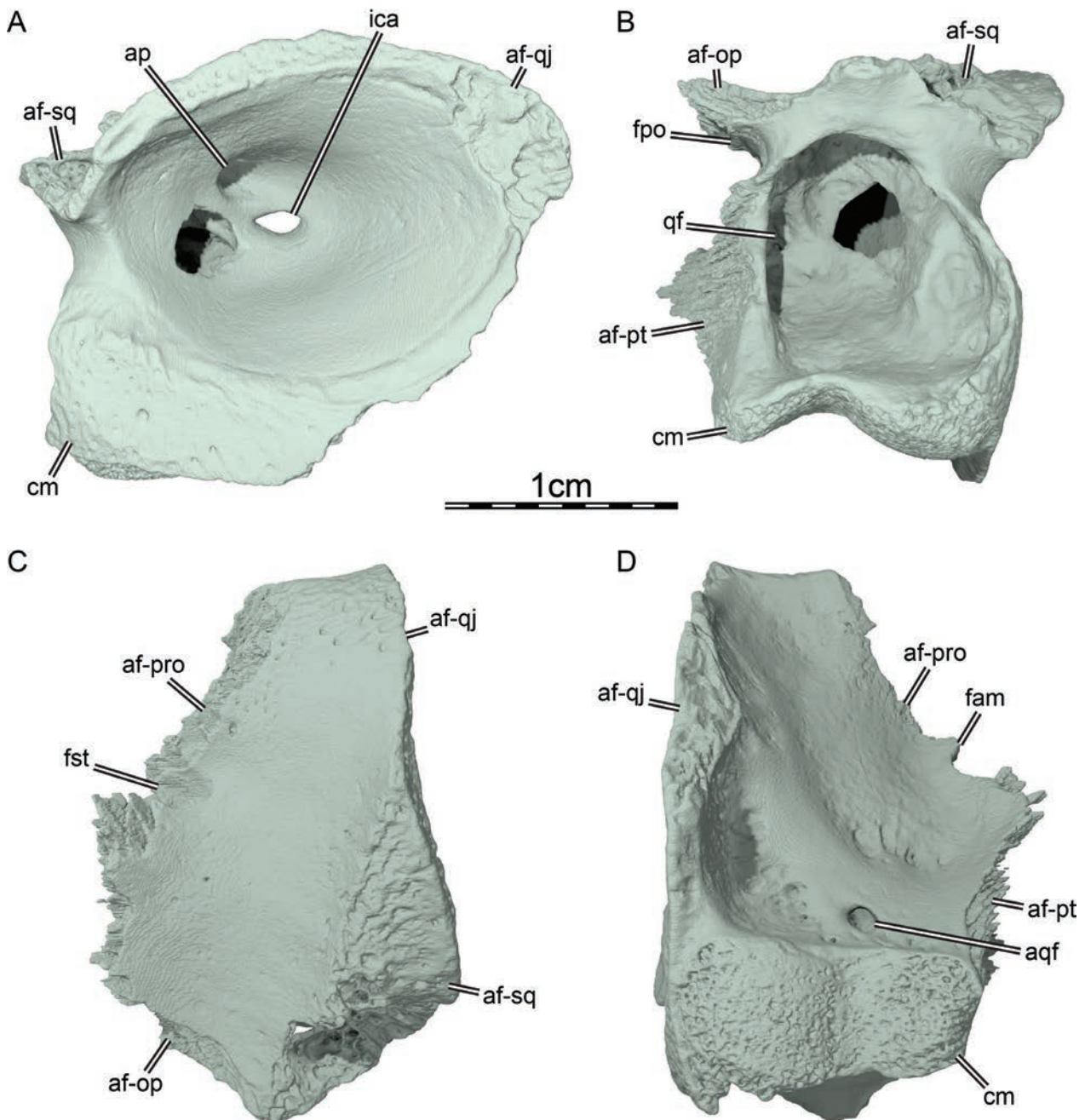


**Figure 4.** Three-dimensional renderings of the right quadrate of BSPG 1991 II 113. **A.** Lateral view; **B.** Posterior view; **C.** Dorsal view; **D.** Ventral view. Abbreviations: af-op, articulation facet for opisthotic; af-pro, articulation facet for prootic; af-pt, articulation facet for pterygoid; af-qj, articulation facet for quadratojugal; af-sq, articulation facet for squamosal; ap, antrum postoticum; aqf, anterior quadrate foramen; cm, condylus mandibularis; fam, foramen arteriomandibulare; fpo, fenestra postotica; fst, foramen stapedio-temporalis; ica, incisura columella auris; qf, quadrate fossa.

incompletely preserved as portions of the prootic are missing posteromedially. Within the fenestra acustico-facialis, only the medial foramen of the canalis nervus facialis is fully preserved. The canalis nervus facialis extends laterally through the prootic and joins the medial margin of the cavum acustico-jugulare. The canal is extremely large in BSPG 1991 II 130. The canalis pro ramo nervi vidiani branches off the canalis nervus facialis just medial to the latter contact and extends ventromedially through the prootic and pterygoid to join the canalis caroticus internus (Fig. 2), which is the common condition in carettochelyids (Joyce et al. 2018; Rollot et al. 2021a). In BSPG 1991 II

130, a likely vidian nerve canal splits from the canalis caroticus internus at the level of its contact with the canalis pro ramo nervi vidiani and extends anteroventrally through the pterygoid. The preserved portion of this proposed vidian canal is, however, extremely short because of the damage that affects the anteroventral region of the cranium. The location of this canal within the pterygoid in that area of the cranium is nevertheless highly indicative of a canalis nervus vidianus. The preserved aspects of the facial nerve pattern in *Allaeochelys libyca* are nevertheless very similar to that of other carettochelyids (Joyce et al. 2018; Rollot et al. 2021a). Canals and foramina for the vestibulocochlear

nerves (CN VIII) are mostly lacking and only the ventral margin of one foramen remains preserved within the fenestra acustico-facialis, just anterodorsal to the medial foramen for the facial nerve canal. The prootic otherwise forms the anterior half of the endosseous labyrinth, the anterior half of the anterior semicircular canal, and the anterior half of the fenestra ovalis. The anterior half of the lateral semicircular canal is not fully enclosed by bone, and the prootic only forms the lateral margin of a groove that contained the anterior portion of the lateral semicircular duct. Lateral to the fenestra ovalis, there is no posterior recess in the prootic, as in *Carettochelys insculpta*. The prootic also forms the anteromedial wall of the cavum acustico-jugulare and the medial half of the canalis stapedio-temporalis. The foramen nervi trigemini *sensu stricto* (see above) is not truly preserved in BSPG 1991 II 130. Although there is an anteriorly concave notch in the anterior surface of the prootic, this likely represents parts of the prootic surface that forms the cavum epiptericum. The remainder of the foramen was likely formed by the epipterygoid, and not by the parietal. This can be inferred as the posterior end of the descending process of the parietal is completely preserved on the right side of BSPG 1991 II 130. Here, the epipterygoid articulated with a small anteroventrally protruding bump of the prootic (Fig. 3A, B), which currently prohibits the parietal to enter the trigeminal foramen margin. In the extant *Carettochelys insculpta*, an exact same bump-like process serves as an articular process for a posterodorsal process of the epipterygoid, which excludes the parietal from the foramen nervi trigemini *sensu stricto*. Below, we argue that the trigeminal foramen *sensu stricto* was likely confluent with an opening for the mandibular artery, which is closely associated with the canalis cavernosus. This canal of turtles is a result of their basicranial evolution: Testudines have modified their cranioquadrate space during their early basicranial evolution (e.g., Gaffney 1990; Sterli and Joyce 2007; Anquetin et al. 2009; Sterli and de la Fuente 2010; Rabi et al. 2013; Ferreira et al. 2020), thereby trapping the lateral head vein in a canal called the canalis cavernosus (Gaffney 1979), which extends from the anterior aspect of the cavum acustico-jugulare between the pterygoid, quadrate and prootic into the secondary braincase of turtles, where the lateral head vein continues medial to the secondary braincase wall that is generally formed by the pterygoid and parietal (Gaffney 1979; Evers et al. 2019; Rollot et al. 2021a). BSPG 1991 II 130 has a morphology of the “cavernous” area that differs strongly from this generalized testudine bauplan. Our examination of comparative material shows that the morphology of BSPG 1991 II 130 is, however, also mirrored in *Carettochelys insculpta*, but the distinctness of this morphology has, to our knowledge, not been noticed or described before. In BSPG 1991 II 130, the most anterior aspect of the cavum acustico-jugulare does not become constricted to a broad canalis cavernosus as is the general condition in turtles. Instead, there is an anteriorly directed, large, circular opening that exits from the cavum acustico-jugulare directly into the vicinity of the mandibular artery foramen. Havlik et al. (2014) identified this opening

as the “posterior” trigeminal nerve foramen. However, the opening cannot be directly associated with the trigeminal nerve, because it is connected to the cavum acustico-jugulare, and not the cavum cranii, which houses the brain from where the cranial nerves stem. Instead, the opening is likely associated with the mandibular artery, which in many turtle groups passes from the cavum acustico-jugulare into the canalis cavernosus, from where it has different courses it can take to reach the mandible. In many turtles, the mandibular artery passes laterally through the trigeminal foramen (Albrecht 1976), but it can also pass through the interorbital foramen as in *Dermatemys mawii* (Evers et al. 2022), or it can pass through a separate foramen opening from the canalis cavernosus into the temporal fossa, as in some testudinids like gopher tortoises, but also as in *Chelonia mydas* (e.g., McDowell 1961; Crumly 1982, 1994; Evers and Benson 2019; Rollot et al. 2021a). In *Carettochelys insculpta*, there is no separate mandibular artery foramen, but the trigeminal foramen is posteroventrally elongated (Fig. 3C, D). Instead of being a nearly circular or slightly oval foramen, the trigeminal opening is stretched and slightly curved. Hereby, the posteroventral aspect of the foramen essentially opens into the canalis cavernosus. This morphology suggests that the elongated trigeminal foramen of *Carettochelys insculpta* essentially incorporates a mandibular foramen. Herein, we call this morphology the “trigeminal foramen *sensu lato*”. The opening from the cavum acustico-jugulare of BSPG 1991 II 130 likely represents the posteroventral part of an incompletely preserved trigeminal foramen *sensu lato*. In BSPG 1991 II 130 and *Carettochelys insculpta*, the trigeminal foramen *sensu lato* is formed largely by the quadrate and prootic, with a ventral contribution of the pterygoid. Whereas in the incompletely preserved BSPG 1991 II 130 it looks like a canalis cavernosus is entirely reduced, the morphology of *Carettochelys insculpta* shows otherwise: in the extant form, the epipterygoid forms a bony bridge from the pterygoid region of the trigeminal foramen *sensu lato* to the descending process of the parietal (Fig. 3C, D). Hereby, the epipterygoid forms the anterolateral wall of a tightly constricted space between the epipterygoid, pterygoid and prootic, which clearly corresponds to a strongly size-reduced canalis cavernosus. In BSPG 1991 II 130, the epipterygoid is not preserved, so that the impression of a complete absence of the canalis cavernosus is given. However, a small process of the prootic in the dorsal margin of the partly preserved trigeminal foramen *sensu lato* of BSPG 1991 II 30 (Fig. 3A, B) suggests that an epipterygoid with similar contacts and shape as in *Carettochelys insculpta* (Fig. 3C–F) was once present. Thus, the large, circular foramen of BSPG 1991 II 130 likely corresponds to the part of the trigeminal foramen *sensu lato* through which the mandibular artery would pass into the temporal cavity, and the likely confluence with the trigeminal foramen is not evident due to the missing epipterygoid, which would have encased a size-reduced canalis cavernosus. An alternative interpretation of the region in BSPG 1991 II 130 would be that the sulcus cavernosus indeed is entirely reduced, and that the mandibular artery and lateral head vein both exit

into the temporal fossa. If the morphology of *Allaeochelys libyca* is informative about the plesiomorphic state of carettochelyid evolution, this scenario would require a complete loss of the canalis cavernosus in *Allaeochelys* and then the re-evolution of a size-reduced canalis cavernosus in *Carettochelys insculpta*, which we think is less likely.

**Opisthotic.** The two opisthotics are damaged and lack their most anteromedial portion, which contributes to the hiatus acusticus, and most of the processus interfenestralis. The opisthotic contacts the prootic anteriorly, the supraoccipital medially, the quadrate laterally, the exoccipital posteroventromedially, and the pterygoid posteroventrolaterally (Fig. 1A, F). A small contact between the basioccipital and processus interfenestralis of the opisthotic might have been present, but is obscured by damage. The opisthotic forms the posterior half of the endosseous labyrinth, the lateral semicircular canal, and the posterior half of the posterior semicircular canal. The most lateral aspect of the left processus interfenestralis is preserved, which allows assessing that the opisthotic forms the posterior half of the fenestra ovalis and that

the processus interfenestralis ventrally contacts the pterygoid. The amount of damage that affects the processus interfenestralis, however, prevents us to observe any other structure to which the process usually contributes in carettochelyids. We are therefore unable to provide any anatomical details about the fenestra perilymphatica or the foramina associated with the glossopharyngeal nerve course. The processus interfenestralis forms the anterior wall of the recessus scalae tympani, which is notably large in BSPG 1991 II 130. Posteriorly, the opisthotic forms the posterior wall to the recessus scalae tympani that ventrally contacts the pterygoid and forms the medial margin of the fenestra postotica (Fig. 5A). At the level of the suture with the pterygoid, the opisthotic forms alongside the latter bone a small canal that extends posterolaterally and joins the back of the cranium by means of a foramen formed by these two bones (Fig. 5A). The canal and foramen may have served as a passage for the glossopharyngeal nerve, as the latter is known to extend posterolaterally within the recessus scalae tympani and through the fenestra postotica in turtles (Soliman 1964; Gaffney 1979).

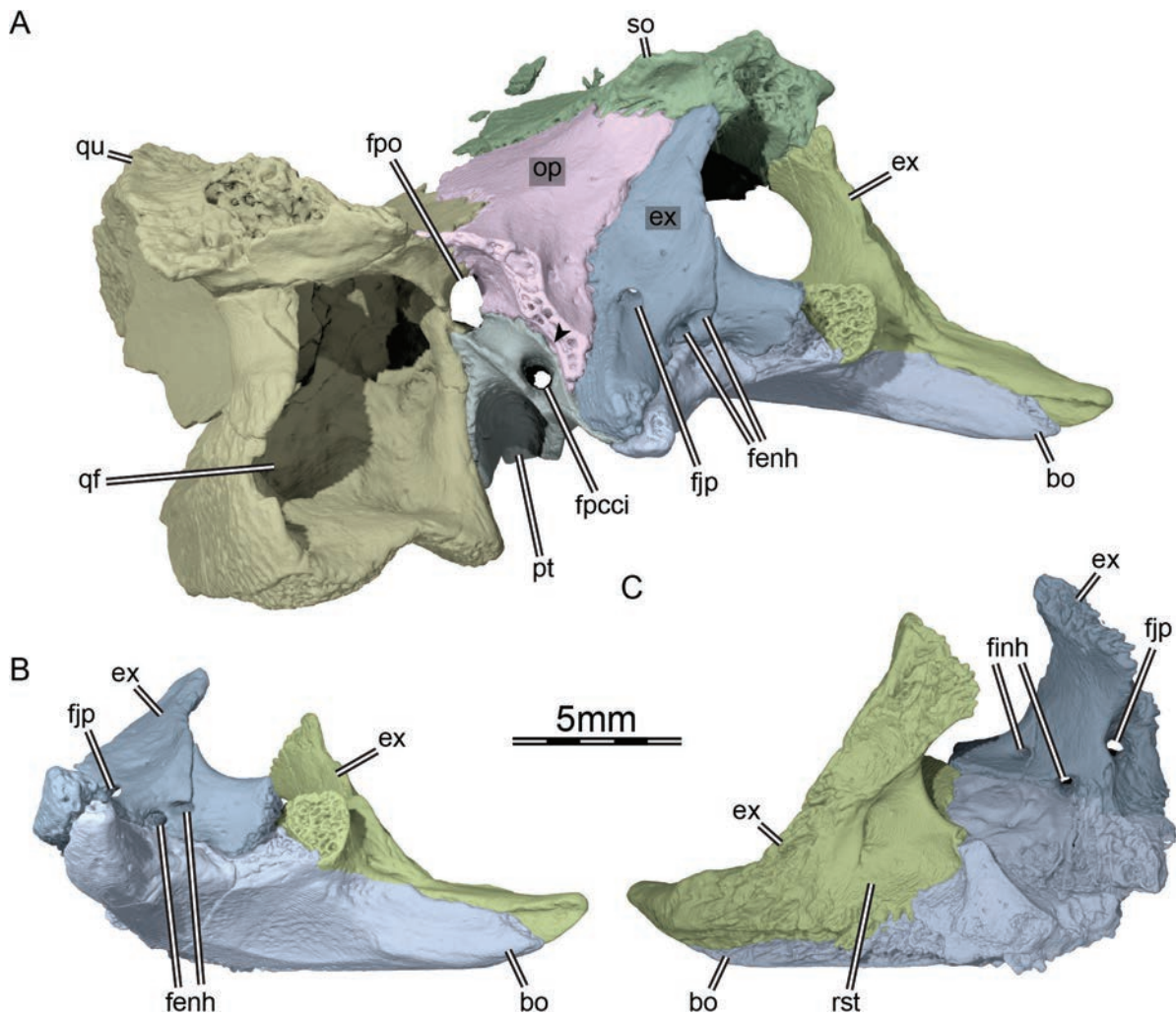


**Figure 5.** Three-dimensional renderings of the left posterior portion of BSPG 1991 II 113. **A.** Posterolateral view; **B.** Posteroventrolateral view; **C.** Anterodorsolateral view. Abbreviations: bo, basioccipital; ex, exoccipital; fenh, foramen externum nervi hypoglossi; finh, foramen internum nervi hypoglossi; fjp, foramen jugulare posterius; fpcci, foramen posterius canalis carotici interni; fpo, fenestra postotica; op, opisthotic; pt, pterygoid; qu, quadrate fossa; qu, quadrate; rst, recessus scalae tympani; so, supraoccipital. Black arrowhead indicates the position of the foramen oropharyngeale.

**Supraoccipital.** The supraoccipital is incomplete, lacking its most anterior and anterodorsal parts and the crista supraoccipitalis almost completely. The supraoccipital contacts the parietal anteriorly, the prootic anterolaterally, the opisthotic posterolaterally, and the exoccipital posteroventrolaterally (Fig. 1A, F). The supraoccipital forms the posterior half of the braincase roof, the posterior half of the anterior semicircular canal, the anterior half of the posterior semicircular canal, the dorsal margin of the hiatus acusticus, and the dorsal margin of the foramen magnum. Although the crista supraoccipitalis is broken off, a small portion of the mediolaterally expanded plate usually seen in carettochelyids is preserved (Fig. 1A). The expanded plate starts posterior to the level of the prootic-opisthotic contact, just medial to the contact between the supraoccipital and opisthotic. In dorsal view, it is apparent that the lateral margins of the preserved portion of the expanded plate are slightly concave, and seem to slightly broaden again towards the posterior (Fig. 1A), suggesting that the expanded plate of the crista supraoccipitalis was broader posteriorly, as in *Carettochelys insculpta* (Joyce 2014), but not *Anosteira pulchra* (Joyce et al. 2018).

**Basioccipital.** The basioccipital is almost complete, only lacking a small portion around the occipital condyle. The basioccipital can generally be differentiated in the CT scans from the exoccipitals, although the suture between the basioccipital and right exoccipital fades away slightly within the right tuberculum basioccipitale. The basioccipital contacts the parabasisphenoid anteriorly, the pterygoid laterally, and the exoccipital posterodorsolaterally and posterodorsally (Figs 1B, F, 5). The contact of the basioccipital with the parabasisphenoid is mediolaterally elongate in ventral view, but is actually restricted to the most central aspect of the two bones more dorsally. This creates a depression lateral to the basioccipital-parabasisphenoid contact that expands the endosseous labyrinth ventrally. A crista basis tubercula basalis is likely absent, although this may be the result of the light damage that affects the anterodorsal surface of the basioccipital (Fig. 5C). In ventral view, the central part of the basioccipital forms a shallow depression that laterally reaches the tubercula basioccipitale, and posteriorly extends up to the occipital condyle (Fig. 1B). The tubercula basioccipitale are posteriorly elongate (Figs 1B, 5), as in *Carettochelys insculpta* (Walther 1922; Joyce 2014) and *Allaeochelys crassesculpta* (Harrassowitz 1922), but different from the short processes seen in *Anosteira pulchra* (Joyce et al. 2018). The occipital condyle is greatly damaged and only the base of the exoccipital lobes is preserved (Figs 1F, 5A, B). The preserved portion neither allows to determine with confidence to which extent each bone contributed to the condyle, nor how many lobes were actually forming the condyle. Although the basioccipital is exposed ventromedially between the exoccipitals, a slight reduction in width of the basioccipital towards the posterior is apparent in the  $\mu$ CT image stack, but our observations are not sufficient to determine with confidence the morphology of the occipital condyle in BSPG 1991 II 130.

**Exoccipital.** The exoccipitals are almost complete, only the portion around the occipital condyle is damaged. The exoccipital contacts the supraoccipital dorsally, the opisthotic laterally, the pterygoid ventrolaterally, and the basioccipital ventrally (Figs 1F, 5). The exoccipital forms the posterolateral wall of the braincase and the lateral margin of the foramen magnum. Within the braincase, the exoccipital forms two internal foramina for the hypoglossal nerve (Fig. 5C). The more anterior foramen is smaller and located just above the suture between the exoccipital and basioccipital. The other foramen is larger and located more posteriorly, at the level of the foramen magnum. Both foramina lead into separate canalis nervi hypoglossi that extend posterolaterally through the exoccipital. The exterior foramina nervi hypoglossi are separate but close to one another, located in a shallow cavity that lies lateral to the occipital condyle and just dorsal to the exoccipital-basioccipital suture (Fig. 5A, B). Our interpretation differs from that of Havlik et al. (2014), who identified three external foramina for the hypoglossal nerve. Cross-examination of the  $\mu$ CT scans available to us reveals that the most ventral of the three foramina identified by the latter authors actually corresponds to some porosity that is externally exposed, and that only two sets of internal and external foramina are present in *Allaeochelys libyca*, as in *Carettochelys insculpta* (Walther 1922) and *Anosteira pulchra* (FMNH PR966). The anteromedial surface of the exoccipital is concave and smooth and forms parts of the posterior wall of the recessus scalae tympani. Within the recessus scalae tympani, the exoccipital forms a moderately large but short canal that extends posterolaterally and joins the posterior surface of the exoccipital by means of the foramen jugulare posterius, which is located just dorso-lateral to the foramina externum nervi hypoglossi (Fig. 5). Medially, the exoccipital forms the posterior margin of the foramen jugulare anterius, i.e., the internal opening between the recessus scalae tympani and the braincase. The exoccipital also forms the dorsal part of the elongate tubercula basioccipitale with an elongated posterolateral process (Figs 1F, 5).

**Parabasisphenoid.** The parabasisphenoid is broken at the anterior limit of the sella turcica. The anterior parts of the otherwise broad and flat rostrum basisphenoidale are therefore missing. The area around the clinoid process and retractor bulbi pits is damaged as well and we are not able to describe these structures. The parabasisphenoid contacts the palatine anteriorly, the pterygoid laterally, the prootic anterodorsolaterally, and the basioccipital posteriorly (Fig. 1B, E). The dorsal surface of the parabasisphenoid is concave and floors the braincase. The parabasisphenoid posteriorly forms a short, thin sheet of bone that underlies the basioccipital and gives the impression of a broad contact between the two bones, but the contact is dorsally limited to the most central portion of both the parabasisphenoid and basioccipital. The parabasisphenoid forms the dorsum sellae, which anteriorly projects to cover the sella turcica. The foramina anterius

canalis carotici basisphenoidalis are located within the lateral corners of the sella turcica and lead into the canalis caroticus basisphenoidalis, which in BSPG 1991 II 130 are the anterior continuation of the canalis caroticus internus (Fig. 2B). The foramina posterius canalis nervi abducentis are located along the dorsal surface of the parabasisphenoid, posterolateral to the dorsum sellae (Fig. 2A). The foramen posterius canalis nervi abducentis leads into the canalis nervus abducentis, which extends anteriorly through the parabasisphenoid. The anterior path of the canal and bony contributions to the foramen anterius canalis nervi abducentis remain unknown as this area is damaged in BSPG 1991 II 130.

**Endosseous labyrinth.** The semicircular canals are thick, with the anterior semicircular canal being the longest of the three and that anteriorly joins the vestibule at the level of the anterior ampulla (Fig. 6). The posterior semicircular canal is shorter than the anterior canal and its posterior third is ventrally confluent with the posterior portion of the lateral semicircular canal, forming a large secondary common crus (Fig. 6B). The common crus is low and dorsally forms an embayment between the anterior and posterior semicircular canals, as in many other turtles (Fig. 6A; see Evers et al. 2019; Martín-Jiménez and Pérez-García 2021, 2022, 2023a, 2023b; Rollot et al. 2021b; Smith et al. 2023). The lateral semicircular canal is the shortest of the three, only forming a proper canal along the posterior half of the labyrinth that is barely detached from the vestibule, which results in a narrow, dorsoventral opening between the lateral canal and the vestibule (Fig. 6C). Anteriorly, the lateral canal merges with a large lateral ampulla. The morphology of the endosseous labyrinth of BSPG 1991 II 130 is extremely similar to that of NHMUK 1903.7.10.1 (*Carettochelys insculpta*). We are only able to identify two very subtle differences between the two endosseous labyrinths, namely a slightly thicker anterior semicircular canal in BSPG 1991 II 130 and a slightly more excavated dorsal embayment of the common crus appears BSPG 1991 II 130.

## Discussion and conclusions

The availability of  $\mu$ CT scans and complete segmentation of BSPG 1991 II 130 allows us to reinterpret several features that were originally misinterpreted by Havlik et al. (2014). The opening originally interpreted as the “posterior” foramen nervi trigemini actually corresponds to the posterior end of a trigeminal foramen *sensu lato*, i.e. the confluent foramina for the trigeminal nerve and mandibular artery. The mandibular artery is inferred to pass directly into the lower temporal fossa by reference to the circulatory system described for *Carettochelys insculpta* by Rollot et al. (2021a). The foramen nervi trigemini *sensu lato* is incompletely preserved in BSPG 1991 II 130, as the epipterygoid is absent. Havlik et al. (2014) identified an epipterygoid beneath the processus trochlearis oticum and between the mandibular artery foramen and foramen nervi trigemini *sensu stricto*. The  $\mu$ CT scans of BSPG 1991 II 130 show that the sutures of this purported epipterygoid with the surrounding bones, i.e., the quadrate, prootic, and pterygoid, actually correspond to a crack, and that the epipterygoid is not preserved. Ironically, we infer that an epipterygoid would have likely sat in a similar area, forming a narrowly constricted and size-reduced canalis cavernosus, as in *Carettochelys insculpta*. This highly unusual ‘cavernous’ area seems to be a derived feature of at least *Carettochelyinae*. The  $\mu$ CT scans and three-dimensional reconstructions also allowed us to confirm the presence of two internal and external hypoglossal foramina with their associated canals, versus the three external foramina labeled by Havlik et al. (2014) in the figures of their contribution. We also reinterpret the suture between the exoccipital and basioccipital, which is nearly horizontal and located more ventrally than interpreted by Havlik et al. (2014), but we note that in the  $\mu$ CT scans, this suture fades away towards the posterior, which likely made its identification on the specimen without back-up from tomographic data difficult. Finally, we identify a small piece of bone located anterior to the right pterygoid-parabasisphenoid suture as a remnant of

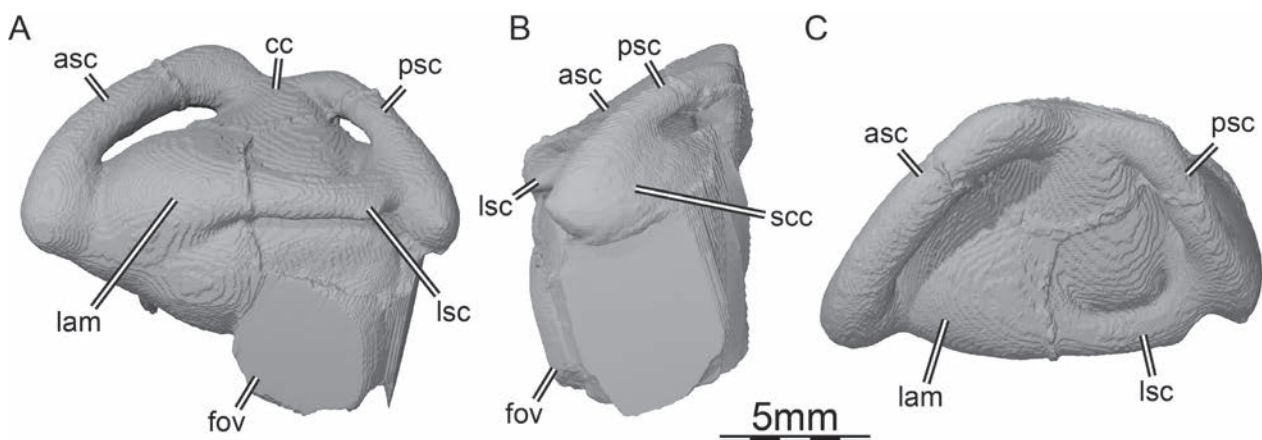


**Figure 6.** Three-dimensional renderings of the left endosseous labyrinth of BSPG 1991 II 113. **A.** Lateral view; **B.** Posterior view; **C.** Dorsal view. Abbreviations: asc, anterior semicircular canal; cc, common crus; fov, fenestra ovalis; lam, lateral ampulla; lsc, lateral semicircular canal; psc, posterior semicircular canal; scc, secondary common crus.

the palatine, but acknowledge that the identification of this bone was only possible thanks to the  $\mu$ CT scans. Our reconstructions of the preserved portions of the facial nerve and internal carotid artery canals also show that the circulatory and innervation systems of *Allaeochelys libyca* are likely identical to that of *Anosteira pulchra* (Joyce et al. 2018) and *Carettochelys insculpta* (Rollot et al. 2021a). Despite differences in the location of the foramen posterius canalis carotici interni, all three taxa share the absence of the canalis caroticus lateralis and the location of the split of the facial nerve into its subordinate branches, i.e., the vidian and hyomandibular nerves, that is located within the prootic. Although the circulatory and innervation systems remain unknown for the most early branching carettochelyids *Kizylkumemys khoratensis* and *Kizylkumemys schultzi*, current knowledge suggests that all carettochelyids likely have very similar systems.

Despite the reinterpretation of several anatomical features and the new information provided in the present contribution, the differences we highlighted between our study and the original work of Havlik et al. (2014) do not challenge the validity of *Allaeochelys libyca*. The insights provided herein will nevertheless be reflected in phylogenetic matrices, as scorings of several characters will have to be updated accordingly (e.g., subdivision of the foramen nervi trigemini). We also believe that some of our observations have the potential to be transcribed into new phylogenetic characters, such as the presence versus absence of a contact between the crista cranii of the frontal and the descending process of the prefrontal, the presence versus absence of an additional canal and associated foramina in the opisthotic for the glossopharyngeal nerve, or the short versus elongate tubercula basioccipitale. Even if scoring changes and new characters are not expected to drastically change the phylogenetic relationships of carettochelyids, they might allow a better resolution within some subclades of carettochelyids. *Anosteira* spp. and *Allaeochelys* spp. are commonly retrieved as unresolved subclades (Havlik et al. 2014; Danilov et al. 2017; Carbot-Chanona et al. 2020), and the inclusion of new characters might allow a better resolution within the latter. The inclusion in phylogenetic matrices of the newly described *Carettochelys niahensis* (White et al. 2023), even if the reported material is fragmentary, might provide novel insights as well.

## Acknowledgments

We thank Tom Davies and Ben Moon (both then at University of Bristol) for helping to CT scan the specimen, and Oliver Rauhut (BSPG) for allowing SWE to loan the material. We also thank the editor Torsten Scheyer, an anonymous reviewer and Adán Pérez-García, who provided useful insights that greatly improved the quality of the manuscript. This work was funded by the SNF grant 50070065 (YR and WGJ) and by the Ambizione SNF grant PZ00P2\_202019/1 (SWE).

## References

- Albrecht PW (1967) The cranial arteries and cranial arterial foramina of the turtle genera *Chrysemys*, *Sternotherus*, and *Trionyx*: a comparative study with analysis of possible evolutionary implications. *Tulane Studies in Zoology* 14(3): 81–99.
- Albrecht PW (1976) The cranial arteries of turtles and their evolutionary significance. *Journal of Morphology* 149(2): 159–182. <https://doi.org/10.1002/jmor.1051490203>
- Anquetin J, Barrett PM, Jones ME, Moore-Fay S, Evans SE (2009) A new stem turtle from the Middle Jurassic of Scotland: new insights into the evolution and palaeoecology of basal turtles. *Proceedings of the Royal Society B: Biological Sciences* 276(1658): 879–886. <https://doi.org/10.1098/rspb.2008.1429>
- Batsch AJGC (1788) Versuch einer Anleitung, zur Kenntniß und Geschichte der Thiere und Mineralien. Akademische Buchhandlung, Jena, 528 pp. <https://doi.org/10.5962/bhl.title.79854>
- Baur G (1889) Note on *Carettochelys*, Ramsay. *American Naturalist* 23(275): 1017. <https://doi.org/10.1086/275045>
- Baur G (1891) On the relations of *Carettochelys*, Ramsay. *American Naturalist* 25(295): 631–639. <https://doi.org/10.1086/275363>
- Carbot-Chanona G, Rivera-Velázquez G, Jiménez-Hidalgo E, Reynoso VH (2020) The first Pan-Carettochelys turtle in the Neogene of the American continent and its paleobiogeographical relevance. *Journal of South American Earth Sciences* 104: 102925. <https://doi.org/10.1016/j.jsames.2020.102925>
- Cope ED (1868) On the origin of genera. *Proceedings of the Academy of Natural Sciences of Philadelphia* 20(1868): 242–300.
- Crumly CR (1982) A cladistic analysis of *Geochelone* using cranial osteology. *Journal of Herpetology* 16(3): 215–234. <https://doi.org/10.2307/1563715>
- Crumly CR (1994) Phylogenetic systematics of North American tortoises (genus *Gopherus*): Evidence for their classification. *Fish and Wildlife Research* 13: 7–32.
- Dacqué E (1912) Die fossilen Schildkröten Aegyptens. *Geologische und Palaeontologische Abhandlungen* 10: 275–337.
- Danilov IG, Obraztsova EM, Chen W, Jianhua J (2017) The cranial morphology of *Anosteira maomingensis* (Testudines, Pan-Carettochelys) and the evolution of pan-carettochelyid turtles. *Journal of Vertebrate Paleontology* 37(4): e1335735. <https://doi.org/10.1080/02724634.2017.1335735>
- Desio A (1935) Studi geologici sulla Sirenaica, sul deserto Libico, sulla Tripolitania e sulle Fezzan orientali. *Missione scientifica della Reale Accademia d'Italia a Cufra 1*: 1–464.
- Evers SW (2021) Project: Evers, 2021, Extant and fossil amniote labyrinth and cranial models. MorphoSource. <https://www.morpho-source.org/projects/000372533>
- Evers SW, Benson RBJ (2019) A new phylogenetic hypothesis of turtles with implications for the timing and number of evolutionary transitions to marine lifestyles in the group. *Palaeontology* 62(1): 93–134. <https://doi.org/10.1111/pala.12384>
- Evers SW, Neenan JM, Ferreira GS, Werneburg I, Barrett PM, Benson RB (2019) Neurovascular anatomy of the protostegid turtle *Rhinochelys pulchriceps* and comparisons of membranous and endosseous labyrinth shape in an extant turtle. *Zoological Journal of the Linnean Society* 187(3): 800–828. <https://doi.org/10.1093/zoolinnean/zlz063>
- Evers SW, Joyce WG, Choiniere JN, Ferreira GS, Foth C, Hermanson G, Yi H, Johnson CM, Werneburg I, Benson RBJ (2022) Independent

- origin of large labyrinth size in turtles. *Nature Communications* 13: 5807. <https://doi.org/10.1038/s41467-022-33091-5>
- Ferreira GS, Lautenschlager S, Evers SW, Pfaff C, Kriwet J, Raselli I, Werneburg I (2020) Feeding biomechanics suggests progressive correlation of skull architecture and neck evolution in turtles. *Scientific Reports* 10(1): 1–11. <https://doi.org/10.1038/s41598-020-62179-5>
- Ferreira GS, Werneburg I, Lautenschlager S, Evers SW (2023) Contrasting brains and bones: neuroanatomical evolution of turtles (Testudinata). In: Dozo MT, Paulina-Carabajal A, Macrini TE, Walsh S (Eds) *Paleoneurology of amniotes: new directions in the study of fossil endocasts*. Springer International Publishing, Cham, 79–121. [https://doi.org/10.1007/978-3-031-13983-3\\_4](https://doi.org/10.1007/978-3-031-13983-3_4)
- Gaffney ES (1972) An illustrated glossary of turtle skull nomenclature. *American Museum Novitates* 2486: 1–33.
- Gaffney ES (1975) A phylogeny and classification of the higher categories of turtles. *Bulletin of the American Museum of Natural History* 155: 387–436.
- Gaffney ES (1979) Comparative cranial morphology of recent and fossil turtles. *Bulletin of the American Museum of Natural History* 164: 65–376.
- Gaffney ES (1990) The comparative osteology of the Triassic turtle *Proganochelys*. *Bulletin of the American Museum of Natural History* 194: 1–263.
- Gill T (1889) A remarkable tortoise. *Annual Report of the Board of Regents of the Smithsonian Institution, for the Year Ending June 30<sup>th</sup> 1887 Part 1*: 509–511.
- Harrasowitz H (1922) Die Schildkrötengattung *Anosteira* von Messel bei Darmstadt und ihre stammesgeschichtliche Bedeutung. *Abhandlungen der Hessischen Geologischen Landesanstalt* 6: 132–239.
- Havlik PE, Joyce WG, Böhme M (2014) *Allaeochelys libyca*, a new carettochelyine turtle from the Middle Miocene (Langhian) of Libya. *Bulletin of the Peabody Museum of Natural History* 55(2): 201–214. <https://doi.org/10.3374/014.055.0207>
- Hirayama R (1992) Fossil turtles from the Neogene strata in the Sinda Basin, eastern Zaire. *African Study Monographs Supplements* 17: 49–65. <https://doi.org/10.14989/68363>
- Joyce WG (2014) A review of the fossil record of turtles of the clade Pan-Carettochelys. *Bulletin of the Peabody Museum of Natural History* 55(1): 3–33. <https://doi.org/10.3374/014.055.0102>
- Joyce WG, Volpato VS, Rollot Y (2018) The skull of the carettochelyid turtle *Anosteira pulchra* from the Eocene (Uintan) of Wyoming and the carotid canal system of carettochelyid turtles. *Fossil Record* 21(2): 301–310. <https://doi.org/10.5194/fr-21-301-2018>
- Lapparent de Broin F de (2000) African chelonians from the Jurassic to the present: Phases of development and preliminary catalogue of the fossil record. *Palaeontologia Africana* 36: 43–82.
- Martín-Jiménez M, Pérez-García A (2021) Neuroanatomical study and three-dimensional reconstruction of the skull of a bothremydid turtle (Pleurodira) based on the European Eocene *Tartaruscola teodorii*. *Diversity* 13(7): 298. <https://doi.org/10.3390/d13070298>
- Martín-Jiménez M, Pérez-García A (2022) The neuroanatomy of the bothremydid pleurodiran turtle *Galianemys*, from the Late Cretaceous (Cenomanian) of Morocco. *The Anatomical Record* 306(6): 1377–1395. <https://doi.org/10.1002/ar.25072>
- Martín-Jiménez M, Pérez-García A (2023a) Neuroanatomical study and three-dimensional cranial reconstruction of the Brazilian Albian pleurodiran turtle *Euraxemys essweini*. *Diversity* 15(3): 374. <https://doi.org/10.3390/d15030374>
- Martín-Jiménez M, Pérez-García A (2023b) Neuroanatomical study of the podocnemidid turtle *Neochelys arenarum* (Pleurodira), from the early Eocene of France. *The Anatomical Record*: 1–13. <https://doi.org/10.1002/ar.25217>
- McDowell SB (1961) On the major arterial canals in the ear region of testudinoid turtles and the classification of the Testudinoidea. *Bulletin of the Museum of Comparative Zoology* 125: 23–39.
- Nessov LA (1976) On the systematics and phylogeny of two clawed turtles. *Vestnik Leningradskogo Universiteta* 9: 7–17.
- Nessov LA (1977) A new genus of pitted-shelled turtle from the Upper Cretaceous of Karakalpakia. *Paleontological Journal* 10: 96–107.
- Noulet JB (1867) Nouveau genre de tortues fossiles proposé sous le nom d'*Allaeochelys*. *Mémoires de l'Académie Impériale des Sciences, Inscriptions et Belles-Lettres de Toulouse* 5: 172–177.
- Rabi M, Zhou CF, Wings O, Ge S, Joyce WG (2013) A new xinjiangchelyid turtle from the Middle Jurassic of Xinjiang, China and the evolution of the basiptyergoid process in Mesozoic turtles. *BMC Evolutionary Biology* 13(1): 1–29. <https://doi.org/10.1186/1471-2148-13-203>
- Ramsay EP (1887) On a new genus and species of fresh water tortoise from the Fly River, New Guinea. *Proceedings of the Linnaean Society of New South Wales 2<sup>nd</sup> series* 1: 158–162. <https://doi.org/10.5962/bhl.part.29176>
- Rollot Y, Evers SW, Joyce WG (2021a) A review of the carotid artery and facial nerve canal systems in extant turtles. *PeerJ* 8: e10475. <https://doi.org/10.7717/peerj.10475>
- Rollot Y, Evers SW, Joyce WG (2021b) A redescription of the Late Jurassic (Tithonian) turtle *Uluops uluops* and a new phylogenetic hypothesis of Paracryptodira. *Swiss Journal of Palaeontology* 140(1): 1–30. <https://doi.org/10.1186/s13358-021-00234-y>
- Smith HF, Berg M, Adrian B (2023) A well-preserved cranium from the Judith River Formation (Montana, USA) reveals the inner ear and neuroanatomy of a Campanian baenid turtle. *The Anatomical Record* 306(6): 1431–1451. <https://doi.org/10.1002/ar.25185>
- Soliman MA (1964) Die Kopfnerven der Schildkröten. *Zeitschrift für Wissenschaftliche Zoologie* 169: 216–312.
- Sterli J, de la Fuente MS (2010) Anatomy of *Condorchelys antiqua* Sterli, 2008, and the origin of the modern jaw closure mechanism in turtles. *Journal of Vertebrate Paleontology* 30(2): 351–366. <https://doi.org/10.1080/02724631003617597>
- Sterli J, Joyce WG (2007) The cranial anatomy of the Early Jurassic turtle *Kayentachelys aprix*. *Acta Palaeontologica Polonica* 52(4): 675–694.
- Thomas H, Sevket S, Khan M, Battail B, Ligabue GC (1982) The Lower Miocene fauna of Al-Sarrar (Eastern Province, Saudi Arabia). *Atlat* 5: 109–136.
- Tong H, Claude J, Buffetaut E, Suteethorn V, Naksri W, Chitsing S (2006) Fossil turtles of Thailand: an updated review. In: Lü JC, Kobayashi Y, Hunag D, Lee YN (Eds) *Papers from the 2005 Heyuan International dinosaur symposium*. Geological Publishing House, Beijing, 183–194.
- Tong H, Suteethorn V, Claude J, Buffetaut E, Jintasakul P (2005) The turtle fauna from the Khok Kruat Formation (Early Cretaceous) of Thailand. *Proceedings of the International Conference on Geology, Geotechnology and Mineral Resources of Indochina, Khon Kaen (Thailand), November 2005*. Khon Kaen University, Khon Kaen, 610–614.

- Tong H, Zhang JY, Li JL (2010) *Anosteira maomingensis* (Testudines: Carettochelyidae) from the Late Eocene of Maoming, Guangdong, southern China: New material and re-description. *Neues Jahrbuch für Geologie und Palaontologie-Abhandlungen* 256(3): 279–290. <https://doi.org/10.1127/0077-7749/2010/0053>
- TTWG, Turtle Taxonomy Working Group [Rhodin AGJ, Iverson JB, Bour R, Fritz U, Georges A, Shaffer HB, van Dijk PP] (2021) *Turtles of the World, 9<sup>th</sup> edition: Annotated Checklist and Atlas of Taxonomy, Synonymy, Distribution, and Conservation Status*. *Chelonian Research Monographs* 8: 1–472.
- Waite ER (1905) The osteology of the New Guinea turtle (*Carettochelys insculpta* Ramsay). *Records of the Australia Museum* 6: 110–118. <https://doi.org/10.3853/j.0067-1975.6.1905.994>
- Walther WG (1922) Die Neu-Guinea-Schildkröte *Carettochelys insculpta* Ramsay. *Nova Guinea* 13: 607–704. <https://doi.org/10.5962/bhl.title.11842>
- Werneburg I, Evers SW, Ferreira G (2021) On the “cartilaginous rider” in the endocasts of turtle brain cavities. *Vertebrate Zoology* 71: 403–418. <https://doi.org/10.3897/vz.71.e66756>
- Wessels W, Fejfar O, Peláez-Campomanes P, van der Meulen A, de Bruijn H (2003) Miocene small mammals from Jebel Zelten, Libya. *Coloquios de Paleontología* 1: 699–715.
- White AW, Archer M, Hand SJ, Godthelp H, Gillespie AK (2023) A new broad-snouted fossil carettochelyid turtle from a previously unknown Caenozoic deposit in Sarawak, Malaysia. *Alcheringa: An Australasian Journal of Palaeontology* 47(2): 1–10. <https://doi.org/10.1080/03115518.2023.2243503>
-

# The oldest teleosts (Teleostei): their early taxonomic, phenotypic, and ecological diversification during the Triassic

Gloria Arratia<sup>1,2</sup>, Hans-Peter Schultze<sup>1</sup>

<sup>1</sup> Biodiversity Institute, University of Kansas, Dyche Hall, 1345 Jayhawk Blvd., Lawrence, Kansas 66045, USA

<sup>2</sup> Department of Ecology and Evolutionary Biology, University of Kansas, Lawrence, Kansas 66045, USA

<https://zoobank.org/AB28819E-2917-4A05-ACD5-ACDB2617580F>

Corresponding author: Gloria Arratia ([garratia@ku.edu](mailto:garratia@ku.edu))

Academic editor: F. Witzmann ♦ Received 18 November 2023 ♦ Accepted 11 December 2023 ♦ Published 4 January 2024

## Abstract

As the fossil record reveals, neopterygians had a major diversification after the great mass extinction at the Permian-Triassic boundary, including the appearance of the major clade Teleostei. Detailed studies of new taxa (*Pseudopholidoctenus germanicus*, *Barschichthys ruedersdorfensis*, and *Ruedersdorfia berlinensis*) from the lower Anisian (middle Muschelkalk) of Germany and their comparisons with other Triassic relatives are presented, including new information concerning size, shape, and diet. Two families, Pholidophoridae and Marcopoloichthyidae, made a modest appearance during the Anisian of Europe and Asia almost simultaneously, with *Pseudopholidoctenus* (and the teleosteomorphs *Barschichthys* and *Ruedersdorfia*) from the Germanic Basin, being the oldest stem teleosts (244 Ma), followed shortly by *Marcopoloichthys ani* from Italy. The early teleostean diversification was fast—already in the late Ladinian three lineages were present: Prohalecitiidae (Europe), Pholidophoridae (Asia, Europe), and Marcopoloichthyidae (Asia, Europe), with ca. 20 species inhabiting the Tethys Ocean during the Middle–Late Triassic. Most Triassic teleosteomorphs were small, ca. 50 mm standard length, and a few as possibly miniature, with torpedo or oblong shapes, and suction feeders—probably a plankton based-diet. These first Triassic radiations were replaced during the early Sinemurian of marine ecosystems of Europe with two major groups: (a) non-monophyletic ‘pholidophoriforms’ and (b) proleptolepids and leptolepids, having an average size (ca. 100 mm SL) longer than Triassic forms, with oblong and fusiform shapes. A fast dispersion from the Tethys to the Paleo-Pacific followed, as demonstrated by the presence of small (ca. 50 mm SL) suction feeder proleptolepids in the early Sinemurian of Chile.

## Key Words

body shape, ecosystems, feeding, Mesozoic, miniaturization, morphology, radiation, systematics, taxonomy

## Introduction

About two hundred years ago, Agassiz (1832) described two species of his new genus *Pholidophorus* (*P. latiusculus* and *P. pusillus*) from the upper part of the middle Norian (Upper Triassic) of Seefeld, Austria (Brandner and Poleschinski 1986). In 1843, he added several Jurassic species to *Pholidophorus*, a list that increased considerably by Woodward (1895), who recognized many Jurassic species, disregarding the Triassic ones; Woodward’s taxonomy was followed by nearly all researchers because of his prestige. His authoritative opinion was taken to the extreme when an Early Jurassic species from the Lower

Lias of Dorsetshire, *Pholidophorus bechei*, was considered by Woodward as the type species, because it was better known, an approach that was followed even by Nybelin (1966) in his review of certain ‘pholidophoriforms’. More recently, Arratia (2013) revalidated the Late Triassic species *Pholidophorus latiusculus* as the type species and removed the Early Jurassic *Ph. bechei* from *Pholidophorus* and placed it in a new genus, *Dorsetichthys* (Arratia 2013: p. 118).

In contrast to the speciose Jurassic so-called ‘pholidophoriforms’ (sensu Arratia 2000), Triassic pholidophorids were described rarely. A Carnian (lower Late Triassic) species was described by Kner (1866), a Norian (Late

Triassic) species by Gortani (1907), and a Rhaetian (Late Triassic) species by Airaghi (1908). Zambelli (1975, 1977, 1980a, b, c, 1990) revised Triassic pholidophorids related to the holotype *Pholidophorus latiusculus* that were recovered in fossiliferous sites near Bergamo, Lombardy, northern Italy (e.g., Cene, Ponte Giurino, and Endenna). He erected several pholidophorid genera (e.g., *Parapholidophorus*, *Pholidoctenus*, *Pholidorhynchodon*, and *Eopholidophorus*) and species from two main Norian localities near Bergamo (Cene and Ponte Giurino). At the same time, Griffith (1977) erected a new pholidophorid genus and species, *Pholidophoretetes salvus*, among other Carnian fishes in the northern Alps (Lunz, Austria). Almost 40 years later, Arratia (2013, 2017) provided detailed taxonomic revisions of previously described Triassic pholidophorids from Europe and erected a few new genera (e.g., *Annaichthys*, *Lombardichthys* and *Zambellichthys*) and species and provided extensive morphological descriptions. Based on these taxa and additional teleosts, Arratia (2013) proposed a phylogenetic hypothesis of these Triassic pholidophorids within Teleosteomorpha or stem-based teleosts. These European Triassic pholidophorids are restricted to the Late Triassic, from the Carnian to the Rhaetian, and to marine deposits in the southern and northern Alps. Research on Middle Triassic (late Ladinian) fishes from southern China has added important information to the knowledge of pholidophorids and early teleosteomorphs, with the discovery of a new genus (*Malingichthys*) with two species, which were interpreted as the oldest pholidophorids and oldest teleosts (Tintori et al. 2015). The new genus *Malingichthys* extended not only the paleogeographic area of pholidophorids to East Asia, but also extended the time, back to middle late Ladinian. Currently, the oldest European teleosteomorph is *Prohalecites porroi* Tintori, 1990, also from the Middle Triassic (late Ladinian; ca. 240 Ma) of Italy. Recently, the range of teleosteomorphs has been enlarged by the description of new taxa: *Marcopoloichthys ani* from the Anisian of China (Tintori et al. 2007), *M. andreotti* and *M. faccii* from the Norian of Italy (Tintori et al. 2007), and *Seinstedtia parva* Schultze et al. (2022) from the Norian Fuchsberg Quarry near Seinstedt, Lower Saxony (Schultze et al. 2022: fig. 2), which is the first described Triassic teleosteomorph for Germany.

Whereas the finds from Italy, Austria and China are from the open marine Tethys, the teleosteomorph specimens from Rüdersdorf are from the restricted marine basin of the Central European Basin (Germanic Basin). Up to 2021, there was a single mention of basal teleosteomorphs for Germany; a skull roof identified as *Pholidoctenus* sp. from Rüdersdorf was figured by Schultze and Kriwet (2021) outside the Tethys (see below for new taxonomic assignment). Only recently, small teleosteomorph fishes were described from an upper Norian/lower Rhaetian locality in the central European Basin (Seinstedt, Lower Saxony; Schultze et al. 2022).

New findings and/or revision of fossiliferous localities or specimens, or the acquisition of new knowledge sometimes

give unexpected results. A single finding that was previously mentioned as *Pholidoctenus* sp. by Schultze and Kriwet (2021), is restudied herein, plus two other new fishes from the same locality (Rüdersdorf near Berlin, Germany). These fishes indicate an even earlier appearance of stem teleosts or teleosteomorphs in the Anisian (lower Middle Triassic) in a paleogeographic region where no teleosteomorphs were previously reported, the European (Germanic) Triassic basin (lower Muschelkalk) of Rüdersdorf near Berlin. These fishes and all other early teleosts, their sizes and body shapes, geographic distributions, and ecosystems are discussed here in the complex framework of early teleostean diversification during the Triassic.

## Geological site

The Muschelkalk Quarry Rüdersdorf, 25 km east of the center of Berlin, is a historic source of building stone and cement for the city of Berlin (Schroeder 2015). The quarry has been in operation for hundreds of years. The Muschelkalk (from upper lower to lower upper Muschelkalk) is exposed as an island in between Pleistocene deposits. The Muschelkalk is moved to the surface by movement of the underlying Zechstein salt. Marine fossils (bivalves, crinoids and many others) are known throughout the sequence. The most common and best known vertebrates are nothosaurids (Raab 1907; Schröder 1914; Rieppel and Wild 1996); single bones are common, but also complete specimens have been found. Schröder (1914) described different species of *Nothosaurus*, but after Rieppel and Wild (1996), only one species, *Nothosaurus marchicus*, is recognized in the Muschelkalk of Rüdersdorf. Other marine reptiles are rare (in the lower Muschelkalk: *Cymatosaurus* according to Huene 1944 and *Omphalosaurus* after Maisch and Lehman 2002), and the black, rounded crushing teeth of *Placodus* are also known. Shark teeth have been found in the middle Muschelkalk (*Acrodus lateralis*, *Hybodus plicatilis*, *Palaeobates* (*Strophodus*) *angustissimus*; see Raab 1907 and Picard 1916) and in the upper Muschelkalk (*Acrodus*, *Palaeobates*; see Raab 1907), as well as actinopterygian teeth in the middle Muschelkalk (*Gyrolepis tenuistriatus* and *Colobodus*; see Raab 1907 and Picard 1916) and upper Muschelkalk (*Colobodus* and *Saurichthys*; see Raab 1907). Additionally, scales broadly assigned to “*Semionotus*” have been known for a long time. Recently, the private collectors, Mr. W.-W. Tornow and Mr. E. Barsch, have found complete and nearly complete fishes from horizons in the Mittlerer Muschelkalk, but most specimens of teleosteomorphs are represented by isolated skull roofs as described below.

## Stratigraphy

Zwenger (1993: see fig. 4.1.26 for Mittlerer Muschelkalk) and Kramm and Hagdorn (2020: tab. 2) described the

System	Series	Stage	Rüdersdorf sequence	Stem teleosts	
TRIASSIC	201.3	Rhaetian		<i>Parapholidophorus caffii</i>	
	208.5	Norian		<i>Seinstedia parva</i> <i>Marcopoloichthys faccii</i> <i>Pholidoctenus</i> spp. <i>Parapholidophorus nybelini</i> <i>Pholidorhynchodon malzannii</i> <i>Lombardichthys gervasuttii</i> <i>Pholidophorus latiusculus</i> <i>Annaichthys pontegiurinnensis</i> <i>Zambellichthys bergamensis</i>	
	227			<i>Knerichthys bronni</i> <i>Pholidophoretetes salvus</i>	
	237	Carnian		<i>Malingichthys</i> spp. <i>Prohalecites porroi</i> <i>Marcopoloichthys furreri</i>	
	MIDDLE	Ladinian	Upper	Glaukonitkalk <i>transversa</i> -Schichten	<i>Marcopoloichthys ani</i>
			Middle	Oberes Karbonat Obere Wechsellagerung Mittleres Karbonat Untere Wechsellagerung with "Fischmergel"	
		Anisian	Middle	Unteres Karbonat ( <i>orbicularis</i> -Schichten)	gen. et sp. nov.: <i>Pseudopholidoctenus germanicus</i> <i>Barschichthys ruedersdorfensis</i> <i>Ruedersdorfia berlinensis</i>
			Lower	Schaumkalk Wellenkalk	
	246.5				

**Scheme 1.** Diagrammatic representation of the Triassic geological system, with special reference to the Rüdersdorf sequence, and a distribution of stem teleosts.

stratigraphic sequence of the Muschelkalk of Rüdersdorf based on earlier accounts. The Muschelkalk of Rüdersdorf reaches from the upper lower Muschelkalk into the lower upper Muschelkalk (Scheme 1). The new fishes described here occur in the lower part of the middle Muschelkalk, in the orbicularis-Schichten (= Unteres Karbonat) and in the above Untere Wechsellagerung. The “Fischmergel” forms the base of the Untere Wechsellagerung and is separated from the underlying orbicularis-Schichten by a 3-m thick bench of dolomite. Few fish remains are known from the Oberer Muschelkalk (Glaukonitkalk). The small specimens described here were collected in the so-called “Fischmergel” near the base of the Untere Wechsellagerung of the middle Muschelkalk, corresponding to middle Anisian (about 244 Ma; Kramm and Hagdorn 2021).

### Material and methods

The described fossil material is deposited in the fish paleontological collection of the Museum of Natural History, Berlin, Germany (**MB**). A broad comparison was done with other Triassic teleosteomorphs deposited

in the Geologische Bundesanstalt Wien Abteilung, Paläontologische Sammlungen, Vienna, Austria (**GBA**); Department of Geology, University of Innsbruck, Innsbruck, Austria (**Innsb**); Civic Museum of Natural Science Enrico Caffi, Bergamo, Italy (**MCSNB**); Geowissenschaftliche Sammlungen, Zentralmagazin Naturwissenschaftlicher Sammlungen, Martin Luther-Universität Halle-Wittenberg, Halle (Saale), Germany (**MLU**); Geological-Paleontological Section of the Naturhistorical Museum, Vienna, Austria (**NHMW**); and the Palaeontological Institut and Museum, University of Zurich, Switzerland (**PIMUZ**).

### Anatomical terminology

The terminology of the skull roof bones is based on homology and ontogeny (Schultze 2008 and Teng et al. 2019 and literature cited therein). The first time that the parietal and postparietal bones are cited in the text, as well as in figures, the traditional terminology is shown in square brackets, e.g., parietal bone [= frontal]; pa [= fr] and postparietal bone [= parietal]; ppa [= pa]. Since most of the

fishes studied herein are represented by skull roof plates, the characteristics of the plates, including measurements and proportions (taken with a digital Vernier caliper), were compared with similar plates in other Triassic pholidophorids. Only complete exposed plates, preserved in dorsal view, were considered to make the values comparable. To avoid misunderstanding concerning these measurements, these are explained below (see Fig. 1).

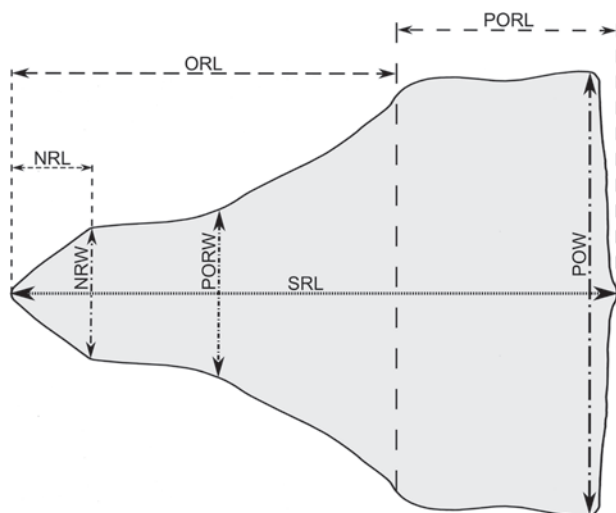


**Figure 1.** Pholidophorid skull roof illustrating possible measurements. See text for explanation.

The **skull roof length** (= SRL) is taken from the most anterior to the most posterior margins of the plate. The **orbital region** is the area of the plate bordering the eyes dorsally; the length of the orbital region or **orbital region length** (= ORL) is taken from the most anterior margin of the plate to the dorso-posterior margin of the orbit, at the region of the plate corresponding to the autosphenotic or sphenotic corner (it includes the parietal [= frontal] bones). The **postorbital region** is the area of the plate extending between the autosphenotic regions to the posterior margin of the plate (it includes the supratemporotabulars [= dermatopterotics] and postparietal [= parietal] bones); the **postorbital region length** (= PORL) is taken from the level of both autosphenotics to the posterior margin of the plate. The **nasal region** is the most anterior area of the plate, usually triangular in shape, and articulating laterally with the nasal bones and occasionally, depending on the taxon, with the rostral; the **nasal region length** (= NRL) is taken from the most anterior tip of the plate to the posterior line forming the triangle. The **nasal region width** (= NRW) is taken at the base of the triangle corresponding to this region. The **mid-orbital region width** (= PORW) is measured at the mid-region of this area, and the postorbital region width is taken at the broadest point of the postorbital region or postparietal plus supratemporotabulars [= dermatopterotic] area. The **postorbital region width** (POW) is measured as the broadest point of the region.

For body size analyses of Triassic stem teleosts, we compiled data on their total and standard lengths (= maximum standard length of Romano et al. 2016)

at species level. Incomplete taxa (e.g., *Zambellichthys* Arratia, 2013 known only by the head) were excluded. Most fishes studied here have hemiheterocercal tails; thus, the standard length was measured from the most anterior tip of the head to the last scale carrying the lateral line and ending approximately at the mid-region between the dorsal and ventral posterior body lobes. Thus, sometimes identification of the last scale carrying the lateral line is not possible due to incomplete preservation or the scales are not preserved or displaced, making any identification difficult. The body shape of the stem Triassic pholidophorids was studied, as well certain anatomical complexes, such as the jaws and their position in the head and their dentition, with the aim to identify possible feeding habits. It is noteworthy to mention that the quality of preservation of most Triassic stem teleosts is generally very good to excellent.

## Illustrations

Illustrations are based directly on the specimens. The drawings were done with the help of a camera lucida attached on a WILD stereomicroscope M5A. Except for the photographs of the new taxa described here, which were taken with a Nikon R9 and 30 mm lens, all others were taken by professional photographers working for the various academic institutions as listed in Acknowledgements.

## Systematic Paleontology

### Teleosteomorpha Arratia, 2001

### Pholidophoriformes sensu Arratia, 2013

### Pholidophoridae Woodward, 1890 sensu Arratia, 2013

#### *Pseudopholidoctenus* gen. nov.

<https://zoobank.org/A3980B26-695C-477E-98E9-1A960AD85DAC>

**Type species.** *Pseudopholidoctenus germanicus* sp. nov.

#### *Pseudopholidoctenus germanicus* sp. nov.

<https://zoobank.org/CC8072F4-A28E-42EA-91D9-3D45809E1BBD>

Figs 2–6

2021 *Pholidoctenus* sp. Schultze and Kriwet: p. 321, fig. 11.

**Diagnosis.** (Based on a unique combination of characters among stem teleosts. Autapomorphies are identified with an asterisk [\*].) Small fish of about 55 mm total length. Skull roof bones covered by small tubercles and ridges of different sizes. The length of the nasal region is about 30% of the midorbital width (Table 1). The length of the postorbital region is about 50% of the orbital region length [\*]. Deep opercle about five times deeper than the subopercle. Suture between opercle and subopercle slightly oblique. Ventral limb of cleithrum straight and

narrow, lacking a posterior expansion at the confluence of both limbs. With a series of large scales or scutes, almost square-shaped, preceding the epaxial lobe of the caudal fin [\*]. Less than 18 principal caudal rays present [\*]. No hypaxial procurrent rays present [\*]. Scales covered with a smooth layer of ganoine. Posterior margin of the scales with a few conspicuous acute projections or serrae.

**Derivatio nominis.** The name refers to the similarity of the skull roof and serrations on bones and scales to the genus *Pholidoctenus* from the Norian of Italy.

**Type material. Holotype.** MB. f. 18641, a well-preserved skull roof including sensory cephalic cranial system.

**Paratypes.** MB. f. 19904, almost complete specimen (missing the anterior part of the head and distal tips of the caudal fin rays), relatively well preserved considering the hardness of the rock and problems cleaning the surface of bones without destroying them. MB. f. 19905 and 19906, skull roofs.

**Provenience.** Opencast mine in Rüdersdorf, 25 km east of the center of Berlin, Germany.

**Age.** Lower Middle Triassic, lower Anisian (middle Muschelkalk).

**Description.** This is a small species of about 55 mm total length and about 36 mm SL. Specimen MB. f. 19904, with the body and squamation preserved in situ, is a rare one in a locality where the fishes are usually preserved as disarticulated bones (Fig. 2). The anterior part of the head is missing, and since the body is slightly bent, it is not possible to estimate its body shape accurately; possibly, it was oblong, and the peduncle depth seems to be half of the predorsal depth. The pectoral fins are missing, and the pelvic fins are incompletely preserved. The dorsal fin is placed at about half the length of the fish, and the anal is placed posteriorly, very close to the ventral margin of the caudal fin.

**Skull roof.** The nicely preserved skull roof (8.3 mm long and 7.5 mm wide at the postorbital region) has all dermal bones fused into a large plate (Fig. 3), with the exception of the rostral and nasal bones that are not preserved. The skull roof plate is almost triangular, being narrow anteriorly at the so-called triangular nasal region and expanding

posteriad, reaching its maximum width at the supratemporotabular [= dermopterotic] level and ending in a straight line (Fig. 3). A posterior process is absent in the posterior margin of the supratemporotabular region. The skull roof looks like a flat plate having a straight profile. Most of the skull roof is formed by the orbital region whose length is about 62% of the total length of the skull roof. The small triangular nasal region is short, and its length is about 11% of the skull roof length (Table 1). The lateral margins of the nasal region would articulate with the nasal bones that are not preserved, but considering the oblique position of both sutures for the nasal bones, it is assumed here that the rostral bone had an anterior position in front of the nasals. The orbital region is narrower than the postorbital region, with the width at its mid-region being ca. 33% of the postorbital region width (Table 1).

The skull roof (Fig. 3) does not show obvious sutures, but there is a slight median overgrowth in the region where both parietals [= frontals] would fuse, a tenuous, incomplete suture where both postparietals [= parietals] would meet, and a tenuous suture separating the short and small right supratemporotabular [= dermopterotic]. According to this interpretation, the parietal region would be the largest component of the skull roof, forming the whole orbital region and extending into the postorbital region. There is no process at the lateral margin at the confluence of the nasal and orbital regions of the plate. The lateral margin of the plate, at the supratemporotabular region, shows an invagination that may be occupied by the dorsal margin of the suborbital or an accessory suborbital, as in *Pholidoctenus serianus* (Zambelli 1977; Arratia 2013) and *Ph. sanpellegrinensis* (Arratia 2017). There is no evidence of a supraoccipital bone and/or epiotics at the posterior region of the plate.

The preorbital region of the skull roof plate that is formed by the fusion of both parietals occupies a significant part of the plate (Table 1). In contrast, the anteriormost narrow orbital region is about 30% of the postorbital region. This gives the skull roof characteristic proportions and shape (see section “Morphological



**Figure 2.** *Pseudopholidoctenus germanicus* gen. et sp. nov. in lateral view (MB. f. 19904) from Rüdersdorf, near Berlin, Germany (central European Basin; Germanic Basin). Scale bar: 1 cm.

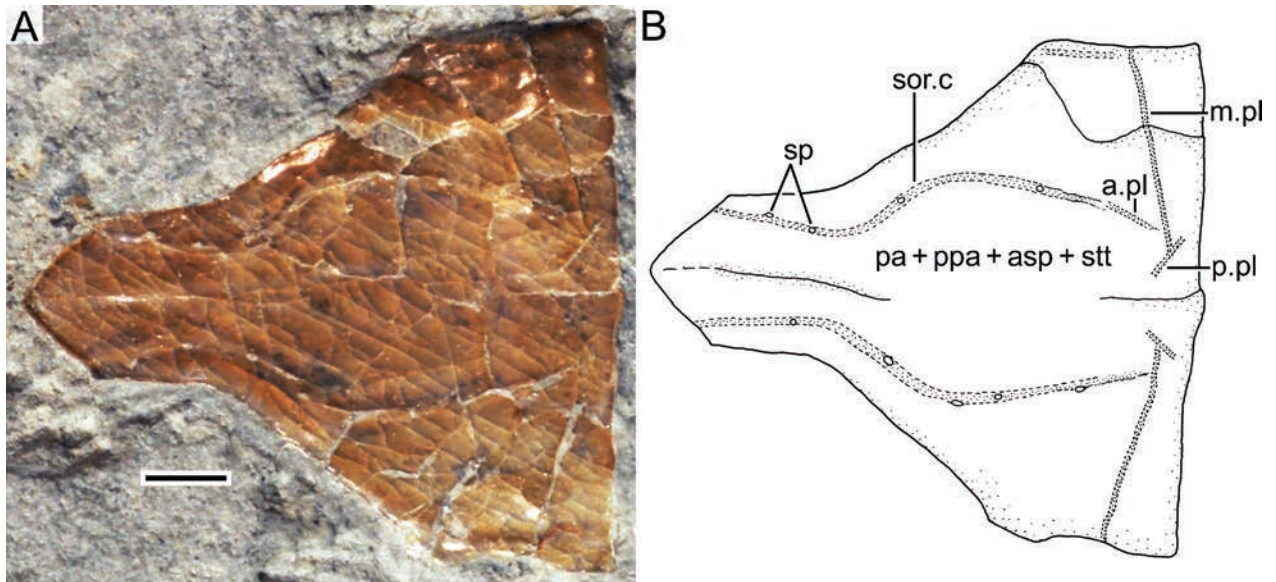


**Figure 3.** *Pseudopholidoctenus germanicus* gen. et sp. nov. (holotype MB. f. 18641) from Rüdersdorf, near Berlin, Germany (central European Basin; Germanic Basin). **A.** Photograph of skull roof. **B.** Interpretative drawing. Abbreviations: a.pl, anterior pitline; m.pl, middle pitline; ot.c, otic canal; pa+ppa+asp+stt [= fr+pa+asp+dpt], parietal+postparietal+autosphenotic + supratemporotabular [= frontal+parietal+autosphenotic+dermopterotic]; ppa.b, postparietal branch; p.pl, posterior pitline; sor.c, supraorbital canal; sp, pore of sensory canal. Scale bar: 1 mm (A).

**Table 1.** Approximate skull roof proportions in certain European stem teleosts with well-preserved skull roofs. The measured specimens are identified by their catalogue numbers. Abbreviations: NRL, nasal region; ORL, orbital region; ORW, orbital mid-region width; PORW, postorbital region; SRL, skull roof length.

Species	ORL/SRL	PORL/ORL	NRL/SRL	NRL/PORW	NRW/PORW	PORW/SRL
<i>Barschichthys ruedersdorfensis</i> gen. et sp. nov. (MB f. 19907)	58%	68%	—	—	150%	35%
<i>Parapholidophorus nybelini</i> (MCSNB 3220)	78%	30%	22%	52%	20%	84%
<i>Pholidoctenus serianus</i> (MCSNB 3095)	73%	36%	16%	43%	32%	96%
<i>Pholidoctenus sanpellegrinensis</i> (MCSNB 13207)	63%	58%	15%	46%	32%	80%
<i>Pholidophoretetes salvus</i> (NHMW 170/0293)	62%	60%	19%	57%	31%	94%
<i>Pseudopholidoctenus germanicus</i> gen. et sp. nov. (MB f. 18641)	62%	50%	11%	33%	32%	93%
<i>Ruedersdorfia berlinensis</i> gen. et sp. nov. (MB f. 19910)	52%	90%	7.7%	22%	86%	34%
<i>Seinstedtia parva</i> (MLU Sei.2010.76)	61%	63%	16.6%	40%	77%	32.8%

comparisons and taxonomic assignments”). The anterior nasal region of the plate is triangular-shaped, and acting as sutural margins for the nasal bones, an interpretation based on other pholidophorids and teleosteomorphs with the bones in situ. Following such an outline and by comparisons with *Pholidoctenus serianus* and *Ph. sanpellegrinensis*, it is hypothesized here that both nasals were medially sutured in part of their medial contact surfaces. The posterolateral corner of the orbital region is the area corresponding to the autosphenotic or sphenotic, which in this case, is fused to the parietal laterally and supratemporotabular [= dermopterotic] posteriorly.

The surface of the skull roof is covered by a thin layer of smooth ganoine; small tubercles and ridges covering the whole skull roof are observed under high magnification.

The supraorbital sensory canal (Fig. 3B) is visible (on both sides) through the bone, with few small pores, irregularly placed and opening on the surface directly on the trajectory of the canal. The supraorbital sensory canal extends posteriad, ending in the postparietal branch, just anterior to the middle pitline. The supraorbital canal,

nically preserved, shows that there is not a lateral connection with the infraorbital canal, neither with the otic canal whose trajectory (and pores) is partially visible in the right supratemporotabular region of the plate. Three pitlines (Fig. 3B) are clearly visible on the postorbital region. The longest one is the middle pitline that extends from near the mid-region of the plate to the lateral margin of the supratemporotabular region. The short anterior pitline is placed in continuation of the postparietal branch, and the posterior pitline, equally short, extends near the posterior margin of the skull roof plate.

**Circumorbital bones and suborbital region.** Only the posterior part of the circumorbital ring is preserved (Fig. 4) and includes the dermosphenotic and two partially preserved dorsoposterior infraorbitals that probably correspond to infraorbitals 4 and 5. The suborbital region, placed between the dorsoposterior infraorbitals anteriorly and the opercle and preopercle posteriorly, is unclear. It could include one large suborbital or two suborbitals.

**Opercular bones.** The opercle and subopercle, and a small fragment of the preopercle (Fig. 4) are preserved.

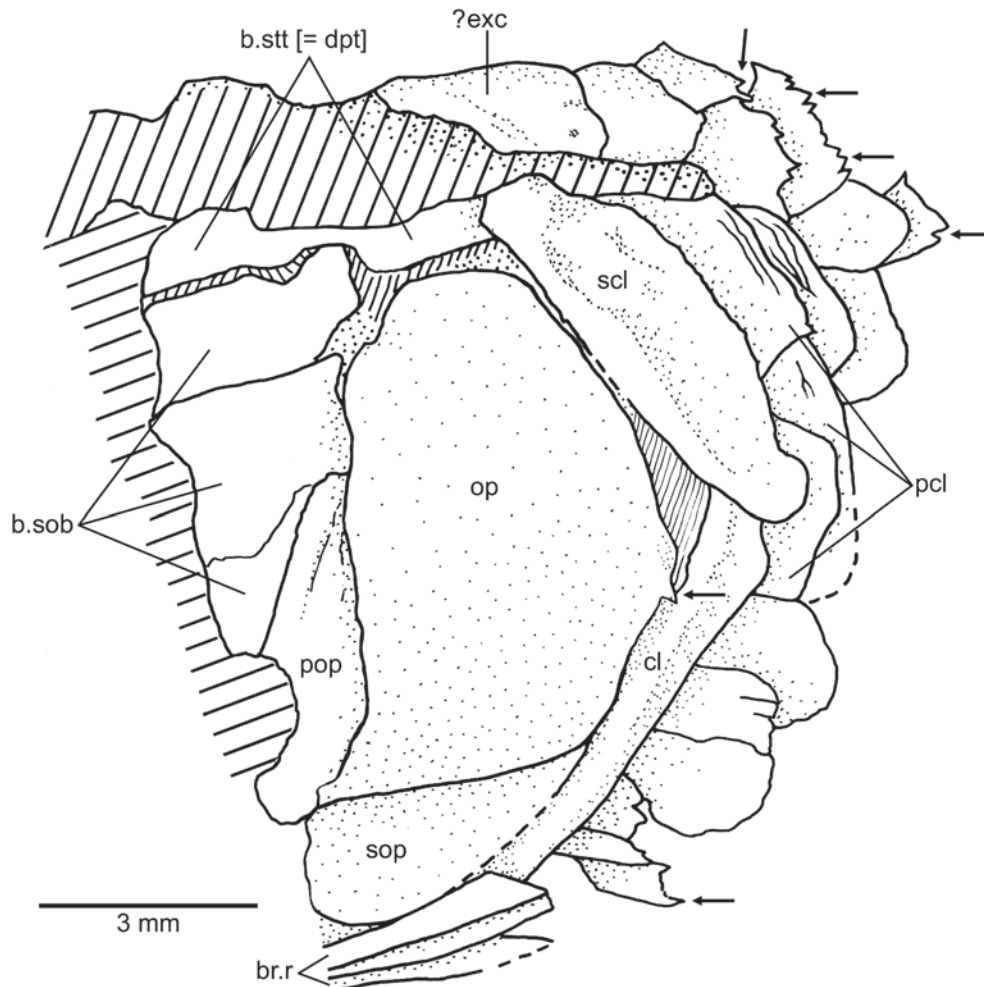


**Figure 4.** *Pseudopholidoctenus germanicus* gen. et sp. nov. (MB. f. 19904) from Rüdersdorf, near Berlin, Germany (central European Basin; Germanic Basin). Drawing of cranium and pectoral girdle in lateral view. Hatched areas represent areas that are destroyed or too poorly preserved to allow a description. Arrows point to small serrations. Abbreviations: br.r, branchiostegal rays; b.sob, broken suborbital; b.stt [= dpt], broken supratemporotabular [= dermopterotic]; cl, cleithrum; ?exc, ?extrascapula; op, opercle; pcl, postcleithra; pop, section of preopercle; scl, supracleithrum; sop, subopercle.

The opercle is a large bone, almost five times deeper than the subopercle. It is almost oval-shaped dorsally, expanding slightly at its mid-region and suturing with the subopercle throughout a slightly oblique suture. One small serration is preserved at the posterior margin.

The small subopercle has an oval-shaped ventral contour; its short anterodorsal process is at the confluence of the preopercle, opercle, and subopercle. The three opercular bones have smooth exposed surfaces. The posterior section of three narrow branchiostegal bones are preserved below the subopercle.

**Paired girdles and fins.** A section of a stout, long and narrow lower arm of the cleithrum (Fig. 4) is preserved; the angle of the lower arm is characteristically shaped and implies that the upper section of the cleithrum was short. An elongate and moderately broad supracleithrum is posterior to the opercle and dorsal part of the cleithrum. The trajectory of the lateral line canal is not visible. Three approximately rectangular-shaped elements, scale-like, are positioned posterior to the supracleithrum and cleithrum and are interpreted here as postcleithra. Postcleithra 2 and 3 are slightly displaced and partially

covering each other. There is no information on other pectoral girdle bones or pectoral rays.

The pelvic basiptyrgium is covered by scales so that information is not available, and the fin is represented by a few, incomplete preserved pelvic rays.

**Dorsal and anal fin.** An incompletely preserved dorsal fin (Fig. 5) is placed slightly anterior to the mid-length of the body trunk, slightly posterior to the incompletely preserved pelvic rays, and it does not oppose the anal fin (Fig. 2). A broad, slightly oval and short scute precedes four paired basal fulcra that are leaf-like and are followed by at least nine dorsal rays, seven with broken bases and two that are displaced. An elongate and broad fringing fulcrum is placed between the last basal fulcrum and the first principal ray, and it is followed by a series of elongated fringing fulcra that decrease in size distally. The first principal ray, only segmented and not branched, has a long base; the following principal rays have also long bases that become thinner posteriad. The bases of the dorsal rays are surrounded by enlarged, thick scales (Fig. 5).

Remains of anal rays (Fig. 6) are preserved posteriorly in the body. Remnants of five anal rays, incompletely

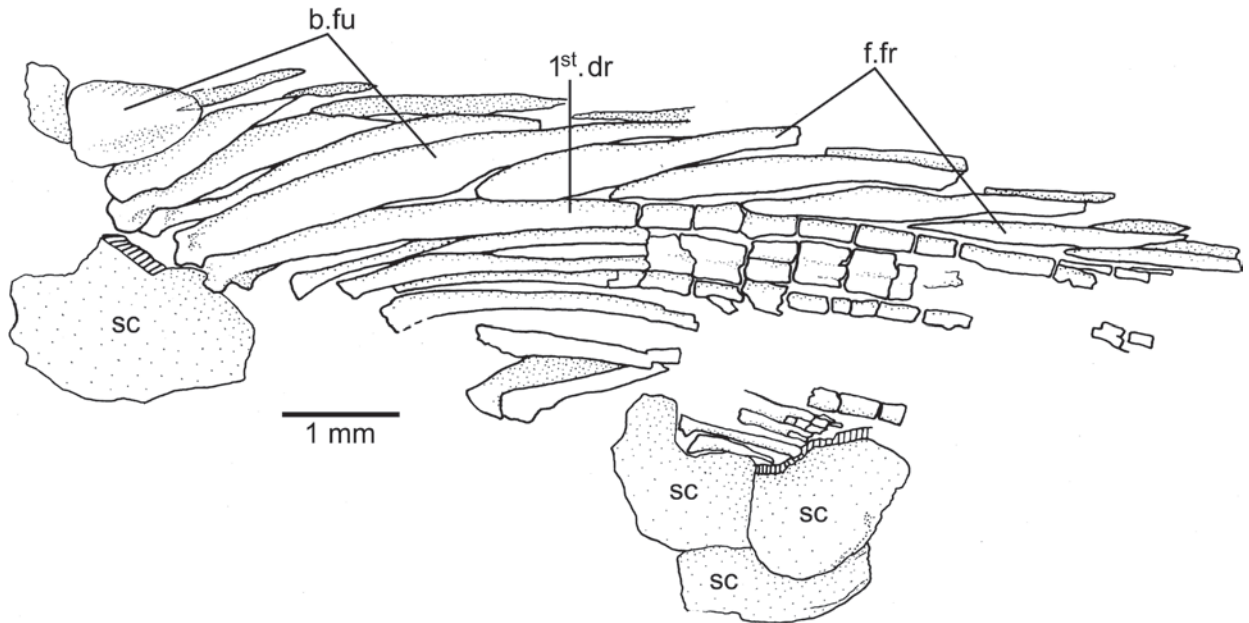


**Figure 5.** *Pseudopholidoctenus germanicus* gen. et sp. nov. (MB. f. 19904) from Rüdersdorf, near Berlin, Germany (central European Basin; Germanic Basin). Dorsal fin and surrounding scales. Abbreviations: b.fu, basal fulcrum; f.fr, fringing fulcrum; sc, scales; 1st.dr, first principal dorsal ray.

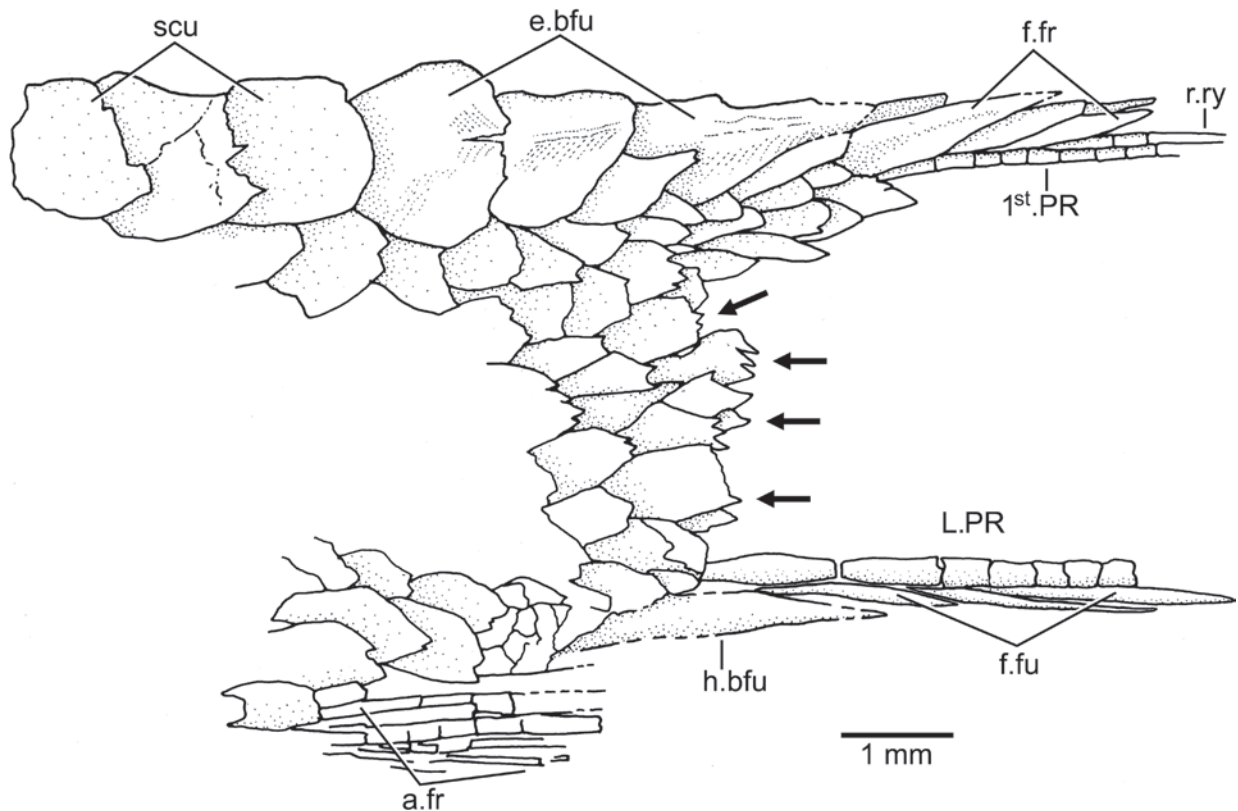


**Figure 6.** *Pseudopholidoctenus germanicus* gen. et sp. nov. (MB. f. 19904) from Rüdersdorf, near Berlin, Germany (central European Basin; Germanic Basin). Posterior part of body illustrating squamation and caudal and anal fins. Arrows point to serrations. Abbreviations: a.fr, anal fin rays; e.bfu, epaxial basal fulcrum; f.fr, fringing fulcrum; h.bfu, hypaxial basal fulcrum; r.ry, rudimentary ray; L.PR, last principal ray; scu, scutes or enlarged scales; 1st.PR, first principal ray.

preserved, almost reach the anterior margin of the hypaxial lobe of the caudal fin.

**Caudal fin.** The fin lacks its middle-posterior part; it seems to be hemiheterocercal, with an abbreviated dorsal

scaly lobe (Fig. 6). Preceding the dorso-anterior margin of the fin is a series of scutes that apparently were in continuation with the posterior part of the dorsal fin, which is missing. The series of scutes is in continuation with three

basal fulcra that are lanceolate in shape with their median posterior margin bifurcated. An incomplete series of elongate fringing fulcra follows. The fin seems to have few principal rays; 14 rays are preserved, and apparently there are not more; their segmentation is mainly straight. The number of principal rays is fewer than in the Italian genus *Pholidoctenus* with 18 to 22 principal rays (Arratia 2013, 2017). Remains of one hypaxial basal fulcrum is preserved; this fulcrum is followed by a series of elongate fringing fulcra. According to the preservation, procurrent rays are absent in the hypaxial lobe of the caudal fin, which is another major difference with species of *Pholidoctenus*.

**Scales and scutes.** Ganoid scales of lepisosteid-type of different sizes and shapes cover the body. Most scales of the dorsal and ventral rows of the flank are rhombic, rectangular or even square-shaped, with a variable number of small serrations at their posterior margin. Apparently, the three main rows of the flank, just posterior to the upper half of the opercle, are deeper and larger than other posterior scales (Fig. 2). The scales decrease in size posterior and have different shapes, but they are not preserved well enough for a detailed description.

The scales at the posterior region of the dorsal margin anterior to the dorsal fin seem to be enlarged in comparison to dorsolateral scales (Figs 2, 5). The median scales placed posterior to the dorsal fin are incompletely preserved, but there are at least four large, square-shaped scales preceding the epaxial basal fulcra (Fig. 6).

## Teleosteomorpha Arratia, 2001

### Family Barschichthyidae family nov.

<https://zoobank.org/D155CF4E-8F48-436B-B35F-65D6DCAD8C06>

**Diagnosis.** (Based on a unique combination of characters among stem teleosts. Autapomorphies are identified with an asterisk [\*].) Small fishes about 80 mm total length. The skull roof plate is unique in that its anterior region lacks the triangular nasal region [\*] present in most Triassic teleosteomorphs. The anterior margin of the skull roof plate is expanded [\*] and markedly lobated [\*], giving a unique aspect to the skull roof among teleosteomorphs (Fig. 7). Anterodorsal profile of head gently rounded. Left and right lateral extrascapulars present. One median extrascapular present [\*]. Extrascapulars lacking the anterior ‘roll-over’ characteristic of pholidophorids. Anterodorsal region of the posttemporal medially positioned. One large, rectangular-shaped suborbital bone. Maxillary blade expanding posteriorly [\*]. A tiny supra-maxilla 1 contrasts with a large supra-maxilla 2 covering most of dorsal margin of maxilla. Lower jaw long, slightly protruding anteriorly, with articulation for quadrate placed posterior to posterior margin of orbit. Skull roof covered with tubercles of ganoine of different sizes. Supramaxilla, maxilla and lower jaw covered with longitudinal ridges of ganoine. Ganoid scales of anterior part of body with few serrations on posterior margin. Markedly difference

in size between lateral line scale row and dorsal scale rows, and slight decrease in size between lateral line scale row and the next two ventral rows; oval-shaped scales or scute-like below pectoral girdles and fins.

### *Barschichthys* gen. nov.

<https://zoobank.org/670FBC57-19CF-44C3-B2ED-01181A82FB7E>

**Type species.** *Barschichthys ruedersdorfensis* sp. nov.

### *Barschichthys ruedersdorfensis* sp. nov.

<https://zoobank.org/D2B43AEC-EA84-42F9-B4CF-407B96671C23>

Figs 7–9

**Diagnosis.** Same as family diagnosis.

**Derivatio nominis.** The names of the family and of the genus are dedicated to Mr. Enrico Barsch, who from an early age (ca. 15 years old) began to collect in the mine of Rüdersdorf, which is characterized by unique but few fossils in durable, hard-to-work stone. Thus, after years of search and careful work, Mr. Barsch has gathered an important collection studied herein and he also donated part of the collection to the Museum of Natural History (MB) in Berlin.

**Type material. Holotype.** MB. f. 19907, a well-preserved skull roof including sensory cephalic cranial system and ornamentation.

**Paratypes.** MB. f. 19908, a well-preserved skull roof including ornamentation. MB. f. 19909, specimen of about 50 mm standard length, preserving the lateral view of the head and part of the trunk, which is interpreted as belonging to the same species due to the orbital region that is expanded anteriorly and broadly expanded posteriorly (though broken), as well as having the same ornamentation as in the holotype and paratype.

**Provenience.** Opencast mine in Rüdersdorf, 25 km east of the center of Berlin, Germany.

**Age.** Lower Middle Triassic, lower Anisian (middle Muschelkalk).

**Description.** The head and anterior part of the body of MB. f. 19909 provide information on cranial bones and the pectoral girdle and their relationships and on the scales of the anterior body (Fig. 8). Patchy regions covered with tubercles are badly preserved on some of the lateral head bones and some scales. The head has its anterodorsal profile almost rounded, and the long lower jaw is slightly protruding anteriorly (Fig. 9). Although the skull roof of the specimen is partially destroyed showing parts of left and right broken bones, it is evident that the head at the level of the extrascapulars is deeper than long. The diameter of the orbit is small, ca. 25% of the head length. Specimens MB. f. 19907 and MB. f. 19908 differ in the distance between orbits or mid orbital region width (PORW), but they are interpreted here as belonging to the same species because they share some unique features such as lacking the nasal region (NRL) of the skull roof

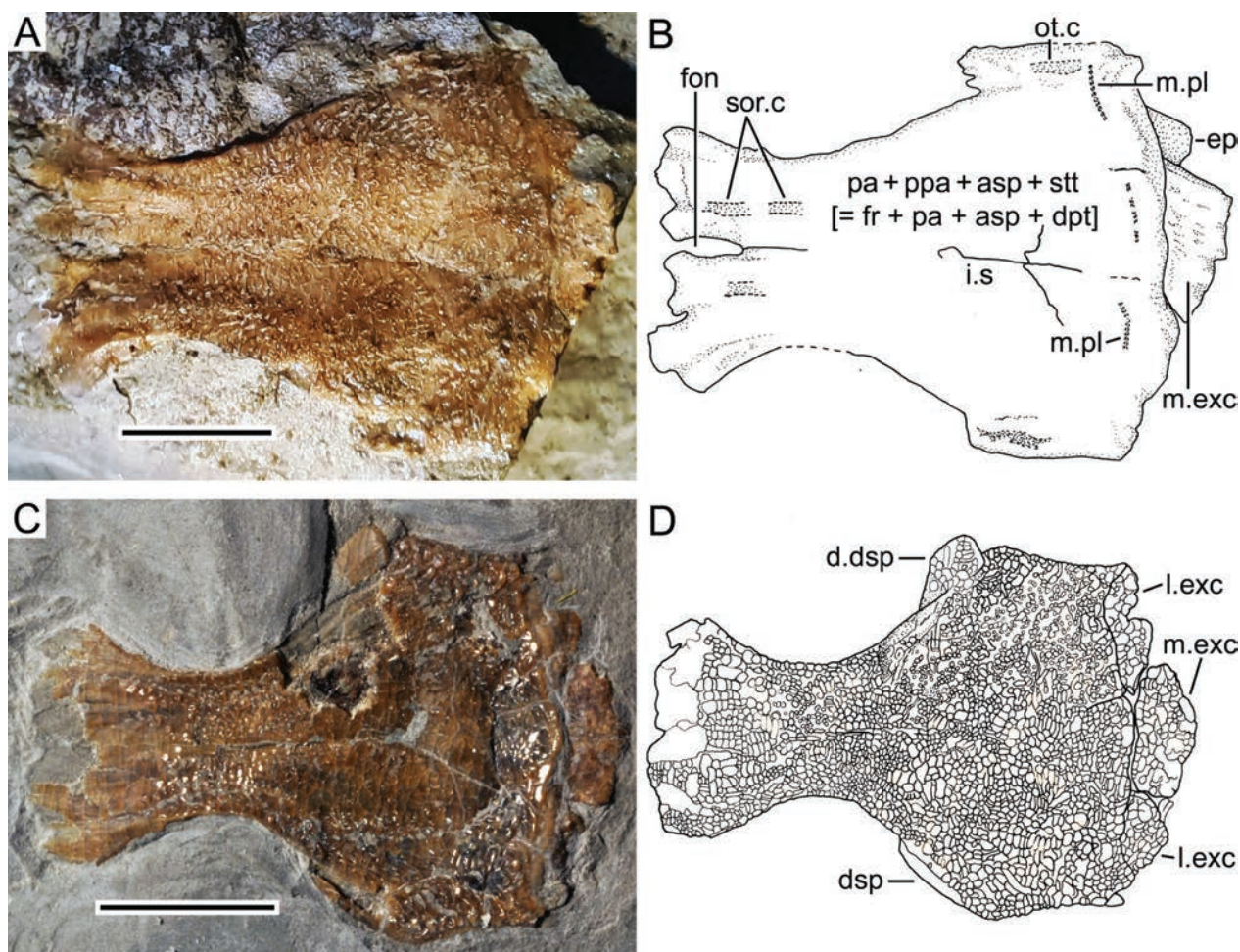


**Figure 7.** *Barschichthys ruedersdorfensis* gen. et sp. nov. from Ruedersdorf, near Berlin, Germany (central European Basin; Germanic Basin). **A.** Photograph of skull roof (holotype MB. f. 19907). **B.** Interpretative drawing. **C.** Photograph of skull roof (MB. f. 19908). **D.** Interpretative drawing. Abbreviations: dsp, dermosphenotic; d.dsp, displaced dermosphenotic; ep, epiotic; fon, anterior cranial fontanel; i.s, incomplete suture; m.exc, median extrascapula; m.pl, middle pitline; ot.c, otic canal; pa+ppa+asp+stt [= fr+pa+asp+dpt], parietal+postparietal+autosphenotic+supratemporotabular [= frontal+parietal+autosphenotic+dermopterotic]; sor.c, supraorbital canal. Scale bars: 5 mm.

plate, having an expanded and undulated anterior margin of the skull roof, and a similar postorbital region structure and proportions and sharing the same characteristic ornamentation. The difference in the mid-orbital region width may indicate sexual differences, a hypothesis that should be tested when more specimens become available.

**Skull roof bones.** Specimen MB. f. 19907 is a nicely preserved skull roof of ca. 19 mm long and 14 mm width at the postorbital region, with all dermal bones fused into a large, characteristically-shaped plate (Fig. 7), with the exception of the rostral and nasal bones that are not preserved. Still, some incomplete suture lines can be observed. Posteriorly, remains of a lateral extrascapula and a median extrascapula are preserved. The skull roof plate is expanded anteriorly, ending on a broadly undulated or lobated margin and expanding posteriad, reaching its maximum width at the supratemporotabular [= dermopterotic] level and ending in a gently curved line. The skull roof looks like a flat plate; however, the first impression is deceptive, because the lateral margins on the

anterior part of the plate are lateroventrally inclined, with the mid-section of the parietal regions of the plate, slightly higher than the lateral orbital margins; the lateral margins of the postorbital region are gently inclined lateroventrally. Most of the skull roof is formed by the orbital region whose length is about 58% of its total length. The small triangular nasal region (Figs 1, 3) present in *Pseudopholidoctenus* gen. nov. is absent here, but the anterior margin is broad; it is ca. 150% of the midregion of the orbital width. Because of the position of the supraorbital sensory canal on the skull roof plate lying closer to the midregion than to the lateral margins, there is the possibility that the nasals were very broad bones, joining at their medial margins and that the rostral bone was anterior to the nasals.

The skull roof (Fig. 7) does not show complete sutures separating bones, but there is a tenuous incomplete suture where both parietals [= frontals] meet, and another tenuous and incomplete suture separating partially the parietal and postparietal regions. Unlike other Triassic teleosteomorphs, a small oval fontanel separates left and right halves of the



**Figure 8.** *Barschichthys ruedersdorfensis* gen. et sp. nov. (MB. f. 19909) from Rüdersdorf, near Berlin, Germany (central European Basin; Germanic Basin) illustrating head and anterior part of trunk in lateral view. Scale bar: 5 mm.

skull plate anteriorly in one skull roof, but it is almost closed in another specimen. As in *Pseudopholidoctenus germanicus* gen. et sp. nov., the parietal region would be the largest component of the skull roof, forming the whole orbital region and extending into the postorbital region. The lateral margins of the plate at the supratemporotabular region are ventrolaterally expanded and carry the otic canal, which is incompletely preserved. There is no evidence of a supraoccipital bone. Suturing with the posterior margin of the plate, there are pieces of the lateral extrascapulae and a median extrascapula preserved (Figs 7, 9). Their anterior margin is smooth and not presenting the so-called thick “roll-over” that characterizes the extrascapulars in pholidophorids, which have only two extrascapulars, not three, as in the case of this fish.

The anterior nasal region of the plate is absent in this fish (compare Fig. 1 and Fig. 7), an interpretation based on other pholidophorids and teleostiomorphs with the region in situ. The broad anterior margin of the skull plate would articulate with the nasal bones, but only one nasal is incompletely preserved, forming an angle of almost 90 degrees with the parasphenoid. The relationship among the anterior margin of the plate, nasals, and rostral (not preserved) is unknown. Due to its size and position, the nasal bone would be part of the anterior region of the circumorbital region. The posterolateral corner of the orbital region is the area corresponding to the autosphenotic or sphenotic, which in this case, is fused to the parietal laterally and supratemporotabular [= dermopterotic] posteriorly.

The surface of most of the skull roof is covered by tubercle-like ornamentation that cannot be described properly due to irregularities in shape and position of the tubercles; however the ornamentation seems to be lacking in the anterior lobated region of the plate.

The supraorbital sensory canal (Fig. 7) and otic canal are visible in certain regions where the ornamentation is not preserved. No sensory pores opening on the surface have been observed. Only discontinuous sections of the middle pitline (Fig. 7) are visible on the postparietal plus supratemporotabular region; these are very difficult to observe because of the density of the ornamentation in the isolated skull roof plates, and the surface is damaged in MB. f. 19907 and MB. f. 19909.

**Braincase.** The braincase is covered by bones, and only sections of the interorbital septum and parasphenoid (Fig. 9) are preserved. A posterior section of the interorbital septum covers half the orbit in specimen MB. f. 19909. A section of the ascendent process of the parasphenoid can be observed in this specimen. Teeth or their sockets are not observed, so they are interpreted as absent. Posteriorly, the parasphenoid expands dorsally, but it is laterally covered by the suborbital so that the extension of the ascendent process is unknown. There is another ventrolateral extension that could be an incompletely preserved basipterygoid process.

**Circumorbital bones and suborbital region.** The description is based on MB. f. 19907 with the circumorbital ring partially preserved (Fig. 9) and includes infraorbitals 1 to 3 and the dermosphenotic. There is no evidence of supraorbital bones. Infraorbital 1 is a large, oval-shaped bone, slightly expanded anterodorsally. Infraorbital 2 is short and triangular-shaped. Infraorbital 3 is a large bone slightly rectangular-shaped and extending below the suborbital, reaching the opercular region. Infraorbitals 4 and 5 are not preserved, but remnants of an incomplete dermosphenotic are preserved in MB. f. 19908 and MB. f. 19909. One large, rectangular-shaped suborbital is surrounded by the dorsoposterior infraorbitals anteriorly (not preserved), the opercle posteriorly, and infraorbital 3 ventrally. The

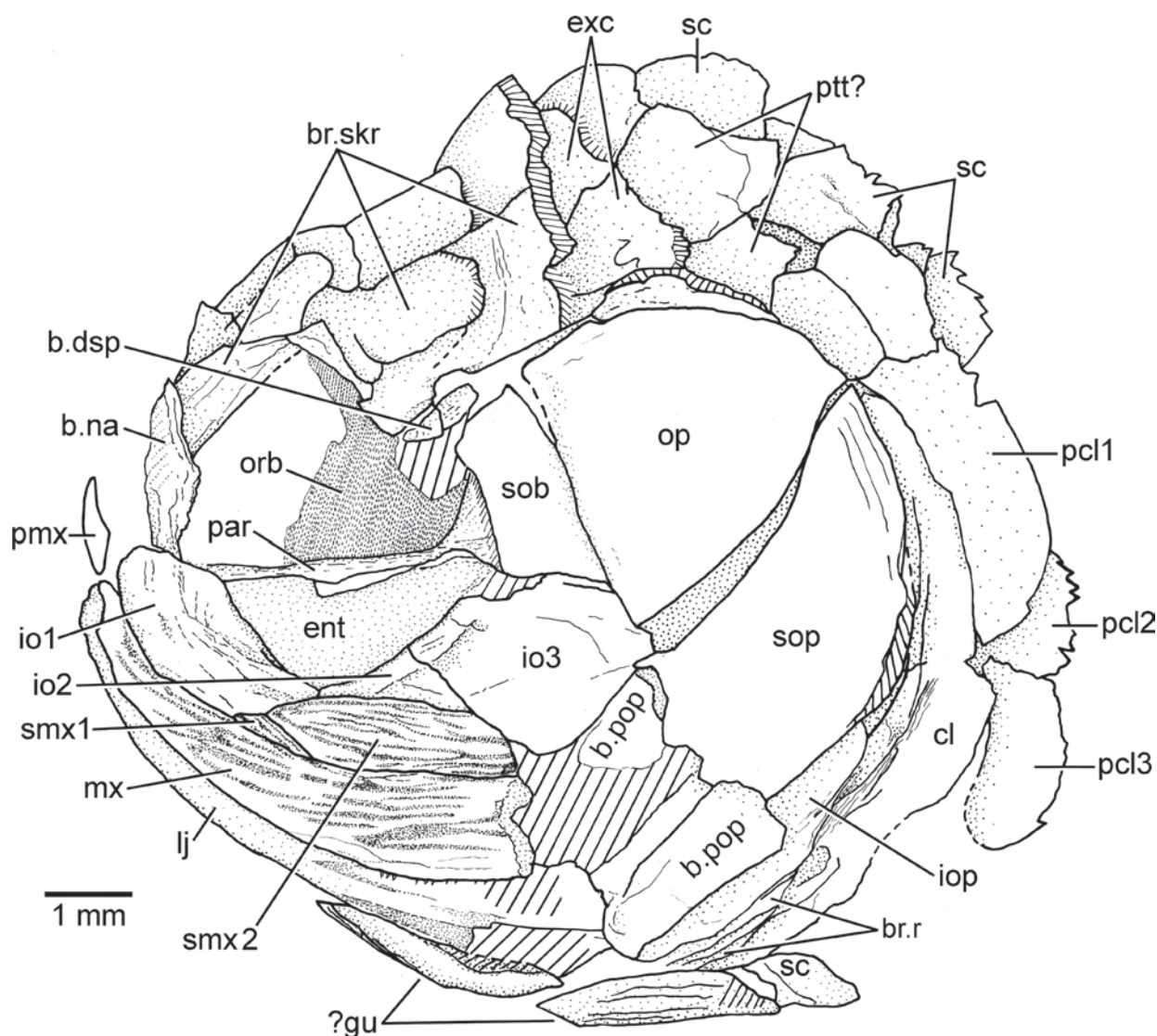


**Figure 9.** *Barschichthys ruedersdorfensis* gen. et sp. nov. from Ruedersdorf, near Berlin, Germany (central European Basin; Germanic Basin). Drawing of skull roof (MB. f. 19909). Hatched marks represent areas that are destroyed or too poorly preserved to allow a description. Abbreviations: b.dsp, broken dermosphenotic; b.na, broken nasal bone; b.pop, broken preopercle; br.r, branchiostegal rays; br.skr, broken skull roof; cl, cleithrum; ent, entopterygoid; exc, extrascapulae; gu?, gular plates?; io1-3, infraorbitals 1-3; iop, interopercle; lj, lower jaw; op, opercle; orb, incomplete orbital septum; par, parasphenoid; pcl1-3, postcleithra 1-3; pmx, premaxilla; ptt, posttemporal; sc, scale; smx1-2, supramaxillae 1-2; sob, suborbital; sop, subopercle.

trajectory of the infraorbital canal can be seen in infraorbitals 1–3, but no branches or pores are visible.

**Upper jaw.** The maxilla and supramaxillae are preserved. An enlarged, narrow premaxilla is preserved as an imprint. The maxilla (Fig. 9) is moderately long, reaching just below the posterior margin of the orbit. However, it is unclear how the posterior margin of the maxilla ended, because the maxilla is broken at its posterior margin. Its anterior articular process is short and narrow in comparison to the maxillary blade that is narrow anteriorly and expands posteriad, with the posterior margin being almost double the depth of the anterior blade. The oral margin (at least at its posterior half) carries small conical teeth; some of these teeth are covered by the oral margin of the bone, but they are seen throughout the bone. The posterior supramaxilla (Fig. 9) is a large, oblong bone that covers about half of the posterior part of the dorsal margin of the maxilla. Below

the anterior end of the supramaxilla, there is a tiny bone that is interpreted here as the anterior supramaxilla. The maxilla and supramaxillae are covered with elongate lines of ganoine, giving both bones a striated aspect.

**Lower jaw.** The lower jaw (Fig. 9) is an elongate bone, with a curved ventral margin, partially exposed below the maxilla, with its posterior region poorly preserved and extending posterior to the maxilla. Consequently, the articulation between lower jaw and suspensorium was posterior to the posterior margin of the orbit. The limit between the dentary and angular is not preserved as well as the trajectory of the mandibular canal. At least, in the posterior part of the jaw, some ridges covered with ganoine are preserved.

**Opercular bones.** The opercle, subopercle, fragment of the preopercle, and an interopercle (Fig. 9) are preserved. The opercle is slightly larger than the subopercle (with its dorsal margin broken; Fig. 9) and characteristically

shaped. Its suture with the subopercle is oblique. The broad subopercle has an almost oblique ventral margin, which becomes slightly rounded posteriorly; its small anterodorsal process is broken and is antieriad directed. The preopercle is represented by some pieces so that a description is not possible, except to propose that the bone was short dorsally because of the position and relationships between the suborbital and opercle. The interopercle is preserved below the preopercle and interopercle, so that it is possible to assume that it was an elongate bone.

**Branchiostegal rays and gular plate.** Remnants of a few, narrow branchiostegal rays are preserved below the interopercle (Fig. 9). Below the posterior part of the lower jaw and opercular region, two elongate bones are preserved, and because of their position, they can be interpreted as being median bones. Thus, these are interpreted here as possibly two gular plates (Fig. 9).

**Pectoral girdle and fin.** It is unclear if one of the scale-like bones that is broken posterior to the extrascapular

bones could be interpreted as a large posttemporal, having a medial position to the supracleithrum (Fig. 9). The dorsal part of the supracleithrum is partially exposed posterodorsal to the opercle. The cleithrum is a long bone whose ventral part is preserved, but the surface of its dorsal, narrower section is partially destroyed. The bone lacks a well-pronounced curvature and extends ventrally below the interopercle and branchiostegal rays, so that it is not possible to observe whether a clavicle was present anteriorly. Remains of the serrated appendage are preserved along the medial, ventral section of the bone. Three scaly types of postcleithra (Figs 9, 10) are present. The first one is the longest of the series and the second one is somewhat oval shaped. Postcleithrum 2 has serrations at its posterior border, but since postcleithra 1 and 3 have their posterior margin poorly preserved, it is unknown whether more serrations were present. There are remains of ornamentation on the lower part of postcleithrum 3 that are shown in Fig. 10.

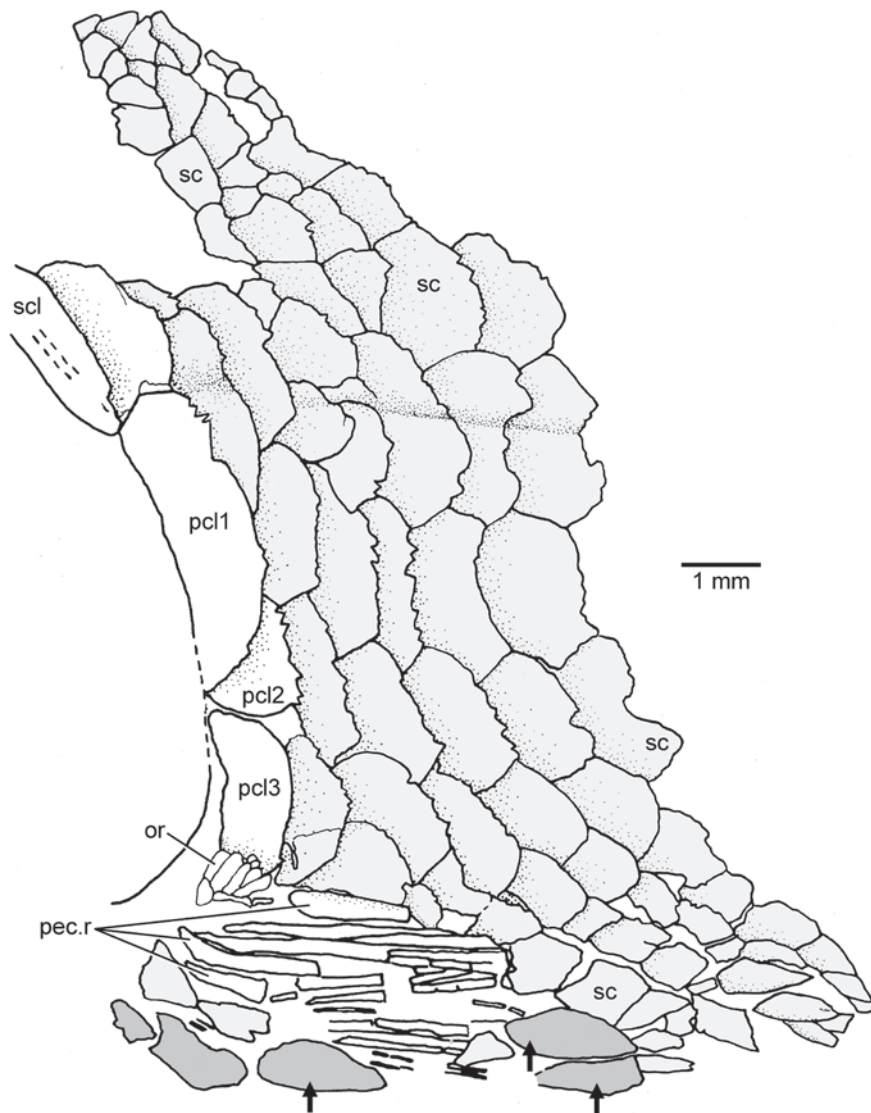


**Figure 10.** *Barschichthys ruedersdorfensis* gen. et sp. nov. from Ruedersdorf, near Berlin, Germany (central European Basin; Germanic Basin). Drawing of a section of the lateral trunk illustrating mainly scales and postcleithral bones (MB. f. 19909). Abbreviations: or, ornamentation (tubercles); pcl1-3, postcleithra 1-3; pec.r, broken pectoral rays; sc, scales; scl, supracleithrum. Arrows point to large oval scales or scutes.

Posterior to the posteroventral curvature of the cleithrum, a few broken rays (Fig. 10) are present, but their poor preservation does not allow a description.

**Scales.** The ganoid type of scales covering the body seem to be thick. There is not a distinct row of scales (Fig. 10) carrying the lateral line that can be described as significantly deeper than the next ventral body scale row; however, there is a significant difference between the lateral line scales and the dorsal series of scales that are smaller. The scales carrying the lateral line and those just above and below are rectangular, with short serrations at their posterior margin that are mostly destroyed. Ventrally, the series of scales become smaller and oval. In the ventral midline, or close to it, below the pectoral girdle and pectoral fin, some larger and oval-shaped scales or scutes are present (Fig. 10). Some of them still have preserved rounded or elongate tubercles of ganoine on their surface.

## Teleosteomorpha Arratia, 2001

### Family incertae sedis

#### *Ruedersdorfia* gen. nov.

<https://zoobank.org/94004D17-F2D9-4962-937E-ADB3724C4C5A>

**Type species.** *Ruedersdorfia berlinensis* sp. nov.

#### *Ruedersdorfia berlinensis* sp. nov.

<https://zoobank.org/F3FFD837-0DBF-4650-AD87-B223884B53C6>

Fig. 11

**Diagnosis.** (Based on a unique combination of characters among stem teleosts. Autapomorphies are identified with an asterisk [\*].) The skull roof plate resulting from the fusion of parietal, postparietal, autosphenotic, and supratemporotabular is characteristic in that the orbital region is almost as long as the postorbital region, and the width of the midorbital region is about half the width of the postorbital region [\*]; Table 1). The length of nasal region is less than 10% of the cranial plate [\*], being a small one among Triassic teleosteomorphs. Middle pitline short, not reaching the lateral margin of the supratemporotabular region [\*]. Skull roof plate covered by a characteristic ornamentation (Fig. 11).

**Derivatio nominis.** The genus name is dedicated to the place of origin (Rüdersdorf) plus the ending “ichthys”, for fish. The species name refers to the town of Berlin, indicating the geographic position of the quarry, that is located 25 km east of the center of Berlin (Germany).

**Type material.** *Holotype.* MB. f. 19910, a well-preserved skull roof including characteristic ornamentation.

*Paratypes.* MB. f. 14888, a skull roof plate preserved as impression. MB. f. 19911, a well-preserved skull roof including sensory canal system.

**Provenience.** Opencast mine in Rüdersdorf, 25 km east of the center of Berlin, Germany.

**Age.** Lower Middle Triassic, lower Anisian (middle Muschelkalk).

**Description.** This taxon is represented by three nicely preserved skull roofs of ca. 18 mm length and 11 mm width at the postorbital region, with all skull dermal bones fused into a plate, with the exception of the rostral and nasal bones that are not preserved. The skull roof plate (Fig. 11) is narrow anteriorly at the so-called triangular nasal region and slightly expands posteriad, reaching its maximum width at the supratemporotabular [= dermopterotic] region; the skull roof plate ends in almost a straight line, with a small process that is exposed at the posterolateral corner of the supratemporotabulars in the paratypes. The skull roof differs from all other taxa studied here and other teleosteomorphs in that the orbital region is as long as the postorbital region (Table 1). The small triangular nasal region is short and its length is about 8% of the skull roof length. Considering the oblique position of both sutural surfaces for the nasal bones and the lateral exits of the supraorbital canal, it is assumed here that nasal bones were placed laterally to the median rostral bone. The orbital region is slightly narrower than the postorbital region, with the width at its mid-region ca. 33% of the postorbital region width (Table 1).

The skull roof (Fig. 11) does not show sutures or incomplete ones. The anteriormost, narrow orbital region is the smallest among the skull roofs studied here, and in addition, its anterior margin is slightly rounded, unlike other pre-orbital regions that commonly are triangular-shaped. This gives the skull roof characteristic proportions and shape (see Table 1 and section on Morphological comparisons and taxonomic assignments). There is no evidence of a supra-occipital bone. The exposed portion of the epiotics at the posteroventral region of the plate are well developed and conic in shape. The surface of the skull roof is covered by a layer of ganoine, characteristically ornamented (Fig. 11).

The supraorbital sensory canal is visible through the bone, with a characteristic trajectory, with few small pores, irregularly placed and opening directly on the surface. The supraorbital sensory canal extends posteriad, ending in the postparietal, just anterior to the middle pitline. Thus, the last section of the canal can be interpreted as its postparietal branch. The supraorbital canal, nicely preserved, shows that there is not a lateral connection with the infra-orbital canal, neither with the otic canal whose trajectory (and pores) is not visible in the supratemporotabular region of the plate. Two pitlines are clearly visible on the postorbital region. One is the middle pitline that is placed posterior to the anterior pitline, and is short, not extending to the lateral surface of the supratemporotabular region. The short anterior pitline is placed in continuation with the postparietal branch of the supraorbital canal, and apparently it does not contact the middle pitline.

## Morphological comparisons and taxonomic assignments

### *Pseudopholidoctenus germanicus* gen. et sp. nov.

A broad comparison of the skull roof plate (Fig. 3) of *Pseudopholidoctenus germanicus* gen. et sp. nov., its

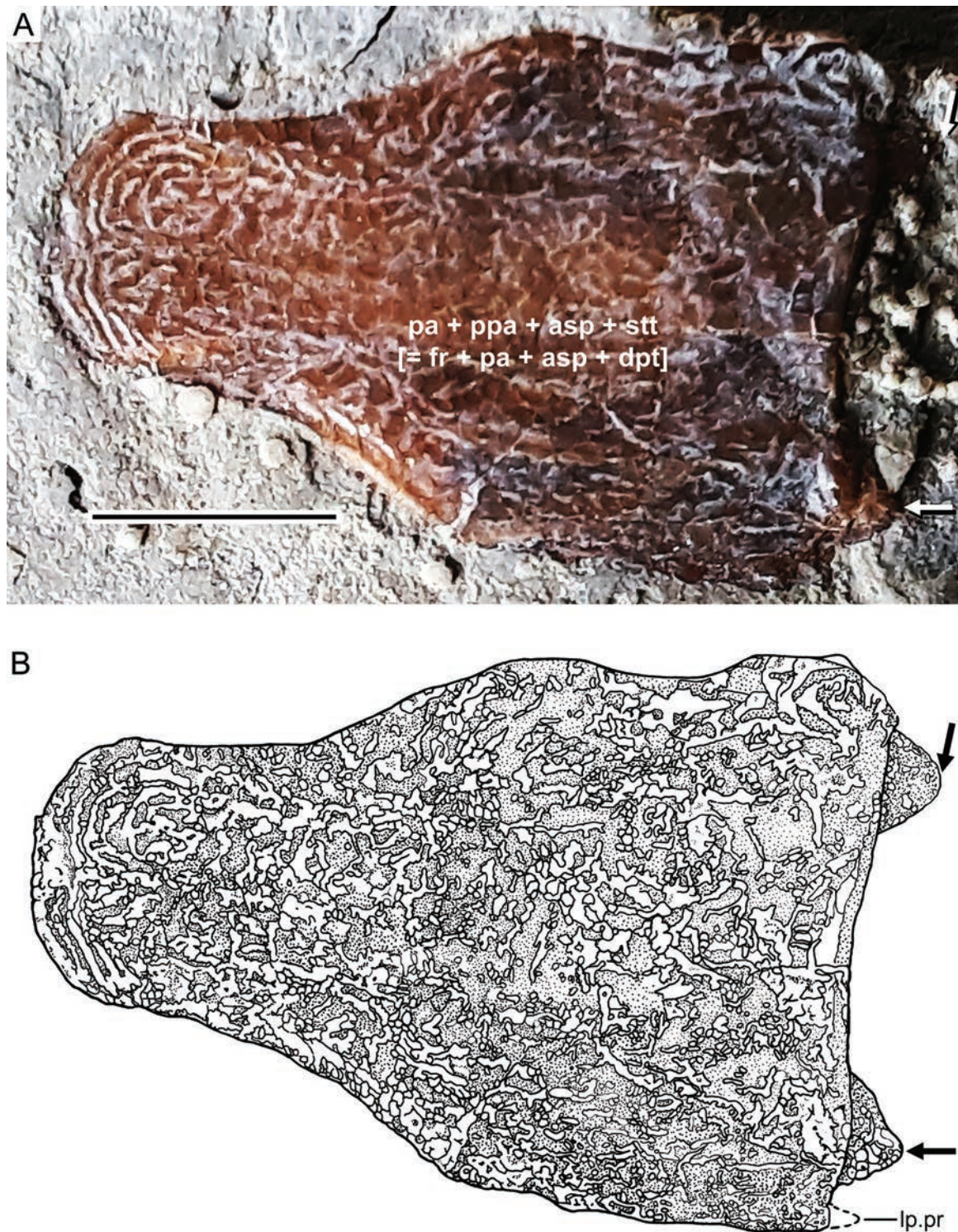


**Figure 11.** *Ruedersdorfia berlinensis* gen. et sp. nov. (holotype MB. f. 19910) from Rüdersdorf, near Berlin, Germany (central European Basin; Germanic Basin). Small arrows point to the epiotics. **A.** Photograph of skull roof plate. **B.** Drawing illustrating details of ornamentation. Sensory canals and pit lines are not observed due to the thickness of the ornamentation. Abbreviation: lp.pr, latero-posterior process of the supratemporotabular area of the skull roof. Scale bar: 5 mm (A).

characteristic triangular shape, proportions and fusion of all bones was performed, including pholidophorids (with the characteristic skull roof, triangular in shape), other stem teleosts from the same locality, and other Triassic teleostomorphs.

Triassic pholidophorids may have the skull roof plate covered with a smooth layer of ganoine or with a layer of

ganoine ornamented with ridges and tubercles of different sizes (e.g., in *Lombardichthys* [*Pholidophorus*] *gervasuttii*, *Annaichthys pontegiuriniensis*, *Pholidorhynchodon malzannii*, and *Knerichthys* [*Pholidophorus*] *bronni*; Arratia 2013). European pholidophorids with a thin ganoine cover and lacking ornamentation on the skull plate as in *Pseudopholidoctenus germanicus* gen. et sp. nov.

are the genera *Pholidoctenus*, *Parapholidophorus*, and the Carnian *Pholidophoretetes* (Arratia 2013). The three genera have slight differences in proportions of their skull roofs (compare Fig. 3 and Fig. 12B; Table 1): (1) *Parapholidophorus* has the longest and narrowest nasal region (Table 1) in contrast to other Triassic European pholidophorids; (2) *Pholidophoretetes* has the shortest and broadest nasal region; and (3) *Parapholidophorus* has an irregular region and/or process at the lateral margin of the parietal region where the supraorbital 1 and nasal bone articulate (see Arratia 2013: figs 59, 61).

In all these European pholidophorids, all bones forming the skull roof are fused (although some specimens still retain incomplete sutures, especially in younger individuals). In contrast, the Chinese pholidophorid *Malingichthys nimaiguensis* (Fig. 12A) has fused parietals medially, while the supratemporotabulars [= dermopterotics] are separated and the postparietals are fused into one element (Tintori et al. 2015: fig. 4); furthermore, the separation of bones is complete in *Malingichthys wanfenglinensis* (Tintori et al. 2015: fig. 7). Although, as in the European pholidophorids, the skull roof is longer than broad, the length of the orbital region is ca. 59% of the total length of the skull roof so that the postorbital region is slightly longer than in European pholidophorids. In parallel, the midsection of the orbital region is comparatively broader (ca. 50%) than the postorbital region width in most European pholidophorids, except *Pholidophoretetes* (see Table 1).

While the trajectory of the supraorbital sensory canal (Fig. 3) is clearly visible and showing a long canal in continuation with the parietal branch, ending just in front of the anterior pitline in *Pseudopholidoctenus germanicus* gen. et sp. nov., the canal is shorter in *Pholidoctenus serianus* and *Ph. sanpellegrinensis* (Arratia 2013: figs 78, 79; Arratia 2017). The number of pores in *Pseudopholidoctenus germanicus* is slightly variable between the left and right sides of the skull roof plate (Fig. 3), and it is also variable in *Pholidoctenus serianus* and *Ph. sanpellegrinensis* (Zambelli 1978; Arratia 2013: figs 78A, 79; Arratia 2017: figs 3, 4A). All mentioned pholidophorids, as well as *Pseudopholidoctenus germanicus*, have small sensory pores, lacking sensory tubules, just opening directly above the canal.

The only other known Triassic teleosteomorphs are *Prohalecites* from Ca' del Frate, northern Italy (Tintori 1990; Tintori and Lombardo 1999; Arratia 2013: fig. 95; Arratia 2017: fig. 9; Arratia 2022; Gouiric-Caballi and Arratia 2022: fig. 14), *Marcopoloichthys* from China, Italy and Switzerland (Tintori et al. 2007; Arratia 2022), and the recently described *Seinstedtia* (Schultze et al. 2022) from Germany. The skull roofs of *Prohalecites* (Fig. 12C) and *Marcopoloichthys* (Arratia 2022: figs 4, 5, 7) are not comparable with that of *Pseudopholidoctenus germanicus* from Rüdersdorf, Germany, because their skull roofs lack the characteristic triangular shape of pholidophorids, with the postorbital region significantly broader than the mid-orbital region. The skull roofs of *Prohalecites* and *Marcopoloichthys* are slightly broader at the postorbital

region in comparison to the orbital region (see Fig. 12C). Additionally, the skull roof of *Prohalecites* has a gently curved profile anteriorly, and most bones are independent. Although the skull roof of *Seinstedtia* has an overall shape similar to that in pholidophorids, its postorbital region is considerably broader than the orbital region (Fig. 12D). Additionally, *Seinstedtia* has several other morphological characters that separate the genus from pholidophorids, so it was interpreted as a teleosteomorph, family undetermined by Schultze et al. (2022).

Thus, the skull roof of *Pseudopholidoctenus germanicus* gen. et sp. nov. from Rüdersdorf, Germany has the characteristic shape found in members of Pholidophoridae sensu Arratia (2013), and in particular it has an overall similarity to those of the Italian *Pholidoctenus serianus* and *Pholidoctenus sanpellegrinensis*, although slight differences in proportions are present in the three species (Table 1). Because of the characteristics of the skull roof in different pholidophorids, we currently interpret the skull roof of MB. f. 18641, previously described as *Pholidoctenus* sp. by Schultze and Kriwet (2021) from the lower Anisian of Rüdersdorf, Germany as belonging to a new genus and species, *Pseudopholidoctenus germanicus*.

#### ***Barschichthys ruedersdorfensis* gen. et sp. nov.**

The other two new stem teleosts, *Barschichthys ruedersdorfensis* and *Ruedersdorfia berlinensis*, described above were recovered together with *Pseudopholidoctenus germanicus* in the same geological site in the middle Anisian (Middle Triassic) of the Germanic Basin (Scheme 1). The two new fishes represented by isolated skull roof plates (and one lateral view of the head and anterior part of the body) are so characteristic that they can be easily separated from each other and also from *Pseudopholidoctenus germanicus*. Although the three taxa share the fusion or incomplete fusion of cranial bones into one plate and the narrowing of the orbital region versus an expanded postorbital region, they have major differences in the nasal region, anterior margin of the skull roof and the trajectory of the supraorbital sensory canal when this canal is observed (compare Figs 3, 7 and Fig. 11).

The lateral view of the head of *Barschichthys ruedersdorfensis* gen. et sp. nov. has some overall similarities with that of members of the Late Jurassic family Archaeomaenidae from Gondwanan continents (e.g., Antarctica, Australia). One of the diagnostic features of archaeomaenids is a “broad cranial roof, with a ventral gently curvature of the antero-dorsal portion of the skull” (Bean 2021: p. 218); however, such apparent similarity is misleading, because the skull roof is also broad, but its shape is completely different from that in archaeomaenids, which lack the expanded anterior margin of the cranial roof plate present in *Barschichthys ruedersdorfensis*. In addition, the anterior margin of the parietal bones in archaeomaenids is straight, while it is irregular in *Barschichthys ruedersdorfensis*. Another diagnostic feature of archaeomaenids is “an almost horizontal suture between opercle and subopercle”, whereas the

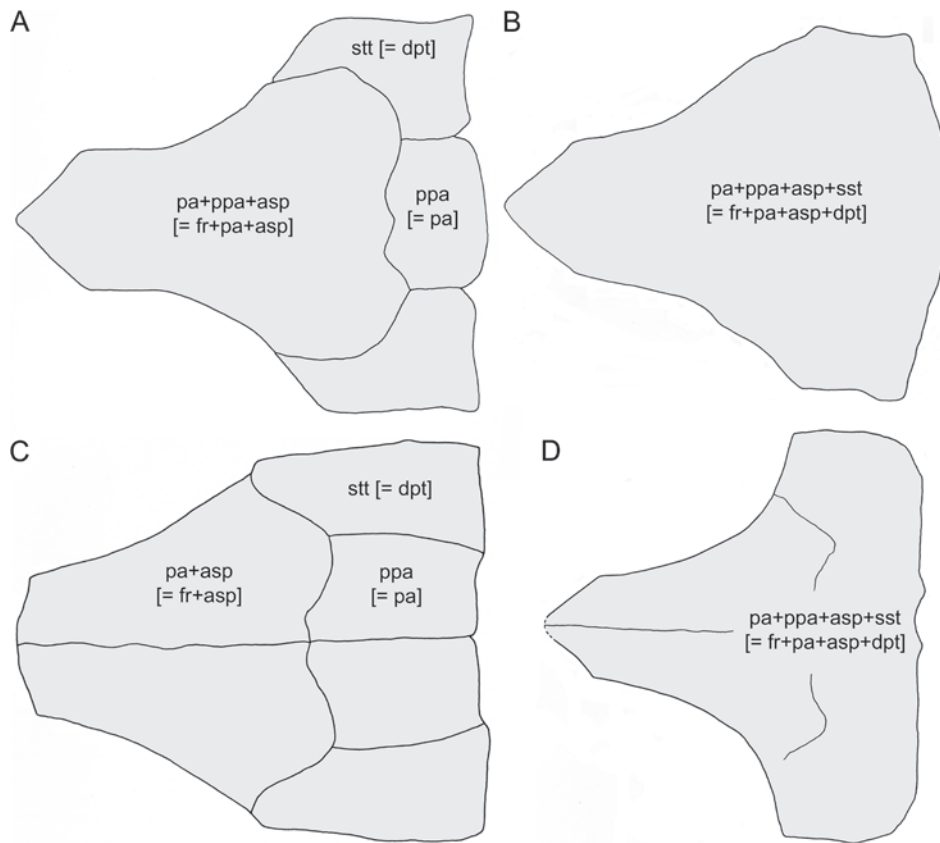


**Figure 12.** Schematic skull roof plates of Triassic teleosteomorphs illustrating variation in shape, proportions and fusion of bones. **A.** Chinese pholidophorid *Malingichthys nimaiguensis*. **B.** Italian pholidophorid *Pholidoctenus serianus*. **C.** Italian prohalecitid *Prohalecites porroi*. **D.** German indeterminate teleosteomorph *Seinstedtia parva*. Abbreviations: pa+asp [= fr+asp], parietal+autosphenotic [= frontal+autosphenotic]; ppa [= pa], postparietal [= parietal]; pa+ppa+asp+stt [= fr+pa+asp+dpt], parietal+postparietal+autosphenotic+supratemporotabular [= frontal+parietal+autosphenotic+dermopterotic]; stt [= dpt], supratemporotabular [= dermopterotic].

**Table 2.** Size, body shape, and paleoenvironments in Triassic pholidophorids.

Taxon	Body size (SL in mm)	Body shape	Geographical distribution	Environment	Age
BARSCHICHTHYIDAE family nov.					
<i>Barschichthys ruedersdorfensis</i> gen. et sp. nov.	?	oblong?	Germany	marine	middle Anisian
PHOLIDOPHORIDAE					
<i>Annaichthys</i>	±60	oblong	Italy	marine	Norian
<i>Knerichthys</i>	±130	oblong	Italy	marine	Carnian
<i>Lombardichthys</i>	±72	oblong	Italy	marine	Norian
<i>Malingichthys maiguensis</i>	±65	fusiform	Asia	marine	late Ladinian
<i>M. wanfenglinensis</i>	±48	fusiform	Asia	marine	late Ladinian
<i>Parapholidophorus caffii</i>	±49	oblong	Italy	marine	Rhaetian
<i>P. nybelini</i>	±60	oblong	Italy	marine	Norian
<i>Pholidoctenus serianus</i>	±55	fusiform/oblong	Italy	marine	Norian
<i>Ph. sanpellegrinensis</i>	±55	fusiform/oblong	Italy	marine	Norian
<i>Pholidophoretas</i>	±72	?	Italy	marine	Carnian
<i>Pholidophorus</i>	±75	oblong	Italy	marine	middle Norian
<i>Pholidorhynchodon</i>	±140	oblong	Italy	marine	Norian
<i>Pseudopholidoctenus germanicus</i> gen. et sp. nov.	±36	oblong	Germany	marine	middle Anisian
MARCOPOLICHTHYIDAE					
<i>Marcopoloichthys ani</i>	35–37	torpedo-like	China	marine	middle Anisian
<i>M. faccii</i>	±37	torpedo-like	Italy	marine	early Carnian
<i>M. furreri</i>	±45	torpedo-like	Switzerland	marine	Ladinian
<i>M. andreotti</i>	±36	torpedo-like	Italy	marine	early Ladinian
PROHALECITIDAE					
<i>Prohalecites</i>	30–36	torpedo-like	Italy	marine	late Ladinian
TELEOSTEOMORPHA INCERTAE SEDIS					
<i>Ruedersdorfia berlinensis</i> gen. et sp. nov.	?	?	Germany	marine	middle Anisian
<i>Seinstedtia parva</i>	38	fusiform	Germany	coastal	Norian

suture is oblique in the Triassic *Barschichthys ruedersdorfensis*, and the shape and size of these bones are also different from those in archaeomaenids. Archaeomaenids have supraorbital bones, whereas they are absent in *Barschichthys ruedersdorfensis*. Thus, the circumorbital ring is closed in archaeomaenids; in contrast, it is open dorsally in *Barschichthys ruedersdorfensis*. The maxilla is comparatively smaller in archaeomaenids than in the German Triassic fish which, in addition, has a unique maxilla among teleosteomorphs, which expands posteriad. The lower jaw of archaeomaenids is short with the quadrate-lower jaw articulation about the middle of the orbit, whereas the lower jaw of the German Triassic fish is long, extending well posteriad to the orbit, and its articulation with the quadrate is placed posterior to the orbit.

The new family described here, Barschichthyidae, differs from members of the Triassic family Pholidophoridae sensu Arratia (2013, 2017) in the same characters cited above for archaeomaenids. And the same can be said if a comparison is done with the Triassic Prohalecitiidae and Marcopoloichthyidae, all with very characteristic crania (Tintori 1990; Tintori et al. 2015; Arratia 2022). Thus, the diagnosis of the new family is supported by several anatomical and morphological features (see Diagnosis) that are unique to this new taxon, as well as its combination of diagnostic characters.

Finally, the diagnosis of the new genus and species, *Ruedersdorfia berlinensis* (Fig. 11), is characterized by a few autapomorphies and a unique combination of characters that justify its creation as a new taxon. However, due to its combination of characters, its position among stem teleosts is unknown and is interpreted here as Teleosteomorpha incertae sedis.

## Discussion

### Size and body shape and oldest teleosteomorphs or stem teleosts

With very few exceptions, Triassic stem teleosts are small-bodied in comparison to some contemporaneous non-teleost fishes, such as *Birgeria* and *Saurichthys*. Except for marcopoloichthyids, other stem teleosts, such as *Prohalecites* and pholidophorids, including *Pseudopholidoctenus germanicus* gen. and sp. nov., have hemiheterocercal tails so that both the maximum body length or total length and the standard length were measured for most taxa studied here. Interpretation as small body size versus an intermediate or large body size fish is somewhat subjective, because of personal differences in taking measurements so that the comparison below is restricted to what can be understood as a ‘small body-sized’ or ‘miniature’ fish in Triassic teleosteomorphs.

Miniaturization, as defined for extant Neotropical fishes by Weitzmann and Vari (1988) and extended thereafter to other fish taxa (e.g., Kottelat et al. 2006) and extant amphibians and reptiles (e.g., Janken 1993; Janken and Wake

1993; Zimkus et al. 2012), involves individuals reaching sexual maturity at 20 mm SL or less and not growing longer than 26 mm SL, and usually exhibiting pedomorphic characters. However, such views are being challenged, because it is considered that after the limitations established by Weitzman and Vari (1988), the threshold is arbitrary. To be considered a miniature, the species needs to present a reduction in body size in comparison with close relatives/sister lineages and the common patterns that follow the miniaturization process, such as reductions and losses of structures (P. Braganca, written comm. November 21, 2022).

Among Permian neopterygians (e.g., the European holosteans *Acentrophorus altus* and *A. glaphyrus*, ca. 40–90 mm total length; Gill 1933; Brandt 2021) and Triassic fossil neopterygians, there are some that are so small that they are candidates to be considered as miniature, such as the European neopterygians *Habroichthys minimus* (ca. 32 mm TL; Bürgin 1992), *Peltolepus notocephalus* (ca. 45 mm TL), *Peltolepus macrodontus* (50 mm TL) (Bürgin 1992), and *Prosantichthys buergeri* (60 mm total length; Arratia and Herzog 2007) and the Asian neopterygians *Frodoichthys luipingensis* and *Gimlichthys dawaziensis* (ca. 40 mm TL; Sun et al. 2016a, b), the thoracopterid *Wushaichthys exquisitus* (ca. 55 mm TL; Xu et al. 2015; Chen and Arratia 2022), the louwoichthyiform *Peltolepus asiaticus* (46 mm TL; Yuan et al. 2022) and the ginglymodian *Diandongichthys ocellatus* (ca. 45 mm TL and ca. 35 mm SL; Xu and Ma 2023). Among European teleosteomorphs, *Pseudopholidoctenus germanicus* gen. et sp. nov. (ca. 36 mm SL), according to current information, would be the smallest pholidophorid (see Table 2). Interestingly, pedomorphic characters have not been mentioned for these fishes.

So far as is known, a few of the oldest stem teleosts can be considered as candidates for miniaturization, because the smallest ones have standard lengths of about 30–36 mm (*Prohalecites porroi*), 35–37 mm SL (Chinese *Marcopoloichthys ani*; Tintori et al. 2007), and 38 mm SL (*Seinstedtia parva*; Schultze et al. 2022). With standard lengths of about 48 and 49 mm *Malingichthys wanfenglinensis* from China and *Parapholidophorus caffii* from Italy are respectively the smallest species among pholidophorids, whereas the Italian *Pholidorhynchodon malzannii* (ca. 140 mm SL) and *Knerichthys bronni* (ca. 130 mm SL) are the longest. Other pholidophorids such as the Italian *Pholidoctenus serianus* and *Ph. sanpellegrinensis*, the Chinese *Malingichthys nimaiguensis* (ca. 55 mm SL), the Italian *Annaichthys pontegiuriniensis* (ca. 59 mm SL), the Austrian *Pholidophorus latiusculus* (ca. 75 mm SL), the Italian *Lombardichthys gervasvasuttii* (ca. 72 mm SL) and the Austrian *Pholidophoretetes salvus* (ca. 72 mm SL) form a group of intermediate small-sized fishes that according to the current information would represent the average length among pholidophorids (Table 2). A comparison among families reveals that Pholidophoridae had the broader size diversification of 36–140 mm SL, whereas the diversity within the family Marcopoloichthyidae was narrower, ranging from 35–55 mm SL. A comparison is

difficult, because these fishes, as part of their phylogenetic position (e.g., Arratia 2013, 2017, 2022), possess several characters that place them among the most primitive teleosts, but according to our results and a survey of the available literature, they do not exhibit features that could be interpreted as paedomorphic.

Comparisons of species lengths of teleosteomorphs versus their geographical distribution point to the fact that the smallest known taxa were living in Europe (*Prohalecites porroi*, *Pseudopholidoctenus germanicus* gen. et sp. nov., and *Seinstedtia parva*) and in Asia (*Marcopoloichthys ani*), but they were not co-existing in a temporal dimension (Table 2). More teleosteomorphs of intermediate and long lengths have been found in Europe, and a few in Asia (Table 1), but this could be biased because Triassic stem teleosts have been explored and studied in Europe for longer periods than in Asia.

Evaluating body shapes of stem teleosteomorphs has also been a difficult task because of differences in interpretation that although subtle, still could be significant. Thus, Fig. 13 illustrates the three shapes that we distinguish here. While there is no conflict separating a fusiform or a torpedo-like fish, sometimes it is difficult to distinguish an oblong fish from a fusiform one. All species of marcopoloichthyids are characterized by a torpedo-like form (Tintori et al. 2007; Arratia 2022); we observe a similar body shape in *Prohalecites*, with its head considerably large compared to its narrow, elongate body. In contrast, *Seinstedtia parva* has a beautiful fusiform body, with its middle body region considerably deeper than the head and the caudal peduncle. Although not as clear as in *Seinstedtia*, the body shape of *Malingichthys imaignensis* and *M. wanfenglinensis* can be also interpreted as fusiform. The body shape of *Pholidophorus latiusculus*, *Pholidoctenus serianus*, *P. sanpellegrinensis*, and others (see Table 1) is better described as oblong, with the body axis longer than its depth.

Among the studied fishes, the body of the German stem teleost *Ruedersdorfia berlinensis* gen. et sp. nov. remains unknown, whereas the body of *Pseudopholidoctenus germanicus* gen. et sp. nov. and *Barschichthys ruedersdorfensis* gen. et sp. nov. is interpreted as probably oblong, and it is covered with ganoid scales. The body of the Eurasian pholidophorids and *Seinstedtia parva* is covered with ganoid scales, adding protection to the inner organs (and body weight); in contrast, *Prohalecites* and *Marcopoloichthys* have naked bodies (Tintori 1990; Tintori et al. 2007; Arratia 2022), but differ in that a series of ganoid scales (= urodermals) is present in the caudal fin of *Prohalecites* (Arratia and Tintori 1999), and that *Marcopoloichthys* has a few large scales around the urogenital region (Tintori et al. 2007; Arratia 2022).

## Buccal morphology and feeding in early teleosteomorphs

The jaws of teleosteomorphs or stem teleosts, either upper or lower jaw, are formed consistently by the same

bones: upper jaw comprising a small, mobile premaxilla, a maxilla, and two supramaxillae, which may be absent in some taxa, and a lower jaw formed laterally by a dentary or dentalosplenic, angular, and surangular. Despite such similarities in bone composition, the jaws of these fishes show some major variations that are outlined below, reflecting differences in feeding mechanisms.

The lower jaw (Fig. 14A) of *Prohalecites* (late Ladinian) is moderate in size, with the coronoid process posteriorly placed, the anterior part of the dentary or dentalosplenic markedly narrower than the posterior half of the jaw, and with its articular region for the quadrate at the level of the posterior margin of the large orbit. The lower and upper jaws are armed with many long, conical teeth. Another interesting character is the absence of a supramaxilla in this fish.

The configuration of the jaw (Fig. 14B) of *Marcopoloichthys* (China, Italy, and Switzerland; Anisian to Ladinian; Tintori et al. 2015; Arratia 2022) is quite different from all other Triassic stem teleosts, especially in its articulation of the quadrate at about the mid-region of the orbit when the fish was not feeding, but at the anterior margin of the orbit when the fish was suction feeding (Arratia 2022: fig. 7). The lower jaw has a characteristic shape, with the high coronoid process placed closer to the mandibular symphysis than posteriorly. Both jaws are edentulous, which is a unique feature among Triassic stem teleosts. *Marcopoloichthys* also lacks a supramaxilla, as in *Prohalecites*.

*Seinstedtia* (Germany; Norian; Schultze et al. 2022) has a characteristic lower jaw (Fig. 14C) with a deeper symphysis than in other Triassic stem teleosts and with its articular region for the quadrate placed below the posterior half of the orbit, so that when the fish has its mouth closed, the anterior profile of the head is almost triangular. At least the premaxilla and dentary carry minuscule, conical teeth. Contrary to other stem teleosts, *Seinstedtia* has only one supramaxilla in its upper jaw.

Among pholidophorids, *Annaichthys pontegiuriniensis* (Norian of Italy; Fig. 14D) is unique in having the maxillary blade almost parallel to the anterior border of the head that is mainly formed by the lower jaw and the most anterior branchiostegal rays; the articulation of the lower jaw with the quadrate is placed almost at the level of the anterior margin of the orbit when the mouth is closed. This configuration corresponds to a protractile lower jaw. Although most specimens of *Pholidophorettes* are not very well preserved, the lower jaw of the holotype also has a position similar to that in *Annaichthys*. In *Pholidoctenus sanpellegrinensis* (Arratia 2017: figs 4, 7C; Fig. 14E), the articulation between lower jaw and quadrate is placed below the anterior half of the orbit when the mouth is closed, giving the lower jaw definite protractility. As in *Annaichthys*, the upper jaw of *P. sanpellegrinensis* has two supramaxillary bones, and both jaws have minuscule conical teeth. The condition is slightly different in *Pholidoctenus serianus* with the articulation between the lower jaw and quadrate placed at the level of the posterior margin of the jaw, which is longer and

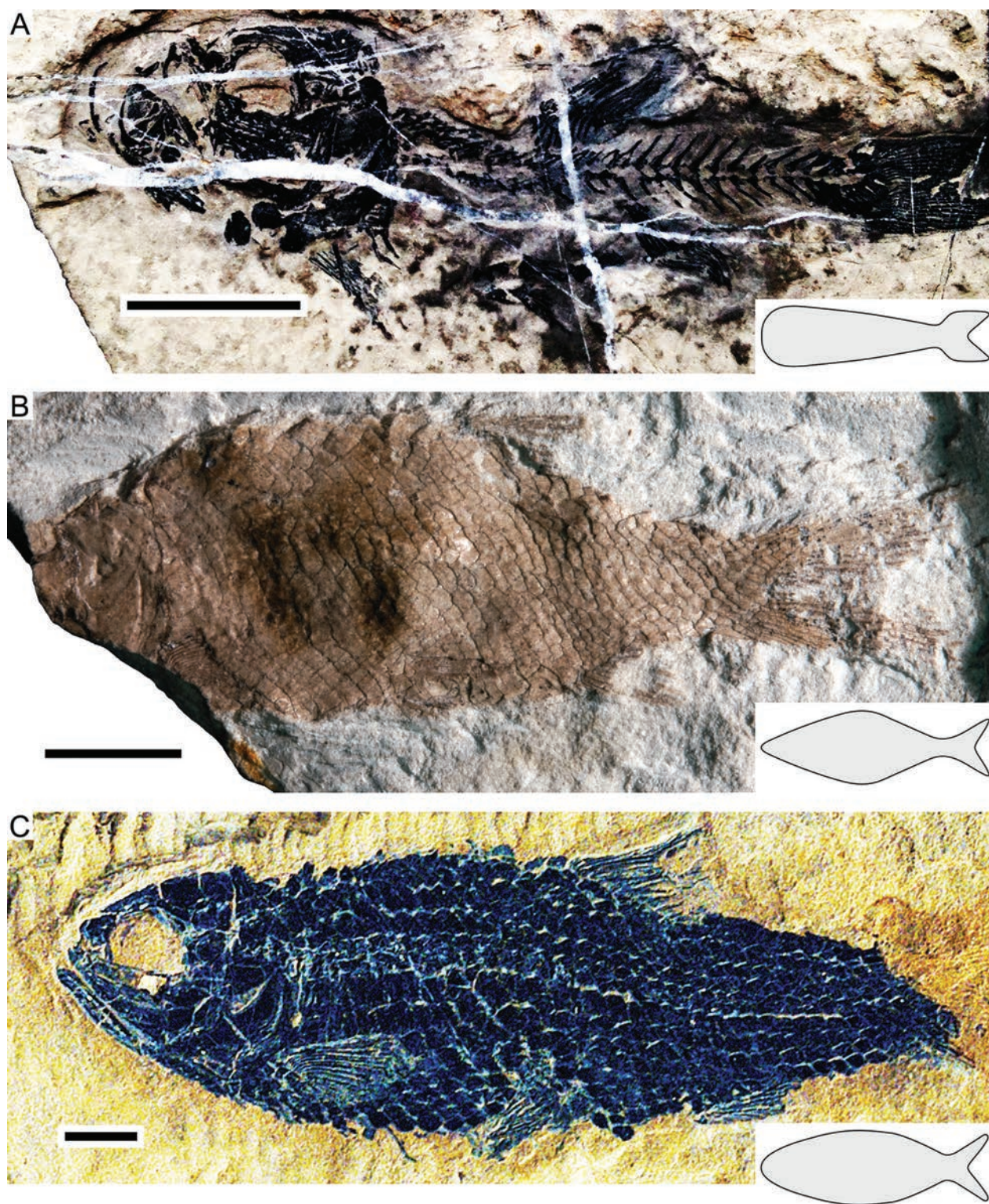


**Figure 13.** Types of body shapes in Triassic teleosteomorphs. **A.** *Marcopoloichthys furreri* (BNM 201166, reversed to the left) illustrating a torpedo-like fish. **B.** *Seinstedtia parva* (MLU Sei.2010.76, reversed to the left) illustrating a fusiform fish. **C.** *Pholidoctenus serianus* (MCSNB 3067) illustrating an oblong fish. Scale bars: 5 mm.

not protractile. In contrast to all other Triassic stem teleosts, *Pholidorhynchodon malzannii* has a long lower jaw, with its articulation with the quadrate lying posterior to the posterior margin of the orbit (Fig. 14F). The long maxilla and long dentary are armed with many small, conical teeth, but in addition, the rostrodermethmoid and lateral

dermethmoid carry powerful, larger conical teeth (Arratia 2013: figs 45, 47A; Arratia 2017: fig. 8). The structure of the jaws and dentition point to carnivorous feeding, a fact that is supported by a few specimens with a small pholidophorid in the mouth. *Pholidorhynchodon*, as far as is known, would be the only carnivorous stem teleost living

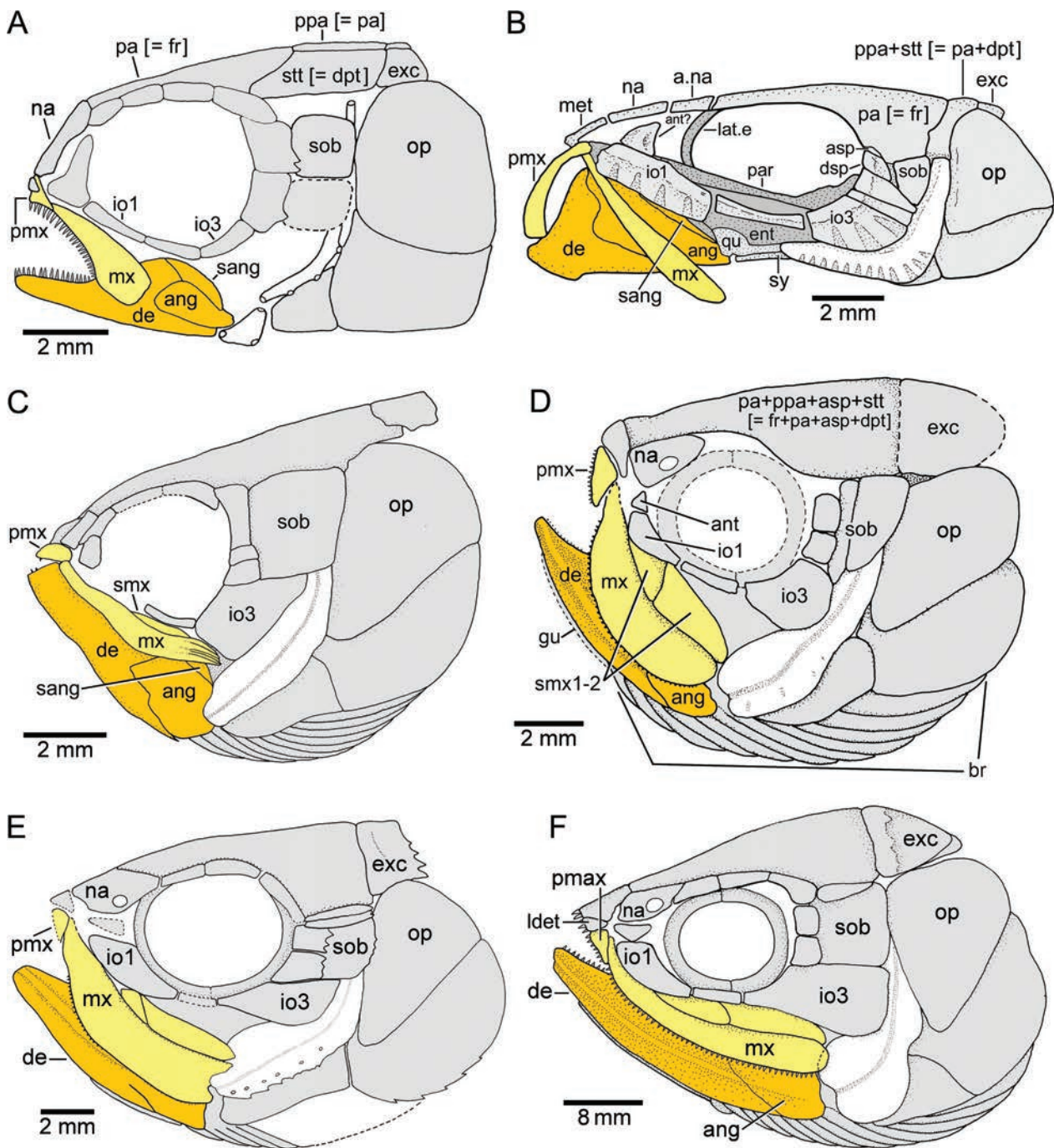


**Figure 14.** Diagram of Triassic teleosteomorph heads in lateral view illustrating the position of the upper and lower jaws with respect to other cranial bones. **A.** *Prohalecites porroi*. **B.** *Marpolochthys furreri*. **C.** *Seinstedtia parva*. **D.** *Annaichthys pontegiuriniensis*. **E.** *Pholidoctenus sanpellegrinensis*. **F.** *Pholidorhynchodon malzannii*. Note the posterior extension of the lower jaw (articulation with quadrate) in relation to the orbit. Abbreviations: a.na, accessory nasal; ang, angular; ant?, antorbital?; asp, autosphenotic; br, branchiostegal rays; de, dentalosplenial or dentary; dsp, dermosphenotic; ent, entopterygoid; exc, extrascapula; gu, gular plate; io1, 3, infraorbitals 1, 3; lat.e, lateral ethmoid; ldet, lateral dermethmoid; mx, maxilla; op, opercle; pa [= fr], parietal [= frontal]; na, nasal; par, parasphenoid; pmx, premaxilla; ppa [= pa], postparietal [= parietal]; qu, quadrate; sang, surangular; smx, supramaxilla; smx1-2, supramaxilla 1–2; sob, suborbital; stt [= dpt], supratemporotabular [= dermopterotic]; sy, symplectic.

in the Late Triassic. The potential food of other species that seem to have protractile mouths is unknown, and considering the structure of the jaws and dentition, we suppose that they were planktivorous, including a variety of small prey; a similar assumption is proposed for the suction-feeding marpolochthyids, who could be also feeding on

phytoplankton. Because of its well-developed dentition, *Prohalecites* is proposed here to have had a carnivorous diet, including small prey. Thus, although there is information concerning the possible feeding mechanisms present in Triassic stem teleosts, except for *Pholidorhynchodon*, specific kinds of prey involved are unknown. Apparently,

a suction-feeding mechanism was widespread among these fishes, including the oldest marcopoloichthyid (*Marcopoloichthys ani*), but a small carnivorous fish (*Prohalecites*) is also among the oldest teleosteomorphs.

### Marine versus freshwater environments and the oldest teleosteomorphs

While marcopoloichthyids and pholidophorids inhabited marine waters in Europe and Asia during the Middle–Late Triassic, *Prohalecites* is only known from marine waters of the Middle Triassic of Italy. The stem teleosts from Italy, Austria and China were inhabitants of the Tethys Ocean, whereas *Pseudopholidoctenus germanicus* gen. et sp. nov. from Rüdersdorf is from the central European Basin (Germanic Basin), and as far as is known, all of these fishes were living in a marine environment. In contrast, the recently described *Seinstedtia* (Schultze et al. 2022) is known from an environment with connection to the sea in the Norian of Germany. The marine aquatic environment (Tethys Ocean) is interpreted here as playing a significant role in the diversification and distribution of stem teleosteomorphs in Eurasia during the Middle–Late Triassic, Europe in the Early Jurassic, and in their dispersion to other latitudes.

The youngest known Triassic teleosteomorph or stem teleost (*Parapholidophorus caffii*) is from the Rhaetian (ca. 208–201 Ma) of Europe, and in the Sinemurian of the Early Jurassic (ca. 199–190 Ma), they are known worldwide, leaving a 2 Ma gap (Hettangian Age) in their history where no teleosteomorphs have been reported, not even other pholidophorids. After this short, apparent gap, there are at least two new radiations of marine stem teleosts in the Sinemurian of Europe represented by:

- 1) *Dorsetichthys bechei* and other ‘pholidophoriforms’, especially from marine environments of the Lower Lias of England and France (Nybelin 1966; Woodward 1985; Arratia 2000, 2004), and
- 2) *Proleptolepis*, with at least four species known from the Lower Lias of England (e.g., Lymes Regis, Dorset, and Charmouth; Nybelin 1974), which, contrary to the Triassic teleosteomorphs, have among their characters a well-developed postero-dorsal process in the quadrate, a well-developed series of uroneurals, and cycloid scales.

Almost simultaneously another radiation of proleptolepids is reported outside Europe, and for this, the Tethys Ocean and its connection with the Paleo-Pacific through the Spanish Corridor (Hallam 1977, 1983) played a major role. The fishes involved are the early to middle Sinemurian proleptolepid-like fishes from northern Chile (Quebrada Vaquillas Altas; Covacevich and Escobar 1979; Naranjo and Covacevich 1979), inhabiting the Paleo-Pacific about 199 to 190 million years ago (Arratia and Schultze 1999). These are represented by at least two

small species of about 50 mm of maximum length, lacking teeth on their jaws (Arratia and Schultze 1999: figs 5, 7, 8) and are assumed here to have been suction feeders.

The Tethys Ocean continued playing a major role during the Upper Lias of Europe with the appearance and diversification of teleosts:

- 1) *Leptolepis* and *Longileptolepis* had about eight species from the Upper Lias of England, France and Germany (Nybelin 1974; Arratia and Thies 2001; Arratia 2003; Konwert and Stumpf 2017), representing another radiation of fishes that are an important landmark in the evolution of teleosts in which many synapomorphies appeared, as for instance the loss of the surangular, prearticular, and coronoid bones in the lower jaw; presence of an autocentrum forming the vertebral centra; 10/9 principal rays in the caudal skeleton; and the first and last segmented and not branched principal ray forming the leading margins of the caudal fin (Arratia 1999, 2013, 2017).
- 2) At the same time (Upper Lias), numerous species previously identified as *Pholidophorus* (Agassiz 1833–1843; Woodward 1895; Nybelin 1966) were present in marine environments of England, France and Germany. All these species should be re-studied, because they belong to the non-monophyletic genus ‘*Pholidophorus*’ sensu Arratia (2000).

It is noteworthy to mention that by the Early to Middle Jurassic (ca. 170–161 Ma), a few stem teleosts reached distant latitudes and occupied other habitats, such *Oreochima ellioti* living in lacustrine freshwater environments from Victoria Land, Antarctica (Schaeffer 1972; Sepkoski 2002; Bean 2021). This fish was first interpreted as an archaeomaenid pholidophoriform by Schaeffer (1972) and more recently archaeomaenids were interpreted as non-pholidophoriform stem teleosts by Bean (2021).

### Age and oldest teleosteomorphs

The interpretation concerning the oldest stem teleost has changed a few times recently due to new findings and/or new interpretation of the fishes. For instance, *Prohalecites porroi* from the Middle Triassic (late Ladinian, ca. 240–237 Ma) of Italy was interpreted as the oldest teleosteomorph by Arratia (2015). However, at the same time two new pholidophorids (*Malingichthys nimaiguensis* and *M. wanfenglinensis*) from the Late Ladinian of China were proposed as the oldest teleosts by Tintori et al. (2015). The new data presented here challenge such interpretations, because the age of *Barschichthys*, *Pseudopholidoctenus* and *Ruedersdorfia* from Rüdersdorf, central European Basin (Germanic Basin) is about 244 Ma, as well as *Marcopoloichthys ani* from Italy, ca. 7 Ma from the Paleozoic/Mesozoic

boundary. A few molecular studies placed the origin of crown teleosts in the Paleozoic (e.g., Near et al. 2012; Broughton et al. 2013; Hughes et al. 2018), many years prior to the earliest fossil record known at that time; however, the new fossil evidence presented here shortens the time difference between the Anisian and Paleozoic (Permian) for the teleostomorphs. Additionally, the results presented above contradict Tintori and other's claim (2015) that China is the center of origin of teleostomorphs. The new information supports Europe in such a role, but we can expect that new discoveries of Triassic fishes in Eurasia may change today's interpretations.

## Acknowledgements

Special thanks to Mr. Enrico Barsch (Berlin) for making specimens of *Barschichthys*, *Pseudopholidoctenus* and *Ruedersdorfia* available for study. To Andrea Tintori (Milan, Italy) for discussion and providing literature on certain Italian geological formations. To Florian Witzmann (Museum für Naturkunde, Berlin, Germany) for assistance with the loan of specimens. Photographs of specimens were kindly taken by John Chorn (Biodiversity Institute, University of Kansas, USA; Figures 2, 3A, 7A, C, 8, 11A, 13B) and by Torsten Schweyer (University of Zurich, Switzerland; Figure 13A). To T. Meehan (Lawrence, Kansas) for revising the English style of the manuscript. Our thanks to one anonymous reviewer and Toni Bürgin (St. Gallen, Switzerland) for reviewing the manuscript.

## References

- Agassiz L (1832) Untersuchungen über die fossilen Fische der Lias-Formation. Jahrbuch für Mineralogie, Geognosie, Geologie und Petrefaktenkunde 3: 139–149.
- Agassiz L (1833–1843) Recherches sur les Poissons fossiles. vol. 2 pt. I: Neuchâtel et Soleure (Petitpierre). <https://doi.org/10.5962/bhl.title.4275>
- Airaghi C (1908) Di un *Pholidophorus* del Retico Lombardo. Rendiconti del Istituto Lombardo, Accademia di Scienze e Lettere, Milano 41: 768–772.
- Arratia G (1999) The monophyly of Teleostei and stem group teleosts. Consensus and disagreements. In: Arratia G, Schultze H-P (Eds) Mesozoic Fishes 2 – Systematics and Fossil Record. Verlag Dr. Friedrich Pfeil, München, 265–334.
- Arratia G (2000) New teleostean fishes from southern Germany and the systematic problems concerning the “pholidophoriforms”. Paläontologische Zeitschrift 74(1/2): 113–143. <https://doi.org/10.1007/BF02987957>
- Arratia G (2001) The sister-group of Teleostei: Consensus and disagreements. Journal of Vertebrate Paleontology 21: 767–773. [https://doi.org/10.1671/0272-4634\(2001\)021\[0767:TSGOTC\]2.0.CO;2](https://doi.org/10.1671/0272-4634(2001)021[0767:TSGOTC]2.0.CO;2)
- Arratia G (2003) *Leptolepis*, *Paraleptolepis* (Teleostei) and a new fish name. Mitteilungen aus dem Museum für Naturkunde in Berlin, Geowissenschaftliche Reihe (= Fossil Record) 6: 157–159. <https://doi.org/10.1002/mmng.20030060108>
- Arratia G (2004) Mesozoic halecostomes and the early radiation of teleosts. In: Arratia G, Tintori A (Eds) Mesozoic Fishes 3 – Systematics, Paleoenvironments and Biodiversity. Verlag Dr. Friedrich Pfeil, München, 279–315.
- Arratia G (2013) Morphology, taxonomy, and phylogeny of Triassic pholidophorid fishes (Actinopterygii, Teleostei). Journal of Vertebrate Paleontology, Memoir 13, 33: 1–138. <https://doi.org/10.1080/02724634.2013.835642>
- Arratia, G (2015) Complexities of early Teleostei and the evolution of particular morphological structures through time. Copeia 103: 999–1025. <https://doi.org/10.1643/CG-14-184>
- Arratia, G (2017) New Triassic teleosts (Actinopterygii, Teleostomorph) from northern Italy and their phylogenetic relationships among the most basal teleosts. Journal of Vertebrate Paleontology 37(6): e131269. <https://doi.org/10.1080/02724634.2017.1312690>
- Arratia G (2022) The outstanding suction-feeder *Marcopoloichthys furreri* n. sp. (Actinopterygii) from the Middle Triassic Tethys Realm of Europe and its implications for early evolution of neopterygian fishes. Fossil Record 25(2): 231–261. <https://doi.org/10.3897/fr.25.85621>
- Arratia G, Herzog AA (2007) A new halecomorph fish from the Middle Triassic of Switzerland and its systematic implications. Journal of Vertebrate Paleontology 27: 838–849. [https://doi.org/10.1671/0272-4634\(2007\)27\[838:ANHFFT\]2.0.CO;2](https://doi.org/10.1671/0272-4634(2007)27[838:ANHFFT]2.0.CO;2)
- Arratia G, Schultze H-P (1999) The Mesozoic fishes from Chile. In: Arratia G, Schultze H-P (Eds) Mesozoic Fishes – Systematics and the Fossil Record. Verlag Dr. Friedrich Pfeil, München, 565–594.
- Arratia G, Thies D (2001) A new teleost (Osteichthyes, Actinopterygii) from the Early Jurassic *Posidonia* shale of Northern Germany. Mitteilungen aus dem Museum für Naturkunde in Berlin, Geowissenschaftliche Reihe (= Fossil Record) 4: 167–187. <https://doi.org/10.5194/fr-4-167-2001>
- Arratia G, Tintori A (1999) The caudal skeleton of the Triassic actinopterygian *Prohalecites* and its phylogenetic relationships. In: Arratia G, Schultze H-P (Eds) Mesozoic Fishes – Systematics and Fossil Record. Verlag Dr. Friedrich Pfeil, München, 121–142.
- Bean L (2021) Revision of the Mesozoic freshwater fish clade Archaeomaenidae. Alcheringa: An Australasian Journal of Palaeontology 45(2): 217–259. <https://doi.org/10.1080/03115518.2021.1937700>
- Brandner R, Posleschinski W (1986) Stratigraphie und Tektonik am Kalkalpen Südrand zwischen Zirl und Seefeld in Tirol (Exkursion D am 3. April 1986). Jahresberichte und Mitteilungen des Oberrheinischen Geologischen Vereins 68: 67–92. <https://doi.org/10.1127/jmoggv/68/1986/67>
- Brandt S (2021) Beschreibung paläozoischer Semionotiden (Holostei) aus dem Oberperm der Dolomiten und Anmerkungen zur Gattung *Acentrophorus* aus dem europäischen Zechstein. In: Wachtler M, Wachtler N (Eds) Permian Fossil Floras and Faunas from the Dolomites Permo-Triassic climate catastrophes as basis for the birth of new life forms. Dolomythos Museum, Innichen, South Tyrol, Italy.
- Broughton RE, Betancur-R R, Li C, Arratia G, Orti G (2013) Multi-locus phylogenetic analysis reveals the pattern and tempo of bony fish evolution. PLoS Currents 5. <https://doi.org/10.1371/currents.tol.2ca8041495ffafd0c92756e75247483e>
- Bürgin T (1992) Basal ray-finned fishes (Osteichthyes; Actinopterygii) from the Middle Triassic of Monte San Giorgio (Canton Tessin, Switzerland). Schweiz Paläontologische Abhandlungen 114: 1–164.

- Covacevich V, Escobar E (1979) Presencia del género *Otapiria* Marwick, 1935 (Mollusca, Bivalvia) en Chile y su distribución en el ámbito circumpacífico. *Actas II Congreso Geológico de Chile* 3: H165–187.
- Gill EL (1923) The Permian fishes of the genus *Acentrophorus*. *Proceedings of the Zoological Society of London* 1923: 19–40. <https://doi.org/10.1111/j.1096-3642.1923.tb02170.x>
- Gortani M (1907) *Pholidophorus faccii* nel Raibliano di Cazzaso in Carnia. *Rivista Italiana de Paleontologia* 13: 117–124.
- Gouiric-Cavalli S, Arratia G (2022) A new †Pachycormiformes (Actinopterygii) from the Upper Jurassic of Gondwana sheds light on the evolutionary history of the group. *Journal of Systematic Palaeontology* 19(21): 1517–1550. <https://doi.org/10.1080/14772019.2022.2049382>
- Griffith J (1977) The Upper Triassic fishes from Polzberg bei Lunz, Austria. *Zoological Journal of the Linnean Society* 60: 1–93. <https://doi.org/10.1111/j.1096-3642.1977.tb00834.x>
- Hallam A (1977) Biogeographic evidence bearing on the creation of Atlantic seaway in the Jurassic. In: West E (Ed) *Palaeontology and Plates Tectonics*. Milwaukee Public Museum, Special Publication Geology 2: 23–34.
- Hallam A (1983) Early and mid-Jurassic molluscan biogeography and the establishment of the central Atlantic seaway. *Palaeogeography, Palaeoclimatology and Palaeoecology* 43: 181–193. [https://doi.org/10.1016/0031-0182\(83\)90010-X](https://doi.org/10.1016/0031-0182(83)90010-X)
- Hanken J (1993) Adaptation of bone growth to miniaturization of body size. In: Hall BK (Ed) *Bone*. Volume 7: Bone Growth-B. CRC Press, Boca Raton, 79–104.
- Hanken J, Wake DB (1993) Miniaturization of body size: organismal consequences and evolutionary significance. *Annual Review of Ecology and Systematics* 24: 501–519. <https://doi.org/10.1146/annurev.es.24.110193.002441>
- Huene Ev (1944) *Cymatosaurus* und seine Beziehungen zu anderen Sauropterygiern. *Neues Jahrbuch für Mineralogie, Geologie und Paläontologie, Monatshefte Abt B* 90: 192–222.
- Hughes LC, Orti G, Huang Y, Sun Y, Baldwin CC, Thompson AW, Arcila D, Betancur-R R, Li C, Becker L, Bellora N, Zhao X, Li X, Wang M, Fang C, Xie B, Zhou Z, Huang H, Chen S, Venkatesh B, Shi Q (2018) Comprehensive phylogeny of ray-finned fishes (Actinopterygii) based on transcriptomic and genomic data. *PNAS* 115: 6249–6254. <https://doi.org/10.1073/pnas.1719358115>
- Kner R (1866) Die fossilen Fische der Asphaltschiefer von Seefeld in Tirol. *Sitzungsberichte der Akademie der Wissenschaften in Wien* 54: 303–334.
- Konwert M, Stumpf S (2017) Exceptionally preserved Leptolepidae (Actinopterygii, Teleostei) from the late Early Jurassic Fossil-Lagerstätten of Grimmen and Dobbartin (Mecklenburg-Western Pomerania, Germany). *Zootaxa* 4243(2): 249–296. <https://doi.org/10.11646/zootaxa.4243.2.2>
- Kottelat M, Britz R, Hui TH, Witte KE (2006) *Paedocypris*, a new genus of Southeast Asian cyprinid fish with a remarkable sexual dimorphism, comprises the world's smallest vertebrate. *Proceedings of the Royal Society B, Biological Sciences* 273: 895–899. <https://doi.org/10.1098/rspb.2005.3419>
- Kramm E, Hagdorn H (2020) Der Muschelkalk im östlichen Brandenburg und in der Lausitz. In: Hagdorn H, Simon T (Ed für die Subkommission PermTrias). *Stratigraphie von Deutschland XIII: Muschelkalk*. Schriftenreihe der Deutschen Gesellschaft für Geowissenschaften. Chapter 9.6: 727–743. Deutsche Geologische Gesellschaft - Geologische Vereinigung.
- Maisch MW, Lehmann J (2002) A new basal omphalosaurid from the Middle Triassic of Germany. *Neues Jahrbuch für Geologie und Paläontologie Monatshefte* 2002: 513–525. <https://doi.org/10.1127/njgpm/2002/2002/513>
- Naranjo JA, Covacevich V (1979) Nuevos antecedentes sobre la geología de la Cordillera de Domeyko en el área de Sierra Vaquillas Altas, Región de Antofagasta. *Actas II Congreso Geológico de Chile* 3: H45–64.
- Near TJ, Eytan RI, Dornburg A, Kuhn KL, Moore JA, Davis MP, Wainwright PC, Friedman M, Smith WL (2010) Resolution of ray-finned fish phylogeny and timing of diversification. *PNAS* 109: 13698–13703. <https://doi.org/10.1073/pnas.1206625109>
- Nybelin O (1966) On certain Triassic and Liassic representatives of the family Pholidophoridae s. str. *Bulletin of the British Museum of Natural History (Geology)* 11: 351–432.
- Nybelin O (1974) A revision of the leptolepid fishes. *Acta Regiae societatis Scientiarum et Litterarum Gothoburgensis, Zoologica* 9, 222 pp.
- Picard EWA (1916) Mitteilungen über den Muschelkalk bei Rüdersdorf. *Jahrbuch der Königlich Preussischen Geologischen Landesanstalt zu Berlin* 35 für 1914: 366–372.
- Raab O (1907) Neue Beobachtungen aus dem Rüdersdorfer Muschelkalk und Diluvium. *Jahrbuch der Königlich Preussischen Geologischen Landesanstalt und Bergakademie zu Berlin* 25, Heft 2 für 1904: 206–217.
- Rieppel O, Wild R (1996) A revision of the genus *Nothosaurus* (Reptilia: Sauropterygia) from the Germanic Triassic, with comments on the status of *Conchiosaurus clavatus*. *Fieldiana Geology New Series* no 34, [IV +] 82 pp. <https://doi.org/10.5962/bhl.title.2691>
- Romano C, Koot M, Kogan I, Brayard A, Minikh AV, Brinkmann W, Bucher H, Kriwet J (2016) Permian-Triassic Osteichthyes (bony fishes): Diversity, dynamics and body size evolution. *Biological Reviews of the Cambridge Philosophical Society* 91(1): 106–147. <https://doi.org/10.1111/brv.12161>
- Schaeffer B (1972) A Jurassic fish from Antarctica. *American Museum Novitates* 2495: 1–17.
- Schröder H (1914) Wirbeltiere der Rüdersdorfer Trias. *Abhandlungen der Königlich Preussischen Geologischen Landesanstalt zu Berlin, Neue Folge* 65: 1–98.
- Schroeder JH [compiler] (2015) *Ruedersdorf Opencast Limestone Mine – A Geo-Highlight near Berlin, Germany*. Selbstverlag Geowissenschaftler in Berlin und Brandenburg e.V. Berlin, Germany, 59 pp.
- Schultze H-P (2008) Nomenclature and homologization of cranial bones in actinopterygians. In: Arratia G, Schultze H-P, Wilson MVH (Eds) *Mesozoic Fishes 4 – Homology and Phylogeny*. Verlag Dr. Friedrich Pfeil, München, 23–48.
- Schultze H-P, Kriwet J (2021) Fische der Germanischen Trias. In: Hauschke N, Franz M, Bachmann GH (Eds) *Trias. Aufbruch in das Erdmittelalter*. Bd. 1. Verlag Dr. Friedrich Pfeil, München, 317–323.
- Schultze H-P, Arratia G, Hauschke N, Wilde V (2022) Osteichthyan fishes from the uppermost Norian (Triassic) of the Fuchsberg near Seinstedt, Lower Saxony (Germany). *Diversity* 2022 14: 901. <https://doi.org/10.3390/d14110901>
- Sepkoski Jr JJ (2002) A compendium of fossil marine animal genera. *Bulletins of American Paleontology* 363: 1–560.

- Shen C-C, Arratia G (2022) Re-description of the sexually dimorphic peltopleuriform fish *Wushaichthys exquisitus* (Middle Triassic, China): taxonomic implications and phylogenetic relationships. *Journal of Systematic Paleontology* 19(19): 1317–1342. <https://doi.org/10.1080/14772019.2022.2029595>
- Sun Z-Y, Jiang D, Ji C, Hao W (2016a) Integrated biochronology for Triassic marine vertebrate faunas of Guizhou Province, South China. *Journal of Asian Earth Sciences* 118: 101–110. <https://doi.org/10.1016/j.jseaes.2016.01.004>
- Sun Z-Y, Tintori A, Lombardo C, Jiang D-Y (2016b) New miniature neopterygians from the Middle Triassic of Yunnan Province, South China. *Neues Jahrbuch für Geologie und Paläontologie, Abhandlungen* 282: 135–156. <https://doi.org/10.1127/njgpa/2016/0610>
- Teng CS, Cavin L, Maxon Jr RE, Sánchez-Villagra MS, Crump JG (2019) Resolving homology in the face of shifting germ layer origins: Lessons from a major skull vault boundary. *eLife* 8: e52814. <https://doi.org/10.7554/eLife.52814>
- Tintori A (1990) The actinopterygian fish *Prohalecites* from the Triassic of Northern Italy. *Palaeontology* 33: 155–174.
- Tintori A, Sun Z-Y, Lombardo C, Jiang D-Y, Sun Y-L, Rusconi M, Hao W-C (2007) New specialized basal neopterygians (Actinopterygii) from Triassic of the Tethys realm. *Geologia Insubrica* 10/2: 13–19.
- Tintori A, Sun Z-Y, Ni P-G, Lombardo C, Jiang D-Y, Ryosuke M-T (2015) Oldest stem Teleostei from the late Ladinian (Middle Triassic) of southern China. *Rivista Italiana di Paleontologia e Stratigrafia* 121(3): 285–296.
- Weitzmann SH, Vari RP (1988) Miniaturization in South American freshwater fishes; and overview and discussion. *Proceedings of the Biological Society of Washington* 101(20): 444–465.
- Woodward AS (1890) The fossil fishes of the Hawkesbury series of Gosford. *Memoirs of the geological survey of New South Wales. Palaeontology* 4: 1–55.
- Woodward AS (1895) *Catalogue of the fossil fishes in the British Museum (Natural History)* 3: xlii + 544 pp. plus 18 pls. British Museum of Natural History, London. <https://doi.org/10.5962/bhl.title.162378>
- Xu G-H, Zhao L-J, Shen C-C (2015) A Middle Triassic Thoracopecterid from China highlights the evolutionary origin of overwater gliding in early-ray finned fishes. *Biology Letters* 11: 183–191. <https://doi.org/10.1098/rsbl.2014.0960>
- Xu G-H, Ma X-Y (2023) A new basal ginglymodian fish (Holostei: Neopterygii) from the Middle Triassic (Anisian) Luoping Biota, Yunnan, China. *Zoological Journal of the Linnean Society* 2023: zlad144. [XX, 1–14] <https://doi.org/10.1093/zoolinnean/zlad144>
- Zambelli R (1975) Note sui Pholidophoriformes. I. *Parapholidophorus nybelini* gen. n. sp. n. *Rendiconti Istituto Lombardo. Accademia di Scienze e Lettere* 109: 3–49.
- Zambelli R (1977) Note sui Pholidophoriformes. II. *Pholidoctenus serianus* gen. n. sp. n. *Rendiconti della Accademia Nazionale dei Lincei*, part 5(3): 101–123.
- Zambelli R (1980a) Note sui Pholidophoriformes. III contributo: *Pholidophorus gervasuttii* sp. n. *Revista del Museo Civico di Scienze Naturali “E. Caffi,” Bergamo* 1: 5–44.
- Zambelli R (1980b) Note sui Pholidophoriformes. IV contributo: *Pholidorhynchodon malzannia* gen. n. sp. n. *Revista del Museo Civico di Scienze Naturali “E. Caffi,” Bergamo* 2: 129–168.
- Zambelli R (1980c) Note sui Pholidophoriformes. V contributo: Pholidophoridae dell’Alta Valvestine (Brescia, Italia). “*Natura Bresciana*”, *Annali del Museo Civico di Storia Naturale, Brescia* 17: 77–88.
- Zambelli R (1990) Note sui Pholidophoriformes. VII contributo. *Eopholidophorus forojuliensis* n. g., n. sp. *Gortiana. Atti del Museo Friulano di Storia Naturale* 11: 63–76.
- Zimkus BM, Lawson L, Loader SP, Hanken J (2012) Terrestrialization, miniaturization and rates of diversification in African puddle frogs (Anura: Phrynobatrachidae). *PLOS ONE* 7(4): e35118. <https://doi.org/10.1371/journal.pone.0035118>



# The new problem of *Chinlestegophis* and the origin of caecilians (Amphibia, Gymnophionomorpha) is highly sensitive to old problems of sampling and character construction

David Marjanović<sup>1</sup>, Hillary C. Maddin<sup>2</sup>, Jennifer C. Olori<sup>3</sup>, Michel Laurin<sup>4</sup>

<sup>1</sup> *Evolutionary Morphology, Dynamics of Nature, Museum für Naturkunde Berlin—Leibniz Institute for Evolution and Biodiversity Science, Invalidenstraße 43, 10115 Berlin, Germany*

<sup>2</sup> *Earth Sciences, Carleton University, 1125 Colonel By Drive, Ottawa, K1S 5B6, ON, Canada*

<sup>3</sup> *Biological Sciences, State University of New York at Oswego, 30 Centennial Dr., 13126 Oswego, NY, USA*

<sup>4</sup> *CR2P (Centre de Recherches en Paléontologie – Paris), CNRS/MNHN/Sorbonne Université, Muséum National d’Histoire Naturelle, 75231 Paris cedex 05, Paris, France*

<https://zoobank.org/B5FBF663-BC46-439A-8DE3-BDE33D91D962>

Corresponding author: David Marjanović ([david.marjanovic@gmx.at](mailto:david.marjanovic@gmx.at))

Academic editor: Florian Witzmann ♦ Received 14 July 2023 ♦ Accepted 2 December 2023 ♦ Published 10 January 2024

## Abstract

The description of the small Late Triassic temnospondyl *Chinlestegophis* ushered in a potentially radically new understanding of the origins of the extant amphibian clades. Together with the fragmentary *Rileymillerus*, *Chinlestegophis* was argued to link extant caecilians to Permo-Triassic stereospondyl temnospondyls rather than to frogs and salamanders (and through them to amphibamiform temnospondyls or to brachystelechid and lysorophian “lepospondyls”). We critically review the comparative description of *Chinlestegophis* and phylogenetic analyses of previous studies. Most of the features previously interpreted to be shared by caecilians, *Chinlestegophis* and/or other stereospondyls have different distributions than scored in the analysis. We also find no evidence for an incipient tentacular sulcus in *Chinlestegophis*, and note that its vertebrae, unreduced ribs and dermal shoulder girdle are unlike those of any extant amphibians (nor their likely sister group, Albanerpetidae). Furthermore, the original matrices contain misscores accrued over more than a decade that likewise influence the results. Some features are coded as multiple redundant characters: the double tooththrow of *Chinlestegophis*, other stereospondyls, and caecilians is represented as seven characters. Analysis of the unmodified matrix yields much less resolution than originally reported, and tree topology is altered by a small change to the taxon sample (the addition of Albanerpetidae), limited revisions of irreproducible scores, and ordering the most obviously clinal characters; any one of these changes removes *Chinlestegophis* from Lissamphibia, and confirms it as a stereospondyl.

## Key Words

Amphibia, *Chinlestegophis*, *Funcusvermis*, Gymnophiona, Gymnophionomorpha, Lissamphibia, majority-rule consensus, phylogenetics, phylogeny

## Introduction

Caecilians have a scanty fossil record (Santos et al. 2020; Kligman et al. 2023); the earliest well-supported stem members are *Funcusvermis gilmorei* Kligman et al., 2023 (Late Triassic), and *Eocaecilia micropodia* Jenkins & Walsh, 1993 (Jenkins and Walsh 1993; Early Jurassic).

*Eocaecilia* retains limbs and some cranial bones that are absent in the caecilian crown group (Gymnophiona; see Wake 2020); partial femora were also assigned to *Funcusvermis* and the Early Cretaceous or, more likely, Late Jurassic (Lasseron et al. 2019) *Rubricacaecilia monbaroni* Evans & Sigogneau-Russell, 2001 (Evans and Sigogneau-Russell 2001; Kligman et al. 2023).

Since *Eocaecilia* was named, a more thorough anatomical study (Jenkins et al. 2007) and many phylogenetic analyses confirmed its position along the caecilian stem (Laurin 1998; Vallin and Laurin 2004; Maddin et al. 2012a; Pardo et al. 2017a: fig. S6). However, despite the absence of serious doubts about the status of *Eocaecilia* in the literature (Evans and Sigogneau-Russell 2001; Carroll 2007: 54; Sigurdson and Bolt 2010: 1373; further corroborated by Kligman et al. 2023), Pardo et al. (2017a: abstract) stated: “The position of *Eocaecilia* within tetrapod phylogeny is controversial, as it already acquired the specialized morphology that characterizes modern caecilians by the Jurassic.” That statement is misleading: all phylogenetic analyses that included *Eocaecilia* support its placement as a stem-caecilian; it is the position of caecilians as a group in the context of its ancestry among extinct tetrapods that remained controversial.

To this controversy, Pardo et al. (2017a) added *Chinlestegophis jenkinsi*, which they named and described as a stem-caecilian from the Late Triassic (slightly younger than *Funcusvermis*: Kligman et al. 2023). Their phylogenetic analyses surprisingly appeared to anchor the caecilians (through *Chinlestegophis*) within the stereospondyl temnospondyls, whereas frogs and salamanders (i.e., batrachians) remained in a more common placement as dissorophoid temnospondyls, producing a new and confidently delivered hypothesis of lissamphibian origins. The captivating notion of the problem of amphibian origins and the evolution of specialized caecilian traits having been “solved” with the discovery of *Chinlestegophis* has already permeated popular zoology textbooks (Pough et al. 2022: figs. 9.2 and 9.5).

Although we agree that *Chinlestegophis* presents an interesting mix of characters, we wish to respond to claims Pardo et al. (2017a) made about *Chinlestegophis* that were incompletely tested in that and subsequent studies (Schoch et al. 2020; Serra Silva and Wilkinson 2021; Gee 2022; Kligman et al. 2023). We find in Pardo et al. (2017a), and review and evaluate below: 1) problems with the matrices used, including narrow taxon sampling, errors and oversights in character construction and modification, and incorrect scores within the original data sets underpinning the resulting matrices; 2) a suboptimal methodology, including reliance on a majority-rule consensus tree and incomplete reporting of tree statistics; and 3) qualitative problems with the diagnostic features linking *Chinlestegophis* (and in some cases *Rileymillerus* Bolt & Chatterjee, 2000) to caecilians. Our reanalyses show that *Chinlestegophis* in particular and stereospondyls in general currently cannot be supported as stem-caecilians and should not be treated as such in textbooks or in secondary analyses, such as molecular estimates of divergence times (as previously stated by Santos et al. 2020 and Kligman et al. 2023).

## Scope

Recent works have investigated selected aspects of the work of Pardo et al. (2017a). Marjanović and Laurin (2018) and Serra Silva and Wilkinson (2021) reanalyzed one of the two matrices, finding that the published majority-rule consensus tree was a highly incomplete presentation of the results. Kligman et al. (2023: supplementary information parts 3–4) reevaluated a large number of scores of that matrix, enlarged the taxon sample and discussed the character states that Pardo et al. (2017a) had used to tie caecilians to *Chinlestegophis* and other stereospondyls, focusing on their distribution in stereospondyls. We focus on their distribution in lissamphibians and so-called lepospondyls, experiment with (and discuss) ordering characters, adding taxa and reevaluating a different set of scores, and first of all we reanalyze the other matrix for the first time, both without and with a topological constraint.

## Nomenclature and terminology

Our usage of the clade names Gymnophiona, Amphibia and Lissamphibia follows Wake (2020) and Laurin et al. (2020a, b); temnospondyl nomenclature follows Schoch (2013, 2018), except for the names Temnospondyli, Euskelia and Limnarchia (Yates and Warren 2000). Whenever practicable, we applied the same set of names to all figures. Junior synonyms are shown in parentheses, and names that cannot be applied to a particular tree (because of qualifying clauses or definitions that restrict their applicability to certain phylogenetic contexts) are not shown on that tree. Schoch (2013) gave identical definitions for Stereospondyli and Stereospondylomorpha; it is obvious that that is an accident and that the intended definition for Stereospondyli can be recovered by replacing “most” by “least”. Misspellings of genus and species names in the matrices and figures of Pardo et al. (2017a) are corrected. See Marjanović and Laurin (2019: 13) for the correction of “Albanerpetontidae” to Albanerpetidae.

We use “caecilians” for crown-group caecilians (Gymnophiona: Wake 2020) and their uncontroversial relatives like *Eocaecilia* and *Funcusvermis*. The names Lepospondyli and Microsauria are used here informally for traditional groupings of taxa; the likely para- or polyphyly of these groupings (supported and reviewed by Marjanović and Laurin 2019) is beyond the scope of this work. For simplicity we present these names without quotation marks throughout.

We use “coding” for the process of choosing and defining the characters and their states, and “scoring” for filling in the matrix. Observed morphology is “miscoded” if, for example, it is represented as two redundant characters in the character sample, but “misscored” if the scores (numbers, state symbols) in the matrix are not what they should be according to the existing state definitions.

## Abbreviations

<b>AMNH FARB</b>	Collection of Fossil Amphibians, Reptiles and Birds at the American Museum of Natural History (New York).
<b>app.</b>	appendix (of cited works).
<b>CI</b>	consistency index.
<b>MPT</b>	most parsimonious tree.
<b>MRC</b>	majority-rule consensus.
<b>OTU</b>	operational taxonomic unit (a line in a data matrix).
<b>RC</b>	rescaled consistency index.
<b>RI</b>	retention index.
<b>supp. inf.</b>	supplementary information (of cited works).

## Matrices, methodologies, and missteps

### Matrix history and taxon sampling

Pardo et al. (2017a) analyzed two matrices: a taxonomically broader, unpublished dataset, and an expanded, published matrix focused on the position of *Chinlestegophis* and *Rileymillerus* within temnospondyls. The originally unpublished matrix (see Suppl. material 1 for a NEXUS file), which generated the trees shown in Pardo et al. (2017a: fig. S6), contains 319 characters (27 of them parsimony-uninformative, including five constant ones) and 71 OTUs; it is based on the matrix of Maddin et al. (2012a), with additions of characters and taxa from Huttenlocker et al. (2013) and several new ones. Those earlier matrices are based on that of Anderson et al. (2008a), but subsequently proposed corrections to that matrix (Marjanović and Laurin 2009; Skutschas and Martin 2011; Sigurdson and Green 2011) were neither included in the resulting composite matrix nor addressed in the text by Pardo et al. (2017a) or any of the references therein. Those changes have considerable influence on the resulting tree topology, as exemplified in Fig. 1.

The published matrix (Pardo et al. 2017a: supporting information part D), which generated the trees shown in Pardo et al. (2017a: fig. 2, 3, S7), has 345 characters (23 parsimony-uninformative) and 76 OTUs. It is built on the unpublished matrix by the deletion of most non-temnospondyl taxa and the addition of characters and taxa taken primarily from Schoch (2013)—see Gee (2022) for a thorough discussion of that lineage of matrices.

It is, of course, common practice to modify and expand existing data sets, and underlying errors are frequently perpetuated into later generations of matrices when first-hand reassessment of specimens is infeasible, detailed comparison to the literature is deemed too time-consuming, or the full history of characters becomes obscured over time, leading to different meanings of the same character for different taxa that were added or revised at different times (Marjanović and Laurin 2019;

Gee 2021, 2022). In those cases, conservative practice is to accept preexisting descriptions and scores as reliable. However, over many iterations of matrices, substantial errors can and do accumulate—this is a known and pervasive problem with large data matrices that are recycled in consecutive studies (Simões et al. 2017; Laurin and Piñeiro 2018; Marjanović and Laurin 2019; Gee 2021, 2022; Kligman et al. 2023: supp. inf. part 4; and see our Discussion section).

The merging of existing matrices can also generate additional problems related to redundant characters and states. As an example, multiple characters related to the lower jaw in the published matrix of Pardo et al. (2017a) carry redundancy (in particular characters 147, 148, 146, 272, 273, 322, 344; see full evaluation below), and because each is strongly associated with specialized morphologies mainly observed in caecilians, they may, even when correctly scored, generate bias by inflating support for the purported relationship between *Chinlestegophis* and caecilians. Moreover, as characters are merged, moved, modified, and added, it becomes increasingly easy to overlook simple mechanical errors, such as state 26(2) being mentioned neither in the list of state labels within the matrix file nor in the character list despite all three states being scored for numerous taxa in the matrix (Pardo et al. 2017a: SI appendix parts C, D).

Robust analyses also may be thwarted by constraints related to the original taxon sampling of the underlying matrices; in other words, matrices compiled by other authors were (implicitly or explicitly) constructed with the intent to apply them to specific problems, and thus any clade may be densely or sparsely sampled depending on the question that was originally addressed, rather than on questions of later interest. Inserting new taxa may be difficult if additional variation is not easily accommodated without major character revisions, and this may limit which taxa can be speedily added. The matrix of Anderson et al. (2008a) is slightly modified from that of Anderson (2007), which is a merger of a matrix that sampled lepospondyls (Anderson 2001) and a matrix that sampled amphibamiform temnospondyls (Anderson et al. 2008b). As a result, all descendants of the matrix of Anderson et al. (2008a), including the unpublished matrix of Pardo et al. (2017a), sample lepospondyls, amphibamiforms, and very little in between; in the case of Pardo et al. (2017a: fig. S6), other than the amphibamiforms and the added taxa *Chinlestegophis* and *Rileymillerus*, taxa include only seven other temnospondyl OTUs (some composite), the colosteid *Greererpeton*, lepospondyls, the diadectomorph pan-amniote *Limnoscelis*, the seymouriamorph *Seymouria* and the anthracosaur *Proterogyrinus*. The taxon sample is completed by the designated outgroup *Acanthostega*, the earliest well-understood limbed vertebrate.

The more narrowly focused published matrix of Pardo et al. (2017a) omits almost all taxa not sampled by Schoch (2013), retaining only temnospondyls,

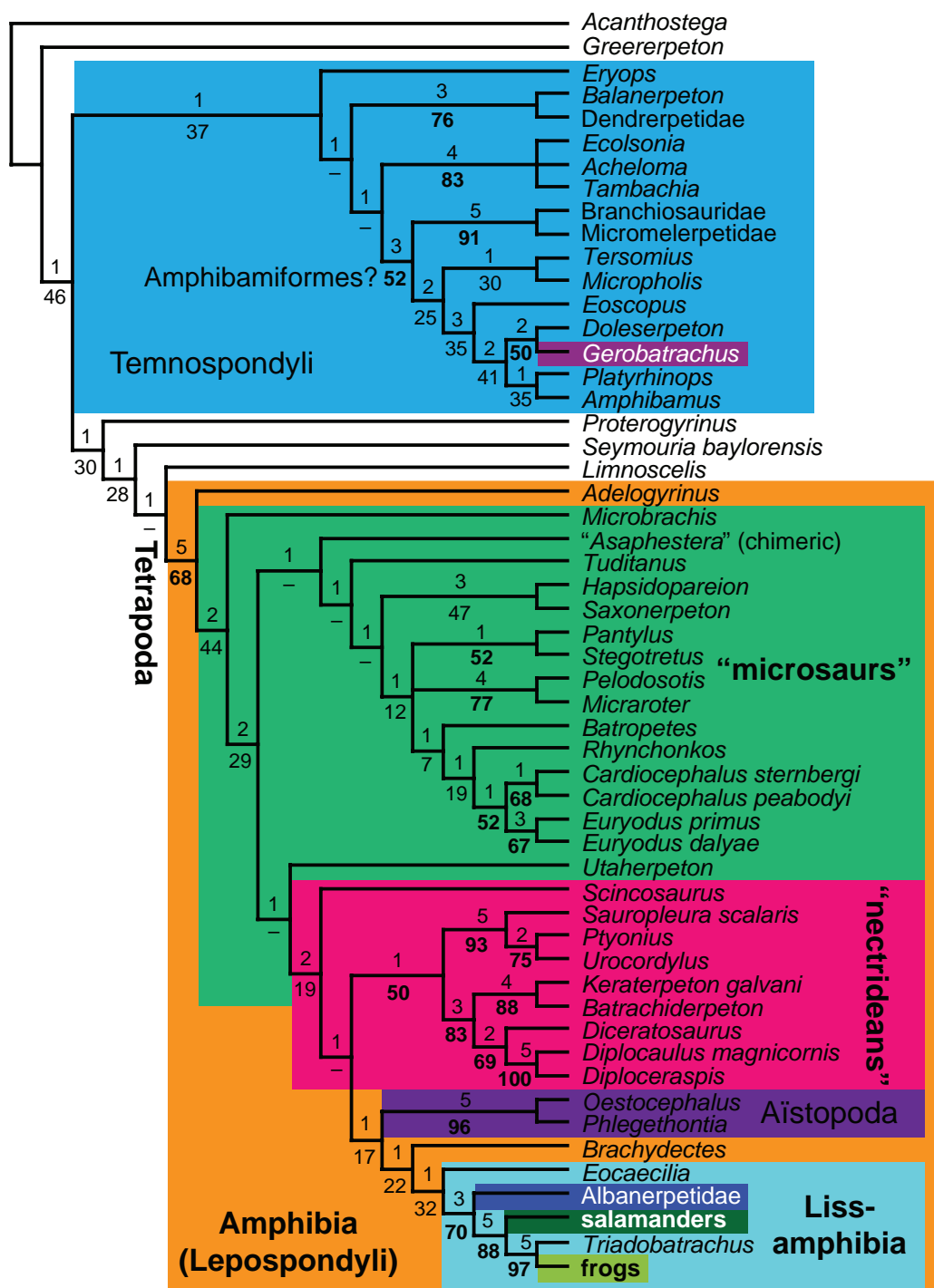


**Figure 1.** Strict consensus of the four MPTs obtained by Marjanović & Laurin (2009: electronic supplementary material 2) from their modified version of the matrix of Anderson et al. (2008a) with ordering of clinal characters. Note that contrary to Anderson et al. (2008a), who had found extant amphibians to be diphylectic, with the stem-caecilian *Eocaecilia* among lepospondyls but *Albanerpetidae*, “salamanders”, *Triadobatrachus* and “frogs” among temnospondyls, Lissamphibia is found as a clade (cyan rectangle) and placed among lepospondyls (orange rectangle). The temnospondyl *Gerobatrachus*, interpreted as a member of the batrachian stem by Anderson et al. (2008a), i.e., closest to frogs and salamanders, is marked with a purple rectangle and white font. The names of extant taxa are in boldface; “frogs” and “salamanders” are composites. The application of the name *Amphibamiformes* is unclear due to the absence of *Dissorophus*. Numbers below internodes are bootstrap percentages (in bold if 50 or higher; “–” indicates clades contradicted by the bootstrap tree, always by clades with bootstrap percentages of 40 or less), numbers above internodes are Bremer values. Some or all of the Bremer values shown as “≥ 5” are probably 5 (Marjanović and Laurin 2009). Note that “*Asaphestera*” as used here is a chimera of the amniote *Asaphestera*, the microsaure *Steenerpeton* Mann et al., 2020, and an indeterminate lower jaw; most of the material belongs to *Steenerpeton*, however (Mann et al. 2020). The *Dendrerpetidae* OTU was originally called “*Dendrerpeton*” but is mostly based on its apparently close relative *Dendrysekos*.

lissamphibians, and the same two outgroups as Schoch (2013), *Proterogyrinus* and *Greererpeton*. The stated reason for this drastic omission of taxa, which eliminated all lepospondyls, *Seymouria* and *Limnoscelis*, was to reduce calculation time for the Bayesian analysis (Pardo et al. 2017a: E5394), after analysis of the unpublished matrix suggested that *Chinlestegophis* and lissamphibians nested within Temnospondyli.

In short, Pardo et al. (2017a) first tested the phylogenetic position of *Chinlestegophis* and the similar *Rileymillerus* (Bolt and Chatterjee 2000) “coarsely” by adding them to a matrix that sampled lepospondyls, amphibamiforms, a few other extinct taxa, and lissamphibians. *Chinlestegophis* and *Rileymillerus* were found as temnospondyls close to, but outside, Amphibamiformes (Pardo et al. 2017a: fig. S6). Accepting the result that *Chinlestegophis*, *Rileymillerus* and lissamphibians were temnospondyls, Pardo et al. (2017a) zoomed in by adding them to a matrix that sampled temnospondyls (and temnospondyl-related characters) more broadly, but omitted most other extinct clades. The question of whether caecilians are lepospondyls or stereospondyl temnospondyls was never adequately tested; the unpublished matrix lacks stereospondyls and uses unrevised scores for lepospondyls that were previously criticized (Marjanović and Laurin 2009; Sigurdson and Green 2011; Skutschas and Martin 2011), whereas the published one lacks lepospondyls altogether.

The published matrix further lacks representation of Albanerpetidae (a member or the sister group of Lissamphibia), despite their presence in the unpublished matrix. Daza et al. (2020) added Albanerpetidae (as a composite taxon with new data) back into the published matrix of Pardo et al. (2017a) and analyzed the result with implied weighting. They found caecilians and batrachians as sister taxa, followed by Karauridae as the next more distant relative, then Albanerpetidae, then the branchiosaurid *Apateon* and then the rest of Amphibamiformes. *Chinlestegophis* and *Rileymillerus* instead formed the sister-group of Brachyopoidea within Stereospondyli (Daza et al. 2020: fig. 4E, S14). Clearly, omitting Albanerpetidae had a large effect on the resulting relationships among extinct taxa and extant amphibians.

## Phylogeny inferred from parsimony

The original parsimony analysis of the published matrix yielded 882 shortest trees (Pardo et al. 2017a; and see below). As often occurs, the strict consensus was poorly resolved. To remedy this, Pardo et al. (2017a: fig. S7B) produced a majority-rule consensus (MRC) tree and used it as the basis for comparison with the tree resulting from a Bayesian analysis of the same matrix (their fig. 2C = S7A). Both the MRC and Bayesian trees show batrachians as amphibamiforms, but caecilians as stereospondyls closest to *Chinlestegophis*, and *Rileymillerus* as sister to caecilians + *Chinlestegophis*. However, none of

the 28 nodes that separate caecilians from batrachians + karaurids have 50% or higher bootstrap support, and none (even the basal caecilian node) occurs in 100% of the shortest trees (Pardo et al. 2017a: fig. S7B). We stress that the percentage of MPTs in which a given node occurs, as long as it is not 0 or 100, is not a support measure in a parsimony analysis (e.g., Serra Silva and Wilkinson 2021; Kligman et al. 2023: supp. inf. part 3); all MPTs are equally parsimonious, and therefore equally optimal by the sole criterion the analysis used. Therefore, the MRC tree provides an incomplete picture of the results of any parsimony analysis, even if there is only a single island of MPTs (see below). Indeed, a fully resolved MRC is not even necessarily identical to any MPT (J. Felsenstein, pers. comm. to D. M. 2017).

Investigating that problem specifically, Serra Silva and Wilkinson (2021) reevaluated the full diversity of MPTs supported by the published matrix of Pardo et al. (2017a), noting in their introductory paragraph that “[d]espite concerns that summarizing MPTs with the majority-rule consensus is potentially misleading [...], some workers still use the majority-rule method as if it were unproblematic (e.g. [...] Pardo et al. 2017[a]).” After briefly describing the reanalysis by Marjanović and Laurin (2018: 57–58; 2019: 144, fig. 30I–K), they demonstrated why the MRC is misleading in the specific case of Pardo et al. (2017a), and why it is important to inspect individual trees when the strict consensus is unsatisfactorily resolved: the 882 trees form islands which are each highly congruent internally, but very different from each other. More than half of the MPTs belong to a single island; therefore, the overall MRC (Pardo et al. 2017a: fig. S7B) is almost entirely identical (Serra Silva and Wilkinson 2021: fig. 2) to the MRC of that one island and fails to represent the MPTs on the other equally parsimonious islands.

Of the other islands, one (figured by Marjanović and Laurin 2019: fig. 30I; Serra Silva and Wilkinson 2021: fig. 3c) agrees with the most popular hypothesis of lissamphibian origins, which is also supported by the previously unpublished matrix of Pardo et al. (2017a: fig. S6): that Lissamphibia (including *Eocaecilia* but excluding *Chinlestegophis* and *Rileymillerus*) nests inside Amphibamiformes, close to *Gerobatrachus* (Atkins et al. 2019; Daza et al. 2020: fig. 4D/S13; Schoch et al. 2020; Kligman et al. 2023). It further differs from the largest island in that the karaurids occupy their usual position as stem-salamanders (corroborated by Jones et al. 2022), not the entirely novel one on the batrachian stem found on the largest island. Moreover, on the stereospondyl side of the tree, *Chinlestegophis* and *Rileymillerus* form the sister-group of Brachyopoidea, rather than being nested in it as on the largest island.

Another island (Marjanović and Laurin 2019: fig. 30K; Serra Silva and Wilkinson 2021: fig. 3b) shows Lissamphibia as the sister-group of *Chinlestegophis* + *Rileymillerus*, together nested within Stereospondyli next to Brachyopoidea. Yet another island (Marjanović and Laurin 2019: fig. 30I; Serra Silva and Wilkinson 2021:

fig. 3a) positions Lissamphibia next to *Gerobatrachus* within Amphibamiformes, and *Chinlestegophis* is nested within the caecilians as the sister-group of *Eocaecilia*, while *Rileymillerus* is placed among the stereospondyls as the sister-group of Brachyopoidea.

In other words, parsimony analysis of the published matrix of Pardo et al. (2017a) supports positions within Amphibamiformes or Stereospondyli equally strongly for *Chinlestegophis*, the undoubted caecilians, and Batrachia (including Karauridae).

## Bayesian inference of phylogeny

With the result of the parsimony analysis of the published matrix wholly inconclusive, an argument can still be made that the topology shown in fig. S7B of Pardo et al. (2017a) should be preferred over the equally parsimonious alternatives because it is congruent with the result of the Bayesian analysis of the same matrix, which is the only result figured in the main paper (Pardo et al. 2017a: figs 2B, C, 3, S7A). However, Bayesian inference as a method of phylogenetic analysis of paleontological matrices has its own sources of error.

The supposed problem of common branch lengths for all characters in previous simulations, pointed out by Goloboff et al. (2017, 2018) and given great weight by Marjanović and Laurin (2019: 98), seems not to be one of them; it was accounted for by the two latest treatments of the question of how best to analyze morphological data (Puttick et al. 2018; Keating et al. 2020) and found to be irrelevant. Yet, those two studies did not simulate any missing data, and the misuse of the MRC to represent the results of parsimony analyses by Puttick et al. (2018) will overestimate the precision but underestimate the accuracy of parsimony, as Keating et al. (2020: fig. 5) demonstrated. Furthermore, the homoplasy distributions in the matrices simulated by Puttick et al. (2018), and probably Keating et al. (2020) as well, do not encompass cases like the matrix of Marjanović and Laurin (2019) at the very least, and evidently not the matrix of Pardo et al. (2017a) either—given the multiple starkly different topologies that it supports as equally parsimonious.

Even more importantly, as paleontological matrices generally do (contrary to the implication by King [2020]), the matrix of Pardo et al. (2017a) contains multiple conflicting signals as well as large amounts of missing data. That combination is known to present a major problem for parametric methods in phylogenetics, including Bayesian inference, whereas parsimony (a non-parametric method) is immune to that particular issue (Simmons 2014; King 2019). Specifically, when character conflict is present (and at least one terminal branch has a positive length), parametric methods give much greater weight to the signal present in characters that are sampled for all taxa than to the signal present in incompletely sampled characters, even if very little information is missing (Simmons 2014; King 2019). Given that there is no reason to assume a correlation

between homoplasy and preservation, we regard this as a flaw of parametric methods for paleontological applications.

We also would like to draw attention to figure 1 of Mongiardino Koch et al. (2021), in which the proportion of quartets in a simulation study that are accurately resolved by undated Bayesian inference (as used by Pardo et al. 2017a) increases when the amount of missing data also increases, or in other words decreases when accurate data are added. Although this startling result is not statistically significant, it seems that undated Bayesian inference was, in that case, right for the wrong reasons, and is likely to be wrong for the same reasons in other circumstances.

Further, by default, parsimony is somewhat less vulnerable than parametric methods to the long-known problem of heterotachy (Crotty et al. 2019, and references therein). That problem was solved, but currently the solution is implemented in only one program, which only performs maximum-likelihood analysis and cannot deal with most features of morphological data (Crotty et al. 2019); a solution remains unavailable for Bayesian inference. On the empirical side, Palci et al. (2019) recovered a plausible topology of total-group snakes when they analyzed their dataset with parsimony, but a highly implausible one, requiring ecologically unmotivated reversals, by Bayesian inference. Thus, we strongly emphasize the conclusion of Marjanović and Laurin (2019: 96–99) that the accuracy of the matrix is much more important than the method of analysis, because no method can compensate for misscoring or miscoding of morphological data, a major issue we document for the matrix published and relied upon by Pardo et al. (2017a).

## Materials and methods

As noted above, Pardo et al. (2017a) performed analyses of two matrices (one published, one unpublished) with similar character samples but different taxon samples. The originally unpublished matrix was kindly shared with us by J. Pardo and A. Huttenlocker, and we publish it here: Suppl. material 1 contains the unaltered matrix in a NEXUS file, with an added PAUP command block that replicates our analyses of it (called a1 and a2 below) when the file is executed in PAUP\*. All of our analyses (Table 1) were run in PAUP\* 4.0a169 (Swofford 2021) for Windows. This includes bootstrap analyses to test the results of selected phylogenetic analyses for robustness; we have relied not only on the bootstrap trees, which we present as figures, but also on the lists of bipartitions in the PAUP\* output (Suppl. material 2: tables S1–S4). The published matrix was modified in Mesquite versions up to 3.70 (Maddison and Maddison 2021). The Kishino/Hasegawa, Templeton and winning-sites tests were employed to assess whether constrained and unconstrained trees resulting from the previously unpublished matrix are significantly different; all three tests are available in PAUP\*.

**Table 1.** Overview of analyses and results presented here.

Analysis	Our figure	Base matrix of Pardo et al. (2017a)	Modifications from Pardo et al. (2017a)	Ordering of clinal characters	inf. char.	Length of MPTs	Topology
–	1	–	n/a	yes	212	1264	Marjanović & Laurin (2009: supplementary figure), matrix modified from Anderson et al. (2008a), clinal characters ordered; LH: Lissamphibia next to <i>Brachydectes</i> (Lysorophia), <i>Gerobatrachus</i> in Amphibamiformes
a1	2	unpublished: SM 1	None	no	292	1450	as in Pardo et al. (2017a: fig. S6B)
a2	3	unpublished: SM 1	constraint de facto for LH	no	292	1454	LH; Lissamphibia contains <i>Gerobatrachus</i> , positions of <i>Chinlestegophis</i> + <i>Rileymillerus</i> as in a1
b	–	published: SM 3	None	no	322	1514	five islands: Lissamphibia, when present, in Amphibamiformes or Stereospondyli; <i>Chinlestegophis</i> in Gymnophionomorpha and/or Stereospondyli; figures in Serra Silva & Wilkinson (2021: fig. 2–4), simplified figures in Marjanović & Laurin (2019: fig. 301–K), only one island figured by Pardo et al. (2017a: fig. S7B)
bootstrap of b	4	published: SM 3	None	no	322	n/a	Diphily of modern amphibians: Karauridae + Batrachia next to <i>Gerobatrachus</i> (43%), caecilians next to <i>Chinlestegophis</i> (52%) in Stereospondyli
c	5	published: SM 3	addition of Albanerpetidae from Daza et al. (2020)	no	329	1565	as in Daza et al. (2020: fig. S14) except for slightly lower resolution; (Albanerpetidae (Karauridae, Lissamphibia) in Amphibamiformes, <i>Chinlestegophis</i> + <i>Rileymillerus</i> in Stereospondyli
d1	6	published: SM 4	None	yes	324	1554	Lissamphibia next to <i>Chinlestegophis</i> + <i>Rileymillerus</i> in Stereospondyli
bootstrap of d1	7	published: SM 4	None	yes	324	n/a	Lissamphibia (46%) next to <i>Chinlestegophis</i> + <i>Rileymillerus</i> (29%); <i>Chinlestegophis</i> as gymnophionomorph not compatible with bootstrap tree (44%)
d2	8	published: SM 4	Albanerpetidae	yes	329	1605	Lissamphibia in Amphibamiformes (closer to <i>Apateon</i> than to <i>Doleserpeton</i> or <i>Gerobatrachus</i> ), <i>Chinlestegophis</i> and <i>Rileymillerus</i> in Stereospondyli
bootstrap of d2	9	published: SM 4	Albanerpetidae	yes	329	n/a	Lissamphibia (52%) next to <i>Chinlestegophis</i> + <i>Rileymillerus</i> (27%); <i>Chinlestegophis</i> as gymnophionomorph not compatible with bootstrap tree (40%)
e1	10–12	published: SM 5	corrections of characters and scores	no	319	1514	seven islands: Lissamphibia either next to <i>Gerobatrachus</i> in Amphibamiformes or next to <i>Chinlestegophis</i> + <i>Rileymillerus</i> in Stereospondyli
e2	13, 14	published: SM 6	corrections of characters and scores	yes	321	1558	Lissamphibia next to <i>Chinlestegophis</i> + <i>Rileymillerus</i> in Stereospondyli
e3	15	published: SM 5	corrections; Albanerpetidae	no	326	1564	(Albanerpetidae (Karauridae, Lissamphibia) in Amphibamiformes, <i>Chinlestegophis</i> + <i>Rileymillerus</i> in Stereospondyli
e4	16, 17	published: SM 6	corrections; Albanerpetidae	yes	326	1601	three islands; Lissamphibia always in Amphibamiformes (closer to <i>Apateon</i> than <i>Doleserpeton</i> or <i>Gerobatrachus</i> ), <i>Chinlestegophis</i> + <i>Rileymillerus</i> in Stereospondyli
bootstrap of e4	18	published: SM 6	corrections; Albanerpetidae	yes	326	n/a	Lissamphibia (77%) in Amphibamiformes (Dissorophoidea: 35%), <i>Chinlestegophis</i> + <i>Rileymillerus</i> in Stereospondyli (34%); <i>Chinlestegophis</i> + <i>Rileymillerus</i> as gymnophionomorphs (15%) or next to Lissamphibia (29%), let alone Lissamphibia in Stereospondyli (10%), not compatible with bootstrap tree

inf. char. = number of parsimony-informative characters; LH = “lepospondyl hypothesis” of lissamphibian origins (*Eocaecilia* closer to *Carrollia* than to *Doleserpeton*); SM = Supplementary material file that contains the matrix and the settings for the analysis in question.

As described below, for some of our analyses of the published matrix, we added Albanerpetidae from Daza et al. (2020, based mainly on *Yaksha* Daza et al., 2020) rather than from Schoch et al. (2020, based on *Celtenham ibericus* McGowan & Evans, 1995, with a few additions from *Shirerpeton* Matsumoto & Evans, 2018). We did not add *Funcusvermis* for any analyses; we consider the effects of adding *Funcusvermis* sufficiently tested by Kligman et al. (2023), who added it to their revision of the matrix of Schoch et al. (2020), which was itself an expansion and slight revision of the published matrix of Pardo et al. (2017a).

### Analyses of the unpublished matrix of Pardo et al. (2017a)

We reanalyzed the originally unpublished matrix (associated with figure S6 of Pardo et al. 2017a) to determine

how many steps are needed to change the results. Two analyses were performed: one (a1) unconstrained, to replicate the original results, and one (a2) constrained to find *Eocaecilia* closer to the lepospondyl *Carrollia* than to the temnospondyl *Doleserpeton*, *de facto* enforcing the “lepospondyl hypothesis” of lissamphibian origins (but not any particular version of it) to enable us to compare the number of necessary extra steps. (The constraint also allows the “polyphyly hypothesis” that was supported by earlier versions of that matrix, most recently Huttenlocker et al. [2013].)

In both analyses, all characters were unordered, and no changes were made to the matrix. The search parameters were as follows: 10,000 random addition sequence replicates (far more than proved necessary) were performed holding one tree at each step, followed by branch swapping using TBR (tree bisection and reconnection) with a reconnection limit of 8 and a limit of 50 million

rearrangements per replicate (which was never hit); steepest descent was not in effect; unlimited automatic increases on the Maxtrees setting; branches collapsed if maximum branch length was 0.

### Analyses of the unmodified previously published matrix

We reanalyzed (analysis b) an unrevised version of the published matrix of Pardo et al. (2017a: supporting information part D; basis for their figures 2, 3 and S7) to verify its replicability and to further inspect the results. We computed consensus trees for each island, rather than for the entire sample of MPTs; unlike Serra Silva and Wilkinson (2021), who computed the MRC of each island, we used the strict consensus. The search settings were as above, except for the use of only 1000 unlimited replicates.

We also present a bootstrap analysis of this matrix (200 bootstrap replicates, each with 500 addition sequence replicates limited to 10 million rearrangements) to enable a better understanding of its support for various hypotheses. Most bootstrap values returned by Pardo et al. (2017a: fig. S7B) were below 50% and not originally published; however, clades supported by moderate bootstrap values (e.g., 45%) may still be better supported than any single alternative.

### Addition of Albanerpetidae to the previously published matrix

Daza et al. (2020: fig. 4E, S14) added Albanerpetidae—as a composite OTU based mainly on *Yaksha*, the new albanerpetid they described—to the published matrix of Pardo et al. (2017a) and analyzed the resulting matrix with implied weighting, using concavity values ( $k$ ) ranging from 10 to 200 in increments of 10. The MRC of the results of all twenty analyses pooled together was presented in Daza et al. (2020: fig. S14); numbers of optimal trees, tree lengths or indices were not published. Although most nodes occur in 100% of the trees (a number that may, however, result from rounding up to the nearest unit in some cases), and although the analysis at  $k = 200$  was practically unweighted (the lower the value of  $k$ , the more strongly are homoplastic characters down-weighted), we ran our single analysis (c) unweighted to be sure which trees the matrix supports at face value. Keating et al. (2020) demonstrated that unweighted parsimony is more accurate than implied-weights parsimony under certain realistic conditions; in addition, a basic assumption of implied weighting—an exponential distribution in which homoplasy-free characters are more common than those with any other number of extra steps—is not likely to be met for this matrix, and the performance of implied weights when that assumption is not met has not been studied (Marjanović and Laurin 2019).

Instead of publishing matrix files, Daza et al. (2020) published only the scores of the albanerpetid OTUs they revised in, or added to, the previously published matrix files they used. They confused the scores they added to the matrix of Pardo et al. (2017a; their reference 22) with the scores of Albanerpetidae they revised in the matrix of Pardo et al. (2017b; their reference 21) and presented these scores for the wrong matrix on pp. 16 and 17 of their supplementary text. The matrix of Pardo et al. (2017a) has 345 characters whereas that of Pardo et al. (2017b) has 370. Unable to add a string of 370 scores to a matrix of 345 characters, we added the string of 345 scores to the matrix of Pardo et al. (2017a) without any changes. The resulting NEXUS file, including a PAUP block that repeats analysis c when executed, is published here as Suppl. material 3. The search settings were as above.

### Ordering continuous characters

In the analyses of both matrices performed by Pardo et al. (2017a), as well as that by Daza et al. (2020), all multistate characters were unordered, even though some represent continuous or meristic morphoclines, which are more appropriately treated as ordered characters (Grand et al. 2013; Rineau et al. 2015, 2018; Marjanović and Laurin 2019; and references therein). Many characters used for phylogenetic analysis represent discretizations of intrinsically continuous variables that represent sizes, shapes and ratios, and the rationale for lumping similar values into a single state to produce discrete states follows the same logic as ordering the resulting states linearly (Wiens 2001). Simulations showed that ordering such states increases resolving power (the ability to recover clades) and reduces the occurrence of erroneous topologies (Grand et al. 2013; Rineau et al. 2015, 2018).

In the process of ordering all such clines in the unmodified published matrix, we discovered (like Kligman et al. 2023: supp. inf. part 4) that state 2 of character 9 is missing from the character list of Pardo et al. (2017a: part C of the supplementary text). In the “charstatelabels” block of the NEXUS file published as part D of the supplementary text, state 2 does occur, but in the matrix it is scored exclusively for *Ichthyophis*. J. Pardo (pers. comm. 2021) explained that state 2, absent from Schoch’s (2013) matrix, was intended to be introduced into the matrix, but this was implemented incompletely and accidentally omitted from the published character list. The states of character 9 (“preorbital region length”) originally were: 0, “less than twice the length of posterior skull table”; 1, “more” (than twice the length); 2, “equal in length”, so that state 2 is a subset of state 0. Gee (2022) and Kligman et al. (2023) noted this, but overlooked the fact that state 2 is scored correctly for *Ichthyophis*; they changed the name of state 2 to “twice as long” but did not rescore *Ichthyophis* or score state 2 for any other taxon. We have instead rescored *Ichthyophis* back to 0 for our ordered analyses, making the character binary.

For characters 3, 26 and 201, the implementation of state 2 as published in part D seems complete even though it is likewise missing from part C in all three cases. Conversely, character 292 has three states in part C, of which state 1 does not occur in the matrix. Characters 301 and 318 have three states in part C as well, of which the matrix lacks state 2.

We performed two parsimony and two bootstrap analyses—without (d1) and with (d2) *Albanerpetidae* as in analyses b and c—ordering the following clinal characters of the published matrix: 67, 75, 110, 143, 145, 158, 163, 170, 182, 187, 191, 201, 205, 209, 213, 214, 221, 226, 229, 242, 243, 262, 264, 266, 269, 271, 273, 279, 298, 300, 302, 304, 327, 328, and 334 (35 ordered out of 345 total characters; 10.1%). We first reordered the states of characters 205, 221, 327 and 328 to allow linear ordering because the original order did not follow the cline: states 0 and 1 of characters 205 and 221 had to be exchanged, as well as states 1 and 2 of characters 327 and 328. The resulting data matrix (and PAUP block) is available as Suppl. material 4.

The search settings were as above. 200 bootstrap replicates were performed, each using 500 random addition sequences. Instead of presenting the bootstrap values on consensus trees, we present the bootstrap trees (including the clades with greater frequencies than their alternatives) with their bootstrap values.

## Evaluation of potential synapomorphies and revisions to the published matrix

Pardo et al. (2017a) suggested various features as synapomorphies of caecilians with either *Chinlestegophis* alone or *Chinlestegophis* and other stereospondyls. Many correspond to characters in the published matrix. Here we evaluate all proposed synapomorphies and explain, where applicable, our revisions of scores in the matrix. We quote and discuss them below in the order in which they appeared in Pardo et al. (2017a). Our intention is not to fully revise the matrix (see Gee 2022), but to demonstrate the strong influence exerted by incorrect scores and compounding errors.

The resulting modified matrix is presented in Suppl. materials 5, 6 and was analyzed (analyses e1–e4: Table 1) using the same parameters applied in our analyses b–d, both without ordering characters (e1, e3; Suppl. material 5) and with the same character ordering used in analysis d (e2, e4; Suppl. material 6), and both without (e1, e2) and with *Albanerpetidae* as in analyses c and d2 (e3, e4). Analysis e4 was bootstrapped using the same parameters as for the bootstraps of analyses b, d1 and d2.

The diagnosis of *Chinlestegophis* states on p. E5389: “A shared feature with stereospondyls and caecilians is opisthotics fused to exoccipitals.” As pointed out by Santos et al. (2020), that feature is universal among lissamphibians except larval and some neotenic

salamanders (e.g., Duellman and Trueb 1994; Jones et al. 2022). It further occurs in the amphibamiform temnospondyl *Doleserpeton* (Sigurdson and Bolt 2010), a few lepospondyls (e.g., Pardo et al. 2015) and some (Maddin et al. 2013; Daza et al. 2020) though apparently not all albanerpetids (Matsumoto and Evans 2018). Among stereospondyls, conversely, it seems to be limited to extremely large and correspondingly unusually highly ossified adults of *Mastodonsaurus giganteus* (Jaeger, 1828) (Kligman et al. 2023: supp. inf. part 3). There is no corresponding character in the published matrix of Pardo et al. (2017a).

“Shared features with brachyopoids and caecilians” were proposed to (p. E5389) “include lacrimal fused to maxilla”. This hypothesis is difficult to evaluate. The maxillopalatine of *Funcusvermis* does not contain the nasolacrimal duct, so there is no evidence that it contains the lacrimal bone (Kligman et al. 2023). In *Chinlestegophis*, a separate lacrimal is absent, and the nasolacrimal duct lies entirely in what would otherwise be called the maxilla (Pardo et al. 2017a); however, the maxilla is dorsoventrally much narrower than expected for a fusion product. (The maxilla is slightly taller in the closely related *Rileymillerus* [Bolt and Chatterjee 2000: fig. 1.3]; however, Kligman et al. [2023: supp. inf. part 3] suggested quite plausibly that the fragmentary supposed nasal of *Rileymillerus* is actually a separate lacrimal.) As a result, fusion of the lacrimal to the maxilla cannot be distinguished from wholesale absence of the lacrimal in the currently known material of *Chinlestegophis*. Similarly, the cause of the absence of a separate lacrimal (loss or fusion) in most brachyopoids and a few other stereospondyls is unknown; even the nasolacrimal canal has not been traced in any of them (see Kligman et al. 2023: supp. inf. part 3 for details). Only in a few gymnophionans, as pointed out by Santos et al. (2020) and discussed by Theska et al. (2018), is ontogenetic fusion of the lacrimal to the maxilla documented (*Hypogeophis rostratus* [Cuvier, 1829]: Müller 2006; *Gegeneophis ramsawamii* Taylor, 1964: Müller et al. 2005; probably *Idiocranium russeli* Parker, 1936: Theska et al. 2018; possibly the “prefrontal” of *Dermophis mexicanus* [Duméril & Bibron, 1841]: Wake and Hanken 1982), although it has generally been hard in gymnophionans to tell the prefrontal, the lacrimal, and even the septomaxilla apart, and it is not clear whether the lacrimal ever forms in most gymnophionans (Theska et al. 2018). It is unclear if the two extant species scored in the matrix, *Epicrionops bicolor* Boulenger, 1883, and *Ichthyophis bannanicus* Yang, 1984, let alone the Early Jurassic *Eocaecilia*, possess(ed) a discrete lacrimal bone during development or not. However, character 21 of the published matrix only describes the presence or absence of the lacrimal, without mentioning the causes of such absence (such as fusion to the maxilla). We interpret this as describing the observed presence or absence of a separate bone in adults and have therefore not changed the scores of these taxa (all “absent”, state 1).

The sentence quoted above continues: “and two small posterior processes (‘horns’) on the occipital exposure of the tabular, just posterior to the otic notch (as in chigutisaurids).” Part B of the supplementary text of Pardo et al. (2017a) expressed some uncertainty about this: “two modest protuberances project from the occipital face of the tabular [of *Chinlestegophis*]. These processes may correspond to a rudimentary tabular horn, but their size and unusual topological relationship to the otic notch makes this homology uncertain. However, it is similar in position to the ‘tabular horn’ of some brachyopoids, particularly *Batrachosuchus* and *Vigilius*” (both of which are brachyopids, not chigutisaurids). Intriguingly, *Batrachosuchus* was scored as lacking “tabular horns” (pointed out by Gee 2022: app. 2.4.2), and see Kligman et al. (2023: supp. inf. part 3) for the doubtful homology of the “tabular horns” of *Chinlestegophis* and any brachyopoids. Later on p. E5390, Pardo et al. (2017a) made clear that tabular “horns” are not known in any caecilians. Indeed, for character 65—“Tabular (horn). Present in some form (0), or entirely absent (1)”—*Eocaecilia* was scored as unknown (?), and *Epicrionops* and *Ichthyophis* were scored as inapplicable (-) because they unambiguously lack tabulars (presence/absence of tabulars is coded by character 239). This means that this character does not hold *Chinlestegophis* and caecilians together in the published matrix. We have kept the scores for the caecilians and only changed the scores of the extant salamanders *Cryptobranchus* and *Hynobius* from unknown to inapplicable because they clearly lack tabulars; this change has no impact on any calculations of relationships.

On the same page, “[s]hared features with *Rileymillerus* and caecilians include the following: orbits small and laterally directed.” Orbit size, not coded in the published matrix, should be quantified before it can be evaluated, but is expected to be convergent among animals that live in darkness. Indeed, the orbits of *Funcusvermis* appear to have been considerably larger than those of other caecilians, *Chinlestegophis* or *Rileymillerus* (Kligman et al. 2023). Orbit location was included as character 26: “Orbit location. Medial, framed by wide jugals laterally (0), or lateral emplacement, framed by very slender jugals (1).” Dilkes (2015) revised the definition of character 26, but focused on the width of the jugal in his modifications. We, instead, interpret the intention of character 26 to be the location of the orbit and suggest rewording this character. Additionally, although three states are scored in the original matrix, only two are given in the character definition. The third state refers to particularly large orbits framed by relatively slender jugals and slender frontals (J. Pardo pers. comm. 2021; Kligman et al. 2023: supp. inf. part 4), but it is scored for batrachians that lack jugals. In order to keep the scores, we have reinterpreted it as referring to the size of the orbit or orbitotemporal fenestra rather than the jugal explicitly. Therefore, like Kligman et al. (2023), we have only changed the score of *Eocaecilia* from 2 to 1. We have further followed Kligman et al. (2023) in changing the scores of two amphibamiforms: *Platyrhinops* from 2 to 1, *Apateon* from 0 to 2.

“Shared features with caecilians include double tooth row on mandible” is stated in the next sentence of Pardo et al. (2017a). This feature is represented in the published matrix as no less than seven characters: 146, 147, 148, 272, 273, 322 and 344.

Character 146 reads: “Symphyseal teeth. No accessory teeth posterior to symphyseal tusks (0), or a transverse row of such teeth (1).” State 1 is found in some stereospondyl taxa. Despite the absence of symphyseal tusks, state 1 also was scored for *Chinlestegophis*, *Eocaecilia* and the two extant caecilians (Pardo et al. 2017a). We changed the score of *Chinlestegophis* to 0 because the lingual tooththrow of the holotype and the referred specimens is restricted to the coronoids, and the coronoids do not participate in the symphyseal region of this animal (Pardo et al. 2017a: fig. S3, movies S4 and S7). The lingual tooththrow of *Eocaecilia*, *Epicrionops* and *Ichthyophis* does reach all the way to the symphysis, so we retained a score of 1 for those, but caution that this likely duplicates scores for the coronoid dentition characters. (As discussed in Marjanović et al. [2023], we provisionally disagree with Kligman et al. [2023] that this tooththrow is borne on the adsymphyseal bone.)

Characters 147 and 148 describe presence/absence of teeth on specific coronoids and are thus redundant with character 272, which describes presence/absence of coronoid teeth in general (Pardo et al. 2017a). Characters 147 and 148 contain potentially important, non-overlapping variation, so we opted to keep that variation over retaining the more general variation captured by character 272, which we have excluded from our analyses. Because it is difficult to identify which coronoid is tooth-bearing in some taxa (i.e., when fewer than three distinguishable coronoids are present), *Doleserpeton* and caecilians in particular, we have, unlike Kligman et al. (2023: supp. inf. part 4), modified the definition of characters 147 and 148 as follows, which allowed us to keep all of the original scores:

- 147. Dentition lingual to distal half of labial tooththrow. Present (0), or absent (1).
- 148. Dentition lingual to mesial half of labial tooththrow. Present (0), or absent (1).

Character 322, “Splenic teeth. Present (0), absent (1)”, was scored 0 exclusively for *Ichthyophis*, *Epicrionops* and the dvinosaurian temnospondyl *Trimerorhachis insignis* Cope, 1878. The scores for the former two refer to the fact that the lingual tooththrow of caecilians has historically been thought to be borne on the splenic (references in Müller 2006; “splenic” was still used in quotation marks by Wilkinson et al. 2021). However, the bone that bears this tooththrow is not in the ventral position of a splenic, but the dorsolingual one of a coronoid, in the three extant caecilians whose development is well enough understood to tell (Müller et al. 2005; Müller 2006; Theska et al. 2018); a splenic has never been positively identified in any caecilian—or

any other lissamphibian. In other words, the scores of 1 for *Triadobatrachus*, *Cryptobranchus*, *Hynobius*, *Ambystoma* and *Leptodactylus* are not correct either; we have followed Gee (2022) in changing the scores of all lissamphibians that were not already scored as unknown to inapplicable (-). Moreover, the existence of teeth (including “denticles”: Gee et al. 2017) on the splenial of any species of *Trimerorhachis* has never been claimed or illustrated in the literature (most recently Milner and Schoch 2013), and D. M. found teeth to be absent there in personal observation of AMNH FARB 4565 (type specimen of *T. insignis*) and AMNH FARB 4572 (referred to the same species). This is not surprising. Only one certain and one possible case of tooth-bearing splenials are known in all of Tetrapodomorpha, if not Gnathostomata, and neither is sampled in any of the matrices we mention here: *Caerorhachis*, in which a “denticle” field extends from the coronoids and the prearticular onto the splenial (Ruta et al. 2002), and the unnamed “Parrsboro jaw”, where the same may or may not be the case (Sookias et al. 2014). In short, we changed the score of *Trimerorhachis* to 1, so that state 0 does not occur in the revised matrix at all; the character is constant and therefore uninformative in a parsimony analysis. Finally, *Chinlestegophis* was scored as unknown; we have corrected this to 1 because Pardo et al. (2017a: fig. S3) depicted the absence of teeth on the splenial.

It is worth mentioning that all three caecilians were correctly scored as lacking splenials in the published matrix of Pardo et al. (2017a: state 2 of character 264). This is contrary to the main text, which erroneously described the pseudodentary as “comprising the dentary, coronoid, splenial, and anterior Meckel’s cartilage” (p. E5391).

Character 344 also appears to target the presence of a lingual row of dentition on the mandible as seen in gymnophionans and taxa like *Chinlestegophis*. The character is defined as: “Dentary marginal dentition. Single row (0), multiple rows (1).” The three caecilian OTUs and *Chinlestegophis*, and no other OTUs, were scored as having multiple rows (1); however, *Chinlestegophis* has only one dentary tooththrow as described and illustrated by Pardo et al. (2017a), and in caecilians, as discussed above, the lingual row of teeth is borne on a coronoid rather than on the dentary. Thus, we rescored those taxa as having a single row of dentary teeth (0), meaning that state 1 does not occur in the revised matrix and this character, too, is uninformative.

Additionally, character 273 is: “Coronoid teeth. Larger than marginal (0), equal to marginal (1), smaller than marginal (2).” State 1 was scored exclusively for the three caecilians, *Chinlestegophis* and the stereospondyl *Benthosuchus*. We rescored *Chinlestegophis* as possessing state 2 because Pardo et al. (2017a: fig. S3) showed that the coronoid teeth are smaller than the marginal teeth.

The next feature listed as shared between *Chinlestegophis* and caecilians is “quadrate completely anterior to ear”, possibly meaning the otic capsules. If so,

this character state—which is not coded in the matrix—is standard among brachystelechid and lysorophian lepospondyls (Maddin et al. 2011; Glienke 2013, 2015; Pardo et al. 2015; Pardo and Anderson 2016) and widespread among lissamphibians as well. For present purposes it is only interesting if caecilians are temnospondyls, which this matrix cannot test.

Next is “broad, parallel-sided parasphenoid cultriform process >20% skull width”. Three characters in the published matrix (112, 114, 343) attempt to capture variation in parasphenoid shape, particularly that of the cultriform process, but “broad” and “parallel-sided” have different distributions. Although the cultriform process of *Chinlestegophis* is even broader than that of *Eocaecilia*, this condition is more or less universal among lissamphibians (references in Marjanović and Laurin 2008: 185–189), occurs prominently in lysorophians (Pardo and Anderson 2016), and also is found in the morphologically most immature dissorophoid temnospondyls (e.g., *Nyranerpeton*: Werneburg 2012).

Character 112 is presented in the character list as having two states: “Cultriform process (width). Base not wider than rest, clearly set off from basal plate (0), or merging continuously into plate (1)” (Pardo et al. 2017a: part C of the supplementary text). In the matrix, however, three states are scored; the first two are as given in the list, and the third (state 2) is called “flaring anteriorly” in the “charstatelabels” block, as in Schoch (2013). We followed Gee (2022) and Kligman et al. (2023) in transferring state 2 to character 343, which originally described whether the cultriform process is “[n]arrow, tapering anteriorly (0)” or “spatulate and parallel-sided (1)”. In other words, character 112 now describes the shape of the caudal end of the cultriform process in two states, and character 343 now describes the shape of the rostral end in three states that form a continuum of widths; character 343 is therefore ordered in our analyses with ordered characters (e2, e4). Our scores for both characters follow those of Gee (2022), which represents an update on Kligman et al. (2023). In addition, we scored *Chinlestegophis* as unknown for character 343; it was reconstructed as having state 1 (Pardo et al. 2017a: fig. 1H) and scored accordingly, but the entire rostral half of the cultriform process appears to be unknown (Pardo et al. 2017a: fig. 1B).

Character 114 is: “Cultriform process (outline). Of similar width throughout (0), or posteriorly expanding abruptly to about twice the width (1).” State 1 was scored only for the two extant caecilian OTUs and for the temnospondyls *Rileymillerus*, *Eryops* and *Onchiodon*. We are not sure if the conditions of those taxa should be considered primarily homologous: the two eryopids have a bulbous expansion near the base of the cultriform process, followed caudally by a constriction and then the basal plate along with its contacts to the pterygoids (Sawin 1941; Boy 1990); *Rileymillerus* has a strongly biconcave cultriform process that gradually expands caudally until it reaches five times its narrowest width where it merges

into the basal plate (Bolt and Chatterjee 2000: fig. 1.2, 2.2); *Epicrionops* and *Ichthyophis* have rostrally pointed cultriform processes that widen rather suddenly at the caudal ends of their contacts with the (maxillo)palatines (Jenkins et al. 2007: fig. 6B, D). But, in any case, *Chinlestegophis* and *Eocaecilia* were correctly scored 0, so (like Gee 2022 and Kligman et al. 2023) we have not modified this character or its scores.

“[O]ccipital condyles extend far beyond posterior edge of skull roof” is the next character state proposed to be shared by *Chinlestegophis* and caecilians (Pardo et al. 2017a: E5390). It is coded in the published matrix as character 137: “Exoccipital condyles. Short and broad base, projecting only with their posterior half behind the rim of the skull table (0), or almost the complete element posterior to level of occipital flange (1)”. State 1 was scored exclusively for most trematosauroids and brachyopoids, *Rileymillerus*, *Chinlestegophis*, *Eocaecilia*, *Cryptobranchus* and *Ambystoma*. However, that state (which appears to be more widespread among stereospondyl and dvinosaurian temnospondyls: Kligman et al. 2023: supp. inf. part 3) can be reached by elongating the condyles, reducing the caudal extent of the skull roof, extending the braincase caudally, or a combination of two or all three factors. The stalked occipital condyles of *Chinlestegophis* (and *Rileymillerus*: Bolt and Chatterjee 2000) are standard for stereospondyls, but are not found in any caecilians; this was beautifully illustrated by Pardo et al. (2017a: fig. 3). Rather, lissamphibians (and albanerpetids: Daza et al. 2020) generally expose large parts of the otic capsules in dorsal view, resulting in the entire occipital condyles lying far beyond the posterior edge of the skull roof. The condyles themselves are weakly elongated in some caecilians and not at all in others, as again shown by Pardo et al. (2017a: fig. 3) and described and illustrated by Jenkins et al. (2007: fig. 1–4, 6). This includes *Eocaecilia*, despite its retention of postparietal and probable tabular bones (Pardo et al. 2017a: fig. 3; Jenkins et al. 2007). Conversely, milder examples of the stereospondyl condition exist in various lepospondyls (Santos et al. 2020, and references therein). Therefore, *Eocaecilia* should not receive the same score as *Chinlestegophis*; we reinterpreted the character as referring to condyle elongation instead of the skull table, limiting state 1 to condyles with a stalked base, and consequently revised the scores of *Eocaecilia*, *Cryptobranchus* and *Ambystoma* to 0.

The last character state proposed to be shared by *Chinlestegophis* and caecilians (Pardo et al. 2017a: E5390) is presence of a “pterygoquadrate”, referring to fusion of the pterygoid and the quadrate bones, as observed in the ontogeny of some extant caecilians (Wake and Hanken 1982; Müller et al. 2005; Müller 2006; Theska et al. 2018: fig. 1c). On the next page, however, *Chinlestegophis* is more cautiously stated to possess, “perhaps, an incipient pterygoquadrate based on the structure of the suspensorium and apparent absence of the quadratojugal.” The full description of the skull (Pardo et al. 2017a: part B of the supplementary text) states the matter in a similarly limited way: “A separate quadrate is not evident in

either side of the skull, but it is likely that the saddle-shaped posterolateral face of the pterygoid represents the articular glenoid, and we hypothesize that this therefore represents a fused pterygoid-quadrate element (pterygoquadrate).” Thus, a pterygoquadrate is not observed in *Chinlestegophis*, and cannot be used to link it to caecilians. The issue is further complicated by *Eocaecilia*, in which the quadrate appears to be fused to the stapes and not to the pterygoid (Jenkins et al. 2007). Additionally, a pterygoquadrate is not universal in Gymnophiona, being absent in non-teresomatans like *Ichthyophis*, *Epicrionops* and *Amazops* (Jenkins et al. 2007: fig. 6B, D; Wilkinson et al. 2021: fig. 3) and the teresomatans *Chikila* (“pterygoid process of the quadrate”, separated from the quadrate by a suture and meeting the maxillopalatine, in Kamei et al. 2012: fig. S2(b)). If the fused pterygoquadrate is not only real in *Chinlestegophis*, but also homologous between *Chinlestegophis* and Teresomata or a subset thereof, it must have been independently lost three successive times in *Eocaecilia*, Rhinatrematidae and Ichthyophiidae, and at least once more in *Chikila*.

The pterygoquadrate may be coded as state 2 of character 318: “Quadrate-maxilla separated by. [sic] Pterygoid (0), small pterygoid and pterygoid process of quadrate (1), by pterygoid process of quadrate only (pterygoid absent) (2).” In agreement with the discussion above, state 2 does not occur in the matrix, which lacks teresomatans.

Pardo et al. (2017a: E5390) also stressed that “[i]n the temporal region, there is a small, round supratemporal that is only loosely articulated to its surrounding calvarial elements. This bone is morphologically and topologically identical to an element identified as the ‘tabular’ in *Eocaecilia*”. As pointed out by Marjanović and Laurin (2019: 151, app. S1: 35), the statement of identity rests entirely on the reconstruction drawing published by Jenkins et al. (2007: fig. 1), which shows almost no uncertainty (by dashed lines, differential shading or any other means), but rather depicts a preferred hypothesis of what an undamaged skull looked like. The text, specimen drawings and photos in Jenkins et al. (2007), further supported by the  $\mu$ CT rendering in Maddin et al. (2012a: fig. 1A), make clear that the morphology and topology of the “?tabular” in the reconstruction are guesses—the presence and independence of the bone are evident, but not its shape or size. In the crushed holotype (Jenkins et al. 2007: fig. 2; Maddin et al. 2012a: fig. 1A), the left “?tabular” is caudally broken, but the right one may well have reached the caudal edge of the skull table (pers. obs. H. M. and D. M.), reopening the possibility that it is, in fact, a tabular and not homologous to the supratemporal of *Chinlestegophis*. Pardo et al. (2017a) actually scored the tabular as present in *Eocaecilia* (state 0 of character 239). However, given the uncertainty surrounding the element, we changed this score to unknown (?), and retained the scores of “unknown” in the tabular-related characters 62, 63 and 65–67. We also followed Gee (2022) and Kligman et al. (2023) in changing the scores of all salamanders to not applicable (-) for the tabular-related character 63, because they clearly lack tabulars, and changed the scores

of all lissamphibians (including *Eocaecilia*) to inapplicable for character 71, which references tabular horns.

The implication later in the same paragraph (Pardo et al. 2017a: E5390) that the real tabular could be part of the *os basale* in *Eocaecilia* is unfounded: there is no reason to think, from their shapes or topological relationships, that the dorsal sides of the *ossa basalia* contain tabulars or any other dermal bones of the skull roof (Jenkins et al. 2007: fig. 2, showing the holotype; compare extant caecilians and their ontogeny: Wake and Hanken 1982; Müller et al. 2005; Müller 2006; Theska et al. 2018).

In their Discussion section, Pardo et al. (2017a: E5393) made a far-reaching claim: “a sulcus associated with the opening of the nasolacrimal duct in the orbit is present in both *Chinlestegophis* and *Eocaecilia* in a similar position to the tentacular sulcus of the basal caecilian *Epicrionops petersi*”, citing Jenkins et al. (2007: fig. 10), which indeed shows the tentacular foramen inside the orbit of the extant *Epicrionops* and a “tentacular sulcus” on the orbital margin of the maxilla of *Eocaecilia*. Evidence of the caecilian tentacle, a body part composed mostly of the nasolacrimal duct and eye musculature and associated with chemosensation in extant caecilians, has not been reported from any vertebrates other than *Gymnophiona* and *Eocaecilia*. In *Chinlestegophis*, the maxilla does not reach the orbit, being excluded by a contact of the prefrontal and the lateral exposure of the palatine (Pardo et al. 2017a: fig. 1, S4). The nasolacrimal duct is housed in the maxilla and meets the orbit in two pores well medial of the skull surface (Pardo et al. 2017a: fig. S4C). Although the sulcus is stated to be in the orbit margin in part F of the supplementary material, it was not reconstructed in fig. 1J, which instead shows an elliptical orbit devoid of any corners; the reconstruction in fig. 1I shows a more angular orbit, fitting the  $\mu$ CT images in fig. 1E–G, but these corners are very wide, obtuse and rounded, offering no evidence of a tentacular sulcus. A nasolacrimal duct that is separated from the surface of the head would not function in sensory reception, and seems unlikely to explain the evolution of the caecilian tentacle. *Funcusvermis* also lacked a tentacular sulcus unless the sulcus had an unusually far dorsal position, i.e., at the dorsoventral midpoint of the rostral orbit margin at minimum (Kligman et al. 2023: fig. 1a, g–i). In any case, no feature relating to the nasolacrimal duct or the shape of the orbit is coded in the published matrix.

## Results

See Table 1 for a brief overview of our analyses and their results.

### Analyses of the unpublished matrix of Pardo et al. (2017a)

Our unconstrained analysis (a1; Fig. 2) found 12 MPTs of 1450 steps, as reported in Part G of the supplementary

information of Pardo et al. (2017a); their previously unreported indices are: CI excluding uninformative characters = 0.2668, RI = 0.6532, RC = 0.1815. The resulting strict consensus is identical to that of Pardo et al. (2017a: fig. S6B), with *Chinlestegophis* and *Rileymillerus* positioned as the sister-group to all other amphibamiform temnospondyls including Lissamphibia, which in turn contains *Eocaecilia* and *Gymnophiona*. Of the 319 characters, 292 are parsimony-informative.

The MPTs form two islands that differ in their resolution of Lissamphibia: (1) *Gerobatrachus* as the sister-group of Lissamphibia, within which “frogs” + *Triadobatrachus* is the sister-group of a clade formed by “salamanders” + *Karaurus* on one side and *Albanerpetidae* + *Eocaecilia* and crown caecilians on the other; (2) crown caecilians + *Eocaecilia* as the sister-group of the other lissamphibians, within which *Gerobatrachus* is the sister-group of a clade formed by “frogs” + *Triadobatrachus* on one side and *Albanerpetidae* + (“salamanders” + *Karaurus*) on the other. Note that only (2) is compatible with phylogenies of extant amphibians based on molecular data (Hime et al. 2020, and references therein).

Constraining *Eocaecilia* to be closer to the lepospondyl *Carrolla* (analysis a2; Fig. 3) than to the temnospondyl *Doleserpeton* produced 48 MPTs of a very similar length (1454 steps) and very similar indices (CI excluding uninformative characters = 0.2661, RI = 0.6519, RC = 0.1807). The positions of *Chinlestegophis* and *Rileymillerus* remain unchanged compared to Pardo et al. (2017a: fig. S6). Although the “lepospondyl hypothesis” is supported in this experiment, Lissamphibia contains *Gerobatrachus*, and it nests far from *Carrolla*, indeed on the other side of the lepospondyl tree—next to the limbless aistopods, followed by the limb-reduced *Brachydectes*, much as in Marjanović and Laurin (2009; Fig. 1) whose matrix has a common ancestor with this one (Anderson et al. 2008a). The strict consensus shows a less well resolved version of the abovementioned topology (2).

The differences in fit to the matrix between the unconstrained and the constrained trees are not significant (Kishino/Hasegawa test:  $p = 0.6284$ ; Templeton test:  $p = 0.6276$ ; winning-sites test:  $p = 0.7160$ ).

### Analyses of the unmodified previously published matrix

Reanalysis of the published matrix (analysis b) yielded identical results to those of Pardo et al. (2017a), Marjanović and Laurin (2019: fig. 30I–K), Serra Silva and Wilkinson (2021) and Gee (2022), returning 882 MPTs with a length of 1,514 steps, CI excluding uninformative characters = 0.2548, RI = 0.6858, RC = 0.1812. Of the 345 characters, 322 are parsimony-informative. The MPTs are spread across the five islands found and described by Serra Silva and Wilkinson (2021) and above (Matrices, Methodologies, and Missteps: Phylogeny inferred from parsimony).

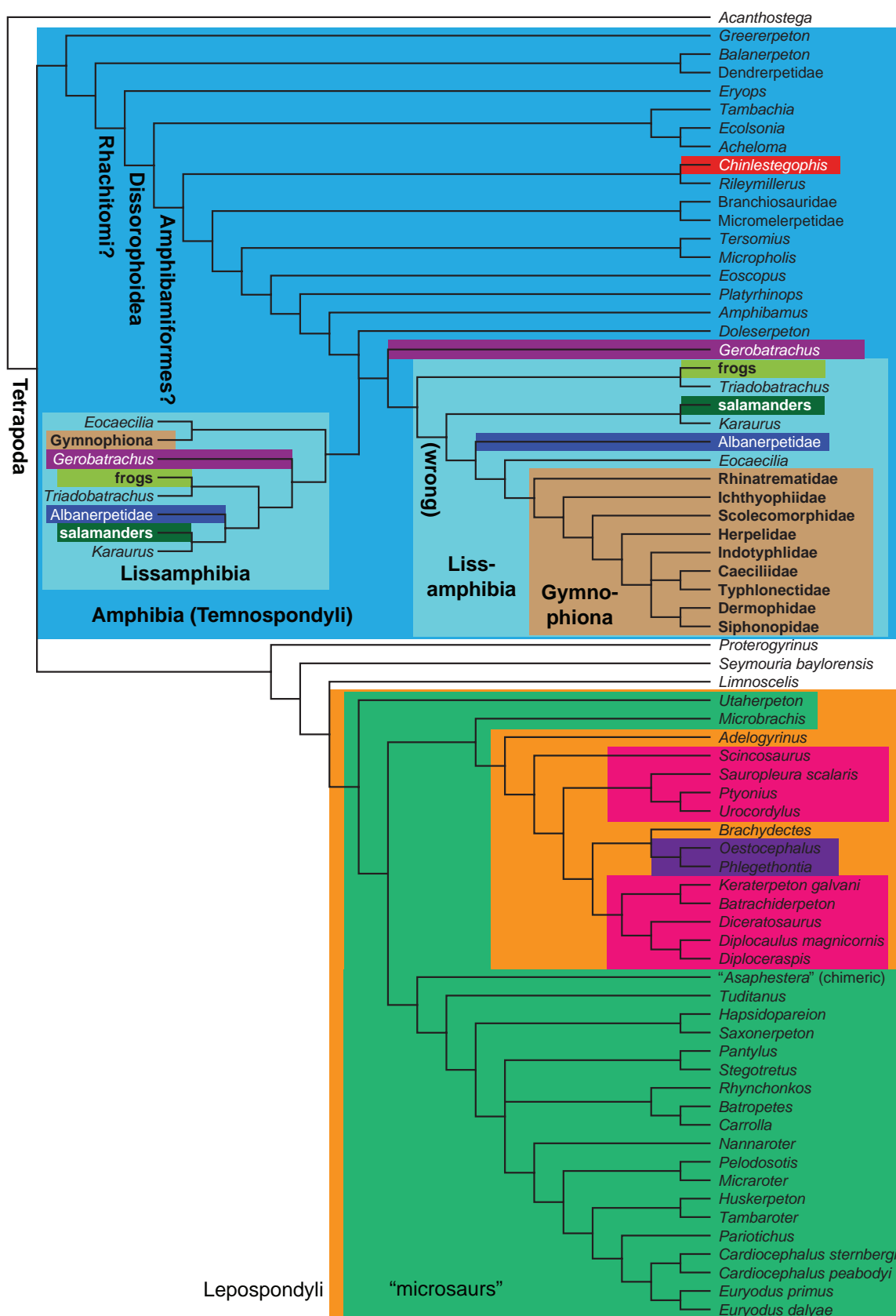


**Figure 2.** Strict consensus of the 12 MPTs obtained from our analysis a1 (see Table 1), using the unpublished matrix used by Pardo et al. (2017a: fig. S6B). The two islands are represented by the duplication of Lissamphibia and its sister-group (on one island) or member (on the other island) *Gerobatrachus*. The branch marked "(wrong)" contradicts the molecular consensus (Hime et al. 2020). Question marks indicate names with uncertain application given the taxon sample. Colored rectangles and boldface, as well as "*Asaphestera*" and *Dendrerpetidae*, as in Fig. 1; red rectangle for *Chinlestegophis*, brown rectangle for crown-group caecilians (*Gymnophiona*).

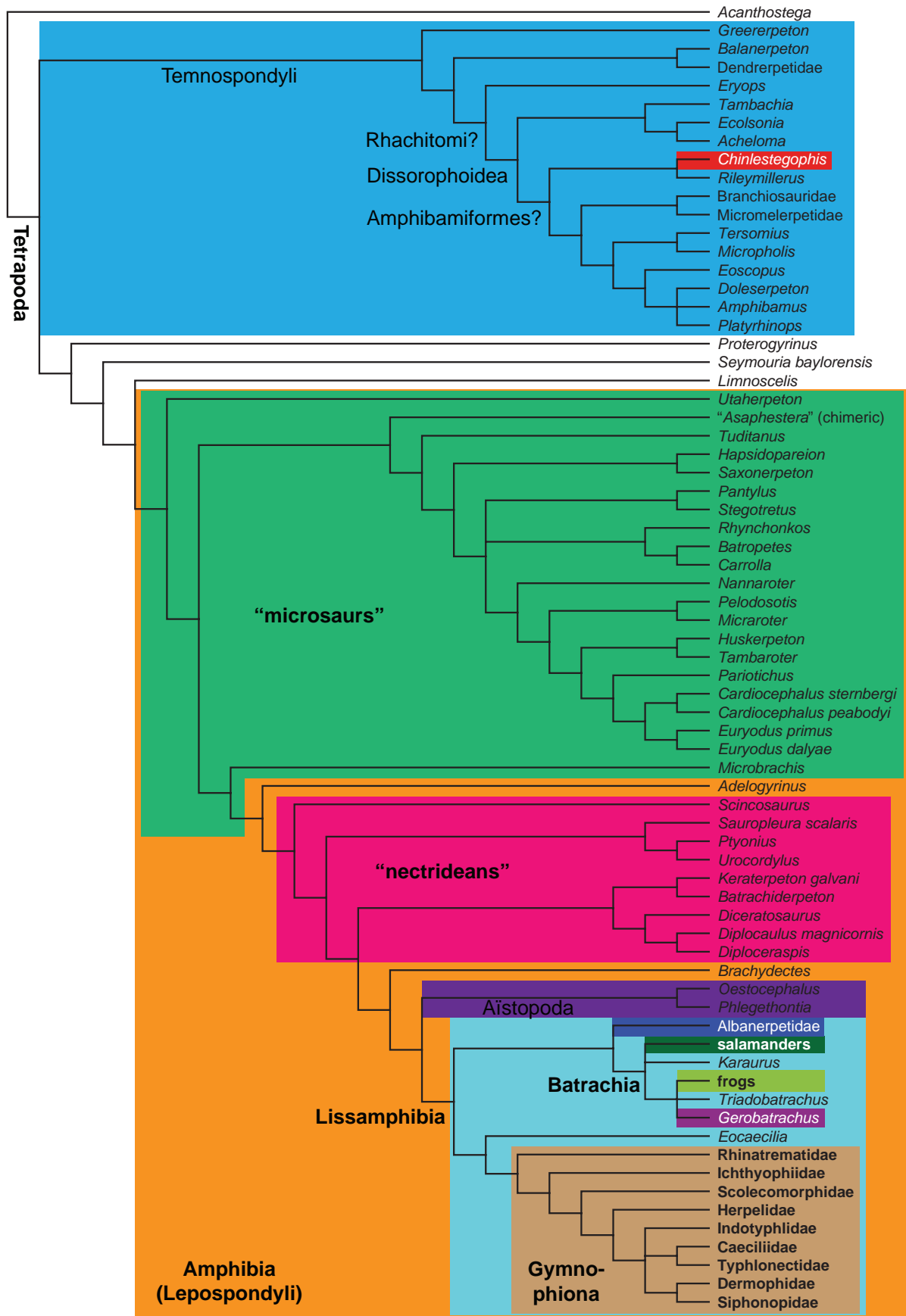


**Figure 3.** Strict consensus of the 48 MPTs obtained from the unpublished matrix used by Pardo et al. (2017a) in an analysis (a2; see Table 1) constrained against the “temnospondyl hypothesis” of lissamphibian origins; a version of the “lepospondyl hypothesis” results. Colors, boldface, “*Asaphestera*” and Dendrerpetidae as in Fig. 2.

The bootstrap tree of analysis b (Fig. 4) shows moderate support for the diphyly of modern amphibians as presented by Pardo et al. (2017a): the three caecilians form the sister-group of the stereospondyl *Chinlestegophis* in 52% of the bootstrap replicates, while the batrachians are found as amphibamiform dissorophoids closest to *Gerobatrachus* in only 43%, and adding any further dissorophoids depresses this value to a maximum of 35%. This latter value is the highest that separates caecilians and batrachians + karaurids; even *Rileymillerus* occurs as the sister-group of *Chinlestegophis* and the caecilians together in only 32%. Most bootstrap values in the rest of the tree, except for the majority of the most highly nested nodes, are even lower.

Inspection of the list of bipartitions in the output of PAUP\* (Suppl. material 2: table S1), including those that are incompatible with the bootstrap tree, shows that Lissamphibia was found in 37% of the bootstrap replicates—support comparable to that for Dissorophoidea including Batrachia (35%), which is shown in the bootstrap tree (Fig. 4). An exclusive clade of all lissamphibians and *Chinlestegophis* occurs in 21% of the replicates and combines with *Rileymillerus* in 20%; all lissamphibians and any or all dissorophoids form an exclusive clade in no more than 16% of the replicates. Stereospondyli excluding *Chinlestegophis* and optionally *Rileymillerus* appears in only 9%, as often as, e.g., an improbable clade of all lissamphibians except *Eocaecilia*. Only 8% group all lissamphibians, *Chinlestegophis* and *Gerobatrachus* exclusively.

### Addition of Albanerpetidae to the previously published matrix

The matrix of Daza et al. (2020: fig. 4E, S14), i.e., the published matrix of Pardo et al. (2017a) with Albanerpetidae added, yielded a single island of 45 MPTs (analysis c; length = 1565 steps, CI excluding uninformative characters = 0.2510, RI = 0.6795, RC = 0.1741). Their strict consensus (Fig. 5) is topologically identical to that of Daza et al. (2020: fig. S14), except for slightly lower resolution: Dissorophidae, Trematopidae, and a node supporting *Edingerella*, *Benthosuchus*, Capitosauroidea and Trematosauroida + Brachyopoidea are unresolved. Interestingly, all nodes marked “95” in the MRC of Daza et al. (2020: fig. S14) are present in the strict consensus of our analysis, whereas a few of those marked “100” are not. Amphibamiformes, including Lissamphibia, is resolved exactly as in Daza et al. (2020: fig. 4E, S14): there is a clade (*Apateon* (Albanerpetidae (Karauridae, Lissamphibia))) which is the sister-group of (*Micropholis* (*Platyrrhinops* (*Amphibamus* (*Doleserpeton*, *Gerobatrachus*)))) within Dissorophoidea. Likewise, *Chinlestegophis* and *Rileymillerus* are positioned as in Daza et al. (2020: fig. S14), as the sister-group to Brachyopoidea within Stereospondyli.

The addition of Albanerpetidae renders seven characters parsimony-informative, so that 329 of the total of 345 now have this status.

### Ordering continuous characters

Ordering of clinal characters (analysis d1) in the otherwise unmodified published matrix of Pardo et al. (2017a) rendered two characters parsimony-informative (for a total of 324 of the 345 characters in the matrix) and resulted in three islands of 270 MPTs in total (length = 1554 steps, CI excluding uninformative characters = 0.2508, RI = 0.6885, RC = 0.1777). The strict consensus is well resolved (Fig. 6) and shows Lissamphibia as the sister-group of the clade formed by *Chinlestegophis* and *Rileymillerus*, nested within the brachyopoid stereospondyls.

The bootstrap tree of analysis d1 (Fig. 7) recovers a rather weakly supported (46% frequency) Lissamphibia with the same sister-group, and the *Chinlestegophis*-*Rileymillerus* clade is again less supported (40%). Affinities between the *Chinlestegophis*-*Rileymillerus* clade and Lissamphibia are slightly better supported than with unordered states, but at 29%, this clade is still weak. The position of *Chinlestegophis* as a stem-caecilian, incompatible with the bootstrap tree, occurs with a frequency of 44% (Suppl. material 2: table S2). Lissamphibia is separated from *Doleserpeton* or *Gerobatrachus* by bootstrap values no higher than 30%; an exclusive clade of frogs, salamanders, karaurids and *Gerobatrachus* has 36% support (less if any other dissorophoids are added) and an exclusive Lissamphibia-*Gerobatrachus* clade only 15% (likewise less if other dissorophoids are added; Suppl. material 2: table S2).

When the clinal characters are ordered and Albanerpetidae is added (analysis d2), 329 characters are parsimony-informative, and the published matrix yields a single island of 30 MPTs (1605 steps, CI excluding uninformative characters = 0.2453, RI = 0.6830, RC = 0.1711). The strict consensus (Fig. 8) shows (*Apateon* (Albanerpetidae (Karauridae, Lissamphibia))) in Amphibamiformes—next to a clade that contains *Doleserpeton* and *Gerobatrachus*—while the *Chinlestegophis*-*Rileymillerus* clade forms the sister-group of the brachyopoid stereospondyls.

Bootstrapping analysis d2 (Fig. 9) shows moderate support for Lissamphibia (52%). Lissamphibia and a clade formed by *Chinlestegophis* and *Rileymillerus* are found as sister groups with low support (27%). Interestingly, both clades together form the sister-group of Dissorophoidea; the support for exclusion from a position close to *Gerobatrachus* or *Doleserpeton* is comparatively high (62%), but the support for exclusion from Trematosauria within Stereospondyli is very low (12%). Noteworthy, on the other hand, is the support (75%) for excluding Karauridae (*Karaurus* and *Kokartus*), universally considered a clade of stem-salamanders (Jones et al. 2022, and references therein), from Batrachia (frogs + salamanders). An exclusive clade of Albanerpetidae, Karauridae and Batrachia has 58% support, moderately contradicting Matsumoto and Evans (2018) and Daza et al. (2020); this may be due to character sampling.

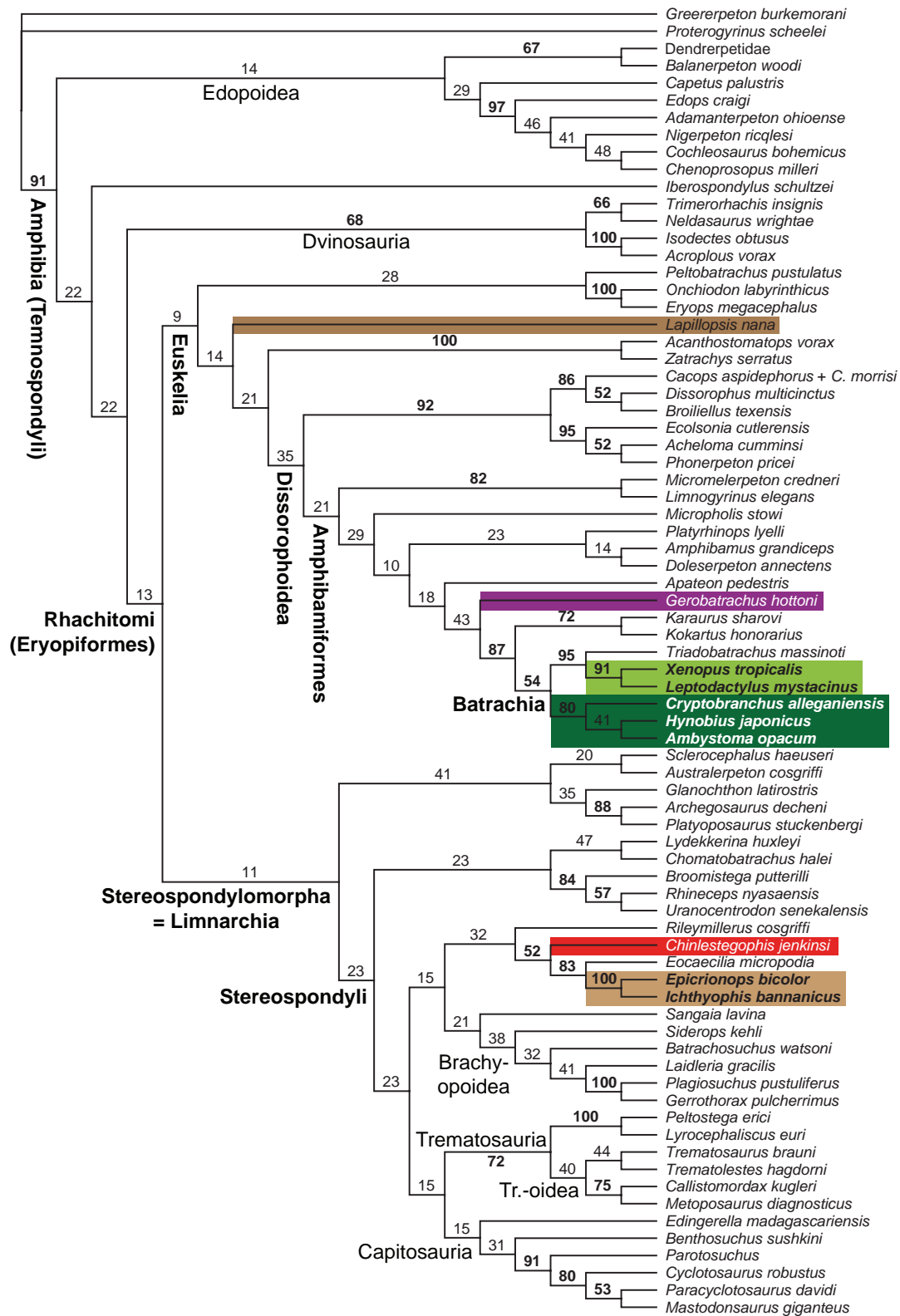


**Figure 4.** Bootstrap tree obtained from the published matrix used by Pardo et al. (2017a) when all characters are unordered (analysis b). The bootstrap tree shows moderate support (52%) for the diphyly of extant amphibians. Colors and boldface as in Fig. 3, bootstrap values  $\geq 50\%$  also in boldface; darker brown rectangle for *Lapillopsis*, a small temnospondyl thought to be a stereospondyl convergent to dissorophoids. The blue rectangle for Temnospondyli is omitted because all OTUs except *Greererpeton* and *Proterogyrinus* are (inferred to be) temnospondyls; the cyan rectangle for Lissamphibia is omitted because the name Lissamphibia does not apply on this tree. Tr.-oidea = Trematosauroida. The Dendrerpetidae OTU was called “*Dendrerpeton acadianum*” by Pardo et al. (2017a) but is mostly based on its apparently close relative *Dendrysekos*. In this and the following figures we have also corrected spelling mistakes in taxon names compared to the matrix and the figures of Pardo et al. (2017a).

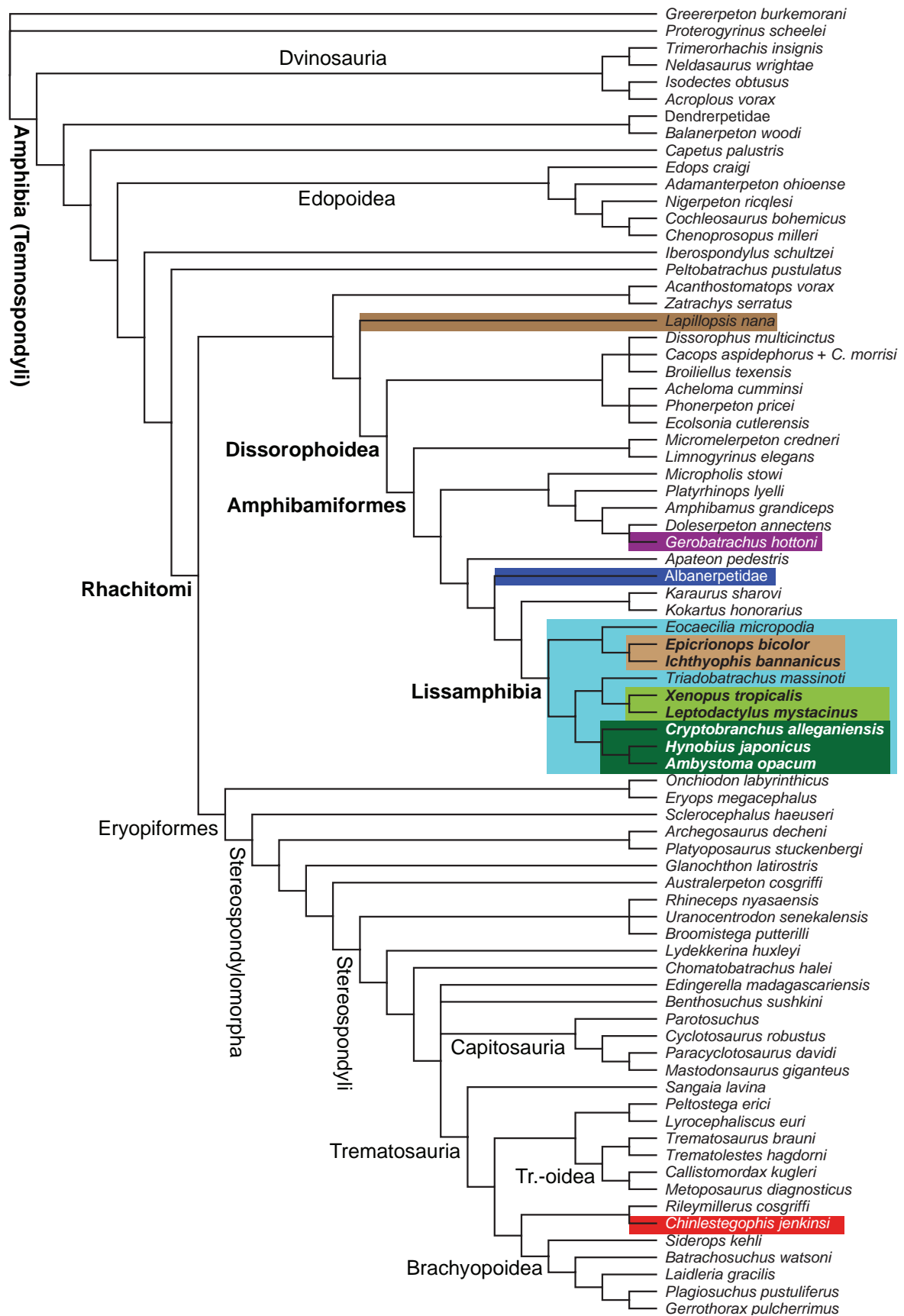


**Figure 5.** Strict consensus of the 45 MPTs obtained from the published matrix of Pardo et al. (2017a) with addition of *Albanoerpetidae* from Daza et al. (2020); all characters are unordered (analysis c). The resolution differs slightly from Daza et al. (2020: fig. S14) because we used parsimony with equal rather than implied weights. Colors, boldface and *Dendrerpetidae* as in Fig. 3 and 4 here and in all following figures; Tr.-oidea = Trematosauroidae.

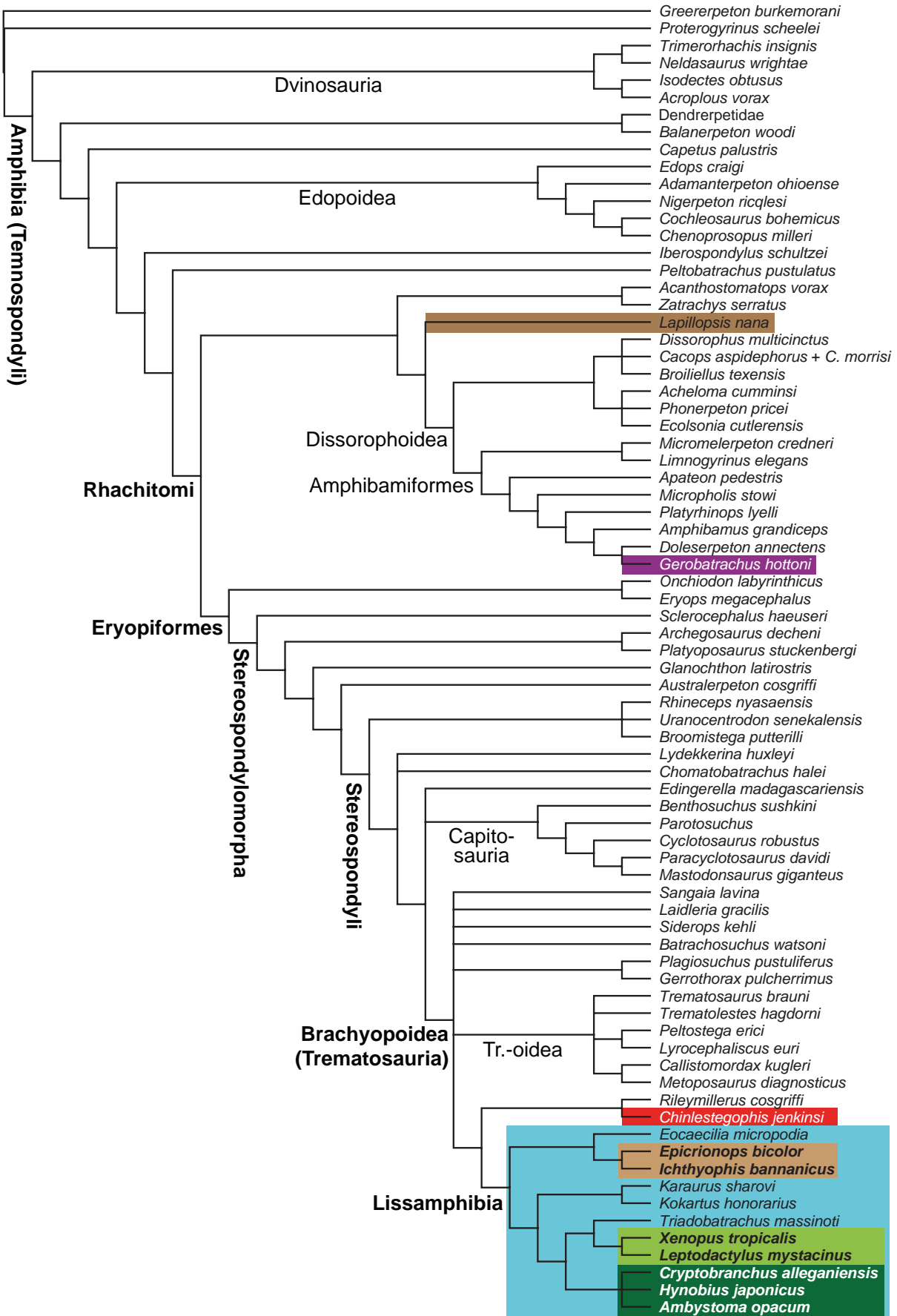


**Figure 6.** Strict consensus of the 270 MPTs obtained from the published matrix of Pardo et al. (2017a) with clinal characters ordered (analysis d1). Tr.-oidea = Trematosauoidea.

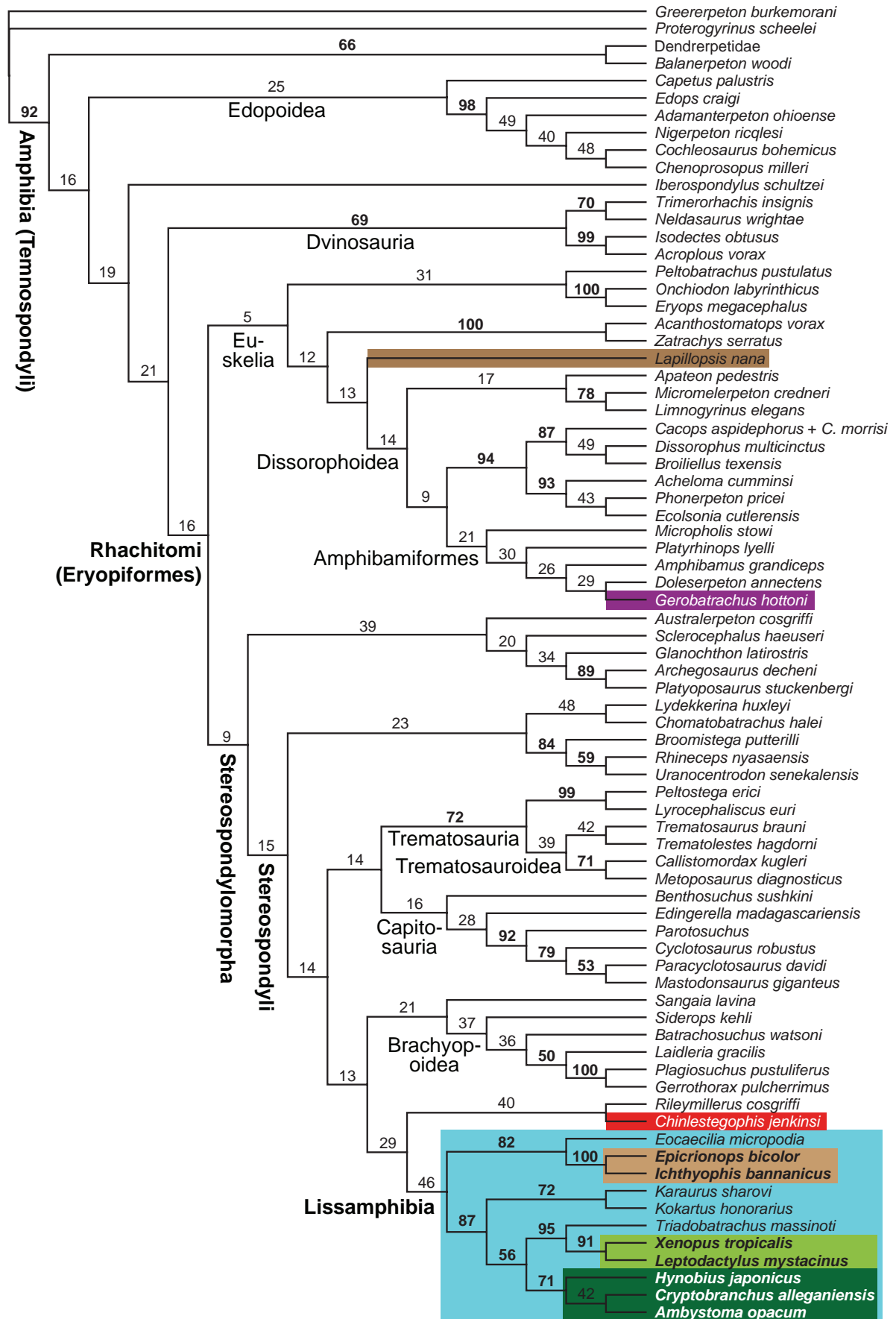


**Figure 7.** Bootstrap tree obtained from the published matrix of Pardo et al. (2017a) with clinal characters ordered (analysis d1). Bootstrap values  $\geq 50\%$  in boldface.

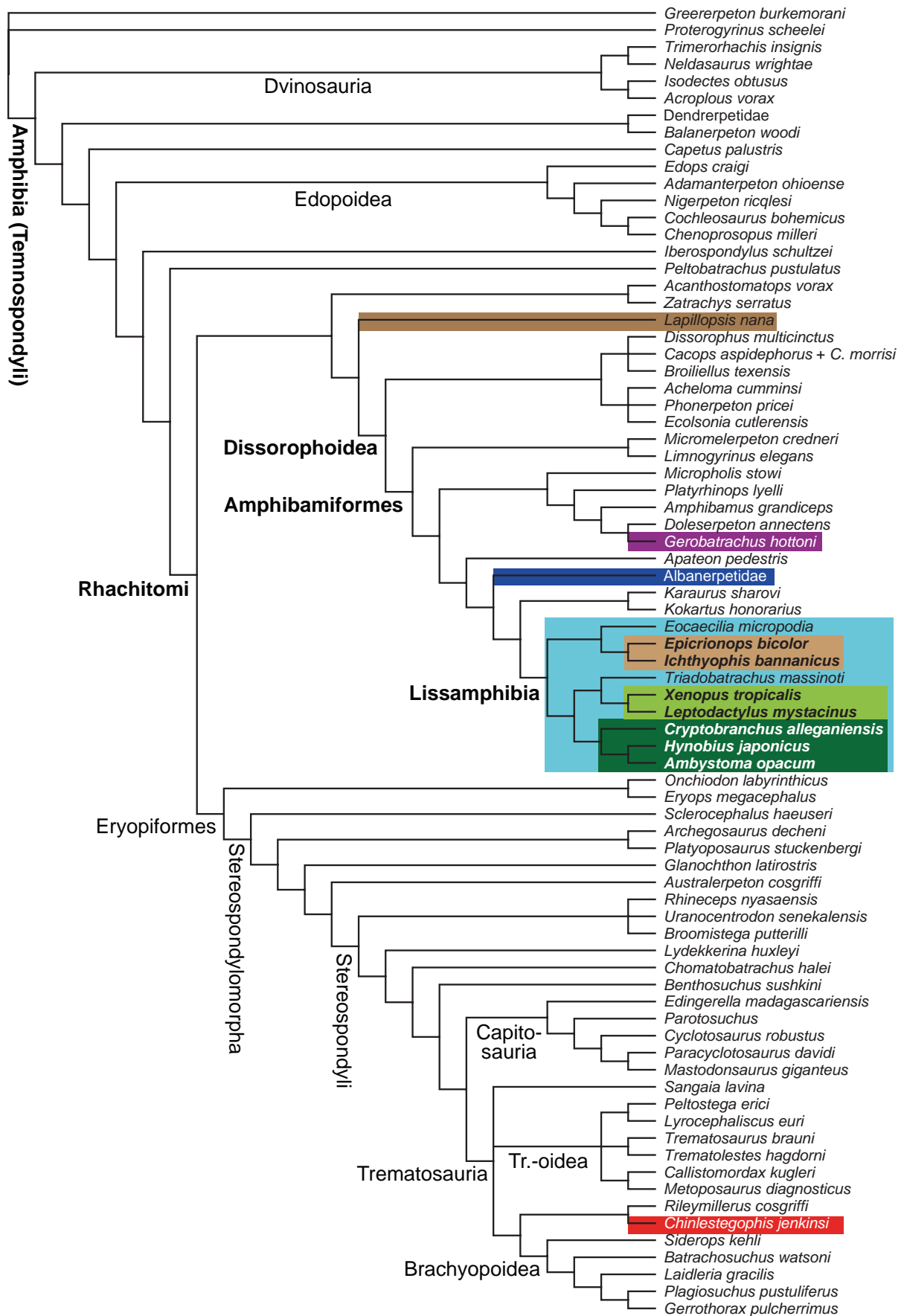


**Figure 8.** Strict consensus of the 30 MPTs obtained from the published matrix of Pardo et al. (2017a) with clinal characters ordered and *Albanerpetidae* added (analysis d2).

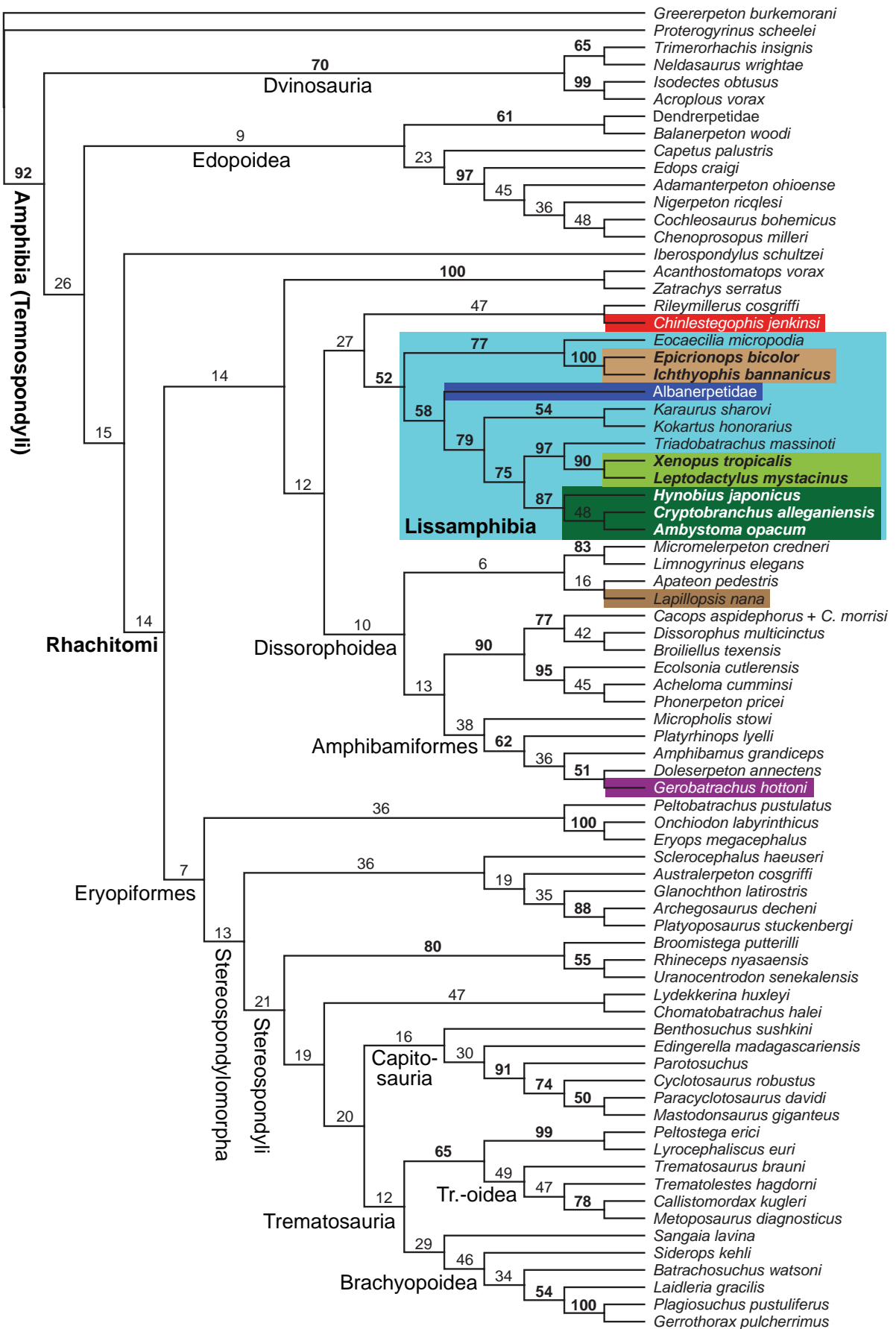


**Figure 9.** Bootstrap tree obtained from the published matrix of Pardo et al. (2017a) with clinal characters ordered and Albanerpetidae added (analysis d2). Bootstrap values  $\geq 50\%$  in boldface. Tr.-oidea = Trematosauroidae.

The list of bipartitions not compatible with the bootstrap tree (Suppl. material 2: table S3) reveals 40% bootstrap support for a clade of *Chinlestegophis* and the three caecilians (slightly more than the 38% without ordering and without Albanerpetidae) and 30% for a clade that includes these four and *Rileymillerus*. *Chinlestegophis* and *Rileymillerus* are excluded from Dissorophoidea + Lissamphibia in 21% of the bootstrap replicates. The support for exclusion of Albanerpetidae from Lissamphibia (17%) is lower than it could be given the 58% for a specific placement in Lissamphibia mentioned above; 12% of the replicates group the caecilians with Albanerpetidae, 6% find all dissorophoids, all batrachians, the karaurids and Albanerpetidae in an exclusive clade.

## Revised published matrix

The matrix including the changes we propose was run both with all characters unordered, as they were in Pardo et al. (2017a), and with the herein proposed characters that form morphological clines ordered; both of these options were used both without and with the addition of Albanerpetidae from Daza et al. (2020). The analysis with all characters unordered and Albanerpetidae excluded (e1) resulted in 1341 MPTs, each with a length of 1514 steps (CI excluding uninformative characters = 0.2535, RI = 0.6849, RC = 0.1801), distributed over seven islands of optimal trees. Of the 344 characters, only 319 are parsimony-informative. In all seven islands, Lissamphibia is recovered and excludes *Chinlestegophis* (as well as *Rileymillerus*). One island (Fig. 10) places (Brachyopoidea (Lissamphibia (*Chinlestegophis*, *Rileymillerus*))) in Stereospondyli, and Karauridae on the batrachian stem; the others recover Lissamphibia next to *Gerobatrachus* in Amphibamiformes while the *Chinlestegophis*-*Rileymillerus* clade remains nested in Stereospondyli next to or inside Brachyopoidea, and Lissamphibia is resolved either as (frogs (karaurids (caecilians, salamanders))) (Fig. 11), contradicting the molecular consensus (Hime et al. 2020), or as (caecilians (frogs (karaurids, salamanders))) (Fig. 12).

The second analysis, using ordered characters (e2), resulted in three islands of 99 MPTs in total (1558 steps; CI excluding parsimony-uninformative characters = 0.2489, RI = 0.6870, RC = 0.1759). 321 characters were parsimony-informative. The well-resolved strict consensus is shown in Figs 13, 14. Lissamphibia is recovered and placed next to a *Rileymillerus* + *Chinlestegophis* clade, which lies next to Plagiosauridae within the brachyopoid stereospondyls; Karauridae lies on the batrachian stem. *Gerobatrachus* remains next to *Doleserpeton* inside a variably resolved Dissorophoidea.

The third and fourth analyses differ from the first and second by the addition of Albanerpetidae (from Daza et al. 2020) as in analysis c. In both, 326 of the 344 characters were parsimony-informative. The unordered analysis e3 yielded 297 MPTs (1564 steps, CI

excluding uninformative characters = 0.2498, RI = 0.6790, RC = 0.1732); PAUP\* groups them as two islands, but these are similar enough that we present the overall strict consensus in Fig. 15. Dissorophoidea including Lissamphibia is resolved as in analysis c; the *Rileymillerus* + *Chinlestegophis* clade is grouped with the poorly resolved brachyopoid stereospondyls.

In the ordered analysis e4, 81 MPTs are recovered (1609 steps, CI without uninformative characters = 0.2434, RI = 0.6817, RC = 0.1695). They all group the *Rileymillerus* + *Chinlestegophis* clade with Brachyopoidea as in analysis e3, while Lissamphibia is nested among the amphibamiform dissorophoids, closer to *Apateon* than to *Gerobatrachus* or *Doleserpeton*. PAUP\* groups the MPTs into three islands depending on how they resolve amphibamiform phylogeny: one island (Fig. 16) has (*Doleserpeton* (*Gerobatrachus* (*Apateon*, Lissamphibia))) inside Amphibamidae, Albanerpetidae on the caecilian stem and Karauridae on the batrachian stem; the other two (Fig. 17) have (*Apateon* (Albanerpetidae (Karauridae, Lissamphibia))) close to but outside Amphibamidae, which contains *Gerobatrachus*; the Early Triassic amphibamiform *Micropholis* is either on the amphibamid or on the lissamphibian side.

Bootstrapping analysis e4 reveals (Fig. 18) considerable support for Lissamphibia (77%), within which Albanerpetidae (43%) and Karauridae (64%) lie on the batrachian stem but not in Batrachia (75%). Lissamphibia is, with limited support, placed next to *Apateon* (22%) in Dissorophoidea (35%); similar support is recovered for placing *Chinlestegophis* (and *Rileymillerus*) close to brachyopoids including plagiosaurids (27%) in Stereospondyli (34%).

Groupings not compatible with the bootstrap tree (Suppl. material 2: table S4) include *Chinlestegophis* + *Rileymillerus* as gymnophionomorphs (15%) or in an exclusive clade with Lissamphibia (29%); comparable support exists for Lissamphibia without Albanerpetidae (30%) or Lissamphibia without Karauridae or Albanerpetidae (20%), both of which are also incompatible with the bootstrap tree. An exclusive clade of lissamphibians and stereospondyls occurs in only 10% of the bootstrap replicates.

## Discussion

### Support for alternative topologies

Our work corroborates some of the results of the analyses performed by Pardo et al. (2017a), but also highlights weaknesses in the phylogenetic signal that was claimed to support caecilian affinities of *Chinlestegophis*. Indeed, Pardo et al. (2017a: abstract) claimed: “Our results place the taxon confidently within lissamphibians.” On the contrary, our results demonstrate that the affinities of *Chinlestegophis* cannot be ascertained with confidence based on either of the two matrices of Pardo et al. (2017a).

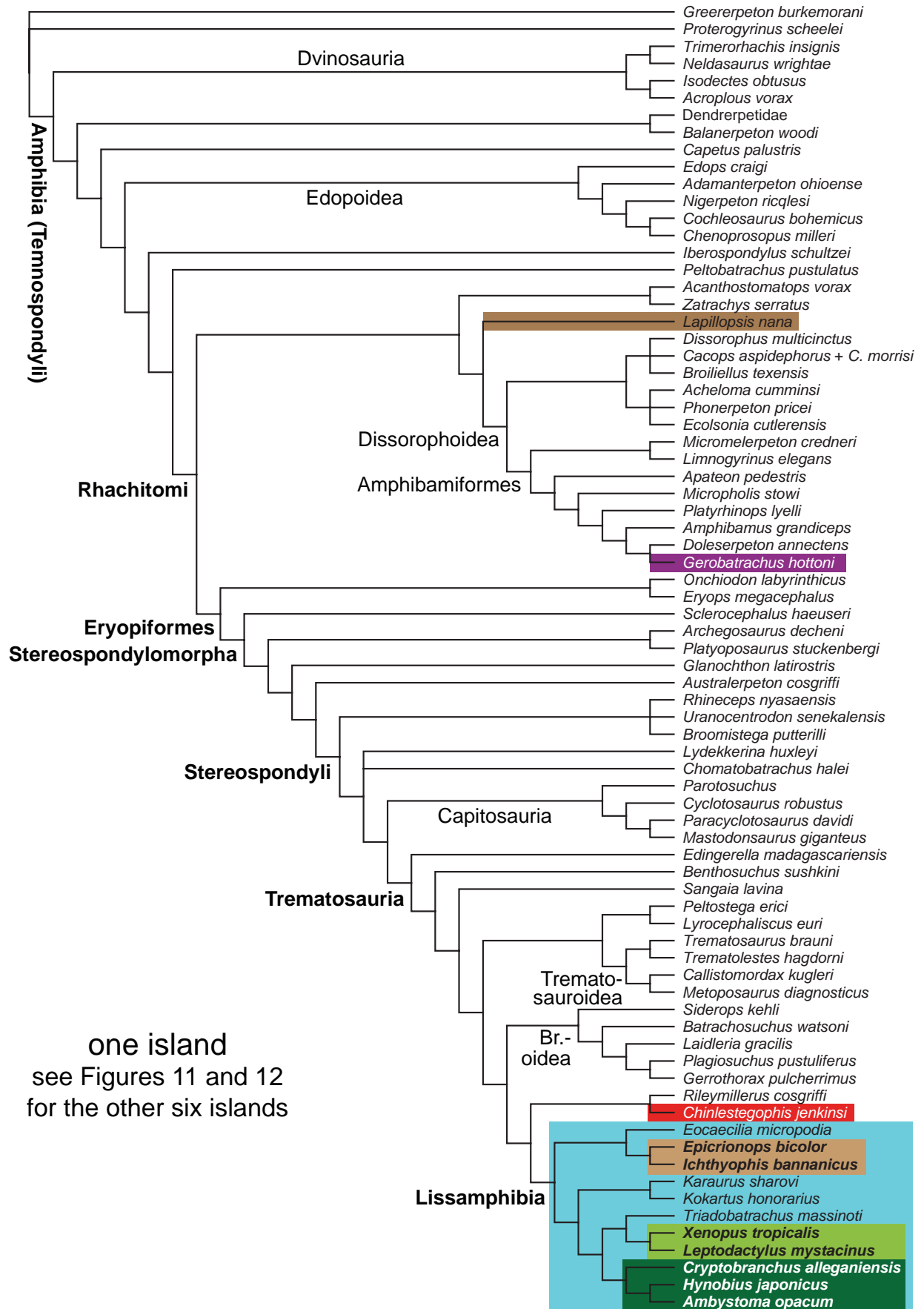


**Figure 10.** Strict consensus tree of some of the 1341 MPTs recovered in analysis e1 (published matrix of Pardo et al. [2017a] after revision, all characters unordered). For the other MPTs, see Figs. 11 and 12. Br.-oidea = Brachyopoidea.

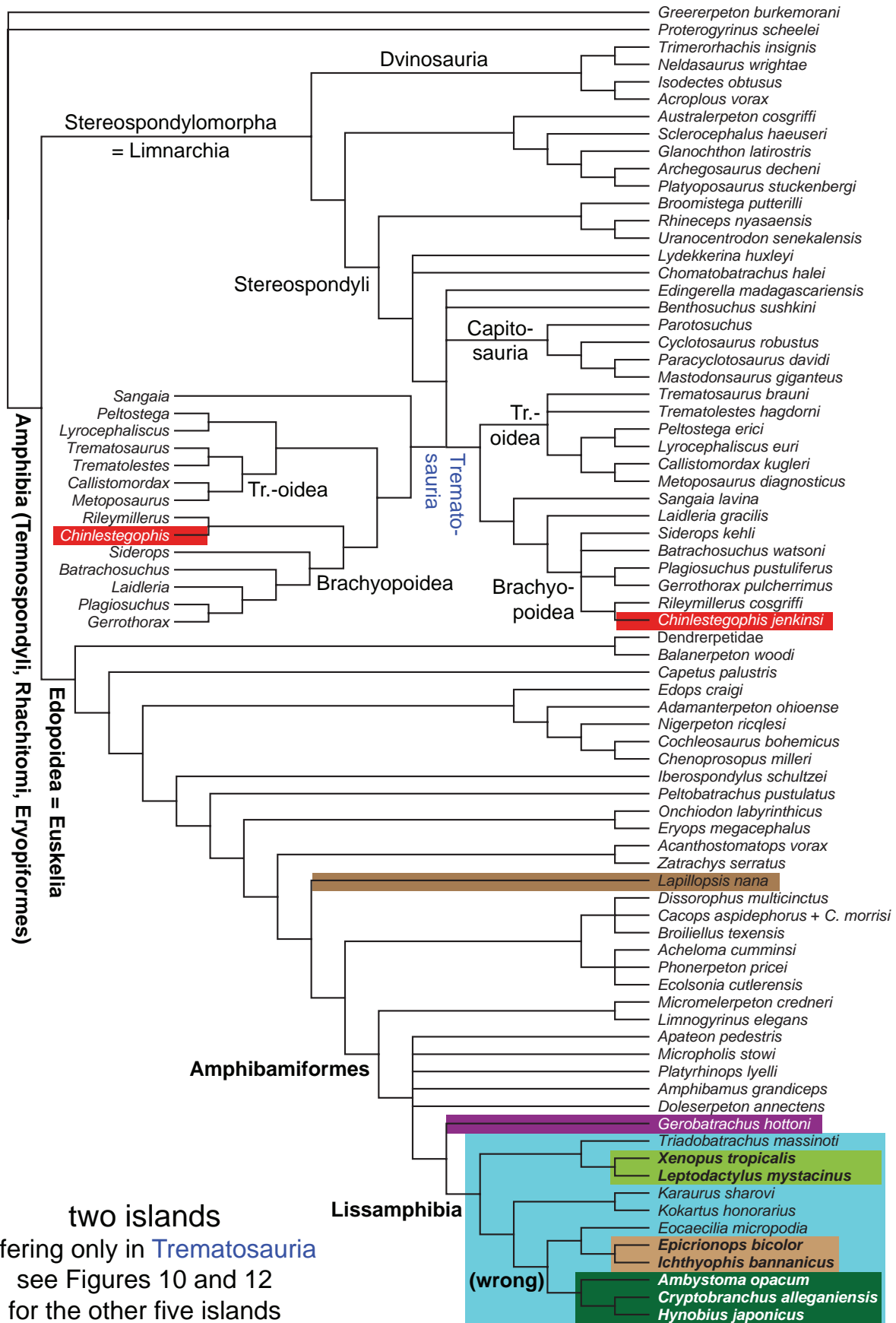
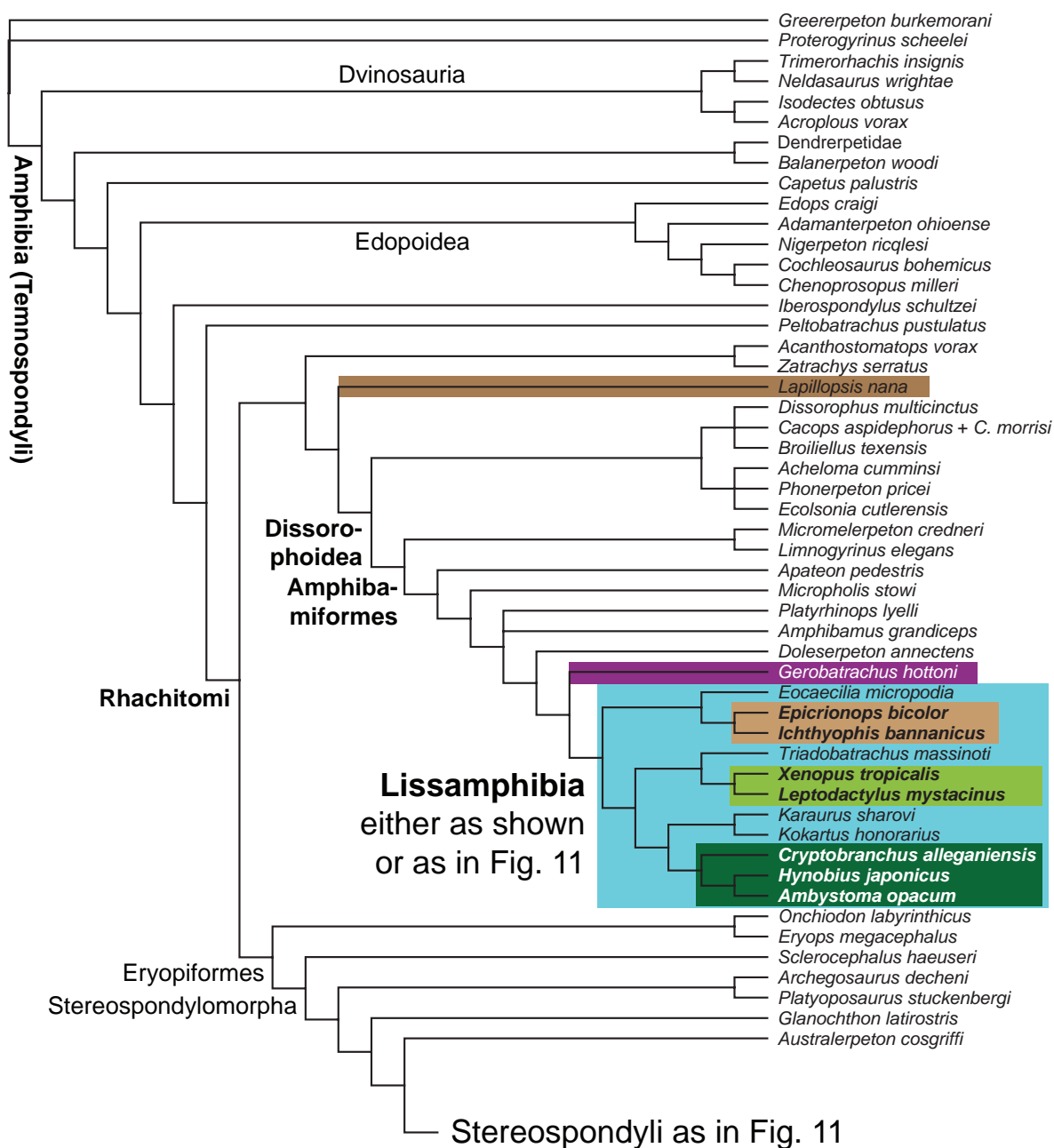


**Figure 11.** Strict consensus of each of two further islands of MPTs from analysis e1. For space reasons, one of the two resolutions of Trematosauria is mirrored and presented without species names. For the other MPTs, see Figs 10, 12. Tr.-oidea = Trematosauroida. The branch marked “(wrong)” contradicts the molecular consensus (Hime et al. 2020).



four islands  
(both combinations of both  
resolutions of Lissamphibia  
and Stereospondyli occur)  
see Figures 10 and 11  
for the other three islands

**Figure 12.** Strict consensus of each of the remaining four islands of MPTs from analysis e1. Except for Lissamphibia, the part depicted here is identical in all four islands; Lissamphibia is resolved either as shown or as in Fig. 11, Stereospondyli is resolved as in Fig. 11 (with both options shown there for Trematosauria). For the other MPTs, see Figs 10, 11.

First, we stress that the unpublished matrix (our analysis a1, see Table 1; Fig. 2; Pardo et al. 2017a: fig. S6) yielded a commonly recovered Lissamphibia, nested within dissorophoids and optionally containing *Gerobatrachus* but never *Chinlestegophis*. This is important because it suggests that

when a broader sample of extinct tetrapods is included, a more mainstream hypothesis of both lissamphibian ancestry and Paleozoic tetrapod relationships is produced, and the stereospondyls represented in this matrix, *Rileymillerus* and *Chinlestegophis*, are distanced from lissamphibian

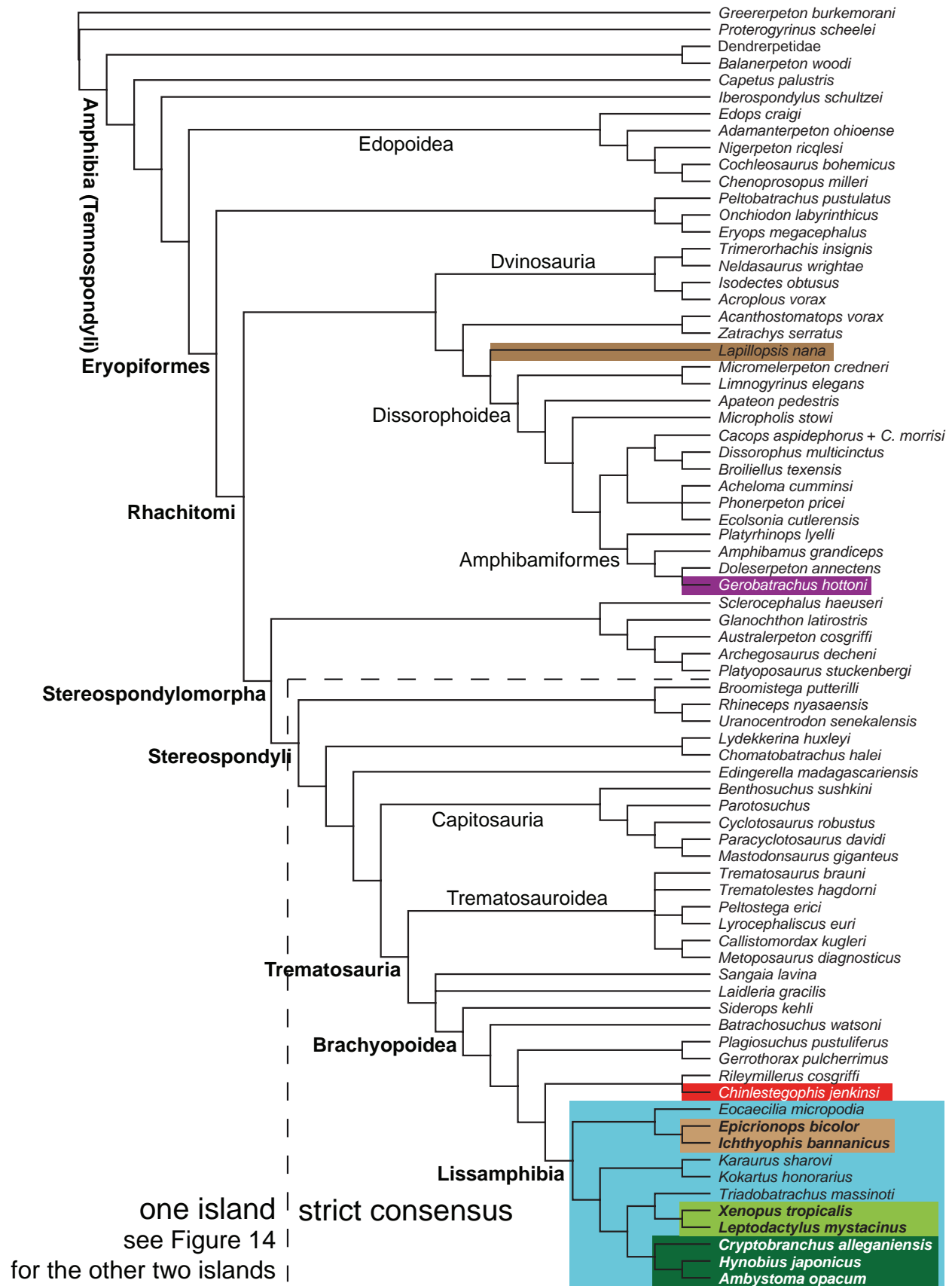


**Figure 13.** Strict consensus of all (to the right and below the dashed line) or some (to the left and above the stippled line) of the 99 MPTs recovered in analysis e2 (published matrix of Pardo et al. [2017a] after revision, clinal characters ordered). See Fig. 14 for the remaining MPTs.

origins. Constraining *Eocaecilia* to nest among lepospondyls (analysis a2; Fig. 3) results in only slightly longer trees (4 steps added to the 1450 of the unconstrained trees) that are not significantly different from the unconstrained trees ( $p$  between 0.62 and 0.72 according to the three usual tests) despite conforming to the “lepospondyl hypothesis” of amphibian origins.

All of our remaining analyses focused on the published matrix of Pardo et al. (2017a). Unsurprisingly, we confirmed (analysis b) the results of Marjanović and Laurin (2019: fig. 30I–K), Serra Silva and Wilkinson (2021) and Gee (2022) that Pardo et al. (2017a) found all MPTs that fit this matrix, that the MRC tree they reported is accurate as such, and that the MRC tree is a highly incomplete representation of the MPTs: it is equally parsimonious for Batrachia and Gymnophiona to lie in Stereospondyli or Amphibamiformes, and for them to form Lissamphibia or not, which may or may not contain *Chinlestegophis*. We further contribute the first fully published bootstrap analysis of this matrix (Fig. 4, Suppl. material 2: table S1); contrary to Pardo et al. (2017a: fig. S7B), it supports diphyly of extant amphibians, although the support is not strong (52% for grouping *Chinlestegophis* with the caecilians; 43% for grouping *Gerobatrachus* with the batrachians; only 35% for grouping all dissorophoids with the batrachians to the exclusion of any caecilians).

Pardo et al. (2017a: fig. S7B) found no bootstrap values of 50% or higher on any node that separates caecilians and batrachians. Differences in bootstrap settings may explain why our results differ somewhat from those of Pardo et al. (2017a); we used 200 bootstrap replicates of 500 addition-sequence replicates each, whereas Pardo et al. (2017a) used 1000 bootstrap replicates of 100 addition-sequence replicates each (J. Pardo pers. comm. 2023; the settings were not published).

However, adding Albanerpetidae to the matrix (analysis c; Fig. 5) confirms the result of Daza et al. (2020): Lissamphibia is found in Amphibamiformes in all MPTs, while *Chinlestegophis* is always a stereospondyl. The omission of albanerpetids from the original matrix was clearly a suboptimal choice, given that all studies published since their discovery over half a century ago support close affinities between albanerpetids and lissamphibians, if not a position among lissamphibians (e.g., Estes 1969; Estes and Hoffstetter 1976; Fox and Naylor 1982; McGowan and Evans 1995; Maddin et al. 2013; Daza et al. 2020; Kligman et al. 2023). Even the most unorthodox analysis of albanerpetid affinities that we know of suggested close affinities to batrachians (McGowan 2002).

The effect of ordering characters within the original published matrix (i.e., without Albanerpetidae and without corrections other than renumbering the states of some ordered characters) (analysis d1; Fig. 6) was to decrease the number of islands from five to one: Lissamphibia (which has 46% bootstrap support) forms the sister group of the stereospondyls *Chinlestegophis* and

*Rileymillerus*. This arrangement only occurs in 29% of the bootstrap replicates, however (Fig. 7; Suppl. material 2: table S2). Adding Albanerpetidae (analysis d2) moved Lissamphibia into the amphibamiform dissorophoids; *Chinlestegophis* and *Rileymillerus* remained brachyopoid stereospondyls (Fig. 8). Bootstrapping this analysis (Fig. 9; Suppl. material 2: table S3) revealed increased, if still modest, support for Lissamphibia (52%) and weak support for any position of that clade, but comparatively strong support against a position close to *Gerobatrachus* or *Doleserpeton* (62%).

A modest revision of the published matrix, without Albanerpetidae, replicated the basic results of analyses c and d1 as equally parsimonious when all characters were unordered (analysis e1; Figs 10–12). Ordering (analysis e2; Figs 13, 14) restricted Lissamphibia to Stereospondyli as in analysis d1 (unmodified matrix, likewise ordered, likewise without Albanerpetidae). Adding Albanerpetidae without ordering (analysis e3; Fig. 15) essentially replicated analysis c; ordering (analysis e4; Figs 16, 17) introduced variation within Lissamphibia but kept it in the same place as in analysis c—with strong bootstrap support: a lissamphibian-stereospondyl clade is not compatible with the bootstrap tree (Fig. 18) and only occurs in 10% of the replicates (Suppl. material 2: table S4). The 77% support for Lissamphibia (with Albanerpetidae) excluding *Chinlestegophis* (or *Rileymillerus*, *Gerobatrachus* or any other traditional non-member) is worth highlighting.

In all four cases, ordering increased the resolution of the results. We interpret this as an example of ordering bringing out phylogenetic signal in data, congruent with results from simulations and some empirical examples; note that ordering does not automatically increase the net resolution (Marjanović and Laurin 2008, 2019; Grand et al. 2013; Rineau et al. 2015, 2018; and references therein).

Strikingly, none of the trees from analyses c, d or e (most parsimonious or bootstrap) support affinities between *Chinlestegophis* and caecilians to the exclusion of other lissamphibians. The bootstrap analysis of the original matrix under original conditions (analysis b; Fig. 4, Suppl. material 2: table S1) only weakly supports diphyly of extant amphibians and an exclusive clade of *Chinlestegophis* and the three caecilians (bootstrap frequency of 52%) or an exclusive clade of frogs, salamanders, karaurids and *Gerobatrachus* (frequency of 43%). Our highly restricted revisions to the published matrix (analyses e1, e2; see Gee 2022 for a generally much more thorough revision), as well as the addition of Albanerpetidae to the taxon sample (analysis c) or the combination of both (analyses e3, e4), resulted in an exclusive clade comprising lissamphibians being nested among dissorophoids (analyses c, e1, e3, e4 and its bootstrap analysis), or Lissamphibia as sister to *Chinlestegophis* + *Rileymillerus* within Stereospondyli (analyses e1, e2). The former is the currently most widespread hypothesis on the origin of the extant amphibian clades; the latter is new, but considerably less novel than extant amphibian diphyly as proposed by Pardo et al. (2017a).

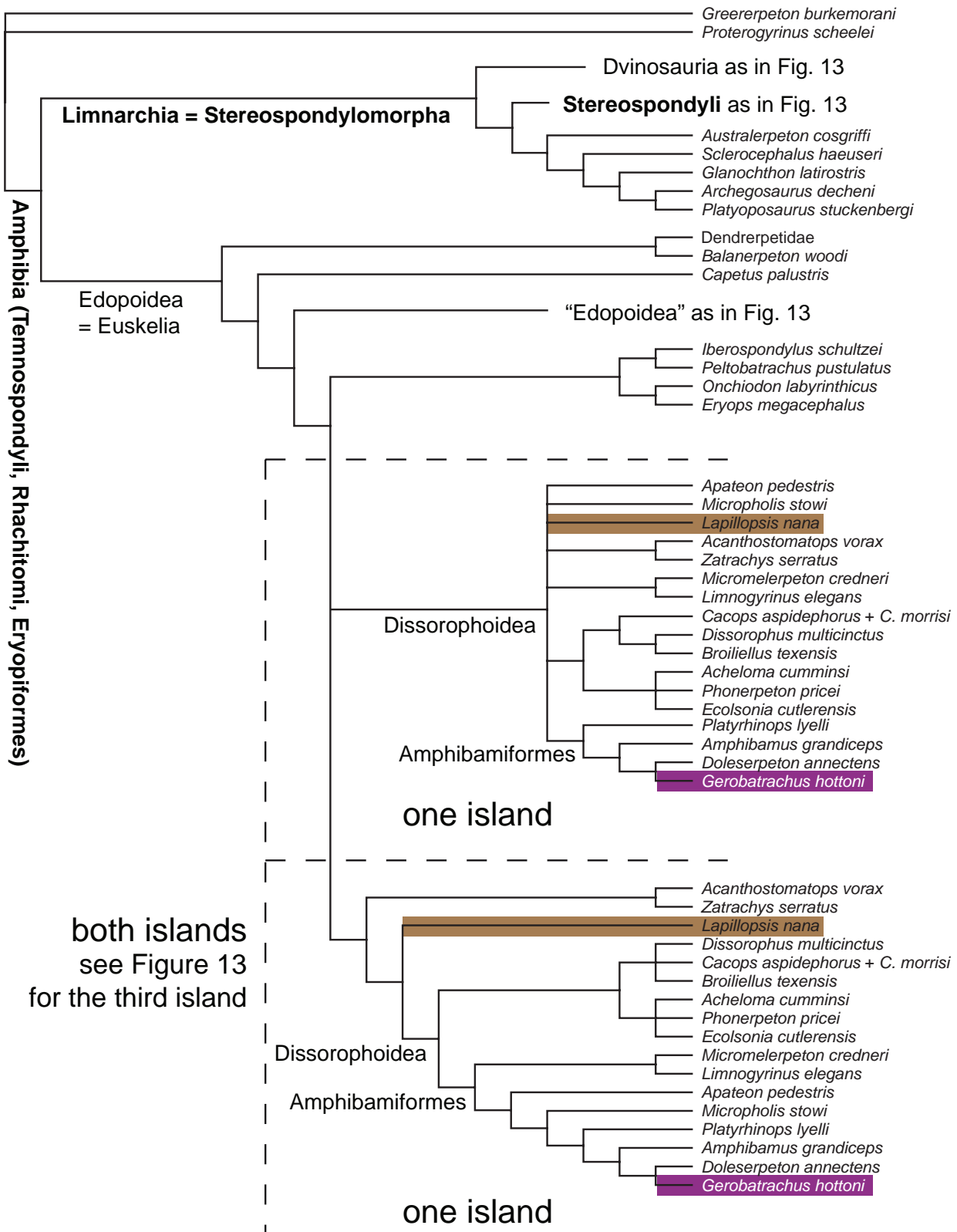


**Figure 14.** Strict consensus of the remaining MPTs recovered in analysis e2 (published matrix of Pardo et al. [2017a] after revision, clinal characters ordered). See Fig. 13 for the MPTs not represented here and for the clades shown collapsed here.

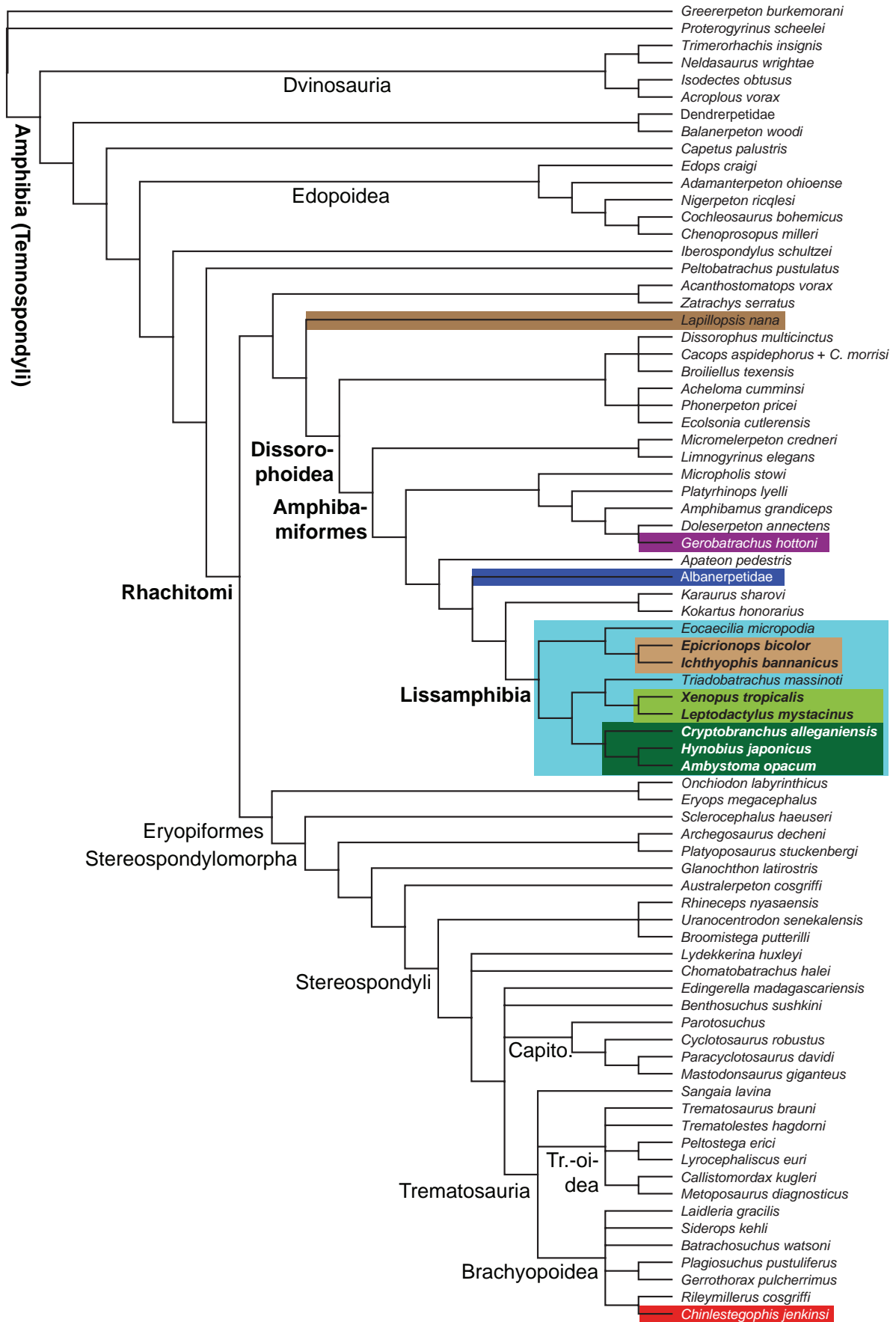


**Figure 15.** Strict consensus of the 297 MPTs recovered in analysis e3 (published matrix of Pardo et al. [2017a] after revision, Albanerpetidae added from Daza et al. [2020], all characters unordered). Capito. = Capitosauria; Tr.-oidea = Trematosauroida.

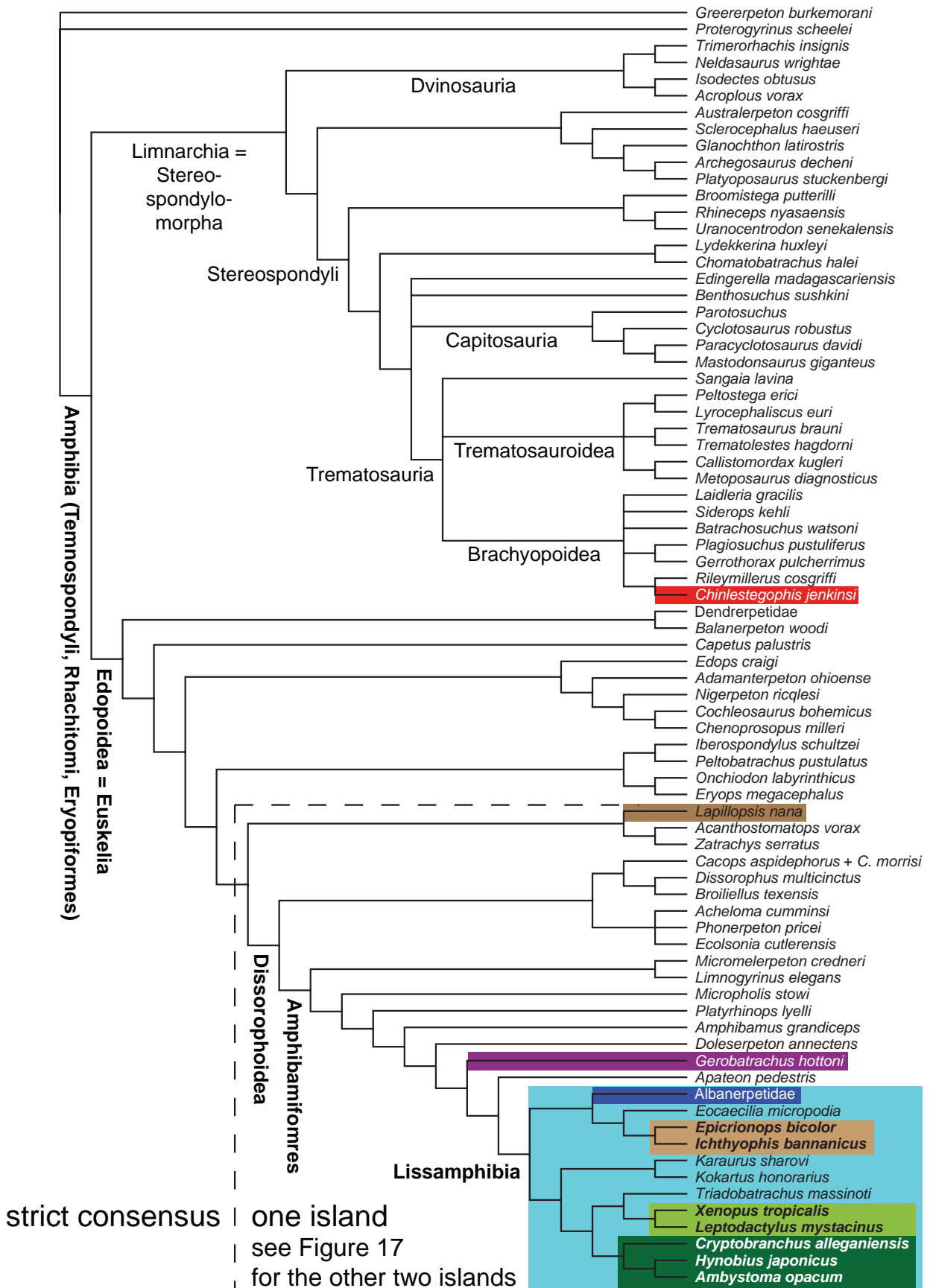


**Figure 16.** Strict consensus of all (to the left and above the stippled line) or some (to the right and below the stippled line) of the 81 MPTs recovered in analysis e4 (published matrix of Pardo et al. [2017a] after revision, Albanerpetidae added from Daza et al. [2020], clinal characters ordered). For the other MPTs, see Fig. 17.

The published matrix of Pardo et al. (2017a) contains some data that suggest affinities between Lissamphibia and the *Chinlestegophis* + *Rileymillerus* clade, always within Stereospondyli, as recovered in analyses b (as one of several equal options), d1 (if only with 29% bootstrap support), e1 (as one of two options) and e2. Although weakly supported, the fact that this result occurred in the original (analyses b, d1) and the revised matrix (analyses e1, 2) suggests that *Chinlestegophis* may contribute important information about amphibian evolution in the context of the “temnospondyl hypothesis”, even if it cannot be supported specifically as a stem-caecilian. More likely, however, it may highlight convergence between the *Chinlestegophis* + *Rileymillerus* clade and lissamphibians in general or caecilians in particular; this is supported to an extent by our bootstrap of analysis e4 (Fig. 18; Suppl. material 2: table S4), where *Chinlestegophis* + *Rileymillerus* were recovered next to Lissamphibia in only 29% and as gymnophionomorphs in only 15% of the bootstrap replicates while a lissamphibian-stereospondyl clade only has 10% bootstrap support (all three groupings are incompatible with the bootstrap tree: Fig. 18), as well as by the bootstrap analysis conducted by Kligman et al. (2023: extended data figure 6), where Lissamphibia excluding *Chinlestegophis* and *Rileymillerus* occurred in 55% of the replicates and Stereospondyli including a *Chinlestegophis* + *Rileymillerus* clade in 57%. Minimally, our results highlight the importance of albanerpetids—sampled in analyses c, d2, e3 and e4—for understanding lissamphibian relationships.

Pardo et al. (2017a) emphasized that the topology they presented was supported by Bayesian inference. As discussed above (Matrices, Methodologies, and Missteps: Bayesian inference of phylogeny), missing data have unpredictable, sometimes very strong, effects on parametric methods of phylogenetics such as Bayesian inference, while the non-parametric method called parsimony is unaffected by this particular issue and therefore safer for paleontological data. Matrix quality remains more important than the method of analysis (Simões et al. 2017; Marjanović and Laurin 2019; Gee 2021, 2022; and references therein).

## Assessment of qualitative arguments

As further support for a close relationship between *Chinlestegophis* and caecilians, Pardo et al. (2017a) proposed a number of features supposedly shared between both taxa, and in some cases with other stereospondyls. Most of them are coded in the matrix in some form. However, our review of these features (Materials and Methods: Evaluation of potential synapomorphies and revisions to the published matrix) finds serious problems in all of them; none supports placing caecilians as the sister taxon of *Chinlestegophis* (or *Chinlestegophis* + *Rileymillerus*), or in stereospondyls in general.

We note several other features, not discussed by Pardo et al. (2017a), by which *Chinlestegophis* resembles other stereospondyls but differs starkly from caecilians. The basicranial articulation in *Chinlestegophis* superficially

resembles that of *Eocaecilia* and Gymnophiona. However, in *Chinlestegophis*, the basicranial joint forms a strong girder, tightly sutured (Pardo et al. 2017a), similar to the condition seen in other stereospondyls. In caecilians, the basicranial joint is instead loosely constructed, with thick cartilage covering the bony joint surfaces of both the *os basale* and the (epi)pterygoid or pterygoquadrate (Maddin et al. 2012b). Furthermore, *Chinlestegophis* has well-developed posttemporal fenestrae, as in brachyopoid stereospondyls, while in lissamphibians and albanerpetids these fenestrae are absent.

What little is known and described of the postcranial skeleton of *Chinlestegophis* (Pardo et al. 2017a: fig. S5) also resembles other stereospondyls but starkly differs from caecilians. The interclavicle of *Chinlestegophis* is a large plate, as usual for stereospondyls; in lissamphibians and albanerpetids, no interclavicle is known. Similarly, the clavicles consist mostly of a large plate and look unremarkable for a stereospondyl in all details of their shape; clavicles are absent in albanerpetids, caecilians (including *Eocaecilia*) and salamanders, and those of frogs are robust curved struts more similar to those of extant amniotes. A few neural arches are preserved in *Chinlestegophis*, but centra are not; this is standard for morphologically immature temnospondyls, but only observable (as presence or absence of ossification) in a very short phase in the ontogeny of frogs and hynobiid salamanders, and not known in caecilians—in *Gegeneophis* and in *Caecilia orientalis* Taylor, 1968, the centra ossify before the neural arches (Müller 2006; Pérez et al. 2009). Indeed, early ossification of the centra (earlier than the neural arches or not long after them), quickly followed by suturing or even fusion to the neural arches, is a synapomorphy of lissamphibians and probably a few amphibamiforms (notably *Doleserpeton* and *Gerobatrachus*) under the “temnospondyl hypothesis”, or of Seymouriamorpha, Chroniosuchia and Tetrapoda under the “lepospondyl hypothesis” (Laurin and Reisz 1997; Danto et al. 2019). Full neurocentral fusion is not found outside these clades (and Albanerpetidae), but is found in all known vertebrae of *Eocaecilia* (Jenkins et al. 2007) and the lone vertebra referred to *Funcusvermis* (Kligman et al. 2023). The ribs of *Chinlestegophis* are, plesiomorphically, longer than three successive vertebrae; they are shorter in amphibamiforms and a few select lepospondyls (Marjanović and Laurin 2008, 2019), and much shorter, about as long as one vertebra, in albanerpetids and all lissamphibians except a few peramorphic salamandrids (Marjanović and Witzmann 2015, and references therein). The only known postcranial similarity to caecilians is body elongation; the massive dermal shoulder girdle does not suggest limb reduction, and indeed the presumed ulna has an unremarkable size.

## Homoplastic rather than stepwise evolution

Interpretations of functional biology and evolutionary trends rely on our perspective of phylogenetic relationships. In the original description of *Chinlestegophis*, once

rest of tree identical to overall strict consensus in Figure 16

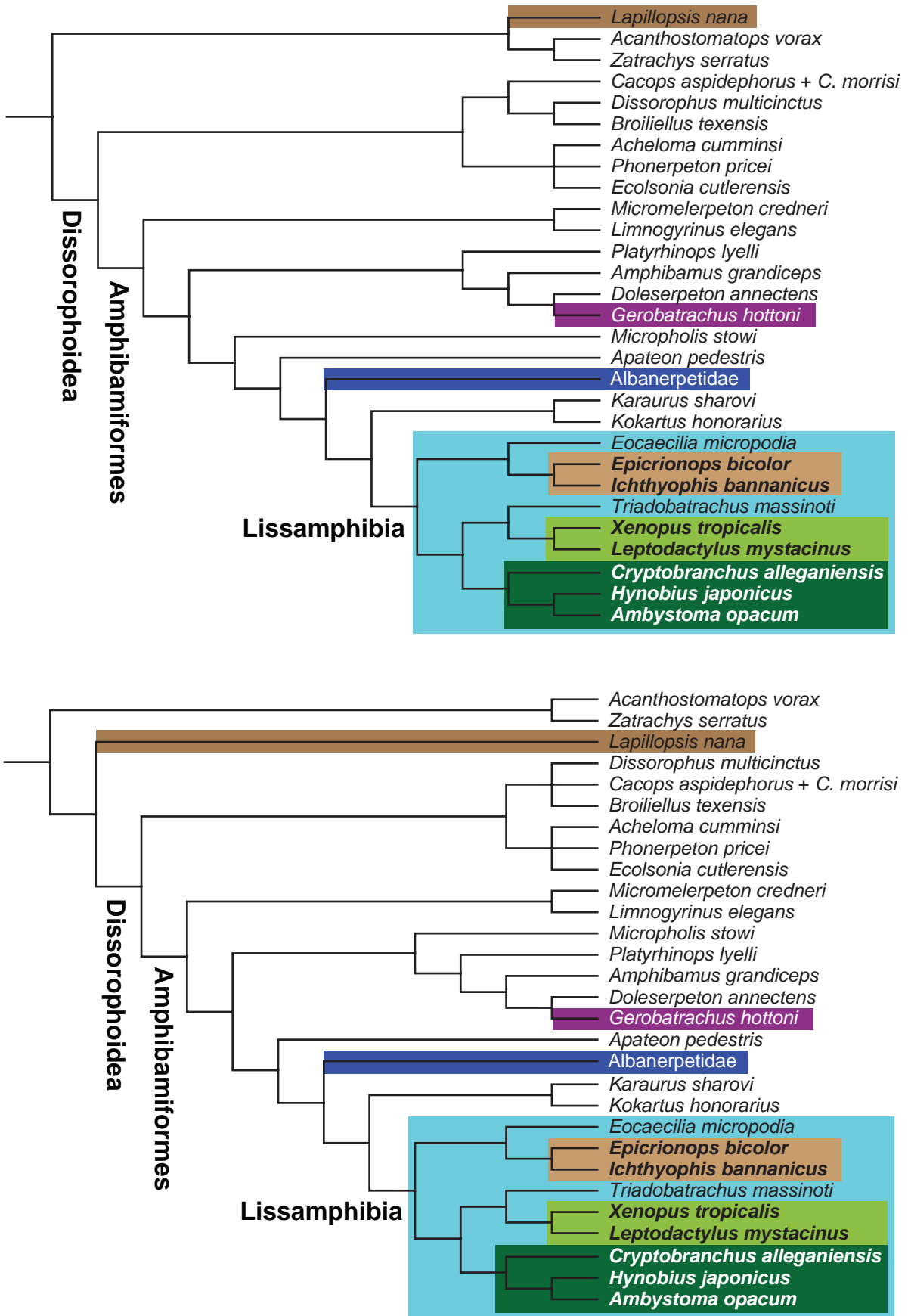


**Figure 17.** Strict consensus of each of the remaining two islands of MPTs from analysis e4. The remainder of the tree is identical in all three islands and not repeated here; see Fig. 16.

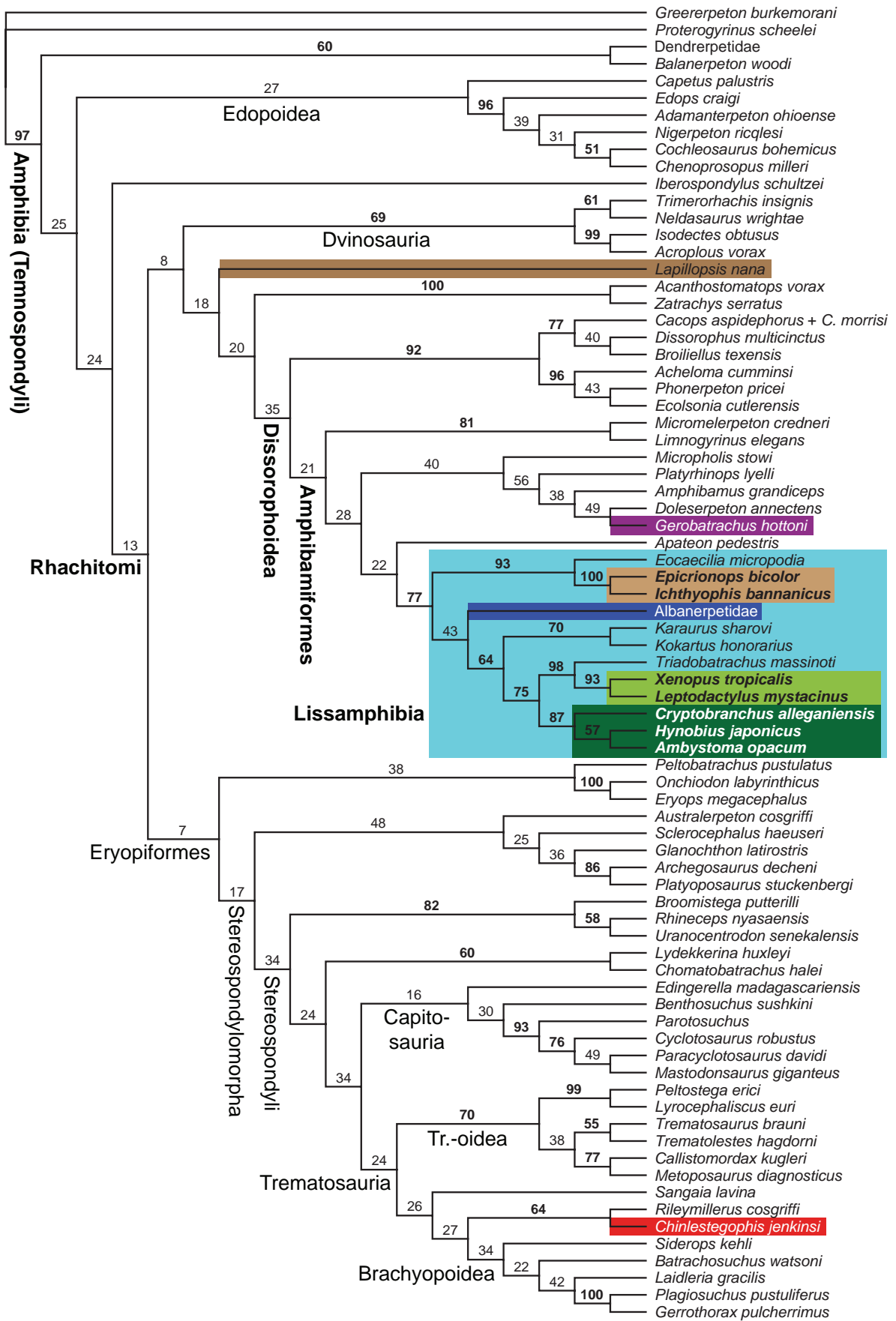


**Figure 18.** Bootstrap tree of analysis e4 (published matrix of Pardo et al. [2017a] after revision, Albanerpetidae added from Daza et al. [2020], clinal characters ordered). Bootstrap values  $\geq 50\%$  in boldface. Tr.-oidea = Trematosauroidae.

a consensus tree was selected and reported, a number of the characteristics used in the matrices and discussed above were used to infer a stepwise evolution of traits toward the specialized fossorial and head-first burrowing lifestyle of caecilians. Those features include fusion of the lacrimal + maxilla and exoccipital + opisthotic (interpreted as stages in the consolidation of the skull), repositioning of the jaw suspension, small and laterally oriented eyes, etc. However, as we demonstrate above, most of those features have a wider distribution across Paleozoic tetrapods or present confounding problems of homoplasy across many disparate clades, extinct and extant.

In particular, we regard as unfortunate the aforementioned removal of all lepospondyls from the unpublished matrix to create the published matrix after the initial recovery of *Chinlestegophis* as a temnospondyl by Pardo et al. (2017a). Potential affinities between lepospondyls and lissamphibians have been controversial for more than two decades (Anderson 2001; Marjanović and Laurin 2008, 2009, 2013, 2019; Laurin et al. 2022; Jansen and Marjanović 2022; Mann et al. 2022; and references therein). Thus, including lepospondyls in tests of the origins of extant amphibians is critical to represent the full range of morphology during the Paleozoic and reveal potential homoplasy. Removing those taxa from analyses could make it more likely that any elongate, fossorial, or burrowing taxa such as *Chinlestegophis* and caecilians be placed together incorrectly in the phylogeny.

Schoch et al. (2020) added three lepospondyls to the published matrix of Pardo et al. (2017a), but they did not add any characters that would help resolve their phylogeny or their relationship to lissamphibians. This was not changed by Kligman et al. (2023), in whose results those three lepospondyls form the sister-group of *Greererpeton* (Kligman et al. 2023: extended data figs 5–7), an Early Carboniferous colosteid that is a more appropriate outgroup than the anthracosaur *Proterogyrinus* that was used as such.

Considering that alternative hypotheses of relationships are equally supported by the published matrix, even without broader taxonomic sampling to include lepospondyls, the proposed stepwise evolution of caecilian features falls apart. Rather than traits linking *Chinlestegophis* and caecilians, those same characteristics appear to represent homoplasy, as shown in trees that place *Chinlestegophis* close to but outside Lissamphibia (our analyses a, d, e2 and some MPTs of b and e1 plus the bootstrap of b) or far away (our analyses c, e3, e4 and some MPTs of b and e1).

## Evolutionary ecology

The grooves for the lateral-line organ identified by Pardo et al. (2017a) on the skull of *Chinlestegophis* indicate an animal that was strictly aquatic for at least part of its adult life. In contrast, there is no evidence of lateral-line grooves or other aquatic features in *Eocaecilia* or the admittedly fragmentary *Funcusvermis*, and among extant caecilians aquatic lifestyles are restricted to larvae

(of those few taxa that have them) and the highly nested clade Typhlonectidae. The inference of an aquatic lifestyle in *Chinlestegophis* is further supported by its poorly ossified vertebral column and probably also by its cranio-caudally elongate plate-like clavicles. Perhaps aquatic vs. terrestrial lifestyles explain why *Chinlestegophis* was able to coexist with caecilians like the slightly older *Funcusvermis*; the wide, flat vertebra referred to the latter lacks a neural spine, interpreted as a fossorial adaptation by Kligman et al. (2023).

## Matrix quality, taxon sampling and character sampling

The discussion above takes at face value both the coding and scoring of the two matrices, and their character and taxon samples, apart from our limited modifications in analyses c, d2 and e; but these issues deserve comments. We have not scrutinized the matrices in full (see Gee 2022 for a cautious but comprehensive treatment of the published matrix of Pardo et al. 2017a), as we wished only to test whether alternative topologies can be equally (or better) supported by the original matrices, and to show the impact of a few scoring changes that were obviously needed. The absence of lepospondyls in the matrix published by Pardo et al. (2017a) prevents us from looking into how many extra steps an origin of lissamphibians among them would imply, compared to an origin among temnospondyls. Similarly, the removal of characters that are variable only among lepospondyls prevents using the published matrix as a starting point for such comparisons; unfortunately, this was not changed by Schoch et al. (2020) or Kligman et al. (2023) despite the former's addition of three lepospondyl OTUs which the latter then retained. The heretofore unpublished precursor matrix remains available for this purpose, but it would need to be updated and greatly enlarged; in its present form, only four extra steps need to be added to the original 1450 to make an odd version of the lepospondyl hypothesis possible.

## Conclusions

Published in one of the most prestigious journals, the description of *Chinlestegophis* (Pardo et al. 2017a) resulted in a new hypothesis about the origins of the extant amphibian clades and a new scenario for the origin of caecilians and their fossorial lifestyle that has attracted attention far beyond that of specialist researchers (Pough et al. 2022). We show that these exciting proposals are poorly supported by the original datasets and the original methods of analysis, as well as by limited revisions to one of the datasets aimed at eliminating the most conspicuous cases of character redundancy and a few questionable anatomical interpretations of *Chinlestegophis* and other taxa. The question of lissamphibian origins

remains unsolved, although our revisions to the matrix reveal further support for Lissamphibia excluding *Chinlestegophis* and any Paleozoic taxa. In any case, we join Kligman et al. (2023) in cautioning against calibrating the divergence of caecilians and batrachians according to the phylogenetic hypothesis of Pardo et al. (2017a), i.e., by using the Late Carboniferous age of certain dissorophoid temnospondyls as the calibration date.

Concerning phylogenetics, we reiterate that the majority-rule consensus is not a useful representation of the result of a parsimony analysis, and that not all issues with Bayesian analysis of matrices with missing data have been solved; but most importantly, matrix quality remains paramount in phylogenetic analysis. This concerns typographic errors, misinterpretations of published literature, redundant characters (in the dataset we revised, the double toothrow in the lower jaw of caecilians was coded as seven characters that an analysis could only treat as independent), characters that represent two or more independently varying features, and inconsistencies in scoring. As previously pointed out (e.g. Marjanović and Laurin 2019; Kligman et al. 2023; and references in both), avoiding, detecting and mitigating these issues is time-consuming but not difficult.

## Acknowledgments

Jason Pardo and Adam Huttenlocker kindly sent us both matrices, and J. Pardo and Ben Kligman discussed certain characters with us. The reviewers Marvalee Wake and Christian Sidor led us to improve the clarity of our writing. D. M.'s understanding of current issues in phylogenetics benefited from a course taught by Tiago Simões and Oksana Vernygora and organized by Transmitting Science.

## References

- Anderson JS (2001) The phylogenetic trunk: maximal inclusion of taxa with missing data in an analysis of the Lepospondyli (Vertebrata, Tetrapoda). *Systematic Biology* 50: 170–193. <https://doi.org/10.1080/10635150119889>
- Anderson JS (2007) Incorporating ontogeny into the matrix: a phylogenetic evaluation of developmental evidence for the origin of modern amphibians. In: Sues H-D, Anderson JS (Eds) *Major transitions in vertebrate evolution*. Indiana University Press, Bloomington, 182–227.
- Anderson JS, Reisz RR, Scott D, Fröbisch NB, Sumida SS (2008a) A stem batrachian from the Early Permian of Texas and the origin of frogs and salamanders. *Nature* 453: 515–518. <https://doi.org/10.1038/nature06865>
- Anderson JS, Henrici AC, Sumida SS, Martens T, Berman DS (2008b) *Georgenthalia clavinasica*, a new genus and species of dissorophoid temnospondyl from the Early Permian of Germany, and the relationships of the family Amphibamidae. *Journal of Vertebrate Paleontology* 28: 61–75. [https://doi.org/10.1671/0272-4634\(2008\)28\[61:G-CANGA\]2.0.CO;2](https://doi.org/10.1671/0272-4634(2008)28[61:G-CANGA]2.0.CO;2)
- Atkins JB, Reisz RR, Maddin HC (2019) Braincase simplification and the origin of lissamphibians. *PLOS ONE* 14: e0213694. <https://doi.org/10.1371/journal.pone.0213694>
- Bolt JR, Chatterjee S (2000) A new temnospondyl amphibian from the Late Triassic of Texas. *Journal of Paleontology* 74: 670–683. [https://doi.org/10.1666/0022-3360\(2000\)074<0670:ANTAFT>2.0.CO;2](https://doi.org/10.1666/0022-3360(2000)074<0670:ANTAFT>2.0.CO;2)
- Boy JA (1990) Über einige Vertreter der Eryopoidea (Amphibia: Temnospondyli) aus dem europäischen Rotliegend (? höchstes Karbon – Perm) 3. *Onchiodon*. *Paläontologische Zeitschrift* 64: 287–312. <https://doi.org/10.1007/BF02985720>
- Carroll RL (2007) The Palaeozoic ancestry of salamanders, frogs and caecilians. *Zoological Journal of the Linnean Society* 150: 1–140. <https://doi.org/10.1111/j.1096-3642.2007.00246.x>
- Crotty SM, Minh BQ, Bean NG, Holland BR, Tuke J, Jeremiin LS, von Haeseler A (2019 [printed 2020]) GHOST: recovering historical signal from heterotachously evolved sequence alignments. *Systematic Biology* 69: 249–264. <https://doi.org/10.1093/sysbio/syz051>
- Danto M, Witzmann F, Kamenz S, Fröbisch N (2019) How informative is vertebral development for the origin of lissamphibians? *Journal of Zoology* 307: 292–305. <https://doi.org/10.1111/jzo.12648>
- Daza JD, Stanley EL, Bolet A, Bauer AM, Arias JS, Čerňanský A, Bevtit JJ, Wagner P, Evans SE (2020) Enigmatic amphibians in mid-Cretaceous amber were chameleon-like ballistic feeders. *Science* 370: 687–691. <https://doi.org/10.1126/science.abb6005>
- Dilkes D (2015 [for 2014]) Carpus and tarsus of Temnospondyli. *Vertebrate Anatomy Morphology Palaeontology* 1: 51–87. <https://doi.org/10.18435/B5MW2Q>
- Duellman WE, Trueb L (1994) *Biology of Amphibians*. Paperback edition. The Johns Hopkins University Press, Baltimore-London, [xxi +] 670 pp. <https://books.google.com/books?id=CzxVvKmrIgC>
- Estes R (1969) Prosirenidae, a new family of fossil salamanders. *Nature* 224: 87–88. <https://doi.org/10.1038/224087a0>
- Estes R, Hoffstetter R (1976) Les urodèles du Miocène de la Grive-Saint-Alban (Isère, France). *Bulletin du Muséum national d'Histoire naturelle, Paris* 57: 297–343.
- Evans SE, Sigogneau-Russell D (2001) A stem-group caecilian (Lissamphibia: Gymnophiona) from the Lower Cretaceous of North Africa. *Palaeontology* 44: 259–273. <https://doi.org/10.1111/1475-4983.00179>
- Fox RC, Naylor BG (1982) A reconsideration of the relationships of the fossil amphibian *Albanerpeton*. *Canadian Journal of Earth Sciences* 19: 118–128. <https://doi.org/10.1139/e82-009>
- Gee BM (2021) Returning to the roots: resolution, reproducibility, and robusticity in the phylogenetic inference of Dissorophidae (Amphibia: Temnospondyli). *PeerJ* 9: e12423. <https://doi.org/10.7717/peerj.12423>
- Gee BM (2022) The disadvantage of derivation: conserved systematic flaws in primary data have repeatedly biased the phylogenetic inference of Temnospondyli (Tetrapoda, Amphibia). *bioRxiv*. <https://doi.org/10.1101/2022.06.22.496729>
- Gee BM, Haridy Y, Reisz RR (2017) Histological characterization of denticulate palatal plates in an Early Permian dissorophoid. *PeerJ* 5: e3727. <https://doi.org/10.7717/peerj.3727>
- Glienke S (2013) A taxonomic revision of *Batropetes* (Amphibia, Microsauria) from the Rotliegend (basal Permian) of Germany. *Neues Jahrbuch für Geologie und Paläontologie – Abhandlungen* 269: 73–96. <https://doi.org/10.1127/0077-7749/2013/0336>
- Glienke S (2015) Two new species of the genus *Batropetes* (Tetrapoda, Lepospondyli) from the Central European Rotliegend (basal Permian) in Germany. *Journal of Vertebrate Paleontology* 35: e918041. <https://doi.org/10.1080/02724634.2014.918041>
- Goloboff PA, Pittman M, Pol D, Xu X (2018 [printed 2019]) Morphological data sets fit a common mechanism much more poorly than

- DNA sequences and call into question the Mkv model. *Systematic Biology* 68: 494–504. <https://doi.org/10.1093/sysbio/syy077>
- Goloboff PA, Torres A, Arias JS (2017 [printed 2018]) Weighted parsimony outperforms other methods of phylogenetic inference under models appropriate for morphology. *Cladistics* 34: 407–437. <https://doi.org/10.1111/cla.12205>
- Grand A, Corvez A, Duque Velez LM, Laurin M (2013) Phylogenetic inference using discrete characters: performance of ordered and unordered parsimony and of three-item statements. *Biological Journal of the Linnean Society* 110: 914–930. <https://doi.org/10.1111/bij.12159>
- Hime PM, Lemmon AR, Lemmon ECM, Prendini E, Brown JM, Thomson RC, Kratochvil JD, Noonan BP, Pyron RA, Peloso PL, Kortyna M, Keogh J, Donnellan S, Lockridge Mueller R, Raxworthy C, Kunte K, Ron S, Das S, Gaitonde N, Green D, Labisko J, Che J, Weisrock D (2020 [printed 2021]) Phylogenomics reveals ancient gene tree discordance in the amphibian tree of life. *Systematic Biology* 70: 49–66. <https://doi.org/10.1093/sysbio/syaa034>
- Huttenlocker AK, Pardo JD, Small BJ, Anderson JS (2013) Cranial morphology of recumbirostrans (Lepospondyli) from the Permian of Kansas and Nebraska, and early morphological evolution inferred by micro-computed tomography. *Journal of Vertebrate Paleontology* 33: 540–552. <https://doi.org/10.1080/02724634.2013.728998>
- Jansen M, Marjanović D (2022) The scratch-digging lifestyle of the Permian “microsauro” *Batropetes* Carroll & Gaskill, 1971 as a model for the exaptive origin of jumping locomotion in frogs. *Comptes Rendus Palevol* 21: 463–488. <https://doi.org/10.5852/cr-palevol-2022v21a23>
- Jenkins FA Jr, Walsh DM (1993) An Early Jurassic caecilian with limbs. *Nature* 365: 246–249. <https://doi.org/10.1038/365246a0>
- Jenkins FA Jr, Walsh DM, Carroll RL (2007) Anatomy of *Eocaecilia micropodia*, a limbed caecilian of the Early Jurassic. *Bulletin of the Museum of Comparative Zoology* 158: 285–365. [https://doi.org/10.3099/0027-4100\(2007\)158\[285:AOEMAL\]2.0.CO;2](https://doi.org/10.3099/0027-4100(2007)158[285:AOEMAL]2.0.CO;2)
- Jones ME, Benson RB, Skutschas P, Hill L, Panciroli E, Schmitt AD, Walsh SA, Evans SE (2022) Middle Jurassic fossils document an early stage in salamander evolution. *Proceedings of the National Academy of Sciences of the United States of America* 119: e2114100119. <https://doi.org/10.1073/pnas.2114100119>
- Kamei RG, Mauro DS, Gower DJ, Van Bocxlaer I, Sherratt E, Thomas A, Babu S, Bossuyt F, Wilkinson M, Biju S (2012) Discovery of a new family of amphibians from northeast India with ancient links to Africa. *Proceedings of the Royal Society B: Biological Sciences* 279: 2396–2401. <https://doi.org/10.1098/rspb.2012.0150>
- Keating JN, Sansom RS, Sutton MD, Knight CG, Garwood RJ (2020) Morphological phylogenetics evaluated using novel evolutionary simulations. *Systematic Biology* 69: 897–912. <https://doi.org/10.1093/sysbio/syaa012>
- King B (2019) Which morphological characters are influential in a Bayesian phylogenetic analysis? Examples from the earliest osteichthyans. *Biology Letters* 15: 20190288. <https://doi.org/10.1098/rsbl.2019.0288>
- King B (2021) Bayesian tip-dated phylogenetics in paleontology: topological effects and stratigraphic fit. *Systematic Biology* 70: 283–294. <https://doi.org/10.1093/sysbio/syaa057>
- Kligman BT, Gee BM, Marsh AD, Nesbitt SJ, Smith ME, Parker WG, Stocker MR (2023) Triassic stem caecilian supports dissorophoid origin of living amphibians. *Nature* 614: 102–107. <https://doi.org/10.1038/s41586-022-05646-5>
- Lasseron M, Allain R, Gheerbrant E, Haddoumi H, Jalil N-E, Métais G, Rage J-C, Vullo R, Zouhri S (2019) New data on the microvertebrate fauna from the Upper Jurassic or lowest Cretaceous of Ksar Metlili (Anoual Syncline, eastern Morocco). *Geological Magazine* 157: 367–392. <https://doi.org/10.1017/S0016756819000761>
- Laurin M (1998) The importance of global parsimony and historical bias in understanding tetrapod evolution. Part I. Systematics, middle ear evolution, and jaw suspension. *Annales des Sciences Naturelles, Zoologie, Paris, 13<sup>e</sup> Série* 19: 1–42. [https://doi.org/10.1016/S0003-4339\(98\)80132-9](https://doi.org/10.1016/S0003-4339(98)80132-9)
- Laurin M, Piñeiro G (2018) Response: Commentary: A reassessment of the taxonomic position of mesosaurs, and a surprising phylogeny of early amniotes. *Frontiers in Earth Science* 6: 220. <https://doi.org/10.3389/feart.2018.00220>
- Laurin M, Reisz RR (1997) A new perspective on tetrapod phylogeny. In: Sumida SS, Martin KLM (Eds) *Amniote origins: completing the transition to land*. Academic Press, San Diego, 9–59. <https://doi.org/10.1016/B978-012676460-4/50003-2>
- Laurin M, Arntzen JW, Báez AM, Bauer AM, Damiani R, Evans SE, Kupfer A, Larson A, Marjanović D, Müller H, Olsson L, Rage J-C, Walsh D (2020a) *Amphibia* C. Linnaeus 1758 [M. Laurin, J. W. Arntzen, A. M. Báez, A. M. Bauer, R. Damiani, S. E. Evans, A. Kupfer, A. Larson, D. Marjanović, H. Müller, L. Olsson, J.-C. Rage and D. Walsh], converted clade name. In: de Queiroz K, Cantino PD, Gauthier JA (Eds) *Phylonoms: An Implementation of PhyloCode*. CRC Press, Boca Raton, Florida, 765–771. <https://doi.org/10.1201/9780429446276>
- Laurin M, Arntzen JW, Báez AM, Bauer AM, Damiani R, Evans SE, Kupfer A, Larson A, Marjanović D, Müller H, Olsson L, Rage J-C, Walsh D (2020b) *Lissamphibia* C. Linnaeus 1758 [M. Laurin, J. W. Arntzen, A. M. Báez, A. M. Bauer, R. Damiani, S. E. Evans, A. Kupfer, A. Larson, D. Marjanović, H. Müller, L. Olsson, J.-C. Rage and D. Walsh], converted clade name. In: de Queiroz K, Cantino PD, Gauthier JA (Eds) *Phylonoms: An Implementation of PhyloCode*. CRC Press, Boca Raton, Florida, 773–778. <https://doi.org/10.1201/9780429446276>
- Laurin M, Lapauze O, Marjanović D (2022) What do ossification sequences tell us about the origin of extant amphibians? *Peer Community Journal* 2: e12. <https://doi.org/10.24072/pcjournal.89>
- Maddin HC, Olori JC, Anderson JS (2011) A redescription of *Carrolla craddocki* (Lepospondyli: Brachystelechidae) based on high-resolution CT, and the impacts of miniaturization and fossoriality on morphology. *Journal of Morphology* 272: 722–743. <https://doi.org/10.1002/jmor.10946>
- Maddin HC, Jenkins FA Jr, Anderson JS (2012a) The braincase of *Eocaecilia micropodia* (Lissamphibia, Gymnophiona) and the origin of caecilians. *PLOS ONE* 7: e50743. <https://doi.org/10.1371/journal.pone.0050743>
- Maddin HC, Russell AP, Anderson JS (2012b) Phylogenetic implications of the morphology of the braincase of caecilian amphibians (Gymnophiona). *Zoological Journal of the Linnean Society* 166: 160–201. <https://doi.org/10.1111/j.1096-3642.2012.00838.x>
- Maddin HC, Venczel M, Gardner JD, Rage J-C (2013) Micro-computed tomography study of a three-dimensionally preserved neurocranium of *Albanerpeton* (Lissamphibia, Albanerpetontidae) from the Pliocene of Hungary. *Journal of Vertebrate Paleontology* 33: 568–587. <https://doi.org/10.1080/02724634.2013.722899>
- Maddison WP, Maddison DR (2021) Mesquite: a modular system for evolutionary analysis. Version 3.70. <http://www.mesquiteproject.org>

- Mann A, Gee BM, Pardo JD, Marjanović D, Adams GR, Calthorpe AS, Maddin HC, Anderson JS (2020) Reassessment of historic ‘microsaurs’ from Joggins, Nova Scotia, reveals hidden diversity in the earliest amniote ecosystem. *Papers in Palaeontology* 6: 605–625. <https://doi.org/10.1002/spp2.1316>
- Mann A, Pardo JD, Sues H-D (2022 [printed 2023]) Osteology and phylogenetic position of the diminutive ‘microsaur’ *Odonterpeton triangulare* from the Pennsylvanian of Linton, Ohio, and major features of recumbirostran phylogeny. *Zoological Journal of the Linnean Society* 197: 641–655. <https://doi.org/10.1093/zoolinnean/zlac043>
- Marjanović D, Laurin M (2008) A reevaluation of the evidence supporting an unorthodox hypothesis on the origin of extant amphibians. *Contributions to Zoology* 77: 149–199. <https://doi.org/10.1163/18759866-07703002>
- Marjanović D, Laurin M (2009) The origin(s) of modern amphibians: a commentary. *Evolutionary Biology* 36: 336–338. <https://doi.org/10.1007/s11692-009-9065-8>
- Marjanović D, Laurin M (2013) The origin(s) of extant amphibians: a review with emphasis on the “lepospondyl hypothesis”. *Geodiversitas* 35: 207–272. <https://doi.org/10.5252/g2013n1a8> [open access: <https://sciencepress.mnhn.fr/en/periodiques/geodiversitas/35/1/les-origines-des-amphibiens-actuels-une-synthese-avec-emp-hase-sur-l-hypothese-lepospondyle>]
- Marjanović D, Laurin M (2018) Reproducibility in phylogenetics: reevaluation of the largest published morphological data matrix for phylogenetic analysis of Paleozoic limbed vertebrates. *PeerJ Preprints* 6: e1596v3. <https://doi.org/10.7287/peerj.preprints.1596v3>
- Marjanović D, Laurin M (2019) Phylogeny of Paleozoic limbed vertebrates reassessed through revision and expansion of the largest published relevant data matrix. *PeerJ* 6: e5565. <https://doi.org/10.7717/peerj.5565>
- Marjanović D, Witzmann F (2015) An extremely peramorphic newt (Urodela: Salamandridae: Pleurodelini) from the latest Oligocene of Germany, and a new phylogenetic analysis of extant and extinct salamandrids. *PLOS ONE* 10: e0137068. <https://doi.org/10.1371/journal.pone.0137068>
- Marjanović D, Maddin HC, Olori JC, Laurin M (2023) The new problem of *Chinlestegophis* and the origin of caecilians (Amphibia, Gymnophionomorpha) is highly sensitive to old problems of sampling and character construction. Version 1 [first preprint of the present article]. *PaleorXiv*. <https://doi.org/10.31233/osf.io/myuv5>
- Matsumoto R, Evans SE (2018) The first record of albanerpetontid amphibians (Amphibia: Albanerpetontidae) from East Asia. *PLOS ONE* 13: e0189767. <https://doi.org/10.1371/journal.pone.0189767>
- McGowan GJ (2002) Albanerpetontid amphibians from the Lower Cretaceous of Spain and Italy: a description and reconsideration of their systematics. *Zoological Journal of the Linnean Society* 135: 1–32. <https://doi.org/10.1046/j.1096-3642.2002.00013.x>
- McGowan G, Evans SE (1995) Albanerpetontid amphibians from the Cretaceous of Spain. *Nature* 373: 143–145. <https://doi.org/10.1038/373143a0>
- Milner AR, Schoch RR (2013) *Trimerorhachis* (Amphibia: Temnospondyli) from the Lower Permian of Texas and New Mexico: cranial osteology, taxonomy and biostratigraphy. *Neues Jahrbuch für Geologie und Paläontologie – Abhandlungen* 270: 91–128. <https://doi.org/10.1127/0077-7749/2013/0360>
- Mongiardino Koch N, Garwood RJ, Parry LA (2021) Fossils improve phylogenetic analyses of morphological characters. *Proceedings of the Royal Society B: Biological Sciences* 288: 20210044. <https://doi.org/10.1098/rspb.2021.0044>
- Müller H (2006) Ontogeny of the skull, lower jaw, and hyobranchial skeleton of *Hypogeophis rostratus* (Amphibia: Gymnophiona: Caeciliidae) revisited. *Journal of Morphology* 267: 968–986. <https://doi.org/10.1002/jmor.10454>
- Müller H, Oommen OV, Bartsch P (2005) Skeletal development of the direct-developing caecilian *Gegeneophis ramsawamii* (Amphibia: Gymnophiona: Caeciliidae). *Zoomorphology* 124: 171–188. <https://doi.org/10.1007/s00435-005-0005-6>
- Palci A, Hutchinson MN, Caldwell MW, Smith KT, Lee MSY (2019 [printed 2020]) The homologies and evolutionary reduction of the pelvis and hindlimbs in snakes, with the first report of ossified pelvic vestiges in an anomalepidid (*Liotyphlops beui*). *Systematic Biology* 188: 630–652. <https://doi.org/10.1093/zoolinnean/zlz098>
- Pardo JD, Anderson JS (2016) Cranial morphology of the Carboniferous–Permian tetrapod *Brachydectes newberryi* (Lepospondyli, Lysorophia): new data from  $\mu$ CT. *PLOS ONE* 11: e0161823. <https://doi.org/10.1371/journal.pone.0161823>
- Pardo JD, Szostakiwskyj M, Anderson JS (2015) Cranial morphology of the brachystelechid ‘microsaur’ *Quasicaecilia texana* Carroll provides new insights into the diversity and evolution of braincase morphology in recumbirostran ‘microsaurs’. *PLOS ONE* 10: e0130359. <https://doi.org/10.1371/journal.pone.0130359>
- Pardo JD, Small BJ, Huttenlocker AK (2017a) Stem caecilian from the Triassic of Colorado sheds light on the origins of Lissamphibia. *Proceedings of the National Academy of Sciences of the United States of America* 114: E5389–E5395. <https://doi.org/10.1073/pnas.1706752114>
- Pardo JD, Szostakiwskyj M, Ahlberg PE, Anderson JS (2017b) Hidden morphological diversity among early tetrapods. *Nature* 546: 642–645. <https://doi.org/10.1038/nature22966>
- Pérez OD, Lai NB, Buckley D, del Pino EM, Wake MH (2009) The morphology of prehatching embryos of *Caecilia orientalis* (Amphibia: Gymnophiona: Caeciliidae). *Journal of Morphology* 270: 1492–1502. <https://doi.org/10.1002/jmor.10772>
- Pough FH, Bemis WE, McGuire B, Janis CM (2022 [for 2023]) *Vertebrate Life*. Eleventh edition. Sinauer Associates/Oxford University Press, Sunderland/Oxford-New York, xvii + 585 + 1 + G12 + 139 pp.
- Puttick MN, O’Reilly JE, Pisani D, Donoghue PC (2018 [printed 2019]) Probabilistic methods outperform parsimony in the phylogenetic analysis of data simulated without a probabilistic model. *Palaeontology* 62: 1–17. <https://doi.org/10.1111/pala.12388>
- Rineau V, Grand A, Zaragüeta R, Laurin M (2015) Experimental systematics: sensitivity of cladistic methods to polarization and character ordering schemes. *Contributions to Zoology* 84: 129–148. <https://doi.org/10.1163/18759866-08402003>
- Rineau V, Zaragüeta i Bagils R, Laurin M (2018) Impact of errors on cladistic inference: simulation-based comparison between parsimony and three-taxon analysis. *Contributions to Zoology* 87: 25–40. <https://doi.org/10.1163/18759866-08701003>
- Ruta M, Milner AC, Coates MI (2002 [for 2001]) The tetrapod *Caerorhachis bairdi* Holmes and Carroll from the Lower Carboniferous of Scotland. *Transactions of the Royal Society of Edinburgh: Earth Sciences* 92: 229–261. <https://doi.org/10.1017/S0263593300000249>
- Santos RO, Laurin M, Zaher H (2020) A review of the fossil record of caecilians (Lissamphibia; Gymnophionomorpha) with comments on its use to calibrate molecular timetrees. *Biological Journal of the Linnean Society* 131: 737–755. <https://doi.org/10.1093/biolinnean/blaa148>
- Sawin HJ (1941) The cranial anatomy of *Eryops megacephalus*. *Bulletin of the Museum of Comparative Zoology at Harvard College* 88: 407–463. <https://www.biodiversitylibrary.org/item/21129#page/451/mode/1up>

- Schoch RR (2013) The evolution of major temnospondyl clades: an inclusive phylogenetic analysis. *Journal of Systematic Palaeontology* 11: 673–705. <https://doi.org/10.1080/14772019.2012.699006>
- Schoch RR (2018 [printed 2019]) The putative lissamphibian stem-group: phylogeny and evolution of the dissorophoid temnospondyls. *Journal of Paleontology* 93: 137–156. <https://doi.org/10.1017/jpa.2018.67>
- Schoch RR, Werneburg R, Voigt S (2020) A Triassic stem-salamander from Kyrgyzstan and the origin of salamanders. *Proceedings of the National Academy of Sciences of the United States of America* 117: 11584–11588. <https://doi.org/10.1073/pnas.2001424117>
- Serra Silva A, Wilkinson M (2021) On defining and finding islands of trees and mitigating large island bias. *Systematic Biology* 70: 1282–1294. <https://doi.org/10.1093/sysbio/syab015>
- Sigurdson T, Bolt JR (2010) The Lower Permian amphibamid *Dole-serpeton* (Temnospondyli: Dissorophoidea), the interrelationships of amphibamids, and the origin of modern amphibians. *Journal of Vertebrate Paleontology* 30: 1360–1377. <https://doi.org/10.1080/02724634.2010.501445>
- Sigurdson T, Green DM (2011) The origin of modern amphibians: a re-evaluation. *Zoological Journal of the Linnean Society* 162: 457–469. <https://doi.org/10.1111/j.1096-3642.2010.00683.x>
- Simmons MP (2014) A confounding effect of missing data on character conflict in maximum likelihood and Bayesian MCMC phylogenetic analyses. *Molecular Phylogeny and Evolution* 80: 267–280. <https://doi.org/10.1016/j.ympev.2014.08.021>
- Simões TR, Caldwell MW, Palci A, Nydam RL (2017) Giant taxon-character matrices: quality of character constructions remains critical regardless of size. *Cladistics* 33: 198–219. <https://doi.org/10.1111/cla.12163>
- Skutschas P, Martin T (2011) Cranial anatomy of the stem salamander *Kokartus honorarius* (Amphibia: Caudata) from the Middle Jurassic of Kyrgyzstan. *Zoological Journal of the Linnean Society* 161: 816–838. <https://doi.org/10.1111/j.1096-3642.2010.00663.x>
- Sookias RB, Böhmer C, Clack JA (2014) Redescription and phylogenetic analysis of the mandible of an enigmatic Pennsylvanian (Late Carboniferous) tetrapod from Nova Scotia, and the lability of Meckelian jaw ossification. *PLOS ONE* 9: e109717. <https://doi.org/10.1371/journal.pone.0109717>
- Swofford D (2021) PAUP\* (\*Phylogenetic Analysis Using PAUP). Version 4.0a169. PhyloSolutions. <http://phylosolutions.com/paup-test/>
- Theska T, Wilkinson M, Gower DJ, Müller H (2018 [printed 2019]) Musculoskeletal development of the Central African caecilian *Idiocranium russeli* (Amphibia: Gymnophiona: Indotyphlidae) and its bearing on the re-evolution of larvae in caecilian amphibians. *Zoomorphology* 138: 137–158. <https://doi.org/10.1007/s00435-018-0420-0>
- Vallin G, Laurin M (2004) Cranial morphology and affinities of *Microbrachis*, and a reappraisal of the phylogeny and lifestyle of the first amphibians. *Journal of Vertebrate Paleontology* 24: 56–72. <https://doi.org/10.1671/5.1>
- Wake MH (2020) *Gymnophiona* J. Müller 1832 [M. H. Wake], converted clade name. In: de Queiroz K, Cantino PD, Gauthier JA (Eds) *Phylogeny: An Implementation of PhyloCode*. CRC Press, Boca Raton, Florida, 779–783. <https://doi.org/10.1201/9780429446276>
- Wake MH, Hanken J (1982) Development of the skull of *Dermophis mexicanus* (Amphibia: Gymnophiona), with comments on skull kinesis and amphibian relationships. *Journal of Morphology* 173: 203–223. <https://doi.org/10.1002/jmor.1051730208>
- Werneburg R (2012) Dissorophoide Amphibien aus dem Westphalian D (Ober-Karbon) von Nýřany in Böhmen (Tschechische Republik)

– der Schlüssel zum Verständnis der frühen ‚Branchiosaurier‘. *Semana* 27: 3–50.

- Wiens JJ (2001) Character analysis in morphological phylogenetics: problems and solutions. *Systematic Biology* 50: 689–699. <https://doi.org/10.1080/106351501753328811>
- Wilkinson M, Reynolds RP, Jacobs JF (2021) A new genus and species of rhinatrematid caecilian (Amphibia: Gymnophiona: Rhinatrematidae) from Ecuador. *Herpetological Journal* 31: 27–34. <https://doi.org/10.33256/31.1.2734>
- Yates AM, Warren A (2000) The phylogeny of the ‘higher’ temnospondyls (Vertebrata: Choanata) and its implications for the monophyly and origins of the Stereospondyli. *Zoological Journal of the Linnean Society* 128: 77–121. <https://doi.org/10.1006/zjls.1998.0184>

## Supplementary material 1

### Mesquite NEXUS file of Pardo et al. (2017a: fig. S6), previously unpublished

Authors: David Marjanović, Hillary C. Maddin, Jennifer C. Olori, Michel Laurin

Data type: nex

Explanation note: We have added a PAUP block that repeats our unconstrained and constrained analyses (a1, a2) if the file is executed in PAUP\*, and a TREES block that contains one tree resulting from each analysis; before conducting the analyses, the PAUP block performs the statistical tests comparing the trees in the TREES block. Otherwise the file remains as provided by J. Pardo and A. Huttenlocker.

Copyright notice: This dataset is made available under the Open Database License (<http://opendatacommons.org/licenses/odbl/1.0>). The Open Database License (ODbL) is a license agreement intended to allow users to freely share, modify, and use this Dataset while maintaining this same freedom for others, provided that the original source and author(s) are credited.

Link: <https://doi.org/10.3897/fr.27.109555.suppl1>

## Supplementary material 2

### Frequencies of bipartitions in our (unrooted) bootstrap analyses

Authors: David Marjanović, Hillary C. Maddin, Jennifer C. Olori, Michel Laurin

Data type: pdf

Explanation note: Tables S1–S4, showing the bootstrap bipartitions corresponding to analyses b, d1, d2 and e4.

Copyright notice: This dataset is made available under the Open Database License (<http://opendatacommons.org/licenses/odbl/1.0>). The Open Database License (ODbL) is a license agreement intended to allow users to freely share, modify, and use this Dataset while maintaining this same freedom for others, provided that the original source and author(s) are credited.

Link: <https://doi.org/10.3897/fr.27.109555.suppl2>

### Supplementary material 3

#### **Mesquite NEXUS file of Pardo et al. (2017a: fig. 2, 3, S7) with the albanerpetid OTU of Daza et al. (2020) added**

Authors: David Marjanović, Hillary C. Maddin, Jennifer C. Olori, Michel Laurin

Data type: nex

Explanation note: No scores are changed, all characters are unordered. We have also added a PAUP block and deleted the CHARSTATELABELS block because Mesquite could not deal with it correctly. If the file is executed in PAUP\*, it repeats our analysis b (without Albanerpetidae), bootstraps it, and repeats analysis c (with Albanerpetidae).

Copyright notice: This dataset is made available under the Open Database License (<http://opendatacommons.org/licenses/odbl/1.0>). The Open Database License (ODbL) is a license agreement intended to allow users to freely share, modify, and use this Dataset while maintaining this same freedom for others, provided that the original source and author(s) are credited.

Link: <https://doi.org/10.3897/fr.27.109555.suppl3>

### Supplementary material 4

#### **Mesquite NEXUS file of Pardo et al. (2017a: fig. 2, 3, S7) with the clinal characters ordered and the albanerpetid OTU of Daza et al. (2020) added**

Authors: David Marjanović, Hillary C. Maddin, Jennifer C. Olori, Michel Laurin

Data type: nex

Explanation note: For characters 205, 221, 327 and 328, the states had to be reordered to allow for linear ordering as described in the text. If executed in PAUP\*, the file repeats our analysis d1 (without Albanerpetidae), bootstraps it, repeats analysis d2 (with Albanerpetidae) and bootstraps it as well.

Copyright notice: This dataset is made available under the Open Database License (<http://opendatacommons.org/licenses/odbl/1.0>). The Open Database License (ODbL) is a license agreement intended to allow users to freely share, modify, and use this Dataset while maintaining this same freedom for others, provided that the original source and author(s) are credited.

Link: <https://doi.org/10.3897/fr.27.109555.suppl4>

### Supplementary material 5

#### **Mesquite NEXUS file of Pardo et al. (2017a: fig. 2, 3, S7) with the modifications to characters and individual scores described in the text and the albanerpetid OTU of Daza et al. (2020) added**

Authors: David Marjanović, Hillary C. Maddin, Jennifer C. Olori, Michel Laurin

Data type: nex

Explanation note: If executed in PAUP\*, the file repeats our analyses e1 (without Albanerpetidae) and e3 (with Albanerpetidae).

Copyright notice: This dataset is made available under the Open Database License (<http://opendatacommons.org/licenses/odbl/1.0>). The Open Database License (ODbL) is a license agreement intended to allow users to freely share, modify, and use this Dataset while maintaining this same freedom for others, provided that the original source and author(s) are credited.

Link: <https://doi.org/10.3897/fr.27.109555.suppl5>

### Supplementary material 6

#### **Mesquite NEXUS file of Pardo et al. (2017a: fig. 2, 3, S7) with the modifications to characters and individual scores described in the text, the albanerpetid OTU of Daza et al. (2020) added and the clinal characters ordered as in Suppl. material 4**

Authors: David Marjanović, Hillary C. Maddin, Jennifer C. Olori, Michel Laurin

Data type: nex

Explanation note: If executed in PAUP\*, the file performs our analyses e2 (without Albanerpetidae) and e4 (with Albanerpetidae) and then bootstraps e4.

Copyright notice: This dataset is made available under the Open Database License (<http://opendatacommons.org/licenses/odbl/1.0>). The Open Database License (ODbL) is a license agreement intended to allow users to freely share, modify, and use this Dataset while maintaining this same freedom for others, provided that the original source and author(s) are credited.

Link: <https://doi.org/10.3897/fr.27.109555.suppl6>

# Coexistence of Oligocene toothed and baleen-assisted mysticetes in the northwestern Pacific

Cheng-Hsiu Tsai<sup>1</sup>, Toshiyuki Kimura<sup>2</sup>, Yoshikazu Hasegawa<sup>2,3</sup>

<sup>1</sup> Department of Life Science, Institute of Ecology and Evolutionary Biology, Museum of Zoology, National Taiwan University, No. 1, Sec. 4, Roosevelt Rd., Taipei, 10617, Taiwan

<sup>2</sup> Gunma Museum of Natural History, 1674-1, Kamikuroiwa, Tomioka, Gunma 370-2345, Japan

<sup>3</sup> Iida City Museum, 2-655-7, Otemachi, Iida, Nagano 395-0034, Japan

<https://zoobank.org/3E4B181B-8B6A-4567-9A58-A4A9ABFAD188>

Corresponding authors: Cheng-Hsiu Tsai ([whaletsai@ntu.edu.tw](mailto:whaletsai@ntu.edu.tw), [craniata@gmail.com](mailto:craniata@gmail.com)); Toshiyuki Kimura ([kimura@gmnh.pref.gunma.jp](mailto:kimura@gmnh.pref.gunma.jp))

Academic editor: Johannes Müller ♦ Received 24 August 2023 ♦ Accepted 22 December 2023 ♦ Published 11 January 2024

## Abstract

Oligocene mysticetes display an unparalleled diversity and morphological disparity in the evolutionary history of Mysticeti. However, their paleoecological aspects, such as the patterns of coexistence of different morphotypes, remain poorly explored. Here we describe an aetiocetid (toothed mysticete) from the Jinnobaru Formation (lower upper Oligocene, about 28 million years ago) of Umashima Island, Kitakyushu, Japan. Our description of a toothed mysticete from the Oligocene of Umashima exemplifies the coexistence of toothed and baleen-assisted mysticetes in the northwestern Pacific. Hopefully, new finds of Oligocene mysticetes will lead to a well-sampled dataset for analyzing this and other related paleoecological traits to understand the demise of “archaic” Oligocene mysticetes and the subsequent rise of the modern-looking baleen-bearing whales in Miocene times.

## Key Words

Aetiocetidae, Chattian, Jinnobaru Formation, Mysticeti, toothed baleen whale, Umashima

## Introduction

The coexistence of closely related species often shows niche partitioning under various mechanisms, such as resource, spatial, and temporal partitioning, habitat differentiation, or size disparity (Schoener 1974). Baleen whales (Cetacea: Mysticeti), the largest animals ever generally avoid intense competition through food partitioning. For example, blue whales consume euphausiids primarily, whereas fin whales predominantly forage on small fishes but also include euphausiids when abundant (Wursig et al. 2018). Yet, coexistence or competition of closely related mysticetes in the deep past has rarely been documented or discussed. The few remarkable examples include a large aetiocetid from the Oligocene of Hokkaido, which implies an early case of niche partitioning by size disparity in toothed mysticetes along the northwestern Pacific coast (Tsai and Ando 2016), and a

likely competitive exclusion between cetotheriid and eschrichtiid whales (Collareta et al. 2021). Here, we describe a newly collected aetiocetid specimen from the Oligocene of Umashima Island (Fukuoka, Japan; Fig. 1). This new specimen represents the first formally recognized toothed “baleen” whale from the Jinnobaru Formation. Given that the Jinnobaru Formation has also produced the well-preserved eomysticetid *Yamatocetus*, our discovery provides an opportunity to discuss the coexistence of different morphotypes of early mysticetes.

## Institutional abbreviations

**UCMP**, University of California Museum of Paleontology, Berkeley, USA; **USNM**, National Museum of Natural History, Smithsonian Institution, Washington, D.C., USA; **YM**, Yamaguchi Prefectural Museum, Yamaguchi, Japan.

## Results

### Systematic paleontology

**Cetacea Brisson, 1762**

**Mysticeti Gray, 1864**

**Aetiocetidae Emlong, 1966**

**Aetiocetidae gen et sp. indet.**

Fig. 2

**Material.** YM-G-100208, including the posterior part of the skull. A 3D file of YM-G-100208 is freely available at: <https://zenodo.org/record/8140997>.

**Locality and age.** YM-G-100208 was collected by Akito Makino on Umashima Island (about ten years ago, 33°57'58"N, 130°51'41"E; Fig. 1), Fukuoka Prefecture, Japan. YM-G-100208 was a floating nodule when discovered, resulting in an uncertain geological horizon. No microfossils, indicative of the geological age, have been recovered from the matrix with YM-G-100208. However, the matrix with YM-G-100208 is grayish and fine-grained sandstone, as typical of the Jinnobaru Formation of the Ashiya Group, which is the only exposed formation on Umashima (Nakae et al. 1998). In addition, YM-G-100208 is extensively eroded but still preserves some skull sutures, suggesting that the specimen was likely not transported far from the original locality. Thus, we regard the geological horizon producing YM-G-100208 to be part of the Jinnobaru Formation of the Ashiya Group. The Ashiya Group includes the Yamaga, Norimatsu, Jinnobaru, Honjo, and Waita formations in ascending order stratigraphically (Ozaki et al. 1993). The geological age of the Ashiya Group ranges from the latest Early to Late Oligocene based on fission-track dating, calcareous nannofossils, and planktonic foraminifera (Saito 1984; Okada 1992; Ozaki

et al. 1993), and the base of the Jinnobaru Formation was dated  $28.91 \pm 0.2$  Ma by the sensitive high-resolution ion microprobe zircon U-Pb method (Sakai et al. 2014). The upper boundary of the Jinnobaru Formation remains uncertain, and we consider YM-G-100208 to be slightly younger than 28 Ma, about the early Late Oligocene, similar to *Yamatocetus canaliculatus*. The Jinnobaru Formation has produced abundant vertebrate fossils, including the eomysticetid *Yamatocetus canaliculatus* (Okazaki 1995; Okazaki 2012), the purported squalodontid "*Metasqualodon*" *symmetricus* (Okazaki 1982), and pterosaurs (Olson and Hasegawa 1996).

**Description.** YM-G-100208 preserves the post-frontal skull. The anteriormost serration likely indicates the frontal-parietal suture. Overall, the preserved part of the skull is eroded, and the natural sutures between bones are barely identifiable; the occipital complex is damaged. The right and left parietals meet at the dorsal midline, and the presence of the sagittal crest remains uncertain due to erosion. The anteriormost edge of the parietal is unclear, but the anteroposterior length of the parietal is much longer than its dorsoventral height. The posterior suture between the parietal and the supraoccipital is also eroded but shows a minor lateral extension of the supraoccipital, leaving a gentle overhang on the squamosal fossa posteriorly. The posterior-most margin of the parietal is also uncertain, but given the preserved morphology, it likely extends further back, only slightly anterior to the occipital condyle.

The supraoccipital is broadly triangular, and the anterior half is concave. Based on the surrounding morphology, the existence of a supraoccipital depression should be regarded as genuine. The suture between the supraoccipital and exoccipital likely remains partly unfused, but the post-mortem damage and compression hinder reliable judgment. The left occipital condyle is missing, but the overall preservation shows an oval shape

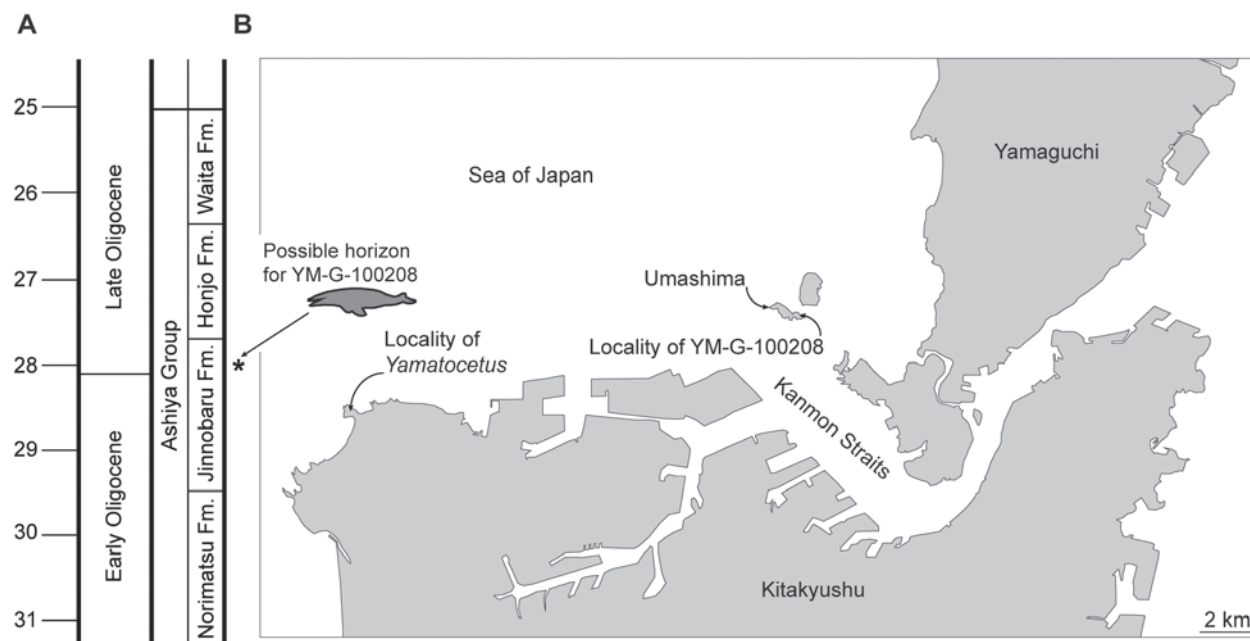


**Figure 1.** Geological horizon and locality of YM-G-100208. (A) Geological column to indicate the collecting horizon. (B) Geographic map to show the collecting locality.

of the magnum foramen (shorter dorsoventral height). Ventrally, the flat surface of the basioccipital is wide (about 63 mm), and the basioccipital crest is massive and bulbous. The basioccipital crest runs posterolaterally.

Anterior to the basioccipital, a partially well-developed keel of the vomer is observed, and the height reaches about 31 mm. The ventral margin of the keel is eroded, but it gently slopes to the surface of the basisphenoid/basioccipital posteriorly from the anterior margin of the pterygoid sinus. The vomer extends posteriorly at least to the level of the basioccipital crest. On the right side of the skull (the left side is eroded), the oval-shaped pterygoid sinus orients anteromedially, being much longer anteroposteriorly than wide. Posteriorly, the periotic is broken and eroded. The shape and degree of protrusion of the anterior process of the periotic remains uncertain due to erosion but shows a contact with the squamosal. The squamosal is also heavily eroded, but the base of the squamosal is robust based on the broken surface.

**Body size and ontogenetic stage.** We estimated that the bizygomatic width of YM-G-100208 is about 28 cm. Based on this estimation, we used Pyenson and Sponberg's equation (2011) for stem mysticetes:

$$\log(\text{TL}) = 0.92 * (\log(\text{BIZYG}[\text{in cm}]) - 1.72) + 2.68$$

to assess the body size of YM-G-100208, resulting in 268 cm – typical for aetiocetids. The skull sutures that can help assess the ontogenetic stage (Walsh and Berta 2011) are broadly eroded. But, given the fusion of some sutures, such as the suture between the basioccipital and basisphenoid, and robustness, we consider that YM-G-100208 represents a subadult at least.

**Comment.** YM-G-100208 shows its aetiocetid affinity by displaying the following combination of characters: body size less than 3 m long, outline of the supraoccipital broadly triangular, an anteriorly-thrust supraoccipital, straight lateral margins of the supraoccipital, a moderate exposure of parietals on the skull roof, and a well-developed basioccipital crest. YM-G-100208 differs from llanocetids in its small body size, lack of the sagittal trough, bulbous basioccipital crests, and the ventral keel of the vomer extending posteriorly to the level of the basioccipital crest. YM-G-100208 further differs from mammalodontids in having a broadly triangular supraoccipital, a less elongate intertemporal region, a well-developed and bulbous basioccipital crests, and the ventral keel of the vomer extending posteriorly to the level of the basioccipital crest. YM-G-100208 differs from eomysticetids in lacking the sagittal crest on the skull roof and the ventral keel of the vomer extending posteriorly to the level of the basioccipital crest. YM-G-100208 further differs from other crown mysticetes in having the parietals exposed on the skull roof. Due to the incompleteness of YM-G-100208, we provisionally identify it as belonging to Aetiocetidae gen. et. sp. indet. This taxonomic identification allows for the first recognition of coexisting toothed and baleen-assisted mysticetes in the northwestern Pacific.

## Discussion

Our description of YM-G-100208 represents a formal recognition of the presence of aetiocetids in the Jinnobaru Formation, likely coexisting with the eomysticetid *Yamatocetus canaliculatus*. Interestingly, “*Metasqualodon*” *symmetricus* was originally named and recognized as an odontocete (Okazaki 1982), but later cladistic analyses suggested its placement in the mysticete lineage (Geisler et al. 2017; Boessenecker et al. 2023). The updated description and formal taxonomic revision of “*Metasqualodon*” *symmetricus*, which require a new generic identification, remain under progress (pers. comm. with Y. Okazaki). In addition, the lack of overlapping materials between YM-G-100208 and the holotype of “*Metasqualodon*” *symmetricus* hinders our interpretations of taxonomic similarities and the detailed composition of the mysticete communities of the Jinnobaru Formation. That said, the description of YM-G-100208 indicates a complex Oligocene ecosystem in the Jinnobaru Formation, with the co-occurrence of baleen-assisted eomysticetids and toothed mysticetes.

In the northwestern Pacific, two units, the Ashiya Group (including Jinnobaru Formation) in Kyushu and the Morawan Formation in Hokkaido, have yielded abundant Oligocene fossil cetaceans. However, the faunal composition of the two fossil whale-rich formations features an apparent discrepancy. Various species of toothed mysticetes were recovered from the Morawan Formation of Hokkaido, but no eomysticetids (Barnes et al. 1995; Tsai and Ando 2016), whereas both toothed mysticetes (this study) and eomysticetids (Okazaki 2012) have been documented (Fig. 2) from the Jinnobaru Formation of the Kyushu area. This faunal discrepancy, coupled with the fact that the Jinnobaru Formation (about 28 Ma) is older than the Morawan Formation (ranging from 26 to 24 Ma), may reflect an evolutionary scenario of the ecosystem structure along the northwestern Pacific. The competition between toothed mysticetes and baleen-assisted eomysticetids should have been less intense (a common resource-dependent niche partitioning). Then, toothed mysticetes may have dispersed north and differentiated to occupy various niches in the Oligocene waters of Hokkaido, resulting in the size disparity of toothed mysticetes (Tsai and Ando 2016).

Alternatively, the faunal discrepancy between the Jinnobaru and Morawan formations may indicate the need for more research effort in the Ashoro area, Hokkaido, which has produced various aetiocetid species but no baleen-assisted mysticetes (Barnes et al. 1995; Tsai and Ando 2016). On the other side of the North Pacific (Fig. 2), abundant Oligocene mysticetes, including both toothed and baleen-assisted species, inhabited both the northern and southern waters of the eastern North Pacific (ranging from Washington of the USA to Mexico) (Barnes et al. 1995; Marx et al. 2015; Peredo and Uhen 2016; Hernández-Cisneros 2022; Hernández-Cisneros and Nava-Sanchez 2022). Of note, a toothed mysticete, *Chonecetus sookensis*, has also been recovered from Canada (Russell 1968). Still, given the geographic locality and geological horizon, *Chonecetus sookensis*

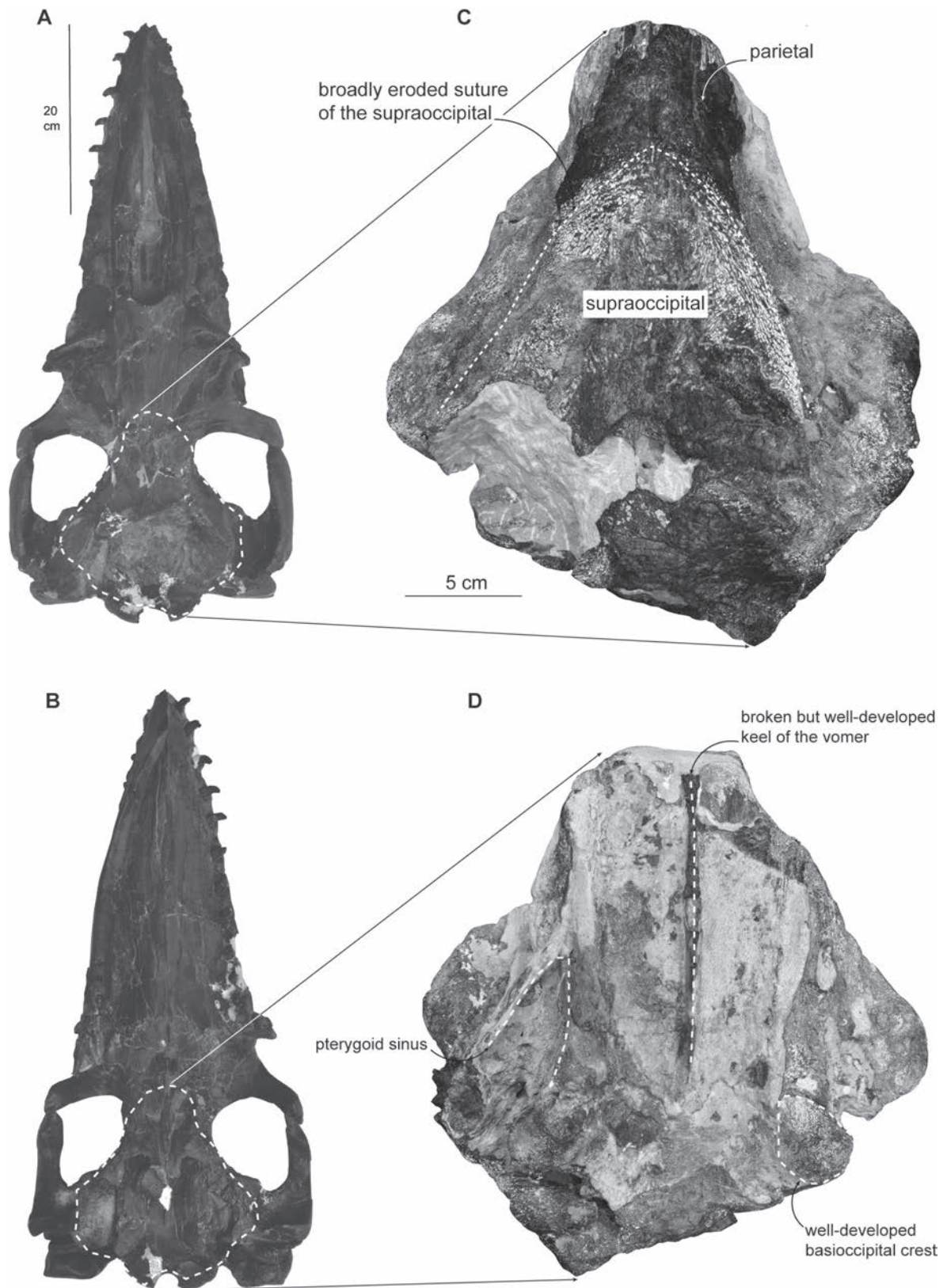


**Figure 2.** The skull of YM-G-100208 and a well-preserved skull of *Aetiocetus weltoni* (UCMP 122900) for comparison. (A) Dorsal view of *Aetiocetus weltoni* (UCMP 122900). (B) Ventral view of *Aetiocetus weltoni* (UCMP 122900). (C) Dorsal view of YM-G-100208. (D) Ventral view of YM-G-100208.

from the Oligocene of Canada can be considered as part of the faunal composition from the Oligocene sediments in Washington, USA. This distribution pattern suggests more abundant Oligocene mysticetes from the western

North Pacific. For example, the Oligocene mysticete composition between New Zealand and Australia also shows a prominent discrepancy; New Zealand includes various baleen-assisted and toothed species (Fordyce and

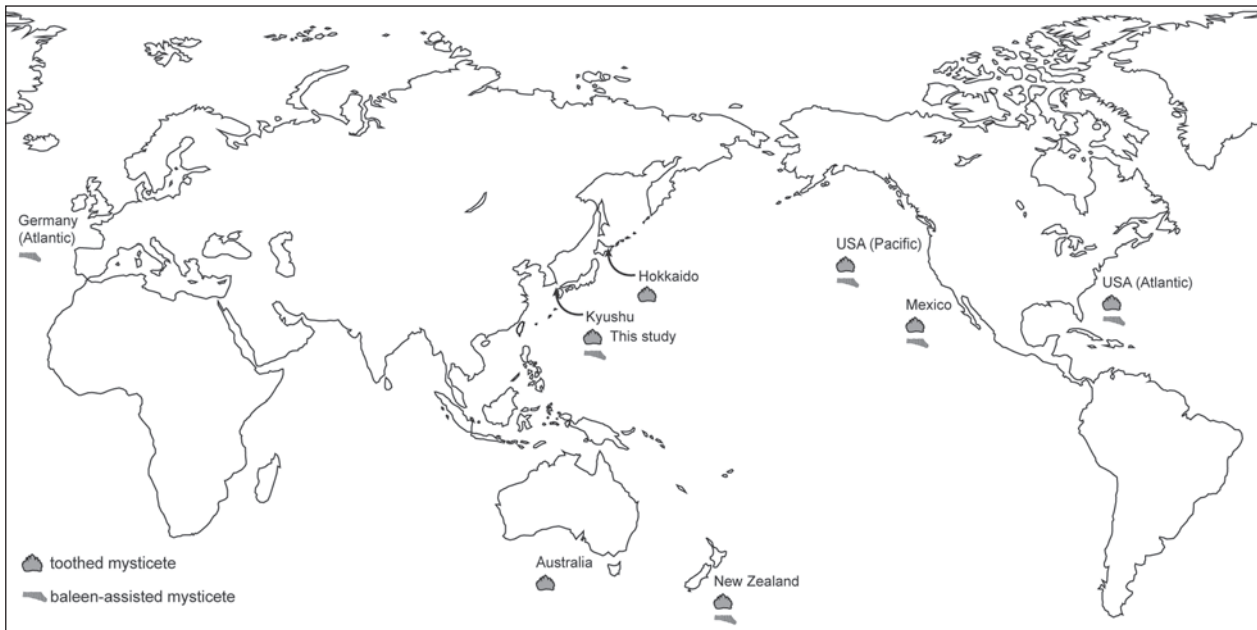


**Figure 3.** The global distribution of Oligocene toothed and baleen-assisted mysticetes.

Marx 2016; Boessenecker and Fordyce 2017; Tsai and Fordyce 2018), whereas toothed mysticetes represent the only Oligocene mysticetes in Australia (Fitzgerald 2006; Fitzgerald 2010). Interestingly, the supplementary information of a recent publication (Marx et al. 2019) listed 12 specimens (earbones: bullae) and identified as eomysticetids or chaemysticetes from the Oligocene of Australia. Future finds should substantiate this identification and provide a better understanding of the Oligocene mysticete communities of the Southern Ocean.

Oligocene mysticetes show an unparalleled diversity and morphological disparity in the evolutionary history of Mysticeti (Barnes et al. 1995; Fitzgerald 2010; Boessenecker and Fordyce 2015; Tsai and Fordyce 2015; Geisler et al. 2017; Peredo et al. 2018; Tsai 2023), and some of the most challenging questions in the mysticete evolution are whether toothed aetiocetids possessed proto-baleen and how the mysticete toothed-baleen transition occurred (Ekdale and Deméré 2022; Peredo et al. 2022). Such a transition in the structure of the feeding apparatus of baleen whales indeed played a critical role and attracts intense research efforts. Our description of a toothed mysticete from the Oligocene of Umashima (Kyushu, Japan) and a compilation of Oligocene mysticetes across the globe (Fig. 3) should draw more attention to finding more Oligocene mysticetes and lead to a well-sampled dataset for analyzing the coexistence pattern or other related paleoecological traits to understand the demise of “archaic” Oligocene mysticetes and give rise to the modern-looking baleen whales.

## Acknowledgments

We thank A. Makino for collecting and donating YM-G-100208; A. Kameya and E. Akazaki of the Yamaguchi Prefectural Museum for access to YM-G-100208; P. Holroyd of the University of California Museum of Paleontology

for access to UCMP 122900; Alberto Collareta and Oliver Hampe for constructive and helpful comments. This research is partly supported by the Taiwan Ministry of Science and Technology (MOST 111-2621-B-002-006, 112-2621-B-002-005; now known as National Science and Technology Council, Taiwan), public donations (NTU FD107028), and Bestland Co., Ltd. based in Tsukuba to CHT.

## References

- Barnes LG, Kimura M, Furusawa H, Sawamura H (1995) Classification and distribution of Oligocene Aetiocetidae (Mammalia; Cetacea; Mysticeti) from western north America and Japan. *Island Arc* 3: 392–431. <https://doi.org/10.1111/j.1440-1738.1994.tb00122.x>
- Boessenecker RW, Beatty BL, Geisler JH (2023) New specimens and species of the Oligocene toothed baleen whale *Coronodon* from South Carolina and the origin of Neoceti. *PeerJ* 11: e14795. <https://doi.org/10.7717/peerj.14795>
- Boessenecker RW, Fordyce RE (2015) A new genus and species of eomysticetid (Cetacea: Mysticeti) and a reinterpretation of ‘*Mauicetus*’ *lophocephalus* Marples, 1956: transitional baleen whales from the upper Oligocene of New Zealand. *Zoological Journal of the Linnean Society* 175: 607–660. <https://doi.org/10.1111/zoj.12297>
- Boessenecker RW, Fordyce RE (2017) A new eomysticetid from the Oligocene Kokoamu Greensand of New Zealand and a review of the Eomysticetidae (Mammalia, Cetacea). *Journal of Systematic Palaeontology* 15: 429–469. <https://doi.org/10.1080/14772019.2016.1191045>
- Brisson AD (1762) *Regnum animale in Classes IX. distributum, sive Synopsis methodica sistens generalem Animalium distributionem in Classibus IX, and duarum primarum Classicum, Quadrupedum scilicet and Cetaceorum, particularem divisionem in Ordines, Sectiones, Genera and Species.* Haak, Leiden, 296 pp. <https://doi.org/10.5962/bhl.title.40361>
- Collareta A, Marx FG, Casati S, Di Cencio A, Merella M, Bianucci G (2021) A cetotheriid whale from the upper Miocene of the Mediterranean. *Neues Jahrbuch für Geologie und Paläontologie* 301: 9–16. <https://doi.org/10.1127/njgpa/2021/0994>

- Ekdale EG, Deméré TA (2022) Neurovascular evidence for a co-occurrence of teeth and baleen in an Oligocene mysticete and the transition to filter-feeding in baleen whales. *Zoological Journal of the Linnean Society* 194: 395–415. <https://doi.org/10.1093/zoolinnea/zlab017>
- Emlong D (1966) A new archaic cetacean from the Oligocene of Northwest Oregon. *Bulletin of the Museum of Natural History, University of Oregon* 3: 1–51.
- Fitzgerald EMG (2006) A bizarre new toothed mysticete (Cetacea) from Australia and the early evolution of baleen whales. *Proceedings of the Royal Society B: Biological Sciences* 273: 2955–2963. <https://doi.org/10.1098/rspb.2006.3664>
- Fitzgerald EMG (2010) The morphology and systematics of *Mammalodon colliveri* (Cetacea: Mysticeti), a toothed mysticete from the Oligocene of Australia. *Zoological Journal of the Linnean Society* 158: 367–476. <https://doi.org/10.1111/j.1096-3642.2009.00572.x>
- Fordyce RE, Marx FG (2016) Mysticetes baring their teeth: a new fossil whale, *Mammalodon hakataramea*, from the Southwest Pacific. *Memoirs of Museum Victoria* 74: 107–116. <https://doi.org/10.24199/j.mmv.2016.74.11>
- Geisler JH, Boessenecker RW, Brown M, Beatty BL (2017) The origin of filter feeding in whales. *Current Biology* 27: 2036–2042. [e2032] <https://doi.org/10.1016/j.cub.2017.06.003>
- Gray JE (1864) On the Cetacea which have been observed in the seas surrounding the British Islands. *Proceedings of the Scientific Meetings of the Zoological Society of London* 1864: 195–248.
- Hernández-Cisneros AE (2022) A new aetiocetid (Cetacea, Mysticeti, Aetiocetidae) from the late Oligocene of Mexico. *Journal of Systematic Palaeontology* 20: 1–15. <https://doi.org/10.1080/14772019.2022.2100725>
- Hernández-Cisneros AE, Nava-Sanchez EH (2022) Oligocene dawn baleen whales in Mexico (Cetacea, Eomysticetidae) and palaeobiogeographic notes. *Paleontologia Mexicana* 11: 1–12.
- Marx FG, Fitzgerald EMG, Fordyce RE (2019) Like phoenix from the ashes: How modern baleen whales arose from a fossil “dark age”. *Acta Palaeontologica Polonica* 64: 231–238. <https://doi.org/10.4202/app.00575.2018>
- Marx FG, Tsai C-H, Fordyce RE (2015) A new Early Oligocene toothed ‘baleen’ whale (Mysticeti: Aetiocetidae) from western North America: one of the oldest and the smallest. *Royal Society Open Science* 2: 150476. <https://doi.org/10.1098/rsos.150476>
- Nakae S, Ozaki M, Ota M, Yabumoto Y, Matsuura H, Tomita S (1998) Geology of the Kokura District. With Geological Sheet Map at 1: 50,000. Geological Survey of Japan, 126 pp.
- Okada H (1992) Calcareous nannofossils and biostratigraphy of the Paleogene sequences of the northern Kyushu, Japan. *Journal of the Geological Society of Japan* 98: 505–528. <https://doi.org/10.5575/geosoc.98.509>
- Okazaki Y (1982) A Lower Miocene squalodontid from the Ashiya Group, Kyushu, Japan. *Bulletin of the Kitakyushu museum of natural history*: 107–112.
- Okazaki Y (1995) A new type of primitive baleen whale (Cetacea; Mysticeti) from Kyushu, Japan. *Island Arc* 3: 432–435. <https://doi.org/10.1111/j.1440-1738.1994.tb00123.x>
- Okazaki Y (2012) A new mysticete from the upper Oligocene Ashiya Group, Kyushu, Japan and its significance to mysticete evolution. *Bulletin of the Kitakyushu Museum of Natural History and Human History, Series A (Natural History)* 10: 129–152.
- Olson SL, Hasegawa Y (1996) A new genus and two new species of gigantic Plotopteridae from Japan (Aves: Pelecaniformes). *Journal of Vertebrate Paleontology* 16: 742–751. <https://doi.org/10.1080/02724634.1996.10011362>
- Ozaki M, Hamasaki S, Yoshii M (1993) Geology of the Orio district with geological sheet map at 1: 50,000. Geological Survey of Japan, 121 pp.
- Peredo CM, Pyenson ND, Marshall CD, Uhen MD (2018) Tooth loss precedes the origin of baleen in whales. *Current Biology* 28: 3992–4000. <https://doi.org/10.1016/j.cub.2018.10.047>
- Peredo CM, Pyenson ND, Uhen MD (2022) Lateral palatal foramina do not indicate baleen in fossil whales. *Scientific Reports* 12: 11448. <https://doi.org/10.1038/s41598-022-15684-8>
- Peredo CM, Uhen MD (2016) A new basal chaeomysticete (Mammalia: Cetacea) from the late Oligocene Pysht Formation of Washington, USA. *Papers in Palaeontology* 2: 533–554. <https://doi.org/10.1002/spp2.1051>
- Pyenson ND, Sponberg SN (2011) Reconstructing body size in extinct crown Cetacea (Neoceti) using allometry, phylogenetic methods and tests from the fossil record. *Journal of Mammalian Evolution* 18: 269–288. <https://doi.org/10.1007/s10914-011-9170-1>
- Russell LS (1968) A new cetacean from the Oligocene Sooke formation of Vancouver Island, British Columbia. *Canadian Journal of Earth Sciences* 5: 929–933. <https://doi.org/10.1139/e68-089>
- Saito T (1984) Oligocene calcareous plankton microbiostratigraphy of the Ashiya Group, North Kyushu. *Biostratigraphy and International correlation of the Paleogene System in Japan*: 85–87.
- Sakai T, Horie K, Takehara M (2014) An outcrop of unconformity at Natsugigahama. Vol. 16, Research Report of Cultural Property of Ashiya Town, 110 pp.
- Schoener TW (1974) Resource partitioning in ecological communities: Research on how similar species divide resources helps reveal the natural regulation of species diversity. *Science* 185: 27–39. <https://doi.org/10.1126/science.185.4145.27>
- Tsai C-H, Ando T (2016) Niche partitioning in Oligocene toothed mysticetes (Mysticeti: Aetiocetidae). *Journal of Mammalian Evolution* 23: 33–41. <https://doi.org/10.1007/s10914-015-9292-y>
- Tsai C-H, Fordyce RE (2015) The earliest gulp-feeding mysticete (Cetacea: Mysticeti) from the Oligocene of New Zealand. *Journal of Mammalian Evolution* 22: 535–560. <https://doi.org/10.1007/s10914-015-9290-0>
- Tsai C-H, Fordyce RE (2018) A new archaic baleen whale *Toipahau-tea waitaki* (early Late Oligocene, New Zealand) and the origins of crown Mysticeti. *Royal Society Open Science* 5: 172453. <https://doi.org/10.1098/rsos.172453>
- Tsai C-H (2023) In search of the origin of crown Mysticeti. *Journal of the Royal Society of New Zealand*. <https://doi.org/10.1080/03036758.2023.2249410>
- Walsh BM, Berta A (2011) Occipital ossification of balaenopteroid mysticetes. *The Anatomical Record* 294: 391–398. <https://doi.org/10.1002/ar.21340>
- Wursig B, Thewissen JGM, Kovacs KM (2018) *Encyclopedia of Marine Mammals*. Academic Press, 1190 pp.

# First 3D reconstruction of a forewing of a fossil Orthoptera: Interpreting the venation pattern in the smallest known cricket with a stridulatory apparatus, †*Picogryllus carentonensis* (Orthoptera, Grylloidea, Oecanthidae)

Jules Ferreira<sup>1</sup>, Hugo Josse<sup>1,2</sup>, Lucas Denadai de Campos<sup>3</sup>, André Nel<sup>1</sup>, Laure Desutter-Grandcolas<sup>1</sup>

<sup>1</sup> Institut de Systématique, Evolution, Biodiversité (ISYEB), Muséum National d'Histoire Naturelle, CNRS, Sorbonne Université, EPHE-PSL, Université des Antilles, CP50, 57 rue Cuvier, 75231 Paris, France

<sup>2</sup> Géosciences Rennes, UMR 6118, Université de Rennes, 35000 Rennes, France

<sup>3</sup> Departamento de Zoologia, Instituto de Biociências, Universidade de São Paulo, São Paulo, Brazil

<https://zoobank.org/65560049-759C-4BD2-A2C7-E3CD3998C6>

Corresponding author: Jules Ferreira ([jules.ferreira27@gmail.com](mailto:jules.ferreira27@gmail.com))

Academic editor: Florian Witzmann ♦ Received 21 September 2023 ♦ Accepted 15 January 2024 ♦ Published 29 January 2024

## Abstract

Fossil insects are valuable indicators of the evolutionary history of the clades to which they belong. According to their state of preservation, fossil insects are often partially described for key morphological characters, such as forewing venation in crickets (Orthoptera, Grylloidea). In parallel, the use of 3D microtomography is increasingly becoming common for studying some fossils, which allowed here the precise reconstruction and interpretation of the venation pattern in the smallest known cricket with a stridulatory apparatus, †*Picogryllus carentonensis*, found in opaque amber. The 3D reconstructions have revealed the general structure of the venation of the forewing and have enabled the identification of all its veins and cells, validating its similarity with that of extant crickets. Putative homologies are established according to previous studies, and some particularities are observed, such as the presence of two crossveins in the mirror, a rare feature in extant crickets that is discussed in the frame of cricket venation evolution. These findings highlight the importance of 3D microtomography as a powerful tool for examining fossil insects and also provide crucial information for taxonomic identification and evolutionary studies, offering a validated morphological basis for future phylogenetic analyses incorporating fossils.

## Key Words

evolution, Grylloidea, homology, microtomography, morphology

## Introduction

Wings have been a main key driver of the evolution of insects since the Devonian-Early Carboniferous (Grimaldi and Engel 2005), and for over two centuries, the venation patterns of the wings of insects have been harshly debated. Neither the number of main veins present in insect wings (e.g., Comstock and Needham 1898, 1899; Snodgrass 1935; Kukulová-Peck 1991), nor the criteria to identify them is yet universally settled and accepted (see Schubnel et al. 2020). This situation resulted in the simultaneous use of different venation

paradigms, impeding the safe reconstruction of wing evolution in the megadiverse clade of insects. The recent use of 3D microtomography helps to reconsider the question for these falsely-flat structures (Schubnel et al. 2023). Microtomography gives access to the very base of the wing, showing the basiventral structures from which veins emerge. Using the basiventral origins of the veins as criteria for vein homology and identification, and combining them with vein polarity *sensu* Kukulová-Peck (1991), Schubnel et al. (2020) studied the venation of a large sample of Neoptera insects and proposed a general pattern of venation with seven main veins, i.e., the costal

(C), subcostal (Sc), radial (R), median (M), cubital (Cu), postcubital (PCu) and anal (A) veins.

Orthoptera (grasshoppers, locusts, katydids, crickets, and their allies) presents a venation pattern to which the theoretical pattern of Schubnel et al. (2020) applies very well. Previously, Béthoux and Nel (2001, 2002) proposed a general venation pattern for the superorder Archaeorthoptera (or total group of Orthoptera), identifying several putative apomorphies of the Orthoptera. Schubnel et al. (2020) validated this pattern, modified by the identification of the PCu vein, and confirmed orthopteran putative apomorphies.

Among Orthoptera, Ensifera has experienced high modifications of wing venation in relation to particular uses of the wings, mainly leaf mimicry (Tettigonioidae: Mugleston et al. 2013, 2016; Garrouste et al. 2016), and acoustic communication (Ensifera: Tettigoniidae and Gryllidae: Desutter-Grandcolas et al. 2017). The rearrangement of the veins in these particular functional and / or selective frames may complicate their identification. This is particularly true when considering fossils, as most adults are preserved

as imprints, except for some smaller species preserved in amber (e.g., Gorochoff 2010; Desutter-Grandcolas et al. 2021), with very often incomplete wings and difficulties in following vein trajectories (Gorochoff 1995). Josse et al. (2023) analysed the pattern of venation of the cricket clade (Ensifera, Gryllidae, Grylloidea and Gryllotalpoidea), well-known for their production of acoustic signals. Sampling both fossil and extant cricket families, and following Schubnel et al. (2020), these authors studied not only the structures responsible for sound production, but the whole forewing venation; they finally proposed hypotheses of vein and cell identities according to precise homology criteria.

The Cretaceous fossil †*Picogryllus carentonensis* Josse and Desutter-Grandcolas, 2023 is the smallest cricket with a full stridulatory apparatus ever described, measuring 3.3 mm in body length. This specimen is exceptionally well-preserved (Fig. 1), enabling a nearly complete description of its body as for an extant species (Desutter-Grandcolas et al. 2023). Its right forewing is damaged, but thanks to the usual superposition of the

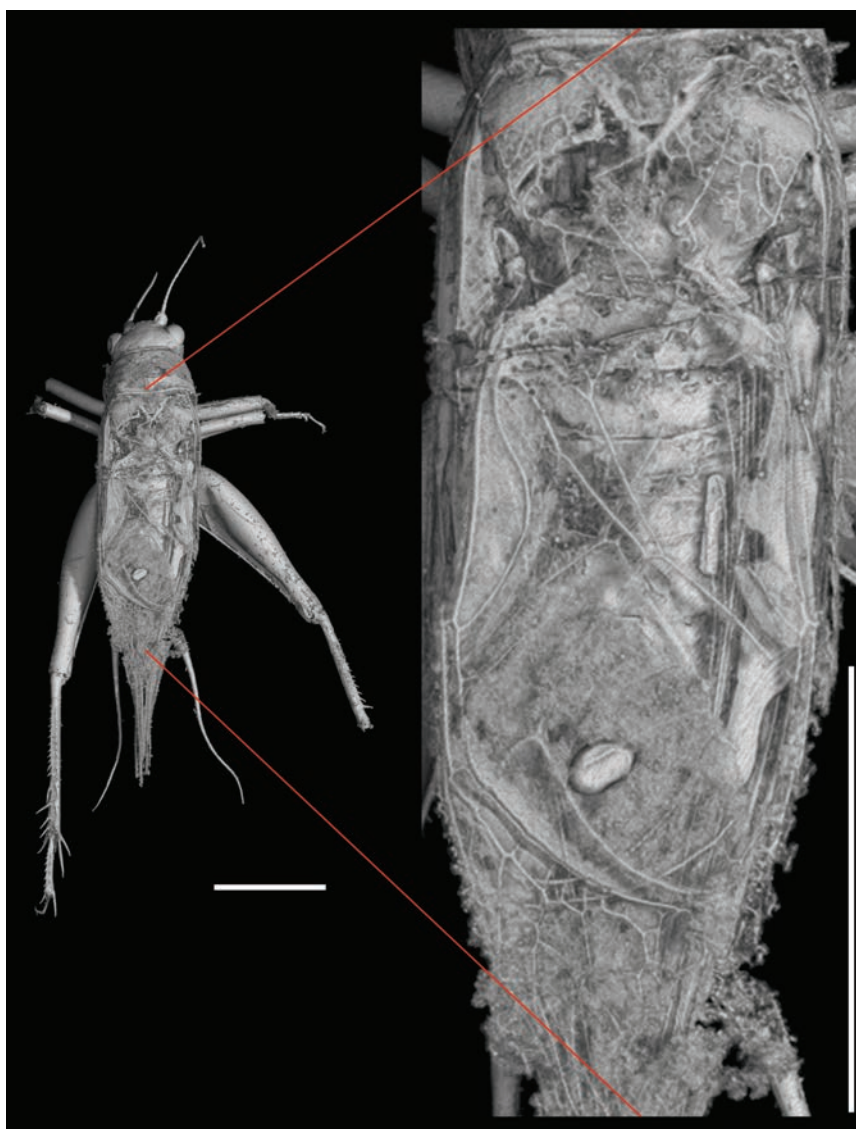


**Figure 1.** 3D reconstruction images of †*Picogryllus carentonensis* in dorsal view (from Desutter-Grandcolas et al. 2023). Scale bars: 1 mm.

right (above) and left (below) forewings in crickets, the left forewing is almost fully complete (Fig. 2A, B).

In the present paper, we present the 3D reconstruction of the left forewing venation of †*P. carentonensis*, which is the first 3D reconstruction of the forewing venation in an ancient fossil cricket. We discussed the application of the venation pattern proposed by Béthoux and Nel (2001, 2002) for orthopteran fossils, Schubnel et al. (2020) for neopteran insects, and Josse et al. (2023) for crickets, identifying its putative synapomorphies with the cricket clades and its putative particularities.

## Material and methods

### Studied material

†*Picogryllus carentonensis* was unearthed from a piece of completely opaque amber retrieved in the A1s1-S layer at the Font-de-Benon quarry in Charente-Maritime, France (Desutter-Grandcolas et al. 2023, see figs 1, 2). This amber piece dated back to the Late Albian to Early Cenomanian period, approximately 100 million years ago (Néraudeau et al. 2002; Dejans and Masure 2005; Peyrot et al. 2005; Polette 2019). It has been described in the Podoscirtinae subfamily of the Oecanthidae family (Campos et al. 2022; Desutter-Grandcolas et al. 2023). The amber piece containing †*P. carentonensis* is deposited at the Institut de Géoscience de Rennes, Université de Rennes, France (reference number IGR.ARC-421.1).

### Fossil imaging and 3D reconstructions

The examination of †*Picogryllus carentonensis* involved propagation phase-contrast X-ray synchrotron microtomography (PPC-SRμCT) at the European Synchrotron Radiation Facility (ESFR) beamline ID19 in Grenoble, France. This technique followed the established procedure outlined by Lak et al. (2008). The scanning parameters were set at 30 keV, a propagation distance of 900 mm, and an isotropic voxel size of 20.24 μm. A total of 2 500 projections were captured over a 180° range, with each projection exposed for 0.2 seconds. For the initial analysis of the tomographic data, VG StudioMax (Volume Graphics) was employed, as detailed in the methodology provided by Desutter-Grandcolas et al. (2023). The data used for reconstructions in this study consisted of 2D microtomographic scans in JPEG 2 000 format. These scans were taken in the three spatial planes: X, Y, and Z, resulting in 1 256 scans for X, 1 347 scans for Y, and 1 037 scans for Z.

The 3D reconstructions of the forewing of †*P. carentonensis* were made using Avizo Lite 9.5.0 software from Thermo Fisher Scientific. The “Surface view” function within the software facilitated the visualization and study of these reconstructions. Utilizing the insights from these 3D reconstructions, illustrations of the left forewing were produced using Microsoft PowerPoint 2021.

### Venation paradigm

We are using the venation pattern of Josse et al. (2023) for crickets (Orthoptera, Gryllidea) and the paradigm proposed by Béthoux and Nel (2001, 2002) modified by Schubnel et al. (2020). Each of the recognized seven main veins is identified along the whole wing length, from the base (basivenal structures) to the tip. The wing is separated into a lateral and a dorsal field, located respectively along and above the body. We also follow the orientation currently used to describe wing venation, separating anterior vs posterior and proximal (= basal) vs distal margins (Fig. 3).

### Abbreviations

The following abbreviations and colours are listed below, and follow Josse et al. (2023):

Main veins and their bifurcations:

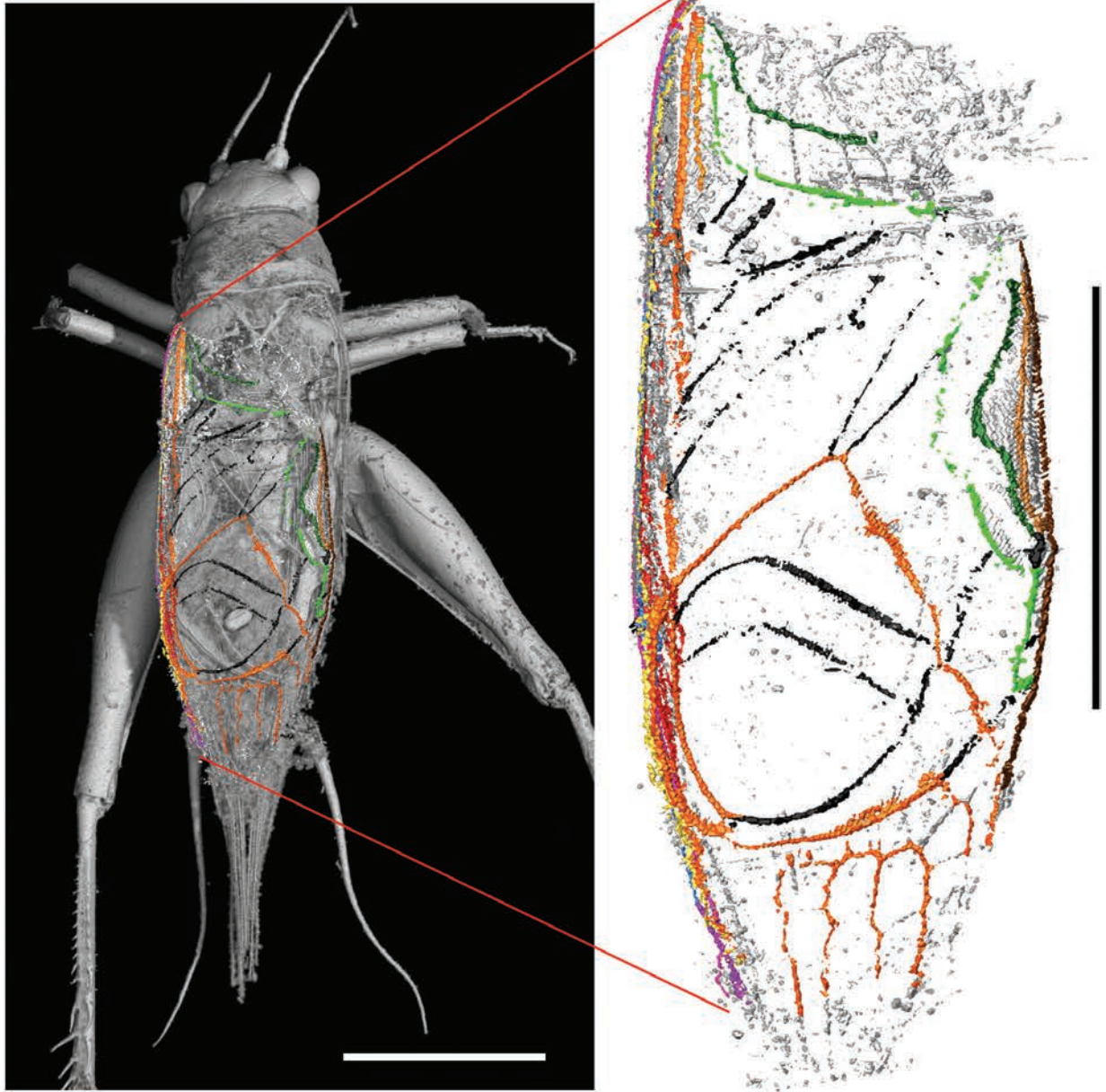
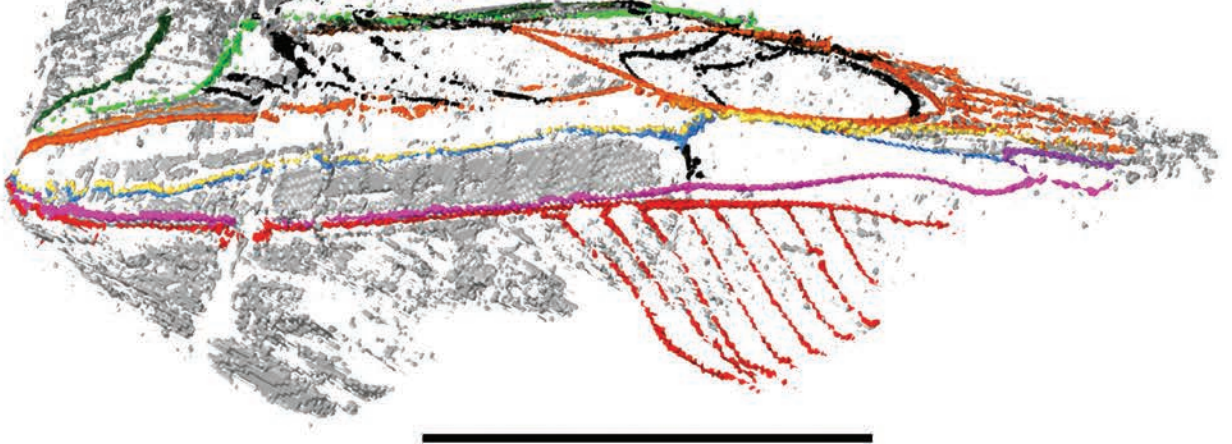
**A:** anal (brown);  
**C:** costa (yellow);  
**Cu:** cubitus (orange);  
**M:** media (blue);  
**PCu:** postcubitus (green);  
**R:** radius (pink);  
**Sc:** subcosta (red);  
**“X”A:** anterior branch of “X” vein (light colour);  
**“X”P:** posterior branch of “X” vein (dark colour);  
**“X”A/P; a, b; α, β; 1, 2:** successive dichotomies of main branches of veins in Orthoptera.

Reinforced crossveins (black in figures):

**d1:** diagonal 1 (crossvein between CuPaα and CuPaβ);  
**d2:** diagonal 2 (crossvein between CuPaβ and PCuA);  
**pi:** or pilar (crossvein between, or close to PCuA and the point of contact of CuPaβ with d2);  
**r-m:** crossveins between R and M;  
**s1, s2:** septum 1 and 2 (crossveins between CuPaα2 and CuPaβ);  
**t1, t2:** transverse 1 and 2 (distal crossveins between CuPaβ and PCuA);  
**t3 to t5:** transverse 3 to 5 (distal crossveins between PCu branches and anal branches).

Forewing (FW) cells:

**ac:** anal cell;  
**c1, c2, c3:** cell 1, 2, 3;  
**ha:** harp;  
**lc:** lanceolate cell;  
**mi:** mirror;  
**para-mi:** para-mirror;  
**sub-c1, c2:** sub-cell 1, 2, located distally to cells c1, c2;  
**sub-mi:** sub-mirror.

**A****B**

**Figure 2.** 3D reconstructions of venation of left forewing of †*Picogryllus carentonensis*. **A.** Dorsal view; **B.** Latero-dorsal view. Scale bars: 1 mm.

## Results

### 3D reconstructions of the venation of the forewing in †*Picogryllus carentonensis*

The left FW of †*Picogryllus carentonensis* has been protected by the right FW. It is nearly complete, except for the base of anal area and the antero-basal area of the lateral field, which could not be completely reconstructed. Also, the teeth of the stridulatory file, located on the PCuA vein, could not be counted, because of the scan precision and the size of the fossil.

The general structure of the FW of †*P. carentonensis* is similar to that of modern crickets, with a dorsal field and a lateral field clearly separated by a median fold located between CuPa and M+CuA. Distally to this fold, the fan, i.e., a thinner part of the wing membrane, extends between the two fields. The fossil has the lateral fields of the forewings vertical along the insect body, nearly at right angle with the dorsal field, which is flat over the insect dorsum (Figs 1, 2).

**Lateral field** (Fig. 3): Wide; maximum width as large as about 3/4<sup>th</sup> of dorsal field maximum width; length about 4/5<sup>th</sup> of dorsal field length. Three main veins and

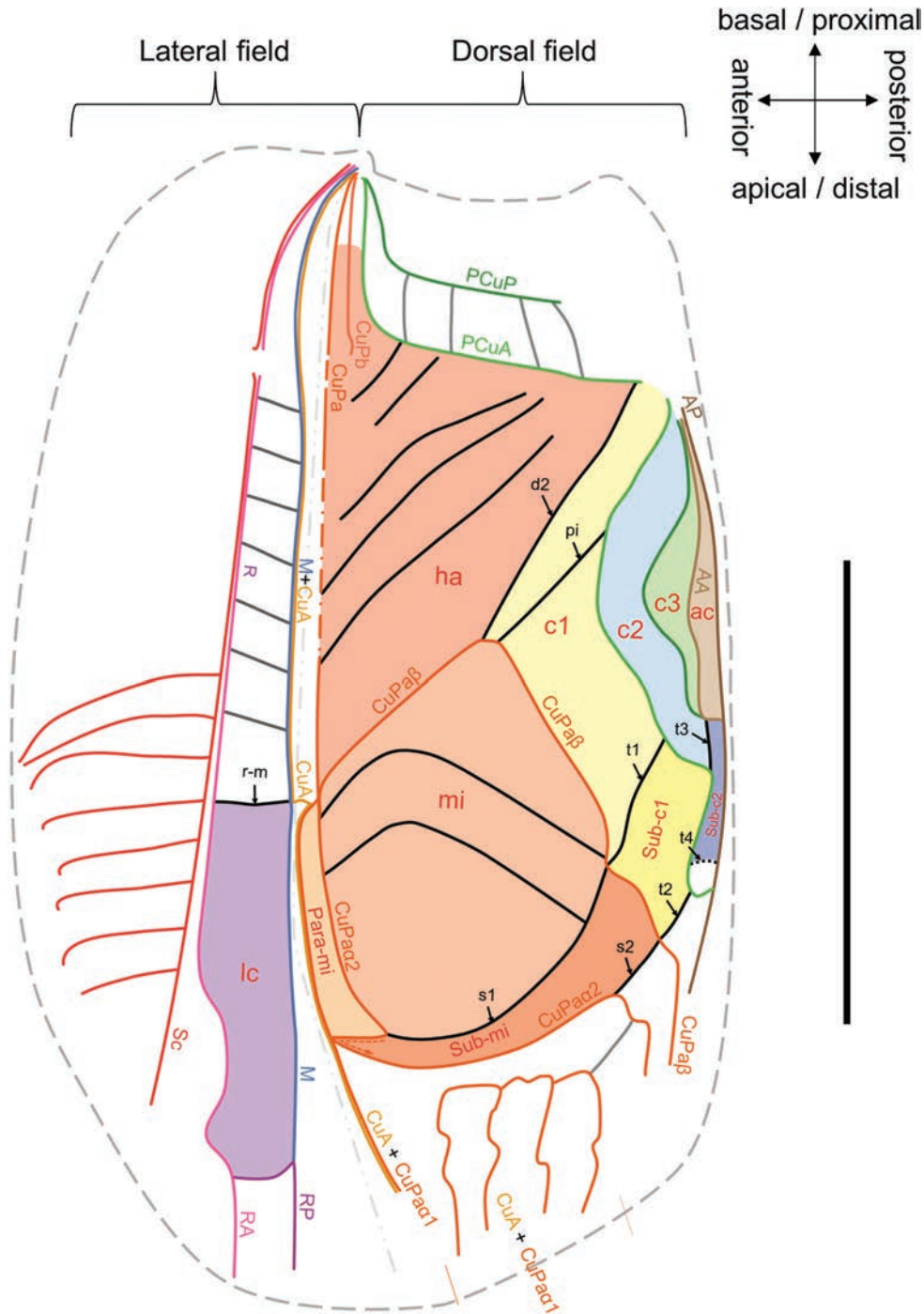


**Figure 3.** Interpretive drawing of venation pattern of left forewing of †*Picogryllus carentonensis*, following terminology and colours as in Josse et al. (2023). Fold separating lateral and dorsal field represented by a dashed-dotted line. Scale bar: 1 mm.

their branches visible, i.e., Sc, R and M+CuA, emerging from very close or maybe merged into bullae basivenal. C not visible or absent. Sc long, reaching lateral field apex, pectinate, with branches directed towards anterior edge of wing and occupying most of lateral field, with at least eight visible distinct oblique branches directed anteriorly. R long, bifurcating into RA and RP very distally, at apical end of lateral field. Sc and R parallel and very close on 3/4<sup>th</sup> of lateral field length. M+CuA long, bifurcated in M and CuA at 2/3<sup>rd</sup> of wing length. R and M+CuA are clearly divergent from their bases becoming almost parallel from 2/4<sup>th</sup> of field length, both veins connected by at least seven oblique, weak crossveins plus a reinforced r-m, limiting basally lanceolate cell; r-m rather perpendicular to R and M. Lanceolate cell long and narrow, located in fan between R and M, approximately 4.5 times longer than wide; with a very slight constriction between R and M at its base at level of r-m. RA straight part directed towards distal end of wing, in continuity of R; RP proximally curved, joining M and merging with it, delimitating apical end of lanceolate cell; distally RP separating again from M and with a distal rectilinear vein in continuity of M. M+CuA bifurcating into M and CuA slightly distal to r-m; M straight towards distal edge of wing and posteriorly limiting lanceolate cell to join and merge with RP distally, in fan. MA or MP not visible or absent. CuA very short, crossing median fold and reaching CuPa posteriorly.

**Dorsal field:** Dorsal field slightly longer and about 1.5 times wider than lateral field. Three main veins and their branches visible: Cu(P), PCu and A. CuP and PCu bases visible, base of Anal veins not visible. CuP bifurcating in CuPa and CuPb from its base. CuPa long, straight, parallel to M+CuA and longitudinal axis of wing over half dorsal field length, bifurcating in CuPaa and CuPaβ at beginning of dorsal field lower 1/3<sup>rd</sup>; CuPaa immediately dividing into CuPaa1 and CuPaa2; CuPaa1 immediately merging with CuA as CuA+CuPaa1, CuPaa2 continuing distally to CuPa with a trajectory parallel to CuA+CuPaa1. CuPb reduced to a short vein (about 1/6<sup>th</sup> of wing length) parallel to CuPa. PCu bifurcating in PCuA and PCuP from its base, both clearly divergent at their base, then curved at 90° before running parallel to the wing posterior edge. Distal to interrupted zone of PCuA and PCuP, both veins with curved and convex anterior trajectories. Anal node and plectrum not visible. Anal veins not preserved at their bases, but visible more distally with trajectories closely following posterior edge of wing. AA slightly curved and convex anteriorly, AP rather straight. Harp longer than wide (Table 1), right-angled and triangle shaped, maximal length greater than half field length; at least five oblique crossveins connecting CuPa to PCuA. ‘Diagonal’ vein (postero-distal limit of harp) composite, made of a part of CuPaβ, proximally curved, and d2, a reinforced crossvein joining ‘elbow’ of CuPaβ to PCuA at anal node. Mirror medium-sized (Table 1), rather rounded distally, but with straighter edge proximally, because of elbow shape of CuPaβ; crossed by two proximally convex crossveins; distal edge flanked by two long and thin cells, i.e., para-mirror and sub-mirror.

Ant-mirror cell absent (d1 absent). Para-mirror longer than wide (Table 1), slightly widening distally, extending along a large part of mirror anterior edge; distally closed by a zig-zag shaped CuPaa, joining CuA+CuPaa1 at one point, before resuming its trajectory towards posterior edge. Sub-mirror longer than wide, longer than para-mirror, gradually widening posteriorly, along distal edge of mirror in continuity with para-mirror, separated from mirror by a long s1. Distal edge of sub-mirror limited by a part of CuPaa2 and a short s2, which connects it with CuPaβ; s2 shorter than s1. Apical field occupied by CuA+CuPa branches, stem vein of CuA+CuPa stronger and in the continuity of CuPa. Posterior field well preserved, with clear c1, c2, c3, sub-c1, sub-c2 and ac. Sub-c3 difficult to see, very small or absent. Cell c1 long and wide, crossed by pi (Table 1), limited distally by a long t1 (Table 1) aligned in continuity with s1; sub-c1 rather large (Table 1), t2 aligned in continuity of s2; c2 longer than wide, narrower than c1, limited distally by t3; sub-c2 longer and narrower; c3 smaller than c1 and c2; ac long and narrow.

**Table 1.** Measurements of veins and cells of left forewing in †*P. carentonensis*.

Veins	Length (in mm)		
Harp anterior edge	1.27		
Harp posterior edge	0.77		
Harp postero-distal edge	1.11		
s1	0.66		
s2	0.13		
Cells	Maximal length (in mm)	Maximum width (in mm)	Ratio length / width
Mirror	0.89	0.65	1.36
Para-mirror	0.54	0.05	10.8
Sub-mirror	0.66	0.18	3.67
c1	0.89	0.22	4.04
Sub-c1	0.42	0.17	2.47

## Discussion

3D reconstructions are increasingly used to examine the venation in insects and propose putative homologies of their veins (e.g., Schubnel et al. 2023). This method can be applied to both extant and fossil taxa, which may facilitate comparative approaches. For fossil crickets, most venation descriptions were made from the observation of imprints. Several well-preserved specimens have been recently described in amber, for which wing venation could be observed and the functional part of the stridulum fully described when present (e.g., Rust et al. 1999; Xu et al. 2020, 2022; Yuan et al. 2022, see fig. 2). Even during the revision process of this paper, Zheng et al. (2023) described two new fossils of Oecanthidae found in Myanmar amber, Cenomanian, upper Cretaceous, i.e., †*Crassicornus maculatus* Zheng, Yuan & Gu, 2023 and †*Ordicalcaratus inconditus* Zheng, Yuan & Gu, 2023, respectively classified in the Oecanthinae and in the Podoscirtinae, and both twice as large as †*P. carentonensis*. These nicely

preserved fossils are described by optic means, thanks to their preservation in clear amber, and increase the number of fossils that are now available to study the Oecanthidae cricket clade. However, optic observations present limitations in terms of resolution and anatomical details, which make homology assessments tricky. Scanning Electronic Microscope has occasionally allowed better observations of wing structures, as demonstrated by the study of the stridulatory vein in a fossil katydid (Gu et al. 2012), the study of the ultrastructure of the wing of an Odonata (Appel et al. 2015), and the study of the wing venation in a Hemiptera (Franielczyk-Pietryra et al. 2023). 3D microtomography is a real progress in the venation study, as shown by the number of papers that use it (e.g., Desutter-Grandcolas et al. 2017; Garwood and Sutton 2010; Walker et al. 2014; Jacquelin et al. 2018; Schubnel et al. 2020, 2023). In the present paper, microtomography allowed the reconstruction of the left forewing of †*P. carentonensis*, although located under the right forewing, and revealed the very details of its venation, despite the precision of the scans not being optimal due to the small size of the specimen. Here, the limitations of microtomography for a specimen of such a small size prevents the reconstruction of the stridulatory file, which in turn could have been used to hypothesize the frequency of the calling song of †*P. carentonensis*. Employing nanotomography for a more detailed scan may be a solution here. However, it is important to note that despite the potential for accessing finer details, the results may not necessarily be better. It would certainly increase the resolution of the reconstructed specimen and that of the interpreted area, but given the apparent damage in these regions, it would probably not help to reconstruct the missing structures. It is anyhow the first time that an almost complete 3D venation pattern is reconstructed in a fossil Orthoptera.

### FW venation in †*Picogryllus carentonensis*

Applying Josse et al. (2023) wing venation patterns for crickets to the reconstruction of the venation of †*Picogryllus carentonensis*, the veins Sc, R, M, Cu, PCu, and A can readily be identified. The base of the Sc is not preserved, which impedes recovering the Costal vein and separates the anterior and posterior branches of Sc. But Sc is pectinate, as observed for ScP in many modern crickets (Josse et al. 2023). †*Picogryllus carentonensis* presents characters identified as synapomorphies of the Orthoptera by Béthoux and Nel (2001, 2002), i.e., the fusion M+CuA and the fusion CuA+CuPa $\alpha$ 1. Also, its two PCu veins (PCuA, PCuP) have the usual shape of these veins, with a strongly curved proximal part (Schubnel et al. 2020).

As in all acoustic crickets, †*P. carentonensis* has a lanceolate cell delimited proximally by r-m and distally by the zigzag-shaped RP; M and CuA separate at the level of the anterior margin of the lanceolate cell; and the two PCu veins run near the posterior margin of the wing, making the so-called chord veins of crickets (Josse et al. 2023). The harp and the c1 cell are separated by

the crossvein d2 (commonly called the diagonal in cricket wing), and the mirror is delimited by CuPa $\alpha$ 2 (anterior margin), CuPa $\beta$  (proximal margins) and the crossvein s1. Finally, an arculus is present, made of the crossvein r-m and the vein CuA after its separation from M (Fig. 3).

As in many Grylloidea, CuP has a posterior branch; when present, CuPb goes usually no further than the most distal harp veins (as in Phalangopsidae crickets for example: see Josse et al. 2023, fig. 3B); in †*P. carentonensis*, CuPb is short, not reaching the most proximal harp veins, as frequently observed in crickets of the supertribe Podoscirtidi (Campos et al. 2022). The mirror is bordered by only two long and narrow cells, i.e., para-mi and sub-mi, and not by the cell sub-c1, which is adjacent to the mirror by one corner. The cell c1 includes the strong crossvein pi, and the mirror is crossed by two parallel, strong crossveins. Finally, the crossvein d1 and the cell ant-mi, sometimes present near the anterior margin of the mirror, are lacking.

Forewing venation in crickets has not been analysed on a firm basis of primary homology setting, although several venation patterns have been hypothesized in the last twenty years (Rasnitsyn and Quicke 2002; Robillard and Desutter-Grandcolas 2004; Béthoux 2008). Josse et al. (2023) proposed a general pattern of FW venation for crickets with acoustic apparatus, which they also apply to male crickets with incomplete apparatus, crickets lacking acoustic structures, and females.

The reconstruction of the FW venation of †*P. carentonensis* generates a pattern that is fully compatible with the proposal of Josse et al. (2023). The homologies proposed by Josse et al. (2023), validated by our own data, will have now to be incorporated in phylogenetic studies of large cricket clades, to test hypotheses of forewing evolution, especially for the shape and limit of the mirror and nearby cells (para-mi, ant-mi, sub-mi), that may delimit vibrating areas. The interpretations of FW venation of †*Crassicorpus maculatus* and †*Ordicalcaratus inconditus* are congruent with our own reconstructions and interpretations of †*P. carentonensis*; the cells around the mirror, not identified individually by Zheng et al. (2023) because of cross-publishing of their work and that of Josse et al. (2023), seem actually present in both fossils, but their identification, and the identification of the veins delimiting and crossing the mirror will have to be checked with more details.

### Particularities in †*Picogryllus carentonensis*?

Although it exhibits a remarkable similarity in wing venation to extant Oecanthidae, †*Picogryllus carentonensis* also displays unique characteristics in its FWs, as the presence of two crossveins in the mirror. Few crickets present two crossveins, or more, in the mirror. The number of crossveins in the cell homologous to the true mirror of crickets varies among the fossils currently classified as †Baissogryllidae, or as †Protogryllidae. This postero-distally cell is open, even enlarged in †Baissogryllidae (Josse et al. 2023, fig. 6), but, it is not closed by a reinforced s1

as in true crickets. Extant phalangopsid crickets, such as *Paragrillus* Guérin-Méneville, 1844, *Rumea* Desutter, 1988, *Paragrillodes* Karny, 1909 and their relatives, have up to six concentric crossveins in their mirror, while winged Phaloriinae have usually two transverse ones, as the Luzarinae *Lerneca fuscipennis* (Saussure, 1874) (Josse et al. 2023, fig. 3B). All these crickets emit loud calls; they also have long, wide, flexible forewings, except *Paragrillodes*, whose forewings do not cover more than half of the abdomen and are somewhat corneous. Some taxa of the Oecanthidi supertribe have been reported with two crossveins in the mirror (Campos et al. 2022), but applying the pattern defined by Josse et al. (2023) to taxa of the genus *Oecanthus* Serville, 1831, shows that the mirror of Oecanthidi has in fact only one crossvein, and that the most proximal cell of the mirror is actually a highly modified c1 cell. In many contemporary crickets, the mirror is involved in sound propagation (Dambach and Gras 1995; Mhatre et al. 2012). The presence of crossveins in the mirror could then be related to wing vibration, as the large, flexible forewings may actually need to be reinforced to resist to vibration. The presence of an arculus revealed by Josse et al. (2023) in singing crickets and mole crickets, but lacking in mute crickets and females, goes in the same direction. Both †*Crassicorpus maculatus* and †*Ordicalcaratus inconditus* present only one vein across the mirror (see Zheng et al. 2023, figs 3B and 4D), but the presence of an arculus will have to be checked on the fossils.

Could this reinforcement hypothesis also apply to †*P. carentonensis*? †*P. carentonensis* is actually the smallest cricket ever found with a stridulatory apparatus, in both the extant and fossil species, measuring only 3.3 mm in body length, and the smallest complete apparatus ever documented. In extant crickets, the smallest species are usually apterous, i.e., ant-loving crickets Myrmecophilidae or some Nemobiinae (Trigonidiidae) crickets, and the smallest singing crickets are much larger than †*P. carentonensis* (Bennet-Clark 1999). As the frequency of the calling song increases with the decrease of cricket size (Bennet-Clark 1999), the crossveins of †*P. carentonensis* may have allowed the call of this species to remain in relatively low frequencies. Detailed studies of wing vibration are now necessary to test the role of these veins as reinforcement structures, whatever the size of the forewings.

Can phylogeny bring information about the evolution of these veins? The †Baissogryllidae, †Protogryllidae, and Phalangopsidae are not closely related to the Oecanthidae (Chintauan-Marquier et al. 2016; Campos et al. 2022), and †*Picogryllus* is nested within the Oecanthidae phylogeny (Ferreira 2023). When comparing the crossveins present in the mirror region of †*P. carentonensis* to those observed in *Lerneca fuscipennis* for example (Phalangopsidae, Luzarinae, see Josse et al. 2023, fig. 3B), it is clear that in both specimens, the crossveins exhibit identical connections: each crossvein is linked to CuPaa2, with one also connected to CuPaβ, and the other connected to s1 crossveins. In the same way, the veins in the mirror

of some †Baissogryllidae and some †Protogryllidae could be homologous to the veins of †*P. carentonensis*, although oriented longitudinally (and not transversally). Nevertheless, the venations of †baissogryllid and †protogryllid differ from that of †*P. carentonensis* by the presence of d1 and of an ant-mirror cell (Josse et al. 2023, fig. 6). These crossveins may support a hypothesis of primary homology, but most probably are homoplastic in the frame of cricket phylogeny.

## Conclusion

The application of 3D microtomography is a real progress in the examination of wing venation in fossil insects. The venation pattern observed in †*Picogryllus carentonensis* is congruent with the pattern proposed by Josse et al. (2023) for crickets, and the synapomorphies of Orthoptera identified by Béthoux and Nel (2001, 2002) for Archaeorthoptera. The reconstruction also highlights unique features of the forewing, like the presence of two crossveins in the mirror, a characteristic not commonly observed in extant crickets, which could be linked to functional properties of the forewing. These findings will support further investigations into the evolution of acoustic structures in crickets. The exquisite preservation of the venation pattern of the fossil †*Picogryllus carentonensis* also holds significant importance for evolutionary biology. It will prove invaluable when constructing a morphological matrix for tip dating (solely reliant on morphological data), total-evidence (incorporating both molecular and morphological data for extant taxa, alongside morphological data for extinct taxa), or total-evidence dating studies (additionally considering ages) (e.g., Ronquist et al. 2012; Jouault et al. 2021, 2022). Fossils lack molecular data, but precise morphological information are most valuable for accurate fossil placements, which contribute to the renewal of morphological phylogenetic studies (e.g., Kealy and Beck 2017; Beck et al. 2023; Coiro et al. 2023).

## Data availability

Untreated CT-scans are available upon request to the corresponding author, and for scientific work at: <https://doi.org/10.5281/zenodo.8270385>.

## Acknowledgments

We are grateful to the two anonymous reviewers for their insights and comments on the first version of the manuscript, which helped us to improve it. Our gratitude also goes to Paul Tafforeau and Malvina Lak (ESRF) for their contribution to the synchrotron imaging of the specimens, as well as Carmen Soriano (ESRF) for the global volume rendering of the specimen. We also thank Patricia Wils

(MNHN, UMS2700 CNRS), who helped us with the use of Avizo Lite, allowing the segmentation of the forewing. Finally, we acknowledge the support of the Museum für Naturkunde, Berlin, for the publication of this paper.

## References

- Appel E, Heepe L, Lin C-P, Gorb SN (2015) Ultrastructure of dragonfly wing veins: composite structure of fibrous material supplemented by resilin. *Journal of Anatomy* 227: 561–582. <https://doi.org/10.1111/joa.12362>
- Beck RMD, de Vries D, Janiak MC, Goodhead IB, Boubli JP (2023) Total evidence phylogeny of platyrrhine primates and a comparison of undated and tip-dating approaches. *Journal of Human Evolution* 174: 103293. <https://doi.org/10.1016/j.jhevol.2022.103293>
- Bennet-Clark HC (1999) Resonators in insect sound production: how insects produce loud pure-tone songs. *Journal of Experimental Biology* 202: 3347–3357. <https://doi.org/10.1242/jeb.202.23.3347>
- Béthoux O (2008) Groundplan, nomenclature, homology, phylogeny, and the question of the insect wing venation pattern. *Alavesia* 2: 219–232.
- Béthoux O, Nel A (2001) Venation pattern of Orthoptera. *Journal of Orthoptera Research* 10: 195–198. [https://doi.org/10.1665/1082-6467\(2001\)010\[0195:VPOO\]2.0.CO;2](https://doi.org/10.1665/1082-6467(2001)010[0195:VPOO]2.0.CO;2)
- Béthoux O, Nel A (2002) Venation pattern and revision of Orthoptera sensu nov. and sister groups. Phylogeny of Palaeozoic and Mesozoic Orthoptera sensu nov. *Zootaxa* 96: 1–88. <https://doi.org/10.11646/zootaxa.96.1.1>
- Campos L, B Souza-Dias P, Audino J, Desutter-Grandcolas L, Nihei S (2022) The fifth family of the true crickets (Insecta: Orthoptera: Ensifera: Grylloidea), Oecanthidae defin. nov.: phylogenetic relationships and divergence times. *Zoological Journal of the Linnean Society* 197: 1–44. <https://doi.org/10.1093/zoolinnean/zlac066>
- Chintauan-Marquier IC, Legendre F, Hugel S, Robillard T, Grandcolas P, Nel A, Zuccon D, Desutter-Grandcolas L (2016) Laying the foundations of evolutionary and systematic studies in crickets (Insecta, Orthoptera): a multilocus phylogenetic analysis. *Cladistics* 32: 54–81. <https://doi.org/10.1111/cla.12114>
- Coiro M, Allio R, Mazet N, Seyfullah LJ, Condamine FL (2023) Reconciling fossils with phylogenies reveals the origin and macroevolutionary processes explaining the global cycad biodiversity. *New Phytologist* 240: 1616–1635. <https://doi.org/10.1111/nph.19010>
- Comstock JH, Needham JG (1898) The wings of insects. *The American Naturalist* 32: 81–89. <https://doi.org/10.1086/276780>
- Comstock JH, Needham JG (1899) The wings of insects. *The American Naturalist* 33: 845–860. <https://doi.org/10.1086/277462>
- Dambach M, Gras A (1995) Bioacoustics of a miniature cricket, *Cycloptiloides canariensis* (Orthoptera: Gryllidae: Mogoplistinae). *Journal of Experimental Biology* 198: 721–728. <https://doi.org/10.1242/jeb.198.3.721>
- Dejax J, Masure E (2005) Analyse palynologique de l'argile lignitifère à ambre de l'Albien terminal d'Archingeay (Charente-Maritime, France). *Comptes Rendus Palevol* 4: 53–65. <https://doi.org/10.1016/j.crpv.2004.12.002>
- Desutter-Grandcolas L, Hugel S, Nel A, Warren B, Souza-Dias P, Chintauan-Marquier IC (2021) Updated diagnoses for the cricket family Trigonidiidae (Insecta: Orthoptera: Grylloidea) and its subfamilies (Trigonidiinae, Nemobiinae), with a review of the fossil record. *Zoologischer Anzeiger* 294: 80–91. <https://doi.org/10.1016/j.jcz.2021.06.004>
- Desutter-Grandcolas L, Josse H, Laurent M, Campos LD de, Hugel S, Soriano C, Nel A, Perrichot V (2023) New Cretaceous crickets of the subfamilies Nemobiinae and Podoscirtinae (Orthoptera, Grylloidea: Trigonidiidae, Oecanthidae) attest the antiquity of these clades. *Geological Magazine* 160: 927–940. <https://doi.org/10.1017/S0016756823000055>
- Desutter-Grandcolas L, Jacquelin L, Hugel S, Boistel R, Garrouste R, Henrotay M, Warren BH, Chintauan-Marquier IC, Nel P, Grandcolas P, Nel A (2017) 3-D imaging reveals four extraordinary cases of convergent evolution of acoustic communication in crickets and allies (Insecta). *Scientific Reports* 7: 7099. <https://doi.org/10.1038/s41598-017-06840-6>
- Ferreira J (2023) Reconstructions 3D d'un fossile de grillon, son incorporation dans une analyse phylogénétique en total-evidence et estimation des dates de divergence de la famille des Oecanthidae (Orthoptera : Grylloidea). Institut de Systématique, Evolution, Biodiversité, Paris, France. Rapport de stage - M1 SEP.
- Franielczyk-Pietryra B, Kalandyk-Kołodziejczyk M, Drohojowska J (2023) Is every vein a real vein? Cross-section of the wing of *Matsucoccus pini* (Insecta, Hemiptera, Coccoidea: Matsucoccidae). *Insects* 14: 390. <https://doi.org/10.3390/insects14040390>
- Garrouste R, Hugel S, Jacquelin L, Rostan P, Steyer J-S, Desutter-Grandcolas L, Nel A (2016) Insect mimicry of plants dates back to the Permian. *Nature Communications* 7: 13735. <https://doi.org/10.1038/ncomms13735>
- Garwood R, Sutton M (2010) X-ray micro-tomography of Carboniferous stem-Dictyoptera: new insights into early insects. *Biology Letters* 6: 699–702. <https://doi.org/10.1098/rsbl.2010.0199>
- Gorochov AV (1995) O sisteme i evolyutsii otrjada pryamokrylykh (Orthoptera) [Contribution to the system and evolution of the order Orthoptera]. *Zoologicheskyy Zhurnal* 74: 39–45. [in Russian]
- Gorochov AV (2010) New and little-known orthopteroid insects (Polyneoptera) from fossil resins: Communication 4. *Paleontological Journal* 44: 657–671. <https://doi.org/10.1134/S0031030110060080>
- Grimaldi D, Engel MS (2005) *Evolution of the insects*. Cambridge University Press, 788 pp.
- Gu J-J, Montealegre-Z F, Robert D, Engel MS, Qiao G-X, Ren D (2012) Wing stridulation in a Jurassic katydid (Insecta, Orthoptera) produced low-pitched musical calls to attract females. *Proceedings of the National Academy of Sciences* 109: 3868–3873. <https://doi.org/10.1073/pnas.1118372109>
- Jacquelin L, Desutter-Grandcolas L, Chintauan-Marquier I, Boistel R, Zheng D, Prokop J, Nel A (2018) New insights on basivenal sclerites using 3D tools and homology of wing veins in Odonatoptera (Insecta). *Scientific Reports* 8: 238. <https://doi.org/10.1038/s41598-017-18615-0>
- Josse H, Faberon L, Schubnel T, Nel A, Desutter-Grandcolas L (2023) Reconciliation between neontology and paleontology in the Gryllidea (Orthoptera, Ensifera): reinterpreting the venation of the stridulatory apparatus in crickets. *Zoosystema* 45: 769–801. <https://doi.org/10.5252/zoosystema2023v45a24>
- Jouault C, Legendre F, Grandcolas P, Nel A (2021) Revising dating estimates and the antiquity of eusociality in termites using the fossilized birth–death process. *Systematic Entomology* 46: 592–610. <https://doi.org/10.1111/syen.12477>

- Jouault C, Maréchal A, Condamine FL, Wang B, Nel A, Legendre F, Perrichot V (2022) Including fossils in phylogeny: a glimpse into the evolution of the superfamily Evanioidea (Hymenoptera: Apo-crita) under tip-dating and the fossilized birth–death process. *Zoological Journal of the Linnean Society* 194: 1396–1423. <https://doi.org/10.1093/zoolinnean/zlab034>
- Kealy S, Beck R (2017) Total evidence phylogeny and evolutionary timescale for Australian faunivorous marsupials (Dasyuromorphia). *BMC Evolutionary Biology* 17: 240. <https://doi.org/10.1186/s12862-017-1090-0>
- Kukulová-Peck J (1991) Chapter 6: Fossil history and the evolution of hexapod structures. In: Naumann ID (Ed.) *The insects of Australia, a textbook for students and research workers* (2<sup>nd</sup> ed.). Melbourne University Press, Melbourne 1: 141–179.
- Lak M, Azar D, Nel A, Néraudeau D, Tafforeau P (2008) The oldest representative of the Trichomyiinae (Diptera : Psychodidae) from the Lower Cenomanian French amber studied with phase-contrast synchrotron X-ray imaging. *Invertebrate Systematics* 22: 471–478. <https://doi.org/10.1071/IS08008>
- Mhatre N, Montealegre-Z F, Balakrishnan R, Robert D (2012) Changing resonator geometry to boost sound power decouples size and song frequency in a small insect. *Proceedings of the National Academy of Sciences* 109: E1444–E1452. <https://doi.org/10.1073/pnas.1200192109>
- Mugleston J, Naegle M, Song H, Bybee SM, Ingleby S, Suvorov A, Whiting MF (2016) Reinventing the leaf: multiple origins of leaf-like wings in katydids (Orthoptera : Tettigoniidae). *Invertebrate Systematics* 30: 335–352. <https://doi.org/10.1071/IS15055>
- Mugleston JD, Song H, Whiting MF (2013) A century of paraphyly: a molecular phylogeny of katydids (Orthoptera: Tettigoniidae) supports multiple origins of leaf-like wings. *Molecular Phylogenetics and Evolution* 69: 1120–1134. <https://doi.org/10.1016/j.ympev.2013.07.014>
- Néraudeau D, Perrichot V, Dejax J, Masure E, Nel A, Philippe M, Moreau P, Guillocheau F, Guyot T (2002) Un nouveau gisement à ambre insectifère et à végétaux (Albien terminal probable) : Archingeay (Charente-Maritime, France). *Geobios* 35: 233–240. [https://doi.org/10.1016/S0016-6995\(02\)00024-4](https://doi.org/10.1016/S0016-6995(02)00024-4)
- Peyrot D, Jolly D, Barrón E (2005) Apport de données palynologiques à la reconstruction paléoenvironnementale de l’Albo-Cénomaniens des Charentes (Sud-Ouest de la France). *Comptes Rendus Palevol* 4: 151–165. <https://doi.org/10.1016/j.crpv.2004.11.016>
- Polette F (2019) Les assemblages palynologiques continentaux du Crétacé inférieur de France (Tithonien–Cénomaniens) : paléoenvironnements, paléoclimats, stratigraphie, et taxonomie. Thèse de doctorat. Rennes 1. [Available from:] <https://www.theses.fr/2019REN1B051> [April 30, 2023]
- Rasnitsyn A, Quicke D (2002) 2.2. Subclass Scarabaeona Laicharting, 1781. The winged insects (= Pterygota Lang, 1888). *History of Insects*. Kluwer Academic Publishers, Dordrecht, 75–83.
- Robillard T, Desutter-Grandcolas L (2004) Phylogeny and the modalities of acoustic diversification in extant Eneopterinae (Insecta, Orthoptera, Grylloidea, Eneopteridae). *Cladistics* 20: 271–293. <https://doi.org/10.1111/j.1096-0031.2004.00025.x>
- Ronquist F, Klopfstein S, Vilhelmsen L, Schulmeister S, Murray DL, Rasnitsyn AP (2012) A total-evidence approach to dating with fossils, applied to the early radiation of the Hymenoptera. *Systematic Biology* 61: 973–999. <https://doi.org/10.1093/sysbio/sys058>
- Rust J, Stumpner A, Gottwald J (1999) Singing and hearing in a Tertiary bushcricket. *Nature* 399: 650–650. <https://doi.org/10.1038/21356>
- Schubnel T, Mazurier A, Nel A, Grandcolas P, Desutter-Grandcolas L, Legendre F, Garrouste R (2023) Flat does not mean 2D: Using X-ray microtomography to study insect wings in 3D as a model for comparative studies. *Methods in Ecology and Evolution* 14: 2036–2048. <https://doi.org/10.1111/2041-210X.14132>
- Schubnel T, Desutter-Grandcolas L, Legendre F, Prokop J, Mazurier A, Garrouste R, Grandcolas P, Nel A (2020) To be or not to be: postcubital vein in insects revealed by microtomography. *Systematic Entomology* 45: 327–336. <https://doi.org/10.1111/syen.12399>
- Snodgrass R (1935) *Principles of insect morphology*, 1935. McGraw-Hill Book Company, New York and London, 667 pp.
- Walker SM, Schwyn DA, Mokso R, Wicklein M, Müller T, Doube M, Stapanoni M, Krapp HG, Taylor GK (2014) In vivo time-resolved microtomography reveals the mechanics of the blowfly flight motor. *PLOS Biology* 12: e1001823. <https://doi.org/10.1371/journal.pbio.1001823>
- Xu C, Zhang H, Jarzembowski EA, Fang Y (2020) The first ground cricket (Orthoptera: Trigonidiidae: Nemobiinae) from mid-Cretaceous Burmese amber. *Cretaceous Research* 115: 104481. <https://doi.org/10.1016/j.cretres.2020.104481>
- Xu C, Wang B, Wappler T, Chen J, Kopylov D, Fang Y, Jarzembowski EA, Zhang H, Engel MS (2022) High acoustic diversity and behavioral complexity of katydids in the Mesozoic soundscape. *Proceedings of the National Academy of Sciences* 119: e2210601119. <https://doi.org/10.1073/pnas.2210601119>
- Yuan W, Zheng C-J, Zheng Y-N, Ma L-B, Gu J-J (2022) The oldest representatives of tree crickets (Orthoptera: Gryllidae; Oecanthinae) from Northern Myanmar. *Insects* 13: 619. <https://doi.org/10.3390/insects13070619>
- Zheng C, Yuan W, Chen H, Gu J-J (2023) Two new genera and species of Oecanthidae (Orthoptera: Grylloidea) from Mid-Cretaceous of Myanmar. *Annales de la Société entomologique de France (N.S.)* 59: 417–427. <https://doi.org/10.1080/00379271.2023.2284172>

# A new species of *Palaeohypotodus* Glückman, 1964 (Chondrichthyes, Lamniformes) from the lower Paleocene (Danian) Porters Creek Formation, Wilcox County, Alabama, USA

Jun A. Ebersole<sup>1</sup>, David J. Cicimurri<sup>2</sup>, T. Lynn Harrell Jr.<sup>3</sup>

<sup>1</sup> McWane Science Center, 200 19th Street North, Birmingham, AL 35203, USA

<sup>2</sup> South Carolina State Museum, 301 Gervais Street, Columbia, SC 29201, USA

<sup>3</sup> Geological Survey of Alabama, Walter Bryan Jones Hall, University of Alabama, Tuscaloosa, AL 35486, USA

<https://zoobank.org/D06A009A-5682-4D42-961D-8B030D5B09AB>

Corresponding author: Jun A. Ebersole ([jebersole@mcwane.org](mailto:jebersole@mcwane.org))

Academic editor: Florian Witzmann ♦ Received 15 September 2023 ♦ Accepted 23 January 2024 ♦ Published 7 February 2024

## Abstract

The historic collection of the Geological Survey of Alabama includes several fossil shark specimens that were recovered from the lower Paleocene Porters Creek Formation in southwestern Alabama, USA. Among these specimens are 17 teeth that we herein recognize as a new species within the extinct Paleogene genus, *Palaeohypotodus*. Detailed examination of these individual teeth, coupled with analyses of the dentitions of various extant lamniform sharks, allowed us to confirm monognathic and dignathic heterodonty within *Palaeohypotodus*. We identified upper and lower anterior and lateral tooth files that can be differentiated from one another by minor variations in morphology. Additionally, numerous isolated teeth from other Danian exposures in Alabama and Arkansas, USA, enhance our understanding of the composition of the dentition and ontogenetic heterodonty of both the new species and the genus as a whole.

## Key Words

Elasmobranchii, Galeomorphi, Gulf Coastal Plain, Paleocene, Shark, Teeth

## Introduction

*Palaeohypotodus* Glückman, 1964 is an extinct lamniform shark genus that has a purported temporal range extending from the Late Cretaceous (Maastrichtian) to the late Eocene (Priabonian), and isolated teeth have been reported from widely disparate localities from around the world (Cappetta 2012; Kriwet et al. 2016). Three species are herein recognized within the genus, including the Cretaceous *Palaeohypotodus bronni* (Agassiz, 1843), and the Paleogene *P. volgensis* Zhelezko in Zhelezko & Kozlov, 1999 and *P. rutoti* (Winkler, 1874). These species are characterized by robust teeth having a combination of erect to strongly distally hooked crown, smooth cutting edges, one or more pairs of lateral cusplets, and distinctive plications along the labial crown foot. *Palaeohypotodus* is known primarily by isolated teeth, but at least one

partially associated skeleton has been reported (Casier 1942). Herein we describe several teeth belonging to a new species of *Palaeohypotodus* that was recently discovered in the historical collections of the Geological Survey of Alabama (Tuscaloosa). These 17 teeth, cataloged under the number GSA–V447, were derived from the lower Paleocene (Danian) Porters Creek Formation of Wilcox County, Alabama, USA. The purpose of this report is to describe and interpret the teeth and dentition of this extinct shark through comparisons with extant lamniform shark jaw sets. Further insights regarding ontogenetic heterodonty and intraspecific variation within the new species were drawn through an analysis of isolated teeth that were recovered from contemporaneous deposits in Alabama and Arkansas. We also comment on the taxonomic history of the genus and the paleobiogeographic distribution of the new species.

## Geological setting

A search through the historical collections at the Geological Survey of Alabama (GSA) in Tuscaloosa by two of the authors (JAE and TLH) resulted in the discovery of 17 teeth belonging to the extinct lamniform shark, *Palaeohypotodus*. The original label associated with these teeth (which were all cataloged together under the number GSA-V447) stated that they were collected from the lower Paleocene (Danian) Porters Creek Formation on the McConnico Plantation near Prairie Creek in Wilcox County, Alabama, USA (Fig. 1). Although the date when the specimens were collected was not recorded, the associated label is of a style used by the GSA during the late 1800s to early 1900s. The exact location of the McConnico Plantation, a historical collecting site located north-northwest of the town of Oak Hill, was rediscovered by examining a property map of Wilcox County that is housed in the GSA archives (Fig. 2a). When this map was overlain on a geologic map of Wilcox County (Fig. 2b), the position of the McConnico Plantation shows that the only area on the property underlain by the Porters Creek Formation is in NW1/4, Sec. 32, T12N, R10E (U.S. Public Land Survey System). As several of the teeth exhibit evidence of sun bleaching and root etching (indicating a prolonged period of surface exposure), we believe that the specimens were collected from an erosional gully in a field rather than a gravel bar in the nearby Prairie Creek. This gully, now evidently filled, exposed strata of the Porters Creek Formation, a Paleocene (Danian/Selandian) unit occurring between the subjacent Clayton Formation and suprajacent Naheola Formation (Fig. 3). In Alabama, the Porters Creek Formation is divided into a lower unnamed member and the overlying Matthews Landing Marl Member. Although we cannot ascertain which member the specimens were derived from, we believe they originated from the unnamed member because 1) the geologic map indicates that the site lies close to the contact with the Clayton Formation, and 2) the Matthews Landing Marl has not been mapped in the immediate vicinity of the McConnico locality. The Porters Creek Formation in Wilcox County, AL consists of approximately 37 m (120 feet) of various fine-grained siliciclastic facies, but a prominent limestone bed occurs in the middle of the unit and carbonate content increases to the east (Raymond et al. 1988). The siliciclastic facies have been described as consisting of micaceous silty sand, massive calcareous clay, and massive black clay, with the Matthews Landing Marl comprised of fossiliferous calcareous clay and glauconitic sandstone (LaMoreaux and Toulmin 1959). Mancini and Tew (1993) reported that the Porters Creek Formation of south-central Alabama attained a thickness of 46 m (150 feet), and they further subdivided the unnamed member into “lower,” “middle,” and “upper” portions. The lower and middle portions were described as consisting of marlstone, limestone, and calcareous silty claystone, whereas the upper portion consists of bioturbated siltstone and marlstone.

The overlying Matthews Landing Marl Member includes fossiliferous, glauconitic sandstone and marlstone (Mancini and Tew 1993), and the unit attains a thickness of 6 m (20 feet) in Wilcox County (Raymond et al. 1988). The geologic formations in Wilcox County dip gently to the south-southwest.

A rather diverse fossil mollusk assemblage from the McConnico Plantation (GSA collection, Table 1) supports an early-to-middle Paleocene age for the Porters Creek Formation. This age is further corroborated biostratigraphically, as the basal portion of the unit in Wilcox County lies within the uppermost P1 (P1c) *Subbotina triloculoides* (Plummer, 1927) planktonic foraminifera interval zone (formerly *Subbotina trinidadensis* (Bolli, 1957) = *Praemurica inconstans* (Subbotina, 1953) interval zone) and the basal portion of the NP4 *Ellipsolithus macellus* (Bramlette & Sullivan, 1961) nannoplankton zone (Mancini 1984; Fluegeman et al. 1990; Mancini and Tew 1993). Zone NP4 was subsequently extended downward into Zone P1 (see Ogg et al. 2016) after Mancini and Tew’s (1993) publication.

**Table 1.** List of historically collected fossil invertebrate taxa in the Geological Survey of Alabama collection that were derived from the Porters Creek Formation at the McConnico Plantation in Wilcox County, AL, USA.

<b>Gastropods</b>	
<i>Eoancilla mediavia</i>	(Harris, 1896)
<i>Natica reversa</i>	Whitfield, 1865
<i>Caricella leana</i>	Dall, 1890
<i>Coronia mediavia</i>	(Harris, 1896)
<i>Exilia pergracilis</i>	Conrad, 1860
<i>Euspira perspecta</i>	(Whitfield, 1865)
<i>Mesalia alabamiensis</i>	(Whitfield, 1865)
<i>Mesalia allentonensis</i>	(Aldrich, 1894)
<i>Orthosurcula longipera</i>	(Harris, 1896)
<i>Turritella alabamiensis</i>	Whitfield, 1865
<i>Turritella humerosa</i>	Conrad, 1835
<i>Turritella levicunea</i>	(Harris, 1896)
<i>Volutocorbis rugatus</i>	(Conrad, 1860)
<b>Bivalves</b>	
<i>Crassatella aquiana</i>	Clark, 1895
<i>Cucullaea macrodonta</i>	Whitfield, 1865
<i>Nucula mediavia</i>	Harris, 1896
<i>Ostrea</i> sp. indet.	Linnaeus, 1758
<i>Venericardia wilcoxensis</i>	Dall, 1903
<b>Scaphopods</b>	
<i>Dentalium mediaviense</i>	Harris, 1896

## Material and methods

The 17 teeth that are the focus of this report are reposited in the collection of the Geological Survey of Alabama in Tuscaloosa and are curated under catalog number GSA-V447. Of these 17 teeth, nine are complete, with the remaining eight consisting of either the main cusp lacking some or all of the root, or complete root with partial main cusp. We herein note the possibility that all 17 teeth cataloged under the number GSA-V447 represent a single individual, in which case the specimens

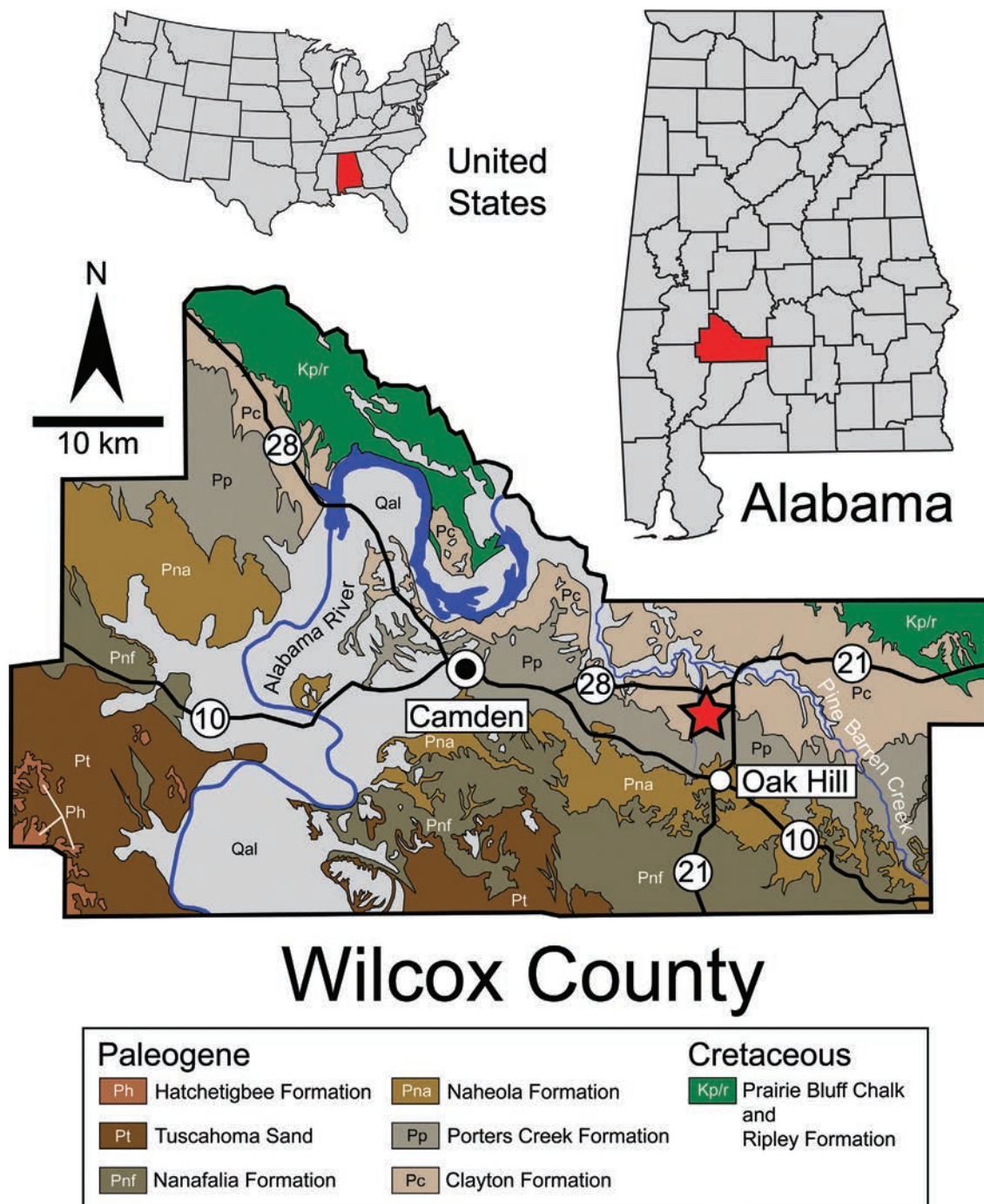


**Figure 1.** Geologic map of Wilcox County showing the approximate location of the McConnico Plantation (indicated by red star). Scale bar applies to Wilcox County map.

represent an associated dentition. However, the lack of unequivocal replacement teeth and associated vertebral centra within the lot perhaps indicates that the 17 teeth are not associated. The consistent preservation amongst the teeth, combined with the relative paucity and low density of vertebrate remains within the Porters Creek Formation (JAE, pers. observation), suggests that these teeth are associated (although this may also be an indication that this taxon is abundant within this particular lithostratigraphic unit). Nevertheless, as GSA–V447 was historically collected and no field notes are available that indicate or contradict the direct association of these 17

teeth, we herein treat them as isolated finds and use the specimens as an artificial tooth set. For the purposes of this report, we herein retain all of the teeth within the original catalog number GSA–V447 but refer to them individually by the use of sub-numbers (i.e., GSA–V447.1–.17).

The teeth of GSA–V447 are believed to represent various tooth positions within the dentition of one taxon, and a standard set of linear measurements (Fig. 4), ratios, and morphological observations were recorded for each tooth to assist with the reconstruction and interpretation of the dentition of this shark. These measurements and observations are as follows:

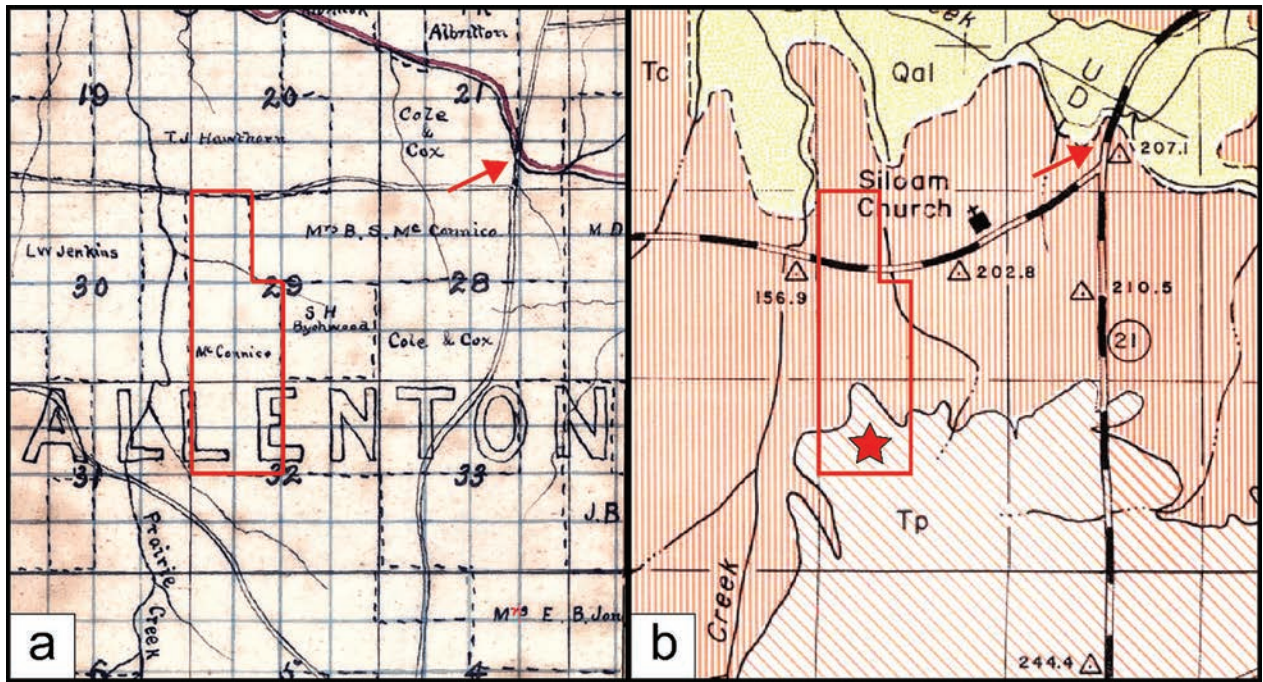


**Figure 2.** Location of McConnico Plantation in Wilcox County, AL, USA; **a.** Portion of a historical property map of Wilcox County, AL (Crump 1870) showing the location of the McConnico Plantation (red polygon). **b.** Portion of a geologic map of Wilcox County, AL (LaMoreaux and Toulmin 1959) showing the location of the McConnico Plantation (red polygon) and the area where GSA-V447 was likely recovered (red star). Arrows indicate the location of Smith’s Bridge which is a landmark for orientation. **Qal** = Quaternary alluvium, **Tc** = Clayton Formation, **Tp** = Porters Creek Formation.

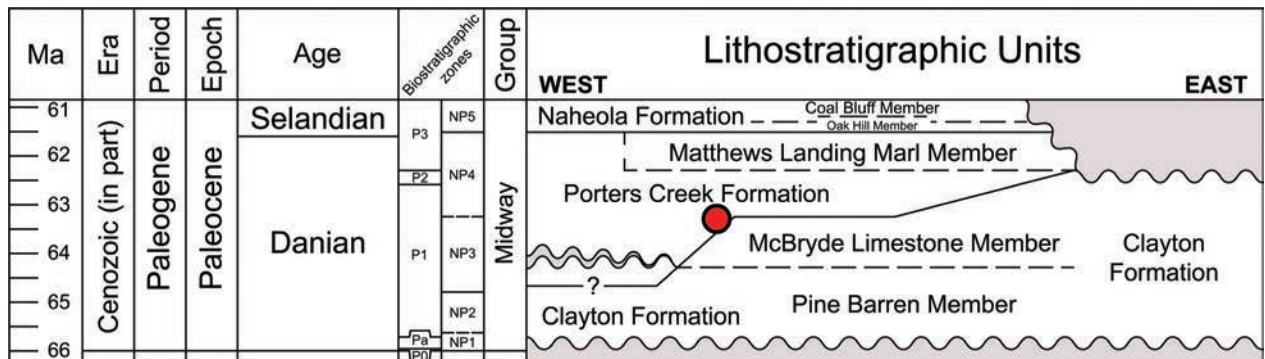


**Figure 3.** Stratigraphic column of early-to-middle Paleocene strata of Alabama. Red dot indicates the likely horizon of GSA-V447. Column is based on Raymond et al. (1988) and modified with data from Gibson et al. (1982), Mancini et al. (1989), Mancini and Tew (1993), and Ogg et al. (2016).

**Total height (TH).** On a complete tooth, this is the maximum apico-basal height measured from the apex of the main cusp to the base of the root lobes (with the tooth positioned so the basal extent of the mesial and distal root lobes are equal).

**Root width (RW).** With the tooth positioned so the basal extent of the mesial and distal root lobes are equal, this is the maximum mesio-distal width measured from the mesial and distal-most extent of the root lobes.

**Main cusp height (MCH).** The maximum apico-basal height of the main cusp measured on the labial face from the medial portion of the crown base to the apex of the main cusp.

**Root height (RH).** Calculated by subtracting the main cusp height from the total height (i.e., TH – MCH).

**Main cusp width (MCW).** Measured on the labial face, the distance between the distal and mesial-most points of the main cusp.

**Main cusp thickness (MCT).** Measured from the medial portion of the lingual crown base to the corresponding point at the labial crown base, inclusive of the neck (aka chevron or dental band), if present.

**Depth of the interlobe area (DIA).** Measured from the apical extent of the interlobe area to the base of the root lobes, with the base of the lobes being equal.

**Root thickness (RT).** The labio-lingual thickness of the root measured from the highest point on the lingual protuberance to the corresponding labial face of the tooth.

**Number of mesial cusplets (#MC).** The total number of mesial cusplets.

**Number of distal cusplets (#DC).** The total number of distal cusplets.

**Labial ornamentation present? (LOP).** A brief description of any ornamentation present along the labial crown foot.

For the nine complete teeth associated with GSA–V447, the standard measurements were used to calculate the three following ratios:

**Ratio of main cusp height to total tooth height (%MCH).** Calculated by dividing the main cusp height by the total height (i.e.,  $MCH \div TH$ ).

**Ratio of root height to total tooth height (%RH).** Calculated by dividing the root height by the total height (i.e.,  $MCH \div TH$ ).

**Ratio of the depth of the interlobe area to total tooth height (%DIA).** Calculated by dividing the depth of the interlobe area by the total height (i.e.,  $DIA \div TH$ ).

An additional 17 isolated teeth of the new *Palaeohypotodus* species were identified in the collections of McWane Science Center (MSC) in Birmingham, AL, USA, and the Mississippi Museum of Natural Science (MMNS) in Jackson, USA (see Referred specimens list below). These specimens were collected from four counties in Alabama (Dallas, Butler, Lowndes, and Wilcox) and one county in Arkansas, USA (Hot Spring County). One of these specimens (MSC 49452) was derived from the type stratum of GSA–V447 (Porters Creek Formation), albeit from Butler County in Alabama. The remaining 16 teeth were recovered from the lower Paleocene (Danian) Clayton Formation (including the Pine Barren Member), a lithostratigraphic unit that is largely temporally equivalent to the lower unnamed member of the Porters Creek Formation (see Fig. 3). Ten of these teeth are complete and were incorporated into our morphological dataset so they could be directly compared with the teeth of GSA–V447. The remaining seven specimens were excluded from our analyses because they are incompletely preserved.

To assist with the dental reconstruction of the *Palaeohypotodus* species, we directly examined the jaws of numerous recent lamniform sharks in the collections of MSC and the South Carolina State Museum in Columbia (SC). These specimens included *Alopias superciliosus* Lowe, 1841 (SC2020.53.12) and *A. pelagicus* Nakamura, 1935 (SC2020.53.19), two *Carcharodon carcharias* (Linnaeus, 1758) (MSC 42596 and SC86.62.1), juvenile and adult *Isurus oxyrinchus* Rafinesque, 1810 (MSC 42606 and SC2020.53.15, respectively), juvenile and adult *I. paucus* Guitart-Manday, 1966 (SC2020.53.22 and SC2020.53.27, respectively), and two *Carcharias taurus* Rafinesque, 1810 (SC86.62.2 and SC2000.120.6). Additionally, we examined a *Lamna nasus* (Bonnaterre, 1788) jaw set from the Gordon Hubbell collection (unnumbered specimen) in Gainesville, FL, USA. Finally, published images of the dentitions of *A. vulpinus*

(Bonnaterre, 1788), *Odontaspis ferox* (Risso, 1810), *O. noronhai* (Maul, 1955), and *Mitsukurina owstoni* Jordan, 1898 were utilized (i.e., Ebert and Dando 2021). The dentitions of the filter-feeding lamniforms, *Cetorhinus* and *Megachasma*, were excluded from our study due to their atypical dentitions.

The terminology used for identifying the jaw position of isolated teeth of elasmobranch fishes has varied greatly in the literature (see Leriche 1905; Applegate 1965; Cappetta 1987, 2012; Cunningham 2000; Shimada 2001, 2002a, b, c, 2004), but herein we follow a combination of Siverson (1999) and Cicimurri et al. (2020) by utilizing the terms anterior, intermediate, lateral, and posterior to identify jaw position in lamniform sharks. Herein, anterior teeth refer to those that develop within the anterior dental hollow in the Meckel's cartilage or palatoquadrate, whereas lateral teeth are those occurring within the upper or lower lateral hollows. Teeth referred to as intermediate are those that occur at the extreme distal end of the anterior hollow or on a cartilage bar located between the upper anterior and lateral dental hollows. These teeth are conspicuously smaller than the preceding anterior and succeeding lateral tooth and may also be strongly distally hooked and/or inclined (more so than in lateral files), which is reflective of the limited space available for tooth development. Posterior teeth are those that comprise files located at the far distal ends of the upper and lower lateral dental hollows and are positioned closest to the jaw commissure. These teeth are significantly smaller and morphologically different from lateral teeth, often mesiodistally as wide as tall (ratio of 1:1) and, in some cases, their width exceeds the overall tooth height (see Cicimurri et al. 2020). The morphological changes across the upper and lower lateral tooth rows are gradational within most lamniform shark dentitions (see Ebert and Dando 2021), and herein we utilize the terms anterolateral and posterolateral to refer to lateral teeth that are located near the anterior or posterior half, respectively, of the lateral dental hollow.

All of the teeth we illustrate were photographed with a Nikon D80 camera and Tamron macro lens. To account for depth of field, specimens were photographed from several focal lengths and the resulting photographs were merged in Adobe Photoshop v. 22.5.9 utilizing the software's auto-align and auto-blend functions. We constructed the figures using the same software.

## Institutional abbreviations

**GIK:** State Darwin Museum, Moscow, Russia. **GSA:** Geological Survey of Alabama, Tuscaloosa, USA. **IRSNB:** Royal Belgian Institute of Natural Sciences, Brussels, Belgium. **MMNS:** Mississippi Museum of Natural Science, Jackson, USA **MSC:** McWane Science Center, Birmingham, Alabama, USA. **SC:** South Carolina State Museum, Columbia, USA.

## Systematic Paleontology

**Class Chondrichthyes Huxley, 1880**

**Subclass Euselachii Hay, 1902**

**Infraclass Elasmobranchii Bonaparte, 1838**

**Division Selachii Cope, 1871**

**Superorder Galeomorphi Compagno, 1973**

**Order Lamniformes Berg, 1958**

**Family Jaekelodontidae Glückman, 1964**

**Genus *Palaeohypotodus* Glückman, 1964**

**Type species.** *Otodus rutoti* Winkler, 1874, Orp Member of the Heers Formation, Orp-le-Grand (Maret), Belgium.

**Emended generic diagnosis.** Lamniform shark with teeth consisting of a triangular main cusp and one to three pairs of lateral cusplets. Enameloid plications occur along the labial crown foot on unworn teeth, and these may coalesce to form transversely oriented ridge-like structures on posterior teeth. Cutting edges are complete on all upper teeth but are incomplete on lower teeth. Although the main cusp is tall and relatively narrow in anterior files, it becomes progressively lower and broader the closer a file is located with respect to the commissure. Upper lateral teeth have a wide triangular and distally hooked main cusp, whereas lower lateral teeth have a narrower and more erect main cusp. Upper third anterior teeth have a basally extended mesial root lobe, the distal cutting edge is more convex than the mesial edge, and the crown appears to be mesially recurved. Teeth have a robust lingual root protuberance that bears a nutritive groove. The root lobes are long and the interlobe area is deep and U-shaped. Upper anterior teeth have shorter and slightly more divergent root lobes compared to those in the lower anterior files.

***Palaeohypotodus bizzocoi* sp. nov.**

<https://zoobank.org/9E51D855-B537-4088-95BE-8F20C549BF6F>

Figs 4–7

**Etymology.** The species is named for the late Bruce D. Bizzoco in honor of his dedicated volunteer service to MSC and his lifelong commitments to education and the preservation of local history in Alabama, USA.

**Hypodigm.** GSA–V447.1 (holotype), upper left anterior tooth (Fig. 5a–d); GSA–V447.2 (paratype), upper right lateral tooth (Fig. 5y–bb); GSA–V447.3 (paratype), upper right lateral tooth (Fig. 5cc–ff); GSA–V447.4 (paratype), lower right anterior tooth (Fig. 6a–d); GSA–V447.5 (paratype), lower left lateral tooth (Fig. 6q–t).

**Referred specimens.** N = 29: GSA–V447.6, upper left anterior tooth, Porters Creek Formation, Wilcox County, AL; GSA–V447.7, upper left anterior tooth, Porters Creek Formation, Wilcox County, AL; GSA–V447.8, upper left lateral tooth, Porters Creek Formation, Wilcox County, AL; GSA–V447.9, upper right lateral tooth, Porters Creek Formation, Wilcox County, AL; GSA–V447.10,

upper left lateral tooth, Porters Creek Formation, Wilcox County, AL; GSA–V447.11, upper anterior tooth, Porters Creek Formation, Wilcox County, AL; GSA–V447.12, lower left anterior tooth, Porters Creek Formation, Wilcox County, AL; GSA–V447.13, lower left anterior tooth, Porters Creek Formation, Wilcox County, AL; GSA–V447.14, lower right lateral tooth, Porters Creek Formation, Wilcox County, AL; GSA–V447.15, lower left lateral tooth, Porters Creek Formation, Wilcox County, AL; GSA–V447.16, lower left lateral tooth, Porters Creek Formation, Wilcox County, AL; GSA–V447.17, lower left lateral tooth, Porters Creek Formation, Wilcox County, AL; MMNS VP–7292.2, upper right lateral tooth, Pine Barren Member of the Clayton Formation, Lowndes County, AL; MMNS VP–7292.3, upper left lateral tooth, Pine Barren Member of the Clayton Formation, Lowndes County, AL; MMNS VP–7292.4, upper right lateral tooth, Pine Barren Member of the Clayton Formation, Lowndes County, AL; MMNS VP–7295.4, upper right posterior tooth, Pine Barren Member of the Clayton Formation, Lowndes County, AL; MMNS VP–7311, lower right lateral tooth, Pine Barren Member of the Clayton Formation, Lowndes County, AL; MMNS VP–8578, upper right lateral tooth, basal Clayton Formation, Hot Spring County, AR; MSC 3020, lower left anterior tooth, lower Clayton Formation, Wilcox County, AL; MSC 42727, upper right lateral tooth, Pine Barren Member of the Clayton Formation, Lowndes County, AL; MSC 42733, upper right lateral tooth, Pine Barren Member of the Clayton Formation, Lowndes County, AL; MSC 42741.4, upper right lateral tooth, Pine Barren Member of the Clayton Formation, Lowndes County, AL; MSC 42741.5, upper right lateral tooth, Pine Barren Member of the Clayton Formation, Lowndes County, AL; MSC 42742.1, upper right lateral tooth, Pine Barren Member of the Clayton Formation, Lowndes County, AL; MSC 42742.2, upper right lateral tooth, Pine Barren Member of the Clayton Formation, Lowndes County, AL; MSC 42742.3, upper right lateral tooth, Pine Barren Member of the Clayton Formation, Lowndes County, AL; MSC 49451, upper left lateral tooth, lower Clayton Formation, Wilcox County, AL; MSC 49452, upper left 3<sup>rd</sup> anterior tooth, Porters Creek Formation, Butler County, AL; MSC 49454, upper left lateral tooth, lower Clayton Formation, Wilcox County, AL.

**Type stratum and age.** Basal unnamed member, Porters Creek Formation, Paleocene, Danian Stage, zones NP3–4 (Fig. 3).

**Type locality.** Historic McConnico Plantation near Prairie Creek in Wilcox County, Alabama, USA, NW1/4, Sec. 32, T12N, R10E (U.S. Public Land Survey System) (Figs 1, 2).

**Description.** Specimen GSA–V447 consists of 17 teeth that are herein assigned to anterior and lateral files of the upper and lower jaws. This assortment of teeth includes nine from the palatoquadrate (upper jaw) and eight from the Meckel's cartilage (lower jaw). Teeth from both the left and right sides of the upper and lower

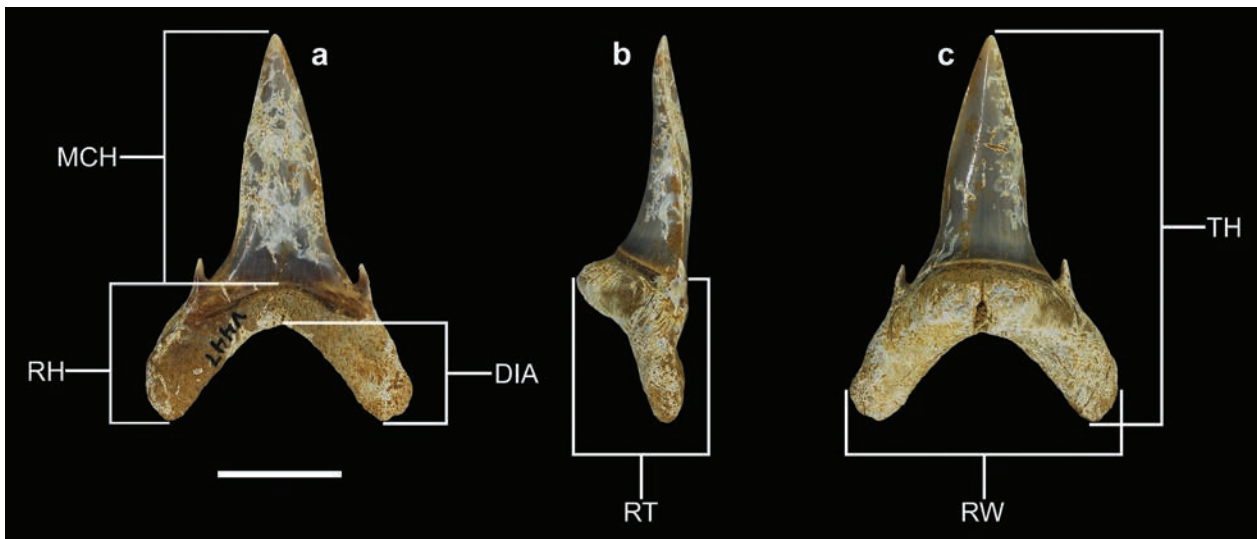


**Figure 4.** Standard tooth measurements. **a–c.** GSA–V447.6, *Palaeohypotodus bizzocoi* sp. nov. upper anterior tooth; **a.** Labial view; **b.** Mesial view; **c.** Lingual view; **DIA** – Depth of the interlobe area; **MCH** – Main cusp height; **RH** – Root height; **RT** – root thickness; **RW** – Root width; **TH** – Total height; Scale bar: 1 cm.

jaws are represented, and it is possible that at least two of the teeth were derived from the same tooth file. Unfortunately, the limited number of teeth included with specimen GSA–V447 did not allow us to determine exactly how many anterior or lateral files were present within the dentition of this taxon, or how many posterior files occurred. However, based on the jaw sets of several extant lamniform sharks like *Carcharodon carcharias*, *Isurus* spp., *Lamna nasus*, and *Odontaspis ferox* (see Materials and Methods), we believe that upper and lower teeth are preserved, and both anterior and lateral tooth files are represented. Tooth morphologies we identified in GSA–V447 include:

**Upper anterior teeth (GSA–V447.1, .6–.7, .11, Fig. 5a–p).** We identified four teeth within this tooth group, including three complete specimens and one with an incomplete main cusp. Unlike the lateral teeth (see below), the sequential position within the jaw of *P. bizzocoi* sp. nov. is unknown because the total tooth height and root width of the upper anterior teeth is extremely variable within the extant lamniform jaws examined. The three complete teeth have a total height (TH) ranging between 28.87 and 29.16 mm and a root width (TW) that ranges from 18.84 to 19.99 mm. The height/width (H/W) ratios vary from 1.44 to 1.55 (Table 2).

The three complete teeth (GSA–V447.1, .6–.7; Fig. 5a–k) have a tall and triangular main cusp. In labial view the main cusp is nearly symmetrical, but the mesial edge is slightly more convex than the distal edge, and this feature allows us to determine if they were derived from the left or right palatoquadrate. The labial face of the main cusp is slightly convex, whereas the lingual face is strongly convex. The mesial and distal cutting edges are complete and extend to the base of the main cusp. The crown enameloid is smooth except for faint plications occurring along the labial crown foot. The main cusp is slightly sinuous in profile view. The teeth have a single

pair of diminutive lateral cusplets that are both medially and lingually hooked. Both lateral cusplets have mesial and distal cutting edges that do not connect to those on the main cusp. The root is bilobate, with lobes being divergent and of nearly equal length and width. The interlobe area is deep, wide, and U-shaped. The teeth have a robust lingual protuberance that is bisected by a deep nutritive groove. The height of the root represents approximately 30% of the total tooth height. Specimen GSA–V447.11 (Fig. 5m–p), the tooth with broken main cusp, is assigned to the upper anterior tooth group because it has a deeper interlobe area (8.44 mm) than any of the upper lateral teeth (see Table 2), the root lobes are shorter and more divergent than those on the lower teeth, and the interlobe area is wider and U-shaped compared to the lower anterior teeth (see additional discussion below).

At least two upper anterior files are represented within GSA–V447 based on the slightly different dimensions and gross morphologies of teeth GSA–V447.6 and GSA–V447.7 (see Table 2). Both teeth have a narrow, triangular main cusp with cutting edges that are sub-parallel except near the apex, where they are biconvex. Tooth GSA–V447.7 (Fig. 5i–l) has a slightly narrower main cusp that is very slightly distally inclined compared to GSA–V447.6 (Fig. 5a–d), and it also has slightly longer root lobes. Teeth GSA–V447.1 and GSA–V447.6 have nearly identical dimensions (see Table 2), suggesting they belong to the same anterior file. Additionally, tooth GSA–V447.11 has a nearly identical root width to that of GSA–V447.7 (Fig. 5i–l), suggesting that these two teeth also represent the same anterior file.

**Upper lateral teeth (GSA–V447.2–.3, .8–.10, Fig. 5q–ii).** Five upper lateral teeth are preserved with GSA–V447, four of which are complete. The basal margins of the root lobes of tooth GSA–V447.9 are not preserved. The crowns of these teeth range in height from 17.64 to 11.4 mm, and the overall height of the complete teeth

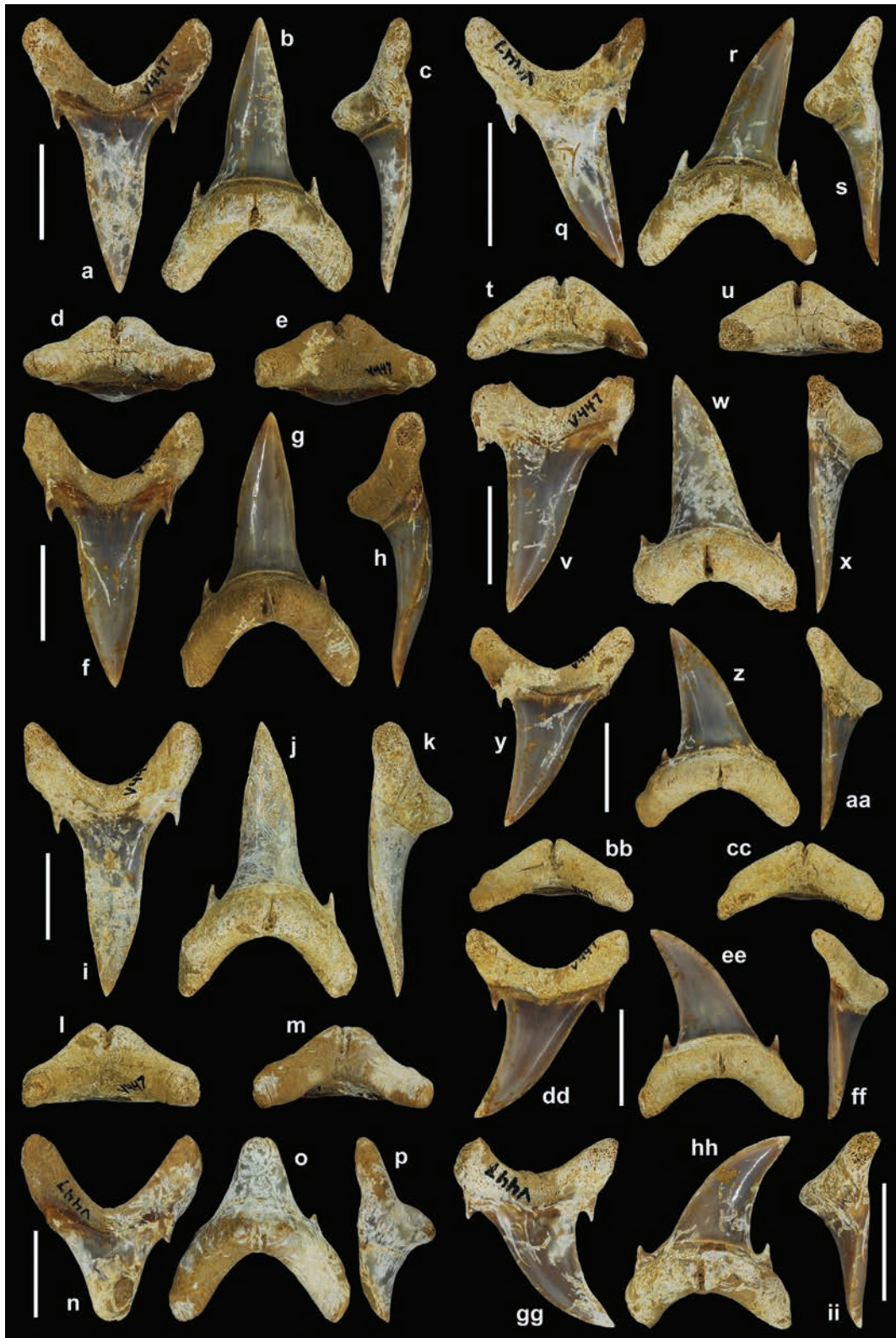


**Figure 5.** (a–ii) *Palaeohypotodus bizzocoi* sp. nov. upper teeth. a–d. GSA–V447.6, upper left anterior tooth; a. Labial view; b. Lingual view; c. Mesial view; d. Basal view. e–h. GSA–V447.1 (holotype), upper left anterior tooth; e. Basal view; f. Labial view; g. Lingual view; h. Mesial view. i–l. GSA–V447.7, upper right anterior tooth; i. Labial view; j. Lingual view; k. Mesial view; l. Basal view. m–p. GSA–V447.11, upper anterior tooth; m. Basal view; n. Labial view; o. Lingual view; p. Profile view. q–t. GSA–V447.8, upper left intermediate or lateral tooth; q. Labial view; r. Lingual view; s. Mesial view; t. Basal view. u–x. GSA–V447.9, upper right lateral tooth; u. Basal view; v. Labial view; w. Lingual view; x. Mesial view. y–bb. GSA–V447.2 (paratype), upper right lateral tooth; y. Labial view; z. Lingual view; aa. Mesial view; bb. Basal view. cc–ff. GSA–V447.3 (paratype), upper right lateral tooth; cc. Basal view; dd. Labial view; ee. Lingual view; ff. Mesial view. gg–ii. GSA–V447.10, upper left lateral tooth; gg. Labial view; hh. Lingual view; ii. Mesial view. Scale bars: 1 cm.

**Table 2.** Measurements, ratios, and observations on the *Palaeohypotodus bizzocoi* sp. nov. teeth associated with GSA–V447. **Abbreviations:** #DC. Number of distal cusplets. **DIA.** Depth of the interlobe area. **H/W Rat.** Height/width ratio; **LOP.** Labial ornamentation present and the nature of the ornamentation; #MC. Number of mesial cusplets; **MCH.** Main cusp height; %MCH. The percentage of the main cusp height in relation to the total tooth height; **MCT.** Main cusp thickness; **MCW.** Main cusp width; **RH.** Root height; %RH. The percentage of the root height in relation to the total tooth height; **RT.** Maximum root thickness; **RW.** Root width; **TH.** Total height. **N/A.** Measurement, ratio, or observation could not be taken due to the incomplete preservation of the tooth.

Number	Tooth Position	TH	RW	H/W Rat	MCH	%MCH	RH	%RH	MCW	MCT	DIA	RT	#MC	#DC	LOP
GSA–V447.6	Upper anterior	29.16	18.84	1.55	20.39	69.9	8.77	30.1	10.53	5.14	6.7	8.63	1	1	Faint across base
GSA–V447.1	Upper anterior	29.11	19.08	1.52	19.98	68.6	9.13	31.4	11.19	5.24	7.18	8.9	1	1	Faint across base
GSA–V447.7	Upper anterior	28.87	19.97	1.44	19.63	67.9	9.24	32.1	11.18	5.28	6.28	8.12	1	1	Faint across base
GSA–V447.11	Upper anterior	N/A	19.99	N/A	N/A	N/A	N/A	N/A	10.26	5.23	8.53	8.44	1	N/A	Faint across base
GSA–V447.8	Upper lateral	20.09	14.54	1.01	14.6	72.6	5.49	27.4	7.34	3.95	5.02	6.1	2	2	Faint across base
GSA–V447.9	Upper lateral	N/A	N/A	N/A	17.64	N/A	N/A	N/A	10.85	4.39	N/A	6.98	1	1	Faint across base
GSA–V447.2	Upper lateral	23.93	19.81	1.21	17.03	71.1	6.9	28.9	11.29	4.64	5.35	6.91	2	2	Faint across base
GSA–V447.3	Upper lateral	19.51	16.94	1.15	14.39	73.7	5.12	26.3	9.52	4.05	4.97	5.91	2	2	Faint across base
GSA–V447.10	Upper lateral	15.59	13.33	1.17	11.4	73.1	4.19	26.9	8.6	3.58	3.78	4.88	1	1	Faint across base
GSA–V447.4	Lower anterior	32.63	17.28	1.89	19.9	60.9	12.73	39.1	9.51	5.48	10.48	9.14	1	1	Faint across base
GSA–V447.12	Lower anterior	N/A	N/A	N/A	18.59	N/A	N/A	N/A	8.8	4.97	N/A	8.16	N/A	N/A	Faint across base
GSA–V447.13	Lower anterior	N/A	N/A	N/A	18.09	N/A	N/A	N/A	10.09	4.79	N/A	N/A	N/A	N/A	Faint across base
GSA–V447.14	Lower lateral	N/A	N/A	N/A	17.53	N/A	N/A	N/A	8.24	4.7	N/A	7.67	1	2	Faint across base
GSA–V447.5	Lower lateral	27.06	15.53	1.74	17.23	63.6	9.83	36.4	8.51	4.59	7.2	7.28	1	1	Faint across base
GSA–V447.15	Lower lateral	N/A	N/A	N/A	14.88	N/A	N/A	N/A	8.49	4.45	N/A	7.06	1	1	Faint across base
GSA–V447.16	Lower lateral	N/A	N/A	N/A	NA	N/A	N/A	N/A	7.96	4.25	N/A	N/A	N/A	1	N/A
GSA–V447.17	Lower lateral	N/A	N/A	N/A	8.74	N/A	N/A	N/A	4.06	2.34	N/A	3.13	N/A	1	Faint across base

ranges from 23.93 to 15.59 mm. The H/W ratios range from 1.01 to 1.21 (Table 2). All the teeth have a triangular main cusp that is distally inclined in the anterolateral positions, but the cusp becomes shorter and more distally hooked the closer a tooth is positioned to the commissure. The labial and lingual faces of the main cusp are almost equally convex. In mesial or distal views, the main cusp is straight except for a slight labial bend at the apex. The crown enameloid is smooth except for very faint plications (visible under magnification) along the labial crown foot. There are one to two pairs of lateral cusplets, and when two pairs are present the larger pair is always positioned medially, and the lateral pair is much reduced in size. The larger pair of cusplets are distinctively hooked both medially and lingually. The main cusp cutting edges are complete and extend to the base of the main cusp. The cutting edges extend across the apical half of the lateral cusplets. A pair of minute mesial and distal denticulations occur between the main cusp and lateral cusplets on specimen GSA–V447.9 (Fig. 5u–x), but such denticles are absent on all other teeth associated with GSA–V447. The bilobate root has short and thin (labio-lingually) lobes that are divergent and rounded at their extremities. The interlobe area is wide and U-shaped. The pronounced lingual protuberance is bisected by a deep nutritive groove.

Teeth GSA–V447.2 and GSA–V447.9 (Fig. 5u–bb) differ somewhat with respect to the degree of distal inclination of the main cusp, with GSA–V447.2 being slightly more inclined. These lateral teeth could be from succeeding lateral files, as for example GSA–V447.9 could be from the second lateral file and GSA–V447.2 the third lateral file. Tooth GSA–V447.3 (Fig. 5cc–ff) is slightly smaller in overall size and has a more distally

inclined and curved crown compared to the other teeth assigned to this group, indicating that it is from a more distally located lateral file. Based on its small size and strongly distally hooked crown, tooth GSA–V447.10 (Fig. 5gg–ii) was likely part of a posterolateral file located closer to the jaw commissure, where the dental hollow is tapered and space for developing teeth is rather limited.

One tooth, GSA–V447.8 (Fig. 5q–t), is believed to be from the upper dentition due to the distal inclination of the crown, and the short length of the root lobes and wide interlobe area. However, it exhibits an unusual morphology as it is significantly smaller than the anterior teeth and it is also conspicuously distally inclined. Additionally, the tooth is smaller than and/or lacks the distal crown curvature exhibited by the lateral teeth. Furthermore, the crown is mesio-distally thinner than all the other upper teeth. Specimen GSA–V447.8 conforms to our observations of the intermediate teeth of the extant lamniform shark dentitions we examined, although we cannot definitively rule out the possibility that it represents a lateral file.

**Lower anterior teeth (GSA–V447.4, Fig. 6a–d).** GSA–V447.4 is the only definitive lower anterior tooth associated with GSA–V447. This tooth measures 32.63 mm in total height and 17.28 mm in root width and has a H/W ratio of 1.89 (Table 2). The main cusp is tall and nearly symmetrical. Its labial face is slightly convex, whereas the lingual face is strongly convex. The crown enameloid is smooth save for faint plications occurring at the labial crown foot. The crown is weakly sigmoidal in mesial and distal views. There is a single pair of short lateral cusplets that are slightly lingually inclined. The mesial and distal cutting edges are incomplete and do

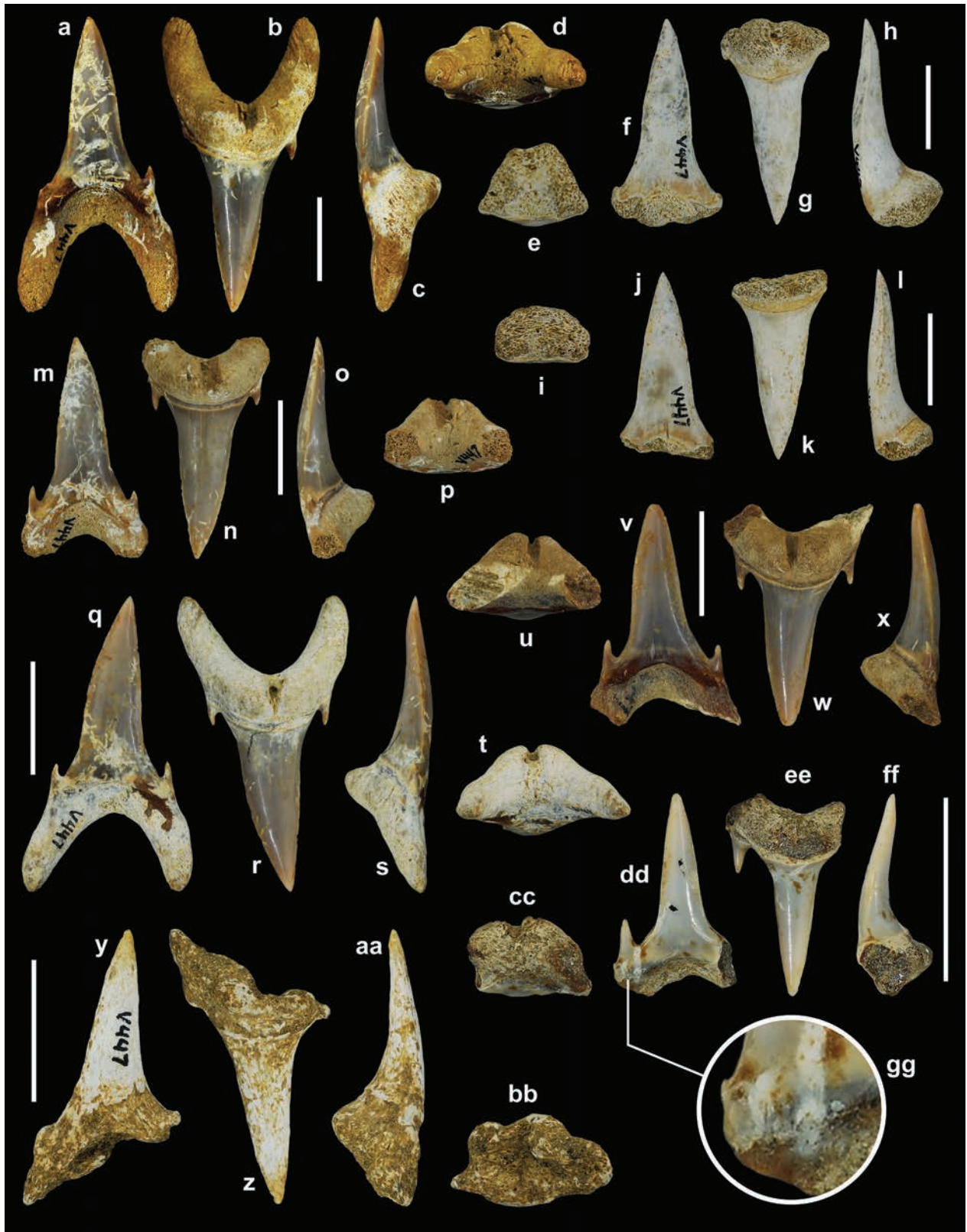


**Figure 6. a–gg.** *Palaeohypotodus bizzocoi* sp. nov. lower teeth. **a–d.** GSA–V447.4 (paratype), lower right anterior tooth; **a.** Labial view; **b.** Lingual view; **c.** Mesial view; **d.** Basal view. **e–h.** GSA–V447.12, lower right anterior tooth; **e.** Basal view; **f.** Labial view; **g.** Lingual view; **h.** Mesial view. **i–l.** GSA–V447.13, lower right anterior tooth; **i.** Basal view; **j.** Labial view; **k.** Lingual view; **l.** Mesial view. **m–p.** GSA–V447.14, lower right lateral tooth; **m.** Labial view; **n.** Lingual view; **o.** Mesial view; **p.** Basal view. **q–t.** GSA–V447.5 (paratype), lower left lateral tooth; **q.** Labial view; **r.** Lingual view; **s.** Mesial view; **t.** Basal view. **u–x.** GSA–V447.15, lower left lateral tooth; **u.** Basal view; **v.** Labial view; **w.** Lingual view; **x.** Mesial view. **y–bb.** GSA–V447.16, lower left lateral tooth; **y.** Labial view; **z.** Lingual view; **aa.** Mesial view; **bb.** Basal view. **cc–gg.** GSA–V447.17, lower right lateral tooth; **cc.** Basal view; **dd.** Labial view; **ee.** Lingual view; **ff.** Mesial view; **gg.** Close-up of labial crown ornamentation. Scale bars: 1 cm.

not extend to the base of the main cusp. Smooth cutting edges extend across the lateral cusplets. The bilobate root has elongated, thin, and rounded lobes that are slightly divergent. The interlobe area is deep and U-shaped. The pronounced lingual protuberance is bisected by a deep nutritive groove. The crown height measures 19.9 mm, and this portion of the tooth comprises approximately 61% of the total height (Table 2).

Two additional teeth associated with GSA–V447, GSA–V447.12–13 (Fig. 6e–l), consist only of the main cusp and a portion of the root. These teeth are attributed to the lower dentition because the main cusp is not as sigmoidal as that of upper anterior teeth, the labial face is less convex compared to upper lateral teeth, and they have incomplete cutting edges. We believe these teeth represent lower anterior files because they have a more symmetrical main cusp compared to lower lateral teeth included with GSA–V447 (see below). Additionally, the main cusp height of these two teeth (18.59 and 18.09 mm, respectively) is greater than that of any lower lateral tooth (17.53 to 8.74 mm) (Table 2).

**Lower lateral teeth (GSA–V447.5, 14–17, Fig. 6m–gg).** Although five lower lateral teeth are part of GSA–V447, only one is complete (GSA–V447.5, Fig. 6q–t). The other four teeth have a complete main cusp but are missing one or both root lobes. These five teeth have a tall and narrow main cusp that has a very slight distal inclination. The slight distal inclination is most evident on the mesial side of the main cusp because the mesial edge is more convex than the distal edge near the apex. This morphology allowed us to determine if the tooth was from the right or left Meckel’s cartilage. The labial face of the main cusp is slightly convex, whereas the lingual face is strongly convex. The crown enameloid is smooth except for very faint plications (seen under magnification) along the labial crown foot. In mesial and distal views, the main cusp has a slight lingual inclination. The teeth generally have a single pair of lateral cusplets, but GSA–V447.1 (Fig. 6m–p) has a second diminutive distal cusplet that is united to the base of the much larger, more medially located cusplet. The lateral cusplets have a slight medial curve and are also lingually inclined. The mesial and distal cutting edges of the main cusp are incomplete, and the cutting edges that extend across the lateral cusplets do not meet the base of the main cusp. The bilobate root has lobes that are narrow, elongated, and slightly divergent. The interlobe area is deep and U-shaped. A robust lingual protuberance is bisected by a deep nutritive groove. The H/W ratio of GSA–V447.2 (complete tooth) is 1.74 (Table 2), and main cusp height on the five teeth ranges from 17.53 to 8.74 mm, indicating that overall tooth size decreased towards the commissure. Tooth GSA–V447.17 (Fig. 6cc–gg) has the shortest main cusp height of any tooth associated with GSA–V447 (Table 2), and this interesting tooth is regarded as a lower posterolateral tooth due to its small size but overall similarity to the other four teeth attributed to the lower lateral tooth group.

**Remarks.** Our analysis of the 17 teeth included with GSA–V447 indicates that monognathic and dignathic

heterodonty were developed within the dentition of *Palaeohypotodus bizzocoi* sp. nov. Our examination of 17 isolated teeth from temporally equivalent strata also indicate a degree of ontogenetic heterodonty within this taxon.

**Monognathic heterodonty.** Some of the variation observed amongst the teeth within GSA–V447 reflects the presence of anterior and lateral tooth files in the palatoquadrate and Meckel’s cartilage of *P. bizzocoi* sp. nov. (Fig. 7). Upper anterior teeth differ from upper lateral teeth by having a taller and mesiodistally narrower main cusp, and the H/W ratios of anterior teeth range from 1.44–1.55 but those of lateral teeth are much lower at 1.01–1.21 (Table 2). The main cusp of anterior teeth is also more erect, more symmetrical, and labiolingually thicker compared to the inclined to strongly distally hooked crown of lateral teeth. Additionally, the anterior teeth have longer and less divergent root lobes and a deeper interlobe area than lateral teeth. The root height is therefore lower on lateral teeth (between 26.3 to 28.9% the height of the tooth) than on anterior teeth (between 30.1 and 32.1%) because of the shorter root lobes. Furthermore, the lateral teeth can have up to two pairs of lateral cusplets but there is only one pair on the anterior teeth. Lastly, although the teeth of the Meckel’s cartilage are similar to one another, the lateral teeth are characterized by the slight distal inclination of the main cusp (Fig. 6). Additionally, the root of GSA–V447.5 shows that lobes are more widely separated compared to the complete anterior tooth (GSA–V447.4).

**Dignathic heterodonty.** The teeth included with GSA–V447 also demonstrate morphological variation between the teeth of the palatoquadrate and Meckel’s cartilage of *P. bizzocoi* sp. nov. (Figs 5, 6). Overall, the upper teeth differ from the lower teeth by having a wider U-shaped interlobe area, as the root lobes on the upper teeth are shorter and more divergent. This is reflected in the H/W ratios among the teeth, which are much higher for lower teeth (1.74 to 1.89) than for the uppers (1.01 to 1.55) (Table 2). In addition, the height of the root constitutes between 26–32% of total tooth height of upper teeth and between 36–39% of lower teeth.

Upper anterior teeth (i.e., GSA–V447.1, 6–7, Fig. 5a–p) are distinguished by their complete cutting edges, whereas those of lower anterior teeth (i.e., GSA–V447.4, Fig. 6a–d) do not reach the main cusp base. In profile view, the upper anterior teeth have a more sigmoidal main cusp compared to the lower anterior files. Additionally, the lateral cusplets on upper anterior teeth are lingually curved but those on the lower anterior teeth have a slight distal inclination. With respect to the tooth root, that of the upper anterior teeth has shorter and more divergent lobes compared to lower anterior teeth, and the interlobe area is resultantly more widely U-shaped on the upper anterior teeth. Furthermore, the root comprises 30–32% of the total height of upper anterior teeth but is close to 40% on the lower anterior tooth GSA–V447.4 (Table 2).

The lower lateral teeth are easily differentiated from upper lateral teeth by their narrower and nearly vertical main cusp with relatively flat labial face. In contrast, the

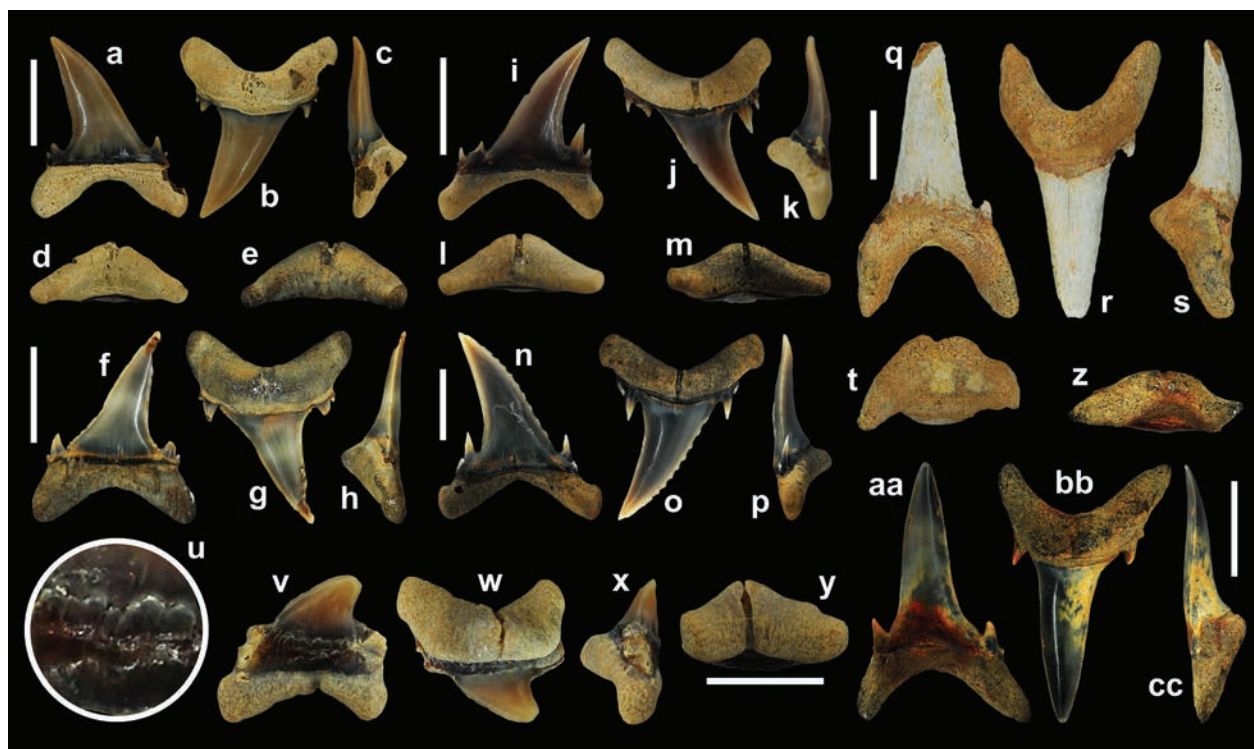


**Figure 7.** *Palaeohypotodus bizzocoi* sp. nov. referred specimens. **a–d.** MSC 49451, upper left lateral tooth, lower Clayton Formation, Wilcox County, AL; **a.** Labial view; **b.** Lingual view; **c.** Mesial view; **d.** Basal view. **e–h.** MMNS VP–8578, upper right lateral tooth, basal Clayton Formation, Hot Spring County, AR; **e.** Basal view; **f.** Labial view; **g.** Lingual view; **h.** Mesial view. **i–l.** MMNS VP–7292.3, upper right lateral tooth, Pine Barren Member of the Clayton Formation, Lowndes County, AL; **i.** Labial view; **j.** Lingual view; **k.** Mesial view; **l.** Basal view. **m–p.** MSC 42733, upper left lateral tooth, Pine Barren Member of the Clayton Formation, Lowndes County, AL; **m.** Basal view; **n.** Labial view; **o.** Lingual view; **p.** Mesial view. **q–t.** MSC 3020, lower left anterior tooth, lower Clayton Formation, Wilcox County, AL; **q.** Labial view; **r.** Lingual view; **s.** Mesial view; **t.** Basal view. **u–y.** MMNS VP–7295.3, upper right posterior tooth, Pine Barren Member of the Clayton Formation, Lowndes County, AL; **u.** Close-up of labial crown ornamentation; **v.** Labial view; **w.** Lingual view; **x.** Mesial view; **y.** Basal view. **z–cc.** MSC 49452, upper left 3<sup>rd</sup> anterior tooth, Porters Creek Formation, Butler County, AL; **z.** Basal view; **aa.** Labial view; **bb.** Lingual view; **cc.** Mesial view. Scale bars: 1 cm (**a–h**, **q–t**, **z–cc**); 5 mm (**i–p**, **v–y**).

upper lateral teeth are conspicuously distally inclined to strongly distally hooked, and the labial crown face is more convex. In addition, the mesial and distal cutting edges of the main cusp on lower lateral teeth are incomplete, whereas they extend to the lateral cusplets on the upper lateral teeth. The main cusp of lower lateral teeth is also slightly curved lingually near the apex, whereas upper lateral teeth have a straighter lingual crown face. Furthermore, the lateral cusplets of lower lateral teeth have a slight distal inclination, whereas those of the upper teeth are distally curved. Moreover, the lateral teeth have a deeper interlobe area due to more elongated but less divergent root lobes compared to the upper lateral teeth. Lastly, the root height of the only complete lower lateral tooth in our sample (GSA–V447.5) constitutes 36.4% of the total tooth height, which far exceeds that on any of the upper lateral teeth (only 26.9% to 28.9%; see Table 2).

**Ontogenetic heterodonty.** The 17 teeth included with GSA–V447 were derived from the Danian Porters Creek Formation in Wilcox County, AL. No additional *P. bizzocoi* sp. nov. specimens are known from the type locality, but the collections at MSC and the MMNS include 17 isolated teeth collected from Alabama and

Arkansas, USA (see Referred specimens above) that we associate with this new species. One of these teeth (MSC 49452) was collected from the type stratum (albeit from a different locality), whereas the other 16 teeth were derived from lithostratigraphic units that are temporally equivalent to the Porters Creek Formation. Two specimens in particular, MSC 49451 and MMNS VP–8578, are morphologically, qualitatively, and quantitatively comparable to teeth within GSA–V447. Specifically, MSC 49451 (Fig. 7a–d) is an upper left lateral tooth that is nearly indistinguishable from the *P. bizzocoi* sp. nov. paratype tooth GSA–V447.3 (Fig. 5cc–ff) in terms of size and gross morphology (see Tables 2, 3). In addition, specimen MMNS VP–8578 (Fig. 7e–h), an upper right lateral tooth, is nearly identical in all respects to *P. bizzocoi* sp. nov. paratype tooth GSA–V447.2 (Fig. 5y–bb). The morphological similarity of the 17 isolated teeth to those included with GSA–V447 leads us to conclude that they represent *P. bizzocoi* sp. nov. and that they reflect intra-specific (ontogenetic) variation within the species.

Ten of the additional 17 isolated teeth referred to *P. bizzocoi* sp. nov. are complete and could be described in their entirety and measured, allowing us to directly

**Table 3.** Measurements, ratios, and observations of *Palaeohypotodus bizzocoi* sp. nov. teeth. Teeth are organized by tooth group and increasing TH. **Column abbreviations:** #DC, Number of distal cusplets; **DIA**, Depth of the interlobe area; **H/W Rat**, Height/width ratio; **LOP**, Labial ornamentation present and the nature of the ornamentation; #MC, Number of mesial cusplets; **MCH**, Main cusp height; %MCH, The percentage of the main cusp height in relation to the total tooth height; **MCT**, Main cusp thickness; **MCW**, Main cusp width; **RH**, Root height; %RH, The percentage of the root height in relation to the total tooth height; **RT**, Maximum root thickness; **RW**, Root width; **TH**, Total height. **N/A**, Measurement, ratio, or observation could not be taken due to the incomplete preservation of the tooth.

	TH	TW	H/W Rat	MCH	%MCH	RH	%RH	MCW	MCT	DIA	RT	#MC	#DC	LOP
<b>Upper anterior teeth</b>														
MSC 49452	23.79	15.87	1.5	18.29	76.9	5.5	23.1	8.34	4.57	4.91	5.54	2	2	Faint across base
MSC 42738	24.55	13.79	1.78	18.13	73.8	6.42	26.2	8.39	5.29	5.99	6.86	1	N/A	Faint across base
GSA–V447.7	28.87	19.97	1.44	19.63	67.9	9.24	32.1	11.18	5.28	6.28	8.12	1	1	Faint across base
GSA–V447.1 (holotype)	29.11	19.08	1.52	19.98	68.6	9.13	31.4	11.19	5.24	7.18	8.9	1	1	Faint across base
GSA–V447.6	29.16	18.84	1.55	20.39	69.9	8.77	30.1	10.53	5.14	6.7	8.63	1	1	Faint across base
<b>Upper lateral teeth</b>														
MMNS VP–7292.3	10.06	9.02	1.12	7.89	78.4	2.17	21.6	3.86	1.88	2.7	3.01	3	3	Faint across base
MMNS VP–7292.4	10.67	9.25	1.15	8.29	77.7	2.38	22.3	4.61	1.91	2.76	3.02	3	3	Faint across base
MSC 42733	12.75	11.21	1.13	10.39	81.5	2.36	18.5	4.98	2.49	3.33	3.66	2	2	Faint across base
MMNS VP–7292.2	12.76	10.42	1.22	9.43	73.9	3.33	26.1	4.78	2.49	4.06	3.78	3	3	Faint across base
GSA–V447.10	15.59	13.33	1.17	11.4	73.1	4.19	26.9	8.6	3.58	3.78	4.88	1	1	Faint across base
GSA–V447.3 (paratype)	19.51	16.94	1.15	14.39	73.7	5.12	26.3	9.52	4.05	4.97	5.91	2	2	Faint across base
MSC 49451	20.5	17.82	1.15	15.38	75	5.12	25	9.77	4.32	5.57	5.99	2	2	Faint across base
GSA–V447.8	20.09	14.54	1.01	14.6	72.6	5.49	27.4	7.34	3.95	5.02	6.1	2	2	Faint across base
MMNS VP–8578	22.01	18.89	1.17	16.16	73.4	5.84	26.6	10.23	4.01	6.24	7.09	2	2	Faint across base
GSA–V447.2 (paratype)	23.93	19.81	1.21	17.03	71.1	6.9	28.9	11.29	4.64	5.35	6.91	2	2	Faint across base
<b>Lower anterior teeth</b>														
GSA–V447.4 (paratype)	32.63	17.28	1.89	18.86	60.9	12.73	39.1	9.67	5.08	10.48	8.65	1	1	N/A
MSC 3020	37.67	22.01	1.71	24.74	65.7	12.93	34.3	11.92	7.29	11.16	10.65	1	1	Faint across base
<b>Lower lateral teeth</b>														
MMNS VP–7311	21.24	14.53	1.46	14.81	69.7	6.43	30.3	9.01	5.06	5.28	6.36	1	2	Faint across base
GSA–VP447.5 (paratype)	27.06	15.53	1.74	14.6	63.6	9.83	36.4	7.45	4.07	7.2	6.29	1	2	N/A

compare them to the teeth of GSA–V447. One of the referred specimens was identified as a posterior tooth (see below) and was excluded from our quantitative analysis due to its atypical morphology.

Our quantitative evaluation of the total tooth sample of *P. bizzocoi* sp. nov. revealed several morphological trends that we interpret to represent ontogenetic heterodonty within the species. Table 3 lists all the complete teeth according to tooth group (i.e., upper and lower anterior and upper and lower lateral) and are presented by ascending order of total tooth height (TH). Our data shows that the teeth associated with GSA–V447 are among the largest in our sample, indicating these specimens likely represent adult individuals (or a single adult individual). Interestingly, specimen MSC 3020 (Fig. 7q–t), a lower anterior tooth, has a TH over 5 mm greater than the largest lower anterior tooth associated with GSA–V447 (paratype tooth GSA–V447.4), indicating that this species could achieve even larger sizes than indicated by the type specimens.

One morphological trend that is evident in Table 3 is the ontogenetic reduction in the number of lateral cusplets on upper teeth. Of the upper anterior teeth in our sample, all the specimens with a TH less than 24 mm have two pairs of lateral cusplets, whereas those with a TH greater than 24 mm only have a single pair. Additionally, the number of lateral cusplets on the upper lateral teeth ranges from one to three pairs, but the occurrence of three pairs is limited to teeth with a TH of 13 mm or less. In contrast, all upper

lateral teeth that exceed 15 mm in TH have a maximum of two lateral cusplet pairs. Similarly, the number of lateral cusplets on each side of the main cusp on lower anterior and lateral teeth also does not exceed two, with most specimens having a single pair regardless of tooth size. We observed that the mesial and distal cusplets on teeth of both the palatoquadrate and Meckel’s cartilage can be unequal in number (Tables 2, 3), particularly on lateral teeth.

Our data shows a general trend across all tooth groups of both the palatoquadrate and Meckel’s cartilage that, as the TH of a tooth increases, the total width (TW), main cusp height (MCH), main cusp width (MCW), root height (RH), root thickness (RT), and depth of the interlobe area (DIA) also increases (see Table 3). These trends reflect ontogenetic change from small and gracile teeth in juvenile stages to large and robust teeth into adulthood. Interestingly, when the ratio of the root to overall tooth height is calculated (%RH) and then compared to that of the main cusp (%MCH), these values show an inverse relationship through ontogeny. As the shark matures the %RH increases and the %MCH decreases, which is a result of an increase in the length of the mesial and distal root lobes through ontogeny. This is also reflected in the DIA (i.e., depth of the interlobe area), which increases (deepens) as the root lobes become elongated (Table 3). Although subtle changes are evident across ontogeny based on the aforementioned values, the height/width ratios (H/W) remain relatively constant. This indicates that juvenile teeth, at least in terms of H/W ratios, are

essentially smaller versions of the larger teeth, with any differences in the values likely being a result of different tooth files within a particular tooth group (for example, a lower second versus lower third anterior).

**Additional tooth files.** In addition to elucidating ontogenetic heterodonty, the sample of 17 isolated *P. bizzocoi* sp. nov. teeth increases our understanding of monognathic and dignathic heterodonty within the species. Included in the sample are two tooth positions that are not represented amongst the teeth associated with GSA–V447. One of these teeth, MSC 49452 (Fig. 7z–cc), has a tall and triangular main cusp, two pairs of lingually curved lateral cusplets, complete mesial and distal cutting edges, plications along the labial crown base, a pronounced lingual root protuberance with nutritive groove, and a deep U-shaped interlobe area, which are all characteristics of *P. bizzocoi* sp. nov. anterior teeth. However, this tooth also has an elongated and mesially extended mesial root lobe, and the distal edge of the main cusp is more convex than the mesial edge, giving the main cusp a slight mesial curve (as opposed to distally inclined or hooked). Of the extant lamniform dentitions we examined, these unique characteristics are remarkably similar to those of the upper third anterior teeth of *Carcharias taurus* and *Mitsukurina owstoni*.

Specimen MMNS VP–7295.4 is herein regarded as an upper posterior tooth of *P. bizzocoi* sp. nov. (Fig. 7u–y). This tooth is very small and measures 5.4 mm in TH and 6.4 mm in RW. The tooth has a short and distally hooked main cusp and although the lateral cusplets are not preserved on this tooth, it appears to have had at least one pair. The mesial and distal cutting edges are complete and extend to the base of the lateral cusplets. The root is robust and, in lingual view, the height of the root (3.8 mm) is more than twice the height of the crown (1.6 mm). The root lobes are short, rounded, divergent, and form a wide and U-shaped interlobe area. The lingual face of the root is bisected by a deep nutritive groove. Perhaps the most conspicuous feature of this tooth is the extensive ornamentation along the labial crown foot, where enameloid plications coalesce into spine-like structures. Similar ornamentation has been reported on posterolateral and posterior teeth of *Palaeohypotodus rutoti* (see Herman 1972, pl. 2, figs 1–3, 5; Herman 1977, pl. 10, fig. 3e; Cappetta 2012, fig. 192h–j), and this specific characteristic was noted by Leriche (1902, 1906) and Herman (1972, 1977). This phenomenon indicates a degree of dental homology and stasis between the temporally younger *P. rutoti* and the Danian *P. bizzocoi* sp. nov.

## Discussion

### Generic assignment of GSA–V447

*Palaeohypotodus* was previously comprised of three valid species, including Cretaceous *P. bronni* (Agassiz, 1843) and Paleogene *P. rutoti* (Winkler, 1874) and *P. volgensis* Zhelezko & Kozlov, 1999. Multiple other species have

been named, like *Palaeohypotodus houzeaui* (Woodward, 1891) and *P. lerichei* Glückman, 1964, but these (and some other) taxa were subsequently synonymized with *P. rutoti* (Cappetta & Nolf, 2005). Still other species, including *P. speyeri* (Darteville & Casier, 1943) and *P. striatula* (Dalinkevicius, 1935), have been referred to other genera (see Cappetta 2012). Several morphological features have been utilized to identify teeth of *Palaeohypotodus*, including; the variable occurrence of one to three pairs of lateral cusplets; upper lateral teeth having a strongly distally inclined to hooked main cusp; upper and lower anterior teeth with tall, triangular and generally symmetrical main cusp; lower lateral teeth with a tall and relatively erect main cusp; upper teeth with complete mesial and distal cutting edges; lower teeth with incomplete cutting edges; a pronounced lingual root protuberance with nutritive groove; and a U-shaped interlobe area. Although many of these features are present on teeth of other taxa, like *Jaekelotodus* Glückman, 1964 and *Odontaspis winkleri* Leriche, 1905, all teeth assigned to *Palaeohypotodus* bear plications across the labial crown foot (particularly on lateral and posterior teeth). Additionally, upper and lower anterior teeth of *Jaekelotodus* have complete cutting edges, and all those of *O. winkleri* have incomplete edges. The teeth included with GSA–V447 all exhibit these characteristics, and their assignment to *Palaeohypotodus* is appropriate.

Of the recognized species, *Palaeohypotodus rutoti* (Winkler, 1874) is the one most often reported in the literature. This species would seem to have a rather long temporal distribution, being variously reported from Danian to Priabonian (late Eocene) strata, as well as an extensive geographic distribution (see Cappetta 2012; Kriwet et al. 2016). Although *P. bronni* (Agassiz, 1843) is predominantly known from the Maastrichtian (Late Cretaceous) of Europe, at least two reports suggest this species may have survived the K/Pg extinction event into the Paleocene (see Leriche 1906; Adolfssen and Ward 2015). To our knowledge, *P. volgensis* has not been identified beyond the type discussion (Zhelezko and Kozlov 1999). Many of the identifications to these species appear to be tentative at best and we believe that these occurrences need further evaluation. Although such a thorough reassessment of *Palaeohypotodus* is beyond the scope of this paper, we present a limited discussion of the morphological criteria that have been used to identify these species so they can be adequately compared to *P. bizzocoi* sp. nov.

### *Palaeohypotodus bronni* (Agassiz, 1843)

This taxon was originally named by Agassiz (1843) based on two teeth collected from Upper Cretaceous (Maastrichtian) deposits in the Mount St. Peter area in Maastricht, Netherlands (pl. 37, figs 8–9), and a third tooth from an unspecified unit in Delaware, USA (fig. 10). Only the outline of the Delaware specimen was provided, and it is difficult to evaluate due to the lack of details. Also, considering that the tooth was collected from a

different continent and the age of the source stratum is unknown, we suggest it be excluded from Agassiz’s (1843) *P. bronni* type suite. Based on our interpretation of the dentition of *P. bizzocoi* sp. nov., the two teeth from Maastricht appear to be from the lower dentition, with that shown in Agassiz’s (1843) figure 8 representing a lower lateral tooth and the one in figure 9 likely being a lower anterior tooth. Agassiz’s (1843) brief description of these teeth stated that they have a symmetrical main cusp, two pairs of lateral cusplets, and plications along the labial crown foot. Unfortunately, these two teeth are embedded in limestone and only the labial face is visible.

Fortunately, additional *P. bronni* specimens from the vicinity of the type locality were subsequently reported by Preim (1897, pl. 1, figs 11–14), Van de Geyn (1937, figs 117–123), Herman (1977, pl. 10, fig. 2a–f), and Cappetta and Corral (1999, fig. 4). Additionally, we examined three teeth from Maastrichtian deposits exposed at the ENCI Quarry in Limburg, Netherlands (MMNS VP–9616, MMNS VP–10577.1–2). This assortment of teeth allows us to gain a better understanding of the dental variation within this species, as it includes anterior and lateral tooth groups from both the palatoquadrate and Meckel’s cartilage (see Table 4). Critical examination of these teeth demonstrated that they are morphologically similar to one another by their having a triangular main cusp that is erect in the anterior and lower lateral files but distally hooked in the upper lateral files, labial plications occur along the crown foot, one to two pairs of lateral cusplets (with the larger pair being positioned closer to the main cusp), a robust root with a pronounced lingual protuberance and nutritive groove, and a relatively deep and U-shaped interlobe area.

**Table 4.** Comparison of the DIA% between *Palaeohypotodus bizzocoi* sp. nov., *P. bronni*, and *P. rutoti*. **DIA%**. Ratio of the depth of the interlobe area in relation to the overall height of the tooth.

<i>Palaeohypotodus bizzocoi</i> sp. nov.		
Source	Tooth Position	DIA%
MSC 49452	Upper 3 <sup>rd</sup> anterior tooth	0.21
MSC 43738	Upper anterior tooth	0.24
MMNS VP–7311	Lower right lateral tooth	0.25
MMNS VP–7292.3	Upper left lateral tooth	0.25
MMNS VP–7292.4	Upper right lateral tooth	0.26
MSC 42733	Upper right lateral tooth	0.26
MSC 49451	Upper left lateral tooth	0.27
MMNS VP–8578	Upper right lateral tooth	0.28
MSC 3020	Lower left anterior tooth	0.3
GSA-VP447.2 (paratype)	Upper lateral tooth	0.31
GSA-VP447.7	Upper anterior tooth	0.32
MMNS VP–7292.2	Upper right lateral tooth	0.32
GSA-VP447.10	Upper lateral tooth	0.33
GSA-VP447.6	Upper anterior tooth	0.33
GSA-VP447.8	Upper lateral tooth	0.34
GSA-VP447.3 (paratype)	Upper lateral tooth	0.35
GSA-VP447.1 (holotype)	Upper anterior tooth	0.36
GSA-VP447.5 (paratype)	Lower lateral tooth	0.42
GSA-VP447.4 (paratype)	Lower anterior tooth	0.53
<b>Mean</b>		<b>0.31</b>

<i>Palaeohypotodus bronni</i>		
Source	Tooth Position	DIA%
MMNS VP–10577.1	Upper lateral tooth	0.16
Van de Geyn (1937) fig. 118	Upper 3 <sup>rd</sup> anterior tooth	0.17
Van de Geyn (1937) fig. 121	Upper anterior tooth	0.17
Herman 1977, pl. 10, fig. 2a	Upper anterior tooth	0.18
Van de Geyn (1937) fig. 120	Lower anterior tooth	0.18
Herman 1977, pl. 10, fig. 2d	Upper lateral tooth	0.19
Agassiz 1843, pl. 37, fig. 8	Lower lateral tooth	0.19
Herman 1977, pl. 10, fig. 2f	Lower lateral tooth	0.19
Preim 1897 pl. 1, fig. 13	Upper anterior tooth	0.19
Preim 1897 pl. 1, fig. 11	Upper lateral tooth	0.2
Agassiz 1843, pl. 37, fig. 9	Upper anterior tooth	0.21
Cappetta and Corral 1999, fig. 4	Upper anterior tooth	0.21
Preim 1897 pl. 1, fig. 14	Upper anterior tooth	0.21
Herman 1977, pl. 10, fig. 2c	Upper anterior tooth	0.21
Van de Geyn (1937) fig. 123	Upper anterior tooth	0.21
MMNS VP–9616	Upper lateral tooth	0.22
Van de Geyn (1937) fig. 117	Lower anterior tooth	0.22
Van de Geyn (1937) fig. 119	Upper lateral tooth	0.23
Herman 1977, pl. 10, fig. 2b	Lower anterior tooth	0.24
Herman 1977, pl. 10, fig. 2e	Upper lateral tooth	0.27
<b>Mean</b>		<b>0.2</b>

<i>Palaeohypotodus rutoti</i>		
Source	Tooth Position	DIA%
Casier 1942, pl. 1, fig. 6	Upper lateral tooth	0.14
Casier 1942, pl. 1, fig. 5	Upper lateral tooth	0.17
Leriche 1951, pl. 42, fig. 8	Upper anterior tooth	0.18
Leriche 1951, pl. 42, fig. 10	Lower anterior tooth	0.19
Leriche 1951, pl. 42, fig. 9	Lower 1 <sup>st</sup> anterior? Tooth	0.2
Herman 1977 pl. 10, fig. 3a	Upper anterior tooth	0.21
Herman 1977 pl. 10, fig. 3d	Upper posterolateral tooth	0.21
Vincent 1876, pl. 6, fig. 1c	Lower anterior tooth	0.21
Casier 1942, pl. 1, fig. 2	Upper 3 <sup>rd</sup> anterior tooth	0.21
Casier 1942, pl. 1, fig. 1	Upper anterior tooth	0.24
Casier 1942, pl. 1, fig. 9	Lower anterior tooth	0.24
Herman 1972, pl. 2, fig. 5	Upper posterolateral	0.24
Herman 1977 pl. 10, fig. 3c	Upper lateral tooth	0.25
Herman 1977 pl. 10, fig. 3e	Upper posterolateral tooth	0.25
Casier 1942, pl. 1, fig. 11	Lower lateral tooth	0.25
Leriche 1951, pl. 42, fig. 11	Lower lateral tooth	0.26
Casier 1942, pl. 1, fig. 12	Lower lateral tooth	0.26
Leriche 1902, pl. 1, fig. 37	Upper anterior tooth	0.26
Leriche 1902, pl. 1, fig. 38	Lower anterior tooth	0.26
Cappetta 2012, fig. 192e	Upper 3 <sup>rd</sup> anterior tooth	0.26
Herman 1977 pl. 10, fig. 3b	Lower anterior tooth	0.28
Vincent 1876, pl. 6, fig. 1d	Upper anterior tooth	0.28
Casier 1942, pl. 1, fig. 10	Lower anterior tooth	0.28
Leriche 1902, pl. 1, fig. 39	Upper lateral tooth	0.28
Vincent 1876, pl. 6, fig. 1a	Upper anterior tooth	0.29
Casier 1950, pl. 2, fig. 1	Lower anterior tooth	0.3
Vincent 1876, pl. 6, fig. 1b	Upper anterolateral tooth	0.34
<b>Mean</b>		<b>0.24</b>

The historical descriptions of *P. bronni* teeth support our observations. For example, Giebel (1848) reiterated that the teeth had one or two pairs of lateral cusplets. Sauvage (1898) also noted the presence of two lateral cusplets on *P. bronni* teeth and he mentioned that Cretaceous specimens from Portugal have conspicuous plications at the labial crown foot. Leriche (1902)

described the teeth as having two pairs of lateral cusplets, with the second pair smaller, and noted that labial folds were small and obsolete on Paleocene specimens he examined (suggesting these latter specimens need to be reevaluated as they may not belong to this genus). From these descriptions, it seems clear that Late Cretaceous teeth from Europe assigned to *P. bronni* have two pairs of lateral cusplets, with the second pair being smaller than the first. Adolfssen and Ward (2015) tentatively reported a Danian record of this taxon, but they specifically noted that the material lacked labial ornamentation and only had a single pair of lateral cusplets. These differences indicate that Paleogene records of *P. bronni* need to be reevaluated, as they may not belong to this genus.

The *P. bronni* teeth we examined are morphologically very similar to those of *P. bizzocoi* sp. nov., but several distinct features distinguish the two species. Adult teeth of *P. bronni* generally have two pairs of rather wide lateral cusplets, whereas *P. bizzocoi* sp. nov. teeth typically have a single pair of relatively narrow cusplets. Overall, teeth of *P. bizzocoi* sp. nov. have one to three pairs of cusplets (adults generally with one pair and juveniles with one to three pairs) that, compared to *P. bronni*, are much shorter, narrower, more needle-like, and diminutive with respect to the size of the main cusp. In addition, the secondary cusplets (i.e., the more labial pair) on *P. bronni* teeth are much larger than those that occur on any *P. bizzocoi* sp. nov. teeth, where on the latter they are generally minute and are largely united to the larger medial cusplet (while they are more clearly separated on *P. bronni*). Furthermore, the root lobes of *P. bronni* teeth are much more robust than those of *P. bizzocoi* sp. nov. On the latter, the root lobes are thin and have consistent width across their length, whereas they widen towards the crown base on *P. bronni* teeth. Lastly, the root lobes are significantly longer on *P. bizzocoi* sp. nov. teeth, resulting in a much deeper interlobe area. This is readily apparent in Table 4, which shows the depth of the interlobe area of *P. bizzocoi* sp. nov. teeth consistently constitutes roughly 25–50% (mean = 31%) of the overall tooth height. This value rarely exceeds 23% on *P. bronni* teeth (mean = 20%). Although we identified the depth of the interlobe area as a characteristic that increases through ontogeny on *P. bizzocoi* sp. nov. teeth, many of the *P. bronni* teeth figured in the literature appear to approach and even exceed the size of the largest *P. bizzocoi* sp. nov. teeth in our sample. This indicates that the extremely elongated root lobes and deep interlobe area are characteristic of *P. bizzocoi* sp. nov. teeth.

Interestingly, Van de Geyn (1937, fig. 118) illustrated a distinct upper anterior tooth with an elongated mesial root lobe and a main cusp that has a distal cutting edge that is more convex than the mesial edge. This tooth is morphologically very similar to the upper third anterior teeth within extant lamniform taxa like *Carcharias taurus* and *Mitsukurina owstoni* and is comparable to an upper third anterior tooth of *P. bizzocoi* sp. nov. we identified in our sample (MSC 49452, Fig. 7z–cc). A comparison of these teeth clearly illustrates the morphological differences

between these two species, as the *P. bronni* tooth figured by Van de Geyn (1937, fig. 118) has root lobes that are wider, the interlobe area is shallower and more V-shaped, and the lateral cusplets are wider, more triangular, and more divergent compared to *P. bizzocoi* sp. nov.

### *Palaeohypotodus rutoti* (Winkler, 1874)

This taxon was named for two teeth (IRSNB P 123 and IRSNB P 124) derived from the Selandian (middle Paleocene) Orp Member of the Heers Formation in Orp-le-Grand (Maret), Belgium (Hovestadt and Steurbaut 2023). Winkler (1874, pl. 1, figs 3–4) illustrated only the lingual view of these two teeth, but Hovestadt and Steurbaut (2023, p. 51) provided high-resolution images of these specimens in labial, lingual, and mesial views. These images show that the type specimens have a distally hooked main cusp, which is indicative of upper lateral teeth. These teeth have two to three pairs of tall and triangular lateral cusplets that are divergent and well separated from one another and from the main cusp. Faint plications occur along the labial crown base on both teeth. Unfortunately, the roots on both type specimens are incomplete, with only the distal lobe preserved on IRSNB P 123 and both lobes are missing from IRSNB P 124. Because the *P. rutoti* type specimens represent only the upper lateral tooth morphology, we expanded our investigation into dental variation in this species by examining published descriptions and illustrations of specimens derived from, or close to, the type locality.

In his type description, Winkler (1874) noted that the teeth have a distally curved main cusp, ‘creases’ along the labial crown base, and two to three pairs of cusplets that decrease in size laterally and are well-delineated from one another. Leriche (1902) described Selandian *P. rutoti* (pl. 1, figs 37–40) teeth as having two or three pairs of slender, sharply pointed lateral cusplets, with the first pair being quite large, and the labial crown foot having numerous short, very closely spaced vertical plications that produced an unbroken line of sharp spines. Vincent (1876) provided a similar description of teeth with a straight to distally curved main cusp, at least one pair of lateral cusplets on anterior teeth and additional pairs on lateral teeth, and small enameloid folds along the base of the labial face. Casier (1942) provided the most thorough description of *P. rutoti* from the Selandian of Belgium based on an associated skeleton consisting of 31 teeth, 58 vertebrae, and three pieces of cartilage that were likely derived from the Meckel’s cartilage or palatoquadrate. Casier (1942) described the teeth as having a slender crown with conspicuous labial folds at the crown base that were “spiniiform” apically. He also noted that the teeth had two to three pairs of distinctly separated and lingually angled lateral cusplets (with most having three pairs), and a robust lingual protuberance. Casier’s (1942) associated specimen included teeth from both the upper and lower jaws, with those in the lower files being described as having a

straighter main cusp. The similarity of these descriptions indicates that Selandian *P. rutoti* from Belgium generally includes: 1) anterior and lower teeth with an erect main cusp; 2) upper lateral teeth with a distally hooked main cusp; 3) teeth with two to three pairs of lateral cusplets; 4) enameloid folds (and at times forming spinose ornamentation) along the labial crown base.

When the previously figured Selandian *P. rutoti* teeth from Belgium (i.e., Winkler 1874, pl. 6, figs 3–4; Vincent 1876, pl. 6, fig. 1; Leriche 1902, pl. 1, figs 37–44; Casier 1942, pl. 1, figs 1–12; Casier 1950, pl. 2, fig. 1; Leriche 1951, pl. 42, figs 8–11; Herman 1972, pl. 2, figs 1–5; Herman 1977, pl. 10, fig. 3; Cappetta 2012, fig. 192e; and Hovestadt and Steurbaut 2023, pg. 51) are compared to those of *P. bizzocoi* sp. nov., several distinct differences become apparent. First, *P. rutoti* teeth generally have two to three pairs of lateral cusplets, with most having three pairs, and at least one figured specimen appears to have four pairs (see Vincent 1876, pl. 6, fig. 1a). On *P. bizzocoi* sp. nov. teeth, the number of pairs of lateral cusplets rarely exceeds two (with three pairs occurring only on small, presumably juvenile, upper lateral teeth), with most teeth having only a single pair. Second, the more medial pair of lateral cusplets on *P. rutoti* teeth, particularly those on the type specimens (see Winkler 1974, pl. 6, figs 3–4, Hovestadt and Steurbaut 2023, pg. 51), are more robust and taller in relation to the height of the main cusp than they are on *P. bizzocoi* sp. nov. teeth. The lateral cusplets on *P. rutoti* teeth are also more widely separated from one another than they are on *P. bizzocoi* sp. nov., with the secondary pair of cusplets on the latter being more closely united to the base of the larger, more medial pair of cusplets. Lastly, the root lobes are generally longer on *P. bizzocoi* sp. nov. teeth, resulting in a deeper interlobe area than on *P. rutoti* specimens. Table 4 shows the ratio of interlobe depth to overall tooth height for *P. bizzocoi* sp. nov., *P. bronni*, and *P. rutoti* for teeth examined first-hand or published in the literature. On *P. bizzocoi* sp. nov. teeth, the depth of the interlobe area constitutes 25–50% (mean = 31%) the overall tooth height, whereas this value rarely exceeds 23% on *P. bronni* teeth (mean = 20%). Although the ratio for *P. rutoti* teeth ranges between 14–34%, which overlaps the low end of that measured on *P. bizzocoi* sp. nov. teeth, they have a significantly lower mean (mean = 24%).

Interestingly, both Casier (1942, pl. 1, fig. 2) and Cappetta (2012, fig. 192e–f) illustrated *P. rutoti* upper third anterior teeth that can be directly compared to specimen MSC 49452 (Fig. 7z–cc), which is herein referred to *P. bizzocoi* sp. nov. Although this tooth position in both taxa has two pairs of lateral cusplets, on *P. rutoti* the outer pair of cusplets is larger and more separated from the medial pair of cusplets than it is on MSC 49452. In contrast, the outer pair of cusplets on MSC 49452 is minute and mostly united to the larger medial pair of cusplets. In addition, in mesial and distal views, the lingual root protuberance on *P. rutoti* teeth is substantially more developed, although this may indicate that specimen MSC 49452 was derived from a replacement row (where the root may be incompletely

developed) or the root shows some signs of erosion. Nevertheless, the labial ornamentation is extremely faint and visible only under magnification on MSC 49452. However, it is visible but inconspicuous on the tooth illustrated in Casier (1942) and is very pronounced on the specimen illustrated by Cappetta (2012).

### *Palaeohypotodus volgensis* Zhelezko in Zhelezko & Kozlov, 1999

Existence of this taxon appears to be limited to the type description, and we are unaware of other published occurrences of this species. The type specimens were derived from the Selandian “lower Saratov beds” exposed along the Volga River near the town of Kamyshin in the Volgograd Oblast of Russia. The type suite consists of a holotype (GIK No. 8057/87) and three paratypes (GIK No. 8057/88–91) that are repositated at the State Darwin Museum in Moscow, Russia. The holotype is an upper left lateral tooth (GIK No. 8057/87; Zhelezko and Kozlov 1999, pl. 1, fig. 5), and the paratypes consist of two upper anterior teeth (pl. 1, fig. 1, 4), an upper lateral tooth (pl. 1, fig. 2), and a lower anterior tooth (pl. 1, fig. 3). Zhelezko and Kozlov (1999) also mentioned the presence of 100 additional teeth belonging to this taxon that were collected from the type locality, but unfortunately none of these specimens were figured and it is unclear whether they also reside within the State Darwin Museum collections.

In their brief description of *P. volgensis*, Zhelezko and Kozlov (1999) stated that the teeth have one to two pairs of conical lateral cusplets, a pronounced lingual root protuberance, pointed root lobes, a deep lingual nutritive groove, and a tall and triangular main cusp. An examination of their figured type specimens corroborates these remarks and also confirms that the *P. volgensis* morphology lacks enameloid plications along the labial crown foot. We considered the possibility that this characteristic was overlooked by the authors or simply not described or visible on the type specimens (pl. 1, figs 1–5), but Zhelezko and Kozlov (1999) prominently mentioned the occurrence of plications in their description of *P. rutoti*, and they are clearly visible on some of the *P. rutoti* teeth that they illustrated (pl. 36, figs 3b, 8b) alongside their *P. volgensis* specimens (pl. 36, figs 12–16). This leads us to believe that labial crown ornamentation is indeed absent on *P. volgensis* teeth, as the authors were clearly aware of this characteristic. Furthermore, the conical lateral cusplets of *P. volgensis* teeth as described by Zhelezko and Kozlov (1999) are a difficult characteristic to evaluate based on the figures they provided. However, their description, in combination with the lack of labial ornamentation, suggests that the specimens require further evaluation because they might not represent *Palaeohypotodus*.

If we consider *P. volgensis* a valid taxon, the figured type specimens are considerably different from teeth of *P. bizzocoi* sp. nov. Not only do *P. volgensis* teeth appear

to lack labial plications along the crown base, but the main cusp on the upper lateral teeth has a much wider base than any of the upper lateral teeth of *P. bizzocoi* sp. nov. In addition, *P. volgensis* lateral teeth have wider and more triangular root lobes, and the root lobes are more pointed on the anterior teeth. In contrast, the root lobes on *P. bizzocoi* sp. nov. teeth are more even in width across their length, and they almost always have rounded basal extremities. Zhelezko and Kozlov (1999) also noted that the root lobes on *P. volgensis* teeth transition from rounded to flattened, whereas they are broadly rounded on all teeth of *P. bizzocoi* sp. nov. Furthermore, Zhelezko and Kozlov (1999) described the lateral cusplets on *P. volgensis* teeth as conical, which could mean that cutting edges are absent. If true, this feature provides additional evidence that *P. volgensis* and *P. bizzocoi* sp. nov. are not conspecific. Lastly, Zhelezko and Kozlov (1999, pl. 36, fig. 16e) showed an interesting characteristic on *P. volgensis* teeth where, in apical view, the crown exhibits conspicuous mesial and distal constrictions between the main cusp and lateral cusplets. This subtle characteristic is absent on all *P. bizzocoi* sp. nov. teeth.

### Stratigraphic and geographic distribution of *Palaeohypotodus bizzocoi* sp. nov.

Although not exhaustive, our review of *Palaeohypotodus* has provided us with a number of morphological characteristics that can be used to differentiate the various species, as well as the means to determine the stratigraphic and paleogeographic range of *P. bizzocoi* sp. nov. The 34 *P. bizzocoi* sp. nov. teeth in our sample (i.e., 17 associated with GSA-V447 and 17 isolated teeth) were collected from four counties in Alabama (Butler, Dallas, Lowndes, and Wilcox counties) and one in Arkansas (Hot Spring County). To determine whether the range of *P. bizzocoi* sp. nov. extends beyond what our sample can elucidate, we examined the published literature for other Paleocene occurrences of *Palaeohypotodus* in Alabama, the Gulf Coastal Plain, and elsewhere in the USA.

Of Alabama occurrences, White (1956), who was later referenced by Thurmond and Jones (1981), reported a tooth identified as *Odontaspis* cf. *rutoti* from the Bartonian Gosport Sand in Clarke County, Alabama. White (1956, p. 148) described this tooth as resembling a lower posterolateral tooth of *Otodus rutoti* (= *Palaeohypotodus rutoti*), but his assignment to the species was tentative because the tooth appeared atypical when compared to those figured by Winkler (1874). Although White (1956) mentioned the presence of fine “puckering” along the labial crown base, he unfortunately did not figure his specimen and we therefore could not confirm its identity. However, no *Palaeohypotodus* specimens were identified by Ebersole et al. (2019) during their extensive study of lower-to-middle Eocene fishes of Alabama, which included the examination of more than 6,000 teeth derived from the Gosport Sand. This leads

us to believe that the tooth reported by White (1956), and Thurmond and Jones (1981) was misidentified, and the only confirmed occurrence of *Palaeohypotodus* in Alabama is that of *P. bizzocoi* sp. nov. reported herein.

Within the Gulf Coastal Plain of the USA, Maisch et al. (2020, figs 8f–m, 12m) figured nine teeth as “*Palaeohypotodus rutoti* [sic]” that were derived from the lower Clayton Formation in Hot Spring County, Arkansas. Of these teeth, the morphology of the teeth illustrated in figs 8h–i and 12m appear better aligned with *Odontaspis* rather than *Palaeohypotodus*, and those figured in fig. 8f, j–n are not well enough preserved to be properly evaluated. Furthermore, the posterior teeth figured in fig. 8j–n have wider and fewer cusplets than those illustrated for *P. rutoti* (see Herman 1972, pl. 2, figs 1–3, 5; Herman 1977, pl. 10, fig. 3e; Cappetta 2012, fig. 192h–j), and the main cusp on the anterior tooth figured in 8f is too narrow and gracile compared to the wide and robust main cusp of typical *Palaeohypotodus* teeth. It is likely these teeth belong to a genus, or genera, other than *Palaeohypotodus*. However, one tooth having a robust main cusp and two pairs of lateral cusplets was figured by these authors (fig. 8g) and morphologically it falls within the range of *P. bizzocoi* sp. nov. The small size of this tooth (1.5 cm), coupled with the extended mesial root lobe and double pair of cusplets, suggests it is an upper third anterior tooth of a juvenile *P. bizzocoi* sp. nov. individual. This tooth, along with specimen MMNS VP–8578, demonstrates the occurrence of this taxon in the Danian of Arkansas. As far as we are aware, the Alabama and Arkansas occurrences of *Palaeohypotodus* represent the only verified accounts of this genus within the entirety of the Gulf Coastal Plain of the USA.

Within Paleocene deposits from elsewhere in the USA, Ward and Wiest (1990) included *P. rutoti* in their list of elasmobranch taxa occurring in Maryland and Virginia. The authors did not figure these specimens and we could not confirm their identity. Cvanara and Hoganson (1993) reported 13 teeth derived from the Danian Cannonball Formation in North Dakota that they referred to *P. rutoti*. They noted the teeth approach nearly 3 cm in height, have two (sometimes three) pairs of large lateral cusplets, and labial plications occur at the crown foot. The cusplets were described as being “conical” but complete cutting edges were clearly visible. In their discussion of the material, Cvanara and Hoganson (1993) expressed their opinion that teeth of *P. bronni* and *P. rutoti* were indistinguishable and they therefore referred the Cannonball Formation teeth to the latter taxon. However, the tooth they illustrated (fig. 3mm–nn) which appears to be an upper lateral tooth, has large, triangular lateral cusplets and shallow interlobe area (19% the height of the tooth) that morphologically falls outside of *P. bizzocoi* sp. nov., *P. rutoti*, and *P. volgensis*. The Cannonball Formation material should be reevaluated using the criteria highlighted herein because the teeth would represent the first verified occurrence of *Palaeohypotodus* in North America and potentially a new species.

Case (1996) referred 24 teeth derived from the Danian part of the Hornerstown Formation in Monmouth County, New Jersey to *P. rutoti*. He illustrated six of these teeth (Case 1996, pl. 2, figs 1–6), all of which have extremely straight, narrow, conical, and needle-like lateral cusplets. The cusplets on some of these teeth (i.e., figs 2, 5, 6) are rather tall with respect to the height of the main cusp when compared to the teeth of *Palaeohypotodus* spp., and these particular specimens are similar to those of extant *Odontaspis* and likely belong to a Paleocene representative of this latter genus. Lastly, Purdy (1998) reported *Odontaspis rutoti* from a temporally mixed Paleocene locality in Berkeley County, South Carolina. Unfortunately, the precise stratigraphic provenience of his material cannot be ascertained, as the entirety of the Williamsburg Formation (Danian to Thanetian) was exposed. However, as his figured specimens (fig. 3) possess lateral cusplets that are taller and more robust than those of *P. bizzocoi* sp. nov. and the interlobe area is shallower, referral of these teeth to *P. rutoti* appears to be appropriate.

The temporal and stratigraphic occurrences noted above establish that *P. bizzocoi* sp. nov. had a paleogeographic range that extended across the northern Gulf Coastal Plain of the USA, at least between Alabama and Arkansas. Future work may yield additional records of the taxon in other northern Gulf states, like Mississippi, Louisiana, and eastern Texas. The occurrence of *P. bizzocoi* sp. nov. is at present confined to three lithostratigraphic units that all date to the Danian Stage (zones NP2–4) of the Paleocene, including the lower Clayton Formation, Pine Barren Member of the Clayton Formation, and the Porters Creek Formation. The occurrence of this taxon within the lowermost Danian units in Alabama and Arkansas (the Pine Barren Member of the Clayton Formation and the equivalent lower beds of the Clayton Formation, respectively) establishes that this taxon was present in the Gulf Coastal Plain of the USA shortly after the K/Pg extinction event. Furthermore, the absence of the species from any Maastrichtian deposits in the region (see Ikejiri et al. 2013) indicates a first occurrence within the lower-most Paleocene. Additionally, the occurrence of *P. bizzocoi* sp. nov. within the upper Danian Porters Creek Formation demonstrates that this species persisted within this region throughout the entirety of the stage. The earliest stratigraphic occurrence of this taxon is well-defined, but its vertical stratigraphic extent is presently unknown due to the lack of systematic vertebrate paleontology work in local Selandian and Thanetian units like the Naheola Formation, Nanafalia Formation, and Tuscahoma Sand.

### Familial placement of *Palaeohypotodus*

When *P. bronni* and *P. rutoti* were originally named by Agassiz (1843) and Winkler (1874), respectively, both were assigned to the genus *Otodus*. Vincent (1876) later contended that the *rutoti* morphology was similar to teeth of extant *Odontaspis* and utilized this generic name

for the species. Although Daimeries (1888) followed Vincent (1876) in the use of *Odontaspis rutoti*, he also noted differences between these teeth and other species assigned to the genus at the time, namely the presence of labial vertical ridges and the greater number of lateral cusplets on the former. A review of the historical literature indicates that both the *bronni* and *rutoti* morphologies were consistently placed within *Odontaspis*, and by extension, within the family Odontaspididae, until Glückman (1964) erected the name *Palaeohypotodus* to include these species. Aside from the occasional usage of *Odontaspis* for these teeth (i.e., Purdy 1998), the *rutoti* and *bronni* morphologies were predominantly assigned to *Palaeohypotodus*, prompting Zhelezko and Kozlov (1999) to assign their *volgensis* morphology to this genus.

In addition to placing the *rutoti* and *bronni* morphologies within *Palaeohypotodus*, Glückman (1964) erected the family Jaekelodontidae to accommodate this genus as well as *Hypotodus*, *Jaekelodus*, and *Anotodus*. Glückman (1964) argued that a new family was warranted for these genera because they all had one to three pairs of lateral cusplets, mesiodistally expanded cusps on the upper lateral teeth, elongated root lobes, and they lacked the elongated anterior tooth morphology typical of other members of the Odontaspididae. However, due to dental similarities and the lack of lateral cusplets on *Anotodus*, this taxon was subsequently reassigned to the Alopiidae (Herman 1979; Cappetta 2012). Zhelezko (1994) later expanded the Jaekelodontidae to include *Mennerotodus*, but reconstructions of the dentition of the genus (Cicimurri et al. 2020) show that this taxon is more appropriately referred to the Carchariidae.

Although Glückman (1964) erected the family Jaekelodontidae to include *Palaeohypotodus*, many subsequent authors continued to place the genus within Odontaspididae (i.e., Cappetta 1987; Cappetta and Nolf 2005; Iserbyt and De Schutter 2012). However, assignment of the genus to Odontaspididae has recently become problematical because of the reintroduction of the family Carchariidae by Shimada et al. (2015) and Stone and Shimada (2019). The latter authors used skeletal data to conduct a phylogenetic analysis of extant “sandtiger” sharks that ultimately corroborated paraphyly within Odontaspididae, which classically included *Odontaspis* and *Carcharias taurus*. The use of Carchariidae is supported to include extant *C. taurus*, whereas Odontaspididae contains only the genus *Odontaspis*. Unfortunately, the application of these family names to fossil species was not addressed by Stone and Shimada (2019), and determining the familial placement of an extinct species is tentative without the aid of associated skeletal material, which is largely lacking for extinct taxa. For example, the Cretaceous tooth morphology *amonensis* was variously assigned to *Odontaspis* (Cappetta & Case, 1975) and *Carcharias* (Cicimurri, 2001), but discovery of a partial skeleton allowed researchers to assign the species to a new genus and determine that it belonged to a new family, Haimrichiidae Vullo et al., 2016.

Although the familial placement of *Palaeohypotodus* has heretofore remained unresolved, it may be elucidated when the suite of teeth we herein assign to *P. bizzocoi* sp. nov., along with other *Palaeohypotodus* teeth reported elsewhere in the literature, are taken into account. For example, Van de Geyn (1937, fig. 118) and Casier (1942, pl. 1, fig. 2) figured upper third anterior teeth for *P. bronni* and *P. rutoti*, respectively, that are very similar to a tooth we assign herein to *P. bizzocoi* sp. nov. (MSC 49452, Fig. 7z–cc). All of these teeth have a distinct combination of an elongated mesial root lobe and a distal cutting edge that is more convex than the mesial edge, which compares more favorably to some teeth in dentitions of extant *C. taurus* rather than *Odontaspis ferox*, suggesting *Palaeohypotodus* is more closely allied with Carchariidae than to Odontaspididae. However, the occurrence of up to three pairs of lateral cusplets on *Palaeohypotodus* teeth is more consistent with teeth of extant *Odontaspis ferox* teeth (which can have one to three pairs), as opposed to *C. taurus* teeth that generally have only a single pair.

Our comparison of *P. bizzocoi* sp. nov., *P. bronni*, and *P. rutoti* teeth to those of extant lamniform sharks revealed similarities between the fossil taxa and both *C. taurus* and *O. ferox*. However, these extant taxa lack both the mesiodistally wide and laterally hooked upper lateral tooth morphology and enameloid plications along the labial crown base, features that have been regarded as characteristic of *Palaeohypotodus* (Herman 1977: 299). Furthermore, the distinct upper lateral tooth crown morphology of *Palaeohypotodus* is comparable to the condition of *Hypotodus* and *Jaekelotodus* (as is the dentition as a whole), suggesting that these taxa are likely closely related (as was suggested by Glückman 1964). The teeth of *Palaeohypotodus*, *Hypotodus*, and *Jaekelotodus* appear to exhibit a combination of features occurring in both Carchariidae and Odontaspididae, and there is no unequivocal modern familial analogue to assign these genera. The dentition of *Palaeohypotodus* spp. also appears to have a condition not present in extant lamniforms, where the upper teeth have complete cutting edges, whereas those in the lower files are incomplete. This characteristic, along with the evidence stated for the other genera indicates that teeth of *Palaeohypotodus*, *Hypotodus*, and *Jaekelotodus* represent an extinct type of lamniform dentition, and we find it appropriate to assign these genera to their own family and herein follow Glückman (1964) by utilizing Jaekelodontidae.

## Conclusions

Our analysis of 34 shark teeth derived from lower Paleocene (Danian) deposits in Alabama and Arkansas, USA, has led to the discovery of a new species, *Palaeohypotodus bizzocoi*, sp. nov. Along with two other previously described members of this genus, *P. bronni* and *P. rutoti*, these species are united by the occurrence of teeth with one to three pairs of lateral cusplets, enameloid plications

along the labial crown base, triangular and distally curved crowns on upper lateral teeth, distinct upper third lateral teeth with elongated mesial root lobe, pronounced lingual root protuberance with deep nutritive groove, and U-shaped interlobe area. A fourth species, *P. volgensis*, is known only by the type specimens. However, the lack of labial plications and the purported conical lateral cusplets on this taxon suggest that it may belong to a different genus. The tooth crowns of *Palaeohypotodus*, *Hypotodus*, and *Jaekelotodus* are similar, and their dental arrangements are comparable to one other, but also dissimilar to those of any extant lamniform sharks. Thus, we resurrect the family Jaekelodontidae Glückman 1964 to accommodate these extinct genera.

Our diagnosis of *P. bizzocoi* sp. nov. was largely based on comparisons with extant lamniform jaw sets and fossil *Palaeohypotodus* specimens derived from, or near to, the type localities for *P. bronni*, *P. rutoti*, and *P. volgensis*. However, our analysis was restricted to these particular occurrences and specimens reported from outside of the type strata/localities should be reevaluated. Our analysis has shed new light on the dental morphology of *Palaeohypotodus* and the various types of heterodonty occurring within the genus (i.e., monognathic, dignathic, ontogenetic), and future reexamination of reported specimens will allow for a better understanding of the stratigraphic and paleobiogeographic ranges of each of the species. For example, *P. rutoti* has been reported from various globally disparate localities (see Cappetta 2012) from deposits ranging in age from the lower Paleocene (Purdy 1998) to upper Eocene (Otero and Soto-Acuña 2015). It would seem unlikely that all of these occurrences represent *P. rutoti*, and our recognition of *P. bizzocoi* sp. nov. indicates a likelihood that the genus was more diverse during the Paleogene than is currently recognized.

## Acknowledgements

The authors wish to thank Dirk Hovestadt for providing us with a copy of Hovestadt and Etienne (2023). George Phillips (MMNS) loaned us teeth of both *Palaeohypotodus bizzocoi* sp. nov. and *P. bronni*. We appreciate the efforts of George Martin, who collected *P. bizzocoi* sp. nov. teeth from Lowndes County, AL and subsequently donated them to the MMNS and MSC collections. Finally, we thank handling editor, Florian Witzmann, and Sebastian Stumpf and Mikael Siverson provided critical reviews that improved an earlier version of this manuscript.

## References

- Adolfsson J, Ward DJ (2015) Neoselachians from the Danian (Early Paleocene) of Denmark. *Acta Palaeontologica Polonica* 60(2): 313–338. <https://doi.org/10.4202/app.2012.0123>
- Agassiz L (1843) *Recherches sur les poissons fossiles*. Jent and Gassman, Soleure, 233 pp. <https://doi.org/10.5962/bhl.title.4275>

- Aldrich TA (1894) The (Midway) Clayton Tertiary section and its fossils. In: Smith EA, Johnson LC, Langdon DW, Jr. (Eds) Report on the geology of the Coastal Plain of Alabama. Geological Survey of Alabama, Special Report 6, 240–248. [https://books.google.com/books?id=BzxAQAAMAAJ&printsec=frontcover&source=gbs\\_ge\\_summary\\_r&cad=0#v=onepage&q&f=false](https://books.google.com/books?id=BzxAQAAMAAJ&printsec=frontcover&source=gbs_ge_summary_r&cad=0#v=onepage&q&f=false)
- Applegate SP (1965) Tooth terminology and variation in sharks with special reference to the sand shark *Carcharias taurus* Rafinesque. Contributions to Science, Los Angeles County Museum 86: 1–18. <https://doi.org/10.5962/p.241076>
- Berg L (1958) System der rezenten und fossilen Fischartigen und Fische. VEB Verlag der Wissenschaften, Berlin, 310 pp. [https://books.google.com/books/about/System\\_der\\_rezenten\\_und\\_fossilen\\_Fischar.html?id=VsoSAQAAMAAJ](https://books.google.com/books/about/System_der_rezenten_und_fossilen_Fischar.html?id=VsoSAQAAMAAJ)
- Bolli HM (1957) The genera *Globigerina* and *Globorotalia* in the Paleocene-Lower Eocene Lizard Springs Formation of Trinidad. In: Loeblich AR, Jr., Tappan H, Beckmann JP, Bolli HM, Montanaro Gallitelli E, Troelsen JC (Eds) Studies in Foraminifera. United States National Museum, Bulletin 215: 61–82. <https://biostor.org/reference/105999>
- Bonaparte CL (1838) Selachorum tabula analytica, Nuovi Annali della Scienze Naturali, Bologna 1: 195–214. <https://www.biodiversitylibrary.org/bibliography/8737>
- Bonnaterre JP (1788) Ichthyologie. Tableau encyclopédique et méthodique des trois règnes de la nature, Paris, 215 pp. <https://www.biodiversitylibrary.org/bibliography/11660>
- Bramlette MN, Sullivan FR (1961) Coccolithophorids and related nanoplankton of the Early Tertiary in California. Micropaleontology 7: 129–188. <https://doi.org/10.2307/1484276>
- Cappetta H (1987) Handbook of Paleoichthyology, Vol. 3B, Chondrichthyes II. Gustav Fischer Verlag, Stuttgart, 193 pp.
- Cappetta H (2012) Chondrichthyes, Mesozoic and Cenozoic Elasmobranchii: Teeth. In: Schultze H-P, Kuhn O (Eds) Handbook of Paleoichthyology, 3E, Friedrich Pfeil, Munich, 512 pp.
- Cappetta H, Case GR (1975) Sélaciens nouveaux du Crétacé du Texas. Géobios 8(4): 303–307. [https://doi.org/10.1016/S0016-6995\(75\)80028-3](https://doi.org/10.1016/S0016-6995(75)80028-3)
- Cappetta H, Corral JC (1999) Upper Maastrichtian selachians from the Condado de Treviño (Basque-Cantabrian region, Iberian peninsula). Estudios del Museo de Ciencias Naturales de Alava 14(1): 339–372. <https://isem-evolution.fr/en/publication/upper-maastrichtian-selachians-from-the-condado-de-trevino-basque-cantabrian-region-iberian-peninsula/>
- Cappetta H, Nolf D (2005) Révision de quelques Odontaspidae (Neoselachii: Lamniformes) du Paléocène et de l'Eocène du Bassin de la Mer du Nord. Bulletin de l'Institut Royal des Sciences Naturelles de Belgique, Science de la Terre 75: 237–266. <https://www.vliz.be/imisdocs/publications/ocrd/99910.pdf>
- Case GR (1996) A new selachian fauna from the Lower Hornerstown Formation (Early Paleocene/Montian) of Monmouth County, New Jersey. Palaeontographica Abteilung A 242: 99–126. <https://doi.org/10.1127/pala/242/1996/1>
- Casier E (1942) Contributions à l'étude des Poissons fossiles de la Belgique. I. Sur d'importants restes d'un Odontaspidé (Odontaspis rutoti T.C. Winkler) du Landénien marin du Tournaisis. Bulletin du Musée Royal d'Histoire Naturelle de Belgique 18(60): 1–12. [https://biblio.naturalsciences.be/rbins-publications/bulletin-of-the-royal-belgian-natural-history-museum/bulletin-of-the-royal-belgian-natural-history-museum-1930-1948/casier\\_contributions\\_1942](https://biblio.naturalsciences.be/rbins-publications/bulletin-of-the-royal-belgian-natural-history-museum/bulletin-of-the-royal-belgian-natural-history-museum-1930-1948/casier_contributions_1942)
- Casier E (1950) Contributions à l'étude des poissons fossiles de la Belgique. IX. La faune des formations dites «paniséliennes». Bulletin de l'Institut Royal des Sciences Naturelles de Belgique 26(42): 1–52. [https://biblio.naturalsciences.be/rbins-publications/bulletin-of-the-royal-belgian-institute-of-natural-sciences/bulletin-of-the-royal-belgian-institute-of-natural-sciences-1949-1970/casier\\_contributions\\_1950](https://biblio.naturalsciences.be/rbins-publications/bulletin-of-the-royal-belgian-institute-of-natural-sciences/bulletin-of-the-royal-belgian-institute-of-natural-sciences-1949-1970/casier_contributions_1950)
- Clark WB (1895) Contributions to the Eocene fauna of the middle Atlantic slope. John Hopkins University Circulars 15(121): 3–6. <https://jscholarship.library.jhu.edu/bitstream/handle/1774.2/32954/1121.PDF>
- Cicimurri DJ (2001) Fossil selachians from the Belle Fourche Shale (Cretaceous, Cenomanian), Black Hills region of South Dakota and Wyoming. Mountain Geologist 38(4): 181–192. <https://archives.datapages.com/data/rmag/mg/2001/cicimurri.htm>
- Cicimurri DJ, Ebersole JA, Martin G (2020) Two new species of *Mennerotodus* Zhelezko, 1994 (Chondrichthyes: Lamniformes: Odontaspidae), from the Paleogene of the southeastern United States. Fossil Record 23: 117–140. <https://doi.org/10.5194/fr-23-117-2020>
- Compagno LJV (1973) Interrelationships of living elasmobranchs. Zoological Journal of the Linnean Society 53(1): 15–61.
- Conrad TA (1835) Observations on a portion of the Atlantic Tertiary region. Transactions of the Geological Society of Pennsylvania 1: 335–341. [https://commons.wikimedia.org/wiki/File:Observations\\_on\\_a\\_portion\\_of\\_the\\_Atlantic\\_tertiary\\_region\\_-\\_with\\_a\\_description\\_of\\_new\\_species\\_of\\_organic\\_remains\\_\(IA\\_101660306.nlm.nih.gov\).pdf](https://commons.wikimedia.org/wiki/File:Observations_on_a_portion_of_the_Atlantic_tertiary_region_-_with_a_description_of_new_species_of_organic_remains_(IA_101660306.nlm.nih.gov).pdf)
- Conrad TA (1860) Description of new species of Cretaceous and Eocene fossils of Mississippi and Alabama. Journal of the Academy of Natural Sciences of Philadelphia, second series 4: 275–298. <https://oliviv.myspecies.info/en/content/descriptions-new-species-cretaceous-and-eocene-fossils-mississippi-and-alabama>
- Cope ED (1871) Contribution to the ichthyology of the Lesser Antilles. Transactions of the American Philosophical Society 14(3): 445–483. <https://doi.org/10.2307/1005256>
- Crump JR (1870) A new map of Wilcox County, Alabama, showing beside the topographical features the proprietorship of the lands according to the assessment of 1870, Scale 1:63,360. Unpublished map on file in the Geological Survey of Alabama library, Tuscaloosa.
- Cunningham S (2000) A comparison of isolated teeth of early Eocene *Striatolamia macrota* (Chondrichthyes, Lamniformes), with those of a Recent sand shark, *Carcharias taurus*. Tertiary Research 20: 17–31. <http://saddlewood33.com/Cunningham2000.pdf>
- Cvancara AM, Hoganson JW (1993) Vertebrates of the Cannonball Formation (Paleocene) in North and South Dakota. Journal of Vertebrate Paleontology 13(1): 1–23. <https://doi.org/10.1080/02724634.1993.10011484>
- Dall WH (1890) Tertiary fauna of Florida with especial reference to the Miocene Silex-beds of Tampa and the Pliocene beds of the Caloosahatchie River, part 1. Transactions of the Wagner Free Institute of Science 3: 1–200. <https://doi.org/10.5962/bhl.title.29760>
- Dall WH (1903) Tertiary fauna of Florida with especial reference to the Miocene Silex-beds of Tampa and the Pliocene beds of the Caloosahatchie River, part 6. Transactions of the Wagner Free Institute of Science 3: 1219–1654. <https://doi.org/10.5962/bhl.title.29760>
- Daimeries A (1888) Notes ichthyologiques (Système Landénien) I. Annales de la Société royale malacologique de Belgique. Bulletin des Séances 23: 42–43.

- Dalinkevicius JA (1935) On the fossil fishes of the Lithuanian Chalk. I. Selachii. Mémoires de la Faculté des Sciences de l'Université de Vytavaus le Grand 9: 243–305.
- Dartevelle E, Casier E (1943) Les poissons fossiles du Bas-Congo et des régions voisines. Annales du Musée du Congo Belge, Sér. A (Minéralogie Géologie, Paléontologie), 3, 2(1): 1–200.
- Ebersole JA, Cicimurri DJ, Stringer GL (2019) Taxonomy and biostratigraphy of the elasmobranchs and bony fishes (Chondrichthyes and Osteichthyes) of the lower-to-middle Eocene (Ypresian to Bartonian) Claiborne Group in Alabama, USA, including an analysis of otoliths. *European Journal of Taxonomy* 585: 1–274. <https://doi.org/10.5852/ejt.2019.585>
- Ebert DA, Dando M (2021) *Field Guide to Sharks, Rays & Chimaeras of Europe and the Mediterranean*. Princeton University Press, New Jersey, 383 pp. <https://doi.org/10.1515/9780691211824>
- Fluegeman Jr RH, Berggren WA, Briskin M (1990) Paleocene foraminiferal biostratigraphy of the Eastern Gulf Coastal Plain. *Micropaleontology* 36: 56–64. <https://doi.org/10.2307/1485664>
- Geibel CG (1848) *Die Fische der Vorwelt mit steter Berücksichtigung der lebenden Fische*. Brockhaus, Leipzig, 467 pp. <https://doi.org/10.5962/bhl.title.24938>
- Gibson TG, Mancini EA, Bybell LM (1982) Paleocene to middle Eocene stratigraphy of Alabama. *Gulf Coast Association of Geological Societies Transactions* 32: 449–458. <https://doi.org/10.1306/03B5A83B-16D1-11D7-8645000102C1865D>
- Glückman LS (1964) *Sharks of Paleogene and their stratigraphic significance*. Nauka Press, Moscow, 229 pp. [In Russian]
- Guitart-Manday DJ (1966) Nuevo nombre para una especie de Tiburón del género *Isurus* (Elasmobranchii: Isuridae) de Aguas Cubanas. *Poeyana, series A* 15: 1–9.
- Harris GD (1896) The Midway stage. *Bulletins of American Paleontology* 1: 115–270. <https://www.biodiversitylibrary.org/item/96050#page/7/mode/1up>
- Hay OP (1902) Bibliography and catalogue of the fossil Vertebrata of North America, *Bulletin of the United States Geological and Geographical Survey of the Territories* 179: 1–868. <https://doi.org/10.5962/bhl.title.20094>
- Herman J (1972) Les vertébrés du Landénien inférieur (Lia ou Heersien) de Maret (Hameau d'Orp-le-Grand). *Bulletin de la Société belge de Géologie, de Paléontologie et d'Hydrologie* 81(3–4): 191–207. <https://docplayer.fr/147612739-Les-vertébres-du-landenien-inferieur-lia-ou-heersien-de-maret-hameau-d-orp-le-grand.html>
- Herman J (1977) Les Sélaciens des terrains néocrétacés et paléocènes de Belgique et des contrées limitrophes. *Eléments d'une biostratigraphie intercontinentale. Mémoires pour servir à l'explication des Cartes géologiques et minières de la Belgique* 15: 1–401. [https://biblio.naturalsciences.be/rbins-publications/memoirs-of-the-geological-survey-of-belgium/bibliographic\\_references/hermanles1977](https://biblio.naturalsciences.be/rbins-publications/memoirs-of-the-geological-survey-of-belgium/bibliographic_references/hermanles1977)
- Herman J (1979) Réflexions sur la systématique des Galeoidei et sur les affinités du genre *Cetorhinus* à l'occasion de la découverte d'éléments de la denture d'un exemplaire fossile dans les sables du Kattendijk à Kallo (Pliocène inférieur, Belgique). *Annales de la société géologique de Belgique* 102: 357–377. <https://popups.uliege.be/0037-9395/index.php?id=4357>
- Hovestadt D, Steurbaut E (2023) Annotated iconography of the type specimens of fossil chondrichthyan fishes in the collection of the Royal Belgian Institute of Natural Sciences, Brussels. *Monographs in Natural Sciences, Royal Belgian Institute of Natural Sciences* 1: 1–122. <https://biblio.naturalsciences.be/library-1/rbins-staff-publications-2023/bookreference.2023-02-15.1152089647>
- Huxley TH (1880) On the application of the laws of evolution to the arrangement of the vertebrata and more particularly of the Mammalia. *Proceedings of the Zoological Society of London* 1880: 649–662.
- Ikejiri T, Ebersole JA, Blewitt HL, Ebersole SM (2013) An overview of Late Cretaceous vertebrates from Alabama. *Bulletin of the Alabama Museum of Natural History* 31(1): 46–66. <https://web.p.ebscohost.com/abstract?direct=true&profile=ehost&scope=site&authtype=crawler&jrn1=01961039&AN=92630768&h=CLzzEnbXkVzWozRXHKPwILpIT0125Jmvg9U9f3AoY-%2fyZShUB9dV8YiW%2bDyICAEtBKzdHNfoOs7Fxo5MV9GvBgA%3d%3d&cr1=c&resultNs=AdminWebAuth&resultLocal=ErrCrINotAuth&cr1hashurl=login.aspx%3fdirect%3dtrue%26profile%3dehost%26scope%3dsite%26authtype%3dcrawler%26jrn1%3d01961039%26AN%3d92630768>
- Iserbyt A, De Schutter PJ (2012) Quantitative analysis of Elasmobranch assemblages from two successive Ypresian (early Eocene) facies at Marke, western Belgium. *Geologica Belgica* 15(3): 146–153.
- Jordan DS (1898) Description of a species of fish (*Mitsukurina owstoni*) from Japan, the type of a distinct family of Lamnoid sharks. *Proceedings of the California Academy of Sciences (Series 3)* 1: 199–202. <https://biostor.org/reference/109813>
- Kriwet J, Engelbrecht A, Mörs T, Reguerod M, Pfaff C (2016) Ultimate Eocene (Priabonian) chondrichthyans (Holocephali, Elasmobranchii) of Antarctica. *Journal of Vertebrate Paleontology* 36(4): e1160911. <https://doi.org/10.1080/02724634.2016.1160911>
- LaMoreaux PE, Toulmin LD (1959) Geology and ground-water resources of Wilcox County, Alabama. *Geological Survey of Alabama, County Report* 4: 1–280.
- Leriche M (1902) Les poissons paléocènes de la Belgique. *Mémoires du Musée Royal d'Histoire Naturelle de Belgique* 2(5): 1–48. <https://biblio.naturalsciences.be/rbins-publications/memoirs-of-the-royal-belgian-institute-of-natural-sciences-first-series/bulletin-of-the-royal-belgian-institute-of-natural-sciences-memoirs-of-the-royal-belgian-institute-of-natural-sciences-first-series/7ead6edc48a74ee49ac2dd3db38fdac>
- Leriche M (1905) Les poissons éocènes de la Belgique, *Mémoires du Musée Royal d'Histoire Naturelle de Belgique* 3: 49–228. <https://biblio.naturalsciences.be/rbins-publications/memoirs-of-the-royal-belgian-institute-of-natural-sciences-first-series/bulletin-of-the-royal-belgian-institute-of-natural-sciences-memoirs-of-the-royal-belgian-institute-of-natural-sciences-first-series/7ead6edc48a74ee49ac2dd3db38fdac>
- Leriche M (1906) Contribution à l'étude des poissons fossils du Nord de la France et des régions voisines. *Mémoires de la Société géologique du Nord* 5: 1–430. <https://gallica.bnf.fr/ark:/12148/bpt-6k3338297m>
- Leriche M (1951) Les poissons tertiaires de la Belgique (Supplément). *Mémoires de l'Institut Royal des Sciences Naturelles de Belgique* 118: 473–600. <https://biblio.naturalsciences.be/rbins-publications/memoirs-of-the-royal-belgian-institute-of-natural-sciences-first-series/bulletin-of-the-royal-belgian-institute-of-natural-sciences-memoirs-of-the-royal-belgian-institute-of-natural-sciences-first-series/7ead6edc48a74ee49ac2dd3db38fdac>
- Linnaeus C (1758) *Systema Naturae per regna tria naturae, regnum animale, secundum classes, ordines, genera, species, cum characteribus differentiis synonymis, locis*. L. Salvius, Stockholm, Sweden, 532 pp. <https://doi.org/10.5962/bhl.title.559>
- Lowe RT (1841) Certain new species of Madeiran fishes. *Proceedings of the Zoological Society of London* 8(89): 36–39. <https://biostor.org/reference/59833>
- Maisch HM, Becker MA, Griffiths ML (2020) Chondrichthyans from the Lower Clayton Limestone Unit of the Midway Group (Paleo-

- cene) near Malvern, Arkansas, USA, with comments on the K/Pg boundary. *Paläontologische Zeitschrift* 94: 561–593. <https://doi.org/10.1007/s12542-019-00494-7>
- Mancini EA (1984) Biostratigraphy of Paleocene strata in southwestern Alabama. *Micropaleontology* 30: 268–291. <https://doi.org/10.2307/1485690>
- Mancini EA, Tew BH (1993) Eustacy versus subsidence: Lower Paleocene depositional sequences from southern Alabama, eastern Gulf Coastal Plain. *Geological Society of America Bulletin* 105: 3–17. [https://doi.org/10.1130/0016-7606\(1993\)105%3C0003:EVSLP-D%3E2.3.CO;2](https://doi.org/10.1130/0016-7606(1993)105%3C0003:EVSLP-D%3E2.3.CO;2)
- Mancini EA, Tew BH, Smith CC (1989) Cretaceous-Tertiary contact, Mississippi and Alabama. *Journal of Foraminiferal Research* 19(2): 93–104. <https://doi.org/10.2113/gsjfr.19.2.93>
- Maul GE (1955) Five species of rare sharks new for Madeira including two new to science. *Notulae Naturae (Philadelphia)* 279: 1–13. <https://books.google.bg/books?id=sjP4NHNPz7sC&pg=PA1&dq=Five%20species%20of%20rare%20sharks%20new%20for%20Madeira%20including%20two%20new%20to%20science&pg=PA1#v=onepage&q=Five%20species%20of%20rare%20sharks%20new%20for%20Madeira%20including%20two%20new%20to%20science&f=false>
- Nakamura H (1935) On the two species of the thresher shark from Formosan waters. *Memoirs Faculty Science Taihoku Imperial University Formosa* 14(1): 1–6.
- Ogg JG, Ogg GM, Gradstein FM (2016) *A Concise Geologic Time Scale*. Elsevier, Amsterdam, 240 pp.
- Otero RA, Soto-Acuña S (2015) New chondrichthyans from Bartonian-Priabonian levels of Río de Las Minas and Sierra Dorotea, Magallanes Basin, Chilean Patagonia. *Andean Geology* 42(2): 268–283. <https://doi.org/10.5027/andgeoV42n2-a06>
- Plummer HJ (1927) Foraminifera of the Midway Formation in Texas. *University of Texas Bulletin* 2644: 1–206. [https://texashistory.unt.edu/ark:/67531/metaph1065563/m2/1/high\\_res\\_d/2644\\_1926nov22.pdf](https://texashistory.unt.edu/ark:/67531/metaph1065563/m2/1/high_res_d/2644_1926nov22.pdf)
- Priem MF (1897) Sur des dents d'élasmodontes de divers gisements sénoniens (Villedieu, Meudon, Foix-les-Caves). *Bulletin de la Société géologique de France* 3(25) 40–56. <http://storage.lib.uchicago.edu/pres/2014/pres2014-0146.pdf>
- Purdy RW (1988) Chondrichthyan Fishes from the Paleocene of South Carolina. *Transactions of the American Philosophical Society, New Series* 88(4): 122–146. <https://doi.org/10.2307/1006671>
- Rafinesque CS (1810) Caratteri di alcuni nuovi generi e nuove specie di animali e pinate della Sicilia, con varie osservazioni sopra i medesimi, lère partie, Per le stampe de Sanfilippo, Palermo, Italy, 106 pp. <https://doi.org/10.5962/bhl.title.104418>
- Raymond DE, Osborne WE, Copeland CW, Neathery TL (1988) Alabama stratigraphy. *Geological Survey of Alabama, Circular* 140: 1–97. <https://www.gsa.state.al.us/Home/DownloadPubDocument/?path=Circulars&fileName=C140.pdf>
- Risso A (1810) *Ichthyologie de Nice, ou histoire naturelle des poissons du département des Alpes Maritimes*. F. Schoell, Paris, 388 pp. <https://doi.org/10.5962/bhl.title.7052>
- Sauvage HE (1898) *Vertébrés fossils du Portugal: contributions à l'étude des poissons et des reptiles du Jurassique et du Crétacique*. Imprimerie de l'Académie Royale des Sciences Lisbon, Portugal, 46 pp. [https://openlibrary.org/books/OL6543329M/...\\_Verte%C3%81bre%CC%81s\\_fossiles\\_du\\_Portugal](https://openlibrary.org/books/OL6543329M/..._Verte%C3%81bre%CC%81s_fossiles_du_Portugal)
- Shimada K (2001) Notes on the dentition of the bigeye sandtiger shark, *Odontaspis noronhai* (Lamniformes: Odontaspidae). *Journal of Fossil Research* 34: 15–17. <https://cir.nii.ac.jp/crid/1520573330898691456>
- Shimada K (2002a) Dental homologies in lamniform sharks (Chondrichthyes: Elasmobranchii). *Journal of Morphology* 251: 38–72. <https://doi.org/10.1002/jmor.1073>
- Shimada K (2002b) The relationship between the tooth size and total body length in the shortfin mako, *Isurus oxyrinchus* (Lamniformes: Lamnidae). *Journal of Fossil Research* 35: 6–9. [http://www.kasekiken.jp/kaishi/kaishi\\_39\(1\)/kasekiken\\_39\(1\)\\_7-11.pdf](http://www.kasekiken.jp/kaishi/kaishi_39(1)/kasekiken_39(1)_7-11.pdf)
- Shimada K (2002c) The relationship between the tooth size and total body length in the white shark, *Carcharodon carcharias* (Lamniformes: Lamnidae). *Journal of Fossil Research* 35: 28–33. <https://www.semanticscholar.org/paper/The-relationship-between-the-tooth-size-and-total-Shimada/d985a21c04b720509b624fe17cec4eb2d2ed8d03>
- Shimada K (2004) The relationship between the tooth size and total body length in the sandtiger shark, *Carcharias taurus* (Lamniformes: Odontaspidae). *Journal of Fossil Research* 37: 76–81. <https://www.semanticscholar.org/paper/The-relationship-between-the-tooth-size-and-total-Shimada/1134aff8e58bccaee72ece673289fae6bac89fd9>
- Shimada K, Popov EV, Siversson M, Welton BJ, Long DJ (2015) A new clade of putative plankton-feeding sharks from the Upper Cretaceous of Russia and the United States. *Journal of Vertebrate Paleontology* 35: e981335. <https://doi.org/10.1080/02724634.2015.981335>
- Siversson M (1999) A new large lamniform from the uppermost Gairle Siltstone (Cenomanian, Late Cretaceous) of Western Australia. *Earth and Environmental Science Transactions of The Royal Society of Edinburgh* 90(1): 49–66. <https://doi.org/10.1017/S0263593300002509>
- Stone NR, Shimada K (2019) Skeletal anatomy of the bigeye sandtiger shark, *Odontaspis noronhai* (Lamniformes: Odontaspidae), and its implications for lamniform phylogeny, taxonomy, and conservation biology. *Copeia* 107(4): 632–652. <https://doi.org/10.1643/CG-18-160>
- Subbotina NN (1953) Fossil foraminifera of the USSR: Globigerinidae, Hantkeninidae and Globorotaliidae. *Proceedings of the Oil Research Geological Institute, new series* 76: 1–96. [In Russian] [https://books.google.com/books/about/Fossil\\_Foraminifera\\_of\\_the\\_USSR.html?id=hNLDzweACAAJ](https://books.google.com/books/about/Fossil_Foraminifera_of_the_USSR.html?id=hNLDzweACAAJ)
- Thurmond JT, Jones DE (1981) *Fossil vertebrates of Alabama*. University of Alabama Press, Tuscaloosa, 244 pp.
- Van de Geyn W (1937) Les élasmodontes du Crétacé Marin du Limbourg Hollandais. *Natuurhistorisch Maandblad Maastricht* 26: 16–21, 28–33, 42–53, 56–60, 66–69. <https://natuurtijdschriften.nl/pub/1009081/NAHM1937026005003.pdf>
- Vincent G (1876) Description de la faune de l'étage Landénien inférieur de Belgique. *Annales de la Société royal malacologique de Belgique* 11: 111–160. [https://books.google.com/books/about/Description\\_de\\_la\\_faune\\_de\\_l\\_%C3%A9tage\\_land.html?id=ltlotR-d1LIC](https://books.google.com/books/about/Description_de_la_faune_de_l_%C3%A9tage_land.html?id=ltlotR-d1LIC)
- Vullo R, Guinot G, Barbe G (2016) The first articulated specimen of the Cretaceous mackerel shark *Haimrichia amonensis* gen. nov. (Haimrichiidae fam. nov.) reveals a novel ecomorphological adaptation within the Lamniformes (Elasmobranchii). *Journal of Systematic Palaeontology* 14(12): 1003–1024. <https://doi.org/10.1080/14772019.2015.1137983>

- Ward DJ, Wiest RL (1990) A checklist of Palaeocene and Eocene sharks and rays (Chondrichthyes) from the Pamunkey Group, Maryland and Virginia, USA. *Tertiary Research* 12(2): 81–88.
- Winkler TC (1874) Mémoire sur quelques restes de poissons du système heersien. *Archives du Musée Teyler* 4: 1–15. <https://books.google.com/books/about/Archives.html?id=dCgXAAAAYAAJ>
- Whitfield RP (1865) Descriptions of new species of Eocene fossils. *American Journal of Conchology* 1: 259–268.
- White EI (1956) The Eocene fishes of Alabama. *Bulletins of American Paleontology* 36(156): 123–150. [https://books.google.com/books/about/The\\_Eocene\\_Fishes\\_of\\_Alabama.html?id=GpTFJwAA-CAAJ](https://books.google.com/books/about/The_Eocene_Fishes_of_Alabama.html?id=GpTFJwAA-CAAJ)
- Woodward AS (1891) Notes on some fish-remains from the lower Tertiary and Upper Cretaceous of Belgium, collected by Monsieur A. Houzeau de Lahaie. *Geological Magazine*, decade 3(8): 104–114. <https://doi.org/10.1017/S0016756800186224>
- Zhelezko VI (1994) Sharks of family Jaekelodontidae of European and middle Asian paleobiogeographic provinces. *Bulletin of the Moscow Society of Naturalists* 69: 47–62. [In Russian]
- Zhelezko VI, Kozlov VA (1999) Elasmobranchii and Palaeogene biostratigraphy of Trans Urals and central Asia. *Russian Academy of Science, Urals Branch* 3: 1–323. [In Russian] [https://books.google.com/books/about/Elasmobranchii\\_and\\_palaeogene\\_biostratig.html?id=4Y6VMgAACAAJ](https://books.google.com/books/about/Elasmobranchii_and_palaeogene_biostratig.html?id=4Y6VMgAACAAJ)
-

# Another one bites the dust: A new *Lithoserix* species (Hymenoptera, Ichneumonidae, Pimplinae) from the early Oligocene in France, with an evaluation of wing morphometrics

Alexandra Viertler<sup>1,2</sup>

<sup>1</sup> Natural History Museum Basel, Augustinergasse 2, CH 4001 Basel, Switzerland

<sup>2</sup> Institute of Ecology and Evolution, University of Bern, Baltzerstrasse 6, CH 3012 Bern, Switzerland

<https://zoobank.org/9D48B90F-748C-4193-9B3E-C7870B0BD821>

Corresponding author: Alexandra Viertler ([viertler49@gmail.com](mailto:viertler49@gmail.com))

Academic editor: Christian Klug ♦ Received 27 November 2023 ♦ Accepted 30 January 2024 ♦ Published 8 February 2024

## Abstract

A new Darwin wasp species, *Lithoserix oublieri* **sp. nov.** is described and illustrated from the early Oligocene limestone formation Calcaires de Campagne-Calavon in the Luberon Region, France. It represents the third species of this extinct genus, which was first described from the late Eocene Florissant Formation in Colorado, US and later found in Aix-en-Provence, France, from the late Oligocene. The taxonomic placement of this genus in the context of tribal classification is analysed and discussed, based on geometric morphometrics of the fore and hind wing venation of fossil and extant Pimplinae species. The results suggest that *Lithoserix* does not belong to the same group as the extinct genus *Crusopimpla*, but rather represents a more basal genus within Pimplini or belongs to an extinct separate tribe, closely related to Pimplini.

## Key Words

Calcaires de Campagne-Calavon Formation, compression fossils, Darwin wasps, fossil record, geometric morphometrics

## Introduction

Pimplinae is a species-rich subfamily of Darwin wasps that began to diversify in the Cretaceous (Kopylov 2009; Kopylov et al. 2010; Spasojevic et al. 2021). Currently, Pimplinae is regarded as paraphyletic (Spasojevic et al. 2021) and consists of four tribes. Pimplini, the tribe that branches off first, is much older than the other pimpline tribes and most other subfamilies in the informal group Pimpliformes (except Diplazontinae). The other three tribes group together, with Ephialtini branching off first, resulting in Delomeristini and the recently resurrected Theroniini being sister groups (Klopfstein et al. 2018). Notably, while no extinct tribes exist in Pimplinae, there are some extinct genera, such as *Crusopimpla*, which was first described from the Tadushi Formation in Russia (Eocene) (Kopylov et al. 2018) and later found in the Fur Formation in Denmark (Eocene) (Klopfstein 2022). Another extinct

pimpline genus is *Lithoserix*, which was first described from the late Eocene Florissant Formation in Colorado (Brown 1986). It was originally placed in Siricidae, but later moved to Ichneumonidae (Kasparyan and Rasnitsyn 1992). The second species of *Lithoserix*, *L. antiquus* (Saussure, 1852), was found in Aix-en-Provence in France (late Oligocene) and only transferred to the genus recently (Spasojevic et al. 2022). Within Darwin wasps, *Lithoserix* was initially placed in Ephialtini by Kasparyan and Rasnitsyn (1992); however, this placement was questioned due to its resemblances to some Delomeristini and Theroniini, as well as to *Xanthopimpla* (Spasojevic et al. 2022). Moreover, many important body characters are not preserved in the *Lithoserix* fossils, making their tribal placement even more difficult (Spasojevic et al. 2022).

In contrast to body characters, which often exhibit varying degrees of preservation in compression fossils, wings and their venation are often consistently well-preserved, making

them an important character system for identifying fossils. Moreover, recent studies have demonstrated that fore wing characteristics can be used to distinguish different subfamilies of Darwin wasps (Li et al. 2020; Meier et al. 2022; Viertler et al. 2022). Within Pimplinae, some tribes are known to possess specific hind wing vein characteristics, such as the interception of the nervellus, which is clearly above the middle in Pimplini, while in Ephialtini, it is often around or below the middle (Gauld et al. 2002). However, it can also be clearly above in quite a few Ephialtini such as *Dolichomitus*, *Ephialtes* etc.

The newly-described fossil species is from the Calcaires de Campagne-Calavon Formation in the Luberon Region of south-eastern France. This formation is around 31–30 million years old (early Oligocene) and includes numerous fossiliferous localities (Ducieux et al. 1985; Duhamel and Louchart 2020; Coster and Legal 2021). Its sedimentary deposits consist mostly of laminated limestones (Coster and Legal 2021) and its paleoenvironment is considered a quiet, calm and shallow lacustrine setting (Duhamel and Louchart 2020). The formation is known for its rich fossil finds, ranging from birds to fish, insects and plant remains (Duhamel and Louchart 2020; Coster and Legal 2021). Most fossil insects are Coleoptera and Diptera (Skartveit and Nel 2017; Nel et al. 2023), while descriptions of Darwin wasps from this location are rather scarce. There is one major publication by Nicolas Théobald (1937), providing an overview of insects in Oligocene formations of France, including two described Darwin wasps (*Pimpla aquensis* Théobald, 1937 and *P. anomalensis* Théobald, 1937) found in Céreste, a locality of Calcaires de Campagne-Calavon. However, *P. anomalensis* probably does not belong to Pimplinae since the areolet seems pentagonal, a feature not found in Pimplinae. Additionally, *P. aquensis* is difficult to assign, but it appears to have a rather petiolate or strongly tapering first tergite, which would be uncommon in Pimplinae.

In this study, I describe and illustrate the third species of the extinct genus *Lithoserix*. Based on a geometric morphometric analysis of wing venation, including extant and fossil species of the four pimpline tribes and the unplaced fossil genus *Crusopimpla*, I discuss the taxonomic placement of *Lithoserix*.

## Materials and methods

### Fossil material

The fossil specimen (PNRL-SIG-216, Signoret collection of the Parc naturel régional du Luberon (PNRL)) is from the Calcaires de Campagne-Calavon Formation. The exact provenance of the locality is unknown.

Photos were taken with a Keyence VHX 600 camera system with a magnification of 50–200. Measurements were then taken with ImageJ (Abràmoff et al. 2004). Using different photos of the specimen as templates, I made interpretative drawings of the fossil in Adobe Photoshop (ver. 25.1.0). Uncertainties of fossil structures are indicated

by dotted lines. Terminology mainly follows Broad et al. (2018), with the exception of the wing venation, which follows Spasojevic et al. (2018). Tergites are abbreviated as “T1”, “T2” etc. For the comparison of the fossil with other taxa, I used identification keys and diagnostic characters from several taxonomic treatments (Townes 1969; Kasparyan and Rasnitsyn 1992; Spasojevic et al. 2022).

The colours of fossils may change due to preservation, requiring consistent patterns for clear interpretation. Colour and colour pattern preservation in ichneumonid fossils were evaluated before and remarkable consistency was found in various holotypes and its paratypes, as well as in parts and counterparts (Klopfstein 2022). Unfortunately, the fossil specimen in this study has no counterpart and there were no paratypes, which complicates confirming colour alterations. Nevertheless, if the new fossil species displays consistent colouration on both body sides (e.g. right and left hind femur), the interpretation is noted in the species description, but should be treated with caution.

### Geometric morphometrics

The landmark dataset of the fore wing encompasses 62 Pimplinae taxa from Viertler et al. (2022), representing all four tribes with 49 of the 79 known genera, plus 10 fossil species. I added the wing venation of the two previously described *Lithoserix* species (see Suppl. material 1 for taxon list), plus of the new species described herein. For the fore wing, 20 fixed landmarks are included in this analysis (Fig. 1A). Viertler et al. (2022) used 21 fixed landmarks, but the location of the first landmark is not certain in the new fossil species and is removed here. The dataset covers all four pimpline tribes, as well as the extinct genera *Crusopimpla* and *Lithoserix*, which are both not placed within a pimpline tribe. Each tribe and each extinct genus are treated as a pimpline “group” in the wing analyses, of which there are six in total.

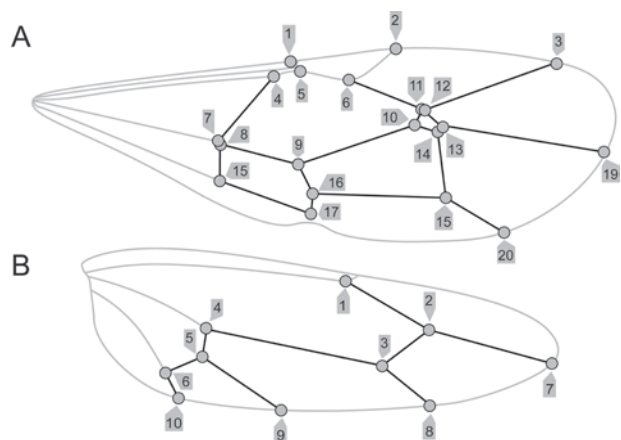


**Figure 1.** Landmark sets of fore- and hind wing. **A.** Schematic representation of a fore wing with 20 landmarks (grey circles) and **B.** hind wing with ten landmarks (grey circles) placed on the respective intersections of the veins. The black lines indicate the veins, which connect the landmarks.

As previously done in Viertler et al. (2022) for the fore wings, the illustrations of the hind wing from Townes (1969) were used to place ten fixed landmarks (Fig. 1B) with the software tpsDig2 (Rohlf 2008). Four *Crusopimpla* species (*C. collina* Klopffstein, 2022, *C. elongata* Klopffstein, 2022, *C. minuta* Klopffstein, 2022 & *C. rettigi* Klopffstein, 2022), *Theronia? nigriscutum* Klopffstein, 2022 and *Lithoserix antiquus* were excluded from the hind-wing dataset, because some landmarks could not be placed due to incomplete hind-wing preservation. Additionally, three taxa, *Zatyptota percontator* (Müller, 1776), *Sinarachna pallipes* (Holmgren, 1980) and *Eriostethus rufus* (Uchida, 1932), belonging to Ephialtini, were removed from the hind-wing dataset since their nervellus is not intercepted and, therefore, LM 5 and LM 9 could not be placed.

Differences in wing venation shape between the groups were evaluated and possible affiliations of *Lithoserix* and *Crusopimpla* to the four pimpline tribes investigated. First, a generalised Procrustes analysis was performed to scale, translate and rotate the landmark configurations using the function gpagen from geomorph (Adams et al. 2022) in R studio (ver. 4.0.2, RStudio Team 2020). To test how size and group affiliation interact with the wing shape, a Procrustes regression for the hind and fore wings was performed with procD.lm. This output was then used in the function plotAllometry, where first the standardised shape scores are calculated from the regression of shape on centroid size and plotted against centroid size. Then the same output is used to plot the predicted values of the first principal component against centroid size, showing the allometric trend per group (package geomorph, Adams et al. (2022)). Additionally, the Procrustes shape coordinates were used to perform a between-group Principal Component Analysis (bgPCA), where the variation of the groups (four pimpline tribes, *Crusopimpla*, and *Lithoserix*) was examined in a leaving-one-out crossvalidation (10,000 permutations) with the function groupPCA from the R package Morpho (Schlager 2017).

Further, a Canonical Variate Analysis (CVA) was conducted using the function CVA from Morpho (Schlager 2017) to gain additional information for evaluation of shape patterns (Renaud et al. 2015; Mennecart et al. 2020). The CVA was applied to the fore and hind wing to visualise the maximised amongst-group variance relative to the within group variance and to evaluate the similarity of the two extinct genera to the extant pimpline tribes.

All data in connection with the geometric morphometric analyses are provided in the Supplementary materials (Suppl. materials 2, 3).

## Results

### Systematic palaeontology

**Order Hymenoptera Linnaeus, 1758**  
**Family Ichneumonidae Latreille, 1802**  
**Subfamily Pimplinae Wesmael, 1845**

### Genus *Lithoserix* Brown, 1986

#### *Lithoserix oublierus* Viertler, sp. nov.

<https://zoobank.org/2E1851F7-0BBF-49DF-8F4A-63CA367ECC28>

Fig. 2

**Type material.** Holotype (PNRL-SIG-216, female, part, no counterpart available).

**Etymology.** Oublierus - from the French word “oublier” (forgotten) because the fossil was in the collection for a long time under the label “wasp” and was overseen, until André Nel and Corentin Jouault saw the wing venation and identified it as a Darwin wasp. The name is dedicated to the possibly numerous Darwin wasp fossils that are overlooked in natural history collections.

**Type locality.** South-eastern France, Calcaires de Campagne-Calavon Formation (Rupelian, 31–30 Ma).

**Systematic placement.** Many characteristics indicate that the fossil belongs to Pimplinae: the stout and short T1 with a lateromedian carina present, a quadratic areolet in the fore wing, 2m-cu slightly bowed outwards and two bullae and a long 2R1 cell. Other strong arguments for this subfamily are found in the hind wing: a long 1Rs relatively to its short rs-m vein, as well as a nervellus that is intercepted clearly above the middle. While the ovipositor of this fossil is only weakly discernible, it appears to project posteriorly from the metasoma, providing further support for its placement in Pimplinae.

The fossil also shows some character combinations that are rare in Pimplinae, but that are found in the extinct genus *Lithoserix*: its rather extensive propodeum carination, the fore wing with an almost triangular areolet, a long 1Rs + M and a sinusoidal 4Rs vein, together with the lateromedian carina on T1 reaching to the posterior end.

**Diagnosis.** There are currently two *Lithoserix* species described, which are both preserved from the dorsal side, while the new species is preserved more laterally. The new fossil specimen differs from both *Lithoserix* by having the vein 1cu-a strongly postfurcal, with 1Cu about 3–4× longer than its width, having 3Cu much longer with twice the length of 2cu-a, 1Rs much longer than vein rs-m in the hind wing and by its narrower hind femurs (Table 1).

Additionally, the new fossil specimen differs from *L. antiquus* by having a nervellus that is intercepted very high up, not having smooth transverse bands on the hind margins of T2–T7 and its lateromedian carina on T1 reaching beyond the middle, maybe even until the posterior end, but this is difficult to interpret. Furthermore, *L. antiquus* has brightly-coloured legs (orange), whereas the new species appears to have dark legs.

Finally, the new fossil species differs from *L. williamsi* by having its antennal segments less stout, at least not in the basal segments. Furthermore, *L. williamsi* is around twice the body size and has strongly impressed notauli, whereas they are only weakly preserved in the new species.

The fossil specimen exhibits shallow notauli and weak pleural, lateral longitudinal and lateromedian carination on the propodeum. The fore wing has a strongly postfurcal nervulus, the nervellus in the hind wing is intercepted

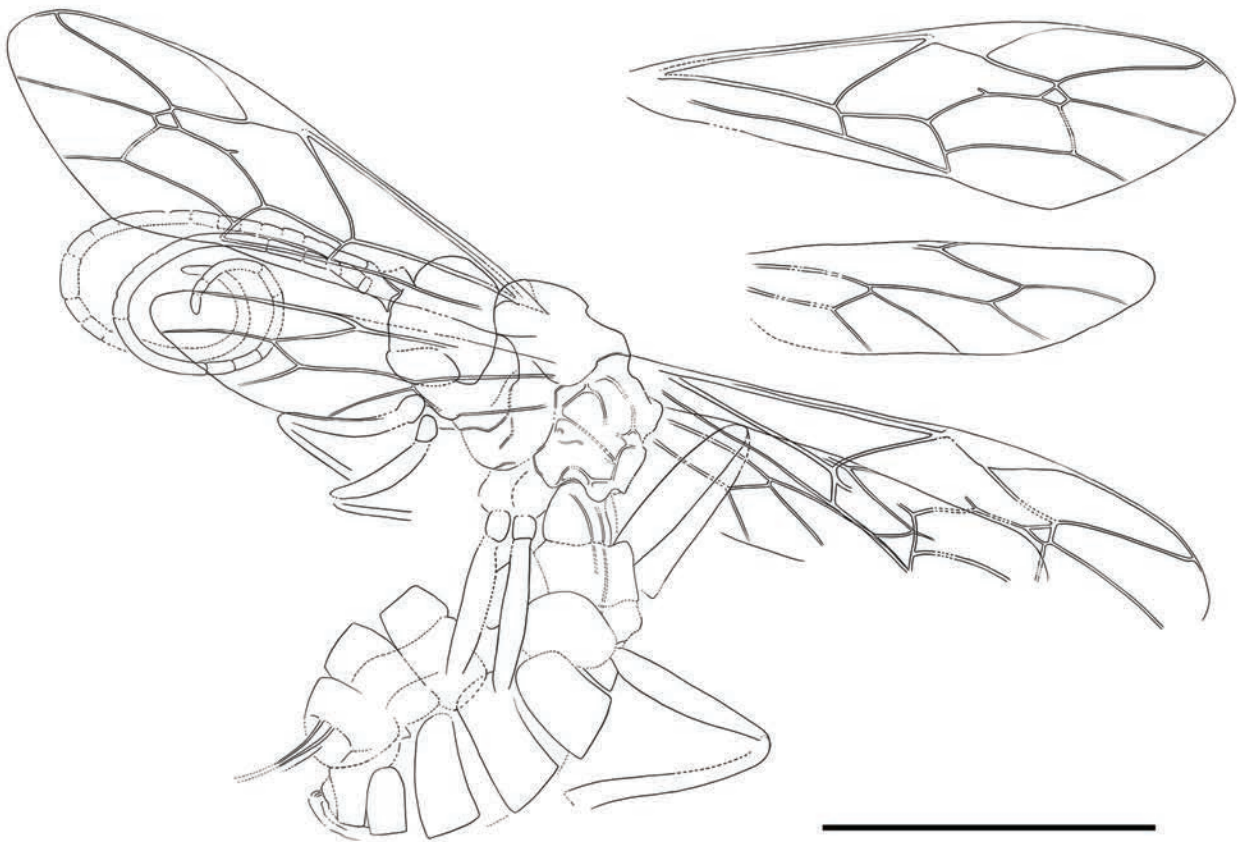


**Figure 2.** Holotype of *Lithoserix oublierus* sp. nov. (PNRL-SIG-216) **A.** Photograph of the holotype; **B.** Interpretative drawing, where dotted lines indicate uncertain interpretations. Scale bars: 5 mm.

in its anterior 0.2 and T1 features lateromedian carinae which reach beyond the middle. The fossil specimen's colouration is interpreted without having a counterpart or paratype, which would increase the certainty of the observed colours. However, the specimen shows both antennae and fore- and mid-coxae with a light colour, but a dark-coloured head, body and femurs. It appears that both hind tibiae have a bright base and a dark apex.

**Table 1.** Overview of differences between the three *Lithoserix* species.

Species	<i>L. williamsi</i>	<i>L. antiquus</i>	<i>L. oublieri</i>
<b>Antennal segments, dimension</b>	Short, only slightly longer than wide	?	1.5–2.5× longer than posteriorly wide
<b>Mesoscutum, notauli</b>	Extending past half of mesoscutum	Extending to basal third of mesoscutum	Weak or absent
<b>Hind femur, dimension</b>	3.4× longer than wide	3.5× longer than wide	4.2× longer than wide
<b>Fore wing, 1cu-a meeting M+Cu</b>	Interstitial	Interstitial	Strongly postfurcal
<b>Fore wing, 3Cu length</b>	1.3× 2cu-a	1× 2cu-a	2× 2cu-a
<b>Fore wing, 4Rs shape</b>	Clearly bowed at base	Little bowed at base and apex	Distally arched and slightly sinusoidal
<b>Hind wing, nervellus</b>	At anterior 0.3	At anterior 0.4	At anterior 0.2
<b>Hind wing, 1Rs length</b>	1.5× rs-m	1.3× rs-m	2.6× rs-m
<b>T1, lateromedian carina</b>	Beyond middle	Basal half	Beyond middle
<b>Body length</b>	22 mm	13.7 mm	12–13 mm

**Description. Preservation.** Holotype in dorso-lateral view. Antenna, head and mesosoma well preserved, but some details are missing or obscured by the very well-preserved fore- and hind wings. Legs are partially preserved, including all femora and fore- and hind tibiae, as well as fore- and mid-trochanters. Propodeal carination visible. Metasoma difficult to interpret since hind coxa and first tergite seem to overlap and the metasoma is preserved rather compressed, which is probably an artefact. Ovipositor partially visible at base, but otherwise indiscernible or broken.

**Body.** 12–13 mm. Fossil dark in colour, either black or dark brown. Antennae seem bright, but scape appears dark. All femurs dark, front tibiae appear bright. Hind tibiae appear bright with lower 0.4 dark.

**Head.** Antenna 10.8 mm, 1.1× fore wing length; without white band; dimensions of segments around 1.5–2.5× longer than posteriorly wide; number of antennal segments unclear, but more than 20; antenna more or less of even thickness throughout.

**Mesosoma.** Dimension unclear. Scutellum with shallow and slightly converging notauli. Metapleuron appears as long as wide, with juxtacoxal carina present. Propodeum rounded posteriorly; about as long as high; with small oval spiracle; traces of pleural carina, lateral longitudinal and lateromedian carina present, at least anteriorly and

posteriorly; posterior transverse carina present. Fore legs slender; hind femur 4.2× as long as wide.

**Wings.** Fore wing 9.7 mm. Areolet closed, slightly petiolate almost triangular, 2-Rs same length as 2-rs-m, 4M 1.1× 2-Rs and 2+3M 0.6× 2-Rs. 2m-cu present, slightly bowed to straight, with two bullae. 4Cu 2× 5Cu. 4Rs distally arched and slightly sinusoidal. 1Rs + M present, longer than width of surrounding veins. 1cu-a distal of 1M+1Rs by more than vein width. Pterostigma length 4.2× width, 0.6× vein 1R1. Cell 2R1 4.1× longer as wide. 5M vein tubular through entire length. 2Cu 0.8× 1M+1Rs, 1.17× r-rs. 1m-cu&2Rs+M vein straight or weakly arched or angled. 3Cu 1.8× 2cu-a. Hind wing with 1Cu very short, 0.15× cu-a. Veins 2Rs and 2Cu tubular through entire length. 2Rs 2.4× rs-m.

**Metasoma.** Dimension unclear, but stout in appearance. T1 broad and short, parallel-sided with slightly narrower base, with lateromedian carina more than half length of tergite. Dimension of T2 unclear, but appears transverse, as do T3–T6. Sternites strongly sclerotised, as dark as tergites. Ovipositor length unknown, but seems to reach past posterior end of metasoma.

## Shape variation in Pimplinae explained by group and size

The regression of shape on centroid size accounted for 30.0% of the fore-wing shape variation in Pimplinae ( $p = 0.001$ ) (Table 2). The remaining shape variation of the fore wing can be explained to 16.7% by the pimpline group affiliation (the four tribes and two extinct genera) ( $p = 0.001$ ); however, no interaction between the two variables could be observed ( $p = 0.218$ ). Hence, despite significant common allometry within groups, differences in shape amongst groups are still observed (Fig. 3A), but are similar for Ephialtini, Delomeristini and Theroniini and similar within Pimplini and *Lithoserix*.

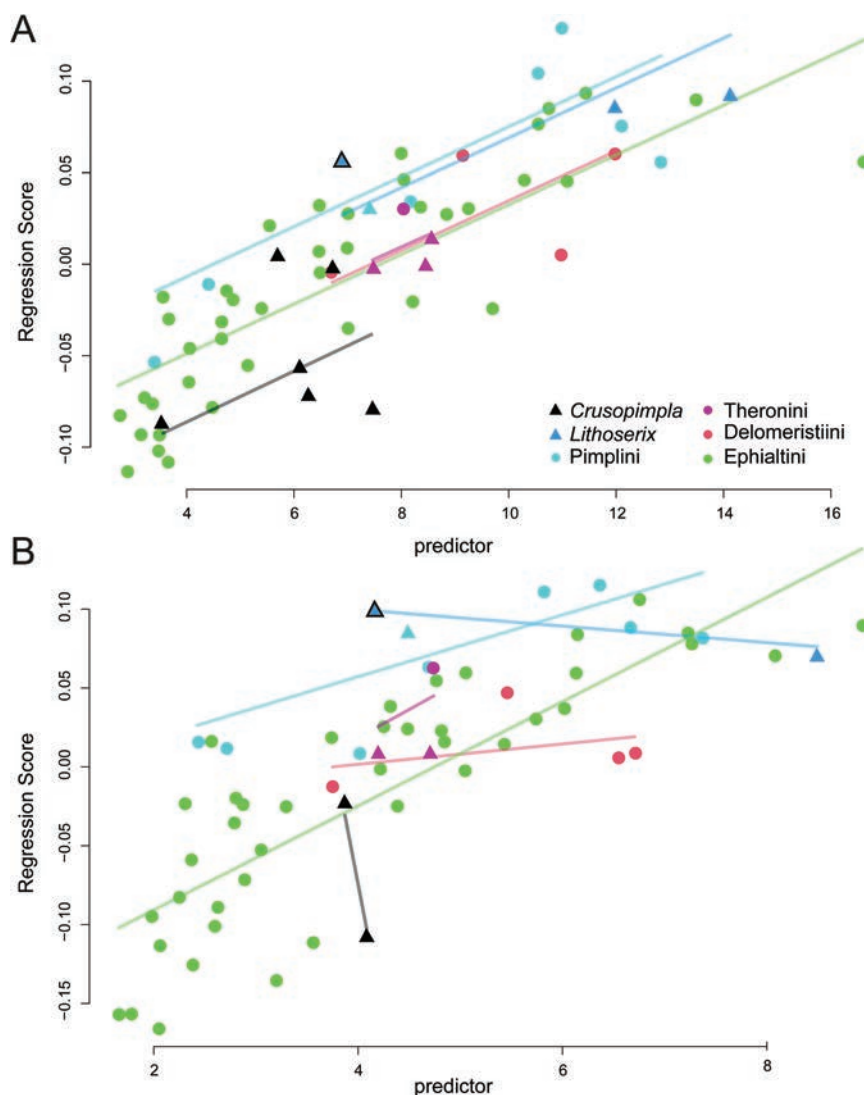
In the hind wing, the shape is explained to 25.9% by the centroid size ( $p = 0.001$ ) and 16.3% by the group affiliation ( $p = 0.001$ ) (Table 2). The shape changes correlated with the interaction of centroid size and group affiliation by 10.3% ( $p = 0.004$ ). Here, an interaction between both was observed ( $p = 0.004$ ), indicating unique allometries in the different groups, while still showing differences in shape amongst tribes (Fig. 3B).

## Pimpline group differences in fore wings

The bgPC1 of the fore wings explains 64.3% of the vein-shape variance associated with the groups, while bgPC2 explains 19.7% of the shape variation (Fig. 4). In those two bgPCA axes, the two extinct genera *Crusopimpla* and *Lithoserix* group separately from the extant tribes with low bgPC2 scores and also seem distinctly different from each other on the bgPC1 axis. The mean shape of *Crusopimpla* appears to have broader and shorter cells,

**Table 2.** Statistical results of Procrustes ANOVA for fore and hind wing. Df (Degree of freedom), (SS) Standard deviations of observed Sums of Squares, MS (mean squares), Rsq (R squares), F (F-value), Z (Z-score), Pr(>F) (*p*-value of F statistic).

<i>Fore wing</i>							
Effect	Df	SS	MS	Rsq	F	Z	Pr(>F)
Centroid size	1	0.16201	0.162014	0.30013	33.24	5.4689	0.001
Group	5	0.09048	0.018096	0.16762	3.713	5.5147	0.001
Centroid size: Group	5	0.02906	0.005813	0.05384	1.193	0.7919	0.218
Residuals	53	0.25825	0.004873	0.47841			
Total	64	0.53981					
<i>Hind wing</i>							
Centroid size	1	0.19919	0.199191	0.25963	26.8507	4.9981	0.001
Group	5	0.12550	0.025100	0.16358	3.3834	3.8758	0.001
Centroid size: Group	5	0.07901	0.015803	0.10299	2.1302	2.5668	0.004
Residuals	49	0.36351	0.007418	0.47380			
Total	60	0.75921					

**Figure 3.** Regression of pimpline wings of shape on size (regression score) plotted against centroid size (predictor). Straight lines show the fitted values of PC1 against centroid size, indicating the allometric trend per tribe in **A**. Fore wing and **B**. Hind wing.

as well as a broad pterostigma and an elongated areolet with vein 3rs-m and 2+3M distinctly longer than 2Rs and 4M. Overall, the fore-wing shape of *Crusopimpla* differs highly significantly from most pimpline groups (Table 3). Additionally, the *Lithoserix* taxa have high bgPC1 scores and their mean shape is characterised by

an overall narrow wing with slender cells as seen in cells 2R1, 1M+1Rs and 2Cu and the areolet not as elongate and more located towards the distal margin of the wing. In addition, although *Lithoserix* does appear to group separately from the extant tribes (Fig. 4), it only shows distinct differences to Ephialtini (Table 3).

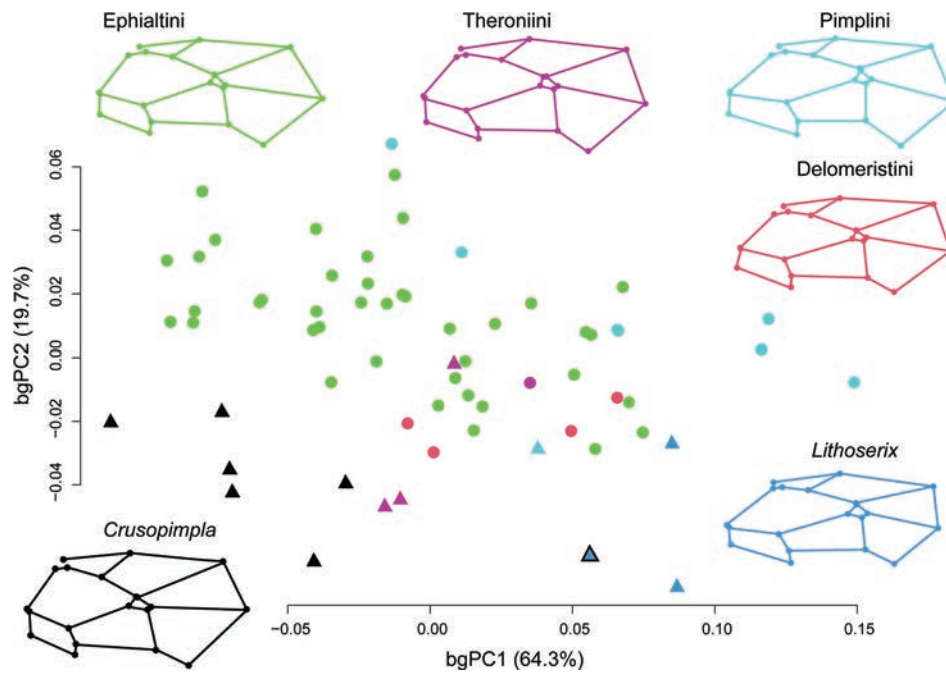


**Figure 4.** BgPCA of the fore wing in all specimens of the four pimpline tribes plus *Lithoserix* and *Crusopimpla*. The mean shape of each tribe/genus is shown in the respective colour. Triangles represent fossil species, whereas the blue triangle with black outline represents *Lithoserix oublieri* sp. nov.

**Table 3.** P-values of pairwise group differences in pimpline wings. Based on permutation testing of the bgPCA of fore wings and hind wings.

<b>Fore wing</b>	<i>Crusopimpla</i>	<i>Delomeristini</i>	<i>Ephialtini</i>	<i>Lithoserix</i>	<i>Pimplini</i>
<i>Delomeristini</i>	0.0118				
<i>Ephialtini</i>	0.0062	0.1425			
<i>Lithoserix</i>	0.0004	0.3245	0.0026		
<i>Pimplini</i>	0.0001	0.1025	0.0002	0.0932	
<i>Theroniini</i>	0.0870	0.4262	0.2375	0.1002	0.0563
<b>Hind wing</b>					
<i>Delomeristini</i>	0.1525				
<i>Ephialtini</i>	0.1970	0.7616			
<i>Lithoserix</i>	0.0358	0.409	0.0539		
<i>Pimplini</i>	0.0054	0.1545	0.0003	0.8323	
<i>Theroniini</i>	0.0505	0.3017	0.0469	0.3888	0.4231

All extant tribes do at least partially overlap in the first two bgPCA axes of the fore-wing variation. Additionally, while the fore wings shapes of *Delomeristini* and *Theroniini* do not differ much from most groups, the two larger extant tribes *Pimplini* and *Ephialtini* exhibit significant differences from each other (Table 3).

### Pimpline group differences in hind wings

BgPC1 explains 79.3% of the overall shape variation, whereas bgPC2 explains 10.5% (Fig. 5). Here, no pimpline group appears to be completely isolated in the morphospace of the bgPCA. However, the two *Crusopimpla* species are located in the higher values of bgPC1 and lower values of bgPC2 and the opposite is observed in *Lithoserix*. Thus, those extinct genera do also distinctly differ from each other in their hind-wing

shape (Table 3). The mean shape of *Crusopimpla* is characterised by their rather long 1M vein and their nervellus. This nervellus is intercepted very low and veins 1Cu and cu-a are rather straight, while this interception is much more angled in the other groups. Those differences of the hind-wing shape are significantly different from *Pimplini* and *Theroniini* (Table 3) and the *Crusopimpla* hind-wing shape seems more similar to *Ephialtini*.

*Lithoserix* are located on the extreme lower value of bgPC1 and are characterised by a relatively long 1Rs compared to rs-m, a relative short 1M and their nervellus intercepted very high up. This is also observed in *Pimplini* and the mean shape of the two *Lithoserix* species is similar to the mean shape of *Pimplini*. There were also no significant differences observed in the pairwise comparison of the Procrustes distances of those two groups (Table 3). However, *Lithoserix* hind wings differ from species of *Ephialtini* (Table 3).

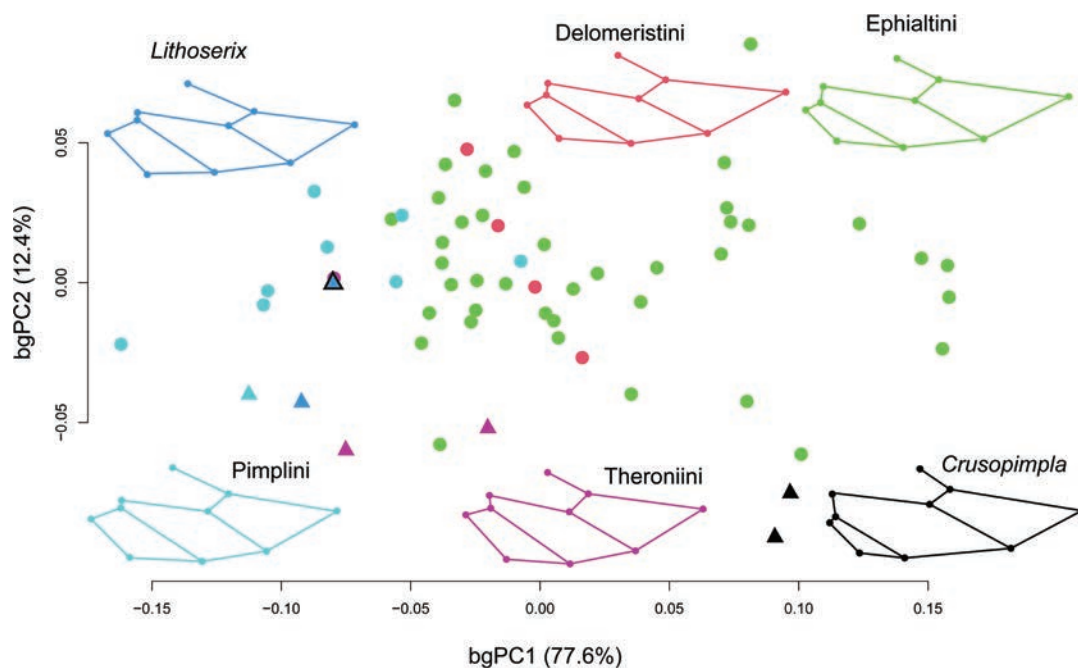


**Figure 5.** BgPCA of the hind wing in all specimens of the four pimpline tribes plus *Lithoserix* and *Crusopimpla*. The mean shape of each tribe/genus is shown in the respective colour. Triangles represent fossil species, whereas the blue triangle with black outline represents *Lithoserix oublieri* sp. nov.

Delomeristini occupies the morphospace mostly within Ephialtini and their hind wing mean shapes do appear similar, with just a slightly upwards shifted nervellus in Delomeristini. The Procrustes distances of their hind wings are not distinctly different (Table 3). The hind-wing shape of Theroniini is different from Ephialtini (Table 3), which appears to be caused by the higher cells M and 2Cu cells.

The CVA confirms the bgPCA results of fore and hind wings and can be found in Suppl. material 4.

## Discussion

The new fossil species is the third species of the extinct pimpline genus *Lithoserix*, which lived from the late Eocene to the late Oligocene. In this study, I described the fossil species *Lithoserix oublieri* sp. nov. and evaluate the placement of *Lithoserix* within Pimplinae using of geometric morphometrics of the fore- and hind wings of extant and fossil pimpline taxa.

While the fore wing is useful to distinguish Pimplinae from other subfamilies (Viertler et al. 2022), it does not seem as straightforward between the tribes of extant Pimplinae, which all partially overlap in the bgPCA analyses. In the hind wings, however, some tribes exhibit a rather specific venation in the analysis. This is in agreement with previous suggestions that some groups can be distinguished through hind-wing venation: in *Crusopimpla*, the nervellus is broken below the middle (Klopfstein 2022) and, in Pimplini, it is broken way above the middle (Gauld et al. 2002). The fact that Pimplini splits in both bgPCA analyses from most Ephialtini,

Delomeristini and Theroniini might support the notion that it is not closely related to the remaining Pimplinae (Klopfstein et al. 2018).

Considering the species diversity of *Crusopimpla* (Klopfstein 2022; Viertler et al. 2022; Manukyan 2023) and its substantial dissimilarities of the wing venation from extant tribes and *Lithoserix* (see results), it is plausible that *Crusopimpla* may belong to an ancestral or basal pimpline tribe.

For *Lithoserix*, important characteristics, such as the clypeus shape or the tarsal claws, are missing to make a confident tribal assignment, as was already discussed with the two previously-described *Lithoserix* species (Spasojevic et al. 2022). However, based on the wing analyses conducted herein, *Lithoserix* should not be placed in the same tribe as *Crusopimpla* and also an affiliation to Ephialtini seems improbable. The wings of *Lithoserix* species are most similar to Pimplini. Both groups change shape similarly with increasing size and no significant shape differences were obtained in either fore- or hind wing. The hind wing with the nervellus intercepted high up, as found in *Lithoserix williamsi* and *Lithoserix oublieri* sp. nov., is often found in the tribe Pimplini, although it is less pronounced in *Lithoserix antiquus*. An argument against Pimplini is the ovipositor length of *Lithoserix*, which is not completely preserved in this fossil, but very long in *Lithoserix williamsi* and *L. antiquus*. This is rather rare in Pimplini, but frequent in Ephialtini (Gauld et al. 2002). However, because Pimplinae probably originated in the Cretaceous (Spasojevic et al. 2021), it would not be surprising to find *Lithoserix* belonging to a stem-lineage within Pimplini or even an extinct tribe, possibly closely-related Pimplini.

## Conclusion

To confidently place *Lithoserix* in Pimplini or to propose a new tribe, a more robust collection of fossils and comprehensive morphological evidence is imperative. The classification of *Lithoserix* presents challenges, as it appears to be situated closest to Pimplini, when considering wing venation, but not according to ovipositor length. To gain information on the evolutionary path of Pimplinae or Darwin wasps, in general, more fossils need to be evaluated.

However, this might be a difficult task. There is not only a lack of researchers studying the astonishing diversity of extant Darwin wasp, but even more so of people working with their fossil taxa. It is probably not rare that undescribed Darwin wasp fossils are labelled “wasp” or “Hymenoptera” in natural history collections and we can only speculate how many fossils in this group are currently overlooked.

## Acknowledgements

I want to thank Tamara Spasojevic (Natural History Museum Basel, Switzerland) and Seraina Klopffstein (Natural History Museum Basel, Switzerland) for valuable feedback and comments on the species *Lithoserix oublierus* sp. nov. Special thanks to Bastien Mennecart (Natural History Museum Basel, Switzerland) and Loic Costeur (Natural History Museum Basel, Switzerland) for taking Tamara Spasojevic and me along to the excavation site in Murs, where we could experience to “dig out” fossil insects first-hand. I am grateful to Pauline Coster (Réserve Naturelle Nationale Géologique du Luberon, France), who helped us on the site and provided access to this fossil, which was waiting for discovery. Many thanks to André Nel (Muséum National d’Histoire Naturelle Paris, France) and Corentin Jouault (Muséum National d’Histoire Naturelle Paris, France) for identifying the fossil as Darwin wasp. A special thanks also to Fabrizia Ronco (University of Basel, Switzerland) for valuable feedback on the wing analyses, to Emmanuel Robert (University of Lyon, France) for providing images of the holotypes of *Pimpla* (?) *anomalousis* and *P. aquensis*, enabling a comparison with this new fossil species and to Adranik Manukyan and Tiago Belintani for their useful comments, which improved the manuscript.

## References

Abràmoff MD, Magalhães PJ, Ram SJ (2004) Image processing with imageJ. *Biophotonics International* 11: 36–41. <https://doi.org/10.1201/9781420005615.ax4>

Adams D, Collyer M, Kaliontzopoulou A, Baken E (2022) Geomorph: Software for geometric morphometric analyses. <https://cran.r-project.org/package=geomorph>

Broad GR, Shaw MR, Fitton MG (2018) Ichneumonid wasps (Hymenoptera: Ichneumonidae): their classification and biology. *Handbooks for the Identification of British Insects* 7(12): 1–418.

Brown FM (1986) *Lithoserix williamsi* (Siricidae: Hymenoptera) a newly recognized fossil horntail from Florissant, Colorado. *Insecta Mundi* 1(3): 119–220.

Coster P, Legal S (2021) An Early Oligocene Fossil Lagerstätten from the Lacustrine Deposits of the Luberon UNESCO Global Geopark. *Geoconservation Research* 4: 604–612. <https://doi.org/10.30486/gcr.2021.1915524.1068>

Ducreux J-L, Huguency M, Truc G (1985) La Formation des Calcaires et Lignites de Sigonce (Oligocène Moyen, Bassin de Forcalquier, Alpes-Haute-Provence): Datation à l’aide des Mammifères: Reconstruction des Milieux de dépôts. *Geobios*: 109–114. [https://doi.org/10.1016/S0016-6995\(85\)80183-2](https://doi.org/10.1016/S0016-6995(85)80183-2)

Duhamel A, Louchart A (2020) Regard sur l’avifaune fossile de l’Oligocène du Parc du Luberon et ses implications paléobiologiques, incluant de nouvelles données fossiles. *Courrier scientifique du Parc naturel régional du Luberon et de la Réserve de biosphère Luberon-Lure*: 98–117.

Gauld ID, Wahl DB, Broad GR (2002) The suprageneric groups of the Pimplinae (Hymenoptera: Ichneumonidae): A cladistic re-evaluation and evolutionary biological study. *Zoological Journal of the Linnean Society* 136: 421–485. <https://doi.org/10.1046/j.1096-3642.2002.00031.x>

Kasparyan DR, Rasnitsyn AP (1992) The Systematic Position of the Oligocene *Lithoserix williamsi* BROWN, (Hymenoptera, Ichneumonidae) from Colorado (USA). *Paleontological Journal* 26: 134–135.

Klopffstein S (2022) High diversity of pimpline parasitoid wasps (Hymenoptera, Ichneumonidae, Pimplinae) from the lowermost Eocene Fur Formation (Denmark). *Geodiversitas* 44: 645–664. <https://doi.org/10.5252/geodiversitas2022v44a23>

Klopffstein S, Langille B, Spasojevic T, Broad GR, Cooper SJB, Austin AD, Niehuis O (2018) Hybrid capture data unravel a rapid radiation of pimpliform parasitoid wasps (Hymenoptera: Ichneumonidae: Pimpliformes). *Systematic Entomology* 44: 361–383. <https://doi.org/10.1111/syen.12333>

Kopylov DS (2009) A new subfamily of ichneumonids from the Lower Cretaceous of Transbaikalia and Mongolia (Insecta: Hymenoptera: Ichneumonidae). *Paleontological Journal* 43: 83–93. <https://doi.org/10.1134/S0031030109010092>

Kopylov DS, Brothers DJ, Rasnitsyn AP (2010) Two New Labenopimpline Ichneumonids (Hymenoptera: Ichneumonidae) from the Upper Cretaceous of Southern Africa. *African Invertebrates* 51: 423–430. <https://doi.org/10.5733/afin.051.0211>

Kopylov DS, Spasojevic T, Klopffstein S (2018) New ichneumonids (Hymenoptera, Ichneumonidae) from the Eocene Tadushi Formation, Russian Far East. *Zootaxa* 4442: 319–330. <https://doi.org/10.11646/zootaxa.4442.2.8>

Li L, Shih PJM, Kopylov DS, Li D, Ren D (2020) Geometric morphometric analysis of Ichneumonidae (Hymenoptera: Apocrita) with two new Mesozoic taxa from Myanmar and China. *Journal of Systematic Palaeontology* 18: 931–943. <https://doi.org/10.1080/14772019.2019.1697903>

Manukyan AR (2023) A new species of the genus *Crusopimpla* Kopylov et al., 2018 (Hymenoptera, Ichneumonidae, Pimplinae) from Upper Eocene Baltic amber. *Paleontological Journal* 57: 84–91. <https://doi.org/10.1134/S0031030123030115>

Meier N, Wacker A, Klopffstein S (2022) New fossil wasp species from the earliest Eocene Fur Formation has its closest relatives in late Eocene ambers (Hymenoptera, Ichneumonidae, Pherhombinae). *Bulletin of the Society of Systematic Biologists* 1. <https://doi.org/10.18061/bssb.v1i1.8427>

- Mennecart B, Guignard C, Dziomber L, Schulz G, Müller B, Costeur L (2020) Allometric and phylogenetic aspects of stapes morphology in Ruminantia (Mammalia, Artiodactyla). *Frontiers in Earth Science* 8: 176. <https://doi.org/10.3389/feart.2020.00176>
- Nel A, Mennecart B, Spasojevic T, Viertler A, Maridet O, Costeur L, Garrouste R, Coster P (2023) The first fossil representative of the water strider subfamily Ptilomerinae (Heteroptera: Gerromorpha: Gerridae) in the Oligocene paleolake of Murs (southern France) with some palaeoecological considerations. *European Journal of Taxonomy* 888: 124–136. <https://doi.org/10.5852/ejt.2023.888.2235>
- Renaud S, Dufour A-B, Hardouin EA, Ledevin R, Auffray J-C (2015) Once upon multivariate analyses: When they tell several stories about biological evolution. *Evans AR (Ed.). PLOS ONE* 10: e0132801. <https://doi.org/10.1371/journal.pone.0132801>
- Rohlf FJ (2008) TPSDIG. <http://www.sbmorphometrics.org/soft-data-acq.html>
- RStudio Team (2020) RStudio: Integrated Development for R. <http://www.rstudio.com/>
- Schlager S (2017) Morpho and Rvcg - Shape Analysis in R. In: Zheng G, Li S, Székely G (Eds) *Statistical Shape and Deformation Analysis*. Academic Press, 217–256. <https://doi.org/10.1016/B978-0-12-810493-4.00011-0>
- Skartveit J, Nel A (2017) Revision of fossil Bibionidae (Insecta: Diptera) from French Oligocene deposits. *Zootaxa* 4225: 1–83. <https://doi.org/10.11646/zootaxa.4225.1.1>
- Spasojevic T, Broad GR, Klopstein S (2022) Revision of 18 ichneumonid fossil species (Hymenoptera, Ichneumonidae) highlights the need for open nomenclature in palaeontology. *Fossil Record* 25: 187–212. <https://doi.org/10.3897/fr.25.83034>
- Spasojevic T, Broad GR, Bennett AMR, Klopstein S (2018) Ichneumonid parasitoid wasps from the Early Eocene Green River Formation: five new species and a revision of the known fauna (Hymenoptera, Ichneumonidae). *PalZ* 92: 35–63. <https://doi.org/10.1007/s12542-017-0365-5>
- Spasojevic T, Broad GR, Sääksjärvi IE, Schwarz M, Ito M, Korenko S, Klopstein S (2021) Mind the outgroup and bare branches in total-evidence dating: A case study of Pimpliform Darwin wasps (Hymenoptera, Ichneumonidae). *Systematic Biology* 70: 322–339. <https://doi.org/10.1093/sysbio/syaa079>
- Théobald N (1937) *Les Insectes fossiles des terrains oligocène de France*. Imprimerie Georges Thomas, Nancy, 473 pp.
- Townes H (1969) The genera of Ichneumonidae, Part 1. *Memoirs of the American Entomological Institute*: 1–300. <https://doi.org/10.1007/BF02027741>
- Viertler A, Baur H, Spasojevic T, Mennecart B, Klopstein S (2022) Classifying fossil Darwin wasps (Hymenoptera: Ichneumonidae) with geometric morphometrics of fore wings. *Schubert M (Ed.). PLOS ONE* 17: e0275570. <https://doi.org/10.1371/journal.pone.0275570>

## Supplementary material 1

### Taxon list

Authors: Alexandra Viertler

Data type: xlsx

Explanation note: This table shows all included extant and fossil taxa that were used in the geometric morphometric analyses of the fore- and hind wings.

Copyright notice: This dataset is made available under the Open Database License (<http://opendatacommons.org/licenses/odbl/1.0>). The Open Database License (ODbL) is a license agreement intended to allow users to freely share, modify, and use this Dataset while maintaining this same freedom for others, provided that the original source and author(s) are credited.

Link: <https://doi.org/10.3897/fr.27.116373.suppl1>

## Supplementary material 2

### TPS dataset of fore wings

Authors: Alexandra Viertler

Data type: tps

Explanation note: This dataset includes 21 fixed landmarks, of which the first landmark was excluded. It also contains two curves: The first curve (eight semi-landmarks) was placed between the landmarks delimiting vein 2m-cu and the second curve (ten semi-landmarks) was placed between the landmarks delimiting vein 1m-cu & 2Rs+M. Both curves were ignored in this analysis

Copyright notice: This dataset is made available under the Open Database License (<http://opendatacommons.org/licenses/odbl/1.0>). The Open Database License (ODbL) is a license agreement intended to allow users to freely share, modify, and use this Dataset while maintaining this same freedom for others, provided that the original source and author(s) are credited.

Link: <https://doi.org/10.3897/fr.27.116373.suppl2>

## Supplementary material 3

### TPS dataset of hind wings

Authors: Alexandra Viertler

Data type: tps

Explanation note: This dataset includes 11 fixed landmarks, of which the first landmark was excluded for this analysis because it represented the start of vein Sc+R on the hind-wing base, which is often not visible in fossil taxa.

Copyright notice: This dataset is made available under the Open Database License (<http://opendatacommons.org/licenses/odbl/1.0>). The Open Database License (ODbL) is a license agreement intended to allow users to freely share, modify, and use this Dataset while maintaining this same freedom for others, provided that the original source and author(s) are credited.

Link: <https://doi.org/10.3897/fr.27.116373.suppl3>

## Supplementary material 4

### Canonical variation analysis (CVA) of fore- and hind wings

Authors: Alexandra Viertler

Data type: tif

Explanation note: This figure shows the CVA of **A.** fore wings and **B.** hind wings of four pimpline tribes and two extinct genera. Both plots show the first two axes of the respective CVA analysis and the extreme shape change along the labelled axes. Triangles represent fossil species, whereas the blue triangle with black outline represents *Lithoserix oublieri* sp. nov. **A.** In the fore wing, CV1 (50.5% explained variance) separates Ephialtini, Pimplini and Delomeristiini from Theronini and the two extinct genera, *Crusopimpla* and *Lithoserix*. The shape change mostly effects the angle of the distal part of the fore wing (LM 3, 19, 20).

CV2 (22.4% explained variance) separates Pimplini to one extreme, *Crusopimpla* to the other extreme from the other groups Ephialtini, Theronini and *Lithoserix*. Here the shape change includes broadening (2R1, 2M) or shortening (1M+1R1, 2Cu) of various cells in the lower values (red outline). **B.** In the hind wing, CV1 (47.4% explained variance) puts *Lithoserix* and many Pimplini in the higher extremes, with the nervellus intercepted above the middle. CV2 (20.3% explained variance) splits mostly *Crusopimpla*, with the nervellus intercepted below the middle, from the other groups. Delomeristiini are situated within Ephialtini.

Copyright notice: This dataset is made available under the Open Database License (<http://opendatacommons.org/licenses/odbl/1.0>). The Open Database License (ODbL) is a license agreement intended to allow users to freely share, modify, and use this Dataset while maintaining this same freedom for others, provided that the original source and author(s) are credited.

Link: <https://doi.org/10.3897/fr.27.116373.suppl4>

## Supplementary material 5

### Results of Canonical variation analysis (CVA) of fore and hind wings

Authors: Alexandra Viertler

Data type: docx

Explanation note: Short results section of the CVA analyses of fore and hind wings in Pimplinae.

Copyright notice: This dataset is made available under the Open Database License (<http://opendatacommons.org/licenses/odbl/1.0>). The Open Database License (ODbL) is a license agreement intended to allow users to freely share, modify, and use this Dataset while maintaining this same freedom for others, provided that the original source and author(s) are credited.

Link: <https://doi.org/10.3897/fr.27.116373.suppl5>



# A phytosaur osteoderm from a late middle Rhaetian bone bed of Bonenburg (North Rhine-Westphalia, Germany): Implications for phytosaur extinction

P. Martin Sander<sup>1,2</sup>, Paul W. Wellnitz<sup>1</sup>

<sup>1</sup> Section Paleontology, Institute of Geosciences, University of Bonn, 53115 Bonn, Germany

<sup>2</sup> The Dinosaur Institute, Natural History Museum of Los Angeles County, Los Angeles, California 90007, USA

<https://zoobank.org/C573EF1B-B2F4-4BCE-953E-D40FE0A4A487>

Corresponding author: P. Martin Sander ([martin.sander@uni-bonn.de](mailto:martin.sander@uni-bonn.de))

Academic editor: Florian Witzmann ♦ Received 23 October 2023 ♦ Accepted 21 February 2024 ♦ Published 13 March 2024

## Abstract

Although there are problematic earliest Jurassic records, phytosaurs are thought to have become extinct during the Rhaetian. A newly-discovered left paramedian phytosaur osteoderm from a clay pit in Bonenburg, Kreis Höxter, North Rhine-Westphalia, Germany, is the youngest, well-dated phytosaur record. This osteoderm was found in a bone bed (Bone Bed 2) in the Contorta Beds of the Rhaetian Exter Formation. Palynology constrains the age of Bone Bed 2 to the late middle Rhaetian (ca. 203.5 million years ago). The Bonenburg osteoderm cannot be assigned to any named species. It most closely resembles some osteoderms from the Rhaetian of Halberstadt in Central Germany. Phytosaurs survived in Europe to at least the late middle Rhaetian, probably falling victim to the end-Triassic extinction event about two million years later.

## Key Words

End-Triassic extinction event, Exter Formation, Germany, osteoderm, Phytosauria, Rhaetian

## Introduction

Phytosaurs are a distinctive clade of predominantly Late Triassic basal archosauriforms with clear adaptations to a semi-aquatic lifestyle (Stocker and Butler 2013). Most phytosaur remains are from fluvial deposits. However, phytosaur habitats occasionally extended into the marine realm as evidenced by phytosaur finds in marine sediments from the Alps (Renesto and Paganoni 1998; Gozzi and Renesto 2003; Renesto 2008; Butler et al. 2019). From the Carnian onwards, phytosaurs were already widespread, being found in many Norian localities of the Triassic Northern Hemisphere (Brusatte et al. 2013; Lucas 2018; Brownstein et al. 2023). However, there are many fewer phytosaur finds from the Triassic Southern Hemisphere (Brusatte et al. 2013; Barrett et al. 2020; Datta and Roy 2023). Phytosaur systematics relies heavily on the well-ossified skulls (Jones and Butler

2018) which are commonly found in isolation. In addition to skulls and skeletons, the phytosaur fossil record consists of their characteristic osteoderms, the subject of the current contribution.

Classical rock units for phytosaur discoveries are the Middle and Upper Keuper sediments of the Germanic Basin. The Keuper can be subdivided into the Lower Keuper (also Lettenkeuper; roughly late Ladinian to Carnian in age), the Middle Keuper (presumed to cover the Norian) and the Upper Keuper (Rhaetian). After the continental conditions of the Middle Keuper, the Upper Keuper is mainly marine-deltaic (Barth et al. 2018), recording the initial marine incursions into the Germanic Basin, followed by its complete inundation in the Early Jurassic. In central and northern Germany, the deposits of the Upper Keuper, traditionally also called *Rhät* as a lithostratigraphic term, are assigned to the Exter Formation (Barth et al. 2018).

## The locality of Bonenburg and its lithostratigraphy

The Bonenburg clay pit (Fig. 1) is a relatively new fossil locality that was put on the map by the unique discovery of a Triassic plesiosaur skeleton (Sander et al. 2016; Wintrich et al. 2017). However, most fossils from Bonenburg come from several bone beds (condensation horizons rich in teeth, fish scales and bones) (Sander et al. 2016).

The stratigraphy of the Bonenburg clay pit (Fig. 1B) presents one of the best examples for the epicontinental Triassic-Jurassic boundary in Europe (Sander et al. 2016; Schobben et al. 2019; Gravendyck et al. 2020), with a continuous section from the Norian to the Sinemurian (Fig. 1B). However, most of the section in the pit pertains to the Rhaetian Exter Formation. The base of the Exter Formation starts out with about 2 m of Postera Beds. No fossils are found in this unit. Next come > 11 m of the Contorta Beds (Sander et al. 2016; Gravendyck et al. 2020). These consist of dark clay- and siltstones and, within them, at least four bone beds are intercalated (Sander et al. 2016; Gravendyck et al. 2020) (Fig. 1B). On top of the Contorta Beds, there are about 16.5 m of the Triletes Beds of the Exter Formation, overlain by marine carbonates and mudstones of Hettangian age, pertaining to the Pylonotenton Formation.

## Biostratigraphic dating of Bone Bed 2

The three best defined bone beds in the Contorta Beds (Fig. 1B) are located 0 m, 7 m and 9 m above the base of the Contorta Beds. Bone Bed 1 is about 1 cm thick, containing mainly small fish and shark teeth (Sander et al. 2016). Bone Bed 2, the source of the osteoderm described in this study, is divided into two parts: the lower Bone Bed 2a and the upper Bone Bed 2b, separated by 8 cm of claystone (Sander et al. 2016). Bone Bed 2 is the most important overall due to its faunal contents. Bone Bed 3 hosts larger bones and is less continuous than Bone Bed 2. The material from Bone Bed 3 is often heavily abraded and encased in phosphate concretions.

Bone Bed 2 contains a vertebrate fauna of Rhaetian age (Sander et al. 2016; Wintrich et al. 2017) and, together with the entire section, has been precisely dated, based on palynomorphs (Fig. 1B). Dense sampling and good palynomorph preservation allowed the subdivision of the palynozones of the North German Basin (Barth et al. 2018) into subzones in the Bonenburg section (Gravendyck et al. 2020). Thus, Bone Bed 2 is situated in the upper half of the RLb subzone of Gravendyck et al. (2020). Subzone RLb is the middle subzone of the *Rhaetipollis-Limbosporites* palynozone (Fig. 1B). The high location of Bone Bed 2 in this subzone indicates that the bone bed is late middle Rhaetian in age (Fig. 1B).

By age interpolation based on the Triassic chronostratigraphic chart of Ogg et al. (2020), Bone Bed 2 is about 203.5 million years old, two million years before the end of the Triassic 201.4 million years ago. This palynologically determined age is consistent with the occurrence

of the conchostracan *Euestheria brodieana* (Kozur and Weems 2010) right below Bone Bed 2 (Schobben et al. 2019), which, according to Ogg et al. (2020, fig. 25.5), occurs in the middle and late Rhaetian.

## Bone Bed 2 faunal contents

The Contorta Beds containing the bone beds are of marine origin (Sander et al. 2016). As the Contorta Beds are a transgressive unit of marine-deltaic deposits (Barth et al. 2018), the bone beds, including Bone Bed 2, were sourced from a very wide range of habitats, from open marine to terrestrial (Sander et al. 2016). In Bone Bed 2, teeth, scales and skull fragments of Chondrichthyes and of Actinopterygii, as well as tooth plates of Dipnoi (Sander et al. 2016) represent fully aquatic, mainly marine habitats. Vertebrae and other remains belonging to ichthyosaurs and plesiosaurs are common (Sander et al. 2016) and represent open marine habitats. Semi-aquatic and terrestrial habitats are represented by a high diversity of tetrapods. Postcranial bones of the putative choristoderan *Pachystropheus* are common and remains of Temnospondyli are moderately common (Sander et al. 2016; Konietzko-Meier et al. 2019). Much rarer finds belong to Cynodontia, Rhynchocephalia, Phytosauria, Pterosauria and Dinosauria (Sander et al. 2016; pers. obs. PMS).

## Phytosaur osteoderms

From sufficiently articulated skeletons, it is known that phytosaurs had a paramedian row of osteoderms running down the neck (on either side of the sagittal plane, thus two rows) and two dorsal paramedian rows of osteoderms (thus four rows altogether), extending from the trunk to at least the base of the tail (Stocker and Butler 2013). In addition, phytosaurs had a gular shield of osteoderms, protecting the neck region ventrally (Huene 1922; Stocker and Butler 2013). All types of osteoderms appear to have been partially overlapping (Huene 1922). However, because the osteoderms are not connected to the skeleton in phytosaurs, they are often found in isolation (e.g., Huene (1922)). Isolated osteoderms can be assigned to either the paramedian or gular series and to one side of the body, based on patterns of asymmetry. Further information on phytosaur osteoderm morphology is found in Suppl. material 1.

## Extinction - the last phytosaurs

Phytosaurs most likely became extinct some time before or at the Triassic-Jurassic boundary. How far phytosaurs ultimately survived into the Rhaetian or even the Jurassic is still a subject of debate. In their review paper on phytosaurs, Stocker and Butler (2013) somewhat apodictically note that 'At present, the confirmed fossil record of the group extends from late Carnian – latest Rhaetian'. Another view is that very few phytosaurs managed to survive into the Rhaetian in the first place (Lucas 2018). This, amongst other things,

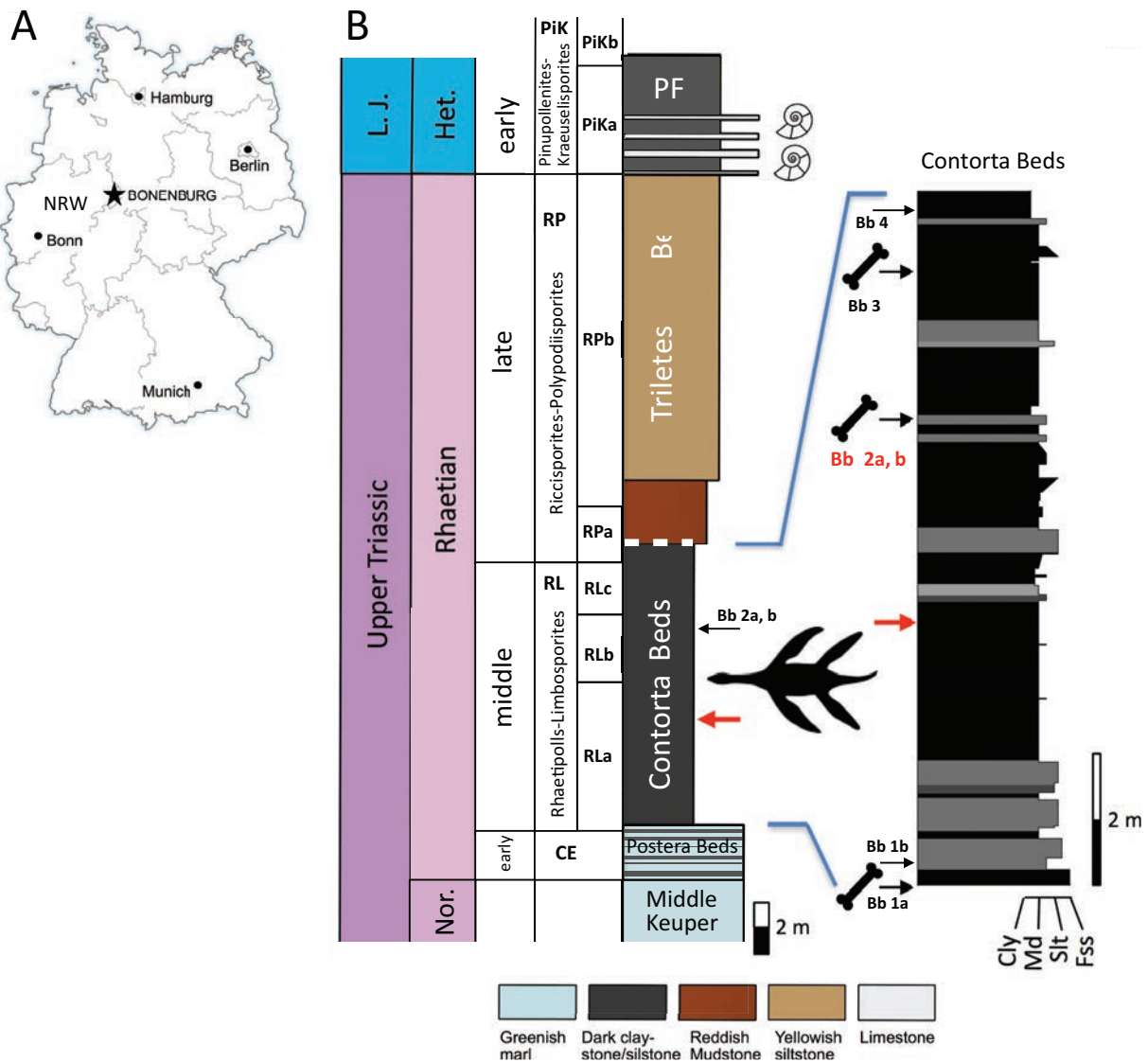


**Figure 1.** Locality and stratigraphy of Bonenburg clay pit #3 of Lücking Brick Company. **A.** Location of the clay pit in the eastern part of the State of North Rhine-Westphalia, Germany; **B.** Simplified stratigraphy of the Norian to Hettangian section exposed at the Bonenburg clay pit, with a special emphasis on the location of the four bone beds and the plesiosaur skeleton in the section. The main part of the section is made up by the Exter Formation which is subdivided into the Postera Beds, Contorta Beds and Triletes Beds, in ascending order. The thick dashed line on top of the Contorta Beds indicates truncation by a low-angle fault. Note that the reddish mudstones above the dashed white line also belong to the Triletes Beds. Colours of the rock types in the main stratigraphic column approximate colours in fresh outcrop. General abbreviations: Bb, bone bed; Cly, claystone; Fss, fine-grained sandstone; Het., Hettangian; L. J., Lower Jurassic; Md, mudstone; Nor., Norian; PF, Pisolententon Formation; Slt, siltstone. Abbreviations of palynozones: CE, *Classopollis-Enzonalasporites* palynozone; RL, *Rhaetipollis-Limbosporites* palynozone; RP, *Riccisporites-Polydidsporites* palynozone; PiK, *Pinuspollenites-Kraeuselisporites* palynozone. Subzones are labelled alphabetically. Modified from Wintrich et al. (2017), palynostratigraphy is from Gravendyck et al. (2020).

led Lucas to conclude for terrestrial tetrapods that ‘There is no compelling evidence of tetrapod mass extinctions at either the Carnian-Norian or the Triassic-Jurassic boundaries’. These diverging statements invite a review of the contender for the ‘last phytosaur’ status and, more generally, of the European record of latest Triassic and earliest Jurassic (if any) phytosaurs (Table 1).

***Machaeroprosozus* from the Wingate Sandstone of Utah**

The phytosaur genus *Machaeroprosozus* (*Redondasaurus*) is known from the Late Triassic of the western

United States (Hunt and Lucas 1993; Lucas 2018; Brownstein 2023). It was first described from the Redonda Formation, the uppermost unit of the Dockum Group (Hunt and Lucas 1993). One specimen of *Machaeroprosozus* (UMNH VP22354), in particular, was noted to be the ‘last phytosaur’ (Lucas et al. 1997) because it was discovered within the Wingate Sandstone of Lisbon Valley, southern Utah (Morales and Ash 1993). The Wingate Sandstone consists of fine-grained eolian sandstones (Martz et al. 2014) and overlies the Church Rock Member, which is the uppermost member of the Chinle Formation (Morales and Ash 1993). It was

**Table 1.** The global record of post-Norian (Rhaetian and Jurassic) phytosaurs, organised by age, youngest occurrences at the top.

Taxon	Collection, Spec. #	Locality	Age	Formation	Material	Remarks	Key references
Phytosauria indet.	?	Hettange-Grande	Hettangian	Bonebed in <i>Angulata</i> Zone	Teeth	May be reworked, may not be phytosaur	Huene and Maubeuge 1954; Buffetaut 1993
? Phytosauria indet.	Various	Southern Germany	Norian to Hettangian	Rhaeto-Liassic Bonebed	Teeth	Teeth named ' <i>Termatosaurus albertii</i> ,' may be sauropterygian.	Maisch and Kapitzke 2010
"cf. <i>Myrstriosuchus</i> "	SMNS	St. Audries Bay, Watchet, UK	Rhaetian to Hettangian	Pre- <i>planorbis</i> Beds, Blue Lias	Rostrum fragment	May be thalattosuchian, not phytosaur	Maisch and Kapitzke 2010
<i>Machaeroprotopus</i> sp.	UMNH VP22354	Lisbon Valley, Utah, USA	Rhaetian (not latest)	Big Indian Rock beds, Wingate Sandstone	Partial skull impression	–	Martz et al. 2014
Phytosauria indet.	WMNM P98442	Bonenburg, Germany	late middle Rhaetian	Upper part of Contorta Beds, middle Exter Formation	Isolated osteoderm	–	This study
<i>Myrstriosuchus</i> sp.	NMB, many	Niederschönthal (today Schönthal, part of Füllinsdorf) near Basel, Switzerland	early to middle Rhaetian	Lower bonebed, Belchen Member of Klettgau Formation	Isolated cranial and postcranial bones, teeth, osteoderms	Huene (1911a, b) called material <i>Myrstriosuchus ruetimeyeri</i> , in Huene (1922) paradigm of <i>Angistorhinops ruetimeyeri</i>	Huene 1911a, b, 1922; Meyer and Wetzel 2021
<i>Myrstriosuchus</i> sp.	MfN MB.R. 2747	Steinlah near Salzgitter, Germany	early Rhaetian	Lower part of Exter Formation	Partial skeleton incl. osteoderms	<i>Angistorhinops ruetimeyeri</i> of Huene. Represents the only substantial Rhaetian phytosaur material from Europe (Jones and Butler 2018)	Schlönbach 1860; Huene 1922; Jones and Butler 2018; Butler et al. 2019; R. Irmis pers. comm.
Phytosauria indet.	MfN MB.R. 4224, 4372.1	Halberstadt, Germany	early Rhaetian	Exter Formation?	Isolated osteoderms	Sculpture similar to Bonenburg osteoderm WMNM P98442	Huene 1922
Phytosauria	MfN, many	Halberstadt, Germany	early Rhaetian	Exter Formation?	Isolated cranial and postcranial bones, teeth, four osteoderms	Contains both "small phytosaur" and <i>Angistorhinops ruetimeyeri</i> of Huene. Some may pertain to <i>Myrstriosuchus</i> sp. nov.	Huene 1922
Phytosauria indet.	Various	UK	early Rhaetian	Rhaetic bone bed	Teeth	–	Storrs 1994; Stocker and Butler 2013; Whiteside and Duffin 2021; Cawthorne et al. 2024
<i>Jupijkam paleofluvialis</i>	Yale Peabody Museum YPM VPPU 7920	Nova Scotia, Canada	late Norian to early Rhaetian	Whitewater Mbr. of Blomidon Fm.	Antorbital skull, single osteoderm	Illustration and description of osteoderm uninformative	Brownstein 2023
Phytosauria indet.	PIMUZ uncat.	Hallau, Switzerland	late Norian to early Rhaetian	Klettgau Formation	Teeth	–	Peyer 1944; Sander 1999; Whiteside et al. 2017
Phytosauria indet.	Institut royal des Sciences naturelles de Belgique uncat.	Saint-Nicolas-de-Port, France	late Norian to early Rhaetian	Grès Infraliasiques Formation	Teeth	–	Cuny 1995; Godefroit and Cuny 1997
Phytosauria indet.	Natural History Museum of Zimbabwe	Zimbabwe	late Norian to early Rhaetian	Tashinga Formation	Mandibular fragments, osteoderms, teeth	Osteoderms surface collected and poorly preserved	Barrett et al. 2020
<i>Myrstriosuchinae</i> indet.	Indian Statistical Institute ISIR276	India	late Norian to Rhaetian	lower Dharmaran Formation	Partial skull	No details given on morphology and age	Datta and Ray 2023
Phytosauria indet.	PIMUZ uncat.	Grisons, Switzerland	late Norian to Rhaetian	Kössen Formation	Dorsal and caudal vertebrae, ilium	–	Furrer 1993, 2023, PMS pers. obs.

previously believed that the Wingate Sandstone was completely Jurassic in age, but later studies suggest that the Wingate encompasses the Triassic-Jurassic boundary, although its exact location within the lower part of the Wingate is not known (Martz et al. 2014). This circumstance makes it difficult to determine the exact age of the 'last phytosaur' find or any other fossil from the basal Big Indian Rock beds of the Wingate. Martz et al. (2014, p.436) conclude that the Big Indian Rock beds are 'probably Rhaetian (though not latest Rhaetian)' in age. Thus, this 'last phytosaur' is no younger than late (but not latest) Rhaetian in age and not Jurassic.

#### cf. *Myrstriosuchus* from the Blue Lias of England

Another contender for the 'last phytosaur' is a rostral fragment assigned to cf. *Myrstriosuchus* (SMNS 55194). This fragment was discovered at St. Audries Bay near Watchet in Somerset, England, in 1986 (Maisch and Kapitzke 2010). It was described as being most comparable to *Myrstriosuchus* in morphology (Maisch and Kapitzke 2010). However, because of the incompleteness of the specimen, the possibility cannot be excluded that the fragment derives from another longirostrine taxon of marine reptile, such as a thalattosuchian crocodylomorph (Maisch and Kapitzke 2010). Arguing against this assignment until recently was

that thalattosuchians were not known from the Hettangian. However, a new Hettangian-Sinemurian teleosaurid (Benani et al. 2023) and an early Pliensbachian stem thalattosuchian (Wilberg et al. 2023) have changed this situation. In fact, Wilberg et al. (2023) provide strong evidence for a Rhaetian or even Norian origin of *Thalattosuchia*, and the rostral fragment from St. Audries Bay thus could pertain to this clade.

The rostral fragment was discovered in-situ within the so-called Pre-*planorbis* Beds, below the first occurrence of *Psiloceras planorbis* (Maisch and Kapitzke 2010). The Pre-*planorbis* Beds are located in the basal part of the Blue Lias Formation (Maisch and Kapitzke 2010). The age estimation was based on dating using ammonites of the genus *Neophyllites* (Maisch and Kapitzke 2010), which seems to indicate the rocks containing the find to be Hettangian in age (Lindström et al. 2017). In other studies, the Triassic/Jurassic boundary was placed within the Pre-*planorbis* Beds (Martin et al. 2015). The debate on the age of the rocks at St. Audries Bay is still ongoing and, thus, is the debate on the age of this potential phytosaur specimen. In fact, in the most recent study (Weedon et al. 2019), the presence of the phytosaur specimen in the beds in question has been used to argue for their Triassic age.

## Aim of the study

The aim of our study is to present clear evidence for the survival of phytosaurs into the late middle Rhaetian, at least in Central Europe, within a million or two years of the end of the Triassic. The evidence is the presence of an unequivocal phytosaur osteoderm found in Bonenburg, Germany. This find would appear to represent the youngest known phytosaur remains, based on clear stratigraphic and morphologic evidence (Table 1).

## Institutional abbreviations

**GPIT**, Paläontologische Sammlungen der Universität Tübingen, Tübingen, Germany; **MCSNB**, Museo Civico di Scienze Naturali di Bergamo, Bergamo, Italy; **MfN**, Museum für Naturkunde, Berlin, Germany; **NMB**, Naturhistorisches Museum Basel, Basel, Switzerland; **PIMUZ**, Paläontologisches Institut und Museum der Universität Zürich, Zurich, Switzerland; **UNMH**, Utah Museum of Natural History, Salt Lake City, USA; **SMNS**, Staatliches Museum für Naturkunde Stuttgart, Stuttgart, Germany; **WMNM**, LWL-Museum für Naturkunde, Münster, Germany.

## Materials and methods

### Materials

The Bonenburg osteoderm WMNM P98442 was found during the annual excavation campaign of the University of Bonn in collaboration with the WMNM at the

Bonenburg clay pit in Bone Bed 2 in 2017. As is typical for the fossils from Bone Bed 2, the osteoderm was found on its own, without any other non-osteodermal bones or similar osteoderms around it.

## Methods

We took size measurements of the osteoderm using dial callipers and documented the morphology of the bone with photographs and interpretive drawings. For comparison, we studied the other published Rhaetian phytosaur material from Europe, in particular MfN MB.R. 2747 from Steinlah, and the Niederschönthal and Halberstadt material (Table 2). In addition, we compared WMNM P98442 to phytosaur osteoderms from the German Middle Keuper at the SMNS and GPIT by personal observation, as well as in the relevant literature. Since the classical genera *Mystriosuchus* and *Nicrosaurus* are the two best known phytosaur genera of the German Keuper (Hungerbühler and Hunt 2000; Hungerbühler 2002; Jones and Butler 2018) and for which osteoderms are well known, we also included those in our research. These two genera are known from the Löwenstein Formation of southern Germany and are middle and late Norian in age (Hungerbühler and Hunt 2000; Hungerbühler 2002; Jones and Butler 2018). Specifically, they are from the middle Stubensandstein, a subunit of the Löwenstein Formation. For understanding the temporal significance of the specimen, it was necessary to compile the stratigraphic range of Rhaetian phytosaurs on a global scale (Table 1).

## Results

### Systematic paleontology

**Archosauriformes Gauthier, Kluge & Rowe, 1988**  
**Phytosauria Jaeger, 1828**

**Phytosauria indet.**

**Material.** One single, slightly damaged left paramedian osteoderm, WMNM P98442.

**Locality and horizon.** Clay pit #3 of Lücking Brick Company, 1 km north of the village of Bonenburg, City of Warburg, North Rhine-Westphalia, Germany (Fig. 1A). The specimen derives from Bone Bed 2 in the dark marine mudstones of the Contorta Beds of the Exter Formation, 7 m in the section above the base of the Contorta Beds and 17.5 m below the Triassic-Jurassic boundary exposed in the pit (Fig. 1B).

**Morphological description.** The external side of the Bonenburg osteoderm WMNM P98442 is extensively sculptured, whereas the internal, or visceral, side is smooth (Fig. 2). The external side is dominated by a rounded ridge or keel, indicating the orientation of the osteoderm relative to the body long axis (Fig. 2A, B). This anteroposterior ridge is offset medially as can be

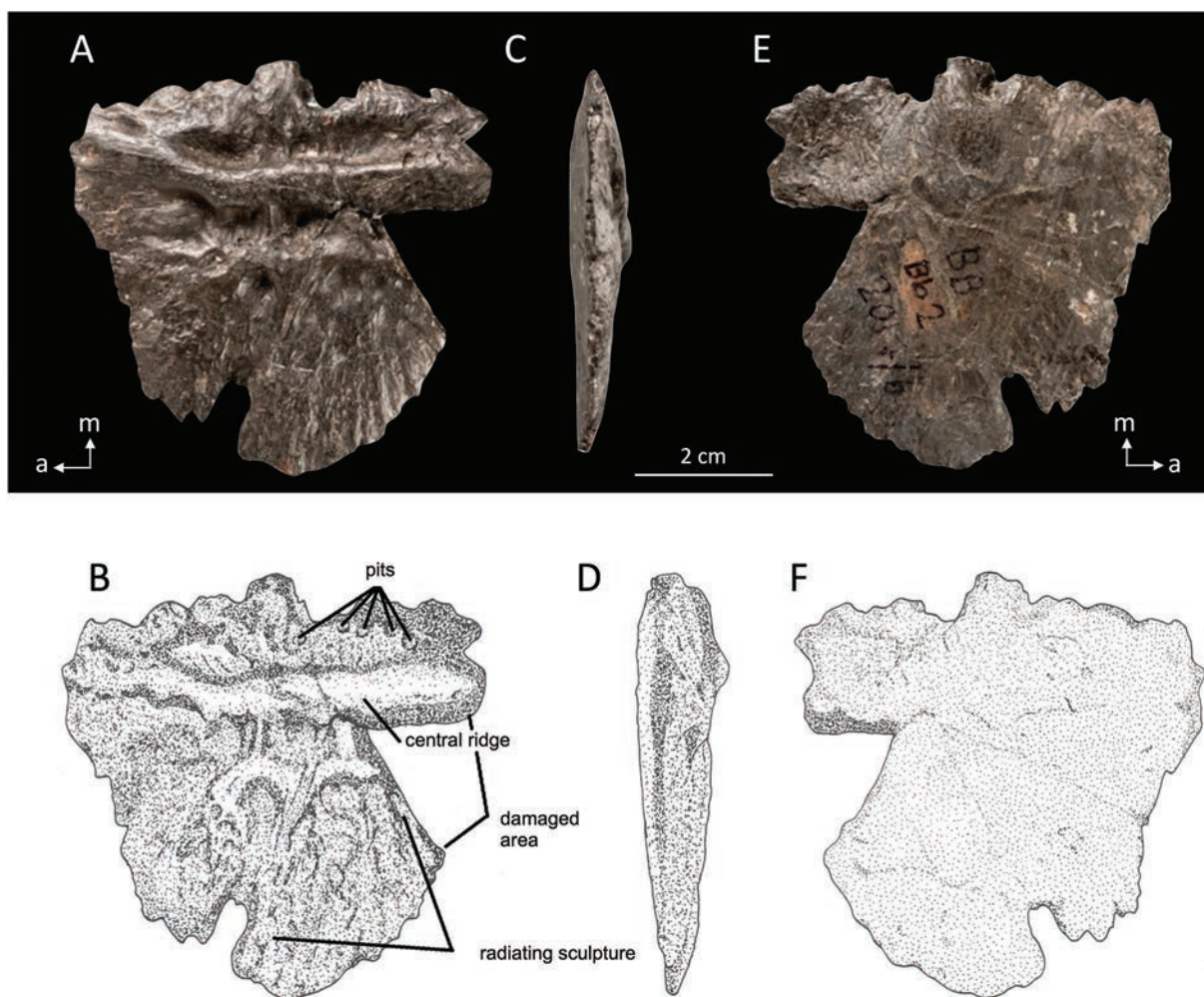


**Figure 2.** Left paramedian phytosaur osteoderm WMNM P98442 from the late middle Rhaetian Bone Bed 2 of the Contorta Beds of the Exter Formation of Bonenburg, North Rhine-Westphalia, Germany. **A, B.** Photograph and drawing of external view showing the typical phytosaur radiating sculpture and the central longitudinal ridge of a paramedian osteoderm. Note that the anterior part (left) is less sculptured and that the ridge does not extend to the anterior edge; **C, D.** Photograph and drawing of anterior view. Note the thinness of the edge which was underlapping the preceding osteoderm; **E, F.** Photograph and drawing of internal view, showing the flat and smooth surface. Abbreviations: a, anterior; m, medial.

seen on articulated phytosaur specimens, providing the medial direction. One end of the ridge extends to the margin of the osteoderm, whereas the other does not. The latter asymmetry indicates anterior because the ridge does not reach the anterior osteoderm margin in phytosaur osteoderms. Together with the asymmetry of the location of the ridge, the location of the anterior margin indicates that the osteoderm is from the left side of the body. The thickness of the osteoderm decreases in anterior and lateral directions (Fig. 2C, D). The osteoderm shows two distinct indentations, one on the lateral and one on the posterior margin (Fig. 2). The latter resulted from damage sustained during discovery. The bone shows no signs of abrasion.

In mediolateral direction, the osteoderm is 62 mm wide and in anteroposterior direction, it is 64 mm long. It shows a maximum thickness of about 13 mm at its centre. Except for the thick ridge, the external sculpture on the osteoderm is of relatively low relief (Fig. 2A, B). Towards lateral, there are some indistinct pits, but there

are no sharp crests or grooves. Only the region medial to the main ridge shows a deep sulcus.

The lateral part of the external surface of the osteoderm, that is not sculptured, shows a radial, fan-like structure on the surface of the bone (Fig. 2A, B). This structure originates in the centre of the bone, right below the middle of the anteroposterior ridge. The fan structure also affects the silhouette of the lateral part of the bone. The internal surface of the osteoderm is completely flat and shows no sculpturing. There are multiple small hole-like structures on the medial part of the external surface of the bone (Fig. 2E, F).

The general morphology of the Bonenburg osteoderm (Fig. 2) fits the description of phytosaur osteoderms in the literature (Huene 1922; Gozzi and Renesto 2003; Scheyer et al. 2014) (Fig. 3). A more detailed investigation of the osteoderms of the Lombardian *Mystriosuchus* specimen MCSNB 10087 (Gozzi and Renesto 2003) and other articulated and osteoderm-bearing phytosaur skeletons might help to further constrain the anatomical position of the Bonenburg osteoderm.

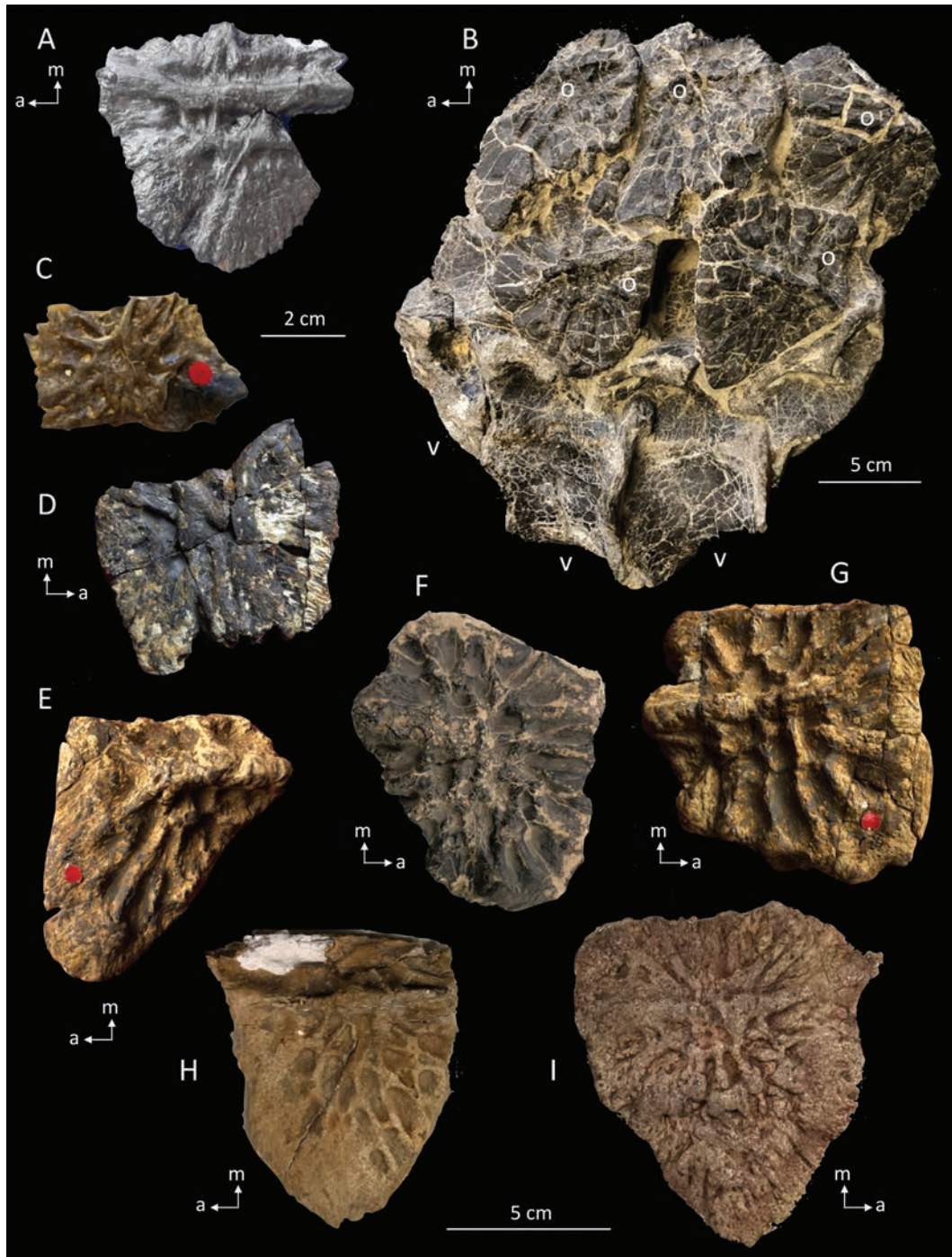


**Figure 3.** Comparison of selected Rhaetian and Norian phytosaur osteoderms in external view. **A.** WMNM P98442, left paramedian osteoderm from the Rhaetian Bone Bed 2, Exter Formation, Bonenburg, Germany. Note the resemblance of sculpture to C and D; **B.** MfN MB.R. 2747, five articulated paramedian osteoderms of the left side in association with anterior dorsal vertebrae of *Myrstriosuchus* sp. (Butler et al. 2019), Exter Formation, Steinlah near Salzgitter, Germany. Note the resemblance of sculpture to F; **C.** Isolated gular osteoderm MfN MB.R. 4224 from the Rhaetian of Halberstadt (Germany) figured by Huene (1922, fig. 112) and assigned to ‘*Angistorhinops ruetimeyeri*’ by him. Note the resemblance of sculpture to A and D; **D.** Isolated left paramedian osteoderm MfN MB.R. 4372.1 from the Rhaetian of Halberstadt, Germany. Note the resemblance of sculpture to A and C; **E.** Isolated left paramedian caudal osteoderm MfN MB.R. 4374.1 from the Rhaetian of Halberstadt (Germany) figured by Huene (1922, fig. 87) and assigned by him to a small indeterminate phytosaur; **F.** Right paramedian osteoderm NHMB N. B. 14 of ‘*Angistorhinops ruetimeyeri*’ from the Rhaetian bone bed of Niederschönthal (northern Switzerland) figured by Huene (1911b, Pl. VIII, fig. 2). Note the resemblance of sculpture to B; **G.** Right paramedian osteoderm MfN MB.R. 4219 from the Rhaetian of Halberstadt (Germany) figured by Huene (1922, fig. 113) and assigned to ‘*Angistorhinops ruetimeyeri*’ by him; **H.** Left paramedian osteoderm SMNS uncatalogued of *Myrstriosuchus* sp. from the middle Norian Stubensandstein of Aixheim, southwestern Germany; **I.** Right paramedian osteoderm SMNS 4063/7 of *Nicrosaurus kapffi* from the middle Norian Stubensandstein of Heslach near Stuttgart, south-western Germany. Abbreviations: a, anterior; m, medial; o, osteoderm; v, vertebra.

**Table 2.** Rhaetian phytosaur osteoderms from Europe personally examined in this study, organised by age, youngest occurrences at the top.

Taxon	Collection, Spec. #	Locality	Age	Formation	Osteoderm Material	Other Material	Remarks	Key references
Phytosauria indet.	WMNM P98442	Bonenburg, Germany	late middle Rhaetian	upper Contorta Beds, middle Exter Formation	Isolated osteoderm	–	–	This study
<i>Mystriosuchus</i> sp.	NMB N. B. 14, N. B. 15, N. B. 31, N. B. 644, N. B. uncat. excavation Strübin 1901	Niederschönthal (today Schönthal, part of Füllinsdorf) near Basel, Switzerland	early to middle Rhaetian	lower bonebed, Belchen Member of Klettgau Formation	Isolated osteoderms	Isolated cranial and postcranial bones, teeth	Huene (1911a, b) called material <i>Mystriosuchus ruetimeyeri</i> , in Huene (1922), hypodigm of <i>Angistorhinops ruetimeyeri</i>	Huene 1911a, b, 1922; Meyer and Wetzel 2021
<i>Mystriosuchus</i> sp.	MB.R. 2747	Steinlah near Salzgitter, Germany	early Rhaetian	lower Exter Formation	Osteoderms with ant. dorsal column	Partial skeleton	<i>Angistorhinops ruetimeyeri</i> of Huene. Represents the only substantial Rhaetian phytosaur material from Europe (Jones and Butler 2018)	Schlönbach 1860; Huene 1922; Jones and Butler 2018; Butler et al. 2019; R. Irmis pers. comm.
Phytosauria indet.	MfN MB.R. 4224, 4372.1	Halberstadt, Germany	early Rhaetian	Exter Formation?	Isolated osteoderms	–	Sculpture similar to Bonenburg osteoderm WMNM P98442	Huene 1922
Phytosauria indet.	MfN MB.R. 4219, 4369.1, 4371.1, 4373.1, 4374.1, 4375.1, 4376.1, 4377.1, 4383.1-2, 4391.1-5	Halberstadt, Germany	early Rhaetian	Exter Formation?	Isolated osteoderms	Isolated cranial and postcranial bones, teeth	Contains both “small phytosaur” and <i>Angistorhinops ruetimeyeri</i> of Huene. Some may pertain to <i>Mystriosuchus</i> sp. nov.	Huene 1922

## Discussion

### Comparisons with skeletally associated phytosaur osteoderms from Europe

#### Rhaetian MfN MB.R. 2747, *Mystriosuchus* sp.

The only skeleton close in age to the Bonenburg find bearing osteoderms is specimen MfN MB.R. 2747, assigned to *Mystriosuchus* sp., from Steinlah near Salzgitter, northern Germany (Tables 1, 2). See also the review of European Rhaetian phytosaurs in Suppl. material 1.

The osteoderms of MfN MB.R. 2747 (Fig. 3B) are from the dorsal region, with representation from all four paramedian rows, as already noted by von Huene (1922). The preservation of the bone of MfN MB.R. 2747 with its black colour and heavy diagenetic cracking makes discerning sculpture somewhat difficult (Fig. 3B). Compared to the Bonenburg osteoderm (Fig. 3A), the osteoderms of MfN MB.R. 2747 are much larger and thicker and have a much coarser sculpture than WMNM P98442 (Fig. 3B). They are clearly not from the same phytosaur taxon.

#### Middle Keuper (Norian) phytosaurs from Germany

There is only one Middle Keuper phytosaur skeleton, SMNS 10260, with associated osteoderms. SMNS 10260 is the anterior half of a skeleton of *Mystriosuchus planirostris*, currently on display at the SMNS. However, note that the complete skull SMNS 13007 was used to replace the partial skull of SMNS 10260 in the display. Osteoderms are still attached to the throat region of the SMNS 10260. Numerous isolated *Mystriosuchus planirostris* osteoderms are also preserved in the SMNS collections (Fig. 3H). None of these osteoderms resembles the Bonenburg osteoderm (Fig. 3A) because their sculpture mainly consists of elongate, radially arranged pits separated by thin ridges and a regularly crenelated margin (Huene 1922, fig. 1; pers. obs. PMS).

A potential second case of association consists of a skull and a single osteoderm from the Stubensandstein of Pfaffenhofen, Baden-Württemberg, both bearing the accession number SMNS 12593. The skull is the holotype of *Nicrosaurus meyeri*. However, Hungerbühler (1998: 146) notes that there are no postcrania with *N. meyeri*, contradicting the label accompanying the osteoderm. The sediment attached to the osteoderm vs. the skull in SMNS 12593 suggests that they came from two different horizons (Rainer Schoch, pers. comm. 2023). Interestingly, though, the sculpture of dermal skull bones of SMNS 12593 and that of the osteoderm match. Similarly, the dermal skull bone sculpture and osteoderm sculpture (Fig. 3I) match in fossils labelled as *Nicrosaurus kapffi* in the SMNS collections. None of the Middle Keuper osteoderms (Fig. 3H, I) resembles the Bonenburg osteoderms (Fig. 3A) in shape and sculpture.

#### Alpine Norian phytosaurs

Records from the Alps are also older than the Bonenburg specimen. Important phytosaur material with associated osteoderms comes from the marine successions of the southern Alps, specifically from the middle Norian Zorzino Limestone (Renesto and Paganoni 1998; Gozzi and Renesto 2003) near Bergamo, northern Italy. The articulated skeleton MCSNB 10087, assigned to the Middle Keuper species *Mystriosuchus planirostris* (Gozzi and Renesto 2003; but see Butler et al. (2019, p. 205)), preserves at least 19 paramedian osteoderms in two regions close to their original location. Gozzi and Renesto (2003) describe two types of osteoderms which differ in shape and sculpturing. The first type is from the medial paramedian rows of the trunk and is oval. The sculpture on its external surface radiates out from the ridge at the centre of the bone. There is no great mediolateral asymmetry (Gozzi and Renesto 2003, fig. 15A; pers. obs. PMS). The second type of osteoderm has a sub-pentagonal to triangular outline and forms the lateral paramedian

row which continues on to the proximal region of the tail, whereas the medial row is restricted to the trunk (Gozzi and Renesto 2003). The sculpturing of these osteoderms is concentrated on the medial part, close to the medially placed anteroposterior ridge (Gozzi and Renesto 2003, fig. 15B; pers. obs. PMS). The asymmetry of this second type of osteoderm is thus similar to WMNM P98442 (Fig. 2A, B). However, the sculpture of the osteoderms of MCSNB 10087 agrees with that of the same species from the Middle Keuper (Fig. 3H), as exemplified by SMNS 10260 and not with the Bonenburg osteoderm (Fig. 3A).

A mass accumulation of *Mystriosuchus steinbergeri* Butler et al. 2019 from the middle Norian marine Dachsteinkalk of the Austrian Alps also includes an osteoderm associated with one of the skulls (Butler et al. 2019). This osteoderm is roughly triangular and shows little sculpture on its outer surface (Butler et al. 2019, figs 15E, F). The bone is roughly of the same size as the Bonenburg osteoderm, but does not offer a good match in terms of sculpture. However, it also appears to be poorly preserved.

## Comparison with isolated Upper Keuper (Rhaetian) osteoderms

### Osteoderms from Niederschönthal, Switzerland

The osteoderms from the Rhaetian bone bed collection from Niederschönthal at the NMB (Table 2) are large to very large and their sculpture (Fig. 3F) does not match with the Bonenburg osteoderm (Fig. 3A). Instead, the size and sculpture of the Niederschönthal osteoderms is rather similar to those of the Steinlah phytosaur MfN MB.R. 2747. Although assignment to the same taxon is hampered by the insufficient understanding of phytosaur osteoderm morphology, the hypothesis of von Huene (1922) of taxonomic identity MfN MB.R. 2747 and the Niederschönthal osteoderms appears plausible from the perspective of osteoderm morphology, but the Bonenburg specimen clearly represents a different taxon.

### Osteoderms from Halberstadt, Central Germany

Huene (1922) assigned skeletal (non-osteoderm) phytosaur material from Halberstadt to a large phytosaur (*A. ruetimeyeri*) and to a small, unnamed taxon (Table 2). In addition, he assigned some isolated osteoderms from the locality to either of these taxa, however, without providing arguments for his assignment beyond size and general resemblance (or lack thereof) to the Steinlah phytosaur MfN MB.R. 2747.

We concur with Huene (1922) that the robust sculpture of most Halberstadt osteoderms is similar to the large osteoderms associated with MfN MB.R. 2747 and the large isolated osteoderms from Niederschönthal. Huene (1922) explicitly included two osteoderms, MfN MB.R. 4373.1 and MfN MB.R. 4374.1 (Fig. 3E), with the smaller unnamed phytosaur. However, the Bonenburg osteoderm

(Fig. 3A) also differs in sculpture and size from those two Halberstadt ones.

On the other hand, one small osteoderm (MfN MB.R. 4224, Fig. 3C) from Halberstadt resembles the Bonenburg one (Fig. 3A) despite being a gular osteoderm and not a paramedian one. The two osteoderms share a similar sculpture and a characteristic frayed margin with bone spicules extending into the former soft skin. Von Huene had already described this feature as ‘*Rand gezackt*’ (jagged edge). Another Halberstadt osteoderm, MfN MB.R. 4372.1, also shows this feature and a similar sculpture (Fig. 3D).

To sum it up, the Bonenburg osteoderm offers a poor match with any named European phytosaur taxon and differs clearly from most other Rhaetian European osteoderms (Fig. 3). Morphological diversity of Rhaetian osteoderms, thus, is consistent with the existence of at least two, if not three, phytosaur taxa during this time period in Europe.

## Comparison with non-European Rhaetian osteoderms

### Osteoderm of *Jupijkam*

There are two reports of probably Rhaetian phytosaur osteoderms from outside Europe. One is a single paramedian osteoderm which is part of the hypodigm of the newly-described mystriosuchine phytosaur *Jupijkam paleofluvialis* (Brownstein 2023) from Nova Scotia, Canada. The fossil is from the upper part of the Whitewater Member of the Blomidon Formation, making it most likely early Rhaetian in age (Brownstein 2023, fig. 1). However, the external sculpture of this osteoderm appears relatively featureless and the illustration (Brownstein 2023, fig. 6) does not allow for a meaningful comparison with the European osteoderms.

Paleogeographically, the find is closest in paleolatitude to the Moroccan osteoderms, well south of the European Keuper phytosaur occurrences and far south of the Lithuanian and Greenland occurrences (Brusatte et al. 2013). This fact makes the statement of Brownstein (2013) that *Jupijkam* represents the northernmost occurrence of Phytosauria puzzling.

### Indeterminate osteoderms from Zimbabwe

Barrett et al. (2020) describe various remains of taxonomically indeterminate phytosaurs from the Tashinga Formation of Zimbabwe. The upper part of this formation is late Norian to early Rhaetian in age, based in part on a radiometric date of 209.4 ± 4.5 Ma from a horizon 7.5 m below a phytosaur-bearing horizon (Barrett et al. 2020, fig. 9). The surface-collected phytosaur remains include seven isolated osteoderm fragments (Barrett et al. 2020). The preservation of these osteoderms, as illustrated by Barrett et al. (2020, fig. 9), is insufficient for a meaningful comparison with the European osteoderms (Fig. 3).

## The Bonenburg osteoderm and phytosaur extinction

### Possible reworking

The importance of the Bonenburg osteoderm for the debate on phytosaur extinction hinges on the assumption that the specimen is not reworked from older beds. This is a natural concern in bone beds which certainly are time-averaged. The possibility of reworking has been raised for another specimen from Bone Bed 2 of Bonenburg before (Konietzko-Meier et al. 2019), the humerus of cf. *Cyclotosaurus*, a large temnospondyl amphibian. As in the case of this humerus, the Bonenburg osteoderm is well preserved and not abraded (Fig. 2) and does not differ in appearance from the other bones in the deposit. Although we currently cannot exclude the possibility of reworking, there is no positive evidence for this process, either.

### Rarity of phytosaur remains in Bonenburg

The rarity of phytosaur remains (the single osteoderm) compared to other vertebrates (Sander et al. 2016; see above) in the Bonenburg bone bed is noteworthy. In particular, the complete lack of phytosaur teeth at Bonenburg is striking, given that teeth are abundant in other Rhaetian European bone beds (Table 1). Taken at face value, the rarity could be interpreted as indicating a decline of phytosaurs by the late middle Rhaetian. However, phytosaurs are not the only faunal element of extreme rarity at Bonenburg and an environmental explanation is equally likely (Suppl. material 1).

## Conclusions

During the 2017 excavation campaign in the Rhaetian bone beds at the Bonenburg clay pit in North Rhine-Westphalia, Germany, a phytosaur osteoderm was found. The host unit of the bone beds are the fine-grained dark clastics of the Contorta Beds of the Exter Formation. The bone bed from which the osteoderm derives, Bone Bed 2, is dated palynologically with high precision (Gravendyck et al. 2020) as late middle Rhaetian.

The osteoderm from Bonenburg is most definitely phytosaurian in origin and pertains to the dorsal paramedian osteoderm rows. However, the osteoderm currently cannot be assigned to a named taxon. This possibly could be rectified by further comparative morphological research, including quantitative approaches and machine-learning, on phytosaur osteoderms aimed at refining the current descriptive terminology, especially of the outer sculpture or ornamentation.

The Bonenburg find indicates the survival of phytosaurs into the late middle Rhaetian, at most two million years before the end of the Triassic. The osteoderm currently is the youngest well-dated evidence for

phytosaurs and, thus, currently lays claim to being ‘the last phytosaur’. Of the other two contenders to this ‘title’, one is not precisely dated and the other may not be a phytosaur. However, that phytosaurs were still thriving a few million years before the end of the Triassic is also suggested by the large body size of the Steinlah phytosaur *Mystriosuchus* sp. (Jones and Butler 2018) and the improved dating of the Rhaetian phytosaur finds from Switzerland (Meyer and Wetzel 2021) and northern Germany. It thus appears likely that phytosaurs fell victim to the end-Triassic extinction event, inconsistent with the view of Lucas (2018) of their gradual extinction in the Late Triassic.

## Acknowledgements

This paper arose from the Bachelor’s thesis of the second author who also executed the drawings in Fig. 2. Despite the small, single fossil this study is based on, so many people contributed to its completion, for which we are very grateful. Tanja Wintrich (University of Bonn, Germany) led the 2017 excavation campaign during which the osteoderm specimen was recovered and we thank her and all the students who participated in the excavation. Citizen scientist Michael Mertens (Schwaney, Germany) supported us as always with locating the bone beds and providing geological information. Olaf Dülfer (University of Bonn, Germany) is thanked for support in the preparation lab and Achim Schwermann (WMNM) is thanked for curatorial support. Rainer Schoch (SMNS) provided access to phytosaur material kept at the SMNS, as did Walter Etter at NHMB and Daniela Schwarz and Oliver Hampe at the MfN. Oliver Hampe also provided a photograph of MfN MB.R. 4224. We thank Dorota Konietzko-Meier and Andrea Prino (University of Bonn, Germany) for discussion on temnospondyl dermal bone. Rainer Schoch was knowledgeable in all questions regarding phytosaurs. The specimen photographs of the Bonenburg osteoderm were taken by Georg Oleschinski (University of Bonn, Germany). We thank Jelle Heijne (University of Bonn, Germany) for photographs of the phytosaur osteoderm collection at GPIT and Alessandro Lania (University of Bonn, Germany) for taking photographs of the osteoderms of the *Mystriosuchus* skeleton MCSNB 10087. These photos clarified the contradiction between the text and the caption of figure 15 in Gozzi and Renesto (2003). Generous funding for the annual Bonenburg excavation campaigns was provided by the Heritage Development Program of the state of NRW through the administrative support of Achim Schwermann (WMNM). This work would not have been possible without the unfaltering and generous support of the owner and operator of the Bonenburg clay pit, August Lücking Ziegelwerke GmbH and Co KG, and especially its CEO, Joachim Thater. We thank Mike Benton (University of Bristol) and an anonymous reviewer for the very helpful reviews of earlier versions of this work.

## References

- Barrett PM, Sciscio L, Viglietti PA, Broderick TJ, Suarez CA, Sharman GR, Jones AS, Munyikwa D, Edwards SF, Chapelle KEJ, Dollman KN, Zondo M, Choiniere JN (2020) The age of the Tashinga Formation (Karoo Supergroup) in the Mid-Zambezi Basin, Zimbabwe and the first phytosaur from mainland sub-Saharan Africa. *Gondwana Research* 81: 445–460. <https://doi.org/10.1016/j.gr.2019.12.008>
- Barth G, Franz M, Heunisch C, Ernst W, Zimmermann J, Wolfgramm M (2018) Marine and terrestrial sedimentation across the T–J transition in the North German Basin. *Palaeogeography, Palaeoclimatology, Palaeoecology* 489: 74–94. <https://doi.org/10.1016/j.palaeo.2017.09.029>
- Benani H, Nehili A, Ouzzaoui LA, Jouve S, Boudad L, Masrouf M, Jalil N, Arrad TY (2023) Discovery of the teleosauroid crocodylomorph from the Early Jurassic of Chaara cave, Middle Atlas of Morocco. *Journal of African Earth Sciences* 198: 104804. <https://doi.org/10.1016/j.jafrearsci.2022.104804>
- Brownstein CD (2023) A late-surviving phytosaur from the northern Atlantic rift reveals climate constraints on Triassic reptile biogeography. *BMC Ecology and Evolution* 23: 33. <https://doi.org/10.1186/s12862-023-02136-8>
- Brusatte SL, Butler RJ, Niedzwiedzki G, Sulej T, Bronowicz R, Satkunas J (2013) First record of Mesozoic terrestrial vertebrates from Lithuania: phytosaurs (Diapsida: Archosauriformes) of probable Late Triassic age, with a review of phytosaur biogeography. *Geological Magazine* 150: 110–122. <https://doi.org/10.1017/S0016756812000428>
- Buffetaut E (1993) Phytosaurs in time and space. *Paleontologia Lombarda, Nuova Serie* 2: 39–44.
- Butler RJ, Jones AS, Buffetaut E, Mandl GW, Scheyer TM, Schultz O (2019) Description and phylogenetic placement of a new marine species of phytosaur (Archosauriformes: Phytosauria) from the Late Triassic of Austria. *Zoological Journal of the Linnean Society* 187: 198–228. <https://doi.org/10.1093/zoolinnean/zlz014>
- Cawthorne M, Whiteside DI, Benton MJ (2024) Latest Triassic terrestrial microvertebrate assemblages from caves on the Mendip palaeoisland, S.W. England, at Emborough, Batscombe and Highcroft Quarries. *Proceedings of the Geologists' Association* 135(1): 105–130. <https://doi.org/10.1016/j.pgeola.2023.12.003>
- Cuny G (1995) French vertebrate faunas and the Triassic–Jurassic boundary. *Palaeogeography, Palaeoclimatology, Palaeoecology* 119: 343–358. [https://doi.org/10.1016/0031-0182\(95\)00017-8](https://doi.org/10.1016/0031-0182(95)00017-8)
- Datta D, Ray S (2023) A giant phytosaur (Diapsida, Archosauria) from the Upper Triassic of India with new insights on phytosaur migration, endemism and extinction. *Papers in Palaeontology* 9: e1476. <https://doi.org/10.1002/spp2.1476>
- Furrer H (1993) *Stratigraphie und Facies der Trias/Jura-Grenzsichten in den oberostalpinen Decken Graubündens*. Dissertation. University of Zurich, Zurich, 114 pp.
- Furrer H (2023) *Meeresgiganten aus der obersten Trias der Schweizer Ostalpen*. *Fossilien* 40: 51–57.
- Godefroit P, Cuny G (1997) Archosauriform teeth from the Upper Triassic of Saint-Nicolas-de-Port (northeastern France). *Palaeovertebrata* 26: 1–34.
- Gauthier J, Kluge AG, Rowe T (1988) The early evolution of Amniota. In: Benton MJ (Ed.) *The Phylogeny and Classification of the Tetrapods, Volume 1: Amphibians, Reptiles, Birds*. Clarendon Press, Oxford, 103–155.
- Gozzi E, Renesto S (2003) A complete specimen of *Mystriosuchus* (Reptilia, Phytosauria) from the Norian (Late Triassic) of Lombardy (Northern Italy). *Rivista Italiana di Paleontologia e Stratigrafia* 109: 475–498.
- Gravendyck J, Schobben M, Bachelier JB, Kürschner WM (2020) Macroecological patterns of the terrestrial vegetation history during the end-Triassic biotic crisis in the central European Basin: A palynological study of the Bonenburg section (NW-Germany) and its supra-regional implications. *Global and Planetary Change* 194: 103286. <https://doi.org/10.1016/j.gloplacha.2020.103286>
- Huene Fv (1911a) *Die jungtriassische Wirbeltierfauna von Niederschönthal bei Basel*. *Centralblatt für Mineralogie, Geologie und Paläontologie* 1911: 422–424.
- Huene Fv (1911b) *Beiträge zur Kenntnis und Beurteilung der Parasuchier*. *Geologische und Paläontologische Abhandlungen, Neue Folge* 10: 67–121.
- Huene Fv (1922) *Neue Beiträge zur Kenntnis der Parasuchier*. *Jahrbuch der Preussischen Geologischen Landesanstalt* 42: 59–160.
- Huene Fv, Maubeuge PL (1954) *Sur quelques restes de sauriens du Rhétien et du Jurassique lorrains*. *Bulletin de la Société Géologique de France, Series 6* 4: 105–109. <https://doi.org/10.2113/gssgfbull.S6-IV.1-3.105>
- Hungerbühler A (1998) *Cranial anatomy and diversity of the Norian phytosaurs from southwest Germany*. Unpublished PhD thesis. University of Bristol, Bristol, 465 pp.
- Hungerbühler A (2002) The Late Triassic phytosaur *Mystriosuchus westphali*, with a revision of the genus. *Palaeontology* 45: 377–418. <https://doi.org/10.1111/1475-4983.00242>
- Hungerbühler A, Hunt AP (2000) Two new phytosaur species (Archosauria, Crurotarsi) from the Upper Triassic of Southwest Germany. *Neues Jahrbuch für Geologie und Paläontologie, Monatshefte* 2000: 467–484. <https://doi.org/10.1127/njgpm/2000/2000/467>
- Hunt AP (1989) Cranial morphology and ecology among phytosaurs. In: Lucas SG, Hunt AP (Eds) *Dawn of the Age of Dinosaurs in the American Southwest*. New Mexico Museum of Natural History, Albuquerque, 349–354.
- Hunt AP, Lucas SG (1993) A new phytosaur (Reptilia: Archosauria) genus from the uppermost Triassic of the western United States and its biochronological significance. *New Mexico Museum of Natural History and Science Bulletin* 3: 193–196.
- Jäger GF (1828) *Über die fossilen Reptilien, welche in Würtemberg aufgefunden worden sind*. Metzler, Stuttgart, 48 pp. <https://doi.org/10.5962/bhl.title.4689>
- Jones AS, Butler RJ (2018) A new phylogenetic analysis of Phytosauria (Archosauria: Pseudosuchia) with the application of continuous and geometric morphometric character coding. *PeerJ* 6: e5901. <https://doi.org/10.7717/peerj.5901>
- Konietzko-Meier D, Werner JD, Wintrich T, Sander PM (2019) A large temnospondyl humerus from the Rhaetian (Late Triassic) of Bonenburg (Westphalia, Germany) and its implications for temnospondyl extinction. *Journal of Iberian Geology* 45: 287–300. <https://doi.org/10.1007/s41513-018-0092-0>
- Kozur HW, Weems RE (2010) *The biostratigraphic importance of conchostracans in the continental Triassic of the northern hemisphere*. Geological Society, London, Special Publications 334: 315–417. <https://doi.org/10.1144/SP334.13>
- Lindström S, van de Schootbrugge B, Hansen KH, Pedersen GK, Alsen P, Thibault N, Dybkjær K, Bjerrum CJ, Nielsen LH (2017) A new correlation of Triassic–Jurassic boundary successions in NW Europe, Nevada and Peru, and the Central Atlantic Magmatic

- Province: A time-line for the end-Triassic mass extinction. *Palaeogeography, Palaeoclimatology, Palaeoecology* 478: 80–102. <https://doi.org/10.1016/j.palaeo.2016.12.025>
- Lucas SG (2018) Late Triassic terrestrial tetrapods: Biostratigraphy, biochronology and biotic events. In: Tanner LH (Ed.) *The Late Triassic World: Earth in a Time of Transition*. Springer International Publishing, Cham, 351–405. [https://doi.org/10.1007/978-3-319-68009-5\\_10](https://doi.org/10.1007/978-3-319-68009-5_10)
- Lucas SG, Heckert AB, Anderson OJ, Estep JW (1997) Phytosaur from the Wingate Sandstone in southeastern Utah and the Triassic-Jurassic boundary on the Colorado Plateau. In: *Southwest Paleontological Symposium Proceedings V 1*. Southwest Paleontological Society and Mesa Southwest Museum, Mesa, Arizona, 49–59.
- Maisch MW, Kapitzke M (2010) A presumably marine phytosaur (Reptilia: Archosauria) from the pre-planorbis beds (Hettangian) of England. *Neues Jahrbuch für Geologie und Paläontologie - Abhandlungen* 257: 373–379. <https://doi.org/10.1127/0077-7749/2010/0076>
- Martin JE, Vincent P, Suan G, Sharpe T, Hodges P, Williams M, Howells C, Fischer V (2015) A mysterious giant ichthyosaur from the lowermost Jurassic of Wales. *Acta Palaeontologica Polonica* 60: 837–842. <https://doi.org/10.4202/app.00062.2014>
- Martz J, Irmis R, Milner A (2014) Lithostratigraphy and biostratigraphy of the Chinle Formation (Upper Triassic) in southern Lisbon Valley, southeastern Utah. In: MacLean JS, Biek RF, Huntoon JE (Eds) *Geology of Utah's Far South*. Utah Geological Association Publication, Salt Lake City, 396–448.
- Meyer CA, Wetzel A (2021) Lebensspuren fossiler See- und Schlangensterne aus der Klettgau-Formation (Belchen-Member, Rhät) des Kantons Basel-Landschaft. *Mitteilungen der Naturforschenden Gesellschaften beider Basel* 20: 3–12.
- Morales M, Ash SR (1993) The last phytosaurs? *New Mexico Museum of Natural History and Science Bulletin* 3: 357–358.
- Ogg JG, Chen ZQ, Orchard MJ, Jiang HS (2020) Chapter 25 - The Triassic Period. In: Gradstein FM, Ogg JG, Schmitz MD, Ogg GM (Eds) *Geologic Time Scale 2020*. Elsevier, Amsterdam, 903–953. <https://doi.org/10.1016/B978-0-12-824360-2.00025-5>
- Peyer B (1944) Über Wirbeltierfunde aus dem Rhät von Hallau. *Eclogae geologicae Helveticae* 36: 260–263.
- Renesto S (2008) Remains of a juvenile phytosaur from the Late Triassic of northern Italy. *Rivista Italiana di Paleontologia e Stratigrafia* 114: 155–160.
- Renesto S, Paganoni A (1998) A phytosaur skull from the Norian (Late Triassic) of Lombardy (northern Italy). *Rivista Italiana di Paleontologia e Stratigrafia* 104: 115–121.
- Sander PM (1999) The microstructure of reptilian tooth enamel: terminology, function, and phylogeny. *Münchener geowissenschaftliche Abhandlungen* 38: 1–102.
- Sander PM, Wintrich T, Schwermann AH, Kindlimann R (2016) Die paläontologische Grabung in der Rhät-Lias-Tongrube der Fa. Lücking bei Warburg-Bonenburg (Kr. Höxter) im Frühjahr 2015. *Geologie und Paläontologie in Westfalen* 88: 11–37.
- Scheyer TM, Desojo JB, Cerda IA (2014) Bone histology of phytosaur, aetosaur, and other achosauriform osteoderms (Eureptilia, Archosauriformes). *The Anatomical Record* 297: 240–260. <https://doi.org/10.1002/ar.22849>
- Schlönbach A (1860) Das Bonebed und seine Lage gegen den sogenannten Obern Keupersandstein im Hannover'schen. *Neues Jahrbuch für Mineralogie, Geologie und Paläontologie* 1860: 513–534.
- Schobben M, Gravendyck J, Mangels F, Struck U, Bussert R, Kürschner WM, Korn D, Sander PM, Aberhan M (2019) A comparative study of total organic carbon- $\delta^{13}\text{C}$  signatures in the Triassic–Jurassic transitional beds of the Central European Basin and western Tethys shelf seas. *Newsletter on Stratigraphy* 2019: 1–25. <https://doi.org/10.1127/nos/2019/0499>
- Stocker MR, Butler RJ (2013) *Phytosauria*. Geological Society, London, Special Publications 379: 91–117. <https://doi.org/10.1144/SP379.5>
- Storrs GW (1994) Fossil vertebrate faunas of the British Rhaetian. *Zoological Journal of the Linnean Society* 112: 217–259. <https://doi.org/10.1111/j.1096-3642.1994.tb00319.x>
- Weedon GP, Page KN, Jenkyns HC (2018) Cyclostratigraphy, stratigraphic gaps and the duration of the Hettangian Stage (Jurassic): insights from the Blue Lias Formation of southern Britain. *Geological Magazine* 156: 1469–1509. <https://doi.org/10.1017/S0016756818000808>
- Whiteside DI, Duffin CJ (2021) New haramiyidan and reptile fossils from a Rhaetian bedded sequence close to the famous 'Microlestes' Quarry of Holwell, UK. *Proceedings of the Geologists' Association* 132: 34–49. <https://doi.org/10.1016/j.pgeola.2020.09.003>
- Wilberg EW, Godoy PL, Griffiths EF, Turner AH, Benson RBJ (2023) A new early diverging thalattosuchian (Crocodylomorpha) from the Early Jurassic (Pliensbachian) of Dorset, U.K. and implications for the origin and evolution of the group. *Journal of Vertebrate Paleontology* 42: e2161909. <https://doi.org/10.1080/02724634.2022.2161909>
- Williams H, Duffin CJ, Hildebrandt C, Parker A, Hutchinson D, Benton MJ (2022) Microvertebrates from the Rhaetian bone beds at Westbury Garden Cliff, near Gloucester, UK. *Proceedings of the Geologists' Association* 133: 119–136. <https://doi.org/10.1016/j.pgeola.2022.01.002>
- Wintrich T, Hayashi S, Houssaye A, Nakajima Y, Sander PM (2017) A Triassic plesiosaurian skeleton and bone histology inform on evolution of a unique body plan. *Sciences Advances* 3: e1701144. <https://doi.org/10.1126/sciadv.1701144>

## Supplementary material 1

### Description of phytosaur osteoderm morphology and discussion of phytosaur rarity at Bonenburg

Authors: P. Martin Sander, Paul W. Wellnitz

Data type: docx

Copyright notice: This dataset is made available under the Open Database License (<http://opendatacommons.org/licenses/odbl/1.0>). The Open Database License (ODbL) is a license agreement intended to allow users to freely share, modify, and use this Dataset while maintaining this same freedom for others, provided that the original source and author(s) are credited.

Link: <https://doi.org/10.3897/fr.27.114601.suppl1>

# Roots of the European Cenozoic ecosystems: lizards from the Paleocene (~MP 5) of Walbeck in Germany

Andrej Čerňanský<sup>1</sup>, Davit Vasilyan<sup>2,3</sup>

<sup>1</sup> Department of Ecology, Laboratory of Evolutionary Biology, Faculty of Natural Sciences, Comenius University in Bratislava, Mlynská dolina, Ilkovičova 6, 842 15 Bratislava, Slovakia

<sup>2</sup> JURASSICA Museum, Route de Fontenais 21, 2900 Porrentruy, Switzerland

<sup>3</sup> Department of Geosciences, University of Fribourg, Chemin du musée 6, 1700, Fribourg, Switzerland

<https://zoobank.org/66166492-B0A7-4887-B51A-42361B1C9FC2>

Corresponding author: Andrej Čerňanský ([cernansky.paleontology@gmail.com](mailto:cernansky.paleontology@gmail.com))

Academic editor: Torsten Scheyer ♦ Received 6 July 2023 ♦ Accepted 11 March 2024 ♦ Published 21 March 2024

## Abstract

We studied at least part of Kuhn's original material of lizards from the Paleocene (~MP 5) of the Walbeck locality in Germany. The collection was considered to be lost but is consistently discussed in the literature due to its importance. We restudied the type material of aff. *Parasauromalus paleocenicus* and aff. *Glyptosaurus walbeckensis* described by Kuhn in 1940. The former was originally allocated to Iguania, the latter to Anguimorpha, though later on these identifications were questioned by several authors. We show such a classification of both cannot be upheld. *P. paleocenicus* resembles the morphology of lacertids showing their presence in Europe already around MP 5. We consider the name *P. paleocenicus* as a nomen dubium. The material of aff. *G. walbeckensis* was later suggested to belong to Lacertidae and also considered as a potential amphisbaenian. Although it differs from modern amphisbaenians, it shares features with one supposed polyodontobaenid – *Camptognathosaurus parisiensis*. The Walbeck form is identical to this species. Since the Walbeck taxon was described in 1940, the principle of priority makes *Camptognathosaurus parisiensis* a junior synonym of the species erected by Kuhn. We propose a new combined name for this form, *Camptognathosaurus walbeckensis* comb. nov. The specimen figured by Kuhn is currently lost, thus we designate a neotype from Walbeck. However, this taxon differs significantly from *Polyodontobaena* and new data doubt the attribution of *Camptognathosaurus* to Amphisbaenia. This taxon is tentatively assigned here to Lacertidae, as further confirmed by phylogenetic analyses. Material of Scincoidea is also described.

## Key Words

early Paleogene, Europe, Lacertidae, Scincoidea, Squamata

## Introduction

Palaeoherpetofaunas of the Paleocene are extremely rare in Europe and, thus, very little is known about squamates from this epoch. We here redescribed and revised lizards from the Paleocene of Walbeck fissure filling in Sachsen-Anhalt in Germany (Fig. 1). The mammalian fauna allowed to correlate the vertebrate assemblage likely to the middle Selandian age and probably corresponding to the European Paleogene mammalian reference interval MP 5 (De Bast et al. 2013; De Bast and Smith 2016). Walbeck is the only known Paleocene fossil site from

Germany and one of the few Paleocene localities known from Europe as a whole. Thus, this locality represents one of the unique and rare exceptions, serving as a window into the late Paleocene world. The fossiliferous sediments of Walbeck with Paleocene continental vertebrates were reworked by a transgressing Oligocene sea and deposited in protected fissures in Muschelkalk limestone (e.g., Storch 2008). Although a reworking of the sediments and fossils of the karstic pocket is present, all studies suggested that the continental vertebrates of Walbeck should have Paleocene age (Russell 1964). The fissure filling was excavated in 1939, and about fifteen tons

of sediment were processed (e.g., Weigelt 1939, 1940, 1942). As the pocket was fully excavated, it cannot be recollected. Dehm (1961) discussed Walbeck and noted how extensive it was: c. 15,000 specimens in a small pocket. The vertebrate fauna was studied already in early 20<sup>th</sup> century (e.g., Kuhn 1940a, b; Russell 1966; Weigelt 1942). Recently mammals and birds have been restudied, and their taxonomy has been revised (Mayr 2002, 2007; Storch 2008; Rose et al. 2015).

Here, we study a part of the original Kuhn's lizard material. In fact, since Kuhn did not use collection numbers, poorly figured only a few specimens, and provided limited descriptions, the recognition of number and allocation of old specimens studied by him is extremely limited. Besides lizards, Kuhn (1940a) also documented the earliest Cenozoic occurrence of Constrictores from Europe [this material is not included here, but Georgalis et al. (2021a) remarked on the size of these snakes]. In any case, the collection was considered to be lost for many years (Estes 1983; Rage and Augé 1993) but mentioned and discussed in the literature for decades due to its importance to our knowledge of the Paleocene (e.g., Estes 1983; Rage and Augé 1993; Augé 2005; Čerňanský and Augé 2013; Čerňanský et al. 2020a; Georgalis et al. 2021b). This material sheds new light on the early evolution of some lizard taxa and demonstrates the palaeodiversity of archaic members of lizard lineages in the late Paleocene of Europe.

Among squamates, for particular reasons, one of the groups one could expect in the Paleocene of Europe

are lacertids. They are the dominant reptilian group in Europe, where the origin of the clade has been also suggested (Arnold et al. 2007, and references therein). This hypothesis has been also supported by the fossil record (Borsuk-Bialynicka et al. 1999; Čerňanský and Augé 2013; Čerňanský and Smith 2018). Descendants of the basal-most divergence in crown Lacertidae, between Gallotiinae and Lacertinae, are also documented from Europe (the Oligocene *Pseudeumeces* and *Dracaenosaurus* and the Miocene *Janosikia*; see Čerňanský et al. 2016a, 2017). Based on molecular analyses, the Lacertidae clade has been estimated to diverge from its sister lineage before the Mesozoic-Cenozoic boundary (Vidal and Hedges 2009). According to Hipsley et al. (2009), modern lacertids arose shortly after the Cretaceous-Paleogene (K/P) transition. In a recent study, crown ages were recovered for Lacertidae in the Paleocene (Garcia-Porta et al. 2019). In any case, their fossil record is unknown in the Mesozoic. In the Paleocene, their fossils are extremely rare, sometimes even doubtful (Rage, 2013). A frontal tentatively allocated to Lacertidae was described from the upper Paleocene locality of Cernay (Čerňanský et al. 2020a; reference locality of MP 6, BiochroM 1997).

In regard to Walbeck, Kuhn (1940a) described isolated vertebra as *Saniwa* aff. *ensidens* and stated its similarity to this American varanoid. He also described an isolated dentary as “aff. *Parasauromalus paleocenicus* sp. nov.”, a new iguanian taxon. Kuhn also referred the species to *Iguanosaurus* (see Kuhn 1944) and to *Iguanosauriscus*



**Figure 1.** Location of Walbeck in Germany and other Paleocene localities of Northern France that yielded *Camptognathosaurus*.

(see Kuhn 1958; see also Estes 1983). Later, it was referred to Lacertidae by Estes (1983), who also tentatively reclassified it into *Plesiolacerta*. However, because the specimens were considered to be probably lost (see Estes 1983), the systematic position of the taxon has remained uncertain. Kuhn (1940a) also established the species aff. *Glyptosaurus walbeckensis*. Kuhn in 1940b better figured two specimens of this species (see Kuhn 1940b: tab II, fig. 4 and tab. III fig. 3). However, Estes (1983) rejected its glyptosaurine affinities and suggested that it was a lacertid as well and tentatively referred it to *Pseudeumeces*. Later, Augé (2005) suggested that it was a potential amphisbaenian and considered it a nomen dubium. Indeed, the Amphisbaenia clade is documented by a relatively rich fossil Paleocene record. Their fossils are known from America (Sullivan 1985; Longrich et al. 2015), Europe (Belgium and France, see Folie et al. 2013) and Africa (Augé and Rage 2006). These reptiles originated most likely in North America (Longrich et al. 2015). Later, they radiated and dispersed in the Paleogene following the Cretaceous-Paleogene (K-P) extinction. It seems that these events were somehow connected to the extinction, which has clearly an impact on squamate faunas as well (see Longrich et al. 2012, 2015).

The study of Walbeck lizards will help to resolve the allocation of the problematic Paleocene lizard taxa. Moreover, it can help better understand the Paleocene - the poorly known epoch which represents the beginning of the Cenozoic.

## Institutional abbreviations

**CR**, Cernay-lès-Reims, collections at the Natural History Museum of Paris, France; **MLU**, the Institut für Geologische Wissenschaften und Geiseltalmuseum, Martin-Luther-Universität Halle-Wittenberg; **NHMW**, the Natural History Museum Vienna, Austria; **RIV PP**, Rivecourt-Petit Pâtis, collection houses at the Compiègne Museum, France; **SMF ME**, Forschungsinstitut und Naturmuseum Senckenberg, Frankfurt, Germany.

## Materials and methods

### Specimens examined, photography and terminology

All studied specimens are housed at the Institut für Geologische Wissenschaften und Geiseltalmuseum, Martin-Luther-Universität Halle-Wittenberg (MLU). The specimens were photographed using a Keyence VHX970 digital light microscope at the JURASSICA Museum (Porrentruy, Switzerland). The image processing program ImageJ (Schneider et al. 2012) was used for measurements. The terminology for teeth follows Richter (1994) and Kosma (2004). The terminology of the individual structures of the vertebrae are primarily from Hoffstetter

and Gasc (1969) and Tschopp (2016). Taxonomy follows Zheng and Wiens (2016) where the clade Lacertoidea includes Lacertidae, Amphisbaenia, Teiidae and Gymnophthalmidae (Laterata sensu Vidal & Hegdes, 2005; Burbrink et al. 2020) and, where Scincoidea consists of Xantusiidae, Gerrhosauridae, Cordylidae and Scincidae. However, others, such as Burbrink et al. (2020), use a different concept of Scincoidea that does not include cordyliforms. The authors unite the families Cordylidae and Gerrhosauridae into a clade Cordyloidea, which is a sister group to Xantusiidae.

The outline figure of the mandible of the holotype (SMF ME 2604) of *Cryptolacerta hassiaca* was redrawn from figures published by Müller et al. (2011: fig. 1). The left dentary of *C. hassiaca* found in the gut of *Paranecrosaurus feisti* was redrawn from figures published by Smith and Habersetzer (2021: fig. 26C-E). GE Phoenix nanotom VR 180 X-ray tomography nano-CTVR system at the Slovak Academy of Sciences in Bratislava was used (Fairfield, CT) for  $\mu$ CT scanning of the holotype left dentary (NHMW 2019/0051/0001) of *Pseudeumeces kyrillomethodicus* (previously published and figured by Georgalis et al. 2021: figs 6, 7). The CT data was analyzed using Avizo 8.1.

## Phylogenetic analysis

To test the relationships of *Camptognathosaurus* within Squamata, we added it to an updated version of the morphological dataset of Gauthier et al. (2012) that included K/Pg-boundary species from the Western Interior of North America assembled by Longrich et al. (2015) and recently published codings for four species in Pan-Lacertidae, three extinct (*Eolacerta robusta*, *Stefanikia siderea*, *Cryptolacerta hassiaca*) and one extant (*Gallotia galloti*) (see Longrich et al. 2015; Čerňanský et al. 2017; Čerňanský and Smith 2018). This morphological data matrix (see Suppl. material 1) was developed and modified using characters taken primarily from Brownstein (2022), in which several errors in the original Gauthier et al. (2012) matrix identified by Simões et al. (2015, 2017) were addressed. In matrix of Brownstein (2022), some species were deleted from this dataset for the purposes of their analysis, including fossorial species such as amphisbaenians. However, because *Camptognathosaurus* was proposed as an amphisbaenian, we returned this group to the matrix. The principal goal of this analysis is to understand the relationship of the Paleocene taxon among Squamata. The data matrix was analysed using maximum parsimony as an optimality criterion in the program TNT and the NT (New Technology) search (Goloboff et al. 2008; Goloboff and Catalano 2016). *Sphenodon punctatus* was specified as an outgroup. All characters were treated as unordered and were equally weighted. Support was estimated through Bremer support indices (Bremer 1994). Mesquite v.2.75 was used to visualize all trees (build 566; Maddison and Maddison 2011).

## Data availability

All specimens from Walbeck are cataloged and accessible in the fossil collection of the Institut für Geologische Wissenschaften und Geiseltalmuseum, Martin-Luther-Universität Halle-Wittenberg (MLU), Germany. Digital surface model of the figured fossil specimen of *Pseudeumeces kyrillomethodicus* is available on Morphosource and Virtual Collections: NHMW 2019/0051/0001: <https://www.morphosource.org/concern/media/000610005?locale=en>.

## Results

### Systematic palaeontology

#### Squamata Opperl, 1811

#### Lacertoidea Opperl, 1811 (sensu Zheng & Wiens, 2016)

#### ?Lacertidae Opperl, 1811

#### *Camptognathosaurus* Folie, Smith & Smith, 2013

**Type species.** *Camptognathosaurus parisiensis* Folie, Smith & Smith, 2013.

#### *Camptognathosaurus walbeckensis* (Kuhn, 1940a), comb. nov.

Figs 2–4

1940a (aff.) *Glyptosaurus walbeckensis*: Kuhn, p. 24, figs 4b, 5b.

1940b „*Glyptosaurus*“ *walbeckensis*: Kuhn, p. 482, tab. II fig. 4, tab. III fig. 3.

1983 *Pseudeumeces? wahlbeckensis*: Estes, p. 104.

2005 *Amphisbaenia incertae sedis*: Augé, p. 301

2013 *Camptognathosaurus parisiensis*: Folie, Smith & Smith, p. 229, fig. 3.

**Neotype.** MLU.GeoS.4045, almost complete left dentary.

**Referred specimens.** Germany (here): Two left maxillae MLU.GeoS.4048–4049; one right maxilla MLU.GeoS.4047; three left dentaries MLU.GeoS.4043–4045, MLU.GeoS.4055, MLU.GeoS.4038, 4039 and 4036; seven right dentaries MLU.GeoS.4051, 4040, 4053, 4037, 4041, 4042, and 4056.

France (see Folie et al. 2013): Two right dentaries RIV PP 413, RIV PP 414; left dentary RIV PP 415, MNHN CR 17420 about fifteen dentaries and maxillae, MNHN CR 17421, right dentary and MNHN CR 17425 left dentary.

**Localities and horizons.** The type locality of *Camptognathosaurus walbeckensis* (Kuhn 1940a), comb. nov. is Walbeck (~MP 5; Germany). This taxon is also known from France: Rivecourt-Petit Pâtis (MP 6b), Cernay-lès-Reims (MP 6a; both France) and, potentially, Montchenot (MP 6).

**Taxonomic comment.** The newly referred dentaries show no evident differences relative to the type material of (aff.) *Glyptosaurus walbeckensis* described from the

same locality (Kuhn 1940a: figs 4b, 5b): in tooth count, tooth morphology, slightly arched ventral margin of the dentary and prominent, dorsally elevated coronoid process. This species has been considered a glyptosaurid (Glyptosauridae sensu Čerňanský et al. 2023a) by Kuhn (1940a). This assignment is untenable given the specimens studied here. Aff. *Glyptosaurus walbeckensis* lacks the following derived characters of Anguioidea (Estes et al. 1988; Gauthier et al. 2012): the splenial anterior inferior alveolar foramen is located between the splenial and the dentary (usually marked by the splenial spine) and the Meckelian canal opens ventrally in the anterior region (not medially for most of length). Moreover, the sulcus dentalis is present, whereas in anguimorphs, the dental crest is shallow and extends medioventrally. The material of aff. *G. walbeckensis* was later suggested to belong to Lacertidae (?*Pseudeumeces*; see Estes 1983). Augé (2005) suggested that it is a potential amphisbaenian and considered it a nomen dubium. In contrast, the new specimens share the following features of Paleocene *Camptognathosaurus parisiensis*: a long dentary bearing ten to twelve teeth, absence of an angle at the mandibular symphysis and robust amblyodont teeth decreasing the size towards the anterior end of the bone.

It should be noted that no holotype for aff. *Glyptosaurus walbeckensis* was explicitly assigned by Kuhn (1940a). He mentioned six dentaries as (aff.) *G. walbeckensis*, but he figured only one and provided a brief description of the dentary features of this taxon. Accordingly, following ICZN (1999: Article 73.2 and Recommendation 73F), all these six specimens mentioned by Kuhn (1940) (and not only the one he figured) are by definition considered as syntypes of the species. As such, the fact that these specimens cannot be adequately identified because they were not listed, figured, or described in detail does not affect their status as syntypes; in fact, a similar situation has been observed in other fossil Cenozoic reptiles as well, such as the constrictor snake *Palaeopython cadurcensis* (see Georgalis et al. 2021a: 22) and the testudinid turtle *Testudo marmorum* (see Vlachos et al. 2020: 3–4). It is difficult to identify the original syntype specimen figured by Kuhn (1940a: fig. 4b, 5b). In the available material studied here, no left dentary seems to be identical to the figured Kuhn's specimen. Unfortunately, the quality of the figure from the original publication is not sufficient to relocate the specimens. The overall shape and morphology of the figured syntype are very similar to MLU.GeoS.4045 (Fig. 3A–D), but a more detailed comparison, especially regarding the arrangement of preserved teeth, does not support the assignment. In Kuhn's (1940a) specimen, there is a small posterior tooth with empty tooth loci anterior to that and five teeth preserved in the row. In MLU.GeoS.4045, six teeth could be counted if we virtually complete the region between the first and last preserved teeth. Another explanation is that the current preservation of Kuhn's specimen is much worse than in 1940. This would make its identification challenging. In such a case, the specimen MLU.GeoS.4039 (Fig. 4F–H) with five

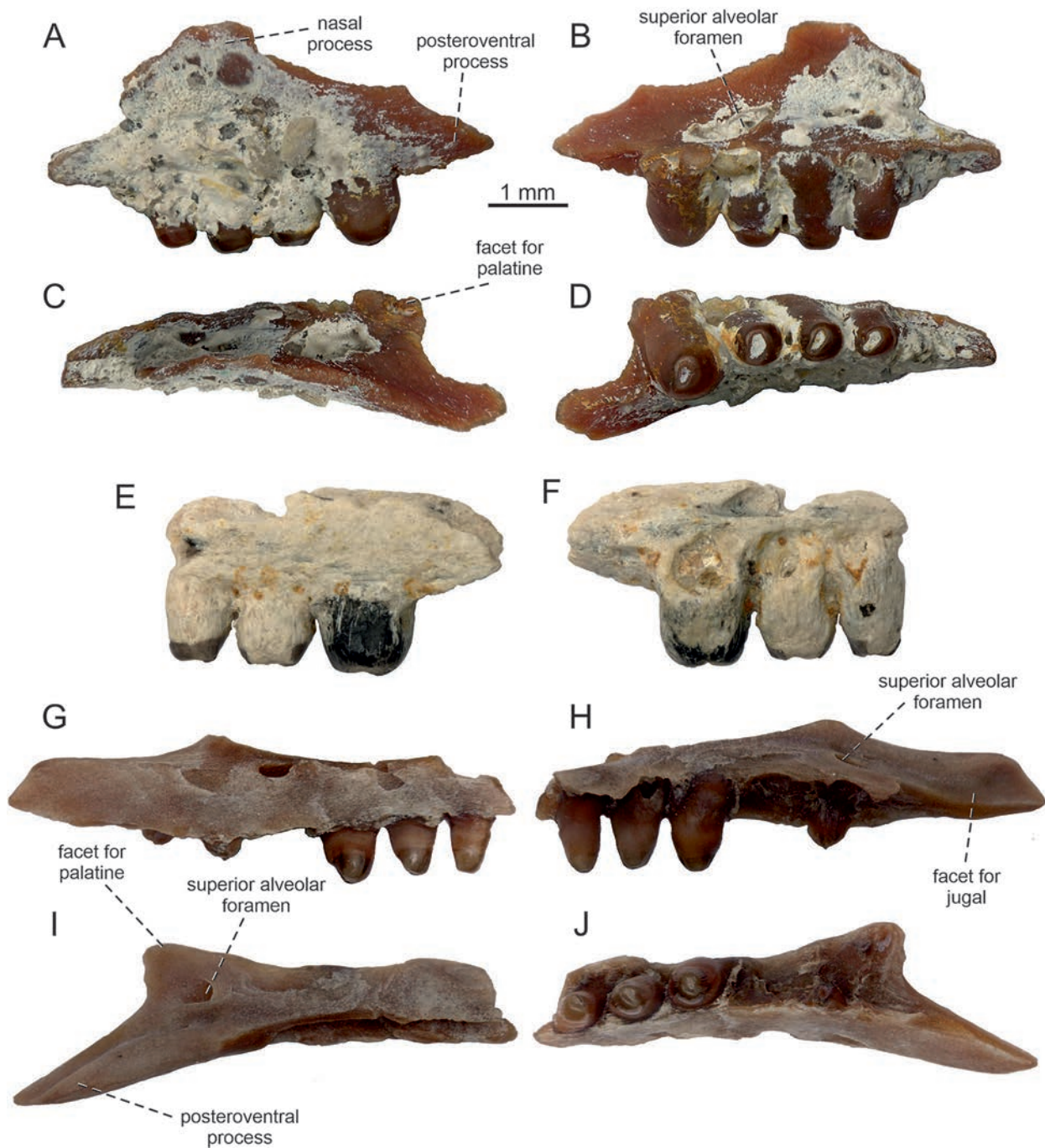


**Figure 2.** *Camptognathosaurus walbeckensis* comb. nov. from the Paleocene Walbeck locality. Two left maxillae MLU.GeoS.4048 (A–D) and MLU.GeoS.4049 (E, F) and right maxilla MLU.GeoS.4047 (G–J) in lateral (A, E, G); medial (B, E, H); dorsal (C, I); and ventral (D, J) views.

preserved teeth (and a total of eleven tooth positions) in a complete row would be a good candidate to represent the original Kuhn's (1940a) figured syntype specimen. In a closer look, however, the anterior portion of this dentary is not identical with the specimen of Kuhn (1940a) – the anterior portion of MLU.GeoS.4039 starts to rise dorsally at the level of the anteriormost preserved tooth (rather than in front of it), the dental crest is preserved in this anterior elevated portion, and the relative mutual size of teeth and their orientation do not match as well. For all these reasons, we cannot confidently exclude an option

that the syntype specimen figured by Kuhn (1940a: fig. 4b, 5b) has been lost.

Furthermore, in the same year, Kuhn (1940b) figured two additional specimens that he referred to aff. *Glyptosaurus walbeckensis*, i.e., a dentary (Kuhn 1940b:pl. II.4) and a maxilla (Kuhn 1940b: pl. III.3), which were both figured in much better quality than the figured syntype specimen in his 1940a publication. The same author further briefly described the maxilla (Kuhn 1940b: 482). However, Kuhn (1940b) did not mention anything that would imply that these two newly figured

specimens were part of the original type material of aff. *Glyptosaurus walbeckensis* that was established in Kuhn (1940a). The fact that Kuhn (1940a) did not mention anything about the existence of a maxilla for this species, renders us to safely regard that the maxilla is not a syntype. As for the dentary, it is impossible to know if this was a newly referred specimen or one of the six syntype dentaries. The same author, in his subsequent compendium of fossil lizards (Kuhn 1963), also did not specify any type material in the respective entry of this taxon. In the absence of any evidence, we have to treat it similarly to the maxilla, i.e., as a referred specimen. In any case, both these 1940b specimens should also be considered as lost: we have three maxillae in our sample but no one is, again, identical to his 1940b figured one, while the 1940b dentary is similar to the right dentary MLU.GeoS. 4042 described and figured herein (Fig. 4A), but a detailed comparison shows that this is not the same specimen.

Estes (1983: p.104) regarded the only figured specimen in Kuhn (1940a: fig. 4b, 5b) as the only type specimen. That action of Estes (1983) rendered him, in fact, as the designator of the lectotype, according to ICZN (1999: Article 74.5). By definition, the remaining five, non-figured, dentaries mentioned in Kuhn (1940a) represent paralectotypes of the species. As for two additional specimens figured by Kuhn (1940b), Estes (1983) regarded them as the “referred specimens” and “topotypic specimens”.

Taking into consideration the poorly figured lectotype of the aff. *Glyptosaurus walbeckensis* in Kuhn (1940a), coupled with the apparent loss of this material and the original brief description, we consider that it is most appropriate to designate a neotype that could render the taxon diagnostic and allow its anatomical features to be properly discerned. *Camptognathosaurus parisiensis* is a junior synonym of the new combination *Camptognathosaurus walbeckensis* and is a type species of the genus *Camptognathosaurus* (the type species of a genus can be a junior synonym of a valid species pertaining to the same genus, see ICZN 1999: Article 67.1.2; e.g., the case with the snake genus *Eryx* Daudin, 1803, but cannot be a non-diagnosable species, which cannot be diagnosed as a member of the genus). One option is to replace the lost one by the holotype of *Camptognathosaurus parisiensis* (RIV PP 413) in the new combination *Camptognathosaurus walbeckensis*. However, we think it is less dangerous to choose a neotype among the specimens from Walbeck (the type locality), some of which are not significantly less well-preserved than those from France. The reason for this is that there are more chances that the neotype we are choosing actually belongs to the same species erected by Kuhn, than if we chose it among specimens from a different region (with a slightly different age and which could ultimately be shown to represent a different species). Currently, only jaw elements are known and caution is needed.

**Revised diagnosis.** Small-sized lizard in regard to skull length (an anteroposterior maximum length of dentary around 10 mm). It differs from other members of Lacertoidea based on a unique combination of features: (1) pleurodont dentition (contra *Trogonophis*); (2) only moderately shortened dentary (as *Polyodontobaena*, *Pseudeumeces*, contra distinctly shortened in all modern amphisbaenians, contra markedly short in *Dracaenosaurus*, contra long in *Lacerta* and *Gallotia*); (3) absence of an angle at the symphysis (as lacertids, *Cryptolacerta*, contra *Cuvieribaena* and all modern amphisbaenians except *Amphisbaena ridleyi*); (4) rounded (arched) ventral margin of dentary (as lacertids, *Cryptolacerta*, contra *Polyodontobaena* and modern amphisbaenians); (5) higher number of labial foramina - around five or six (as *Lacerta*, *Pseudeumeces*, contra eight in *Gallotia*, contra four in *Polyodontobaena*, three in *Blanus* and *Rhineura*, two in *Cuvieribaena*); (6) opening of the alveolar canal beneath tooth row (as *Cryptolacerta*, *Polyodontobaena*, contra all modern amphisbaenians except *Rhineura*); (6) dentary tooth number 10–12 (as Pohl-Perner specimen of *Cryptolacerta* and *Polyodontobaena*; 12–14 in *Dracaena*, 12–17 in *Pseudeumeces*, contra higher tooth count in *Tupinambis* and extant lacertids; contra smaller number - seven or eight in *Dracaenosaurus* and in all modern amphisbaenians); (7) heterodont dentition, teeth increase their size posteriorly (the last tooth/teeth can be smaller) (as *Pseudeumeces*, *Janosikia*, *Polyodontobaena*, contra decreasing tooth size posteriorly in *Cuvieribaena* and usually in modern amphisbaenians – note that in *Blanus*, the third or fourth tooth is smaller); (8) teeth arranged in a single line along the tooth row (contra *Dracaena*); (9) robust, blunt teeth with constricted bases present in the posterior half of the tooth row (as *Dracaenosaurus*, *Pseudeumeces*, contra presence of robust and blunt teeth without constriction in the anterior region of the tooth row in *Cuvieribaena*); (10) absence of cementum deposits (contra teiids); (11) moderately low dental crest, teeth exceed the dental crest by more-or-less the half of the tooth length [as *Cryptolacerta*, contra high dental crest (most of the ventral tooth length laterally cover by the crest) in *Pseudeumeces*, *Dracaenosaurus*, *Janosikia* and *Lacerta*, contra low dental crest, shallowly pleurodont (most of the tooth length exposed laterally) in *Polyodontobaena* and most amphisbaenians]; (12) large, dorsally distinctly elevated coronoid process of dentary, which appears to cover, at least partly, the anterolateral part of the coronoid (as *Cryptolacerta* and many amphisbaenians, contra basal Rhineuridae); (13) open Meckelian canal (contra *Rhineura*); (14) fossa for adductor musculature well developed, extensive, running well below the dentary tooth row (as *Cryptolacerta*, *?Cuvieribaena*, contra *Polyodontobaena* and extant amphisbaenians) and (15) posteroventral process of maxilla long (as lacertids, *Cryptolacerta*, contra derived state in modern amphisbaenians).

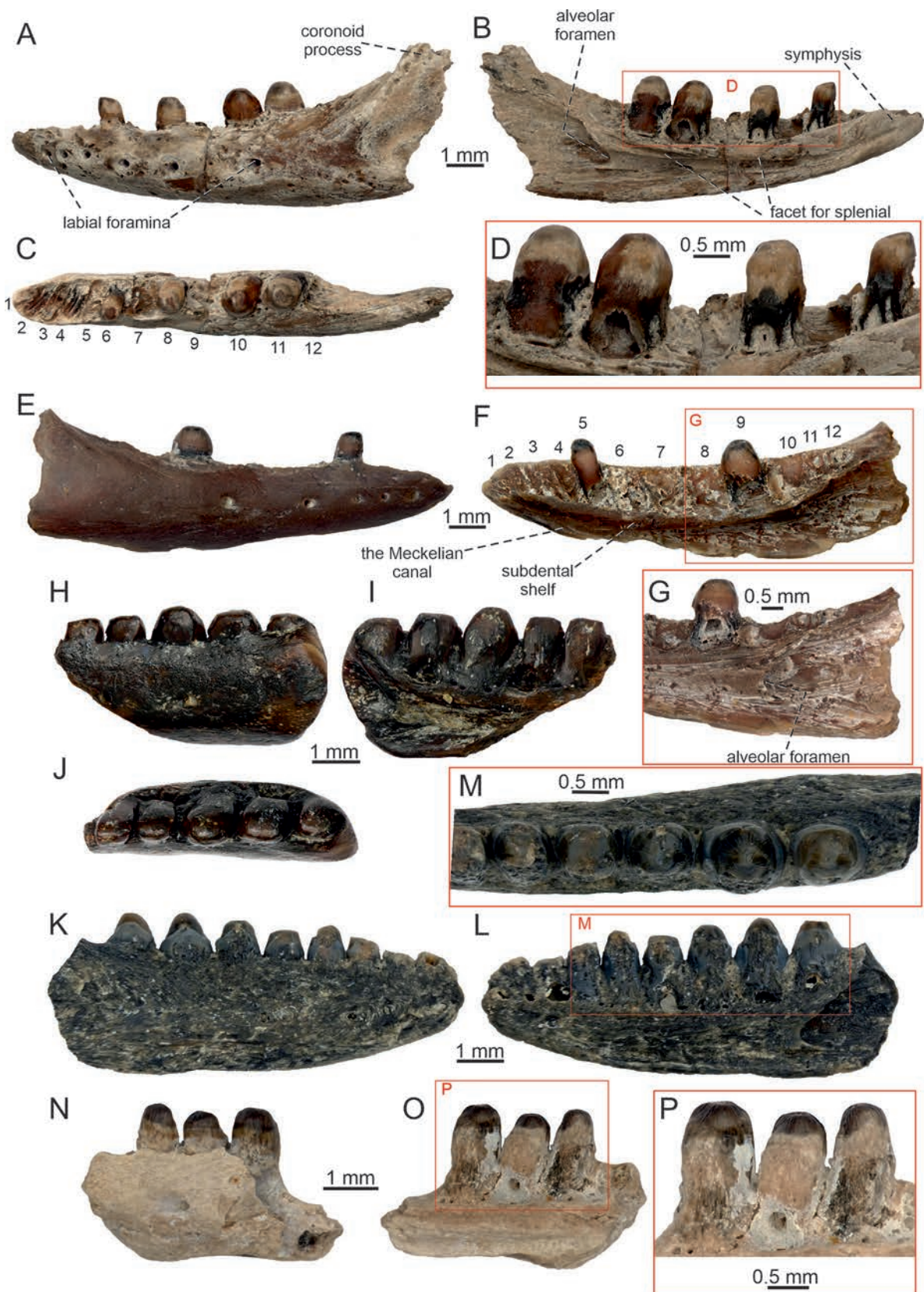


**Figure 3.** *Camptognathosaurus walbeckensis* comb. nov. from the Paleocene Walbeck locality. The neotypic left dentary MLU.GeoS.4045 in lateral (A), medial (B), dorsal (C) views; and tooth detail in medial (D) view. Right dentary MLU.GeoS.4051 in lateral (E) and medial (F) views; and detail of the area around the alveolar foramen in ventromedial (G) view. Left dentary MLU.GeoS.4055 in lateral (H), medial (I) and dorsal (J) views. Right dentary MLU.GeoS.4037 in lateral (K) and medial (L) views; and teeth in dorsal (M) view. Left dentary MLU.GeoS.4043 in lateral (N) and medial (O) views; and detail of teeth in medial (P) view.

**Description. Maxilla.** Three maxillae (two left, one right) are available in the material (Fig. 2A–F). The specimen MLU.GeoS.4048 is better preserved, whereas 4049 is represented only by a posterior fragment bearing three teeth. MLU.GeoS.4048 possesses six or seven tooth positions (see remarks) with four teeth still attached. The preserved portion of the maxilla appears to be anteroposteriorly short rather than long. Note, however, that it is incomplete and the true length of the element cannot be determined (but see remarks for Kuhn 1940b). It consists of two major portions: the dental portion bearing the marginal dentition and the dorsally extending nasal process (facial process sensu Evans 2008). In dorsal view, the bone gradually widens posteriorly except for the posteroventral process. A short process bearing a facet for the palatine extends posteromedially. Further posteriorly, the bone continues into the posteroventral process. The process is not pointed but forms a low perpendicular wall. The external side of the maxilla is slightly concave. In lateral view, the external surface of the bone is mostly covered by adhering sediment. The partly exposed areas are more-or-less smooth (the same is true for MLU.GeoS.4049 which, however, represents only a ventral portion of the maxilla, see below). The nasal process is small (note that the anterior part of the process is broken off) and slightly dorsally expanded. Its posterior portion is well demarcated from the further posterior portion of the maxilla by a recess.

Further posteriorly, the bone gradually decreases, but note that the dorsal margin of this part is slightly concave. The anterior region of the maxilla is damaged. In medial view, the partly damaged supradental shelf is well-developed and moderately expanded medially. Its maximum medial expansion, corresponding to the palatine process of the maxilla, can be seen at the level of the last posterior preserved tooth. The portion situated further posteriorly appears to be damaged. However, it can be assumed that the process did not protrude distinctly further posteriorly (Fig. 2C). The large posterior opening of the superior alveolar canal is located in the posterior region at the level of the fifth tooth position (counted from anterior).

The specimen MLU.GeoS.4047 represents a partly preserved right maxilla. It appears to be somewhat long (relative to amphisbaenians), but its dorsal portion, including the nasal process, is completely broken off. The anterior portion is missing as well. The preserved external surface of this specimen is smooth. Only a ventral half of one supralabial foramen is preserved. The bone extends posteriorly into the more-or-less long posteroventral process. The process is slightly inclined laterally relative to the anteriorly located portion of the maxilla (Fig. 2I, J; the same condition can be seen in MLU.GeoS.4049). The preserved maxilla bears six tooth positions where four teeth are still attached to the bone. The medial margin of the supradental shelf is damaged, although its sharp stepped end around the end of the tooth row is visible. It forms the medially expanded portion. In this area, the facet for the palatine is present. The posterior opening of

the superior alveolar canal is located at the level of the penultimate tooth position. The posteroventral process of maxilla is long rather than short. In lateral and medial views (Fig. 2G, H), its dorsal margin is concave and the posteroventral process forms a low perpendicular wall. The ventral margin of this wall reaches only slightly more posteriorly than its dorsal margin. From the level of the superior alveolar foramen, the posteroventral process is also slightly rotated ventrolaterally. Thus, its lateral surface is partly visible when the maxilla is observed in ventral view (Fig. 2J). The posterior region of the maxilla appears to bear a facet for jugal (Fig. 2H).

**Remarks.** All three maxillae, despite some small differences, are allocated to the same species. They share several features, such as robust teeth of which a robustness increases posteriorly; the location of the palatine process; and the presence of well-developed posteroventral process (in contrast to modern amphisbaenians). Identical dentition in this type of element helps to recognize that they most likely belong to the same taxon as dentaries described below. Moreover, they are comparable in size and come from the same locality. It seems to be unlikely that maxillae belong to a form for which dentaries have not been recorded in the locality. The small differences among maxillae are considered individual variability and/or may reflect ontogenetic differences (see Discussion). Therefore, until the intraspecific variability and ontogeny is better understood in this form, we prefer to provisionally refer the new maxillae to the species *Camptognathosaurus walbeckensis* comb. nov.

The tooth number in the tooth row is difficult to estimate because the region of the last posterior tooth in MLU.GeoS.4048 is damaged. It seems that there could be a place for one additional tooth. But in such case, this tooth, if present, would be much smaller than the last preserved (potentially penultimate) tooth. Actually, this would not be unusual and cannot be excluded (although nothing indicates such a condition in MLU.GeoS.4049). In such a case, the maxillary tooth number in a preserved (not complete) tooth row of this specimen is seven.

Besides these three specimens, there is an additional right maxilla figured by Kuhn (1940b: tab II fig. 4). This Kuhn's specimen is much more complete, but is not present in the material available to us (according to Estes 1983, it is lost). There are similarities with our material, such as an amblyodont dentition and a long posteroventral process with a concave dorsal margin, although it is difficult to be absolutely sure without proper study that this specimen represents the same taxon (*Camptognathosaurus*). Only its lateral aspect is figured and according to Kuhn (1940b), it has 11 mm in length (it is moderately long rather than short) and possesses seven teeth (the tooth count of a complete tooth row was ten). Its external surface (including the nasal process) is pierced by numerous small foramina. The posteriormost supralabial foramen is located at the level of the fourth tooth position. The nasal process is anteroposteriorly long but dorsally low. Its dorsal margin is rounded, whereas

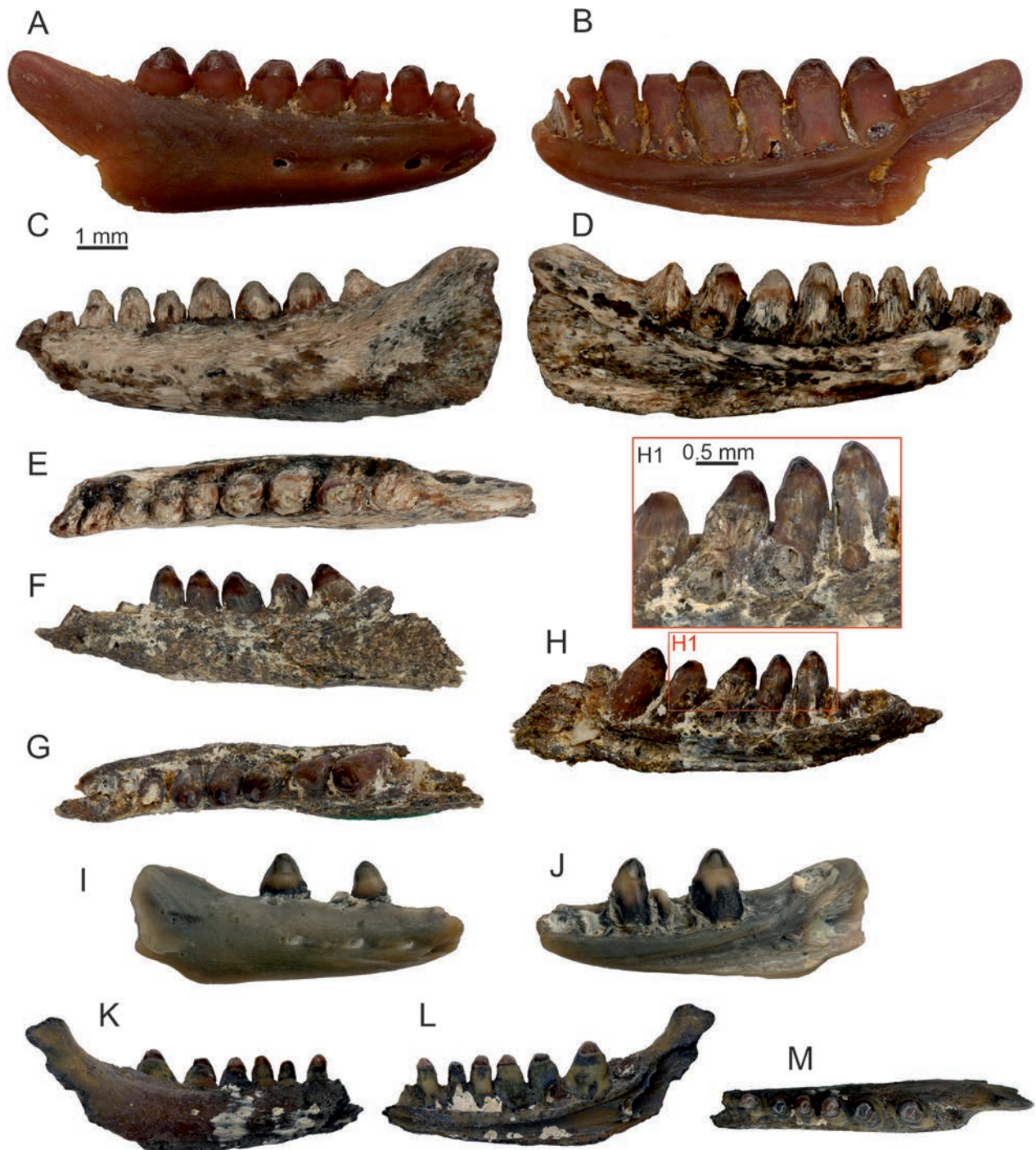


**Figure 4.** *Campptognathosaurus walbeckensis* comb. nov. from the Paleocene Walbeck locality. Right dentary MLU.GeoS. 4042 in lateral (A) and medial (B) views. Left dentary MLU.GeoS.4038 in lateral (C), medial (D) and dorsal (E) views. Left dentary MLU.GeoS. 4039 in lateral (F), dorsal (G) and medial (H) views and with detail of teeth (H1). Right dentary MLU.GeoS. 4056 in lateral (I) and medial (J) views. Right dentary MLU.GeoS. 4041 in lateral (K), medial (L), and dorsal (M) views.

its posterior portion slightly protrudes posteriorly. This portion is triangular, pointed and posteriorly directed. Estes (1983) stated that there is a weak sculpture reflecting osteodermal attachment on the nasal process.

**Dentary.** Several dentaries are preserved. Most of them are, however, only fragmentary (Figs 3, 4). The complete tooth row is preserved in the dentaries MLU.GeoS. 4045 (neotype) and 4051 (Fig. 3A–G). The specimens bear

twelve tooth positions (two teeth are still attached to the bone in 4051, see Fig. 3E, F; whereas four are preserved in 4045, see Fig. 3A–C). Some smaller dentaries bear eleven or perhaps ten tooth positions – this estimation is based on MLU.GeoS.4038, where only the anterior-most portion is broken off, but nine tooth positions are preserved (seven more-or-less complete teeth and half of two anteriormost ones are preserved in this specimen).

The otherwise smooth lateral surface is pierced by a single row of five (in MLU.GeoS.4051) to six (in 4045) labial foramina (in some cases four, e.g., MLU.GeoS.4042 – note, however, that these specimens are incomplete; Fig. 4A). The foramina are located in the mid-line of the bone and gradually increase in size posteriorly. The posteriormost foramen is located at the level of the fifth tooth position (counted from posterior) in MLU.GeoS.4051, but at the third in 4045 (note, however, that this is not a result of a different placement for the foramen in the dentary, but of the closely packed posteriormost teeth in 4051). In the posterior region of the dentary, there is a well-developed, wedge-shaped fossa for the adductor musculature. This structure is extensive, running well below the tooth row.

In medial view, the Meckelian canal is fully open, although narrow in the anterior region – the canal gradually widens posteriorly. The intramandibular septum, which separates the Meckelian canal from the alveolar canal, extends posteriorly almost to the end of the tooth row, but does not surpass it. The septum reaches the level of the third tooth position (counted from posterior) in MLU.GeoS.4051, whereas it reaches the level of the last tooth position in 4045 (this is likely related to the two additional posterior teeth in 4051, not a true shift in the structure position). The ventral margin of the septum forms a small and narrow crest (Fig. 3B). This crest is not free but is ventrolaterally fused to the bone (thus, this is not identical to a free posteroventral margin of the intramandibular septum sensu Gauthier 1982). Dorsally, the opening of the alveolar canal (i.e., alveolar foramen) is located. A subdental shelf roofs the Meckelian canal. Dorsally, the subdental shelf bears the sulcus dentalis (the sulcus becomes shallower posteriorly). The shelf is robust in the anterior section (Fig. 3B), but it distinctly narrows posteriorly due to the presence of the facets for the splenial and large facet for the coronoid on its ventromedial surface. The splenial facet is medially exposed and visible at the level of the third tooth position (counted from posterior; this condition is present in all specimens in which this feature can be observed). Then, it turns more ventrally and reaches far anteriorly, extending to the level of the sixth tooth position counted from posterior or the seventh tooth position if counted from anterior. The symphyseal region is preserved in MLU.GeoS.4045. It is slightly dorsally elevated relative to the mid-section of the shelf (the subdental shelf is slightly dorsally concave). The symphysis is small and rectangular in shape. The facet for the splenial is also present on the ventral margin, but the margin itself is weathered, worn or corroded in the specimens so it is difficult to estimate its anterior termination. The ventral margin of the bone is slightly arched. The posterior region of the bone (posterior to the end of the tooth row) distinctly rises dorsally to form a dorsally elevated and prominent coronoid process. It appears that it covered, at least partly, the anterolateral part of the coronoid. The coronoid itself is not preserved, so this cannot be fully

confirmed. The coronoid process of the dentary is fairly preserved in MLU.GeoS.4045. Only its dorsal portion is slightly damaged. The process reaches clearly higher than the level of the tooth apices of the largest teeth. The ventral posterior ends of all dentaries are damaged. At least a short angular process can be identified in MLU.GeoS.4045 (Fig. 3A, B). However, this appears to be only the base of the process, so its real length is unclear. The same is true for MLU.GeoS.4036, a left dentary without teeth.

**Dentition.** The tooth implantation is pleurodont. Teeth are tall (relative to the overall size of the jaw), over-arching the moderately low dental crest by more-or-less the half of the tooth length. Tooth size (robustness) in both maxilla and dentary gradually increases posteriorly. Note, however, that the last and/or penultimate tooth can be somewhat smaller again relative to the next anteriorly located tooth. The teeth are straight (not recurved) and slightly inclined anteriorly. In general, they are robust with blunt apices. The large teeth in the posterior region are extremely blunt, amblyodont and have rounded apical portions forming robust cylinders. Some specimens bear well-preserved fine radial striations of the crowns (Fig. 3M, O). The teeth are slightly constricted at their bases. Here, large circular resorption pits are located.

Although teeth are robust in some specimens, they have a slightly pointed appearance rather than being rounded and distinctly blunt. In some of these specimens, tooth crowns (however not all of them) have rounded mesial and slightly concave distal margins (Fig. 4H; note that this is also present in the penultimate preserved tooth of MLU.GeoS.4045, although in lesser form; see Fig. 3D). This feature (weak pointedness), however, can somehow vary among individuals and even in a single tooth row. Moreover, the conditions in the MLU.GeoS.4047 maxilla and 4042 dentary rather reflect an intermediate stage (Figs 2H, 4B; see remarks and Discussion).

**Remarks.** The material described here shares morphological features with the material of *Camptognathosaurus parisiensis* described by Folie et al. (2013: fig. 3) from France (MP 6b, Rivecourt-Petit Pâtis; MP 6a, Cernay-lès-Reims). The dentary RIV PP 413 (the holotype in Folie et al. 2013) is markedly similar to the specimen MLU.GeoS.4045 we describe here (Fig. 3A–D). All specimens from Germany and France (all localities are geographically relatively close to each other, see Fig. 1) share the following combination of features: (1) slightly rounded (arched) ventral margin of dentary; (2) number of labial foramina; (3) position of the alveolar foramen; (4) heterodont dentition in regard to size; (5) robust, blunt teeth with slightly constricted bases present in the posterior half of the tooth row (the last tooth/teeth can be smaller); (6) large, dorsally distinctly elevated coronoid process; and (7) similar tooth number – the specimen RIV PP 413, which is represented by a nearly complete right dentary from Rivecourt-Petit Pâtis, bears eleven tooth positions. Both paratypes CR 17420 and CR 17425 are, however, incomplete.

It should be noted that some dentaries described here show several small differences (or variation) among them: (1) size; (2) blunt tooth crown vs. slightly more pointed (although still robust); (3) slightly lower tooth number (twelve vs. eleven or ? ten tooth positions); and (4) potentially also the shape of the coronoid process. If the coronoid process is robust, dorsally rising in those dentaries with the well-preserved posterior portion (Fig. 3), the shape of this process is difficult to demonstrate clearly in some other dentaries. Namely, it is not markedly dorsally elevated in MLU.GeoS.4042 (Fig. 4A, B) and 4038 (Fig. 4C, D). It is clearly unrelated to the early ontogeny because the dorsally distinctly protruding process is observed in a small specimen MLU.GeoS.4041 (Fig. 4K, L). However, the left dentary MLU.GeoS.4038 is eroded. The relatively lower process in these two mentioned specimens seems to reflect only an artefact of preservation. All other differences seem to fall into the normal individual (and/or ontogenetic) variation; thus, all specimens studied here represent most likely a single taxon (see Discussion).

### Lacertidae indet.

Figs 5, 6

1940a aff. *Parasauromalus paleocenicus*: Kuhn, p. 24, figs 4a, 5a nomen dubium.

1944 aff. *Iguanosaurus paleocenicus*: Kuhn, tab. 20, fig. 7 nomen dubium.

1958 *Iguanosauriscus paleocenicus*: Kuhn, p. 382 nomen dubium.

1983 *Plesiolacerta? paleocenica* new comb.: Estes, p 104 nomen dubium.

**Material.** One left dentary MLU.GeoS.4059; seven isolated dorsal vertebrae MLU.GeoS.4067, 4066, 4061–4064, 4068.

**Description.** *Dentary.* The specimen MLU.GeoS.4059 represents a left dentary (Fig. 5). It is in fair condition. Only the anterior region is missing. The smooth lateral surface of the bone is pierced by a line of labial foramina, four of which are preserved (Fig. 5A). In the anterior region, these foramina are located at mid-height on the dentary, but as the dentary deepens posteriorly, the last two foramina are located more-or-less in the dorsal one-third of the bone. The posteriormost foramen is located at the level of the eleventh tooth position (counted from posterior). The alveolar shelf supports 21 tooth positions. Seven complete teeth are still attached to the bone and eight teeth have partly preserved tooth bases. However, since its anterior region is missing, the total number of teeth is unknown, but it certainly would have been slightly higher. The Meckelian canal is fully open and exposed medially (Fig. 5B). It is narrow in the anterior region and widens slightly posteriorly. In the posterior region, it is only moderately broad. The alveolar canal (Fig. 5D) opens at the level of the seventh tooth position (counted from posterior). The intramandibular

septum forms the ventromedial wall, separating this canal from the Meckelian canal. The ventral margin of the bone is nearly straight. Note, however, that its posterior portion is damaged. The subdental shelf roofs the Meckelian canal (sensu Rage and Augé 2010), which is only slightly concave in medial view – the shelf is more-or-less straight in the anterior section, whereas it rises slightly dorsally from the ninth tooth position (counted from posterior). It gradually becomes thinner posteriorly due to the presence of the facet for the splenial on its ventromedial surface. This facet is present on the ventral margin as well. Unfortunately, the posterior section of the shelf is damaged. The sulcus dentalis is developed, mainly in the anterior region of the dorsal surface of the shelf. Posterior to the tooth row, the bone tapers into the narrow and pointed coronoid process, which rises slightly dorsally. On the dorsolateral surface of the posterior end, the articulation for the coronoid is preserved, showing that the coronoid overlapped the dentary dorsally.

**Dentition.** The tooth implantation is pleurodont. The teeth are tall and heterodont, ranging from monocuspid in the anterior region of the dentary to bicuspid with a dominant, triangular (pointed) and slightly recurved main cusp and an additional smaller, well-separated mesial cusp (Fig. 5D–F). The bicuspidity starts around the 14<sup>th</sup> tooth position (counted from posterior). Note, however, that only one tooth (14<sup>th</sup>) is preserved in this region, possessing an incipient mesial cusp. The tooth crowns are lingually slightly concave. Weak, delicate radial striations (converge at the tip of the main cusp) are present on the lingual side of, at least, some of the tooth crowns (well seen especially in the teeth located in the mid-portion of the dentary; see Fig. 5F). In some cases, two dominant striae form a slightly developed lingual cusp. The tooth neck is slightly swollen lingually. Small circular resorption pits are present on the lingual aspects of tooth bases in some teeth. The narrow inter-dental gaps of the preserved teeth indicate that the teeth were closely spaced.

**Remarks.** The specimen MLU.GeoS.4059 is identical to the left dentary on which Kuhn (1940a: figs 4a, 5a) established the new species aff. *Parasauromalus paleocenicus*, although one anterior tooth subsequently broke off. The specimen is undoubtedly the same one described by Kuhn. It was also figured by Kuhn in 1944 (see Kuhn 1944: tab. 20, fig. 7).

The specimen MLU.GeoS.4059 represents a lacertid since it exhibits the synapomorphies of the family (Estes et al. 1988; Gauthier et al. 2012), such as sulcus dentalis and lateral overlap of the posterodorsal margin of the dentary by the coronoid. The tooth morphology also indicates a lacertid rather than other groups: presence of bicuspid teeth, weak striations and sometimes a weakly-developed lingual cusp is common among members of Lacertidae, including *Lacerta* (see Kosma 2004; Čerňanský and Syromyatnikova 2019). Among scincoids, the lingual cusp is usually well separated. In scincids, the lingual cusp is usually framed by broadly mesially and distally running cristae lingualis anterior

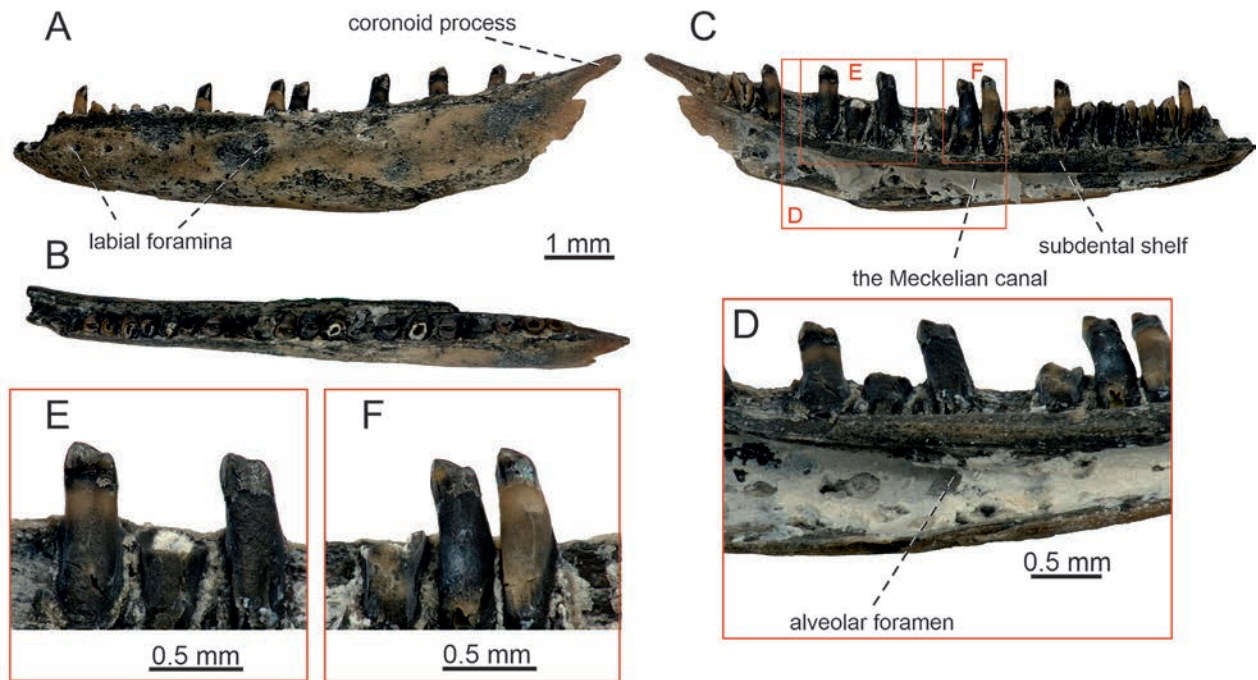


**Figure 5.** Lacertidae indet. from the Paleocene Walbeck locality. (A–F) Left dentary MLU.GeoS.4059 in lateral (A), medial (B) and dorsal (C) views. Detailed photographs of the area around the alveolar foramen in ventromedial (D) and detail of teeth in medial (E, F) views.

and posterior rather than more-or-less vertical striae dominans anterior and posterior (e.g., Caputo 2004; Kosma 2004; Čerňanský et al. 2020b; Čerňanský and Syromyatnikova 2021). Moreover, bicuspid teeth among scincoids are rare but present only in some cordyliformes (Estes, 1983) - bicuspid teeth are present in, e.g., *Gerrhosaurus flavigularis* and *Zonosaurus quadri-lineatus*, tricuspid teeth with dominant central cusp are present in, e.g., *Tracheloptychus*, and even multicusp teeth are present in a herbivorous gerrhosaurid - the posterior teeth of *Gerrhosaurus (Angolosaurus) skoogi* possess up to seven cusps Kosma 2004; Nance 2007). The presence of bicuspid and faintly tricuspid teeth is reported in a potential cordyliform *Deccansaurus* from the Deccan intertrappean strata (uppermost Cretaceous – lowermost Paleocene; Yadav et al. 2023). However, this taxon differs from the Walbeck lacertid by many aspects, e.g., the Meckelian canal is distinctly narrow (shallow) and exposed ventrally rather than medially, and a splenial is short. In teiids, the tricuspid teeth have extensive cementum depositions on tooth bases (Estes 1983).

**Vertebrae.** Seven vertebrae are available in the material (three of them are figured, see Fig. 6). The neural spine is moderately high (MLU.GeoS.4067; the short vertebrae with tall neural spines tend to be cervicals and thoracics) or rather low (MLU.GeoS.6066, 4061 and 4063) (Fig. 6) and slightly inclined posteriorly. It originates on the anterior border of the neural arch, forming a median ridge here (prespinal lamina sensu Tschopp 2016). It rises progressively posteriorly, and its top is slightly rounded. This part is wider and drop-shaped in dorsal view. The neural canal is large and pentagonal in outline.

The well-developed prezygapophyses are distinctly inclined dorsally, having well-defined, roughly elliptical articulation surfaces at the level of which the vertebra reaches its greater width. The postzygapophyses are oval in shape. Both pre- and postzygapophyses are slightly elongated and oriented obliquely but more anteroposteriorly than mediolaterally. The vertebrae are only slightly constricted between the pre- and postzygapophyses and consequently, they are relatively broad in dorsal view. In lateral view, the interzygapophyseal ridge (postzygoprezygapophyseal lamina sensu Tschopp 2016) is visible as a sharp ridge, connecting both pre- and postzygapophyses laterally. The synapophyses are well-developed, being located in the anterior region. The centrum gradually narrows posteriorly. In ventral view, it has a triangular shape. Its relative length varies among vertebrae, being short in MLU.GeoS.4067 and 4068, but rather long in MLU.GeoS.4066 and 4061. The ventral margin of the centrum is concave in lateral view. In ventral view, the centrum is pierced by two small foramina in its anterior third. The cotyle and condyle are mainly preserved in MLU.GeoS.4067 and 4066. They are moderately large, being rounded in MLU.GeoS.4067, but slightly depressed in 4066. The condyle is well demarcated from the centrum - the condyle (especially where the cartilage has been stripped from it) is narrower than the centrum. Note, however, that the true precondylar constriction seen in varanids (the width of the condyle is greater than the width of the centrum immediately anterior to it, e.g., Rieppel 1980; Estes 1983; Smith et al. 2008; Holmes et al. 2010; Čerňanský et al. 2022a) is absent in the herein described material.

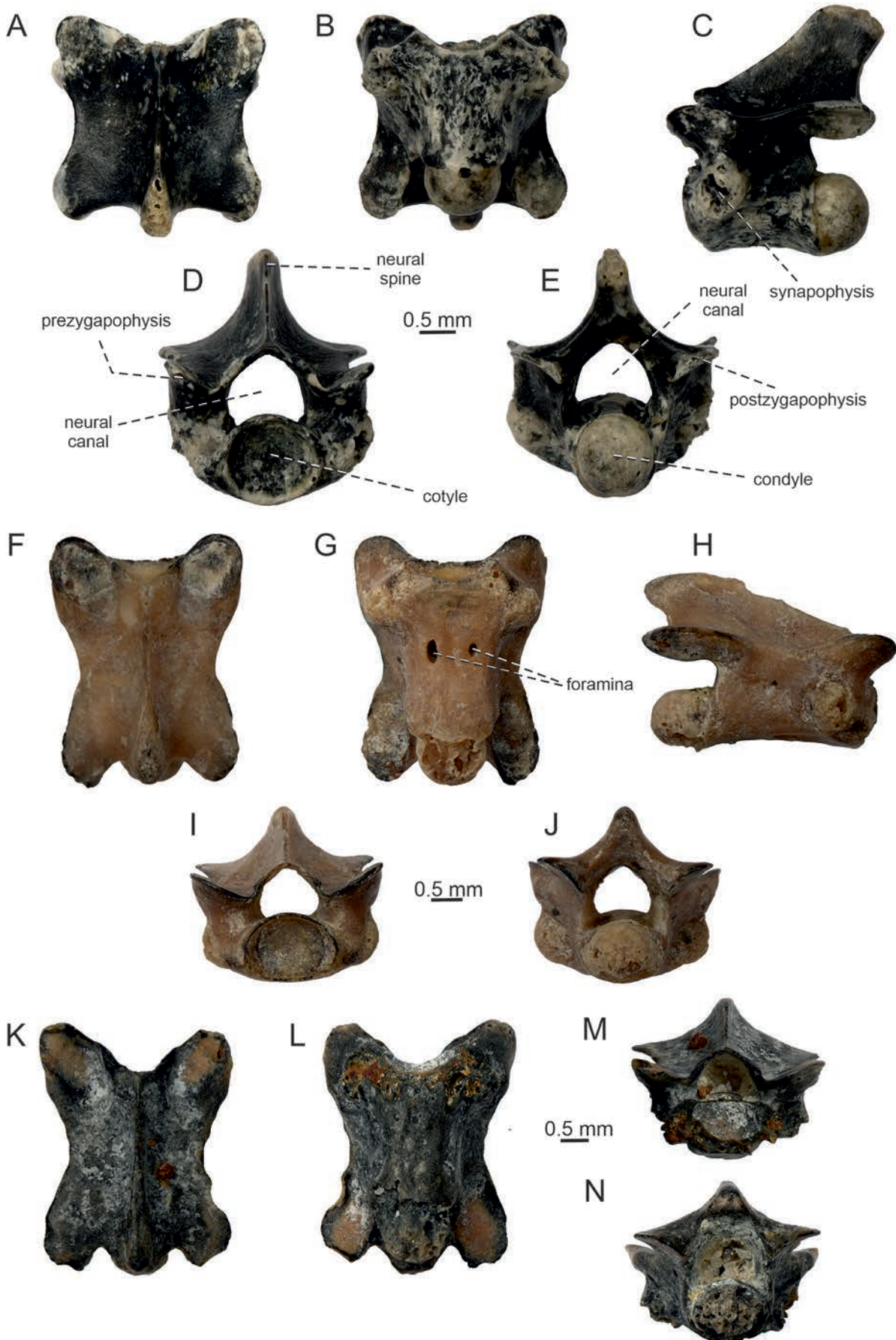


**Figure 6.** Lacertidae indet. from the Paleocene Walbeck locality. Isolated dorsal vertebrae MLU.GeoS.4067 (A–E), MLU.GeoS.4066 (F–J), MLU.GeoS.4061 (K–N) in dorsal (A, F, K), ventral (B, G, L), lateral (C, H), anterior (D, I, M) and posterior (E, J, N) views.

**Remarks.** Kuhn (1940a) originally described an isolated dorsal vertebra as *Saniwa* aff. *ensidens*, although stated that the specimen is by two-thirds smaller than a vertebra of this American varanoid. The vertebra described and figured by Kuhn (1940a: fig. 3) is identical to the material we describe here, although one cannot be sure if one of the vertebrae represents the same specimen Kuhn described. Thus, the oldest occurrence of *Saniwa* in Europe should be considered to be younger, namely from the earliest Eocene age locality Dormaal (Augé et al. 2022). For the identification of the vertebrae described here, see Discussion.

### Scincoidea Oppel, 1811 (sensu Zheng & Wiens, 2016)

Fig. 7

? Scincoidea indet.

**Material.** One right maxilla MLU.GeoS.4057, one left maxilla MLU.GeoS.4058.

**Description. Maxilla.** Two maxillae are preserved. The specimen MLU.GeoS.4057 is larger and represents a fragment of the right maxilla around the superior alveolar foramen (Fig. 7A, B). The anterior and posterior portions are broken off. The specimen possesses nine-and-a-half tooth positions (eight teeth are still attached). The lateral surface is eroded, but it can be estimated that the preserved portion was smooth. It is pierced by three supralabial foramina. The nasal process of the maxilla forms an almost perpendicular wall, although note that it is only partly preserved. It expands almost to the posterior end of the preserved portion of the bone. This posterior margin appears not to be stepped but gradually decreases posteriorly. In medial view, the supradental shelf is almost straight, only slightly expanded medially – however, it is heavily damaged. The superior alveolar opening is at the level of the sixth tooth position (counted from posterior). However, the exact number of teeth is unknown in this specimen due to the missing portions. Posterior to the opening, the bony dorsolateral wall is damaged, and thus, the area ventral to it, is exposed.

The specimen MLU.GeoS.4058 is smaller and slightly in overall better condition than 4057. It represents the left maxilla (Fig. 7C–H) around the region of the superior alveolar foramen, but here, the posterior region is preserved. The lateral surface is smooth. It is pierced by three supralabial foramina: the first anterior is located at the level of the seventh tooth position; the second is at the level of the sixth tooth position and the last posterior one lies at the level of the third tooth position (all counted from posterior). The first two are moderately large, whereas the posterior one is smaller. The dental crest is well-developed, reaching more-or-less the half the tooth height. Nine tooth positions are preserved (six teeth are still attached). The supradental shelf is only partly preserved, especially in the posterior section of the bone. The opening of the superior alveolar canal is

located at the level of the sixth tooth position (counted from posterior). However, the anterodorsal margin of the bone, which demarcates the opening, appears to be partially damaged. Due to this, the original opening might be slightly more posteriorly located, approximately at the level between the fifth and sixth tooth positions. The further posterior region is well-excavated, forming a longitudinal depression. The nasal process is partly preserved. Only its ventral portion remained intact. Its posterior margin appears to be stepped, but this region is partly broken off. Thus, an actual outline is unknown. The posterior portion protrudes into a short and narrow posteroventral process. It is bluntly ended.

**Dentition.** The tooth implantation is pleurodont. The teeth are tall, although the posterior last ones are slightly smaller (the last and penultimate teeth in MLU.GeoS.4058). The teeth are robust; the robustness increases posteriorly. They are slightly inclined posteriorly, being closely spaced with small interdental gaps. The apices are more-or-less rounded and blunt rather than having a sharp and pointed appearance (although it should be noted that the sixth tooth in MLU.GeoS.4058 has a roughly triangular appearance). The tooth crowns in MLU.GeoS.4057 are eroded, and some preservational artefact makes crowns look more rounded (plausibly because of digestion). The tooth crowns in MLU.GeoS.4058 are fairly preserved. In this specimen, the lingual surface of the crown in these teeth is concave, being curved inwards, whereas the labial one is distinctly convex. The lingual aspect of the crown is bordered by the culmen lateris anterior and culmen lateris posterior. No apicobasal crown striation can be recognized. The tooth crowns possess labial and lingual cusps, being transversally bicuspid. Note that this morphology is less noticeable, possibly due to preservation (the enamel appears to be slightly eroded – as occurs, for example, when teeth pass through stomach acid). However, further structures on enamel, such as striae, would be also affected (see Smith et al. 2021). The labial cusps form a somewhat rounded labial edge. For this reason, the overall appearance of these teeth is blunt. These labial cusps are slightly bent inwards – lingually, which is well-visible mainly in the tooth at the sixth tooth position (counted from posterior). Most tooth crowns show some longitudinal asymmetry (the mesial portion is longer than the distal one). The lingual cusps are small and hardly recognizable. They appear to be framed by short, mesially and distally running cristae lingualis dominans anterior and posterior. The tooth bases are well-expanded medially relative to the rest of the tooth shafts. The bases are pierced by oval resorption pits. A few teeth have huge pits, reaching almost over the half of their length. This feature is probably related to an artefact of preservation.

**Remarks.** The material resembles mostly scincid, where the lingual cusp is usually framed by the broadly mesially and distally running cristae lingualis anterior and posterior rather than more-or-less vertical striae dominans anterior and posterior (e.g., Kosma 2004) – the

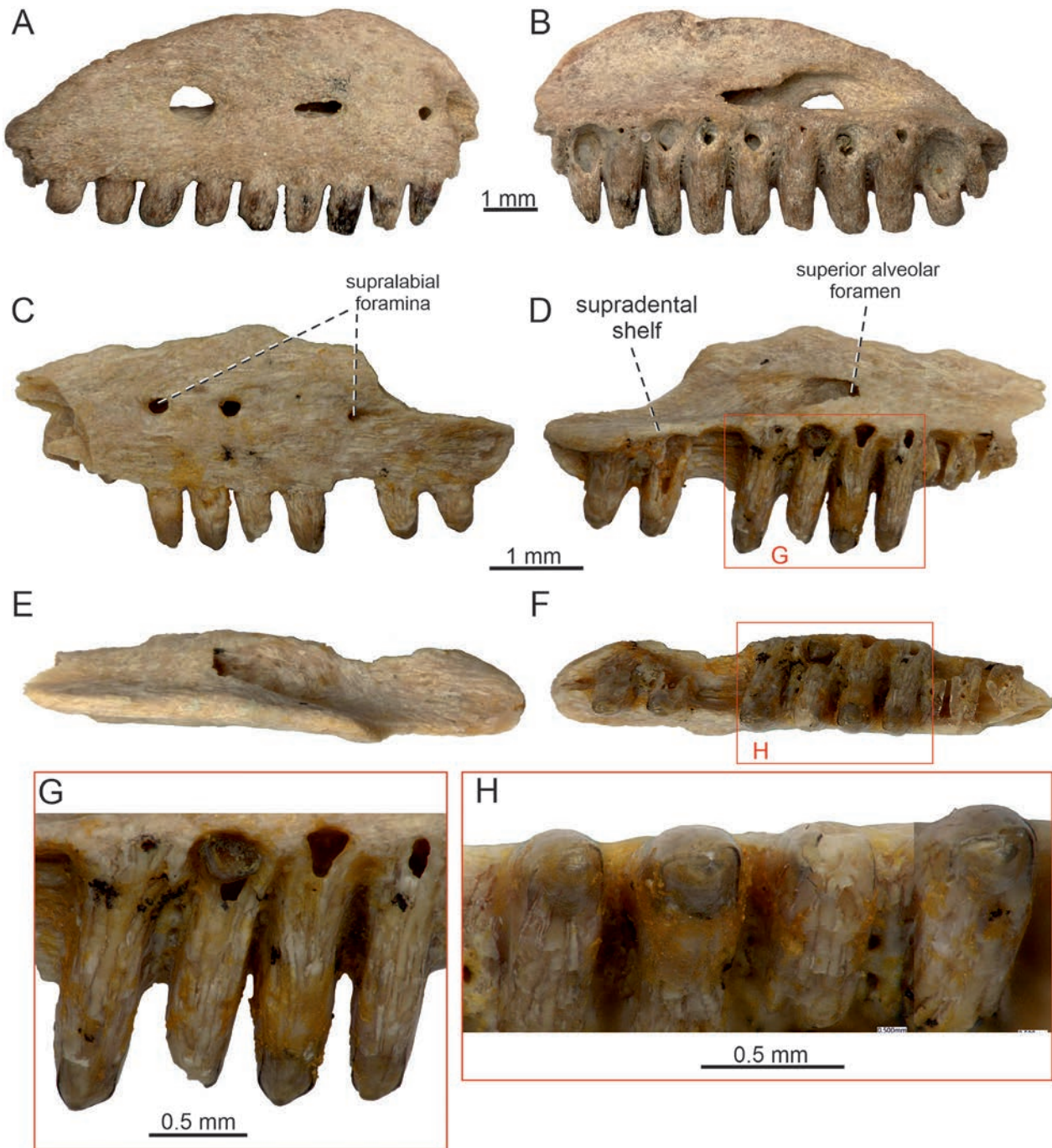


**Figure 7.** ?*Scincoidea* indet. from the Paleocene Walbeck locality. Right maxilla MLU.GeoS.4057 (**A**, **B**) and left maxilla MLU.GeoS.4058 (**C–H**) in lateral (**A**, **C**), medial (**B**, **D**), dorsal (**E**) and ventral (**F**) views. Detail of teeth of MLU.GeoS.4058 in medial (**G**) and ventromedial (**H**) views.

presence of the lingual, well-separated cusp is more common among the cordylids than the scincids (Folie et al. 2005). Transversely bicuspid teeth can be present in some gekkotans, e.g., eublepharids (Sumida and Murphy 1987). In contrast to the robust Walbeck specimens, gekkotans have lightly built skeletons, which reflects their rarity in the fossil record (Evans 2003, 2008). Transversely bicuspid teeth can be also present in teiids (in members of this group; in contrast to the Walbeck material, the teeth have extensive cementum depositions

at tooth bases, see Estes 1983) and polyglyphanodontids, but the lingual cusp is much better developed in these taxa than the small cusp of the Walbeck material and scincoideans (see Nydam 1999). In lacertids, the lingual cusp, if present, is only weakly developed. Moreover, crown lacertids usually have bi- and tricuspid tooth crowns (Čerňanský and Syromyatnikova 2019).

We cannot be certain whether both Walbeck specimens belong to the same taxon (because true crown morphology is only known for the well-preserved one

–MLU.GeoS.4058). In fact, some features do not support an allocation to a single taxon (the supralabial foramina appear to be much larger in the poorly preserved specimen MLU.GeoS.4057, teeth look a little bit more robust). However, these differences can be related to the level of preservation, ontogenetic and/or individual variability. In any case, we provisionally allocated both specimens together as ? *Scincoidea* indet.

### Phylogenetic analysis of *Camptognathosaurus walbeckensis*

The phylogenetic tree presented here is based on limited fossil material – the jaws, and thus more complete fossil specimens of this taxon are needed to draw more robust conclusions. The results of the phylogenetic showed that *Camptognathosaurus* was consistently recovered as a lacertid lizard. A New Technology (NT) search in TNT produced two equally parsimonious trees (for a consensus tree, see Fig. 8). *Camptognathosaurus walbeckensis* was placed as sister to *Gallotia atlantica* (Bremer value 1, relative Bremer 25; see Suppl. material 2). The sister group relationship between *C. walbeckensis* and *G. atlantica* was supported by 4 characters (present unambiguously in all trees, namely: characters 356, 417, 419, and 420). They together are sister to the clade [[*Cryptolacerta hassiaca* + *Lacerta viridis*] + *Takydromus ocellatus*], forming all together the clade Lacertidae (Bremer value 1, relative Bremer 33). Eolacertidae are recovered as being sister to Lacertidae. Interestingly, *Cryptolacerta* is recovered as sister to *Lacerta* (Bremer value 1, relative Bremer 25); in contrast to results of Brownstein et al. (2022), where *Cryptolacerta* was placed as sister to *Gallotia* [the phylogenies of Brownstein et al. 2022: figs S9–11 differ somewhat in the topology of Lacertidae (fig. S9–10 a polytomy, but S11 with *Gallotia* and *Takydromus* as sister-taxa, which contravenes the assumption that Gallotiinae and Lacertinae are the basal divergence].

Overall, although this may be true or not, the support for the clade is very low and thus, the interpretation of the *Camptognathosaurus* relationship among Lacertidae needs to be met with caution (*Camptognathosaurus* is represented by a very limited fossil material). In the event that future studies based on more complete material of *Camptognathosaurus* would support its closer relationship to members of Gallotiinae, this would show the presence of this lineage already in the Paleocene. In our analysis, in any case, this Paleocene taxon was never recovered as an amphisbaenian. According to morphological data, many studies show them grouping with snakes and other limbless squamates (e.g., Rage 1982; Estes et al. 1988; Conrad 2008; Gauthier et al. 2012). However, recent molecular analyses using DNA sequencing suggest that amphisbaenians is the sister group to Lacertidae (e.g., Townsend et al. 2004; Vidal and Hedges 2005; Pyron et al. 2013; Reeder et al. 2015; Zheng and Wiens 2016; Burbrink et al. 2020).

## Discussion

Although Walbeck fossil lizards are represented only by isolated elements (this is the case of most Paleogene assemblages in Europe, except of, e.g., Messel), they form an important dataset on the evolution of terrestrial herpetofauna in Europe during the late Paleocene. The paleodiversity of squamates from this locality is low. Regarding the number of specimens, this seems to be not a result of sampling or taphonomic bias. Lizards are represented only by small forms with some unusual features (*Camptognathosaurus*, for its revision, see chapter below), and some, in contrast, have very modern appearances (MLU.GeoS.4059 – Lacertidae indet).

The fauna is different in many aspects (diversity, types, etc.) relative to the faunas described from slightly younger, earliest Eocene localities, such as Dormaal in Belgium (Augé 1990, 1992; Augé and Smith 1997, 2002; Sullivan et al. 2012; Folie et al. 2013; Čerňanský et al. 2022b, 2023b; Augé et al. 2022), Cos in France (Čerňanský et al. 2023a, c) and localities in Spain (Bolet 2017).

Overall, this is consistent with the previous statement of Rage (2013) that squamates were rare and poorly diverse during the Paleocene. This is true at least according to the few known localities. However, our knowledge about this geological epoch is limited. It is worth considering a possibility that there is a bias towards selected groups, and that other faunas that were present are not recorded. However, records are still too sketchy to allow much speculation regarding the reasons for the missing groups. The Walbeck fossils provide us with the rare opportunity to observe, although only partly, the composition of herpetofaunas during this crucial interval in Europe.

In any case, a few taxa can be identified in Walbeck – Lacertidae, *Camptognathosaurus* (a lacertoid that forms the dominant group of lizards in regard to the number of elements), and (provisionally) *Scincoidea*. However, immigrants that occurred later in Europe are absent. This is in sharp contradiction with an original statement of Kuhn (1940a) that the Walbeck lizards show very close relationships with North American faunas. Although this herpetofauna of Walbeck is limited, it forms one of the few initial discoveries for our understanding of the Paleocene and the roots of the European Cenozoic ecosystems. Nevertheless, many aspects can be resolved only by future systematic research on new localities and studies of further new material from this part of the Earth history.

### *Camptognathosaurus*

Although Lacertoidea (the clade Lacertoidea includes Lacertidae, Amphisbaenia, Teiidae and Gymnophthalmidae, see Zheng and Wiens 2016; Laterata sensu Vidal & Hedges, 2005; Burbrink et al. 2020) have a well-documented Eocene record in Europe (e.g., Augé 2005, 2012; Folie et al. 2013; Čerňanský et al. 2015b;

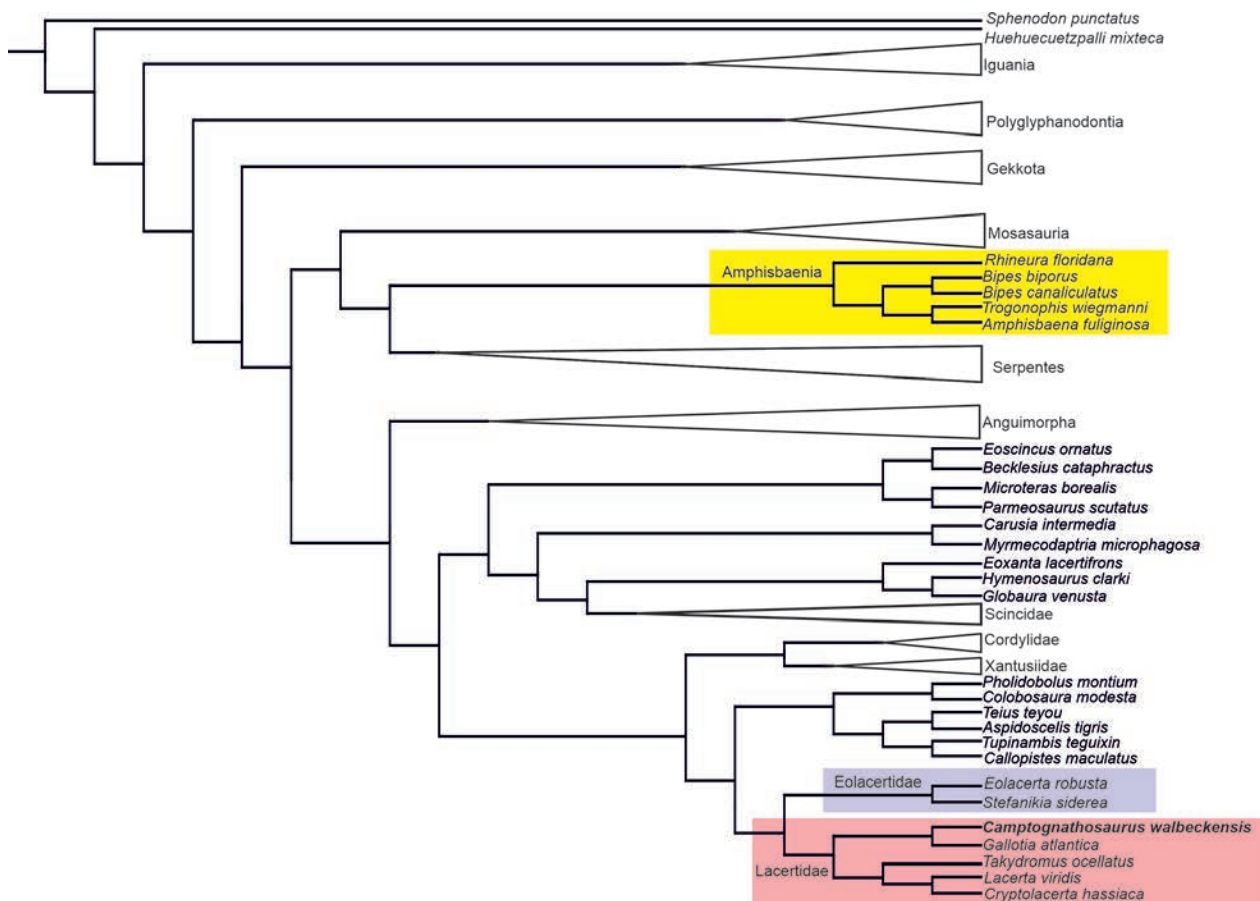


**Figure 8.** Parsimony phylogenetic analysis of *Camptognathosaurus*. Strict consensus topology generated in parsimony analysis of dataset in TNT v. 1.5. showing the potential position of the Paleocene species within Lacertidae.

Rage and Augé 2015; Čerňanský and Smith 2018), they have only rarely been reported from Paleocene deposits (Augé 2005; Folie et al. 2013; Čerňanský et al. 2020a). In regards to quantity, as previously mentioned, *Camptognathosaurus* forms a dominant component of the late Paleocene lizard fossils in Walbeck assemblage. However, in contrast to that, species diversity appears to be low – only one taxon is identified. A huge amount of individuals in the record might point to a very successful population (considering that this is not caused simply by the fact that the jaws of this taxon are more robust than those of other lizards and, therefore, more resistant to destructive processes related to fossilization processes, as also reflected in their resistance to destruction by digestion of predators). Low diversity of fauna might eventually cause less competition for a species in regard of its particular lifestyle. In any case, this potentially shows that lacertids (pan-lacertids sensu Čerňanský and Smith 2018), not amphisbaenians (see below), formed likely a dominant group of the Paleocene lizard fauna in Europe.

### Revision of *Camptognathosaurus*

In regard to aff. *Glyptosaurus walbeckensis* described by Kuhn (1940a), Estes (1983) rejected its glyptosaurid affinities and suggested that it was a lacertid and

tentatively referred it to *Pseudeumeces*. Later, Augé (2005) suggested it was a potential amphisbaenian and considered it a nomen dubium. Indeed, it could appear to be a polyodontobaenid based on the combination of the following features (see diagnosis in Folie et al. 2013:227): (1) the tooth number (10–12); (2) an absence of an angle at the symphysis (the presence of this feature is related to fossoriality, see Gans 1974); and (3) teeth increase in size posteriorly. Thus, the posterior teeth are robust and massively built. The first is, however, a plesiomorphy. The second is also a plesiomorphy that is not shared with *Polyodontobaena* – one of the important features included by Longrich et al. (2015) in their study was the “kink” in the ventral margin of the dentary associated with the expansion of the symphysis below the Meckelian canal. Such a morphology is seen in *Polyodontobaena*, but not in *Camptognathosaurus*. The third is important but hardly determinative, as such dentition has arisen numerous times in Squamata. It evolved independently in various lineages such as Lacertidae, Amphisbaenia, Iguanidae, Teiidae, Scincidae, Xantusiidae, Anguillidae, Varanidae and Mosasauridae (Estes and Williams 1984). Polyodontobaenidae deserves a comment here. Although Folie et al. (2013) mentioned the presumed archaic features of polyodontobaenids („primitive amphisbaenians“), the fact is that in the most extensive phylogenetic analysis of

amphisbaenians (Longrich et al. 2015) *Polyodontobaena* is sister to the clade Blanidae, more derived than rhineurids. Thus, “a primitive morphology” in *Polyodontobaena* can be seen only in regard to crown members of Blanidae.

The stratigraphically older species *Polyodontobaena belgica* from the early Paleocene of Belgium (MP 1–5, Hainin) is, however, very different from *Camptognathosaurus* by the following features: (1) pointed tooth crowns are present (Folie et al. 2013); (2) the dentition is shallowly pleurodont (most of the tooth length is exposed from the lateral side as well – the condition seen in amphisbaenians); (3) the dentary of the Belgian taxon is slender and its ventral dentary margin is straight (except for the kink); (4) the Meckelian canal is narrow; (5) the intramandibular septum reaches the level of the last tooth position posteriorly; (6) the fossa for the adductor musculature is located behind the tooth row; (7) lower number of labial foramina.

The dentaries of *Camptognathosaurus* clearly possess several interesting features that are in contrast to members of Amphisbaenia: (1) absence of an angle at the symphysis (an angle is present at the symphysis of the dentary in most amphisbaenians, e.g., Gans 1974; Gans and Montero 2008); (2) high number of teeth (the presence of ten or fewer teeth is synapomorphic of Amphisbaenia, see Smith 2009; although not unique to them among squamates. The amphisbaenian skull is short and robustly built, and the reduced dentary of modern forms bears five to nine teeth, see Kearney 2003); (3) moderately low dental crest [teeth exceed the dental crest by more-or-less the half of their length in contrast to amphisbaenians, in which the tooth implantation is shallowly pleurodont (acrodont in Trogonophiidae) - the dental crest is markedly low]; (4) sulcus dentalis is well developed (in amphisbaenians, it is usually only slightly developed; see, e.g., Bolet et al. 2014); (5) splenial reaches the anterior section of the dentary (among amphisbaenians, the presence of a splenial is restricted to members of Blanidae – the splenial in the extant *Blanus* is a tiny splint of bone, partly covering the Meckelian canal medially and barely leaves an imprint on the medial side of the subdental shelf, see Gans and Montero 2008; Bolet et al. 2014; Villa et al. 2019; although note that the splenial is relatively large in the Eocene *Cuvieribaena*, see Čerňanský et al. 2015b); (6) intramandibular septum does not reach the end of the tooth row posteriorly (the intramandibular septum extends along the entire tooth row in amphisbaenians, except of *Rhineura*, see Smith 2009; Čerňanský 2019); (7) wedge-shaped fossa for the adductor musculature is extensive, running well below the tooth row (although this can be simply connected to a stronger bite force connected to amblyodont teeth; in *Polyodontobaena* and extant Amphisbaenia, it is usually behind the tooth row); (8) high number of labial foramina (five or six instead of usually three in amphisbaenians, see Gans and Montero 2008; Čerňanský 2019; Villa et al. 2019) and (9) the largest amblyodont teeth in Walbeck specimens are present in the posterior section of the

jawbone. This is in sharp contrast to stratigraphically younger amphisbaenians with amblyodont dentition, in which the largest teeth are in the anterior region (see Čerňanský et al. 2015b; Čerňanský 2023). Thus, by having robust teeth in the posterior rather than anterior region of the tooth row, these Paleocene forms resemble members of the clade Lacertidae (see, e.g., Čerňanský et al. 2016a,b, 2017). If *Camptognathosaurus* would be an amphisbaenian, then this would be a plesiomorphic condition for Amphisbaenia. The position of the largest teeth in a tooth row is not random but reflects the lever mechanism of the mandible to be more effective. The postdentary position of the articulation area of the mandible with the quadrate is directly determined by the length and the orientation of the posterior region of the mandible, which influences the tooth row and mandibular geometry and mechanics. The lever mechanism in a typical amphisbaenian mandible is more effective when the larger teeth are in the anterior region rather than posteriorly (Čerňanský et al. 2015b; note that the condition in amphisbaenians represents rather a novel adaptation among lacertoids). Overall, it seems likely that the mandibular mechanism of *Camptognathosaurus* was more similar to lacertids rather than to amphisbaenians (in regard, see *Cuvieribaena* from the Eocene of France described by Čerňanský et al. 2015b). Note, however, that the largest teeth in the posterior section of the tooth row are also present in the extant *Amphisbaena ridleyi* (see Pregill 1984: fig. 1A). The mandible of this species is rather atypical for amphisbaenians. The whole mandible of *A. ridleyi* is concave dorsally, and the typical feature of most amphisbaenian dentaries - an angle at the symphysis (e.g., Gans 1974; Gans and Montero 2008; Longrich et al. 2015), is absent. In fact, however, the condition in lacertids such as *Pseudeumeces cadurcensis*, *Dracaenosaurus croizeti*, *Janosikia ulmensis*, *Maioricalacerta rafelinensis*, is also common in other lizards – amblyodont teeth in most durophagous lizards are in the posterior or mid-posterior region of the dentary, as in, e.g., *Dracaena guianensis*, *Tiliqua scincoides*, *Eumeces schneideri*, *Paraplacosauriops quercyi*, *Pseudopus apodus*, and *Varanus niloticus* (Dalrymple 1979; Rieppel and Labhardt 1979; Pregill 1984; Augé 2005; Bailon et al. 2014; Klembara et al. 2014; Čerňanský et al. 2016a, b, 2017; Čerňanský and Syromyatnikova 2021; Georgalis et al. 2021b).

Both maxillae MLU.GeoS.4047 and 4048 possess some very interesting features. In all modern amphisbaenians (including Miocene forms), the posteroventral process is reduced, whereas the posterior section is formed by the posteriorly distinctly protruded ectopterygoid process (sensu Bolet et al. 2014) of the maxilla (see Gans and Montero 2008; Bolet et al. 2014; Čerňanský 2019; Villa et al. 2019). This is an opposite condition to the Walbeck maxillae. Moreover, the delicate, well-developed, pre-terminal palatine process is not known in any crown amphisbaenian, and the flaring of the maxilla posteriorly is also unknown (except in *Trogonophis*). One

feature deserves a comment: the posterior region of the maxilla implies the presence of a jugal. If this is correct, a jugal is present in known crown amphisbaenians only in Rhineuridae (Gans and Montero 2008). Moreover, Estes (1983) stated that there is a weak sculpture reflecting osteodermal attachment on the nasal process of the specimen figured by Kuhn (1940b: tab. II fig. 4), although this specimen cannot be allocated to *Camptognathosaurus* without doubts, since it is figured only in lateral view.

Thus, while this seemed possible based on the holotype dentary from France, the detailed study of the Walbeck dentary and especially maxillae reveals a stunningly primitive morphology for anything but a hypothetically basal-most stem amphisbaenian. Although *Polyodontobaena* appears to belong to Amphisbaenia, possibly representing a stem blanid (it is recovered as the sister taxon to Blanidae, see Longrich et al. 2015), there are serious doubts that the same is true for *Camptognathosaurus*. Indeed, the latter one resembles more, in some features, the Eocene *Cryptolacerta* from the classic Messel locality in Germany. *Cryptolacerta* was considered as being closest to the amphisbaenian ancestor (Müller et al. 2011), but this was put in doubt in several studies and the phylogenetic analyses placed it with Lacertidae (Longrich et al. 2015; Tałanda 2016; Brownstein et al. 2022). *Camptognathosaurus* shares the following features with *Cryptolacerta* (see Müller et al. 2011; Smith and Habersetzer 2021; Fig. 9A–C here): (1) the large coronoid process that, at least partly, might cover the anterolateral part of the coronoid; (2) the slightly arched ventral margin; (3) the rounded subdental shelf; (4) the absence of an angle at the mandibular symphysis; (5) the Meckelian canal is fully open and exposed medially, being narrow in the anterior region and widens slightly posteriorly; (6) the position of the alveolar foramen relative to the tooth row; (7) the around five labial foramina; (8) the well-developed, wedge-shaped fossa for the adductor musculature; (9) the moderately low dental crest; (10) the heterodont dentition; (11) the short tooth row (fourteen tooth positions are present in the holotype, but only eleven in the second specimen; Müller et al. 2011; Smith and Habersetzer 2021); (12) the enlarged posterior teeth; (13) the posteroventral process of maxilla long rather than short; (14) the maxillary tooth row does not reach the posterior end of the bone but leaves a small posterior toothless portion; and (15) the presence of jugal. There are, however, important differences as well, such as the presence of bicuspid tooth crowns in *Cryptolacerta*. In fact, most of these character states suggest lacertid affinities in general or, among them, of durophagous lacertids (most of them are widespread among lacertids, particularly amblyodont lacertids like *Dracaenosaurus* and *Pseudeumeces*). Interestingly, however, the first character state (the large coronoid process that, at least partly, might cover the anterolateral part of the coronoid) is absent in crown lacertids, in which a lateral overlap of the posterodorsal margin of the dentary by the coronoid is present. The condition in *Cryptolacerta* and

*Camptognathosaurus* is rather typical of amphisbaenians (not in *Rhineura*, see Gans and Montero 2008; Čerňanský 2019). However, this feature is not restricted to them and is also present in, e.g., dibamids (Čerňanský 2019) and in skinks, such as *Acontias*, *Ophiomorus*, *Heremites*, *Tiliqua* and *Eumeces* (Čerňanský 2019; Čerňanský et al. 2020b; Čerňanský and Syromyatnikova 2021). The last two taxa also have amblyodont dentition, although *Tiliqua* has a closed Meckelian canal. In fact, the tendency toward closure of the Meckelian canal is a characteristic of many scincid lizards (Greer 1970, 1974; Rieppel 1981; Estes 1983; Evans 2008; Augé and Smith 2009; Hutchinson and Scanlon 2009; Gauthier et al. 2012; Čerňanský et al. 2020b; Čerňanský and Syromyatnikova 2021). Although members of *Eumeces* have an open Meckelian canal in dentary and amblyodont teeth, they differ from *Camptognathosaurus* in many aspects (see Čerňanský et al. 2020b), e.g., (1) higher tooth number (around 18); (2) higher dental crest relative to the tooth size; (3) although splenial is well developed, its dorsal portion attached to the subdental shelf reaches only to the half of the tooth row; and (4) the maxillary tooth row reaches almost the posterior end of maxilla. So the conclusion is that although *Camptognathosaurus* has amblyodont teeth, it does not seem to have any characteristics that would indicate its allocation to skinks.

Thus, in general, all the new data bring serious concerns about the attribution of *Camptognathosaurus* to Amphisbaenia. It seems much reasonable to suggest its relationship being closer to lacertids, e.g., to forms such as *Pseudeumeces* or *Cryptolacerta*. Unfortunately, *Cryptolacerta* requires a detailed revision of its anatomy and phylogenetic relationship. As mentioned above, its current status is considered to be a lacertid (Longrich et al. 2015; Tałanda 2016; Brownstein et al. 2022). It may be a specialized lacertid with burrowing adaptations (see, e.g., Tałanda 2016). Based on current data, we can suggest the hypothetical possibility that *Camptognathosaurus* is related to *Cryptolacerta* rather than to *Blanus*, and that both these early Paleogene taxa might be lacertids (at least pan-lacertids). *Camptognathosaurus* is too incomplete, but can be assigned to clade Lacertoidea without doubt. Based on the overall bone morphology, *Camptognathosaurus* is provisionally assigned here to the total clade Lacertidae. It shares the following combination of features with Lacertidae (see Estes et al. 1988; Čerňanský and Syromyatnikova 2019; Villa and Delfino 2019): (1) well-developed sulcus dentalis; (2) subdental shelf of the dentary (without splenial spine) is well protruded medially; (3) wide medially open Meckelian canal (restricted in eolacertids, see Čerňanský and Smith 2018, 2019); (4) an arched dentary, with concave tooth row, subdental shelf, and ventral edge; (5) pleurodont implantation and replacement areas located at the center of the tooth bases; (6) dentary tooth number 10–12; the number spans well among the number of the amblyodont lacertids such as the Paleogene *Pseudeumeces* and *Dracaenosaurus*; (7) well-developed and continuous

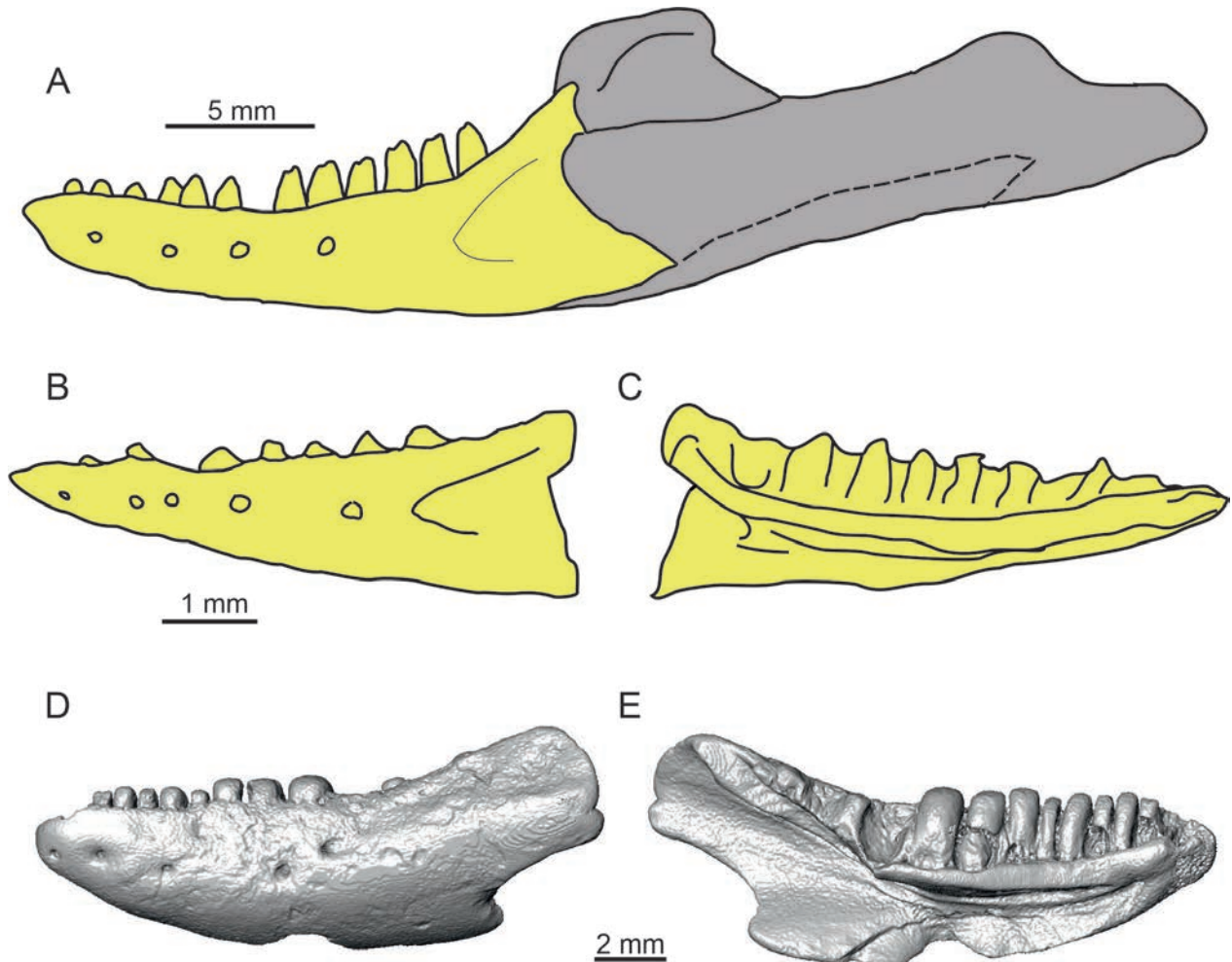


**Figure 9.** Paleogene lacertoids – the Eocene *Cryptolacerta hassiaca* (A–C) from Messel and the Oligocene *Pseudeumeces kyrillo-methodicus* from Quercy (D, E). Left mandible of the holotype SMF ME 2604 in lateral (A) view (modified from Müller et al. 2011); left dentary of the specimen found in the gut of *Paranecrosaurus feisti* in lateral (B) and ventral (C) views (modified from Smith and Habersetzer 2021). Virtual 3D models of the holotype left dentary NHMW 2019/0051/0001 in lateral (D) and medial (E) views.

splenic facet on the medioventral edge of the subdental shelf; (8) splenic is large and long, reaching the anterior region of dentary; (9) the maxillary tooth row does not reach the posterior end of the bone but leaves a small posterior toothless portion (contra, e.g., teiids and skinks) and, (10) potentially, assumed presence of osteoderms fused to the lateral side of the facial process of maxilla (suggested by Estes 1983). The presence of all these features indicates lacertid lizards rather than members of other groups. Note, however, that there are some differences between this Paleocene form and crown lacertids such as a large coronoid process of the dentary mentioned above. On the other hand, although this condition is not the same, a large and slightly dorsally elevated coronoid process is also present in crown lacertids with amblyodont dentition such as *Pseudeumeces* (Fig. 9D, E), *Dracaenosaurus* and *Janosikia* (all members of Gallotiinae; see Čerňanský et al. 2016a, b, 2017; Georgalis et al. 2021b). Thus, in fact, this might be potentially related to the amblyodont dentition, rather than being a character suggesting this form is out of the crown. In any case, this hypothesis about the

relationship of *Camptognathosaurus* to lacertids needs to be met with caution and should be tested by future studies of new, more complete fossil record of this taxon.

In general, our hypothesis would support the model proposed by Čerňanský and Smith (2018) about the origin and early history of Lacertidae that the Paleogene of Europe, rather than being dominated by archaic forms only distantly related to Lacertidae (e.g., Mayer and Benyr 1994; Müller et al. 2011), in fact, hosted large radiation of pan-lacertids - the total clade including Lacertidae [Pan-Lacertidae sensu Čerňanský and Smith 2018, the stem-based clade. Note that this name was originally used in Čerňanský and Smith (2018), later in Čerňanský et al. (2020a) and Brownstein et al. (2022), however, has never been officially erected. It should include extant Lacertidae and all extinct taxa descended from its last common ancestor, as well as stem lacertids that diverged prior to the origin of the crown. *Camptognathosaurus walbeckensis* is only questionably referred here to lacertids based on its morphology (as further confirmed by phylogenetic analyses) and also overall similarity to forms such

as *Pseudeumeces* and *Cryptolacerta*, following studies of the latter taxon (Longrich et al. 2015; Tałanda 2016; Brownstein et al. 2022), in which, *Cryptolacerta* is a crown lacertid]. In other words, the Paleogene of Europe does not only contain members of the stem, but a mixture of members of the stem (*Eolacerta*, *Stefanikia*), and crown groups (see Čerňanský and Augé 2013; Čerňanský et al. 2016a, 2017; Čerňanský and Smith 2018). Note that the position of *Cryptolacerta* and *Camptognathosaurus* is uncertain. They could, hypothetically, represent stem members (more closely related to the crown than to eolacertids), but as mentioned above, in regard to *Cryptolacerta*, the Brownstein et al. (2022) reference phylogenies all find it as a sister-taxon to *Gallotia atlantica*, i.e., in crown Lacertidae. Longrich et al. (2015) do not necessarily contradict this assignment, because they did not include any extant member of Gallotiinae. In our analysis, *Cryptolacerta* is sister to *Lacerta* and *Camptognathosaurus* is sister to *Gallotia* (Fig. 8). So as far as the current reference phylogenies are concerned, both *Cryptolacerta* and *Camptognathosaurus* appear to be crown Lacertidae. But again, this Messel taxon requires a detailed revision to resolve its exact phylogenetic position and more complete fossil specimens of *Camptognathosaurus* are needed to draw more robust conclusions.

### Kuhn's „*Glyptosaurus walbeckensis*“ vs. „*Camptognathosaurus parisiensis*“

Kuhn (1940a) diagnosed „(aff.) *Glyptosaurus walbeckensis*“ as:

1. having a maximum of ten tooth positions. Although it is possible since some dentaries from Walbeck could possess ten tooth positions, we can doubt it based on Kuhn's figures. It seems to be more likely (based on comparison with herein studied specimens) that his specimen has eleven tooth positions (the teeth in the anterior region are much smaller). Based on the figures of Kuhn (1940a, b), Estes (1983) also regarded the number of teeth as 10–12.
2. the amblyodont dentition, the last teeth gradually decrease in size.
3. the strongly elevated “coronoid” (Kuhn used the term coronoid, but because the coronoid bone is not preserved in the material, we suggest that he probably thought the coronoid process of dentary), i.g., the same as the form described here as *Camptognathosaurus*.

The specimen figured by Kuhn (1940a: fig. 4b, 5b) is very similar to the specimen RIV PP 413 selected by Folie et al. (2013: fig. 3A) as the holotype of *Camptognathosaurus parisiensis* from the French localities. Moreover, the dentary RIV PP 413 shares the same features with the Walbeck specimen MLU.GeoS.4045 described here (Fig. 3A–D; see remarks

above). The principle of priority regarding the scientific name of the International Code of Zoological Nomenclature ICZN (1999) makes *Camptognathosaurus parisiensis* a junior synonym of the species described by Kuhn (1940a). Thus, this taxon gets a combined name, *Camptognathosaurus walbeckensis* comb. nov., because Kuhn used *Glyptosaurus* as a generic name. It does not matter if the older type species is a junior synonym – it is clear in ICZN (Article 67.1.2: “The name of a type species remains unchanged even when it is a junior synonym or homonym, or a suppressed name”).

### Problem of morphotypes in Walbeck

Paleocene lizards from Europe are described based only on the isolated jaws, whereas more complete specimens, which would shed more light on their morphology and taxonomy, are currently unknown. Potentially, one could suggest that two morphotypes can be identified in Walbeck. They can be distinguished by a slightly different tooth count and tooth crown morphology. Regarding the second character, we prefer not to describe two forms based on minor differences (see argumentations below). We suggest two hypothetical explanations:

1. the jaws with slightly more pointed teeth represent different taxon.
2. more probably – the Walbeck material with slightly more pointed teeth represents younger, juvenile ontogenetic stages (at least some of them, e.g., MLU.GeoS.4041; see Fig. 4K–M) of *Camptognathosaurus walbeckensis* comb. nov. (e.g., Fig. 3A–D). Some minor differences can be also caused by individual variability and taphonomic alteration. In any case, all differences in tooth crown morphology can be explained. It is important to note that specimens with intermediate conditions are present in the material, and no strict border clearly separating two morphotypes could be found:
  - a. pointedness: this feature varies among individuals and even in a single tooth row. There are many intermediate stages, for example, the robust teeth in MLU.GeoS.4042 (Fig. 4A, B). Moreover, the concave distal margin of the tooth crown is also present in the penultimate preserved tooth of MLU.GeoS.4045, although less pronounced (see Fig. 3D). The same condition can be seen in the type material of *Camptognathosaurus parisiensis* described by Folie et al. (2013: fig. 3). The change in tooth crown morphology during ontogeny is well documented for many lizards, even in a much higher degree. For example, dental complexity decreases during ontogeny in *Ctenosaura* (*C. pectinata* and *C. similis*), which is generally insectivorous as a juvenile and herbivorous as an adult (Christensen and Melstrom 2021). Among anguines, the apices

of teeth are more-or-less pointed in juveniles of *Pseudopus* (both extant *P. apodus*, see Klembara et al. 2014 and fossil *P. panonicus*, see Loréal et al. 2023), whereas adults have robust amblyodont teeth. In extant lacertids, an ontogenetic change in the tooth morphology is sometimes observed, as in *Gallotia stehlini*, where the juvenile tricuspid teeth are replaced by multicuspids in the adult (Barahona et al. 2000). Among fossil lacertids, this was observed in the Early Miocene *Janosikia* – although amblyodont dentition is present in the juvenile specimen (as in adults), vestiges of mesial cusps are present on some anterior maxillary teeth (see Čerňanský et al. 2016a).

- b. tooth count: note that the original holotype of *Camptognathosaurus parisiensis*, RIV PP 413, has eleven tooth positions (Folie et al. 2013). This observation falls within the variability range of the Walbeck specimens. Moreover, the number of teeth and labial foramina in all lizards is variable and in general size-related, so these numbers should not be regarded as absolute differentiation.

In any case, all differences are too small to be considered as distinguishing features.

For all these reasons, we regard them to be intraspecific and/or ontogenetic variations, some of them are caused by poor preservation and, thus, should represent the same taxon. It should be noted, however, that the biological (not just taxonomic) conspecificity of two populations – based on fragmentary dentaries – is not 100% secure.

### Paleoecology

Nowadays, true feeding specialists among lizards are rare. The problem is also that although squamates seem to be ideal subjects for investigating relationships between diet and dental patterns, studies exploring patterns between tooth shape and diet are remarkably rare for squamates (Christensen and Melstrom 2021). The dentition of *Camptognathosaurus* indicates durophagous specialist. Although it may have preferred to eat hard-shelled invertebrates, as is generally the case in amblyodont lizards (Dalrymple 1979; Rieppel and Labhardt 1979; Estes and Willams 1984), the presence of amblyodont teeth does not demonstrate that *Camptognathosaurus* fed solely on shelled invertebrates, because durophagy is not restricted to such prey. Most fossil taxa with amblyodont dentition (except of, e.g., *Dracaenosaurus* with its extremely durophagous specialization, see Čerňanský et al. 2017) were probably faunivorous (or even more likely omnivorous, as it is seen in the extant scincid *Tiliqua*, see, e.g., Christian et al. 2003; Shea 2006). In fact, only a few durophagous specialists exist worldwide nowadays. Among Tupinambinae, for example, only *Dracaena* is a truly durophagous form, whereas other teiids with

amblyodont teeth are omnivorous (Mercolli and Yanosky 1994; Kiefer and Sazima 2002).

Interestingly, snails are highly unusual in the diets of modern amphisbaenian species and have been reported as the main prey for only two species: *Amphisbaena ridleyi* (Pregill 1984), which has robust, but still somewhat pointed teeth and *Trogonophis wiegmanni* (Gans 1960; Martín et al. 2013), which has robust, blunt teeth, with acrodont implantation. Teeth indicative of durophagy have been observed in the Eocene amphisbaenians *Cuvieribaena* from France (Čerňanský et al. 2015b) and the North American *Oligodontosaurus wyomingensis* (Estes 1975; although in this latter species the teeth are somewhat pointed). On the other hand, amblyodont teeth repeatedly occur among lacertid members during different periods of the European Cenozoic (Augé 2005; Bailon et al. 2014; Čerňanský et al. 2016a, b, 2017). Amblyodonty is certainly adaptive and can respond to several environmental cues and climate change might be one of them. Paleogene terrestrial ecosystems faced significant changes and reorganisations. If *Camptognathosaurus* is a lacertid, then this type of ecology shows a tendency in members of the clade already in the Paleocene. This is interesting because present-day lacertids are more uniform (no lacertid species with amblyodont dentition is known to exist today). The interpretation of *Cryptolacerta* as a member of the total clade of Lacertidae (Longrich et al. 2015; Tałanda 2016; Brownstein et al. 2022) suggests that members of the clade was also able to evolve modifications such as partially reduced both fore- and hindlimbs (Tałanda 2016). It seems that lacertids were able to respond to changes by evolving different types of adaptations which allowed them to occupy different ecological niches (much broader than seen in present-day members of this lineage). As already stated by Čerňanský and Smith (2018), the ecological breadth of pan-lacertids is amply demonstrated by the differences in size and body form (e.g. small semifossorial forms like *Cryptolacerta*, mid-sized and large terrestrial forms like *Stefanikia* and *Eolacerta*). Some of these (*Succinilacerta*, *Plesiolacerta*) were more closely related to crown Lacertidae than others, and even crown representatives may have been present (Borsuk-Bialynicka et al. 1999; Čerňanský and Augé 2013; Čerňanský et al. 2016a). Most of these lineages became extinct until only members of the crown remained. Meanwhile, one lineage (Lacertinae) radiated magnificently in the Neogene, uplifting Lacertidae as the dominating group of reptiles in present day Europe (Čerňanský and Smith 2018).

### “aff. *Parasauromalus paleocenicus*” as Lacertidae

As mentioned in the Introduction, Kuhn (1940a) established the species “aff. *Parasauromalus paleocenicus*” based on an isolated left dentary. This dentary has been identified among the material studied herein (Fig. 5).

However, the left dentary MLU.GeoS.4059 clearly does not correspond to an iguanian (for *Parasauromalus* see Smith and Gauthier 2013: fig. 8C). The same is true for isolated vertebrae, which do not belong to either an iguanian or a varanoid. Indeed, as Estes (1983) suggested, the dentary can be allocated to Lacertidae. However, its reclassification to *Plesiolacerta*, questionably suggested by Estes (1983), cannot be supported. That Eocene taxon is characterized (see Čerňanský and Augé 2013; Čerňanský and Syromyatnikova 2019) by: (1) heterodont dentition, including mono-, bi- and tricuspid teeth; (2) dentary with an overall prominently arched shape; and (3) widely open and large Meckelian groove. If lacertid vertebrae (at least some of them) belong to the same taxon as the dentary, then their morphology could be a further argument against its allocation to *Plesiolacerta*, in which the vertebrae are characterized by a strongly-developed zygosphene and zygantum (Čerňanský and Augé 2013). The dentary morphology resembles the one present in typical crown insectivorous lacertids (see, e.g., Čerňanský et al. 2015a: fig. 3a,b; Čerňanský and Syromyatnikova 2019, although it cannot be fully excluded that this dentary belonged to a taxon which is on the stem of Lacertidae, just closer than other forms described so far from the Paleocene). Therefore, the name „*aff. Parasauromalus paleocenicus*“ should be considered as a nomen dubium. In any case, this record forms an important evidence because it strongly supports the presence of Lacertidae in Europe already in ~MP 5. This is consistent with recent molecular analyses in which the crown ages were recovered for Lacertidae in the Paleocene or around the Cretaceous-Tertiary (K/T) transition (Vidal and Hedges 2009; Hipsley et al. 2009; Garcia-Porta et al. 2019).

All vertebrae described here are allocated to Lacertidae, because their morphology resembles the one present in lacertids (see, e.g., Čerňanský et al. 2015a: fig. 4I-M for a fossil one, Tschopp 2016 for extant ones), but more precise allocation is impossible. It should be noted, however, that the vertebral morphology of *Camptognathosaurus* is currently unknown. In fact, it cannot be fully excluded that some specimens, like MLU.GeoS. 4066, might belong to *Camptognathosaurus*. Two reasons might support it: (1) this taxon is the most numerous in regard to preserved elements in Walbeck, and (2) the presence of a low neural spine is reported for *Cryptolacerta* too (Müller et al. 2011), which is similar to *Camptognathosaurus* in many aspects (see comparison above).

One question arises regarding the original attribution of *Camptognathosaurus* to amphisbaenians by Folie et al. (2013). Vertebrae of modern amphisbaenians can be easily recognized in the fossil record (although an allocation at the family level is very difficult) by the following combinations of features (see Estes 1983): (1) depressed centrum with a flat ventral surface; (2) roughly parallel lateral margins in ventral aspect; (3) massive synapophyses; (4) absence of zygosphene; and (5) and a sinusoidal neural arch lacking a neural spine. No vertebra from Walbeck possesses a combination of these features. One

can argue that according to Folie et al. (2013), the members of polyodontobaenids (if *Camptognathosaurus* belonged to this clade) exhibit many plesiomorphic features in jaws. Thus, this could also be expected from elements from other body parts. Some specimens, such as MLU.GeoS. 4066 are interesting. It possesses roughly parallel lateral margins in ventral view and quite large subcentral foramina (Fig. 6G). Other morphological character states (i.e., the presence of the neural spine), however, do not support an allocation of any vertebrae currently known from Walbeck to Amphisbania but rather show affinity to lacertids. For this reason, in this study, we prefer to assign tentatively all herein-described vertebrae as Lacertidae. Moreover, if *Camptognathosaurus* belongs not to crown Lacertidae, but, at least, to the total clade, such an allocation would not be entirely inconsistent even if some of these vertebrae would prove to belong to this taxon.

## Scincoidea

The allocation of the right (MLU.GeoS.4057) and left (MLU.GeoS.4058) maxillae to Scincoidea (the clade includes Scincidae, Cordyliformes and Xantusiidae, see Zheng and Wiens 2016) is supported (see remarks above). Previously, Folie et al. (2005) described material from the middle Paleocene of Belgium as *Scincoideus haininensis*. Although the crown tips of this taxon do not possess striae similar to the Walbeck material, and the tooth apices also have a rather blunt appearance, some differences still can be observed. For example, the last posterior supralabial foramen is located at the level of the eighth tooth position (counted from posterior), whereas in the maxilla from Walbeck it is located at the level of the third tooth position (in MLU.GeoS.4058). However, the Belgian material requires a detailed revision because there are doubts about its allocation to Scincoidea. This taxon is rather considered to be a member of Lacertoidea (see Smith and Gauthier 2013; Čerňanský et al. 2020a). More complete Walbeck specimens are needed for a proper comparison.

## Palaeogeographic note for the Paleocene

Besides Walbeck in Germany and Rivecourt-Petit Pâtis (MP 6b) and Cernay-lès-Reims (MP 6a) both France, the material of “*cf. Camptognathosaurus parisiensis*” is also described from the locality Montchenot (Paris Basin, MP 6; Augé et al. 2021). This locality is geographically close to Cernay. Based on the occurrence of the same taxon, it might seem likely that the whole area, including the French localities and the German Walbeck locality, might have formed one palaeogeographical unit (e.g., an island or part of the continent above the sea level) in the Paleocene. Note, however, that a dispersion over sea cannot be fully excluded as this is not uncommon for lizards (e.g., Losos 2009; Čerňanský et al. 2020c),

in which even fossorial forms such as amphisbaenians are found on islands. Although palaeodistribution of *Campygnathosaurus* is important, it is difficult to make the strong argument that today's northern France and Germany were really united by a land connection on this basis. Future research of new localities and various types of organisms might shed light on the paleogeography of Europe during the Paleocene.

## Acknowledgments

This work was supported by the Scientific Grant Agency of the Ministry of Education of Slovak Republic and Slovak Academy of Sciences, Grant Nr. 1/0160/24 (A. Č). For advice about ICZN rules, we thank Georgios Georgalis (Polish Academy of Sciences). We thank Krister T. Smith (Senckenberg Research Institute, Germany) and one anonymous reviewer for critically reading of the manuscript.

## References

- Arnold EN, Arribas O, Carranza S (2007) Systematics of the Palaearctic and Oriental lizard tribe Lacertini (Squamata: Lacertidae: Lacertinae), with descriptions of eight new genera. *Zootaxa* 1430: 1–86. <https://doi.org/10.11646/zootaxa.1430.1.1>
- Augé ML (1990) La faune de lézards et d'amphisbènes (Reptilia, Squamata) du gisement de Dormaal (Belgique, Eocène inférieur). *Bulletin de l'Institut Royal des Sciences Naturelles de Belgique, Sciences de la Terre* 60: 161–173.
- Augé ML (1992) *Campinosaurus woutersi* n.g. n.sp., Anguimorphe nouveau (Lacertilia) de l'Éocène inférieur de Dormaal (Belgique). Une relique éocène des Dorsetisauridae du Jurassique terminal/Crétacé basal? *Comptes rendus de l'Académie des Sciences* 315: 885–889.
- Augé ML (2005) Évolution des lézards du Paléogène en Europe. *Mémoires du Muséum national d'Histoire naturelle* 192: 1–369.
- Augé ML, Rage J-C (2006) Herpetofaunas from the upper Paleocene and lower Eocene of Morocco. *Annales de Paléontologie* 92: 235–253. <https://doi.org/10.1016/j.annpal.2005.09.001>
- Augé ML, Smith R (1997) Les Agamidae (Reptilia, Squamata) du Paléogène d'Europe occidentale. *Belgian Journal of Zoology* 127: 123–138.
- Augé M, Smith R (2009) An assemblage of early Oligocene lizards (Squamata) from the locality of Boutersem (Belgium), with comments on the Eocene-Oligocene transition. *Zoological Journal of the Linnean Society* 155: 148–170. <https://doi.org/10.1111/j.1096-3642.2008.00435.x>
- Augé ML, Dion M, Phélizon A (2021) The lizard (Reptilia, Squamata) assemblage from the Paleocene of Montchenot (Paris Basin, MP6). In: Steyer JS, Augé ML, Métais G (Eds) *Memorial Jean-Claude Rage: A life of paleo-herpetologist*. *Geodiversitas* 43(17): 645–661. <https://doi.org/10.5252/geodiversitas2021v43a17>
- Augé ML, Folie A, Smith R, Phélizon A, Gigase P, Smith T (2022) Revision of the oldest varanid, *Saniwa orsmaelensis* Dollo, 1923, from the earliest Eocene of northwest Europe. *Comptes Rendus Palevol* 21(25): 511–529. <https://doi.org/10.5852/cr-palevol-2022v21a25>
- Bailon S, Boistel R, Bover P, Alcover JA (2014) *Maiorialacerta rafe-linensis*, gen. et sp. nov. (Squamata, Lacertidae), from the early Pliocene of Mallorca (Balearic Islands, western Mediterranean Sea). *Journal of Vertebrate Paleontology* 34: 318–326. <https://doi.org/10.1080/02724634.2013.799481>
- Barahona F, Evans SE, Mateo JA, García-Márquez M, López-Jurado LF (2000) Endemism, gigantism and extinction in island lizards: the genus *Gallotia* on the Canary Islands. *Journal of Zoology, London* 250: 373–388. <https://doi.org/10.1111/j.1469-7998.2000.tb00781.x>
- Biochro M (1997) Synthèse et tableaux de corrélations; In: Aguilar JP, Legendre S, Michaux J (Eds) *Actes du Congrès BiochroM'97, Mémoires et Travaux de l'EPHE. Institut de Montpellier* 21, April 14–17, 1997, Montpellier, France, 769–805.
- Bolet A (2017) First early Eocene lizards from Spain and a study of the compositional changes between late Mesozoic and early Cenozoic Iberian lizard assemblages. *Palaeontologia Electronica* 20.2.20A: 1–22. <https://doi.org/10.26879/695>
- Bolet A, Delfino M, Fortuny J, Almécija S, Robles JM, Alba DM, Rook L (2014) An amphisbaenian skull from the European Miocene and the evolution of Mediterranean worm lizards. *PLOS ONE* 9: e98082. <https://doi.org/10.1371/journal.pone.0098082>
- Borsuk-Białynicka M, Lubka M, Böhme W (1999) A lizard from baltic amber (Eocene) and the ancestry of the crown group lacertids. *Acta Palaeontologica Polonica* 44: 349–382.
- Bremer K (1994) Branch support and tree stability. *Cladistics* 10: 295–304. <https://doi.org/10.1111/j.1096-0031.1994.tb00179.x>
- Brownstein CD, Meyer DL, Fabbri M, Bhullar B-AS, Gauthier JA (2022) Evolutionary origins of the prolonged extant squamate radiation. *Nature Communications* 13: 7087. <https://doi.org/10.1038/s41467-022-34217-5>
- Burbrink FT, Grazziotin FG, Pyron AR, Cundall D, Donnellan S, Irish F, Keogh SJ, Kraus F, Murphy RW, Noonan B, Raxworthy ChJ (2020) Interrogating genomic-scale data for Squamata (lizards, snakes, and amphisbaenians) shows no support for key traditional morphological relationships. *Systematic Biology* 69(3): 502–520. <https://doi.org/10.1093/sysbio/syz062>
- Caputo V (2004) The cranial osteology and dentition in the scincid lizards of the genus *Chalcides* (Reptilia, Scincidae). *Italian Journal of Zoology* 2: 35–45. <https://doi.org/10.1080/11250000409356604>
- Čerňanský A (2019) The first potential fossil record of a dibamid reptile (Squamata: Dibamidae): a new taxon from the early Oligocene of Central Mongolia. *Zoological Journal of the Linnean Society* 187: 782–799. <https://doi.org/10.1093/zoolinnean/zlz047>
- Čerňanský A (2023) New lizard material from two Early Miocene localities in France: Montaigu-le-Blin (MN 2) and Crémat (MN 3). *Geobios* 80: 15–28. <https://doi.org/10.1016/j.geobios.2023.06.007>
- Čerňanský A, Augé ML (2013) New species of the genus *Plesiolacerta* (Squamata: Lacertidae) from the upper Oligocene (MP 28) of southern Germany and a revision of the type species *Plesiolacerta lydekkeri*. *Palaeontology* 56: 79–94. <https://doi.org/10.1111/j.1475-4983.2012.01167.x>
- Čerňanský A, Smith KT (2018) Eolacertidae: a new extinct clade of lizards from the Palaeogene; with comments on the origin of the dominant European reptile group - Lacertidae. *Historical Biology* 30: 994–1014. <https://doi.org/10.1080/08912963.2017.1327530>
- Čerňanský A, Smith KT (2019) The first juvenile specimen of *Eolacerta* (Squamata: Eolacertidae) from the early-middle Eocene of the Messel Pit (Germany). *Comptes Rendus Palevol* 18: 735–745. <https://doi.org/10.1016/j.crpv.2019.04.004>

- Čerňanský A, Syromyatnikova EV (2019) The first Miocene fossils of *Lacerta* cf. *trilineata* (Squamata, Lacertidae) with a comparative study of the main cranial osteological differences in green lizards and their relatives. PLOS ONE 14(8): e0216191. <https://doi.org/10.1371/journal.pone.0216191>
- Čerňanský A, Syromyatnikova EV (2021) The first Pre-Quaternary fossil record of the clade Mabuyidae with a comment on the enclosure of the Meckelian canal in skins. Papers in Palaeontology 7: 195–215. <https://doi.org/10.1002/spp2.1279>
- Čerňanský A, Augé ML, Phelizon A (2020a) Dawn of Lacertids (Squamata, Lacertidae): New Finds from the Upper Paleocene and the Lower Eocene. Journal of Vertebrate Paleontology 40: e1768539. <https://doi.org/10.1080/02724634.2020.1768539>
- Čerňanský A, Augé M, Rage J-C (2015b) A complete mandible of a new Amphisbaenian reptile (Squamata, Amphisbaenia) from the late Middle Eocene (Bartonian, MP 16) of France. Journal of Vertebrate Paleontology 35: e902379. <https://doi.org/10.1080/02724634.2014.902379>
- Čerňanský A, Klembara K, Müller J (2016b) The new rare record of the late Oligocene lizards and amphisbaenians from Germany and its impact on our knowledge of the European terminal Palaeogene. Palaeobiodiversity and Palaeoenvironments 96: 559–587. <https://doi.org/10.1007/s12549-015-0226-8>
- Čerňanský A, Klembara K, Smith KT (2016a) Fossil lizard from central Europe resolves the origin of large body size and herbivory in giant Canary Island lacertids. Zoological Journal of the Linnean Society 176: 861–877. <https://doi.org/10.1111/zoj.12340>
- Čerňanský A, Rage J-C, Klembara J (2015a) The early Miocene squamates of Amöneburg (Germany): the first stages of modern squamates in Europe. Journal of Systematic Palaeontology 13: 97–128. <https://doi.org/10.1080/14772019.2014.897266>
- Čerňanský A, Tabuce R, Vidalenc D (2023a) Anguimorph lizards from the lower Eocene (MP 10–11) of the Cos locality, Phosphorites du Quercy, France, and the early evolution of Glyptosaurinae in Europe. Journal of Vertebrate Paleontology 42(5): e2211646. <https://doi.org/10.1080/02724634.2023.2211646>
- Čerňanský A, Smith R, Smith T, Folie A (2023b) Iguanian lizards (Acrodonta and Pleurodonta) from the earliest Eocene (MP 7) of Dormaal, Belgium: the first stages of these iconic reptiles in Europe. Journal of Vertebrate Paleontology 42(4): e2184696. <https://doi.org/10.1080/02724634.2023.2184696>
- Čerňanský A, Syromyatnikova EV, Kovalenko ES, Podurets KM, Kalyan AA (2020b) The key to understanding the European Miocene *Chalcides* (Squamata, Scincidae) comes from Asia: the lizards of the East Siberian Tagay locality (Baikal Lake) in Russia. The Anatomical Record - Advances in Integrative Anatomy and Evolutionary Biology 303: 1901–1934. <https://doi.org/10.1002/ar.24289>
- Čerňanský A, Daza JD, Tabuce R, Saxton E, Vidalenc D (2023c) An early Eocene pan-gekkotan from France could represent an extra squamate group that survived the K/Pg extinction. Acta Palaeontologica Polonica 68(4): 695–708. <https://doi.org/10.4202/app.01083.2023>
- Čerňanský A, Bolet A, Müller J, Rage J-C, Augé ML, Herrel A (2017) A new exceptionally preserved specimen of *Dracaenosaurus* (Squamata, Lacertidae) from the Oligocene of France as revealed by micro-computed tomography. Journal of Vertebrate Paleontology 37: e1384738. <https://doi.org/10.1080/02724634.2017.1384738>
- Čerňanský A, Daza JD, Smith R, Bauer AM, Smith T, Folie A (2022b) A new gecko from the earliest Eocene of Dormaal, Belgium - a thermophilic element of the “greenhouse world”. Royal Society Open Science 9: 220429. <https://doi.org/10.1098/rsos.220429>
- Čerňanský A, Herrel A, Kinii JM, Anderson CV, Boistel R, Lehmann T (2020c) The only complete articulated early Miocene chameleon skull (Rusinga Island, Kenya) suggests an African origin for Madagascar’s endemic chameleons. Scientific Reports 10: 109. <https://doi.org/10.1038/s41598-019-57014-5>
- Čerňanský A, Singh NP, Patnaik R, Sharma KM, Tiwari RP, Sehgal RK, Singh NA, Choudhary D (2022a) The Miocene fossil lizards from Kutch (Gujarat), India: a rare window to the past diversity of this subcontinent. Journal of Paleontology 96: 213–223. <https://doi.org/10.1017/jpa.2021.85>
- Christian KA, Webb JK, Schultz TJ (2003) Energetics of bluetongue lizards (*Tiliqua scincoides*) in a seasonal tropical environment. Oecologia 136: 515–523. <https://doi.org/10.1007/s00442-003-1301-9>
- Christensen K, Melstrom KM (2021) Quantitative analyses of squamate dentition demonstrate novel morphological patterns. PLOS ONE 16(9): e0257427. <https://doi.org/10.1371/journal.pone.0257427>
- Conrad JL (2008) Phylogeny and systematics of Squamata (Reptilia) based on morphology. Bulletin of the American Museum of Natural History 310: 1–182. <https://doi.org/10.1206/310.1>
- Dalrymple GH (1979) On the jaw mechanism of the snail-crushing lizards, *Dracaena* Daudin 1802 (Reptilia, Lacertilia, Teiidae). Journal of Herpetology 13: 303–311. <https://doi.org/10.2307/1563324>
- De Bast E, Steurbaut E, Smith T (2013) New mammals from the marine Selandian of Maret, Belgium, and their implications for the age of the Paleocene continental deposits of Walbeck, Germany. Geologica Belgica 16: 236–244.
- De Bast E, Smith T (2017) The oldest Cenozoic mammal fauna of Europe: implication of the Hainin reference fauna for mammalian evolution and dispersals during the Paleocene. Journal of Systematic Palaeontology 15: 741–785. <https://doi.org/10.1080/14772019.2016.1237582>
- Dehm R (1961) Spaltenfüllungen als Lagerstätten fossiler Landwirbeltiere. Mitteilungen der Bayerischen Staatssammlung für Paläontologie und Historische Geologie 1: 57–72.
- de Queiroz K, Cantino PD (2020) International Code of Phylogenetic Nomenclature (PhyloCode). CRC Press, Boca Raton, FL, 190 pp. <https://doi.org/10.1201/9780429446320>
- Estes R (1975) Lower vertebrates from the Fort Union Formation, Late Paleocene, Big Horn Basin, Wyoming. Herpetologica 31: 365–385.
- Estes R (1983) Sauria terrestria, Amphisbaenia, Handbuch Der Paläoherpetologie, Part 10A. Gustav Fischer Verlag, Stuttgart, Germany, 249 pp.
- Estes R, Williams E (1984) Ontogenetic variations in the molariform teeth of lizards. Journal of Vertebrate Paleontology 4: 96–107. <https://doi.org/10.1080/02724634.1984.10011989>
- Estes R, de Queiroz K, Gauthier JA (1988). Phylogenetic relationships within squamata. In: Estes R, Pregill GK (Eds) Phylogenetic relationships of the lizard families. Stanford: Stanford University Press, 119–281.
- Evans SE (2003) At the feet of the dinosaurs: The origin, evolution and early diversification of squamate reptiles (Lepidosauria: Diapsida). Biological Reviews 78: 513–551. <https://doi.org/10.1017/S1464793103006134>
- Evans SE (2008) The skull of lizards and tuatara. In: Gans C, Gaunt AS, Adler K (Eds) Biology of the Reptilia. Volume 20 (Morphology H, The skull of Lepidosauria). Ithaca (NY): Society for the Study of Reptiles and Amphibians, 1–348.
- Folie A, Sigé B, Smith T (2005) A new scincomorph lizard from the Paleocene of Belgium and the origin of Scincoidea in Europe. Naturwissenschaften 92: 542–546.

- Folie A, Smith R, Smith T (2013) New amphisbaenian lizards from the Early Paleogene of Europe and their implications for the early evolution of modern amphisbaenians. *Geologica Belgica* 16: 227–235. <https://popups.uliege.be/1374-8505/index.php?id=4265>
- Gans C (1960) Studies on amphisbaenids (Amphisbaenia, Reptilia) 1. A taxonomic revision of the Trogonophinae, and a functional interpretation of the amphisbaenid adaptive pattern. *Bulletin of the American Museum of Natural History* 119: 133–204.
- Gans C (1974) Biomechanics, an approach to vertebrate biology. J. B. Lippincott, Philadelphia, 261 pp.
- Gans C, Montero R (2008) An atlas of amphisbaenian skull anatomy. In: Gans C, Gaunt AS, Adler K (Eds) *Biology of the Reptilia*. Volume 21, Morphology I. Society for the Study of Amphibians and Reptiles, Ithaca, New York, 621–738.
- García-Porta J, Irisarri I, Kirchner M, Rodríguez A, Kirchof S, Brown JL, MacLeod A, Turner A, Ahmadzadeh F, Albaladejo G, Crnobrnja-Isailovic J, De la Riva I, Fawzi A, Galán P, Göçmen B, Harris DJ, Jiménez-Robles O, Joger U, Jovanović Glavaš O, Karis M, Koziel G, Künzel S, Lyra M, Miles D, Nogales M, Oğuz MA, Pafilis P, Rancilhac L, Rodríguez N, Rodríguez Concepción B, Sanchez E, Salvi D, Slimani T, S'khifa A, Qashqaei AT, Žagar A, Lemmon A, Moriarty Lemmon E, Carretero MA, Carranza S, Philippe H, Sinervo B, Müller J, Vences M, Wollenberg Valero KC (2019) Environmental temperatures shape thermal physiology as well as diversification and genomewide substitution rates in lizards. *Nature Communications* 10: 4077. <https://doi.org/10.1038/s41467-019-11943-x>
- Gauthier JA (1982) Fossil xenosaurid and anguid lizards from the early Eocene Wasatch Formation, southeast Wyoming, and a revision of the Anguioidea. *Contributions to Geology, University of Wyoming* 21: 7–54.
- Gauthier JA, Kearney M, Maisano JA, Rieppel O, Behlke ADB (2012) Assembling the Squamate Tree of Life: Perspectives from the Phenotype and the Fossil Record. *Bulletin of the Peabody Museum of Natural History* 53: 3–308. <https://doi.org/10.3374/014.053.0101>
- Georgalis GL, Rabi M, Smith KT (2021a) Taxonomic revision of the snakes of the genera *Palaeopython* and *Paleryx* (Serpentes, Constrictores) from the Paleogene of Europe. *Swiss Journal of Paleontology* 140: 18. <https://doi.org/10.1186/s13358-021-00224-0>
- Georgalis GL, Čerňanský A, Klembara J (2021b) Osteological atlas of new lizards from the Phosphorites du Quercy (France), based on historical, forgotten, fossil material. In: Steyer J-S, Augé ML, Métais G (Eds) *Memorial Jean-Claude Rage: A life of paleo-herpetologist*. *Geodiversitas* 43(9): 219–293. <https://doi.org/10.5252/geodiversitas2021v43a9>
- Greer AE (1970) A subfamilial classification of scincid lizards. *Bulletin of the Museum of Comparative Zoology at Harvard College* 139: 151–184.
- Greer AE (1974) The generic relationships of the scincid lizard genus *Leiopisma* and its relatives. *Australian Journal of Zoology* 31: 1–67. <https://doi.org/10.1071/AJZS031>
- Goloboff P, Catalano S (2016) TNT version 1.5, including full implementation of phylogenetic morphometrics. *Cladistics* 32: 221–238. <https://doi.org/10.1111/cla.12160>
- Goloboff PA, Farris JS, Nixon KC (2008) T.N.T., a free program for phylogenetic analysis. *Cladistics* 24: 774–786. <https://doi.org/10.1111/j.1096-0031.2008.00217.x>
- Hipsley CA, Himmelmann L, Metzler D, Müller J (2009) Integration of Bayesian molecular clock methods and fossil-based soft bounds reveals early Cenozoic colonization of African lacertid lizards. *BMC Evolutionary Biology* 9: 151. <https://doi.org/10.1186/1471-2148-9-151>
- Hoffstetter P, Gasc JP. 1969. Vertebrae and ribs of modern reptiles. In: Gans C (Ed.) *Biology of the reptilia*. Volume 1, Morphology A. New York: Academic Press, 201–210.
- Holmes RB, Murray AM, Yousry S, Attia YS, Simons EL, Chatrath P (2010) Oldest known *Varanus* (Squamata: Varanidae) from the upper Eocene and lower Oligocene of Egypt: support for an African origin of the genus. *Palaeontology* 53: 1099–1110. <https://doi.org/10.1111/j.1475-4983.2010.00994.x>
- Hutchinson MN, Scanlon JD (2009) New and unusual Plio-Pleistocene lizard (Reptilia: Scincidae) from Wellington Caves, New South Wales, Australia. *Journal of Herpetology* 43:139–147. <https://doi.org/10.1670/08-126R.1>
- International Commission on Zoological Nomenclature (1999) *International Code of Zoological Nomenclature*. 4th edn. The International Trust for Zoological Nomenclature, London, 306 pp.
- Kearney M (2003) Systematics of the Amphisbaenia (Lepidosauria: Squamata) based on morphological evidence from recent and fossil forms. *Herpetological Monographs* 17: 1–74. [https://doi.org/10.1655/0733-1347\(2003\)017\[0001:SOTALB\]2.0.CO;2](https://doi.org/10.1655/0733-1347(2003)017[0001:SOTALB]2.0.CO;2)
- Kiefer MC, Sazima I (2002) Diet of juvenile *Tupinambis merianae* (Teiidae) in southeastern Brazil. *Amphibia-Reptilia* 23: 105–108.
- Klembara J, Hain M, Dobiašová K (2014) Comparative anatomy of the lower jaw and dentition of *Pseudopus apodus* and the interrelationships of species of subfamily Anguinae (Anguimorpha, Anguinae): Anatomy of lower jaw and teeth of Anguinae. *The Anatomical Record* 297: 516–544. <https://doi.org/10.1002/ar.22854>
- Kuhn O (1940a) Crocodilier- und Squamatenreste aus dem oberen Palaeocän von Walbeck. *Sonder-Abdruck aus dem Zentralblatt für Mineralogie und Paläontologie, Abteilung B* 1: 21–25.
- Kuhn O (1940b) Die Placosauriden und Anguiden aus dem mittleren Eozän des Geiseltales. *Nova Acta Leopoldina (n. f.)* 8: 461–486.
- Kuhn O (1944) Weitere Lacertilien, insbesondere Iguaniden aus dem Eozän des Geiseltales. *Paläontologische Zeitschrift* 23: 360–366. <https://doi.org/10.1007/BF03160444>
- Kuhn O (1958) Ein neuer lacertilien aus dem frankischen Lithographieschiefer. *Neues Jahrbuch für Geologie und Paläontologie, Monatshefte* 1958: 380–382.
- Kuhn O (1963) Sauria (Supplementum I). *Fossilium Catalogus I: Animalia*. W. Junk, The Hague, pars 104: 1–87.
- Kosma R (2004) The dentitions of recent and fossil scincomorph lizard (Lacertilia, Squamata). Systematics, functional morphology, paleoecology. Ph.D. dissertation, University of Hannover, Hannover, Germany, 229 pp.
- Longrich NR, Bhullar BAS, Gauthier JA (2012) Mass extinction of lizards and snakes at the Cretaceous–Paleogene boundary. *Proceedings of the National Academy of Sciences* 109: 21396–21401. <https://doi.org/10.1073/pnas.1211526110>
- Longrich NR, Vinther J, Pyron RA, Pisani D, Gauthier JA (2015) Biogeography of worm lizards (Amphisbaenia) driven by end-Cretaceous mass extinction. *Proceedings of the Royal Society B: Biological Sciences* 282: 20143034. <https://doi.org/10.1098/rspb.2014.3034>
- Loréal E, Syromyatnikova EV, Danilov IG, Čerňanský A (2023) The easternmost record of the largest anguine lizard that has ever lived – *Pseudopus pannonicus* (Squamata, Anguinae): new fossils from the late Neogene of Eastern Europe. *Fossil Record* 26 (1): 51–84. <https://doi.org/10.3897/fr.26.100059>
- Losos JB (2009) *Lizards in an evolutionary tree: ecology and adaptive radiation of anoles*. University of California Press,

- Oakland, California, 528 pp. <https://doi.org/10.1525/california/9780520255913.001.0001>
- Maddison WP, Maddison DR (2011) Mesquite: a modular system for evolutionary analysis. Version 2.75. <http://mesquiteproject.org/>
- Martín J, Ortega J, López P, Pérez-Cembranos A, Pérez-Mellado V (2013) Fossorial life does not constrain diet selection in the amphisbaenian *Trogonophis wiegmanni*. *Journal of Zoology* 291: 226–233. <https://doi.org/10.1111/jzo.12064>
- Mayer W, Benyr G (1994) Albumin-evolution und phylogenese in der familie lacertidae (Reptilia: Sauria). *Annalen des Naturhistorischen Museum in Wien* 96B: 621–648.
- Mayr G (2002) An owl from the Paleocene of Walbeck, Germany. *Mitteilungen aus dem Museum für Naturkunde in Berlin, Geowissenschaftliche Reihe* 5: 283–288. <https://doi.org/10.1002/mmng.4860050117>
- Mayr G (2007) The birds from the Paleocene fissure filling of Walbeck (Germany). *Journal of Vertebrate Paleontology* 27(2): 394–408. [https://doi.org/10.1671/0272-4634\(2007\)27\[394:TBFTPF\]2.0.CO;2](https://doi.org/10.1671/0272-4634(2007)27[394:TBFTPF]2.0.CO;2)
- Mercolli C, Yanosky AA (1994) The diet of adult *Tupinambis teguixin* (Sauria, Teiidae) in the eastern chaco of Argentina. *Herpetological Journal* 4: 15–19. <https://doi.org/10.1007/BF00993696>
- Müller J, Hipsley CA, Head JJ, Kardjilov N, Hilger A, Wuttke M, Reisz RR (2011) Eocene lizard from Germany reveals amphisbaenian origins. *Nature* 473: 364–367. <https://doi.org/10.1038/nature09919>
- Nance HA (2007) Cranial osteology of the African gerrhosaurid *Angolosaurus skoogi* (Squamata: Gerrhosauridae). *African Journal of Herpetology* 56: 39–75. <https://doi.org/10.1080/21564574.2007.9635552>
- Nydam RL (1999) Polyglyphanodontinae (Squamata: Teiidae) from the medial and Late Cretaceous: New records from Utah, U.S.A. and Baja California del Norte, Mexico. In: Gillette DD (Ed.) *Vertebrate Paleontology in Utah*. Utah Geological Survey Miscellaneous Publication, 99–1, Utah Geological Survey, Salt Lake City, 303–317.
- Pregill G (1984) Durophagous feeding adaptations in an amphisbaenid. *Journal of Herpetology* 18: 186–191. <https://doi.org/10.2307/1563747>
- Pyron AR, Burbrink FT, Wiens JJ (2013) A phylogeny and revised classification of Squamata, including 4161 species of lizards and snakes. *BMC Evolutionary Biology* 13: 93. <https://doi.org/10.1186/1471-2148-13-93>
- Rage JC (1982) La phylogénie des Lépidosauriens (Reptilia): une approche cladistique. *Comptes Rendus de l'Académie des Sciences* 294: 563–566.
- Rage JC, Augé M (1993) Squamates from the Cainozoic of the western part of Europe. A review. *Revue de Paléobiologie* 7: 199–216.
- Rage J-C, Augé ML (2010) Squamate reptiles from the middle Eocene of Lissieu (France) A landmark in the middle Eocene of Europe. *Geobios* 43: 253–268. <https://doi.org/10.1016/j.geobios.2009.08.002>
- Rage J-C, Augé ML (2015) Valbro: A new site of vertebrates from the early Oligocene (MP 22) of France (Quercy) III – Amphibians and squamates. *Annales de Paléontologie* 101: 29–41. <https://doi.org/10.1016/j.annpal.2014.10.002>
- Reeder TW, Townsend TM, Mulcahy DG, Noonan BP, Wood Jr PL, Sites Jr JW, Wiens JJ (2015) Integrated Analyses Resolve Conflicts over Squamate Reptile Phylogeny and Reveal Unexpected Placements for Fossil Taxa. *PLOS ONE* 10(3): e0118199. <https://doi.org/10.1371/journal.pone.0118199>
- Richter A (1994) Lacertilia aus der Unteren Kreide von Una und Galve (Spanien) und Anoual (Marokko). *Berliner geowissenschaftliche Abhandlungen (E: Paläobiologie)* 14: 1–147.
- Rieppel O (1980) The postcranial skeleton of *Lanthanotus borneensis* (Reptilia, Lacertilia). *Amphibia-Reptilia* 1: 95–111. <https://doi.org/10.1163/156853880X00105>
- Rieppel O (1981). The skull and jaw adductor musculature in some burrowing scincomorph lizards of the genera *Aconias*, *Typhlosaurus* and *Feylinia*. *Journal of Zoology, London* 195: 493–528. <https://doi.org/10.1111/j.1469-7998.1981.tb03480.x>
- Rieppel O, Labhardt L (1979) Mandibular mechanics in *Varanus niloticus* (Reptilia: Lacertilia). *Herpetologica* 35: 158–163.
- Rose KD, Storch G, Krohman K (2015) Small-mammal postcrania from the middle Paleocene of Walbeck, Germany. *Paläontologische Zeitschrift* 89: 95–124. <https://doi.org/10.1007/s12542-013-0211-3>
- Russell DE (1964) Les mammifères paléocènes d'Europe. Editions du Muséum, Université de Paris, Paris, 324 pp.
- Simões TR, Caldwell MW, Nydam RL, Jiménez-Huidobro P (2017) Osteology, phylogeny, and functional morphology of two Jurassic lizard species and the early evolution of scansoriality in geckoes. *Zoological Journal of the Linnean Society* 180: 216–241. <https://doi.org/10.1111/zoj.12487>
- Simões TR, Wilner E, Caldwell MW, Weinschütz LC, Kellner AW (2015) A stem acrodontan lizard in the Cretaceous of Brazil revises early lizard evolution in Gondwana. *Nature Communications* 6: 1–8. <https://doi.org/10.1038/ncomms9149>
- Schneider CA, Rasband WS, Eliceiri KW (2012) NIH Image to ImageJ: 25 years of image analysis. *Nature Methods* 9: 671–675. <https://doi.org/10.1038/nmeth.2089>
- Shea GM (2006) Diet of two species of bluetongue skink, *Tiliqua multifasciata* and *Tiliqua occipitalis* (Squamata: Scincidae). *Australian Zoologist* 33: 359–368. <https://doi.org/10.7882/AZ.2006.009>
- Smith KT (2009) A new lizard assemblage from the Earliest Eocene (zone Wa0) of the Bighorn Basin, Wyoming, USA: biogeography during the warmest interval of the Cenozoic. *Journal of Systematic Palaeontology* 7: 299–358. <https://doi.org/10.1017/S1477201909002752>
- Smith KT, Bhullar BAS, Holroyd PA (2008) Earliest African record of the *Varanus* stem clade (Squamata: Varanidae) from the early Oligocene of Egypt. *Journal of Vertebrate Paleontology* 28: 909–913. [https://doi.org/10.1671/0272-4634\(2008\)28\[909:EAROTV\]2.0.CO;2](https://doi.org/10.1671/0272-4634(2008)28[909:EAROTV]2.0.CO;2)
- Smith KT, Gauthier JA (2013) Early Eocene lizards of the Wasatch Formation near Bitter Creek, Wyoming: diversity and paleoenvironment during an interval of global warming. *Bulletin of the Peabody Museum of Natural History* 54(2): 135–230. <https://doi.org/10.3374/014.054.0205>
- Smith KT, Habersetzer J (2021) The anatomy, phylogenetic relationships, and autecology of the carnivorous lizard “*Saniwa*” *feisti* from the Eocene of Messel, Germany. *Comptes Rendus Palevol* 20(23): 441–506. <https://doi.org/10.5852/cr-palevol2021v20a23>
- Smith KT, Comay O, Maul L, Wegmüller F, Le Tensorer JM, Dayan T (2021) A model of digestive tooth corrosion in lizards: experimental tests and taphonomic implications. *Scientific Reports* 11(1): 12877. <https://doi.org/10.1038/s41598-021-92326-5>
- Sumida SS, Murphy RW (1987) Form and function of the tooth crown structure in gekkonid lizards (Reptilia, Squamata, Gekkonidae). *Canadian Journal of Zoology* 65: 2886–2892. <https://doi.org/10.1139/z87-438>
- Storch G (2008) Skeletal remains of a diminutive primate from the Paleocene of Germany. *Naturwissenschaften* 95: 927–930. <https://doi.org/10.1007/s00114-008-0401-0>

- Sullivan RM (1985) A new middle Paleocene (Torrejonian) rhineurid amphisbaenian, *Plesiorhineura tsentasi* new genus, new species, from the San Juan Basin, New Mexico. *Journal of Paleontology* 59: 1481–1485.
- Sullivan RM, Augé ML, Wille E, Smith R (2012) A new glyptosaurine lizard from the earliest Eocene of Dormaal, Belgium. *Bulletin de la Société géologique de France* 183: 629–635. <https://doi.org/10.2113/gssgfbull.183.6.627>
- Talanda M (2016) Cretaceous roots of amphisbaenian lizards. *Zoologica Scripta* 45: 1–8. <https://doi.org/10.1111/zsc.12138>
- Tschopp E (2016) Nomenclature of vertebral laminae in lizards, with comments on ontogenetic and serial variation in Lacertini (Squamata, Lacertidae). *PLOS ONE* 11(2): e0149445. <https://doi.org/10.1371/journal.pone.0149445>
- Townsend TM, Larson A, Louis E, Macey JR (2004) Molecular phylogenetics of Squamata: the position of snakes, amphisbaenians and dibamids, and the root of the squamate tree. *Systematic Biology* 53: 735–757. <https://doi.org/10.1080/10635150490522340>
- Uetz P, Freed P, Hošek J (2022) The Reptile Database. <http://www.reptile-database.org> [accessed October 2023]
- Vidal N, Hedges SB (2005) The phylogeny of squamate reptiles (lizards, snakes, and amphisbaenians) inferred from nine nuclear protein-coding genes. *Comptes Rendus Biologies* 328: 1000–1008. <https://doi.org/10.1016/j.crv.2005.10.001>
- Vidal N, Hedges SB (2009) The molecular evolutionary tree of lizards, snakes, and amphisbaenians. *Comptes Rendus Biologies* 332: 129–139. <https://doi.org/10.1016/j.crv.2008.07.010>
- Villa A, Delfino M (2019) A comparative atlas of the skull osteology of European lizards (Reptilia: Squamata). *Zoological Journal of the Linnean Society*, 187(3): 828–928. <https://doi.org/10.1093/zoolinnean/zlz035>
- Villa A, Kirchner M, Alba DM, Bernardini F, Bolet A, Luján ÀH, Fortuny J, Hipsley CA, Müller J, Sindaco R, Tuniz C, Delfino M (2019) Comparative cranial osteology of *Blanus* (Squamata: Amphisbaenia). *Zoological Journal of the Linnean Society* 185: 693–716. <https://doi.org/10.1093/zoolinnean/zly082>
- Vlachos E, Georgalis GL, Roussiakis S, Böhme M, Theodorou G (2020) The Pliocene tortoises (Testudines, Testudinidae) from the late Miocene of the South Balkans. *Journal of Vertebrate Paleontology* 39(5): e1711520. <https://doi.org/10.1080/02724634.2019.1711520>
- Weigelt J (1939) Die Aufdeckung der bisher ältesten tertiären Säugetierfauna Deutschlands. *Nova Acta Leopoldina, N.S.* 7: 515–528.
- Weigelt J (1940) Die Entdeckung paleozöner Säugetiere im deutschen Heimatboden. *Naturwissenschaften* 28: 620–623. <https://doi.org/10.1007/BF01475222>
- Weigelt J (1942) Die alttertiären Säugetiere Mitteldeutschlands nach den Hallenser Grabungen im Geiseltal und bei Walbeck. de Gruyter, Berlin, 48 pp. <https://doi.org/10.1515/9783111668871>
- Yadav R, Bajpai S, Maurya AS, Čerňanský A (2023) The first potential cordyliform (Squamata, Scincoidea) from India (uppermost Cretaceous – lowermost Paleocene): an African lizard clade brings possible implications for Indo-Madagascar biogeographic links. *Cretaceous Research* 150: 105606. <https://doi.org/10.1016/j.cretres.2023.105606>
- Zheng Y, Wiens JJ (2016) Combining phylogenomic and supermatrix approaches, and a time-calibrated phylogeny for squamate reptiles (lizards and snakes) based on 52 genes and 4162 species. *Molecular Phylogenetics and Evolution* 94: 537–547. <https://doi.org/10.1016/j.ympev.2015.10.009>

## Supplementary material 1

### Updated phylogenetic matrices

Authors: Andrej Čerňanský, Davit Vasilyan

Data type: nexus

Explanation note: Updated phylogenetic matrices in TNT. file format used for the phylogenetic analyses in this study.

Copyright notice: This dataset is made available under the Open Database License (<http://opendatacommons.org/licenses/odbl/1.0>). The Open Database License (ODbL) is a license agreement intended to allow users to freely share, modify, and use this Dataset while maintaining this same freedom for others, provided that the original source and author(s) are credited.

Link: <https://doi.org/10.3897/fr.27.109123.suppl1>

## Supplementary material 2

### Consensus tree with Bremer values

Authors: Andrej Čerňanský, Davit Vasilyan

Data type: tif

Explanation note: A New Technology (NT) search in TNT produced two equally parsimonious trees. Here is the consensus tree of these two trees.

Copyright notice: This dataset is made available under the Open Database License (<http://opendatacommons.org/licenses/odbl/1.0>). The Open Database License (ODbL) is a license agreement intended to allow users to freely share, modify, and use this Dataset while maintaining this same freedom for others, provided that the original source and author(s) are credited.

Link: <https://doi.org/10.3897/fr.27.109123.suppl2>

## Supplementary material 3

### Parsimonious tree with Bremer values

Authors: Andrej Čerňanský, Davit Vasilyan

Data type: tif

Explanation note: A New Technology (NT) search in TNT produced two equally parsimonious trees. Here is the tree with Bremer values.

Copyright notice: This dataset is made available under the Open Database License (<http://opendatacommons.org/licenses/odbl/1.0>). The Open Database License (ODbL) is a license agreement intended to allow users to freely share, modify, and use this Dataset while maintaining this same freedom for others, provided that the original source and author(s) are credited.

Link: <https://doi.org/10.3897/fr.27.109123.suppl3>

# Cauca: megafaunal and felid fossils (Mammalia) from a Pleistocene site in northwest Venezuela

Jorge Domingo Carrillo-Briceño<sup>1</sup>, Damián Ruiz-Ramoni<sup>2,3</sup>, Rodolfo Sánchez<sup>4</sup>, Arturo Jaimes<sup>5</sup>, Edwin Chávez-Aponte<sup>6,7,8</sup>, Francisco Juan Prevosti<sup>2,9</sup>, Valentina Segura<sup>2,10</sup>, Alfredo Armando Carlini<sup>11</sup>, Lisa Garbé<sup>12</sup>, Olivier Tombret<sup>12</sup>, Antoine Zazzo<sup>12</sup>, Marcelo Ricardo Sánchez-Villagra<sup>1</sup>

1 Universität Zürich, Paläontologisches Institut, Karl-Schmid-Straße 4, 8006 Zürich, Switzerland

2 Consejo Nacional de Investigaciones Científicas y Técnicas (CONICET), Buenos Aires, Argentina

3 Instituto Argentino de Nivología, Glaciología y Ciencias Ambientales (IANIGLA), Av. Ruiz Leal s/n, Parque Gral. San Martín, 5500, Mendoza, Argentina

4 Museo Paleontológico de Urumaco, Calle Bolívar s/n, Urumaco, Estado Falcón, Venezuela

5 Centro de Antropología, Instituto Venezolano de Investigaciones Científicas, Km. 11 Altos de Pipe, Parroquia Macarao 1204, Miranda, Venezuela

6 Sistema Nacional de Museos, Fundación Museos Nacionales (FMN), Museo de la Estampa y el Diseño “Carlos Cruz Diez”, ZP 1011, El Silencio, Caracas, Venezuela

7 Fundación Nacional de Parques Zoológicos, Zoocriaderos y Acuarios (FUNPZZA) y Universidad Popular del Ambiente “Fruto Vivas”, del Ministerio del P.P. para el Ecosocialismo, ZP 1010, Caracas, Venezuela

8 Parque Zoológico El Pinar, Instituto Nacional de Parques, ZP 1010, Caracas, Venezuela

9 Museo de Ciencias Antropológicas y Naturales, Universidad Nacional de La Rioja (UNLaR), Av. Luis M. de la Fuente s/n, 5300, La Rioja, Argentina

10 Unidad Ejecutora Lillo (CONICET-Fundación Miguel Lillo), Miguel Lillo 251, CP 4000, San Miguel De Tucumán, Tucumán, Argentina

11 Laboratorio de Morfología Evolutiva y Desarrollo (Morphos), Facultad de Cs. Naturales y Museo, UNLP, La Plata, Argentina

12 Archéozoologie, Archéobotanique, Sociétés, Pratiques et Environnements (AASPE), UMR 7209, Muséum national d’Histoire naturelle, CNRS, Paris, France

<https://zoobank.org/739CC1FF-7E28-4678-AD10-09E6412EB960>

Corresponding authors: Jorge Domingo Carrillo-Briceño ([jorge.carrillo@pim.uzh.ch](mailto:jorge.carrillo@pim.uzh.ch), [jorgedcb100@gmail.com](mailto:jorgedcb100@gmail.com)); Marcelo Ricardo Sánchez-Villagra ([m.sanchez@pim.uzh.ch](mailto:m.sanchez@pim.uzh.ch))

Academic editor: Johannes Müller ♦ Received 31 January 2024 ♦ Accepted 15 March 2024 ♦ Published 11 April 2024

## Abstract

Numerous surveys and three excavation and surface collection field seasons resulted in the discovery of numerous megafaunal remains and that of a medium-sized felid in a new site located on the coastal plain of the Gulf of Venezuela, in Western Falcón State. The faunal assemblage is represented by South American natives such as megatheres (cf. *Eremotherium laurillardii*), an indeterminate mylodontid and a glyptodont (probably related to *Glyptotherium*) and Nearctic representatives such as gomphotheres (*Notiomastodon platensis*), equids (*Equus* sp.) and a feline (Felidae cf. *Leopardus pardalis*), providing novel information for the distribution of some of these mammals. Radiocarbon indicates that this deposit is at least 40,000 years old. Lithic artefacts of a kind reported for other Pleistocene sites in the region document the presence of humans in Cauca, but as these cultural remains were found on the surface, their association with the fauna is uncertain.

## Key Words

Carnivora, cf. *Leopardus pardalis*, *Eremotherium*, *Equus*, Megaherbivores, Mylodontidae, *Notiomastodon*, South America

## Introduction

The north-western region of Venezuela (specifically the Falcón State; Figs 1, 2) is characterised by a semi-arid landscape in which multiple sites preserve rich fossil deposits. The Urumaco sedimentary sequence (ca. 23–1 Ma) preserves the largest succession of strata with vertebrate remains that exemplify the faunal changes of the last 23 Ma (Aguilera 2004; Linares 2004; Sánchez-Villagra et al. 2010; Carrillo-Briceño et al. 2021). In the same region, numerous sites of archaeological significance preserve megafaunal (taxa with a body mass greater than or equal to 44 kg) and cultural remains of the Late Pleistocene and the Early Holocene (e.g. Royo y Gómez (1959, 1960); Bryan et al. (1978); Ochsenius and Gruhn (1979); Aguilera (2006); Carrillo-Briceño (2015); Carlini et al. (2022); amongst others). Compared to other parts of Venezuela, the northwest region has a great Pleistocene fossiliferous record with abundant remains of reptiles, birds and especially mammals (Royo y Gómez 1960; Bocquentin-Villanueva 1979, 1982; Ochsenius 1980; Aguilera 2006; Prevosti and Rincón 2007; Rincón and White 2007; Carlini et al. 2008; Carrillo-Briceño et al. 2008a; Carlini and Zurita 2010; Chávez-Aponte and Carrillo-Briceño 2012; Ruiz-Ramoni et al. 2013, 2022; Carrillo-Briceño 2015; Rincón et al. 2021; Reyes-Céspedes et al. 2023; amongst others; see Fig. 2).

In the Falcón State, various types of evidence indicate the co-existence of early South American humans with now-extinct fauna and inferred interactions between humans and megaherbivores documented at the Muaco, Taima-Taima and Cucuruchú sites (Cruxent 1970; Bryan et al. 1978; Ochsenius and Gruhn 1979; Oliver and Alexander 2003; Carrillo-Briceño 2015; Carlini et al. 2022). In the excavations carried out at these sites, projectiles and other artefacts produced with bone and lithic materials were reported, in some cases proposed in direct association with the remains of megafauna (Rouse and Cruxent 1963; Cruxent 1967, 1979; Ochsenius and Gruhn 1979). Since the last excavations carried out at the Taima-Taima site in the 1990s (Aguilera 2006; Carrillo-Briceño 2015), no other systematic excavations at Pleistocene sites in the Falcón State have been carried out. In the present contribution, we provide palaeontological evidence from a new site assigned by its content and radiocarbon dating to the Late Pleistocene, which we have named “Cauca”. This new locality presents an association of extinct mammals and evidence of lithic artefacts near the excavations is also reported (e.g. Jaimes et al. (2024a)).

## Geographic and geological context

The site, Cauca (11°18'51"N, 70°17'41"W), was so named because of its proximity to the homonymous fishing village, in the coastal area of the Gulf of Venezuela. It is located approximately 14.6 km northwest of the Town

of Urumaco, Urumaco Municipality, following the dirt road that connects Urumaco with the hamlets of Cauca and Río Seco (Fig. 1). The site is on the western coastal plain about 2.3 km south of the coastal zone and approximately 12 metres above sea level. Currently, this plain is influenced by the trade winds (“vientos alisios”), whose incidence generates a semi-arid or arid, seasonal climate with prolonged periods of water deficit, with rainfall that ranges between 200 and 600 mm annually, average temperatures of 30 °C and a predominantly xerophytic vegetation (Matteucci et al. 1999).

The area is affected by an intermittent runoff system, generating laminar erosion of the sediments. The geology is represented by a not formally defined sedimentary unit, characterised mainly by facies of unconsolidated fine to coarse sands of light brown to ochre colour, with underlying coastal palaeodunes. The level of oxidation of the sand and clay layers carrying the bone assemblages suggests that Cauca was probably deposited in a low-energy more humid environment, contrasting with the environmental conditions currently present in the area. For now, there is no precise evidence of whether this deposition environment was a permanent or intermittent body of water. The coastal plains of Falcón State were subject to a negative water balance during the Late Pleistocene (Ochsenius 1980) and the Cauca site could have offered attractive water resources for animals with swamp patch areas. An example of archaeological sites, such as Muaco, Taima-Taima and Cucuruchú, which were deposited in sedimentary environments influenced by the action of resurgent springs, offer an oasis that may have attracted animals during dry periods (Cruxent 1970; Ochsenius and Gruhn 1979; Ochsenius 1980).

## Excavations at the Cauca site

The fossiliferous site covers an area of approximately 1600 m<sup>2</sup>, where eight groupings of bone remains have been identified emerging on the surface (Figs 1B, 3). The first reports from this locality were made by one of the authors (R.S.) from the Palaeontology Department of the Alcaldía Bolivariana del Municipio Urumaco, in January 2004. During a survey of the site on 16 November 2019, several of the authors (J.D.C.B., A.J. and R.S.) collected from surface partial lithic projectiles and other preformatted artefacts in the vicinity of the Cauca site (see Jaimes et al. (2024a)). Thanks to the support and legal authorisation from the Alcaldía Bolivariana del Municipio Urumaco and the Instituto del Patrimonio Cultural de Venezuela (permits N° 00019-01/31/2020, 00110-04/09/2021, 00178-07/14/2021 and 00522-08/18/2022) the first systematic excavations were planned at the Cauca site.

To date, three excavation field seasons have been carried out between 2021 and 2022, totalling five work areas. These excavations were under the direction of A.J. and R.S., excavating only the outcropping bone groupings defined as 1, 3–5 and 8 (see Fig. 1B). The five

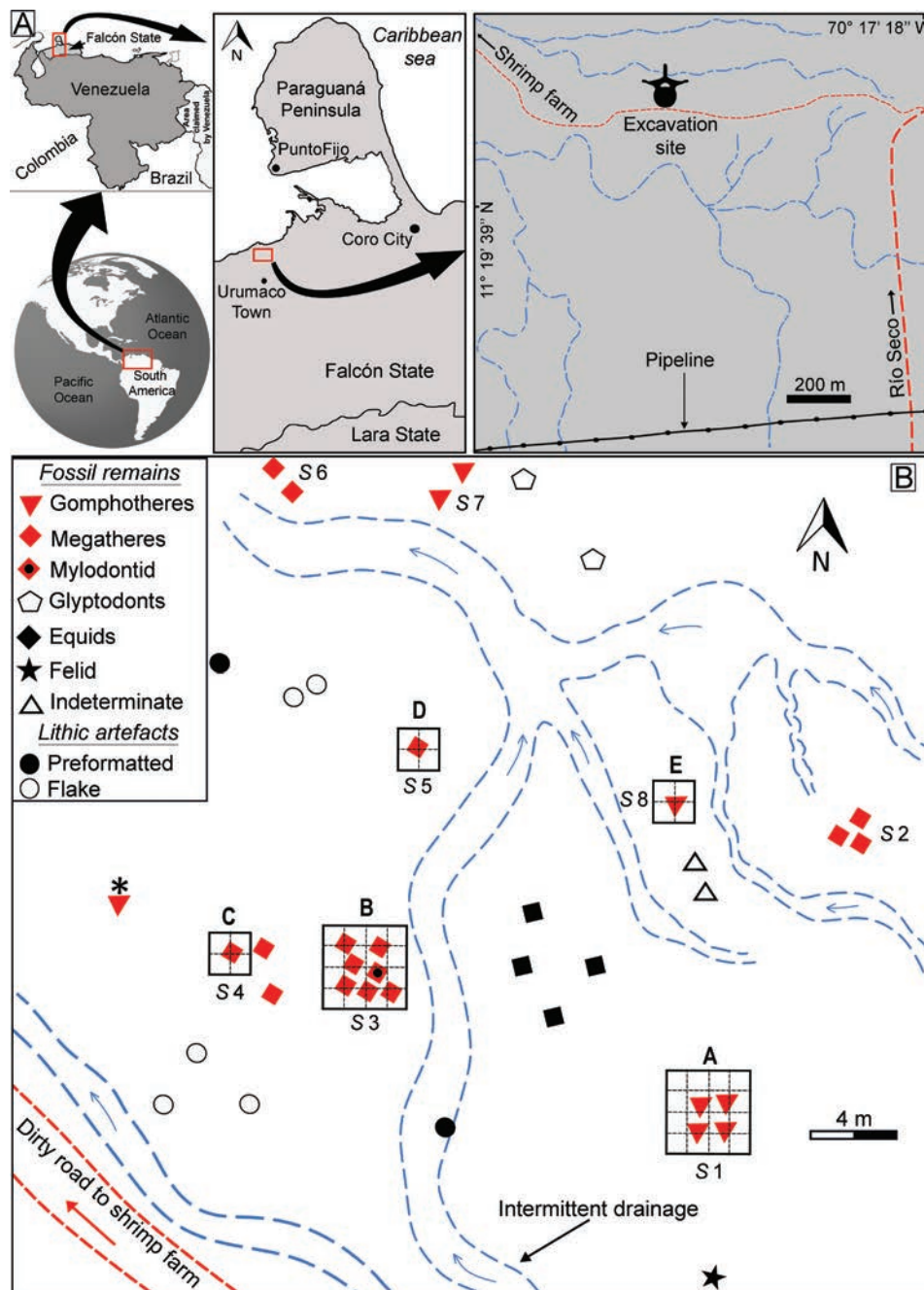


**Figure 1.** Geographic location of the Cauca site (A) and the excavation area (B). The different bone groupings are referred to as “S” and the excavations as “A–E”. The M2 isolated from a juvenile *Notiomastodon platensis* (AMU-CURS-1045) is referred to with a triangle and \*. Lithic artefacts referred to here are illustrated in Fig. 9.

excavations include: 1) Cauca “A”, carried out between 3 and 4 August 2021, with a 4 × 4 m grid (Fig. 4B); 2) Cauca “B”, carried out between 4 and 26 October 2021, with a 4 × 4 m grid (Fig. 4B), and 3) Cauca “C”, “D” and “E” carried out between 3 and 20 November 2022, and all with 2 × 2 m grids (Figs 1B, 4B).

The depth of all excavations did not exceed 40 cm because that is the thickness of the bearing layer (e.g. Fig. 4B, C). There is no evidence of fossil under/below this layer. The stratigraphy of the site, based on the five excavations and from the top or surface to the excavated base, is characterised by at least three well-defined

layers. The first is the surface layer, about 5 cm thick and composed of unconsolidated sediments that include pellets and other small clasts that are transported by rain runoff and wind action that occurs from east to west. The second layer varies between 20 and 35 cm thick, composed of fine silt-clayey sands, heterogeneous, compact, and well-defined with colours between light brown and ochre, with evidence of oxidation. In Cauca “D”, specifically grid “C”, the sediments showed a greater clay composition, which could be related to its accumulation in the lowest deposition area in the northern section of the site. The deposit of this second layer may have occurred in

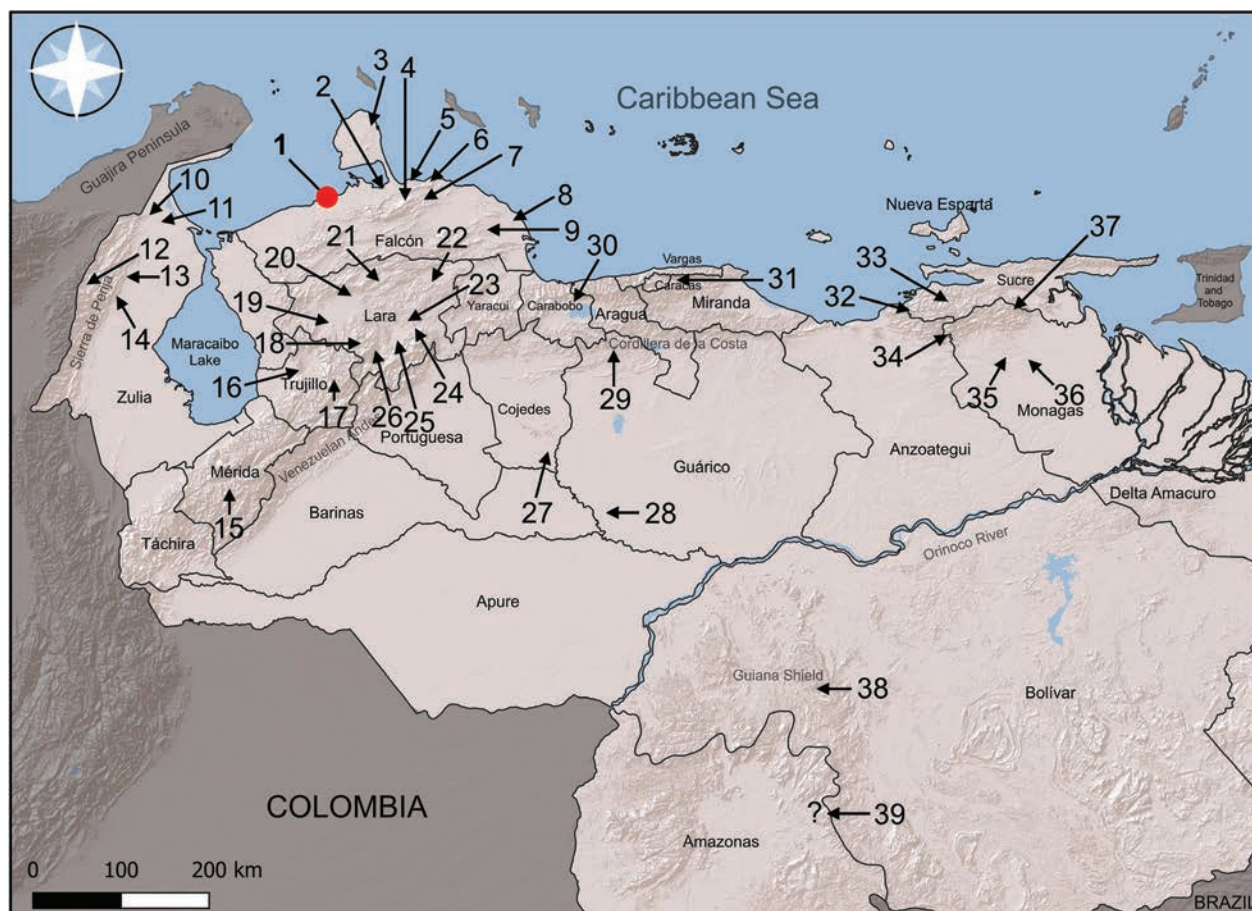


**Figure 2.** Map of Quaternary fossil mammal sites in Venezuela. Falcón State; 1) Cauca; 2) Coro; 3) La Ciénega, Pueblo Nuevo; 4) Cueva del Cerro La Chapa; 5) Muaco; 6) Taima-Taima; 7) Quebrada Cucuruchú; 8) Cueva el Zumbador; 9) Cueva del Miedo. Zulia State; 10) Minas de Guasare-Socuy; 11) El Mene de Inciarte; 12) Cerro Pintado; 13) Cueva de los Huesos; 14) Sierra de Perijá. Mérida State; 15) Llano el Anís. Trujillo State; 16) Agua Viva; 17) Los Guamos. Lara State; 18) La Hundición; 19) El Vano; 20) Carora; 21) Quebrada de Guadalupe; 22) La Cruz, Guardagallos, La Represa, Quebrada del Totumo, Las Faldas, Las Veras, La Ruezga; 23) Campo Alegre, Urama; 24) San Miguel; 25) Quíbor; 26) Barbacoas. Cojedes State; 27) Zanja de Lira. Guárico State; 28) Camaguán; 29) San Juan de los Morros; Carabobo State; 30) Río Las Tunitas, Río Los Guayos y Río Guacara. Miranda State; 31) Cueva de Iglesias. Sucre State; 32) Cueva de los Escorpiones; 33) Caiguire Abajo, Cumanacoa. Monagas State; 34) Mundo Nuevo; 35) El Breal de Orocuál (ORS 16 and ORS 20); 36) Maturín; 37) Cueva del Guácharo. Bolívar State; 38) Minas de Guaniamo. Amazonas State; 39) Sierra de Maigualida (\*D.R.R., pers. obs.).

a water-saturated, or intermittent, very low-energy environment, favoured by the low inclination of the terrain ( $\sim 10^\circ$ ). This second layer is the carrier of the bone remains and it could have had a greater thickness, which was likely eroded by laminar erosion, explaining the large amount of fossil bones exposed on the surface. The third layer, or the basal part, is characterised by an ancient relief of slightly more consolidated dark and oxidised sands, in which no remains of vertebrates or other micro/macrofossil organisms have been found.

Most of the bone and dental remains identified on the surface in different surveys (pre-excavation) were practically disintegrated or in a state of fragmentation that did not allow any type of surface rescue (Fig. 3A–C). Possibly, this was because of its exposure to environmental factors for decades before the first survey at the site. In pre-excavation activities, only the relatively complete crown of an M2 molar from a gomphothere and

fragments of equid teeth were recovered on the surface by the authors (J.D.C.B., R.S.) in 2013.

## Referred materials and methods

A total of 41 cranial and postcranial elements of fossil mammals were collected in the Cauca site and deposited in the palaeontological collection of Alcaldía Bolivariana del Municipio Urumaco (AMU-CURS). All fossils outcropping on the surface and in the excavations were treated in situ with consolidation of the Paraloid B72 type diluted to 10% in thinner solvent. Given the high degree of deterioration of the fossil elements, only the remains in the best state of preservation were recovered and transported in plaster jackets (e.g. Fig. 4D). The restoration and preparation of the fossil specimens was carried out in the palaeontology laboratory of the Urumaco Museum.

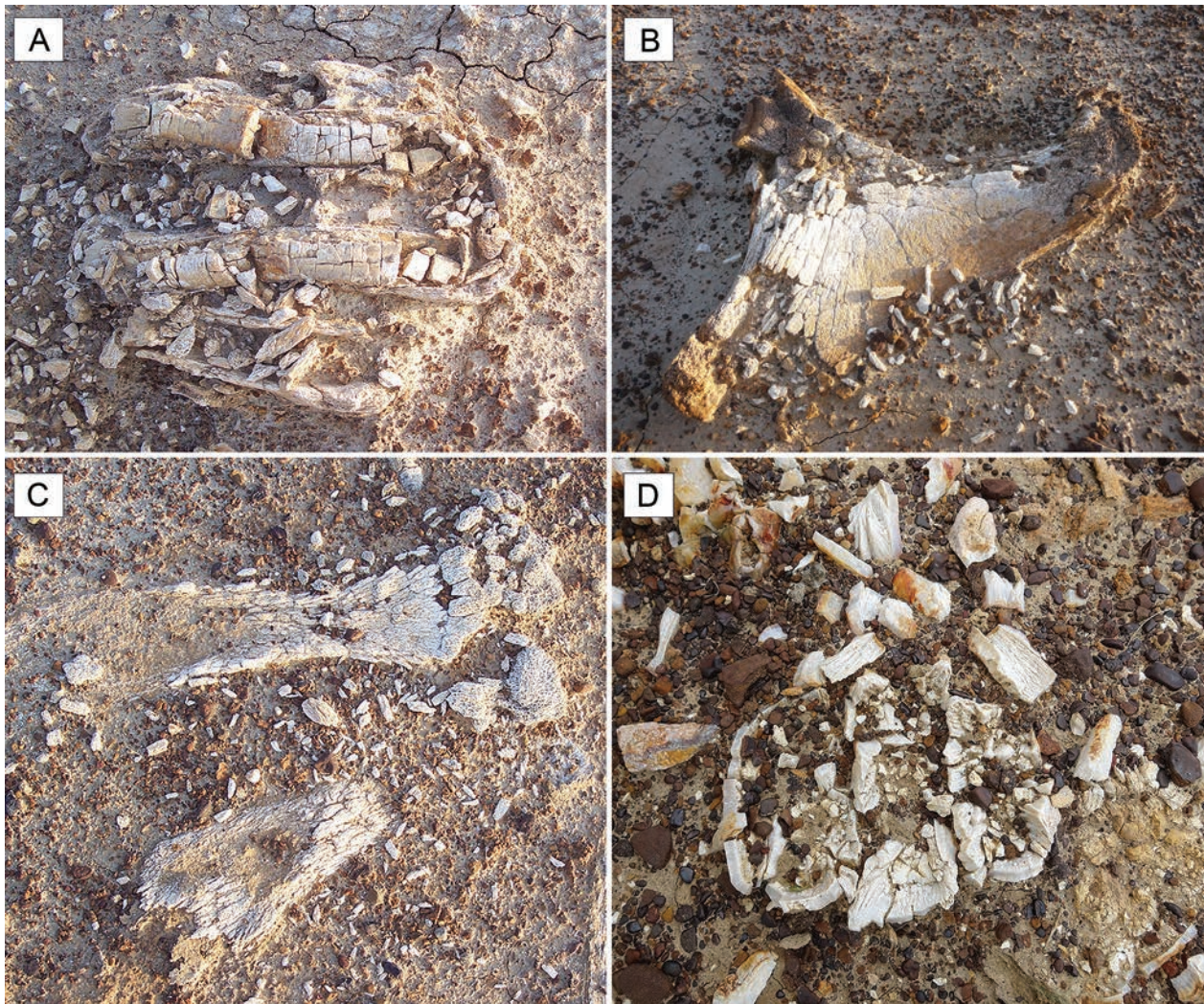


**Figure 3.** Remains of fossil vertebrates emerging on the surface at the Cauca site. Skull (A), pelvis (B) and appendicular elements (C) of megatheriid *Eremotherium*. A, C. correspond to unexcavated S2 (see Fig. 1B). Upper molars (D) of gomphoteriid *Notiomastodon platensis*, with the root completely eroded, associated with the mandible AMU-CURS-1269 from Cauca “A” (Fig. 1B).

The taxonomic identification involved an extensive bibliographic review and comparisons with fossil and extant specimens housed in: Argentina [Centro Regional de Investigaciones y Transferencia Tecnológica de La Rioja (CRILAR); Museo Argentino de Ciencias Naturales “Bernardino Rivadavia” (MACN); Museo de La Plata (MP)], France [Muséum national d’Histoire naturelle, Paris (MNHN)], México [Instituto Nacional de Antropología e Historia (INAH)], Switzerland [Natural History Museum of Basel (NMB); Palaeontological Institute of the University of Zurich (PIMUZ)] and Venezuela [Centro de Investigaciones Antropológicas, Arqueológicas y Paleontológicas (CIAAP) de la Universidad Experimental Francisco de Miranda (UNEFM), Falcón; Museo de Ciencias de Caracas (MCNC); Museo Geológico Royo y Gómez de la Universidad Central de Venezuela (UCV); Fundación La Salle de Ciencias Naturales, San Carlos, Cojedes State]. Additionally, the material was compared with images shared by collaborators and available on the web (e.g. [www.boneid.net](http://www.boneid.net)).

Most of the fossiliferous localities presented on the map in Fig. 2 are based on the following references: Schaub (1935); Nectario María (1937, 1941); Simpson (1939); Von der Osten (1947); Royo y Gómez (1960); Bocquentin-Villanueva (1979, 1982); Ochsenius (1980); Linares (1983); Linares and Bruni (1993); Odreman (1997); Aguilera (2006); Rincón et al. (2006, 2021); Prevosti and Rincón (2007); Rincón and White (2007); Carrillo-Briceño et al. (2008a, 2016); Chávez-Aponte et al. (2008a, 2008b); Chávez-Aponte and Carrillo-Briceño (2012); Ruiz-Ramoni et al. (2013, 2022); Carrillo-Briceño (2015); Solórzano et al. (2015); Steadman et al. (2015); Ruiz-Ramoni (2016); Meneses and Gordones (2021); Chávez-Aponte (2022); Jaimes et al. (2024b) and references therein. Names of localities referred to with (\*) in Fig. 2 are mentioned here for the first time.

Anatomical and measurement abbreviations. (mf) lower molariforms, (Mf) upper molariforms, (m) lower molar, (M), upper molar, (TI) total length.



**Figure 4.** Excavations at the Cauca site. Cauca “A” (A), Cauca “B” (B), and Cauca “E” (C), showing the defence of *Notiomastodon platensis* (AMU-CURS-1359) *in situ*. Mandible of *N. platensis* in plaster jacket in Cauca “A” (D). Cauca “D” with remains (tibia and ribs) of cf. *Eremotherium laurillardi* (E).

### Radiocarbon dating of the Cauca site

Two dental fossil samples were selected for radiocarbon dating (Table 1). The dated material comes from a *Notiomastodon platensis* mandible (AMU-CURS-1269) found in excavation Cauca “A” and an isolated tooth of *Equus* sp. (AMU-CURS-1365), found in the vicinity of the latter (Fig. 1B). Both specimens correspond

stratigraphically to the most superficial or exposed part of what we recognise here as the second layer.

In the absence of bone collagen, tooth enamel was selected from these two fossils. The enamel surface was cleaned and the dentine was removed with a dremel to isolate the enamel from the rest of the dental tissue. The enamel (approx. 2 g) was then ground using a steel mortar and pestle, followed by grinding in an agate mortar to a

**Table 1.** Measured and calibrated <sup>14</sup>C ages of the fossil samples from Cauca.

Sample id	species	<sup>14</sup> C age	Error	Target ID	Cal BP (95.4% proba)	
Cauca 3-23-2 AMU-CURS-1269	<i>Notiomastodon platensis</i>	33750	350	5545.1.1	39584	37540
Cauca 4-21 AMU-CURS-1365	<i>Equus</i> sp.	37050	500	5547.1.1	42310	41175

particle size of < 100 microns. The powder was then further ground using a McCrone Microniser Retsch following the methodology described in Wood et al. (2016). Briefly, this approach enables better separation of crystallite clusters and increases the efficiency of the acetic acid pre-treatment aimed at removing diagenetic carbonates. To achieve this, the powder was ground three times for 10 min, with a 5 min pause between each stage to avoid heating. For some samples, part of the hand-milled fraction (< 100 microns) was retained for comparison with the conventional pre-treatment approach. The resulting powder was pre-treated under light vacuum for 20 h with a solution of 1 N acetic acid (1 ml acetic acid for approx. 50 mg powder). The extraction yields were comprised between 70–80%. The pre-treated powder was then rinsed with milliQ water and dried at 50 °C in an oven. About 250 mg of powder was then reacted under vacuum with orthophosphoric acid at 70 °C for around 20 min. The CO<sub>2</sub> released was then separated cryogenically from the water produced and chemically purified, thanks to several passages through a trap filled with a copper-silver wool mixture. The CO<sub>2</sub> gas was then reduced in the presence of hydrogen and iron to produce graphite. Samples were then pressed into targets and <sup>14</sup>C ages were measured on the compact AMS ECHoMicadas (Archéozoologie, Archéobotanique, Sociétés, Pratiques et Environnements, Equipe SAPOA, France).

## Results

### Faunistic assemblage

Five mammal taxa are reported here, including three xenarthrans, one proboscidean, an equid and a felid. Other fragmentary and no diagnostic elements are referred to here as indeterminate mammals.

#### **Xenarthra Cope, 1889**

#### **Phyllophaga Owen, 1842**

#### †**Megatheriidae Gray, 1821**

#### †**Eremotherium Spillmann, 1948**

#### †**cf. Eremotherium laurillardii (Lund, 1842)**

Fig. 5

**Referred material.** Remains of *Eremotherium* cf. *E. laurillardii* have been recovered at the Cauca site in bone groupings 2–6, with only groupings 3–5 being excavated (Fig. 1B). Fourteen cranial and postcranial remains that include a right hemi-mandible (with mf 1 to 4), skull (with right Mf 1 to 5 and left Mf 2 to 4), right clavicle, right radius, presumably left navicular, cuneiform, IV left

metatarsal, a worn element that we presume corresponds to a scaphoid, fragment of pelvis with acetabulum and part of the pubic ramus and five incomplete vertebrae, from excavation Cauca “B” (Fig. 4B) and assigned to catalogue number AMU-CURS-1268. A probable right tibia (AMU-CURS-sn) and seven rib fragments were found in Cauca “D”. The other cranial and postcranial elements identified in Cauca “C” and unexcavated groupings 2 and 6 were not collected due to their poor state of preservation, being in some cases disintegrated (Fig. 3A–C).

**Descriptions.** The 14 disarticulated cranial and postcranial elements recovered in Cauca “B” most probably belong to the same individual (AMU-CURS-1268). The cranial material is composed of only the skull (AMU-CURS-1268a) (Fig. 5A1–A4) and the right hemi-mandible (AMU-CURS-1268b) (Fig. 5B1, B2). The skull has a TL of 580 mm and preserves only the palatal section, since part of the cranial vault, nasal bones and part of the maxilla bones were destroyed by erosive processes. The palatal section is relatively well preserved, with both the right Mf1–Mf5 and the left series Mf2–4 and the alveolus of left Mf1 and Mf5. The hemi-mandible has a TL of 450 mm, preserving the four molariforms mf1–mf4 (Fig. 5B2). This hemi-mandible has a convex ventral margin and projects downwards at the level of the first molars, forming a moderate mandibular protuberance. The molariforms preserved in the skull and hemi-mandible are of quadrangular section with crowns characterised by two transverse and parallel ridges, separated by a “V”-shaped valley. Measurements of the molariforms are presented in Table 2. Associated with these cranial remains were recovered the right clavicle with a TL of 240 mm (AMU-CURS-1268c; Fig. 5D1, D2), complete right radius with a TL of 700 mm (AMU-CURS-1268d; Fig. 5C1–C3), presumably left navicular (AMU-CURS-1268e), cuneiform (AMU-CURS-1268f), IV left metatarsal (AMU-CURS-1268g; Fig. 5G), a worn element that we presume corresponds to a scaphoid (AMU-CURS-1268h), fragment of pelvis with the acetabulum and part of the pubic ramus (AMU-CURS-1268i) and five incomplete vertebrae (AMU-CURS-1268j–n; Fig. 5E1–F). Other small, fragmented and indeterminate bone elements were observed during the excavation and presumably could be associated with the same individual.

In Cauca “C”, only a few remains of postcranial elements of an *Eremotherium*, were found emerging on the surface. These were identified as vertebrae, ribs, pelvis fragments and other small indeterminate fragments. However, the poor state of preservation and disintegration in some cases, did not allow their recovery. Due to the proximity of these materials to the individual collected in Cauca “B”, a possible association amongst them is not ruled out here. In Cauca “D”, an association of seven fragments of ribs

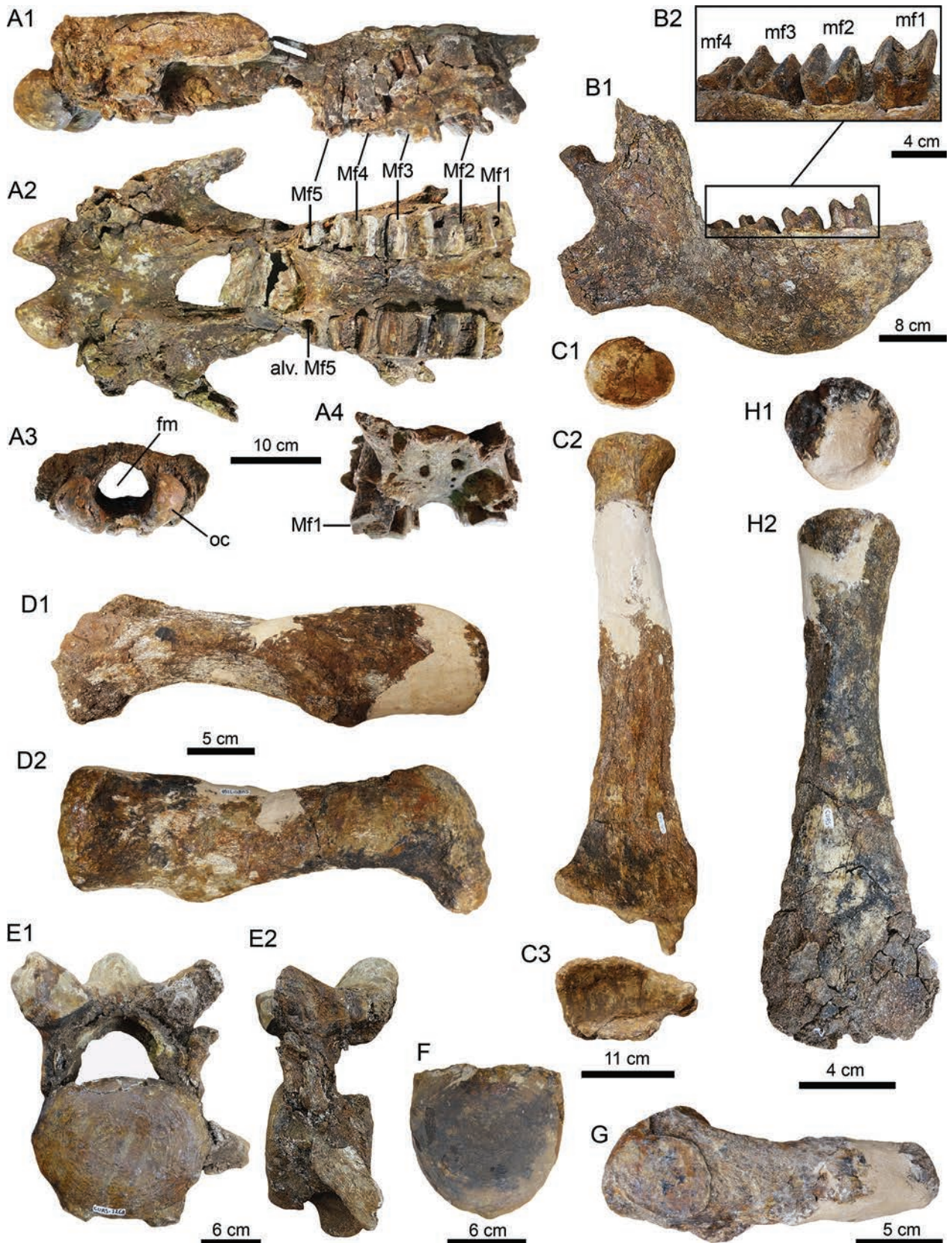


**Figure 5.** Megatheres (A1–G) and mylodontids (H1, H2) from the Cauca site. A1–A4. Skull of cf. *Eremotherium laurillardardi* (AMU-CURS-1268a) in right lateral, ventral, posterior and anteroventral view; B1, B2. Right hemi-mandible (AMU-CURS-1268b) in right lateral view; C1–C3. Right radius (AMU-CURS-1268d) in proximal, dorsal and distal view; D1, D2. Right clavicle (AMU-CURS-1268c); E1, E2. Thoracic vertebra (AMU-CURS-1268j) in anterior and left lateral view; F. Thoracic or lumbar vertebral centrum (AMU-CURS-1268k) in anterior view; G. Left IV metatarsal (AMU-CURS-1268g); H1, H2. cf. *Mylodontidae*, proximal and dorsal right radius (AMU-CURS-1363). Abbreviations: (alv.) alveolus, (fm) foramen magnum, (mf) lower molariform, (Mf) upper molariform, (oc) occipital condyle.

**Table 2.** Dental measurements of cf. *Eremotherium laurillardii* (AMU-CURS-1269a, b) collected at the Cauca site. Abbreviations: upper molariform (Mf), lower molariform (mf), right (d), left (i). (\*): incomplete or missing pieces. Measures in millimeters.

	Mfr1	Mfr2	Mfr3	Mfr4	Mfr5*	Mfl1	Mfl2	Mfl3	Mfl4	Mfl5*	mfr1	mfr2	mfr3	mfr4
Long	25	35	35	35	20	25	35	35	37	20	40	40	40	30
Width	36	50	47	40	25	35	45	47	40	15	44	45	42	40
Height	40	32	22	10	5	10	10	27	20	–	40	30	10	10

and a right tibia were recovered, also in a poor state of preservation (Fig. 4E). This bone accumulation is located about 8 m north of the Cauca “B” individual, so a possible association with the latter would not be unlikely.

Bone grouping 2 (Fig. 1B) was not excavated due to the partial or total disintegration in very little scraps of bones of the outcropping materials. However, a skull in a state of fragmentation (Fig. 3A) still offers evidence that allows us to identify this association as a second specimen of *Eremotherium*. In bone grouping 6 (not excavated) to the northwest of Cauca “D”, a humerus of *Eremotherium* was also identified, but its poor state of preservation prevented collection or conservation *in situ*.

**Remarks.** The ground sloth *Eremotherium laurillardii* distributed from south-eastern USA to Brazil, is the only species of the genus known from the Late Pleistocene in the Americas (Cartelle and De Iuliis 1995). The taxonomic validity of *Eremotherium rusconi* Schaub, 1935, another species from the Late Pleistocene of South America, is questionable (Cartelle and De Iuliis 1995; Faure et al. 2014; Cartelle et al. 2015).

Remains referable to *Eremotherium* are common and widely referred to in the Pleistocene fossil record of Venezuela (e.g. Schaub (1935); Simpson (1939); Nectario Maria (1941); Aguilera (2006); Carrillo-Briceño (2015); Carrillo-Briceño et al. (2016); Chávez-Aponte (2022) and references therein); specific taxonomic assignments of many of these specimens are still uncertain and should be clarified.

Remains assigned to cf. *Eremotherium laurillardii* have been reported in Venezuelan territory in palaeontological and archaeological sites ranging from sea level (e.g. Muaco, Taima-Taima and Cucuruchú; see Aguilera (2006); Carrillo-Briceño (2015); J.D.C.B pers. obs. (2022)), to mountain areas above 1200 m (e.g. El Vano; Jaimes et al. (2024b)).

The cranial and postcranial materials of *Eremotherium* collected from Cauca likely belong to an adult individual. The assignment of these specimens to the genus *Eremotherium* is based on the Hypsodontic index (HI) known for ground sloths. According to Bargo et al. (2006), HI is an element that is quantified by using the depth of the mandible (DM) (below the third molariform tooth) divided by the length of the molariform tooth row (LTR). In the right hemi-mandible collected in Cauca “B” (AMU-CURS-1268b), the DM is 140 mm and the LTR is 180 mm, with a resulting IH equal to 0.77, a value that coincides with *Eremotherium* whose range oscillates between 0.73 and 0.83 (De Iuliis 1996; Bargo et al. 2006). Based on the taxonomic validity of the Late Pleistocene *Eremotherium* species suggested by Cartelle and De Iuliis (1995) and Cartelle et al. (2015), we tentatively suggest assigning the specimens collected at the Cauca site as cf. *Eremotherium laurillardii*.

## †Mylodontidae Gill, 1872

### cf. Mylodontidae

Fig. 5

**Referred material.** The right radius (AMU-CURS-1363) collected in Cauca “B” (Fig. 4B).

**Descriptions.** The AMU-CURS-1363 radius is incomplete in its distal part and has a TL of 430 mm (Fig. 5H1, H2). This specimen differs in dimensions and morphology with reference to the left radius of cf. *Eremotherium laurillardii* (AMU-CURS-1268d; Fig. 5C1–C3) found in the same excavation. AMU-CURS-1363 is proportionally thicker and shorter compared to Megatheriidae and Megalonychidae (e.g. McAfee (2007)), being narrow at the proximal end and laterally expanded at the distal end, which is fragmented and deteriorated. The proximal articular head is concave, narrow, and semicircular with a maximum diameter of 40 mm. The axes are relatively straight, and a prominent laterally expanded pronator ridge is not observed, as occurs in Scelidotherinae and some Lestodontinae. These characteristics lead us to consider AMU-CURS-1363 as belonging likely to a mylodontid (Mylodontinae) indet.

**Remarks.** The incompleteness and state of preservation of AMU-CURS-1363 does not allow for a more precise taxonomic determination. Mylodontid remains reported for the Late Pleistocene of Falcón State come from the Muaco and Taima-Taima sites and some of these have been referred to as *Glossotherium tropicorum* Hoffstetter, 1952, by Bocquentin-Villanueva (1979), Aguilera (2006) and Carrillo-Briceño (2015); although De Iuliis et al. (2017) noted that those specimens from Falcón appear to be distinct from the *G. tropicorum* material known from Ecuador and Peru. A taxonomic re-evaluation of the *Glossotherium* materials found in Falcón, as well as in other regions of Venezuela (Carrillo-Briceño 2015; Chávez-Aponte 2022), would be relevant for new clues about the stratigraphic range and geographic distribution of the three valid species of *Glossotherium* recognised for the Pleistocene of South America (see Cartelle et al. (2019)).

## Cingulata Illiger, 1811

### †Glyptodontidae Gray, 1869

#### †Glyptodontidae indet.

Fig. 6

**Referred material.** Two isolated osteoderms (AMU-CURS-1047 and -1360) were collected on the surface at the Cauca site (Fig. 1B).

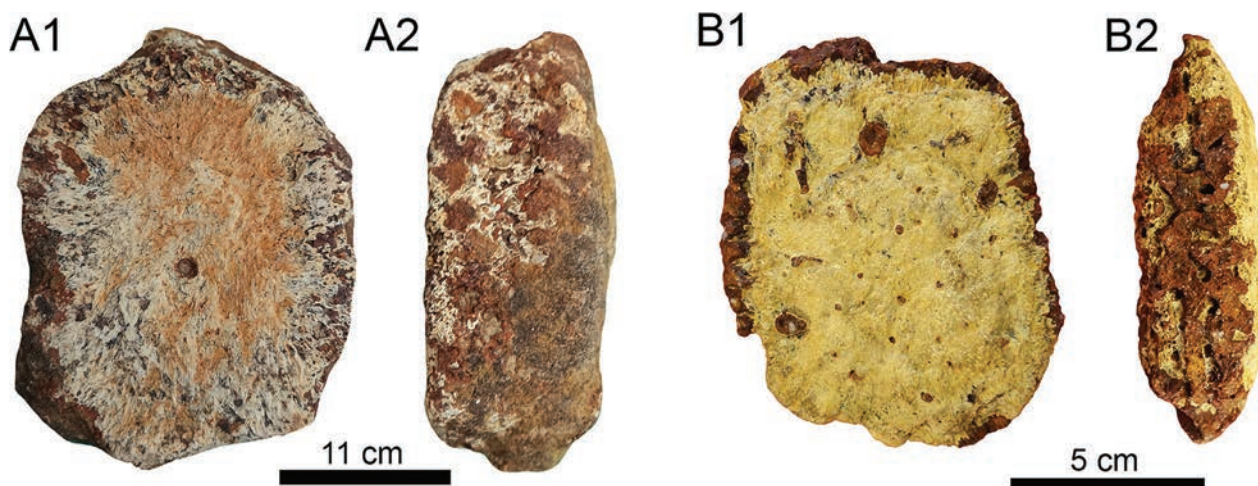


**Figure 6.** Indeterminate Glyptodontidae osteoderms from Cauca site. **A1, A2.** AMU-CURS-1047; **B1, B2.** AMU-CURS-1360; both in external and transversal view.

**Descriptions.** Both isolated osteoderms are from the shell. AMU-CURS-1047 has a TI of 47 mm and is eroded on both the internal and external faces, which does not allow the identification of the ornamentation pattern (Fig. 6A1, A2). AMU-CURS-1360 possibly corresponds to an osteoderm from the anterior lateral region of the shell and this has a TI of 31 mm; it is also eroded on the inner face, and partially preserving the ornamentation of the outer face with a central figure of irregular polygonal shape, preserving some foramina that could belong to hair follicles and surrounded by a groove (Fig. 6B1, B2).

**Remarks.** The state of preservation of these two osteoderms does not allow a more precise taxonomic determination than Glyptodontidae, Glyptodontinae. However, these osteoderms could belong to the genus *Glyptotherium*, widely known in the Late Pleistocene of the Falcón State, especially at the sites of Muaco and Taima-Taima (Carlini et al. 2008, 2022). A recent report suggests that these *Glyptotherium*-related armadillos had a broader distribution in what is now Venezuela during the Late Pleistocene, with reports including mountain areas above 1200 m altitude (see Jaimes et al. (2024b)).

### Proboscidea Illiger, 1811

#### †Gomphotheriidae Hay, 1922

#### †*Notiomastodon* Cabrera, 1929

#### †*Notiomastodon platensis* (Ameghino, 1888)

Fig. 7

**Referred material.** A mandible (Fig. 7A1), the proximal part of a humerus and the distal end of the radius with what appears to be parts of very deteriorated carpals and metacarpals, all assigned as AMU-CURS-1269 and collected from Cauca “A” (Fig. 4A). An isolated M2 (AMU-CURS-1045) collected about 5 m northwest of Cauca “C” (Fig. 1B) and a complete and isolated tusk (AMU-CURS-1359) (Fig. 7C) from Cauca “E” (Fig. 4C).

Other dental and postcranial fragments (see below) in a very poor state of preservation could not be collected.

**Descriptions.** The mandible AMU-CURS-1269 (Fig. 7A1) preserves the complete right m2 (Fig. 7A1–A3, A5) and erupted m3 (Fig. 7A1, A4) and erupted left m2 and m3 in a fragmentary state (Fig. 7A1, A5). Part of the mandibular ramus and condylar processes are not preserved. The right m2 is a bunodont and trilophodont molar with a well-defined heel and cingulum (Fig. 7A2, A3); it is 150 mm in TI. This molar presents a wear state of “3” (following Mothé et al. (2010)), which suggests that it could correspond to a subadult/adult individual. Abundant fragments referring to upper molars M2–M3 of the same individual were recovered on the mandibular remains (Fig. 3D). A small portion of a tusk was also found a few centimetres from the specimen, which was not collected due to the high degree of disintegration. Of the postcranial remains associated with the lower jaw, the proximal part of a right humerus is only preserved in the posterior section and what appears to be the distal end of the radius with carpal and metacarpal fragments are in a very poor state of preservation.

The isolated tusk AMU-CURS-1359 (Fig. 7C), whose position on the skull is undetermined, measures about 1700 mm long and could belong to an adult. It is curved, although it shows no apparent natural twist and lacks an enamel band. The tusk lies about 14 m north of the Cauca “A” site and its association with the jaw and the other elements is uncertain. Near the collection site of this tusk and on the surface, some fragmented and indeterminate postcranial bones were observed.

A few metres northeast of the Cauca “D” and “E” excavations, a tusk and bone fragments were found emerging on the surface. However, these were not collected due to the poor state of preservation (grouping 7; Fig. 1B). In addition, small fragments of gomphotherid molars were scattered on the surface of the site, possibly because of transport by runoff. A possible upper left M2 (AMU-CURS-1045) not worn and with ~ 96 mm in TI

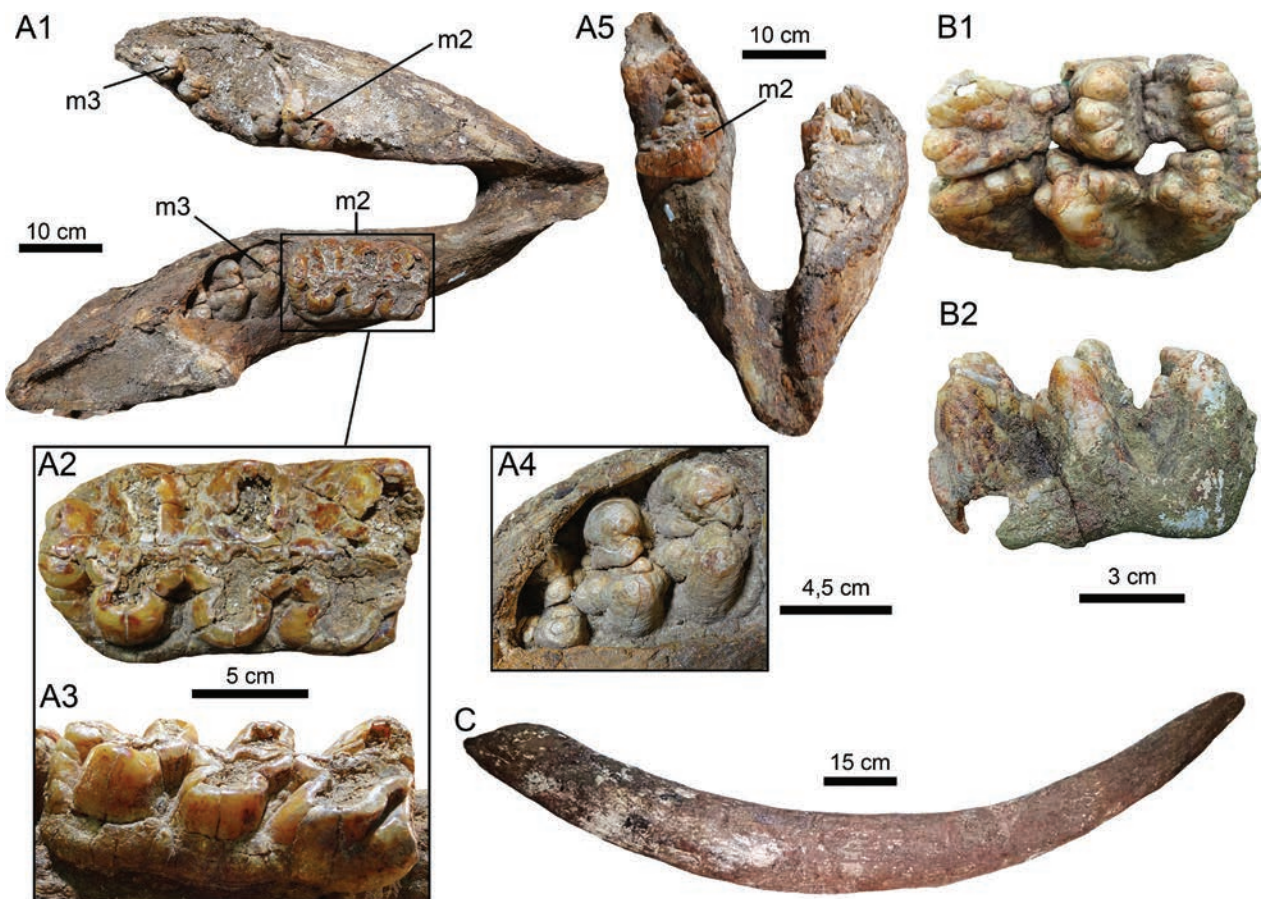


**Figure 7.** *Notiomastodon platensis* remains from Cauca site. **A1, A5.** Dorsal and anterodorsal views of the mandible (AMU-CURS-1269); **A2, A3.** Occlusal and labial views of preserved right m2 and (**A4**), occlusal view of m3; **B1, B2.** Occlusal and lateral view of M2 (AMU-CURS-1045). **C.** lateral view of tusk (AMU-CURS-1359).

(Fig. 7B1, B2), was collected a few metres northeast of excavation “C”, suggesting the probable presence of a juvenile individual at the site. On the other hand, we do not have any evidence that allows us to associate the cranial and dental remains found in Cauca “A”, with the other gomphothere elements reported herein, resulting in an uncertain number of adult individuals present at the site.

**Remarks.** In recent times, consensus has emerged suggesting the validity of only two genera of gomphothere in the southern continent, *Cuvieronius hyodon* Fischer, 1814 and *Notiomastodon platensis* (= *Stegomastodon platensis*) (e.g. Mothé et al. (2012, 2013, 2017a); Alberdi and Prado (2022)). The stratigraphic and geographic distribution, as well as the diagnostic features that have been used to differentiate both genera, which are based on the skull and mandibular symphysis morphology and upper tusk and molars, are discussed in detail by Mothé et al. (2016, 2017a, 2017b), Alberdi and Prado (2022) and Carrillo-Briceño et al. (2023).

Based on the taxonomic differences mentioned above and used to differentiate both genera of gomphotheres in South America, we assigned the better-preserved specimens referred to in this section to *N. platensis*. This assignment is supported by: 1) the double to

single clover wear pattern present in the right m2 of the AMU-CURS-1269 (Fig. 7A2), which resembles the pattern present in molars with advanced wear state in *N. platensis* (e.g. Mothé et al. (2012, 2013, 2017a) and references therein); 2) the robustness, curved shape and lack of twist and enamel bands in the tusk AMU-CURS-1359 (Fig. 7C), which contrast with the shape and morphology of the *C. hyodon* tusk (Mothé et al. 2012, 2013; Mothé and Avilla 2015); and 3) a jaw with no trace of lower tusks; meanwhile, *C. hyodon* presents a pair of lower incisors or its corresponding vestigial alveoli (Mothé and Avilla 2015). By analogy, we believe the other remains of gomphotheres found at the Cauca site (e.g. tooth fragments and probably postcranial elements), and with a poor state of preservation (for example these from grouping 7) could also belong to *N. platensis*.

Abundant specimens of gomphotheres have been reported for several locations in the Falcón State and other sites in Venezuela (Carrillo-Briceño et al. 2008a, 2008b; Chávez-Aponte et al. 2008; Carrillo-Briceño 2012, 2015); however, their taxonomic assignment should be re-evaluated. The gomphothere remains collected from the palaeontological/archaeological sites of Muaco, Taima-Taima and Cucuruchú in Falcón State, should be assigned to *N. platensis* (e.g. J.D.C.B., pers. obs. (2022)).

**Perissodactyla Owen, 1848**  
**Equidae Gray, 1821**  
**Equus Linnaeus, 1758**

**Equus sp. and Equidae indet.**

Fig. 8

**Referred material.** The equid material corresponds to isolated dental elements collected on the surface of the second layer (Fig. 1B) and is represented by a complete m3 (AMU-CURS-1365) and another five molar fragments (AMU-CURS-523: n = 2, and AMU-CURS-1046: n = 3).

**Descriptions.** The left m3 AMU-CURS-1365 is almost complete, only missing part of the mesial surface (Fig. 8A1). The occlusal surface of the m3 is relatively well preserved with a length of 28 mm and it is characterised by a subtriangular protoconid, an oval hypoconid, a metaconid and metastylid forming a more rounded double knot, an oval postflexid and the presence of a well-defined pli caballinid fold. The rest of the five fragments could belong to both upper and lower molars; however, the poor state of preservation of these prevents a more detailed taxonomic identification.

**Remarks.** The occlusal pattern, present in the m3 with a subtriangular protoconid, an oval hypoconid and the presence of a pli caballinid fold, can likely be associated more with *Equus* than *Hippidion* Owen, 1869 (see Prado and Alberdi (2017); Carrillo-Briceño et al. (2023) and references therein). The poor state of preservation of the other dental elements does not allow them to be assigned beyond Equidae for now.

For the Pleistocene of Falcón State, equid remains assigned to *Equus neogeus* Lund, 1840 and *Equus santaeelenae* Spillmann, 1938, have been reported for the sites of Muaco, Taima-Taima, Cucuruchú and Quebrada Ocando (Royo and Gómez 1960; Aguilera 2006; Rincón et al. 2006). Other reports of fossil equids from Venezuela have also been referred to by Rincón et al. (2006) and Carrillo-Briceño (2015).

Prado and Alberdi (2017), based on an extensive review of the morphological and morphometric characters of cranial and postcranial elements of fossil horses from South America, recognise only three species as valid (e.g. *E. andium*, *E. insulatus* and *E. neogeus*). Machado and Avilla (2019) questioned the diagnoses and taxonomic validity of the three valid species proposed by Alberdi and Prado (2017), suggesting the possibility of a single *Equus* species of South America which should be recognised as *E. neogeus*. In the case of our specimens, only the m3 AMU-CURS-1365 is likely associated here with *Equus*; despite this, until now, as there is no consensus on the taxonomy of the valid *Equus* species of South America and the lack of more diagnostic characters in our specimen, it is appropriate to keep this assignment tentatively as *Equus* sp.

**Carnivora Bowdich, 1821**  
**Felidae Fischer, 1817**  
**Felinae Fischer, 1817**

**cf. *Leopardus pardalis* (Linnaeus, 1758)**

Fig. 8

**Referred material.** A right astragalus (AMU-CURS-1361; Fig. 8B1–B3). This specimen was collected, exposed on the surface about six metres south of the Cauca “A” excavation (Fig. 1B) and we believe that it also comes from the upper part of the second layer that has been affected by laminar erosion. The preservation of the astragalus is good, except for partial erosion of the fibular facet and the distal end of the lateral lip of the trochlea that is broken.

**Description.** AMU-CURS-1361 has a maximum length of 23.23 mm and a maximum width at the trochlea of 12.59 mm, which corresponds to a medium-sized mammal. The astragalus head is projected distally, but its media border is more displaced medially than the trochlea. The head is wide and, in the distal view, it has an elliptical shape that is slightly inclined medially. The trochlea is well-marked, with a sharp medial lip and a laterally inclined lateral lip. It differs from that of canids in that the trochlea is less excavated, the head is less inclined and not subtriangular in shape in the distal view. Canids have a bony shelf distal to the trochlea that connects with the neck of the head, which is not present in the AMU-CURS-1361, in felids and other carnivorans. Other carnivorans, like procyonids and mustelids, have a different astragalus shape, with a flatter trochlea and a wider and rounded head that is more medially directed. Although we did not observe diagnostic features at the genus level in the context of medium-sized felines in the astragalus, AMU-CURS-1361 exhibits a morphology resembling *Leopardus pardalis* and *Lynx rufus* Schreber, 1777.

**Remarks.** We note some differences between AMU-CURS-1361 and *Lynx rufus*. In the revised specimens of the bobcat (INAH 7776; NMB 6111; and one at BonelD.net), the head of the astragalus is proportionally shorter and the distal border of the sustentacular facet is interrupted by a sharp incision. These features were also observed in some individuals of *Leopardus pardalis* (e.g. MACN-Ma 30866), while in other *Le. pardalis*, this facet contacts the navicular facet (e.g. MACN-Ma 27888, 30695 and 30698). Thus, based on the size and shape of the astragalus, AMU-CURS-1361 has a greater morphological affinity with *Le. pardalis* than with *Ly. rufus*, but given the small size of the comparison sample, it is not possible to make a more precise taxonomic conclusion.

**Mammalia indet.**

Fig. 8

**Note.** A bone of the foot of an indeterminate mammal (Fig. 8C) with a Tl of 30 mm (AMU-CURS-1362) was collected on the surface about three metres north of

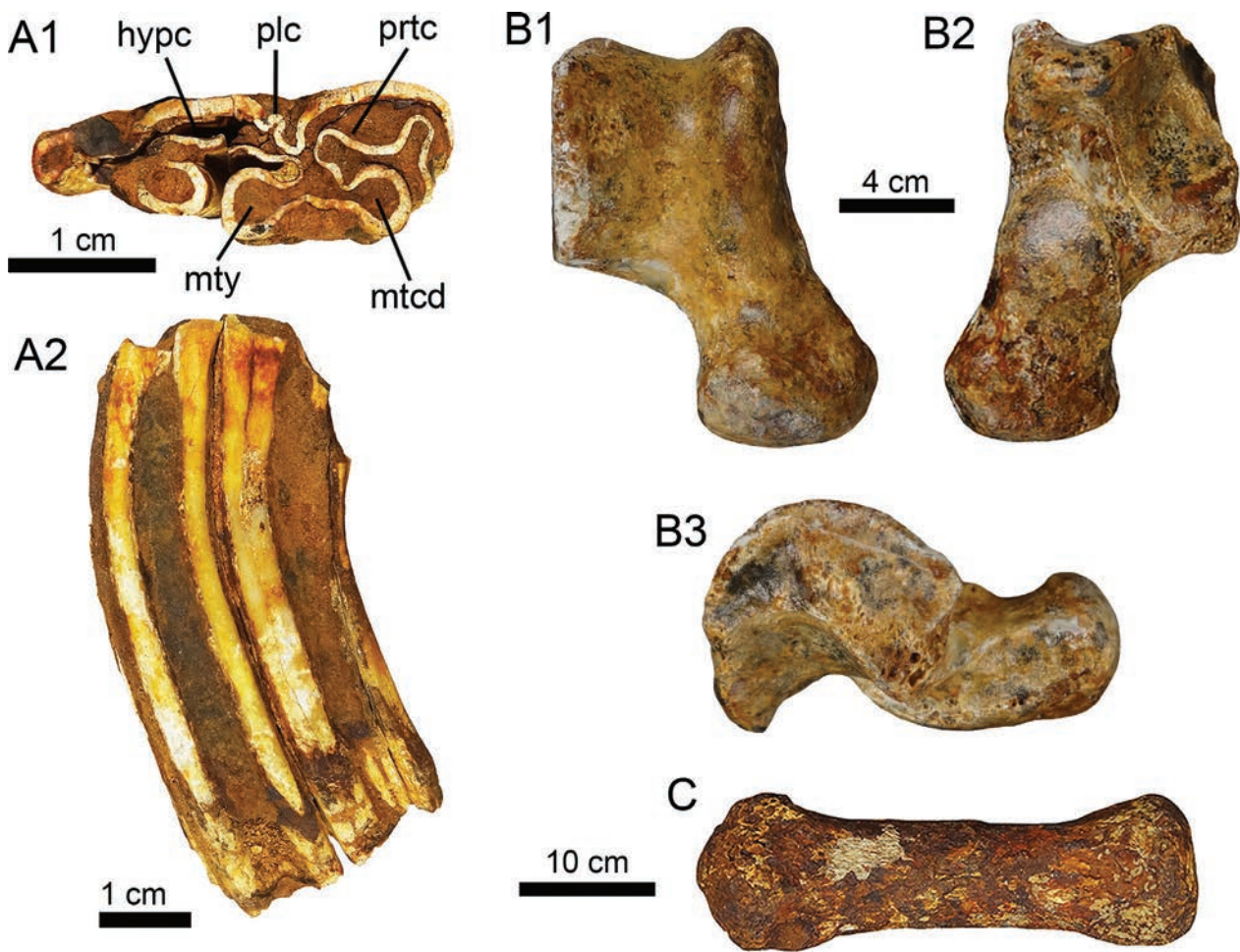


**Figure 8.** Equids, felids, and indeterminate mammals from Cauca site. **A1, A2.** Left m3 of *Equus* sp. (AMU-CURS-1365) in occlusal and labial view; **B1–B3.** Right astragalus of cf. *Leopardus pardalis* (AMU-CURS-1361) in dorsal, plantar and lateral view; **C.** A bone of the foot of an indeterminate mammal (AMU-CURS-1362). Abbreviations: (hypc) hypoconid, (mtcd) metaconid, (mty) metastylid, (plc) pli caballini fold, (prtc) protoconid.

Cauca “A”. The state of preservation of the specimen is poor and it lacks diagnostic elements that do not allow a more precise taxonomic determination.

### Dating of the Cauca Site

Radiocarbon age of  $33750 \pm 350$  and  $37050 \pm 500$  BP were obtained from teeth of *Notiomastodon platensis* and *Equus* sp., respectively. Results were then calibrated using OxCal 4.4 (Bronk Ramsey 2009) and indicate that the *Notiomastodon* is 37.5–39.5 ka cal. BP and that the *Equus* is 41.3–42.3 ka cal. BP. These dates are amongst the oldest dates ever produced on bioapatite (see Cherkinsky (2009)) and are close to the limit of the radiocarbon dating technique. It is important to note here that these are minimum ages because diagenesis makes bioapatite samples look younger due to carbon isotope exchange between soil dissolved carbonates and bone carbonate (Zazzo and Saliège 2011; Zazzo 2014). It is, thus, very likely that these samples are older than 40 ka.

### Lithic artefacts and early human evidence in the area

Preformatted lithic artefacts, on the surface and without evidence of discrete accumulations, were in the adjacent areas of the Cauca “B–D” excavations (Fig. 1B). None of these artefacts was recovered in direct association with the bone materials in the fossil-bearing stratum or layer. These artefacts are represented by a chopper (AMU-12-1; Fig. 9A–B2), a planoconvex scraper (AMU-12; Fig. 9C–D3) and three flakes or lithic debris (AMU-12-2; Fig. 9E).

Between 100 and 150 m northeast of the Cauca excavation site, we have found a relatively flat area with the presence of abundant preformatted lithic artefacts on the surface. The carrier layer corresponds to unconsolidated fine to coarse sand facies of light brown and ochre colour that underlie palaeodunes. This area and its surroundings have been prospected by members of our team since 2019 and, in it, we have collected at least three different typologies of lithic projectiles that include El Jobo, Clovis and Fish Tail technologies, amongst other lithic artefacts (Jaimes et al. 2024a). However, so far, we do not have

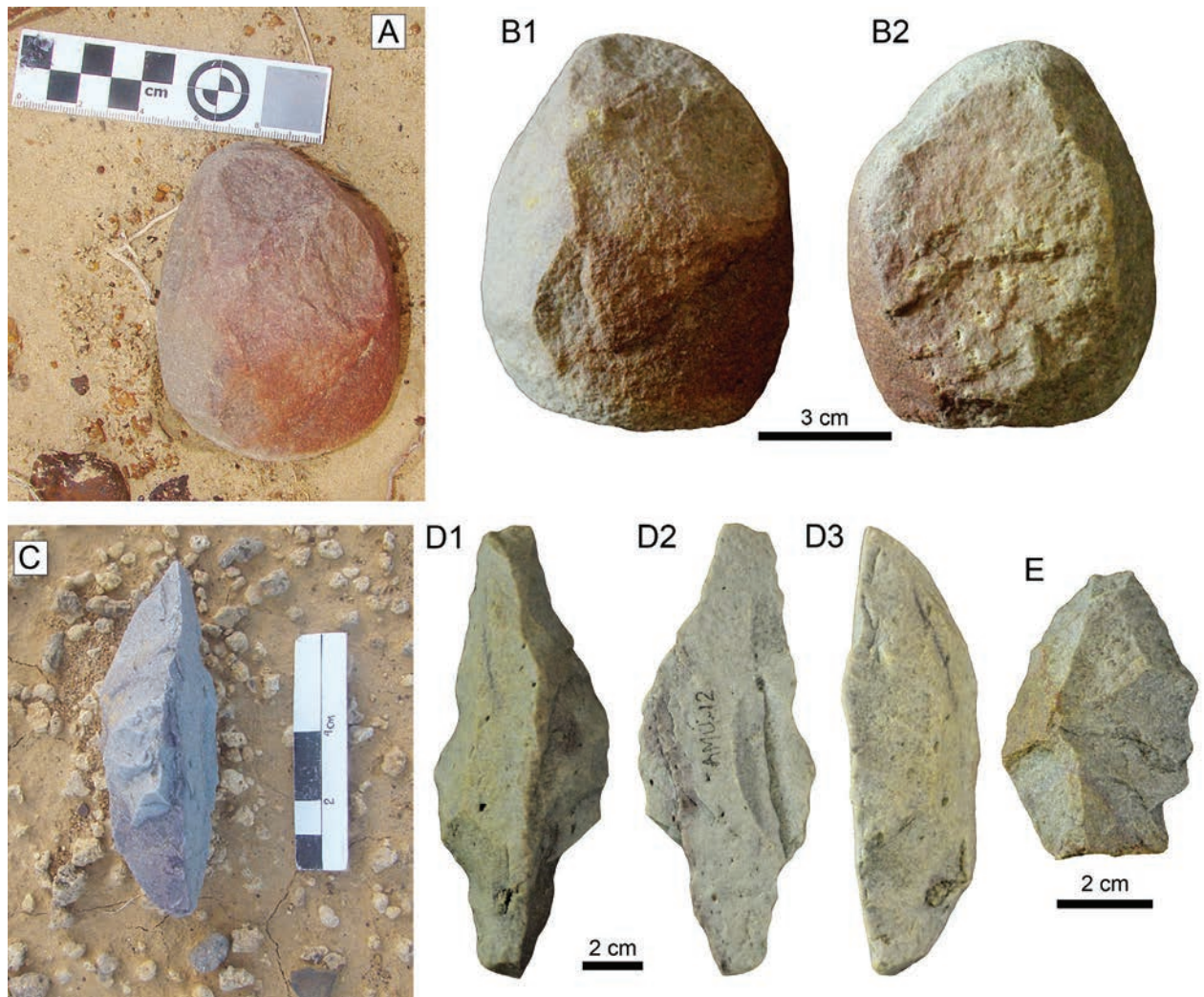


**Figure 9.** Lithic artefacts found in the vicinity of the excavations at the Cauca site (see Fig. 1B). **A**, **C**. *in situ* artefacts. Chopper (AMU-12-1; **B1**, **B2**), planoconvex scraper (AMU-12; **D1–D3**) and flake (AMU-12-2; **E**).

precise evidence that allows us to put this diversity of lithic technologies around the Cauca site in a chronological and stratigraphic context or in any relationship with the megafauna reported for the place.

According to Jaimes et al. (2024a), the contemporaneity of these three projectile typologies in the surroundings of Cauca in such a small area remains an uncertainty and their presence there could probably be due to erosion/laminar washing of the most overlying layers which may have generated decanting and mixing of artefacts corresponding to different antiquities. There is no doubt that the site of Cauca and its surroundings have been subjected to these processes of laminar erosion and this could be inferred by the flat characteristics of the terrain and the almost null evidence of transportation shown by both the fossils and the lithic artefacts (Jaimes et al. 2024a).

## Discussion

Prospecting and excavations in Cauca have resulted in a varied association of fossil mammals represented by South American natives, such as megatheres (cf. *Eremotherium*

*laurillardi*), an indeterminate mylodontid and a glyptodont (probably related to *Glyptotherium*) and Nearctic representatives, such as gomphotheres (*Notiomastodon platensis*), equids (*Equus* sp.) and a feline (Felidae cf. *Leopardus pardalis*), expanding the geographic distribution of some taxa.

Megaherbivores reported for the Cauca site such as megatheres, glyptodontids, gomphotheres and equids, have also been widely referred to in the Pleistocene fossil record of Venezuela, with distributions that cover a large part of the national territory, from sea level to almost 2000 m above sea level and even south of the Orinoco River (see Linares and Bruni (1993); Carrillo-Briceño et al. (2008a, 2008b); Carrillo-Briceño (2015); Chávez-Aponte (2022); see Fig. 2). The sympatry amongst megaherbivores in Cauca (i.e. *Notiomastodon* and *Eremotherium*) also characterises other sites in Venezuela, including some in the Cordillera de Mérida (Simpson 1939), the basin of Lake Valencia (Del Valle and Salazar 2009) and the sites of Taima-Taima, Muaco and Cucuruchú in Falcón State (Royo y Gómez 1959, 1960; Ochsenius and Gruhn 1979; Bocquentin-Villanueva 1982; Aguilera 2006; Carrillo-Briceño 2015).

The only medium-sized predator recovered so far at the locality corresponds to a material classified as Felidae cf. *Leopardus pardalis*. Records are scarce for medium-sized felids in the northern neotropics, which is why the report of cf. *Leopardus pardalis* in Cauca is notable, as this taxon was previously undocumented in north-western Venezuela. Royo y Gómez (1960) mentioned the presence of “*Felis (Lynx) cf. rufus?*” in the locality of Muaco and acknowledged that, despite this lineage not having been recognised in South America, the collected material (Nº. 24 on the author’s published list) exhibits similarities. Later, the identification presented by Royo y Gómez was questioned by Marshall et al. (1984) because the author did not present figures or descriptions of the studied fossil felid. Unfortunately, the current location of this material is unknown (D.R.R., pers. obs.), so this record cannot be confirmed and likely does not correspond to the *Lynx* genus. A left P3 and a lumbar vertebra from the Late Pleistocene El Mene de Inciarte locality in Eastern Venezuela were referred to cf. *Leopardus* sp. (Ruiz-Ramoni 2016). The P3 could correspond to a deciduous tooth of an undetermined feline and the study of the vertebra’s morphology further questioned this allocation to *Leopardus* (D.R.R., pers. obs.). Finally, Linares (1998) mentioned “remains” of *Le. pardalis* in archaeological sites (Pre-Columbian Age) on Margarita Island, the Eastern Cordillera and the Central Cordillera, but this taxonomic assignation was not justified and the specimens were not figured (see Prevosti and Forasiepi (2018)).

Currently, the medium-sized felines in the north of South America region are *Le. pardalis*, *Le. tigrinus*, *Le. wiedii* and *Herpailurus yagouaroundi* (Linares 1998; Sánchez and Lew 2012; Boher et al. 2023; Ruiz-García et al. 2023). The ocelot, or cunaguaro, *Le. pardalis* has a large distribution during the present (see Paviolo et al. (2015)) and during the Late Pleistocene (see Werdelin (1985); Seymour (1999); Prevosti and Forasiepi (2018); Prevosti et al. (2021); Manzuetti et al. (2023)) which is congruent with its presence in Venezuela deposition of Cauca sediments. On the other hand, the current distribution of *Ly. rufus* is limited to the northern half of México to Canada (Larivière and Walton 1997) and there are no fossils or living records of this genus in South America.

On the other hand, the sedimentary characteristics of some Late Pleistocene archaeological sites, such as Muaco and Taima-Taima (Ochsenius and Gruhn 1979; Carlini et al. 2022) and El Vano, in the Andean region of Venezuela (Jaimes 2003, 2005; Jaimes et al. 2024b), suggest that these sites were deposited in environments characterised by bodies of water that attracted animals. Specifically, Muaco and Taima-Taima have been referred to as resurgent springs, offering an oasis during dry periods (Ochsenius and Gruhn 1979; Ochsenius 1980). At the Cauca site, the bone remains are concentrated in a defined area (Fig. 1B) and the sedimentary conditions allow us to infer that the site was deposited in a humid, probably low-energy environment. However, the high degree of alteration and degradation of the site due to its exposure to extant (epidiagenetic) weathering is a limitation that

prevents us from inferring more precise evidence about possible extension and permeance/seasonality of the body of water. During the Late Pleistocene, the coastal plains of the Falcón State were subject to a negative water balance (Ochsenius 1980) and the ancient body of water in Cauca could have offered attractive water resources for the fauna that roamed in the area. The extension of these coastal plains in the region was greater than at present because of the glaciations and the consequent variations in sea level that occurred along the coastal zone. These now submerged plains extended from western Falcón to the Guajira Peninsula (see fig. 8 in Carrillo-Briceño (2015)), offering natural corridors that facilitated faunal and human movements along the Caribbean coast.

### Age of the Cauca site

The bioapatite dating of two fossil remains from Cauca provided an age of at least 40,000 cal. BP. In contrast, a biochronological approach of the site using identified fossil taxa does not offer a more precise age due to a wide chronological record for these taxa. For example: 1) Late Pleistocene for *Eremotherium laurillardii* (Cartelle and De Iuliis 1995), 2) Pliocene (~ 3.8 Ma, only for North America)–Late Pleistocene (for South America) for *Glyptotherium* (Carlini and Zurita 2010; Gillette et al. 2016; Zurita et al. 2018), 3) Early Pleistocene (1.2–0.4 Ma)–Late Pleistocene (~ 11,770 years BP) for *N. platensis* (Alberdi and Prado 2022) and 4) Middle Pleistocene (~ 2 Ma)–Early Holocene (~ 8,000 years BP) for *Equus* (MacFadden 2013; Prado and Alberdi 2017; Villavicencio et al. 2019).

### Taphonomic aspects and potential human-megafauna interactions at the Cauca site

Fossil bone elements emerging on the surface at the Cauca site were categorised within conservation stage “5” on the scale of Behrensmeyer (1978) (i.e. as the bone is fragile and breaks easily, it may lose the original shape of the bone). These materials could not be collected or identified in most cases due to their degree of fragmentation or total or partial disintegration (e.g. Fig. 3A–C). In contrast, the elements of the excavated groupings (not exposed) present a conservation stage of “3 to 4”, on the scale of Behrensmeyer (1978). These specimens have a thick fibrous surface, rough texture, large and small splinters that tend to break off when the bone is moved. Weathering has penetrated the internal cavities. The cracks are open and chipped with rounded edges and, in some cases, there is an incursion of sediment and biological activity (plant roots). These taphonomic preservation conditions limit the identification of micro modifications of animal or anthropogenic origin on the bone surface. Some specimens recovered from excavations are fractured or incomplete, where the missing part was exposed on the surface and eroded.

The factors that influenced the arrangement, alteration and disarticulation of the bones could be related to natural processes (meteoric and animal action) or human action (Fernández-Jalvo and Andrews 2016). At the Cauca site, indirect evidence of disarticulation was observed. An example is the postcranial remains of a probable adult individual assigned as cf. *E. laurillardi* and identified in excavation groupings 3 (Cauca “B”), 4 (Cauca “C”) and 5 (Cauca “D”) (Fig. 1B). In Cauca “B”, only the skull, right hemi-mandible, and a few other postcranial elements of the individual (see the faunal assemblage section) were identified. Other remains that probably belong to the same individual from Cauca “B” are found scattered between Cauca “C” and “D”. In Cauca “C”, a badly deteriorated fragment of the pelvis and other fragments of ribs and vertebrae were identified less than six metres west of Cauca “B”. In Cauca “D”, about 12 m north of Cauca “B”, a grouping of fragments of disarticulated ribs and a right tibia were recovered (Fig. 4E). These ribs show high fragmentation, with an arrangement pattern where some are on top of others and very close to the tibia.

At the Cauca site, large, compact and dense postcranial elements such as humeri and femurs of large megaherbivores (e.g. *Eremotherium* or *mylodontids*, *Notiomastodon*), both on the surface and in excavated groupings 1–5 (Cauca “A–D”), are scarce. Some examples are the tibia reported in Cauca “C”, the humerus in very poor condition observed in grouping 6 and what appear to be fragments of large bones destroyed amongst the remains of the *Eremotherium* identified in unexcavated grouping 2 (Fig. 3C). Gravitational dispersion models of large mammal carcasses in deposition environments with inclinations greater than 20° and subjected to hydraulic forces of 152 cm/s, considered a high rate (Voorhies 1969), are easier to disperse, starting with phalanges, ribs, teeth and jaw, while the last to be transferred from the place of death would be the skull. Although gravitational dispersion can organise and select bones for transport, others tend to anchor especially in clay environments with a lower inclination and subject to lower rates of hydraulic currents (Fernández-Jalvo and Andrews 2016). However, the spatial arrangement of the bone elements of the probable same individual from the cf. *Eremotherium laurillardi* in Cauca “B–D” breaks with the natural anatomical pattern that could be expected in high-energy deposition environments. The same could be inferred from the remains of *Notiomastodon platensis* from Cauca “A” and the tusk found in Cauca “E” if there is a possible relationship between them. Despite this, we do not rule out the possibility that most of the large bones and other cranial and postcranial elements have been eroded and destroyed before or after the biostratigraphic and fossil-diagenetic processes. As mentioned above, many fossils that remain on the surface have suffered fragmentation and disintegration due to the direct action of meteoric processes (e.g. very dry environment with concentrated rain) once they were exposed due to the erosion of the carrier layer and a clear example is the unexcavated grouping 2 (Fig. 3A, C).

The greatest disadvantage present when identifying potential evidence of direct action by animals (predators and scavengers) or humans in the skeletal remains of the Cauca site, as well as in their distribution pattern, includes: 1) the poor state of preservation of the remains, which limits the identification of micro modifications of anthropogenic origin on the surface of the bones, 2) absence of direct association of lithic artefacts and the remains of fossil fauna and 3) the high degree of exposure of the site to the external agents (e.g. laminar erosion) that, for years or decades, has eroded and degraded its sedimentary context. This last limitation prevents us from putting into stratigraphic context the few preformatted lithic instruments found in the vicinity of excavations B–D (Fig. 9). The origin of the pruning layer of these artefacts is uncertain and its association with the site’s megafauna is speculative and cannot be ratified, especially if the radiocarbon ages obtained for the site (40,000 cal. BP.) are taken into consideration. The latter would contrast with new cultural evidence for the American continent with ranges within the Last Glacial Maximum (LMG) (e.g. Pansani et al. (2023)).

The presence of lithic artefacts in adjacent areas of the excavations and surroundings of the Cauca site, with different lithic typologies, such as El Jobo, Clovis and Fish Tail (Jaimes et al. 2024a), undoubtedly sheds new light on technologies and distribution of the artefacts used by the megafauna hunters who roamed the region at the end of the Pleistocene. However, the lack of a chronological and stratigraphic context of the layers carrying the lithic also prevents a secure association with the megafauna of the Cauca site. The only known sites with an association of megafauna and humans from the Late Pleistocene of Venezuela (with dating), are Muaco, Cucuruchú, Taima-Taima and El Vano (see Cruxent (1970); Bryan (1973); Carrillo-Briceño (2015); Carlini et al. (2022)). In Taima-Taima (Bryan et al. 1978; Haynes 2023) and El Vano (Jaimes 1998, 1999, 2003, 2005; Jaimes et al. 2024b), there is evidence of hunting/butchering of gomphotherids (*Notiomastodon platensis*) and megatheres (cf. *Eremotherium laurillardi*), respectively, are evident. At both sites, lithic points associated with the Jobo typology were found in association with the bone remains (Cruxent 1967, 1970, 1979; Bryan et al. 1978; Jaimes 1998, 2003, 2005). Meneses and Gordones (2021) recently suggested the existence of early human presence alongside megafauna (*Notiomastodon* sp.) at the El Llano del Anís site in Mérida State (Fig. 2). However, the absence of precise dating, comprehensive palaeontological examinations of the site’s fossil material and substantial evidence of human involvement in the bone remains pose limitations in interpreting the site.

## Conclusions

Despite thorough investigations into the Pleistocene mammals of South America, significant knowledge gaps persist, particularly in the northern region of the continent.

In this contribution, we report the first fossil records of mammals from the new coastal locality called Cauca in Falcón State, with the objective of revaluing this region in the context of the evolution of fauna in the continent. The fossil assemblage from the Cauca site is characterised by at least five megaherbivores that includes the terrestrial sloths cf. *Eremotherium laurillardi*, an indeterminate mylodontid, a glyptodont probably related to *Glyptotherium*, the proboscidean *Notiomastodon platensis* and the equid *Equus* sp. The only medium-sized taxon corresponds to a predator, identified here as Felidae cf. *Leopardus pardalis* and its report is notable due to the undocumented fossil record of this taxon in north-western Venezuela and the region. The bioapatite dating of two fossil remains from Cauca provided an age of at least 40,000 years old.

Lithic artefacts of a kind reported in the vicinity of the Cauca excavation and in other adjacent Pleistocene sites (Jaimes et al. 2024a), document the presence of humans in the region, but as these cultural remains were found on the surface, their association with the fossil fauna is uncertain.

Cauca is part of the Coro coastal plain that has been interpreted as one of the natural corridors that allowed the expansion of territories by different species during the Pleistocene, associated with the Great American Biotic Interchange (Webb 1978, 1991). Cauca, like sites such as Muaco, Taima-Taima, Cucuruchú and El Vano, has records of the existence of faunas subsequently extinct following environmental transformation in which probably both climate change and humans played a synergistic role (see Barnosky et al. (2016); Metcalf et al. (2016); MacPhee (2018)).

## Acknowledgements

The authors would like to thank D.J. Gutiérrez, R.I. Sánchez, M. González, J.L. Sánchez, A. Palencia and R. Rojas for their valuable support in field activities. To the Sánchez family and community of Urumaco for the valuable support they have always shown. Loic Costeur for managing photographic archives for comparative purposes. To the Instituto del Patrimonio Cultural de Venezuela, The Alcaldía Bolivariana de Urumaco who kindly provided support and permits for field activities. We would like to thank M. Morales from the Instituto Nacional de Antropología e Historia (INAH), México, S. Lucero from the Museo Argentino de Ciencias Naturales “Bernardino Rivadavia”, C. Gaitán from the Unidad Ejecutora Lillo (UEL), Argentina, T. Fariñas from the Centro Regional de Investigaciones Científicas y Transferencia Tecnológica de La Rioja (CRILAR), Argentina and J. Madurell from the Institut Català de Paleontologia “Miquel Crusafont” (ICP), Catalonia for providing access to photos and materials that were used during the comparison of this specimen. We thank F. Thil from the Laboratoire des Sciences du Climat et de l’Environnement for help with the radiocarbon dating of the samples using the ECHOmicadas compact radiocarbon

system. We also thank the Latin American Center at the University of Zurich for its support with the GRC Travel Grant 2019 and Mobility Grant 2022 approved to J.D.C.B. This work was supported by a Research Partnership Grant from the Leading House for the Latin American Region RPG2385 (‘A palaeontological, archaeological and genomic study of early humans in northern South America’) and SNF Grant IZSTZ0\_208545 (South American Pleistocene Megafaunal Diversification and Extinction – An Evaluation of the Historical Roth collection in Zurich) to MRS-V. To the two anonymous reviewers and the editorial team, many thanks for their comments and suggestions.

## References

- Aguilera OA (2004) Tesoros Paleontológicos de Venezuela: Urumaco, Patrimonio Natural de La Humanidad. Universidad Nacional Experimental Francisco De Miranda, Venezuela, Editorial Arte, Caracas, 148 pp.
- Aguilera OA (2006) Tesoros Paleontológicos de Venezuela. El Cuaternario del Estado Falcón. Ministerio de la Cultura, Instituto de Patrimonio Cultural, Editorial Arte, Caracas, 120 pp.
- Alberdi MT, Prado JL (2022) Diversity of the fossil gomphotheres from South America. *Historical Biology* 34(8): 1685–1691. <https://doi.org/10.1080/08912963.2022.2067754>
- Ameghino F (1888) Rápidas diagnosis de algunos mamíferos fósiles nuevos de la República Argentina. *Obras Completas, Buenos Aires* 5: 469–480.
- Bargo MS, De Iullis G, Vizcaíno S (2006) Hypsodonty in Pleistocene ground sloth. *Acta Palaeontologica Polonica* 51(1): 53–61.
- Barnosky AD, Lindsey EL, Villavicencio NA, Bostelmann E, Hadly EA, Wanket J, Marshal CR (2016) Variable impact of late-Quaternary megafaunal extinction in causing ecological state shifts in North and South America. *PNAS* 113(4): 856–861. <https://doi.org/10.1073/pnas.1505295112>
- Behrensmeyer AK (1978) Taphonomic and ecologic information from bone weathering. *Paleobiology* 4(2): 150–162. <https://doi.org/10.1017/S0094837300005820>
- Bocquentin-Villanueva J (1979) Mammifères fossiles du Pléistocène supérieur de Muaco, état de Falcón, Venezuela. PhD Thesis, l’Université Pierre et Marie Curie, Paris.
- Bocquentin-Villanueva J (1982) Notas sobre la fauna del Pleistoceno Superior de Taima-Taima depositada en el Museo del Hombre de Coro, estado Falcón, Venezuela. *Acta Científica Venezolana* 33: 479–487.
- Boher Benti S, Salazar Candelle M, Ferreira Marques C (2023) Mamíferos de Venezuela: lista actualizada 2023 y comentarios taxonómicos. *Anartia* 36: 7–35. <https://doi.org/10.5281/zenodo.10433912>
- Bowdich TE (1821) An Analysis of the Natural Classification of Mammalia: for the Use of Students and Travelers. J. Smith, Paris, 115 pp.
- Bronk Ramsey C (2009) Bayesian analysis of radiocarbon dates. *Radiocarbon* 51(1): 337–360. <https://doi.org/10.1017/S0033822200033865>
- Bryan AL (1973) Paleoenvironments and Cultural Diversity in Late Pleistocene South America. *Quaternary Research* 3: 237–256. [https://doi.org/10.1016/0033-5894\(73\)90043-4](https://doi.org/10.1016/0033-5894(73)90043-4)

- Bryan AL, Casamiquela R, Crucent JM, Gruhn R, Ochsenius C (1978) An El Jobo mastodon kill at Taima-Taima, Venezuela. *Science* 200(4347): 1275–1277. <https://doi.org/10.1126/science.200.4347.1275>
- Cabrera A (1929) Una revisión de los mastodontes argentinos. *Revista Del Museo De La Plata* 32: 61–144.
- Carlini AA, Zurita AE (2010) An introduction to Cingulate evolution and their evolutionary history during the Great American Biotic Interchange: biogeographical clues from Venezuela. In: Sánchez-Villagra MR, Aguilera OA, Carlini F (Eds) *Uruguay and Venezuelan paleontology*. Indiana Press University, St. Gallen, 233–235.
- Carlini AA, Zurita AE, Aguilera OA (2008) North American Glyptodontines (Xenarthra, Mammalia) in the Upper Pleistocene of northern South America. *Paläontologische Zeitschrift* 82(2): 125–138. <https://doi.org/10.1007/BF02988404>
- Carlini AA, Carrillo-Briceño JD, Jaimes A, Aguilera OA, Zurita AE, Iriarte J, Sánchez-Villagra MR (2022) Damaged glyptodontid skulls from Late Pleistocene sites of northwestern Venezuela: evidence of hunting by humans? *Swiss Journal of Palaeontology* 141(1): 11. <https://doi.org/10.1186/s13358-022-00253-3>
- Carrillo-Briceño JD (2012) Los Mastodontes y sus Parientes: El Registro Fósil de los Proboscídeos. In: Sánchez-Villagra MR (Ed.) *Venezuela Paleontológica: Evolución de la diversidad en el pasado*. Printwork Art GmbH, St. Gallen, 313–322.
- Carrillo-Briceño JD (2015) Bestias Prehistóricas de Venezuela “Colosos de la Edad de Hielo”. Río Verde, Caracas, 287 pp.
- Carrillo-Briceño JD, Chávez-Aponte AE, Alfonso HI (2008a) Notas preliminares sobre los mastodontes gonfoterios (Mammalia: Proboscidea) del Cuaternario venezolano. *Boletín Antropológico* 26(74): 233–266. <http://www.saber.ula.ve/handle/123456789/30824>
- Carrillo-Briceño JD, Alfonso-Hernández I, Chávez-Aponte EO (2008b) Primer registro paleontológico de Gomphotheriidae (Mammalia Proboscidea) para la Serranía de Trujillo, Estado Trujillo. *Boletín del Centro de Historia del Estado Trujillo* 17(63): 33–44.
- Carrillo-Briceño JD, Amson E, Zurita A, Sánchez-Villagra MR (2016) Hermann Karsten (1817–1908): a German naturalist in the Neotropics and the significance of his paleovertebrate collection. *Fossil Record* 20(1): 21–36. <https://doi.org/10.5194/fr-20-21-2016>
- Carrillo-Briceño JD, Sánchez R, Scheyer TM, Carrillo JD, Delfino M, Georgalis GL, Kerber L, Ruiz-Ramoni D, Birindelli JLO, Cadena E-A, Rincón AF, Chavez-Hoffmeister M, Carlini AA, Carvalho MR, Trejos-Tamayo R, Vallejo F, Jaramillo C, Jones DS, Sánchez-Villagra MR (2021) A Pliocene–Pleistocene continental biota from Venezuela. *Swiss Journal of Palaeontology* 140(1): 9. <https://doi.org/10.1186/s13358-020-00216-6>
- Carrillo-Briceño JD, Vezzosi RI, Ming KM, Christen ZM, Mothé D, Ruiz-Ramoni D, Sánchez-Villagra MR (2023) Nearctic Pleistocene ungulates from the Pampean region (Argentina) in the historical collections of Santiago Roth in Switzerland: an overview. *Swiss Journal of Palaeontology* 142(1): 12–26. <https://doi.org/10.1186/s13358-023-00273-7>
- Cartelle C, De Iuliis G (1995) *Eremotherium laurillardi*: the panamerican Late Pleistocene megatheriid sloth. *Journal of Vertebrate Paleontology* 15(4): 830–841. <https://www.jstor.org/stable/4523673>
- Cartelle C, De Iuliis G, Pujos F (2015) *Eremotherium laurillardi* (Lund, 1842) (Xenarthra, Megatheriinae) is the only valid megatheriine sloth species in the Pleistocene of intertropical Brazil: A response to Faure et al., 2014. *Comptes Rendus Palevol* 14(1): 15–23. <https://doi.org/10.1016/j.crpv.2014.09.002>
- Cartelle C, De Iuliis G, Boscaini A, Pujos F (2019) Anatomy, possible sexual dimorphism, and phylogenetic affinities of a new mylodontine sloth from the Late Pleistocene of intertropical Brazil. *Journal of Systematic Palaeontology* 17(23): 1957–1988. <https://doi.org/10.1080/14772019.2019.1574406>
- Chávez-Aponte EO (2022) Los Megamamíferos de Venezuela: la megafauna del Pleistoceno en el Sur del estado Cojedes. *Fundación de Educación Ambiental – Editorial Amalivaca, Caracas*, 220 pp.
- Chávez-Aponte EO, Carrillo-Briceño JD (2012) Los Carnívoros del Pleistoceno. In: Sánchez-Villagra MR (Ed.) *Venezuela Paleontológica: Evolución de la diversidad en el pasado*. Printwork Art GmbH, St. Gallen, 323–334.
- Chávez-Aponte EO, Alfonso-Hernández I, Carrillo-Briceño JD (2008a) Morfología Dentaria de los Gonfoterios de la Localidad de Muaco, Estado Falcón, Venezuela. *INTERCIENCIA* 33(10): 771–775.
- Chávez-Aponte EO, Alfonso-Hernández I, Finol H, Barrios C, Boada A, Carrillo-Briceño JD (2008b) Histología y Ultraestructura de los Osteodermos Fósiles de *Glyptodon clavipes* y *Holmesina* sp. (Xenarthra Cingulata). *INTERCIENCIA* 33(8): 616–619.
- Cherkinsky A (2009) Can we get a good radiocarbon age from “bad bone”? Determining the reliability of radiocarbon age from biapatite. *Radiocarbon* 51(2): 647–655. <https://doi.org/10.1017/S0033822200055995>
- Cope E (1889) The Edentata of North America. *American Naturalist* 23: 657–664. <https://doi.org/10.1086/274985>
- Crucent JM (1967) El paleo-indio en Taima-Taima, Estado Falcón, Venezuela. *Acta Científica Venezolana* 3: 3–17.
- Crucent JM (1970) Projectile points with Pleistocene mammals in Venezuela. *Antiquity* 44(175): 223–225. <https://doi.org/10.1017/S0003598X00104624>
- Crucent JM (1979) Stone and bone artifacts from Taima-Taima. In: Ochsenius C, Gruhn R (Eds) *Taima-Taima: A Late Pleistocene Paleo-indian kill site in Northernmost South America Final reports of 1976 excavation*. CIPICS/South American Quaternary Documentation Program, Saarbrücken, Germany, 77–89.
- De Iuliis G (1996) A Systematic Review of the Megatheriinae (Mammalia: Xenarthra: Megatheriidae). PhD Thesis, University of Toronto, Toronto, Canada.
- De Iuliis G, Cartelle C, McDonald HG, Pujos F (2017) The mylodontine ground sloth *Glossotherium tropicorum* from the Late Pleistocene of Ecuador and Peru. *Papers in Palaeontology* 3(4): 613–636. <https://doi.org/10.1002/spp2.1088>
- Del Valle C, Salazar C (2009) La Prehistoria en la Cuenca del Lago: Carabobo y Aragua, Venezuela. *Enriqueta Peñalver Gómez colecciones. Cosmográfica, Valencia*, 483 pp.
- Faure M, Guérin C, Parenti F (2014) Sur l’existence de deux espèces d’*Eremotherium* *E. rusconii* (Schaub, 1935) et *E. laurillardii* (Lund, 1842) dans le Pléistocène supérieur du Brésil intertropical. *Comptes Rendus Palevol* 13(4): 259–266. <https://doi.org/10.1016/j.crpv.2013.11.001>
- Fernández-Jalvo Y, Andrews, P (2016) Pits and perforations. In: Eric D, Eric JS (Eds) *Atlas of taphonomic identifications*. Springer, Dordrecht, Netherlands, 101–153. [https://doi.org/10.1007/978-94-017-7432-1\\_4](https://doi.org/10.1007/978-94-017-7432-1_4)
- Fischer G (1814) *Zoognosia tabulis synopticis illustrata*. Typis Nicolai Sergeidis Vsevolozsky, Moscow.
- Fischer G (1817) *Adversaria Zoologica*. Mémoire Société Impériale Naturelle 5: 368–428.

- Gill T (1872) Arrangements of the families of Mammals, with analytical tables. *Smithsonian Miscellaneous Collections* 11: 1–98. <https://doi.org/10.5962/bhl.title.14607>
- Gillette DD, Carranza-Castaneda O, White Jr RS., Morgan, GS, Thrasher C, McCord R, McCullough G (2016) Ontogeny and sexual dimorphism of *Glyptotherium texanum* (Xenarthra, Cingulata) from the Pliocene and Pleistocene (Blancan and Irvingtonian NALMA) of Arizona, New México, and México. *Journal of Mammalian Evolution* 22: 133–154. <https://doi.org/10.1007/s10914-015-9309-6>
- Gray JE (1821) On the natural arrangement of vertebrate animals. *London Medical Repository* 15(1): 296–310.
- Gray JE (1842) Descriptions of some new genera and fifty unrecorded species of Mammalia. *Journal of Natural History* 10(65): 255–267. <https://doi.org/10.1080/03745484209445232>
- Gray JE (1869) Catalogue of carnivorous, pachydermatous and edentate mammalia in the British Museum. Trustees of the British Museum, London, 398 pp.
- Hay OP (1922) Further observations on some extinct elephants. *Proceedings of the Biological Society of Washington* 35: 97–102.
- Haynes G (2022) Sites in the Americas with Possible or Probable Evidence for the Butchering of Proboscideans. *PaleoAmerica* 8(3): 187–214. <https://doi.org/10.1080/20555563.2022.2057834>
- Hoffstetter R (1952) Les Mammifères Pléistocène de la République de l'Équateur. *Mémoires de la Société Géologique de France* 66: 1–391.
- Illiger C (1811) *Prodromus systematis Mammalium et Avium additis terminis zoographicis utriusque classis*. C. Salfeld, Berlin, 301 pp. <https://doi.org/10.5962/bhl.title.106965>
- Jaimes A (1998) El Vano, Venezuela: El Jobo traditions in a Megatherium Hill Site. *Current Research in the Pleistocene* 15: 25–27.
- Jaimes A (1999) Nuevas evidencias de cazadores-recolectores y aproximación al entendimiento del uso del espacio geográfico en el noroccidente de Venezuela. Sus implicaciones en el contexto suramericano. *Arqueología del Área Intermedia* 1: 83–120.
- Jaimes A (2003) El Vano una nueva localidad paleo-india en el noroccidente de Venezuela. *Maguaré* 17: 46–64.
- Jaimes A (2005) Condiciones tafonómicas, huesos modificados y comportamiento humano en los sitios de matanza de El Vano (Tradición Jobo) y Lange/Ferguson (Tradición Clovis). *Boletín de Antropología Americana* 41: 159–184. <https://www.jstor.org/stable/40978248>
- Jaimes A, Carrillo-Briceño JD, de Jesús I, Martín La Riva CA, Sánchez-Villagra MR (2024a) Diversidad tecnológica en proyectiles del Cuaternario en el norte de Venezuela. In: Sánchez-Villagra MR, Carrillo-Briceño JD, Jaimes A, Arvelo L (Eds) *Contribuciones en Venezuela Arqueológica*. Scindinge Hall, Tübingen.
- Jaimes A, Sánchez-Villagra MR, Carrillo-Briceño JD (2024b) Fósiles y artefactos en el sitio de matanza de megafauna El Vano, Pleistoceno tardío de Venezuela. In: Sánchez-Villagra MR, Carrillo-Briceño JD, Jaimes A, Arvelo L (Eds) *Contribuciones en Venezuela Arqueológica*. Scindinge Hall, Tübingen.
- Larivière S, Walton LR (1997) *Lynx rufus*. *Mammalian species* 563: 1–8. <https://doi.org/10.2307/3504533>
- Linares OJ (1983) Mamíferos fósiles del Pleistoceno de Venezuela. Museo Arqueológico de Quíbor –FUNDACULTURA, Quíbor, Venezuela, 17 pp.
- Linares OJ (1998) Mamíferos de Venezuela. Sociedad Conservacionista Audubon de Venezuela, Caracas, 691 pp.
- Linares OJ (2004) Bioestratigrafía de la fauna de mamíferos de las Formaciones Socorro, Urumaco y Codore (Mioceno medio-Plioceno temprano) de la región de Urumaco, Falcón, Venezuela. *Paleobiología Neotropical* 1: 1–26.
- Linares OJ, Bruni A (1993) Sobre la presencia de un mastodonte en las minas de Guaniamo, estado Bolívar, Venezuela: implicaciones paleo-ecológicas para el límite sabana-bosque en la amazonia. *International Symposium on “The Quaternary of Amazonia”*, Manaus.
- Linnaeus C (1758) *Systema Naturae per regna tria naturae, secundum classes, ordines, genera, species; cum characteribus, differentiis, synonymis, locis* (10<sup>th</sup> edn.). Larentii Salvii, 824 pp. <https://doi.org/10.5962/bhl.title.542>
- Lund PW (1840) Nouvelles recherches sur la faune fossile du Brésil. *Annales Des Sciences Naturelles* 13: 310–319.
- Lund PW (1842) Blyk paa Brasiliens Dyreverden før den Sidste Jordomvaeltning. Fjerde Afhandling: Fortsættelse af Pattedyrene. Det Kongelige Danske Videnskabernes Selskbas Naturvidenskabelige og Mathematisk Afhandlinger 9: 137–208.
- Machado H, Avilla L (2019) The diversity of South American Equus: did size really matter? *Frontiers in Ecology and Evolution* 7: 235. <https://doi.org/10.3389/fevo.2019.00235>
- MacFadden BJ (2013) Dispersal of Pleistocene *Equus* (Family Equidae) into South America and calibration of GABI 3 based on evidence from Tarija, Bolivia. *PLoS ONE* 8(3): e59277. <https://doi.org/10.1371/journal.pone.0059277>
- MacPhee RDE (2018) *End of the Megafauna: The Fate of the World's Hugest, Fiercest, and Strangest Animals*. W.W. Norton and Company, New York-London, 256 pp.
- McAfee RK (2007) *Reassessing the taxonomy and affinities of the Mylodontinae sloths, Glossotherium and Paramylodon* (Mammalia: Xenarthra: Tardigrada). PhD Thesis, Northern Illinois University, Illinois, USA.
- Manzuetti A, Ubilla M, Jones W, Perea D, Prevosti FJ (2023) The ocelot *Leopardus pardalis* (Linnaeus, 1758) (Carnivora, Felidae) in the Late Pleistocene of Uruguay. *Historical Biology* 35(1): 108–115. <https://doi.org/10.1080/08912963.2021.2023140>
- Marshall LG, Berta A, Hoffstetter R, Pascual R, Reig OA, Bombin M, Mones A (1984) Mammals and stratigraphy: geochronology of the continental mammal-bearing Quaternary of South America. *Palaeovertebrata* 13: 1–76.
- Matteucci SD, Colma A, Pla L (1999) Bosques secos tropicales del estado Falcón, Venezuela. In: Matteucci SD, Solbrig OT, Morello J, Halffter G (Eds) *Biodiversidad y uso de la tierra. Conceptos y ejemplos de Latinoamérica*. Buenos EUDEBA (Editorial de la Universidad de Buenos Aires), Buenos Aires, 399–420.
- Meneses L, Gordones G (2021) Evidencias arqueológicas de la ocupación humana temprana de la Cordillera Andina de Mérida: El Llano del Anís. *Boletín Antropológico* 39(102): 366–398. <https://doi.org/10.53766/BA/2021.02.102.05>
- Metcalf JL, Turney C, Barnett R, Martin F, Bray SC, Vilstrup JT, Orlando L, Salas-Gismondi R, Loponte D, Medina M, De Nigris M, Civalero T, Fernández PM, Gasco A, Duran V, Seymour KL, Otaola C, Gil A, Paunero R, Prevosti FJ, Bradshaw CJA, Wheeler JC, Borrero L, Austin JJ, Cooper A (2016) Synergistic Roles of Climate Warming and Human Occupation in Patagonian Megafaunal Extinctions During the Last Deglaciation. *Science Advances* 2(6): e1501682. <https://doi.org/10.1126/sciadv.1501682>
- Mothé D, Avilla L (2015) Mythbusting evolutionary issues on South American Gomphotheriidae (Mammalia: Proboscidea). *Quaternary Science Reviews* 110: 23–35. <https://doi.org/10.1016/j.quascirev.2014.12.013>

- Mothé D, Avilla LS, Winck GR (2010) Population structure of the gomphotheres *Stegomastodon waringi* (Mammalia: Proboscidea: Gomphotheriidae) from the Pleistocene of Brazil. *Anais da Academia Brasileira de Ciências* 82(4): 983–996. <https://doi.org/10.1590/S0001-37652010005000001>
- Mothé D, Avilla LS, Cozzuol MA, Winck GR (2012) Taxonomic revision of the Quaternary gomphotheres (Mammalia: Proboscidea: Gomphotheriidae) from the South America lowlands. *Quaternary International* 276–277: 2–7. <https://doi.org/10.1016/j.quaint.2011.05.018>
- Mothé D, Avilla LS, Cozzuol MA (2013) The South American gomphotheres (Mammalia, Proboscidea, Gomphotheriidae): taxonomy, phylogeny and biogeography. *Journal of Mammalian Evolution* 20: 23–32. <https://doi.org/10.1007/s10914-012-9192-3>
- Mothé D, Marco PF, Avilla LS, Beatty BL (2016) The dance of tusks: rediscovery of lower incisors in the Pan-American Proboscidean *Cuvieronius hyodon* revises incisor evolution in Elephantimorpha. *PLoS ONE* 11(1): e0147009. <https://doi.org/10.1371/journal.pone.0147009>
- Mothé D, Ferretti MP, Avilla L (2017a) Running over the same old ground: *Stegomastodon* never roamed South America. *Journal of Mammalian Evolution* 26: 165–177. <https://doi.org/10.1007/s10914-017-9392-y>
- Mothé D, Aguanta WF, Belatto SL, Avilla L (2017b) First record of *Notiomastodon platensis* (Mammalia, Proboscidea) from Bolivia. *Revista Brasileira de Paleontologia* 20(1): 149–152. <https://doi.org/10.4072/rbp.2017.1.12>
- Nectario María H (1937) Los grandes mamíferos fósiles de la región de Barquisimeto. *Boletín de Geología y Minería* 1(2–4): 301–317.
- Nectario María H (1941) El *Megatherium larensis* de Venezuela. *Revista Geográfica Americana* 16(98): 6.
- Ochsenius C (1980) Cuaternario en Venezuela. Introducción a la paleoecología en el norte de Sudamérica. Universidad Nacional Experimental Francisco de Miranda, Coro, 68 pp.
- Ochsenius C, Gruhn R (1979) Taima-Taima: A Late Pleistocene Paleo-indian kill site in Northernmost South America Final reports of 1976 excavation. CIPICS/South American Quaternary Documentation Program, Saarbrücken, Germany, 137 pp.
- Odreman ROE (1997) Lista actualizada de los fósiles de Venezuela. In: La Marca E (Ed.) Vertebrados actuales y fósiles de Venezuela. Serie Catálogo Zoológico de Venezuela vol.1. Museo de Ciencias y Tecnología de Mérida, Mérida, Venezuela, 231–243.
- Oliver JR, Alexander CS (2003) Ocupaciones humanas del Pleistoceno terminal en el occidente de Venezuela. *Maguaré* 17: 83–246.
- Owen R (1842) Description of the skeleton of an extinct gigantic sloth, *Myiodon robustus*, Owen, with observations on the osteology, natural affinities, and probable habits of the megatheriid quadruped in general, Owen, with observations on the osteology, natural affinities, and probable habits of the megatheriid quadruped in general. R. & J. Taylor, London, 278 pp.
- Owen R (1848) Description of teeth and portions of jaws of two extinct anthracotheriid quadrupeds (*Hyopotamus vecrianus* and *H. bovinus*) discovered by the Marchioness of Hastings in the Eocene deposits on the NW coast of the Isle of Wight, with an attempt to develop Cuvier's idea of the classification of pachyderms by the number of their toes. *Quarterly Journal of Geology Society of London* 4: 103–141. <https://doi.org/10.1144/GSL.JGS.1848.004.01-02.21>
- Owen R (1869) On fossil remains of equines from Central and South America referable to *Equus Conversidens*, Ow., *Equus tau*, Ow., and *Equus arcidens*, Ow. *Philosophical Transactions of the Royal Society of London* 69: 569–573. <https://doi.org/10.1098/rstl.1869.0020>
- Pansani TR, Pobiner B, Gueriau P, Thoury M, Tafforeau P, Baranger E, Vialou ÁV, Vialou D, McSparron C, de Castro Mariela C, Dantas Mário AT, Bertrand L, Pacheco MLAF (2023) Evidence of artefacts made of giant sloth bones in central Brazil around the last glacial maximum. *Proceedings of the Royal Society B: Biological Sciences* 290(2002): 20230316. <https://doi.org/10.1098/rspb.2023.0316>
- Paviolo A, Crawshaw P, Caso A, de Oliveira T, Lopez-Gonzalez CA, Kelly M, De Angelo C, Payan E (2015) *Leopardus pardalis* (errata version published in 2016). The IUCN Red List of Threatened Species 2015: e.T11509A97212355. <https://doi.org/10.2305/IUCN.UK.2015-4.RLTS.T11509A50653476.en>
- Prado JL, Alberdi MT (2017) Fossil Horses of South America. Springer International Publishing, Cham, Switzerland, 150 pp. <https://doi.org/10.1007/978-3-319-55877-6>
- Prevosti FJ, Forasiepi AM (2018) Evolution of South American Mammalian Predators during the Cenozoic: Paleobiogeographic and Paleoenvironmental Contingencies. Springer International Publishing, Cham, Switzerland, 196 pp. <https://doi.org/10.1007/978-3-319-03701-1>
- Prevosti FJ, Rincón AD (2007) A new fossil canid assemblage from the Late Pleistocene of Northern South America: the canids of the Inciarte Asphalt Pit (Zulia, Venezuela), Fossil Record and Biogeography. *Journal of Paleontology* 81(5): 1053–1065. <https://doi.org/10.1666/pleo05-143.1>
- Prevosti FJ, Méndez C, Schiaffini M, Cirignoli S, Contreras S, Zurita AE, Luna CA (2021) The fossil record of the ocelot *Leopardus pardalis* (Carnivora, Felidae): a new record from the southern range of its distribution and its paleoenvironmental context. *Journal of Vertebrate Paleontology* 41(1): e1922867. <https://doi.org/10.1080/02724634.2021.1922867>
- Reyes-Céspedes AE, Carlini AA, Carrillo-Briceño JD (2023) New record of *Pachymatherium* (Cingulata: Pachymatheriidae) from the Late Pleistocene in Venezuela. *ANARTIA* 35: 7–13. <https://doi.org/10.5281/zenodo.7951590>
- Rincón AD, White RS (2007) Los Xenarthra Cingulata del Pleistoceno Tardío (Lujanense) de Cerro Misión, estado Falcón, Venezuela. *Boletín de la Sociedad Venezolana de Espeleología* 41: 2–12.
- Rincón AD, Alberdi MT, Prado JL (2006) Nuevo registro de *Equus (Amerhippus) santaeeleanae* (Mammalia, Perissodactyla) del pozo de asfalto de Inciarte (Pleistoceno Superior), estado Zulia, Venezuela. *Ameghiniana* 43(3): 529–38. <https://www.ameghiniana.org.ar/index.php/ameghiniana/article/view/777>
- Rincón AD, Lemoine LA, McDonald HG (2021) A new addition to Pleistocene megalonychid sloth diversity in the northern Neotropics. *Journal of South American Earth Sciences* 110: 103379. <https://doi.org/10.1016/j.jsames.2021.103379>
- Ruiz-García M, Pinedo-Castro M, Shostell JM (2023) Morphological and genetics support for a hitherto undescribed spotted cat species (Genus *Leopardus*; Felidae, Carnivora) from the Southern Colombian Andes. *Genes* 14(6): 1266. <https://doi.org/10.3390/genes14061266>
- Ruiz-Ramoni D (2016) Paleobiología y ecología evolutiva de los carnívoros fósiles (Eutheria: Mammalia) de los pozos de asfalto El Breal de Orocuai y Mene de Inciarte en Venezuela. PhD Thesis, Instituto Venezolano de Investigaciones Científicas, Miranda, Venezuela.

- Ruiz-Ramoni D, Rincón AD, Solórzano A, Sánchez L, Mendoza J (2013) Nueva asociación de vertebrados continentales del Pleistoceno del estado Lara, Venezuela. X Congreso Venezolano e Ecología: Integrando Saberes ante la crisis ambiental, Mérida, 858 pp.
- Ruiz-Ramoni D, Wang X, Rincón AD (2022) Canids (Caninae) from the Past of Venezuela. *Ameghiniana* 59(1): 97–116. <https://doi.org/10.5710/AMGH.16.09.2021.3448>
- Rouse I, Crucent JM (1963) Venezuelan archaeology. Yale University Press, New Haven and London, 179 pp.
- Royo y Gómez J (1959) Geology and paleontology of the beds with artifacts at Muaco, state of Falcon. *Boletín Informativo de la Sociedad Venezolana de Geología, Minería y Petróleo* 2(9): 257–258.
- Royo y Gómez J (1960) Características paleontológicas y geológicas del yacimiento de vertebrados de Muaco, estado Falcón, con industria lítica humana. *Memorias del III Congreso Geológico Venezolano* 2: 501–505.
- Sánchez J, Lew D (2012) Lista actualizada y comentada de los mamíferos de Venezuela. *Memoria de la Fundación La Salle de Ciencias Naturales* 70(173): 173–238.
- Sánchez-Villagra MR, Aguilera OA, Carlini F (2010) *Urumaco and Venezuelan paleontology*. Indiana Press University, St. Gallen, 286 pp.
- Schaub S. (1935) Säugetierfunde aus Venezuela und Trinidad. *Abhandlungen der Schweizerischen Paläontologischen Gesellschaft* 55: 1–21.
- Schreber JCD (1777) *Die Säugethiere in Abbildungen nach der Natur, mit Beschreibungen*. Wolfgang Walther, Erlangen, 1112 pp.
- Seymour KL (1999) Taxonomy, morphology, paleontology and phylogeny of the South American small cats (Mammalia: Felidae). PhD Thesis, University of Toronto, Canada.
- Simpson G (1939) Estudio sobre vertebrados fósiles en Venezuela. *Revista de Fomento* Año II(8): 275–283.
- Solórzano A, Rincón AD, McDonald HG (2015) A new mammal assemblage from the Late Pleistocene El Breal de Orocuá, northeast of Venezuela. In: Harris JM (Ed.) *La Brea and beyond: the paleontology of Asphalt-preserved biotas*. Science series, vol. 42, Natural History Museum of Los Angeles County, Los Angeles, 125–150.
- Spillmann F (1938) Die fossilen Pferde Ekuadors der Gattung *Neohippus*. *Palaeobiologica* 6: 372–393.
- Spillmann F (1948) Beiträge zur Kenntnis eines neuen gravigraden Riesensteppentieres (*Eremotherium carolinense*, gen et sp. nov.), seines Lebensraumes und seiner Lebensweise. *Palaeobiologica* 8: 231–279.
- Steadman DW, Oswald JA, Rincón AD (2015) The diversity and biogeography of late Pleistocene birds from the lowland Neotropics. *Quaternary Research* 83(3): 555–564. <https://doi.org/10.1016/j.yqres.2015.02.001>
- Villavicencio NA, Corcoran D, Marquet PA (2019) Assessing the causes behind the Late Quaternary extinction of horses in South America using species distribution models. *Frontiers in Ecology and Evolution* 7: 226. <https://doi.org/10.3389/fevo.2019.00226>
- Von der Osten E (1947) Resumen de la paleontología vertebrada de Venezuela. *Memorias de la Sociedad de Ciencias Naturales La Salle* 19: 153–170.
- Voorhies MR (1969) Taphonomy and population dynamics of an Early Pleistocene Vertebrate Fauna, Knox County, Nebraska. University of Wyoming Contributions to Geology Special Paper 1: 1–69. [https://doi.org/10.2113/gsrocky.8.special\\_paper\\_1.1](https://doi.org/10.2113/gsrocky.8.special_paper_1.1)
- Webb SD (1978) A history of savanna vertebrates in the New World. Part II: South America and the Great Interchange. *Annual Review of Ecology and Systematics* 9(1): 393–426. <https://doi.org/10.1146/annurev.es.09.110178.002141>
- Webb SD (1991) Ecogeography and the great American interchange. *Paleobiology* 17(3): 266–280. <https://doi.org/10.1017/S0094837300010605>
- Werdelin L (1985) Small Pleistocene felines of North America. *Journal of Vertebrate Paleontology* 5: 94–210. <https://doi.org/10.1080/02724634.1985.10011858>
- Wood R, Duval M, Thi Mai Huong N, Tuan N, Bacon AM, Demeter F, Düringer P, Oxenham M, Piper P (2016) The effect of grain size on carbonate contaminant removal from tooth enamel: towards an improved pretreatment for radiocarbon dating. *Quaternary Geochronology* 36: 174–187. <https://doi.org/10.1016/j.quageo.2016.08.010>
- Zazzo A, Saliège J-F (2011) Radiocarbon dating of biological apatites: a review. *Palaeogeography, Palaeoclimatology, Palaeoecology* 310: 52–61. <https://doi.org/10.1016/j.palaeo.2010.12.004>
- Zazzo A (2014) Bone and enamel diagenesis: a radiocarbon prospective. *Palaeogeography, Palaeoclimatology, Palaeoecology* 416: 168–178. <https://doi.org/10.1016/j.palaeo.2014.05.006>
- Zurita AE, Gillette DD, Cuadrelli F, Carlini AA (2018) A tale of two clades: Comparative study of *Glyptodon* Owen and *Glyptotherium* Osborn (Xenarthra, Cingulata, Glyptodontidae). *Geobios* 51(2018): 247–258. <https://doi.org/10.1016/j.geobios.2018.04.004>



# Fossil flying squirrels (Petauristinae, Sciuridae, Rodentia) from the Yumidong Cave in Wushan County, Chongqing, China

Li-bo Pang<sup>1</sup>, Shao-kun Chen<sup>1</sup>, Xin Hu<sup>2</sup>, Yan Wu<sup>2</sup>, Guang-biao Wei<sup>3</sup>

1 Hebei International Joint Research Center for Paleoanthropology, College of Earth Sciences, Hebei GEO University, Shijiazhuang 050031, Hebei, China

2 China Three Gorges Museum, Chongqing 400015, China

3 Chongqing Institute of Geological Survey, Chongqing 401122, China

<https://zoobank.org/4886C6AC-2F7E-4C8D-B0E9-5A361EF622DB>

Corresponding author: Shao-kun Chen ([cskcsk2000@163.com](mailto:cskcsk2000@163.com))

Academic editor: Hui-ting Wu ♦ Received 13 November 2023 ♦ Accepted 22 April 2024 ♦ Published 21 May 2024

## Abstract

Flying squirrels are important forest environment indicators. There have been many reports on them from fossil localities of the Late Cenozoic in southwest China, but relatively few detailed studies have been carried out on them. Numerous flying squirrel fossils of the Mid-Late Pleistocene were unearthed from the Yumidong Cave in Wushan County, Chongqing Municipality, China, providing excellent materials for morphological comparison and further research on this group. Four species have been recognised from this locality, including *Pteromys volans*, *Trogopterus xanthipes*, *Belomys pearsonii* and *Aeretes melanopterus*. *P. volans* and *A. melanopterus* are Palearctic species, which adapted to the cold environment and had been completely extinct in the study area since the Holocene Megathermal period. Based on the analyses of paleozoogeography and paleoecology of these four species, it could be concluded that the Yumidong Cave area was dominated by subalpine evergreen coniferous forest or coniferous and broad-leaved mixed forest during MIS 2 and MIS 4 periods, which were colder and had more coniferous forest than now, while the vegetation landscape of MIS 3 and MIS 5 periods were similar to that of nowadays.

## Key Words

Mid-Late Pleistocene, paleoenvironment, Petauristinae, Yumidong Cave

## Introduction

The subfamily Petauristinae is also known as flying squirrels for they can use their membrane between the fore- and hind-legs to glide. They are strictly arboreal animals. According to fossil records, flying squirrels firstly appeared in Sihong, Jiangsu Province in the Early Miocene (Qiu 2015) and then gradually radiated to other areas in China. Nowadays there are 7–9 genera and 17–20 species of flying squirrels living in China, mostly in east and southwest China (Huang et al. 1995; Jiang et al. 2015a, b; Li Q et al. 2019b, 2021). Zheng (1993) made a systematic description on the flying squirrel fossils from cave and fissure deposits of the Pleistocene in southwest China. However, in later studies, researchers usually just

listed them in the fauna or only made limited descriptions — even so, there were still many misidentifications. Therefore, it is very meaningful to conduct a detailed morphological research on this category. Furthermore, flying squirrels can be used as indicators for the forest paleoenvironment due to their typical arboreal habits.

The Miaoyu Basin in Wushan County, Chongqing Municipality, China is located at the northern foot of the Wushan Mountains, having a subtropical monsoon climate now. The zoogeographical zone is of the Sino-India Subrealm of the Oriental Realm. Topographically, the Miaoyu Basin and its surrounding area are dominated by low-medium mountains and the terrain is high in the south and low in the north with altitudes between 200 m and 2046 m. The Wushan Mountains are in the

transition zone from the second step to the third step of Chinese topography. During the neotectonic movement, three stages of karst planation were formed here: the Exi planation surface, the Shanyuan planation surface and the Yumeng planation surface (Xie 1990). Many ancient hominin and mammalian fossil localities, represented by the Longgupo Cave, the Longgudong Cave, the Baotansi Cave and the Yumidong Cave, make the Miaoyu Basin and its surrounding area one of the most important areas for the study of Quaternary paleontology in China (Huang and Fang 1991; Zheng 2004; Chen et al. 2017).

The Yumidong Cave (Fig. 1) is developed in a limestone hill named Dongbao in the southern part of the Miaoyu Basin (30°50'44.39"N, 109°38'09.22"E), about 4 km away from the Longgupo Cave and the Baotansi Cave. It is a horizontal karst cave with an elevation about 1100 m at the entrance. The background and lithostratigraphic sections of this locality were described by Wei et al. (2017), Chen et al. (2017) and the Chongqing China Three Gorges Museum (2018). Dating results and faunal comparisons showed an age of Mid-Late Pleistocene for the sections. The interbeds of sandy clay and limestone breccia of the sections represented four warm periods (layers ②-1, ③, ⑤, ⑦) and four cool periods (layers ②-2, ④, ⑥, ⑧ and below), which could be correlated to MIS 8 ~ ,1 respectively (Chen et al. 2017; Wei et al. 2017; Shao et al. 2022). A great number of mammalian fossils were collected from this cave (Chen et al. 2017;

Chongqing China Three Gorges Museum 2018), amongst which flying squirrel is one of the groups with the most abundant species and specimens in the fauna, providing excellent materials for the study of this group.

The fossils mentioned in the article (Suppl. material 1: table S1) were excavated from the layer ②-2 and below in the Yumidong Cave and are all stored in the Chongqing China Three Gorges Museum.

The dental terminologies follow Zheng (1993) and Li CK et al. (2019a). Abbreviations used in this paper: ac, anterocone; acd, anteroconid; alf, anterolingual flexus; anl, anteroloph; anld, anterolophid; ap, angular process; asd, anterobuccal sinusid; av, anterior valley; bv, buccal valley; cdp, condylar process; crp, coronoid process; cv, central valley; ds, diastema; eald, ectolophid; end, entoconid; enld, entolophid; hy, hypocone; hyd, hypoconid; hycud, hypoconulid; hyld, hypolophid; mdf, mandibular foramen; me, metacone; mecu, metaconule; med, metaconid; mel, metaloph; meld, metalophid; mestd, mesostylid; mmf, masseter muscle fossa; mmmr, masseter muscle ridge; mn, mandibular notch; msd, mesoconid; msld, mesolophid; msst, mesostyle; msstd, mesostylid; mtf, mental foramen; pa, paracone; past, parastyle; peld, extra posterolophid; plf, posterolingual flexus; pmf, pterygoid muscle fossa; pol, posteroloph; pold, posterolophid; pr, protocone; prcu, protoconule; prd, protoconid; prl, protoloph; prlpl, protolophule; prlpld, protolophulid; prst, protostyle; pv, posterior valley; vn, vascular notch.

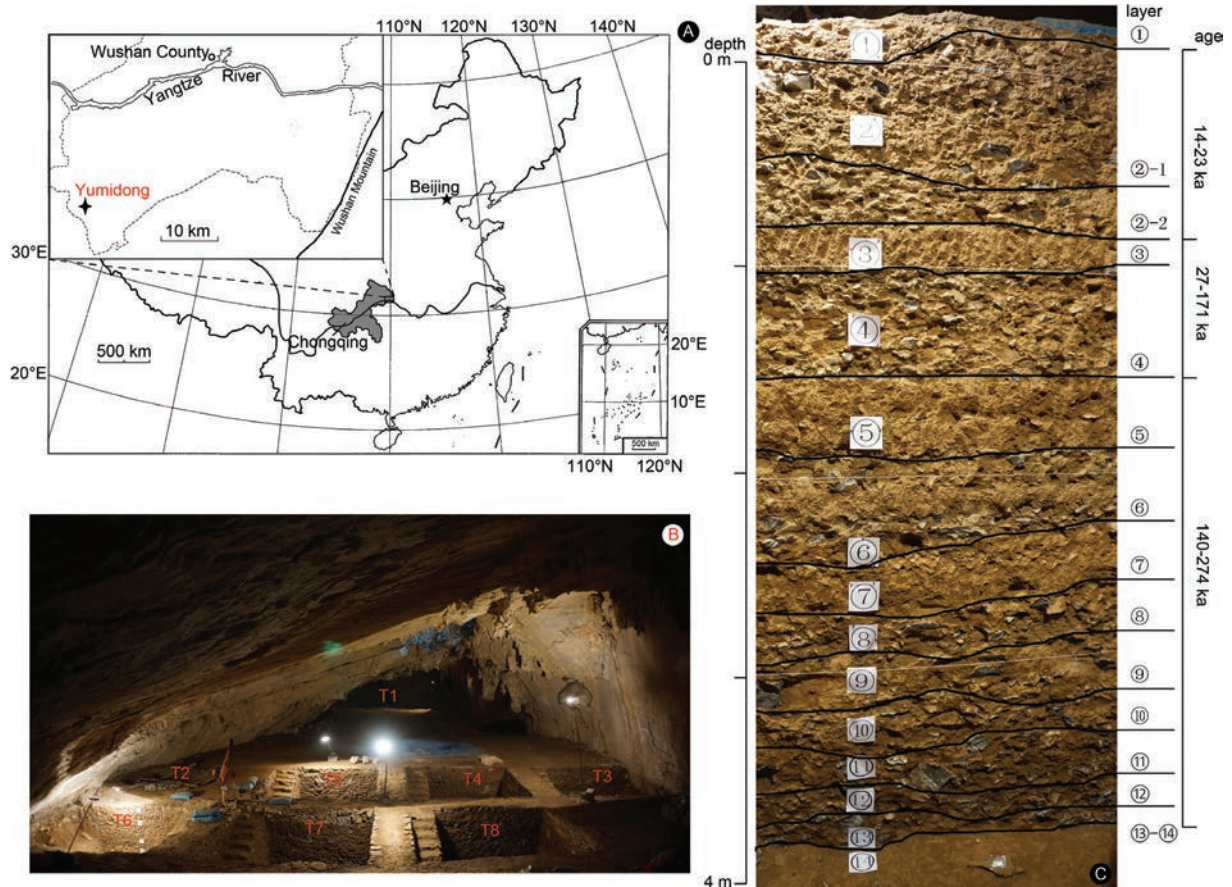


**Figure 1.** Geographical location (A), excavation units (B), stratigraphic sequence of T6 and their age (C) of the Yumidong Cave. The age is based on Shao et al. (2022).

## Systematic paleontology

### Order Rodentia Bowdich, 1821

### Family Sciuridae Fischer von Waldheim, 1817

### Subfamily Petauristinae Brandt, 1855

### Genus *Pteromys* Cuvier, 1800

#### *Pteromys volans* (Linnaeus, 1758)

Fig. 2; Suppl. material 1: table S2

**Materials.** As in Suppl. material 1: table S1, there are four maxillary bones, 27 mandibular bones and one isolated tooth from the layer ②-2 and 23 maxillary bones, 21 mandibular bones and 10 isolated teeth from the layer ④.

**Description.** The mandible is very short and its length is close to the height. The incisor is relatively narrow and curves towards the labial side. Its tip is slightly lower than the worn surface of the cheek teeth. Its posterior end lies under the mandibular foramen. The diastema is deep and short. A single large and round mental foramen locates at the buccal side of the lowest part of the diastema, closer to p4 than the incisor. Both the upper and lower masseter muscle ridges are obvious with the anterior angle at the level of the middle part of p4. The masseter muscle fossa is very wide and relatively deep. The angular process is particularly marked and wider than the ascending ramus. Its upper part is curved to the buccal side, while the inferior margin is curved to the lingual side. The lower and posterior edges are ridge-like. The pterygoid muscle fossa at the lingual side is very deep; its anterior end is at the level of the middle part of m3. The mandibular foramen is relatively large, oval in shape and positioned more dorsally than the worn surface of the cheek teeth. The ascending ramus is very thin. The condylar process and coronoid process are rarely preserved.

P3 is small, single-rooted and cylinder-shaped. Its crown surface is oval, with a central main cusp at the buccal side and one or two small accessory cusps at the lingual side. Viewing from the buccal side, P3 cannot be covered by P4 completely.

P4 is molariformed. Its crown surface is close to trapezoid: the buccal side is longer than the lingual side and the antero-lingual corner is shrunk. In occlusal view, the tooth is mainly composed of four transverse ridges (anteroloph, protoloph, metaloph and posteroloph) and two cusps at the lingual side (protocone and hypocone). The parastyle is large and the anteroloph is very low and short. The protoloph starts at the tip of the paracone and ends at the base of the protocone. The protoconule is not obvious. The metaloph is somewhat short and ends at the developed metaconule. A crista stretches out from the metaconule to the posteroloph. The posteroloph is low and there is a V-shaped groove between it and the hypocone. The hypocone is the smallest amongst the main cusps, isolated when unworn, but connected with the postprotocrista after being worn. The protocone is well developed, occupying 3/4 of the length of the lingual side. The anterior valley and the central valley are both V-shaped and much wider and deeper than the posterior valley. The extra anteroloph is absent,

while a weak protolophule is permanent. The cingulum is well developed at the lingual side, but cannot be checked at other sides.

The main structure of M1 is the same as that of P4, but the anteroloph is more developed, making the occlusal outline almost quadrate. The parastyle is quite degenerate and merges with the anteroloph. The protoloph is high, starting at the tip of the paracone and ending at the preprotocrista. The protoconule is tiny, but clear. The metaloph is short and low, ending at the middle of the metaconule. The metaconule is well developed and its posterior edge connects with the posteroloph. The posteroloph is very low. The protocone is like a longitudinal ridge, occupying 4/5 or more of the length of the lingual side. The hypocone is small and only occupies the posterolingual corner of the tooth. The extra anteroloph and the protolophule are present in most of the specimens.

M2 is very similar to M1 in size and shape.

The occlusal outline of M3 is close to a rounded triangle. The anterior lobe is very similar to that of M1/2, but the posterior lobe is much degenerate and shrunk. The metacone is almost isolated and there is no obvious metaloph and metaconule. The posteroloph is very short and low and connects with the posterior base of the metacone. The hypocone is tiny and locates at the middle of the posterior side of the tooth.

The occlusal outline of dp4 is an irregular quadrilateral with a narrow anterior lobe and a wide posterior lobe. A single anteroconid is obvious and the anterolophid is very weak. The protoconid is near to the metaconid, but somewhat larger. The mesoconid is small and locates behind the protoconid. There is no trace of the metalophid and the mesolophid is very short. The hypoconid is almost the same as the protoconid in size. The posterolophid is curved and connects the entoconid with a small hypoconulid between them. The morphological structure of p4 is similar to dp4, except its slightly wider anterior lobe.

The occlusal outline of m1 is close to an oblique rhomboid. The metaconid and the hypoconid are stronger than the protoconid and the entoconid. The mesoconid is permanent, while the mesostylid is relatively weak. Amongst the four transverse ridges on the occlusal surface, the anterolophid is continuous and highest. The posterolophid is also continuous, but lower than the anterolophid. The metalophid is variable. It may be very short on some specimens, while it may reach to the base of the metaconid on the others. The mesolophid is not well developed. The trigonid basin is much narrower than the talonid basin and not closed. The anterobuccal sinusid is very shallow. The buccal valley is wide.

The occlusal structure of m2 is similar to that of m1, except the anterior lobe of m1 is narrower than that of m2.

m3 is the longest cheek tooth and its anterior lobe is almost the same as m2. On the posterior lobe, a prominent hypolophid connects the hypoconid and the entoconid. The posterolophid is well developed and convex backwards.

**Comparison.** The size (in Suppl. material 1: table S2) and occlusal structure show these specimens belong to

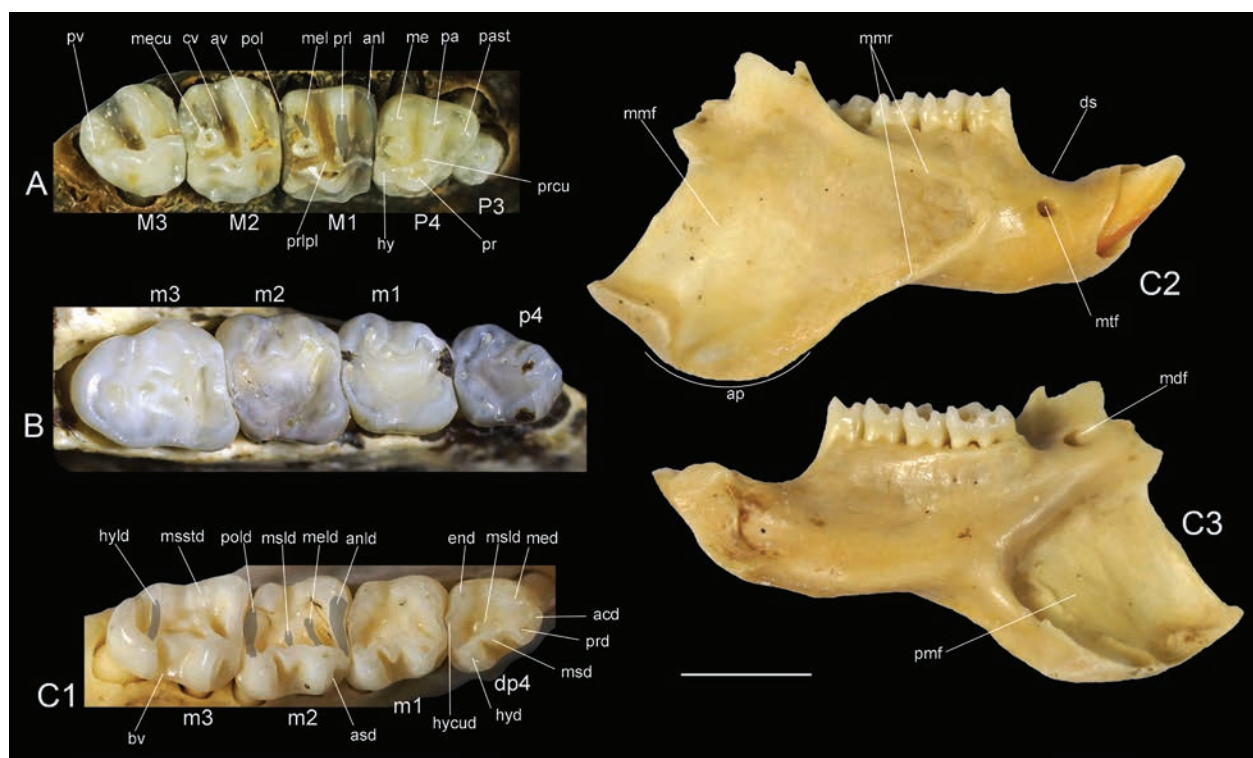


**Figure 2.** *Pteromys volans* from the Yumidong Cave. **A.** 12YMDT4②35.18, right P3-M3, occlusal view; **B.** 12YMDT4②35.286, left p4-m3, occlusal view; **C.** 12YMDT4②4.1, right mandible with dp4-m3, occlusal (1), labial (2) and lingual (3) view. Scale bar: 2 mm (A, B, C1); 4 mm (C2, C3).

a species of small flying squirrel. Until now, two genera and three species of Pleistocene small flying squirrels have been known in south China, these being *Hylopetes electilis*, *Pteromys huananensis* and *P. volans*.

*Hylopetes electilis* is an extant species and its fossils were only reported from the Middle Pleistocene deposits of the Wazhuwan Cave and the Tianmen Cave in Tongzi, Guizhou Province (Zheng 1993). The most typical character for this species is the pitted enamel of its cheek teeth. In addition, this species has weaker entoconid and more developed mesoconid and mesostylid than *Pteromys volans*.

*Pteromys huananensis* was only known from the Early Pleistocene Longgupo Cave in Wushan, Chongqing Municipality (Huang and Fang 1991). The validity of this species is yet to be discussed. Its M3 has clear metacone, protoconule, mesostyle and metaloph, which is different from the specimens described here.

The fossils of *Pteromys volans* were excavated from the Longgupo Cave of the Early Pleistocene, the Xinglong Cave, the Puding Cave, the Yanhui Cave, the Tianmen Cave and the Upper Pingba Cave of the Middle Pleistocene and the Xitaiping Cave of the Late Pleistocene (Zheng 1993; Huang et al. 2002; Tong et al. 2008). The dental diagnosis of this species includes (modified from Li CK et al. (2019a)): cheek teeth brachyodont; P3 small, but with differentiated cusps; P4 molarised; hypocone and metaconule of P4-M2 well developed; the extra anteroloph and the protolophule present; M3 without metaloph and metaconule; the mesoconid and the entoconid of

lower cheek teeth permanent; the trigonid basin not closed; m3 elongated obviously. Morphologically, the specimens described herein resemble *P. volans* and should be assigned to this species.

### Genus *Trogopterus* Heude, 1898

#### *Trogopterus xanthipes* (Milne-Edwards, 1867)

Fig. 3A–C; Suppl. material 1: table S3

**Materials.** As in Suppl. material 1: table S1, there are two maxillary bones, 12 mandibular bones and three isolated teeth from the layer ②-2, one maxillary bone and three isolated teeth from the layer ④ and one mandibular bone from the layer ⑥.

**Description.** The mandible is high and strong. The tip of the incisor is slightly lower than or as high as the worn surface of the cheek teeth. The transversal section of incisor is close to a triangle. The diastema is deep and short. A single mental foramen, small and open forwards, locates at the buccal side of the lowest part of the diastema. The lower masseter muscle ridge is weak and the upper masseter muscle ridge is almost undetectable. The masseter muscle fossa is relatively shallow. The inferior margin of the horizontal ramus is straight. The vascular notch is extensive. The angular process is usually badly preserved. Based on the preserved part, this process should extend downwards significantly. The pterygoid muscle fossa at the lingual side is very deep and wide with its anterior end terminates at the

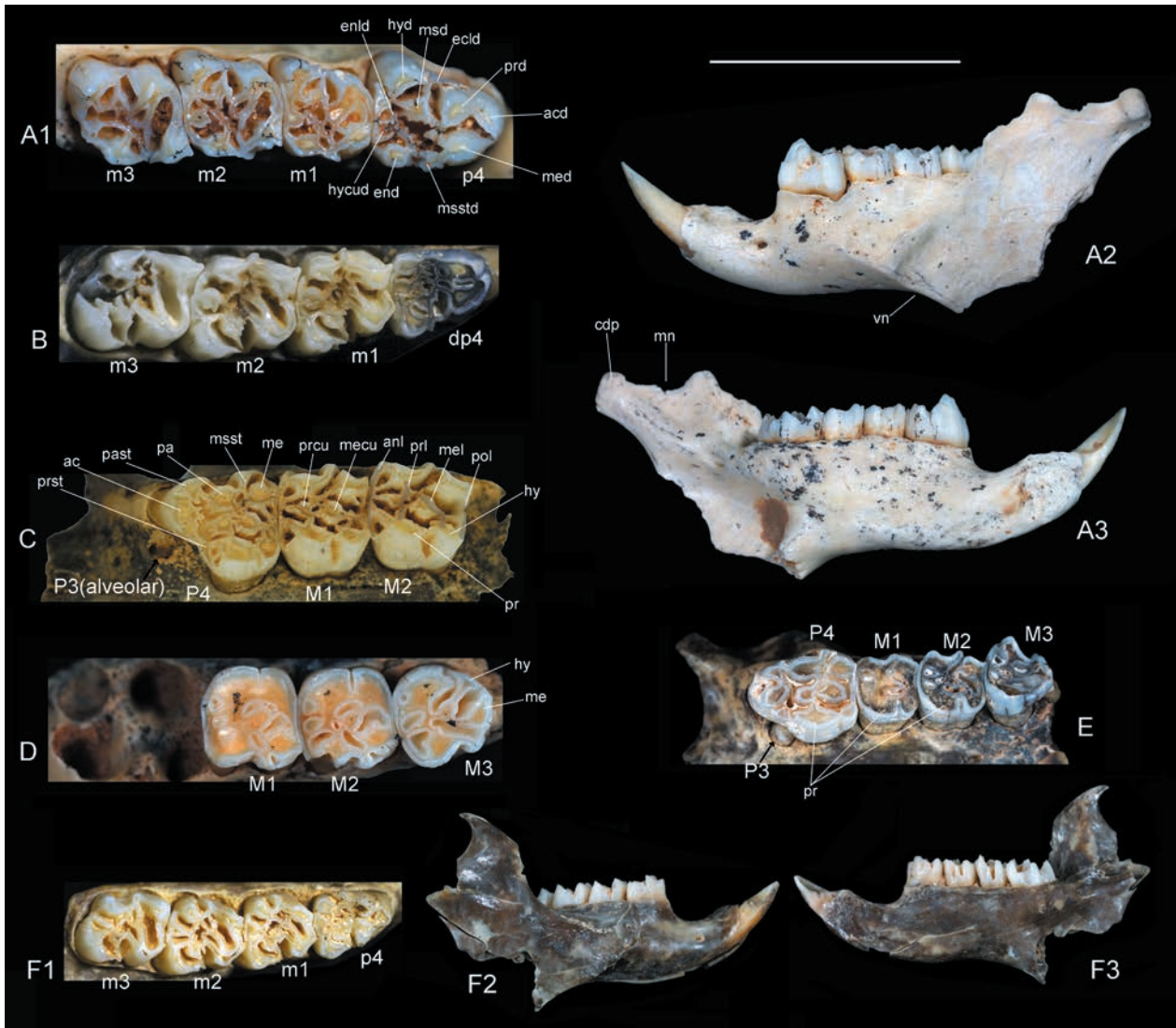


**Figure 3.** *Trogopterus xanthipes* (A–D) and *Belomys pearsonii* (E, F) from the Yumidong Cave. **A.** 12YMDT4②30.2, left mandible with lower incisor and p4–m3, occlusal (1), labial (2) and lingual (3) view; **B.** 12YMDT4②35.1, right dp4–m3, occlusal view; **C.** 12YMDT4②35.7, left P4–M2, occlusal view; **D.** 12YMDT4②60.3, right M1–M3, occlusal view; **E.** 12YMDT4②35.9, left P3–M3, occlusal view; **F.** 12YMDT4②35.8, right mandible with lower incisor and p4–m3, occlusal (1), labial (2) and lingual (3) view. Scale bar: 5 mm (A1, B–E, F1); 10 mm (A2, A3, F2, F3).

level of the middle part of m3. The mandibular foramen is low, relatively small, round in shape and open backwards. The ascending ramus is moderately strong and starts near the m2/m3 boundary. The coronoid process is not preserved on any of the specimens of this species, but should be higher than the condylar process. The condylar process is a transverse axis and its neck is somewhat obvious. The mandibular notch is an obtuse angle.

P3 is tiny, single-rooted and very near to the anterolingual corner of P4. P4 is three-rooted and larger than other cheek teeth. Its occlusal outline is a trapezoid with a narrow anterior lobe and a wide posterior lobe. The anteroloph is formed by four independent cusps which are separated by three small grooves and the anterocone is the highest amongst them. The parastyle is located at the anterobuccal side of the paracone and is the buccal end of the anteroloph. The paracone and the metacone are similar

in size. The mesostyle is well developed and connects with the paracone and the metacone. The protocone is very strong, with a small protostyle at its anterolingual side. The hypocone is relatively slender, located at the posterolingual corner of the teeth. The protocone and the hypocone are separated by a shallow groove at the lingual side. The protoconule and the metaconule are both obvious, but the metaconule is more enlarged and prominent. The protoloph is continuous, starting from the paracone to the protocone via the protoconule. The metaloph becomes vestigial for the enlarged metaconule. The posteroloph is continuous and low. There are many cristae in the anterior and the posterior valleys, dividing them into several enamel loops.

The anteroloph of M1 is low, straight and smooth and the protostyle is absent, which are different from P4. Other than these, the posterior part of M1 is very similar

with that of P4. M2 is very similar to M1 in size and shape. The anterior part of M3 is very similar to M1/2, but its posterior part is somewhat shrunk. The hypocone is reduced, but still permanent, connecting with the metaconule by a straight metaloph. The posteroloph is absent and the metacone transfers to the back of the tooth.

The occlusal outline of p4 is close to a trapezoid, narrow in the anterior part and wide in the posterior part. p4 is the largest in lower cheek teeth. Its anteroconid is transversely oval-shaped, connected to the preprotocristid and separated from the metaconid by a narrow groove. The metaconid and the protoconid are higher than the hypoconid and the entoconid. A narrow ridge extends from the posterolingual side of the protoconid to the prehypocristid, forming the ectolophid. The mesoconid is prominent and three short ridges extend from it: the anterior one (the premesocristid) connects with the postprotocristid; the posterior one (the postmesocristid) connects with the posthypocristid; the buccal one (the ectomesolophid) connects with the ectolophid at the tip of the prehypocristid. The mesostylid is somewhat developed and parallel to the teeth row, but does not connect with the entoconid, making the talonid basin open. The transverse section of entoconid is almost round. The entolophid is thin and there are three cristae on it. The hypoconid is L-shaped, located at the posterobuccal corner of the tooth. There are two cusps on the posterolophid: the small one is at the buccal side and is separated from the hypoconid by a shallow groove; the large one is the hypoconulid, which is almost as large as the entoconid and is separated from the entoconid by a very deep groove. dp4 is similar to p4 in morphology, except there is no obvious anteroconid. The size of dp4 does not exceed m1.

The occlusal outline of lower molars is oblique quadrilateral. The main structure is similar to p4, except the anteroconid is fused with the anterolophid. At the unworn stage, the posterolophid and the ectolophid are separated by a groove. With moderate wear, the anterolophid, the posterolophid, the ectolophid and a lingual lophid are connected via the mesostylid and the entolophid, forming a complete occlusal outline of the tooth. The anterobuccal corner of the tooth is curved and smooth. There is no trace of the anterobuccal cingulum and sinusid. One or two metalophids and several folds are developed in the talonid basin, making the occlusal surface more complex than p4. The mesostylid is not well developed and stretches forward obliquely. m3 is not shrunk. Its posterolophid somewhat curves and the hypoconulid is weaker than that of m1/2.

**Comparison.** The size (in Suppl. material 1: table S3), complex occlusal surface and developed enamel folds show these specimens belong to a species of medium-large-sized flying squirrel. In the Quaternary of south China, four genera of medium-large-sized flying squirrels have been known so far, which are *Petaurista*, *Aeretes*, *Belomys* and *Trogopterus*.

The cheek teeth of *Petaurista* and *Aeretes* are obviously different from the described specimens. Their occlusal surfaces are relatively simple. There are no mesostyles,

but well-developed hypoconules on the upper cheek teeth and the transverse ridges are more notable. In addition, M1/2 of *Petaurista* has no hypocone (Li CK et al. 2019a), while it is always present on the Yumidong specimens. The hypocone on P4-M2 of *Aeretes* is present, but always very near to the protocone (Zheng 1993; Tong 2007; Tong et al. 2008; Li CK et al. 2019a).

*Belomys* resembles *Trogopterus* in occlusal structures more than other flying squirrels (Zheng 1993; Tong 2007). One of the most obvious differences between them is the significantly larger size of *Trogopterus*. The specimens described here are relatively similar to *Trogopterus* morphologically and their size matches *Trogopterus* better than *Belomys*. Only one species of *Trogopterus* has been known until now, the extant *T. xanthipes*. Therefore, the specimens could be identified as *T. xanthipes*.

## Genus *Belomys* Thomas, 1908

### *Belomys pearsonii* (Gray, 1842)

Fig. 3D, E; Suppl. material 1: table S4

**Materials.** As in Suppl. material 1: table S1, there are one maxillary bone and 11 mandibular bones from the layer ②-2, one mandibular bone from the layer ③, two mandibular bones from the layer ④, two mandibular bones from the layer ⑤, one mandibular bone from the layer ⑥ and one mandibular bone from the layer ⑩.

**Description and comparison.** The mandible and teeth of *Belomys pearsonii* are very similar to *Trogopterus xanthipes*, but there are still some differences. The most obvious is their size: *T. xanthipes* is much larger than *B. pearsonii* and there is almost no overlap of the measurements of their cheek teeth (Suppl. material 1: tables S3, S4). Additionally, there are discernible differences of cheek tooth characteristics between these two species: 1) *B. pearsonii* is more lower-crowned than *T. xanthipes*; 2) P3 of *B. pearsonii* is closer to the protocone of P4 than that of *T. xanthipes*; 3) compared with *B. pearsonii*, P4/p4 of *T. xanthipes* is much larger than upper/lower molars; 4) the protocone of P4-M2 of *B. pearsonii* is more developed than that of *T. xanthipes*, but the hypocone is somewhat weaker; 5) the hypocone of M3 of *T. xanthipes* is permanent and connects with the metaconule by a straight metaloph, but the hypocone and the metaloph of M3 of *B. pearsonii* are absent.

There are three species in the genus *Belomys*, *B. pearsonii*, *B. parapearsoni* and *B. thamkaewi*. *B. parapearsoni* is only known from the Early Pleistocene. It is smaller than *B. pearsonii*, with lower tooth crown, less developed mesostyle, less developed mesostylid and more developed hypoconid. *B. thamkaewi* was unearthed from cave deposits of the Late Pleistocene in Thailand and its validity is yet to be discussed. Chaimanee and Jaeger (2000) thought it was very similar to *B. pearsonii*, except the somewhat larger size. However, their measurements seem doubtful, but even so, the data do not exceed the data range of fossil *B. pearsonii* from China.

## Genus *Aeretes* Allen, 1940

### *Aeretes melanopterus* (Milne-Edwards, 1867)

Fig. 4; Suppl. material 1: table S5

**Materials.** As in Suppl. material 1: table S1, there are one isolated tooth from the layer ②-2 and three maxillary bones and two mandibular bones from the layer ④.

**Description.** The mandible is robust and the diastemal portion is short. The tip of the incisor is slightly higher than the worn surface of the cheek teeth. Its posterior end lies under the posterior root of m3. The diastema is short and a medium-sized mental foramen is located at the middle part of the buccal side of the diastema. The inferior margin of the horizontal ramus is smoothly curved. A vascular notch is obvious and under the masseter muscle fossa. The masseter muscle fossa is relatively shallow with a weak ridge. Its anterior angle is at the level of the anterior root of m1. The pterygoid muscle fossa at the lingual side is very wide and deep. Its anterior end is at the level of the posterior part of m3. The mandibular foramen is large, oval-shaped and positioned more ventrally than the worn surface of the cheek teeth. The angular process is broken, but the preserved part shows it should be almost as wide as the ascending ramus. The upper part of the ascending ramus is badly preserved, but it seems not very high. The condylar process is a short transverse axis and its neck is long. The coronoid process is thin and higher than the condylar process.

DP4 is smaller than P4 and M1. Its occlusal outline is triangular. The parastyle is fused with the anteroloph, forming a high and isolated anterolingual corner. Besides the parastyle, the paracone, the metacone and the protocone are all well developed on the crown surface. The protostyle is invisible. The hypocone is very weak, close behind the protocone. The protoloph is short and straight. No obvious protoconule. The metaloph bends back at the metaconule. The enlarged metaconule is connected with the posteroloph by a short ridge, forming a small hypoconule on the posteroloph and dividing the posterior valley into two. The posteroloph is low. The posterolingual flexus is narrow and closed after being moderately worn. The anterior valley and the central valley are short and the anterior one is wider than the central one. There are one large root at the lingual side and two small ones at the buccal side.

P3 is not preserved. On the basis of the alveolar, it should be single-rooted, not particularly small and visible from the buccal side.

P4 is molariformed. Its lingual side is much shorter than the buccal side, making its occlusal outline triangular. The lingual wall is wrinkled and higher than the buccal wall. The protocone is small and separated from the developed hypocone by a vertical groove (the anterolingual flexus) which extends to the base of the tooth crown. The anterolingual flexus is shallow, visible after being moderately worn. The posterolingual flexus is quite deep and narrow. There are four transverse ridges on the crown surface (the anteroloph, the protoloph, the metaloph and the posteroloph).

The anteroloph is well developed and the parastyle is fused with it. The anteroloph is connected with the protocone at the slightly worn stage, but separated after being moderately worn by the anterolingual flexus. The protoloph is relatively straight. There are two ridges extending from the protoconule, the smaller one backwards and the larger one forwards. The metaconule is marked and the metaloph bends back at the metaconule. There are three small ridges extending backwards from the metaloph and two of them are connected with the posteroloph. The posteroloph is continuous and is connected with the hypocone only after being very deeply worn. Three roots, one larger at the lingual side and two smaller at the buccal side.

The occlusal outline of M1 is close to a square. The occlusal structure is mainly composed of four cusps (the paracone, the metacone, the protocone and the hypocone) and four transverse ridges (the anteroloph, the protoloph, the metaloph and the posteroloph). The anteroloph and the posteroloph are lower than the protoloph and the metaloph. The protocone is not completely separated from the hypocone and both of them are ridge-shaped. The anteroloph and the protoloph converge with the protocone. The metaloph is connected with the hypocone. The paraconule and the metaconule are small. The main structure of the posterior lobe is similar to that of DP4.

The occlusal outline of p4 is a trapezoid with a narrow anterior lobe and a wide posterior lobe. The anteroconid is small, located at the anterobuccal side of the metaconid. The metaconid is the highest amongst all cusps of the tooth. The metastylid is barely visible and is separated from the well-developed mesostylid by a deep groove. The protoconid is weaker than the metaconid, but larger than other cusps. The anterobuccal sinusid is shallow and V-shaped. The buccal valley is wide. The mesoconid is obvious. The mesolophid divides the talonid basin into two. The protolophulid is tiny and the extra posterolophid is short. The posterolophid is curved. Two roots.

The lower molars have similar occlusal structure with p4. The anterolophid is developed and connected with the anteroconid and the metaconid. The anterobuccal sinusid is much deeper than that of p4. The mesoconid is connected with the protoconid. The metalophid is more developed than that of p4. The posterior lobe of m3 tapers obviously with a weak entoconid. Four roots.

**Comparison.** Based on the dental dimensions (in Suppl. material 1: table S5), the described fossils should be a large species of flying squirrel, which is most likely to belong to either *Aeretes* or *Petaurista*.

In *Petaurista*, M1/2 lacks the hypocone and the lower cheek teeth have marked anterobuccal sinusid, which can be used for generic diagnosis and are obviously different from the features of the described fossils.

The diagnosis of the genus *Aeretes* includes (summarised by Li CK et al. (2019a)): P3 small, P4 larger than molars, the hypocone of P4-M2 weak and located close behind the protocone, the protoconule and the metaconule weak, the hypoconule well developed, the posterolingual flexus very deep, the entoconid of lower molars small, the mesostylid

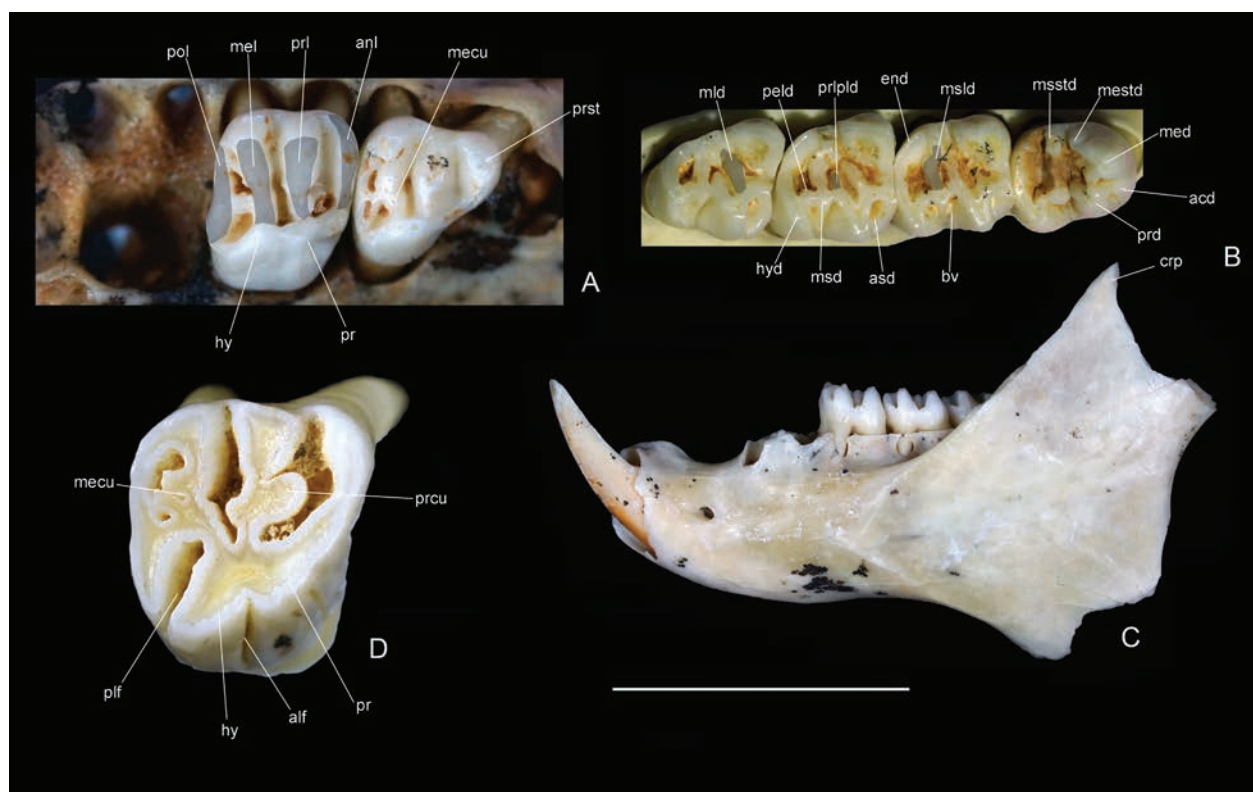


**Figure 4.** *Aeretes melanopterus* from the Yumidong Cave. **A.** 12YMDT4④60.54, right DP4-M1, occlusal view; **B.** 12YMDT4②35.81, right P4, occlusal view; **C.** 12YMDT4④60.1, left mandible, labial view; **D.** 12YMDT4④60.2, right p4-m3, occlusal view. Scale bar: 5 mm (A, B, D); 10 mm (C).

developed and separated from the metastylid and entoconid by deep grooves and the mesoconid small. The described fossils resemble *Aeretes*.

There are three species in the genus *Aeretes*, *A. premelanopterus*, *A. grandidens* and *A. melanopterus*. The primitive *A. premelanopterus* has weak protoconule, but strong metaconule; *A. grandidens* has stronger protoconule and metaconule than *A. premelanopterus*. The protoconule and metaconule of *A. melanopterus* from different regions varies in morphology: specimens from Chongqing and Guizhou have a very weak protoconule and developed metaconule (Zheng 1993), while specimens from Beijing have a marked protoconule and metaconule (Tong 2007). The Yumidong specimens are most similar to *A. melanopterus* from Beijing. Furthermore, comparing the Yumidong specimens with *A. melanopterus* from the Baotansi Cave in Chongqing, there is another obvious dental morphological difference: the lingual vertical groove of P4 is clear on the Yumidong specimens, but unclear on the Baotansi specimens.

Compared with the *Aeretes melanopterus* from the Tianyuan Cave and extant specimens (based on Tong (2007)), the morphological structure of the described specimens falls within their variable range. Based on dimensions, the described specimens are much smaller than the Tianyuan Cave specimens and fall within the variable range of the living species. It is reasonable to attribute these fossils to *A. melanopterus*. Tong (2007) mentioned the diagnosis of this species, including: cheek teeth subhypsodont, enamel slightly rugose, the lingual

wall of upper cheek teeth higher than the buccal wall, the posterolingual flexus very narrow and deep.

## Discussion

### Paleoenvironmental analysis

The evergreen forest covers the area around the Yumidong Cave and the character of vertical zonality of this area is clear nowadays. In areas below 700 m above sea level, the vegetation type is dominated by evergreen broad-leaved and deciduous broad-leaved mixed forest. With increasing elevation, the proportion of coniferous and broad-leaved mixed forest increases. In areas above 2000 m, with only a limited range of peaks in the Wushan Mountains higher than this altitude, the coniferous and broad-leaved mixed forest becomes dominant. It was thought that the drastic climate changes during the Late Pleistocene intensely affected the distribution patterns of flora and fauna (Zhang 2011a, b). What was the paleoenvironment like in the Late Pleistocene in this area? Fossil flying squirrels from the Yumidong Cave provide a clue for this question. The environmental changes in the Pleistocene undoubtedly impacted the paleozoogeographic process of flying squirrels (Lu et al. 2013). Two species of flying squirrel, *Petaurista alborufus* and *Trogopterus xanthipes*, are still surviving in this area and the latter is on the list of fossil flying squirrels excavated from the Yumidong Cave. The other three species of fossil flying squirrels excavated

from the Yumidong Cave have completely disappeared in this area now (Fig. 5), which could reflect a different environment in the Late Pleistocene in this area.

*Pteromys volans* is a Palearctic cold-adapted species, widely distributed in forest zones from northeast Europe to the Korean Peninsula, even to the Hokkaido Island of Japan nowadays (Nowak 1991; Huang et al. 1995). In China, it is mainly distributed in the north of Xinjiang, north and north-east China and lives in the temperate and cold-temperate alpine coniferous forest or coniferous and broad-leaved mixed forest. A small group of this species was listed in the subalpine coniferous forest of the north-eastern margin of the Qinghai-Tibet Plateau (Hu and Wang 1984; Huang et al. 1995), but it has not been confirmed. It was also listed in the Nanling Mountains of Hunan (Liu and Yuan 1981), but Fu (1987) removed it from the list when he summed up the report of the Nanling mammal expedition. Fossils of this species were described from deposits of several caves in Guizhou, Chongqing and Beijing, ranging from the Early to the Late Pleistocene (Zheng 1993; Huang et al. 2002; Tong et al. 2008). However, inexplicably, fossils of *P. volans* have never been reported in northeast China, which is one of its current distribution areas, while in other areas of the world, except in southwest China, its fossil records are not earlier than the late Middle Pleistocene (Yalkovskaya et al. 2015). Specimens of *P. volans* are abundant in the Yumidong Cave, making up 9% of small mammalian fossils in layer ②-2 and 46% in layer ④. This phenomenon indicates the existence of temperate and cold-temperate alpine coniferous forest or coniferous and broad-leaved mixed forest during MIS 2 and MIS 4 in the researched area.

*Trogopterus xanthipes* is an endemic species in China, living from temperate subalpine coniferous forest to subtropical broad-leaved forest at an altitude of 1360 m–2750 m (Hu and Wang 1984). This species is still living in the researched area at the present time. As a fossil species, it was only known from Guizhou, Chongqing and Beijing (Zheng 1993; Tong et al. 2008).

The extant *Belomys pearsonii* is widely distributed in south China, north-eastern South Asia and Southeast Asia (Molur 2016), but it has completely disappeared from the researched area. However, the subfossils of this species have been reported from the Neolithic Dahekou site in Chongqing (Wang et al. 2021). As a fossil species, it is one of the most common flying squirrel species in southwest China (Zheng 1993; Wu 2006).

The extant *Aeretes melanopterus* is mainly distributed in the north-eastern Qinghai-Tibet Plateau, the Hengduan Mountains and the Qinling Mountains and a small population is also known in Beijing. This species inhabits the coniferous and broad-leaved mixed forest at altitudes of 2500 m–3000 m and prefers to nest on high trees (Allen 1940; Hu and Wang 1984; Chen et al. 2002; Zheng and Song 2010).

Throughout the current habitats of extant species of fossil Petauristinae from the Yumidong Cave, all the four species can adapt to coniferous and broad-leaved mixed forest and alpine coniferous forest. *Pteromys volans* and *Aeretes melanopterus* have completely disappeared from

the researched area and its vicinity. Now they live in temperate and cold-temperate zones at higher latitudes or inhabit areas of middle to high altitudes at latitudes similar to the Yumidong Cave (Fig. 5). All the species of flying squirrel described here were mainly excavated from the layer ②-2 and the layer ④ of the Yumidong Cave. They may indicate a paleoenvironment of subalpine evergreen coniferous forest or coniferous and broad-leaved mixed forest during MIS 2 and MIS 4, which was colder and of more coniferous forest than nowadays in this area. It is similar to the vegetation landscape on the peaks of the Wushan Mountains over 2000 m above sea level now. However, the regional extinct species *P. volans* and *A. melanopterus* were not found from the layer ③ and the layer ⑤ of the Yumidong Cave, probably representing a vegetation landscape similar to nowadays.

### Extinction of cold-adapted Petauristinae in the Three Gorges area

The species combination of the flying squirrels from the Baotansi Cave 4 km away is consistent with the Yumidong Cave. It was thought that the age of the Baotansi deposits was the Middle Pleistocene on the basis of an ambiguous specimen of *Allocrietus* sp. (Zheng 1993), but we believe that its main deposits are from about the latest Pleistocene by our survey at the locality. Another latest Pleistocene fossil locality nearby is the Migong Cave (Pang et al. 2017). Small mammal fossils from this locality also supported a cool paleoenvironment, but the forest would have been relatively sparse because there was no trace of flying squirrel fossils at all (Pang et al. 2017). These two localities are near the Yumidong Cave and their strata were formed at the same period with the layer ②-2 of the Yumidong Cave. The main reason for their different paleoenvironments is the difference in altitudes. The Yumidong Cave is about 1100 m in altitude; the Baotansi Cave is about 820 m; the Midong Cave is about 160 m–200 m. It is concluded that the different habitats in mountains and valleys caused by the vertical zonality resulted in the fauna divergence during the latest Pleistocene in the Three Gorges area.

The distribution pattern of Petauristinae fossils in the strata of the Yumidong Cave might indicate that the cold-adapted flying squirrels spread southwards during the glacial periods and disappeared in this area during the interglacial periods. It is speculated that cold-adapted flying squirrels lived at the middle zone of the Wushan Mountains during the latest Pleistocene or the Last Glacial Maximum. When the Holocene Megathermal period came, their habitats might have contracted to higher peaks, which were very limited ecological spaces and could not support their survival in the following period. As a result, these cold-adapted flying squirrels died out in this area.

Specimens of flying squirrels were also reported from the Holocene Dahekou Site in Fuling District of Chongqing (Wang et al. 2021). However, the specimens originally identified as *Trogopterus xanthipes* should be *Belomys pearsonii*. The specimens of *Petaurista petaurista* and

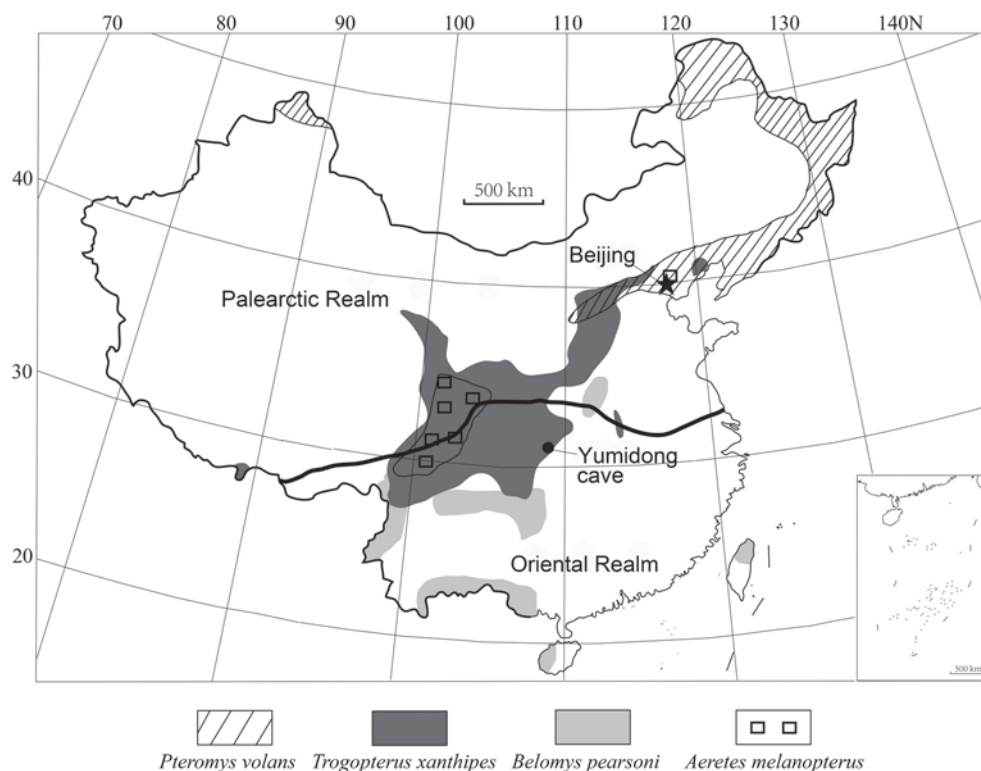


**Figure 5.** Distribution patterns of the living forms of Petauristinae from the Yumidong Cave.

*Aeretes melanopterus* seem to be an undetermined species of the genus *Petauristas*. The specimens of *Hylopetes alboniger* should belong to Sciurinae and resemble *Tamiops swinhoei*. That is to say, current evidence cannot prove the cold-adapted flying squirrels, such as *Pteromys volans*, *Trogopterus xanthipes* and *Aeretes melanopterus*, survived through the Last Glacial to the Holocene in the Three Gorges area.

## Conclusion

Numerous flying squirrel fossils of the Mid-Late Pleistocene were unearthed from the Yumidong Cave in Wushan County, Chongqing Municipality, China. According to the morphological characteristics, these specimens can be identified as *Pteromys volans*, *Trogopterus xanthipes*, *Belomys pearsonii* and *Aeretes melanopterus*, four species of four genera in total, making the Yumidong Cave one of the richest flying squirrel localities of the Quaternary in China. Throughout the current habitats of extant species of fossil Petauristinae from the Yumidong Cave, all the four species could adapt to coniferous and broad-leaved mixed forest and alpine coniferous forest. Their distribution in the strata indicates that the landscapes around the Yumidong Cave during MIS 2 and MIS 4 were dominated by subalpine evergreen coniferous forest or coniferous and broad-leaved mixed forest, similar to the environment of the peaks of the Wushan Mountains above 2000 m nowadays, while the landscapes during MIS 3 and MIS 5 were similar to the environment around the Yumidong Cave at present.

## Acknowledgements

Special thanks to Shao-hua Zheng of IVPP for his kind help on the study of small mammalian fossils. This work was supported by the National Key Research and Development Program of China (No. 2023YFF0804501), the Chinese Academy of Sciences (XDB26000000) and the Talent Program of Chongqing (cstc2022ycjh-bgzxm0170).

## References

- Allen GM (1940) The mammals of China and Mongolia. *Natural History of Central Asia* 11: 621–1350.
- Chaimanee Y, Jaeger JJ (2000) A new flying squirrel *Belomys thamkaewi* n. sp. (Mammalia: Rodentia) from the Pleistocene of West Thailand and its biogeography. *Mammalia* 64: 307–318. <https://doi.org/10.1515/mamm.2000.64.3.307>
- Chen SK, Pei J, Yi J, Wei GB, Pang LB, Wu Y, Hu X (2017) Preliminary report on the mammalian fauna from Yumidong Cave, Wushan, Chongqing, and its chronological analysis. *Quaternary Science* 37: 845–852.
- Chen W, Gao W, Fu BQ (2002) *Beijing Fauna*. Beijing Press, Beijing, 304 pp.
- Chongqing China Three Gorges Museum (2018) The Excavation of the Yumidong Site of the Paleolithic Age in Wushan County, Chongqing Municipality. *Archaeology* 1: 3–16.
- Fu TZ (1987) Notes on the Nanling mammals. *Chinese Journal of Zoology* 1: 36–38.
- Hu JC, Wang YZ (1984) *Sichuan Fauna Economica*. Volume 2: Mammals. Sichuan Science and Technology Press, Chengdu, 365 pp.
- Huang WB, Fang QR (1991) *Wushan Man Site*. China Ocean Press, Beijing, 230 pp.

- Huang WB, Zheng SH, Gao X, Xu ZQ, Gu YM, Wang XZ, Ma ZB, Zhao GL (2002) The Fengjie Man of 140, 000 years old: An ancient human site found at Tiankeng-Difeng Region. Zhonghua Book Company, Beijing, 83 pp.
- Huang WJ, Chen YX, Wen YX (1995) Rodents in China. Fudan University Press, Shanghai, 308 pp.
- Jiang ZG, Ma Y, Wu Y, Wang YX, Feng ZJ, Zhou KY, Liu SY, Luo ZH, Li CW (2015a) China's mammalian diversity. Biodiversity Science 23: 351–364. <https://doi.org/10.17520/biods.2014202>
- Jiang ZG, Ma Y, Wu Y, Wang YX, Zhou KY, Liu SY, Feng JZ (2015b) China's mammal diversity and geographic distribution. Science Press, Beijing, 400 pp.
- Li CK, Qiu ZD, Tong YS, Wang BY, Wu WY, Li Q, Li Q, Wang Y (2019a) Palaeovertebrata Sinica. Volume III Fascicle 5 (1) Glires II: Rodentia I. Science Press, Beijing, 545 pp.
- Li Q, Cheng F, Jackson SM, Helgen KM, Song WY, Liu SY, Sanamxay D, Li S, Fei Li, Xiong Y, Sun J, Wang HJ, Jiang XL (2021) Phylogenetic and morphological significance of an overlooked flying squirrel (Pteromyini, Rodentia) from the eastern Himalayas with the description of a new genus. Zoological Research 42: 389–400. <https://doi.org/10.24272/j.issn.2095-8137.2021.039>
- Li Q, Li XY, Jackson SM, Li F, Jiang M, Zhao W, Song WY, Jiang XL (2019b) Discovery and description of a mysterious Asian flying squirrel (Rodentia, Sciuridae, *Biswamoyopterus*) from Mount Gaoligong, southwest China. Zookeys 864: 147–160. <https://doi.org/10.3897/zookeys.864.33678>
- Liu ZH, Yuan XC (1981) Survey of animal resources of Nanling (mammals of southern Jiangxi and Hunan). Yearly report of Guangdong Institute of Entomology, 83–86.
- Lu X, Ge D, Xia L, Zhang ZQ, Li S, Yang QS (2013) The evolution and paleobiogeography of flying squirrels (Sciuridae, Pteromyini) in response to global environmental change. Evolutionary Biology 40: 117–132. <https://doi.org/10.1007/s11692-012-9191-6>
- Molur S (2016) *Belomys pearsonii*. The IUCN Red List of Threatened Species 2016: e.T2756A22256636. <https://doi.org/10.2305/IUCN.UK.2016-1.RLTS.T2756A22256636.en>
- Nowak RM (1991) Walker's Mammals of the World. 5<sup>th</sup> ed. Vol. 1. Johns Hopkins University Press, Baltimore, 642 pp.
- Pang LB, Chen SK, Huang WB, Wu Y, Wei GB (2017) Paleoenvironmental and chronological analysis of the mammalian fauna from Migong Cave in the Three Gorges Area, China. Quaternary International 434: 25–31. <https://doi.org/10.1016/j.quaint.2014.11.039>
- Qiu ZD (2015) Revision and supplementary note on Miocene sciurid fauna of Sihong, China. Vertebrata Palasiatica 53: 219–237.
- Shao QF, Philippe A, He CD, Jin MG, Huang MJ, Jiao YN, Voinchet P, Lin M, Bahaind J-J (2022) Applying a Bayesian approach for refining the chronostratigraphy of the Yumidong site in the Three Gorges region, central China. Quaternary Geochronology 70: 101304. <https://doi.org/10.1016/j.quageo.2022.101304>
- Tong HW (2007) *Aeretes melanopterus* (Pteromyinae, Rodentia) from Tianyuan Cave near Zhoukoudian (Choukoutien) in China. Geobios 40: 219–230. <https://doi.org/10.1016/j.geobios.2006.04.006>
- Tong HW, Zhang SQ, Li Q, Xu ZJ (2008) Late Pleistocene mammalian fossils from the Xitaiping Cave, Shidu, Beijing. Vertebrata Palasiatica 46: 53–72.
- Wang YF, Yang H, Li DD (2021) Record of flying squirrels and its significance from Dahekou site of Chongqing, China. Quaternary Science 46: 224–234.
- Wei GB, Huang WB, Boëda E, Forestier H, He CD, Chen SK, Zhao JX, Li YH, Hou YM, Pang LB (2017) Recent discovery of a unique Palaeolithic industry from the Yumidong Cave site in the Three Gorges region of Yangtze River, southwest China. Quaternary International, 434: 107–120. <https://doi.org/10.1016/j.quaint.2014.11.048>
- Wu XZ (2006) Yunxi Man—A report of the excavation of Huanglongdong Site. Science Press, Beijing, 271 pp.
- Xie M (1990) Neotectonic uplift velocity and type along the Changjiang River during Quaternary. Quaternary Sciences 10(4): 308–315.
- Yalkovskaya LE, Bol'Shakov VN, Sibiryakov PA, Bolobin AV (2015) Phylogeography of the Siberian flying squirrel (*Pteromys volans* L. 1785) and the history of the formation of the modern species range: new data. Dokl Biochem Biophys 462: 181–184. <https://doi.org/10.1134/S1607672915030114>
- Zhang RZ (2011a) Geological events and mammalian distribution in China. Acta Zoologica Sinica 48: 141–153.
- Zhang RZ (2011b) Zoogeography of China. Science Press, Beijing, 330 pp.
- Zheng SH (1993) Quaternary rodents of Sichuan-Guizhou area, China. Science Press, Beijing, 270 pp.
- Zheng SH (2004) Jianshi Hominid Site. Science Press, Beijing, 412 pp.
- Zheng SW, Song SY (2010) Qinling fauna. China Forestry Publishing House, Beijing, 454 pp.

## Supplementary material 1

### Flying squirrel fossils described in the article from the Yumidong cave

Authors: Li-bo Pang, Shao-kun Chen, Xin Hu, Yan W, Guang-biao Wei

Data type: docx

Explanation note: **table S1**: Flying squirrel fossils described in the article from the Yumidong cave; **table S2**: Measurements of *Pteromys volans* fossils from the Yumidong cave and comparisons with related specimens (in mm); **table S3**: Measurements of *Trogopterus xanthipes* fossils from the Yumidong cave and comparisons with related specimens (in mm); **table S4**: Measurements of *Belomys pearsonii* fossils from the Yumidong cave and comparisons with related specimens (in mm); **table S5**: Measurements of *Aeretes melanopterus* fossils from the Yumidong cave and comparisons with related specimens (in mm).

Copyright notice: This dataset is made available under the Open Database License (<http://opendatacommons.org/licenses/odbl/1.0>). The Open Database License (ODbL) is a license agreement intended to allow users to freely share, modify, and use this Dataset while maintaining this same freedom for others, provided that the original source and author(s) are credited.

Link: <https://doi.org/10.3897/fr.27.115693.suppl1>



# The Eocene to Oligocene boundary and paleoclimatic indications based on calcareous nannofossils of Tonasa Formation, South Sulawesi, Indonesia

Meutia Farida<sup>1</sup>, Asri Jaya<sup>1</sup>, Asmita Ahmad<sup>2</sup>, Jimmi Nugraha<sup>3</sup>

<sup>1</sup> Geological Engineering Department, Hasanuddin University, Jl. Malino Km. 6, Bontomarannu, Somba Opu, Gowa, South Sulawesi, 92171, Indonesia

<sup>2</sup> Soil Science Department, Hasanuddin University, Jl. Perintis Kemerdekaan Km. 10, Makassar, South Sulawesi, 90245, Indonesia

<sup>3</sup> Indonesia Agency for Meteorology Climatology and Geophysics, Jl. Angkasa I No. 2 Jakarta, 10610, Indonesia

<https://zoobank.org/836BFB30-A3FA-4D8D-A5C1-25EA44881E11>

Corresponding author: Meutia Farida ([meutia.farida@unhas.ac.id](mailto:meutia.farida@unhas.ac.id))

Academic editor: Florian Witzmann ♦ Received 13 November 2022 ♦ Accepted 9 May 2024 ♦ Published 10 June 2024

## Abstract

The biostratigraphy of the Tonasa Formation in the Jeneponto Regency of South Sulawesi, Indonesia, is still poorly known, and there are barren ages, such as much of the Oligocene to Early Miocene. The Tonasa Formation is well exposed along the coast of the Jeneponto Regency, in which the Karama area consists of the most important outcrops of this formation which in this area consists of interbedded marl and limestone. Our study focuses on the biostratigraphy of the Karama area section A based on nannofossil. Samples were collected by measured stratigraphy methods and then subjected to investigation using smear slides. The assemblages of species were determined by semiquantitative analysis. Data analysis obtained three nannofossil datums (boundaries): The First Occurrence (FO) of *Sphenolithus pseudoradians* NP19/NP20, the First Occurrence of *Sphenolithus distentus* (CP.16/CP.17), and the Last Occurrence (LO) *Sphenolithus predistentus* (NP.23/NP.24). The zonal boundary was determined based on calcareous nannoplankton; the Late Eocene to Middle Oligocene boundary of the Tonasa Formation was found in this section. Interestingly, throughout this period, the marker species in this section is *Sphenolithus*. In addition, the presence of *Sphenolithus*, *Discoaster*, and *Zygrhablithus bijugatus* indicated that the basin was in warm water condition.

## Key Words

Calcareous nannoplankton, Carbonate platform, Nannofossil datum, Tonasa Formation, Warm water

## Introduction

Indonesia is located between three major plates: the Pacific Plate from the east, the Indo-Australia Plate moving to the north, and the Eurasia Plate, which is relatively passive. They have been actively moving, have caused complex geological conditions, and they have strongly influenced the geological history. One of the results of the collision of the three plates is the formation of Sulawesi Island with its unique K-shaped outline. The consequences of this geological condition are reflected in the stratigraphic setting that is found on Sulawesi Island.

The stratigraphic sequence of the southern arm of Sulawesi is from the Late Cretaceous to the present (Van Leeuwen 1981; Sukamto 1982). One of the widely studied formations is the Tonasa Formation that developed during the Cenozoic era. This formation has significant benefits and is one of the most beautiful karst topography in the world. However, its stratigraphic succession has not been recorded in some area. For example, the Oligocene to Early Miocene strata are poorly exposed in the Jeneponto area (Wilson and Bosence 1997), although the carbonate succession in this area ranges from the Late Eocene to the Middle Miocene (Sukamto and Supriatna 1982). and from the Middle Eocene to the Early Miocene based

on nannofossil assemblages in the Barru area (Farida et al. 2022a). A stratigraphic correlation of the Tonasa Formation was obtained between the Pangkajene and Jeneponto areas.

The age of the Tonasa Formation in Karama area is latest Eocene (P17) based on planktonic foraminifera (Supardi and Barianto 2017). Preliminary studies documented the abundance and diversity of nannofossils in the Karama Traverse (B) area (Farida et al. 2022b). Other sites of the Tonasa Formation have a good stratigraphic succession record. Therefore, we were interested in examining the Eocene/Oligocene boundary based on calcareous nannofossil assemblages in the Jeneponto area. High-resolution biostratigraphy with nannofossils can provide the ages of rocks with higher precision and is one of the most powerful biostratigraphical tools in carbonate sediments (Agnini et al. 2017). This applies also to the investigation of the paleoenvironment, paleoclimate, paleoceanography, and other aspects (Perch-Nielsen 1985; Persico and Villa 2004; De Vargas et al. 2007; Villa et al. 2008; Ali 2009; Sato and Chiyonobu 2009). The biozonation of calcareous nannofossils during the Paleogene has been proposed by some authors. For this study area, we used calcareous nannofossils zonation as proposed by Martini (1971), and Okada and Bukry (1980). The Tonasa Formation consists of interbedded

limestone and *Globigerina* marl (Sukanto and Supriatna 1982). It is well-exposed in the Karama area, which we call the Karama A and Karama B sections. The study area in Karama A section (Fig. 1) mainly consists of interbedded limestone and marl.

One of the most important components of carbonate rock is nannofossils, which were primary producers. They are useful as a tool for determining the biostratigraphy, paleoceanography, and paleoclimate of marine sediments (Perch-Nielsen 1985; De Vargas et al. 2007; Sato and Chiyonobu 2009). The distribution patterns of nannoplankton are strongly related to surface water temperature and nutrients (Imai et al. 2015; Kanungo et al. 2017). The Cenozoic climate development is characterized by the transition between Greenhouse and Icehouse conditions, particularly at the Eocene/Oligocene boundary (Zachos et al. 2001; Fornaciari et al. 2010). Climatic changes in the Cenozoic are accompanied by tectonic and biotic events. The most obvious change is the temperature decrease during the Eocene – Oligocene, which caused a decrease in biodiversity (Berggren and Phrotero 1992; Zachos et al. 2001). A major deterioration in global climate occurred through the Eocene and Oligocene, which was characterized by long-term cooling in both terrestrial and marine environments (Villa et al. 2008). In addition, the presence of certain species indicated a specific water condition.

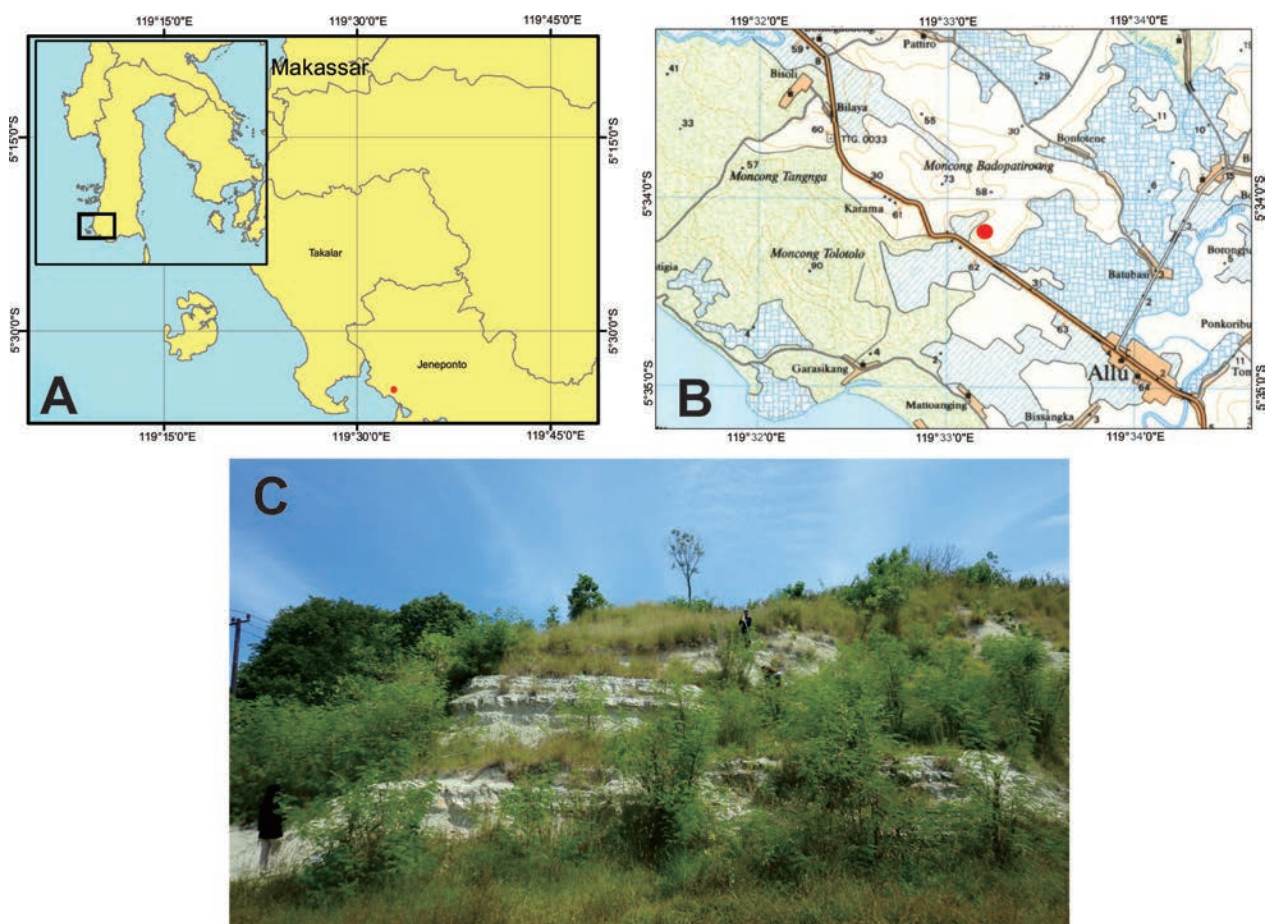


**Figure 1.** A. Map of South Sulawesi-Indonesia. B. Map showing the location of the study area, Karama A section (from Bakosurtal 1991). C. Outcrop of the Tonasa Formation composed of interbedded between limestone and marl.

For example, *Discoaster* was considered an indicator of warm oligotrophic waters, being a lower photic zone species (Bukry 1973; Aubry 1992; Farida et al. 2012; Imai et al. 2015).

### Geology of the study area

Carbonate rocks are widely distributed in the southern arm of Sulawesi (Fig. 2), thereby indicating that this area was under marine conditions. The carbonate platform was dominated by foraminifera and a ramp-type southern margin, and subsidence was the dominant control of accommodation space on the Tonasa Carbonate Platform (Wilson and Bosence 1997). The Tonasa Formation is one of the most widely distributed and has a thickness of 1750–3000 m (Sukamto 1982; Sukamto and Supriatna 1982).

Regionally, the Tonasa Formation is composed of partly layered and massive limestone, coral bioclastic, and

calcarenite with *Globigerina* marl intercalation (Sukamto and Supriatna 1982). This formation discordantly overlies the older volcanic sediments of the Camba Formation (Sukamto 1982; Sukamto and Supriatna 1982). Carbonate platforms in the north and south of South Sulawesi are separated by the Camba Formation.

Stratigraphically, the southern part of Sulawesi is composed of rock formations from the Mesozoic to the Cenozoic. Tertiary-aged rocks are most widely distributed in this area. The Tertiary stratigraphy of the western part of South Sulawesi is divided into (1) the Tonasa Formation that was deposited interfingering with the Early Eocene Malawa Formation, and (2) the Camba Formation that was deposited above the Tonasa Formation during the Middle to Late Miocene. Carbonate development was terminated by the influx of volcanoclastic materials. In the eastern part of South Sulawesi, the Tonasa Formation interfingered with the middle part of the Salo Kalupang Formation around the Middle Eocene, and an unconformity was found at the upper part of the Tonasa

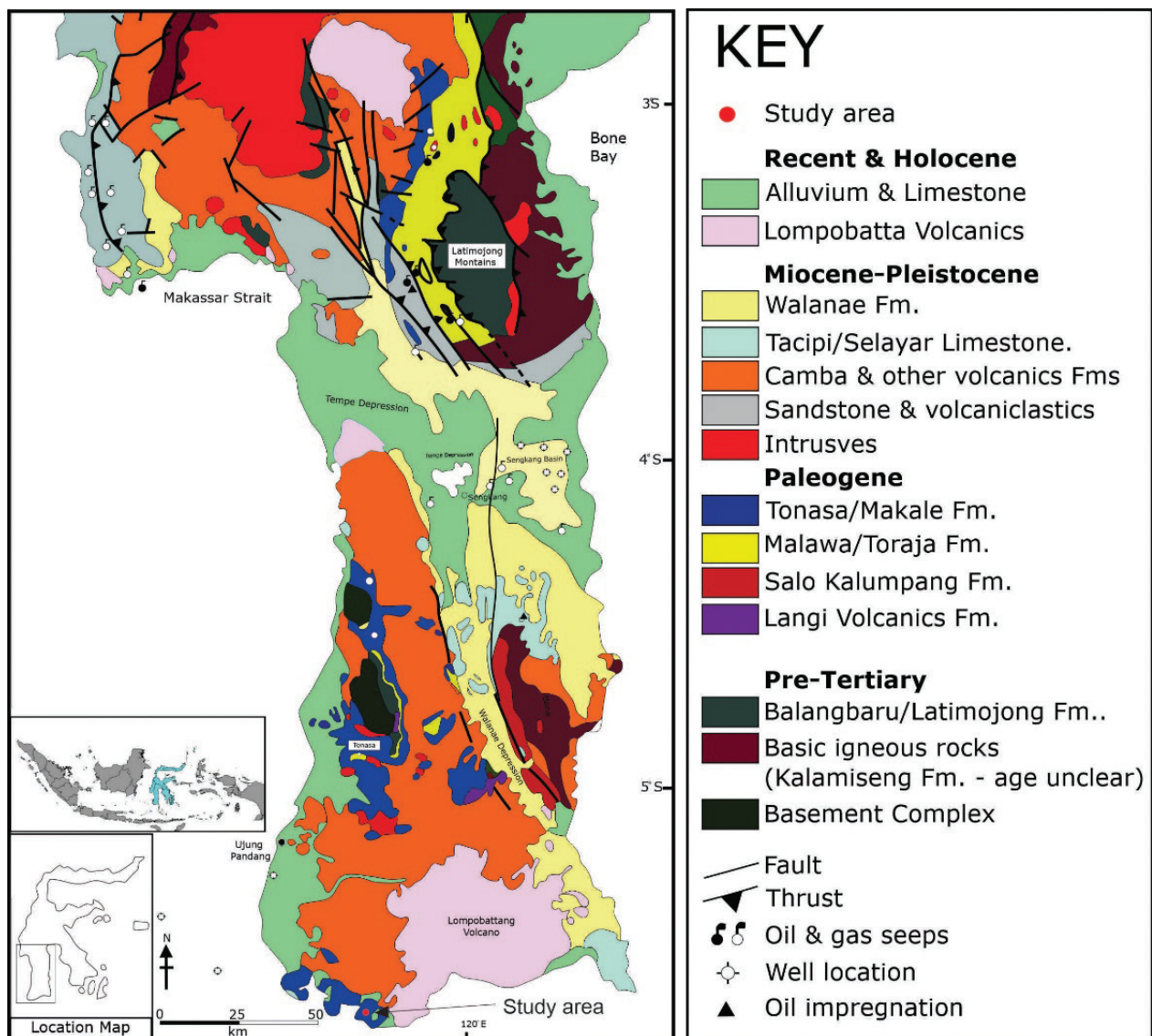
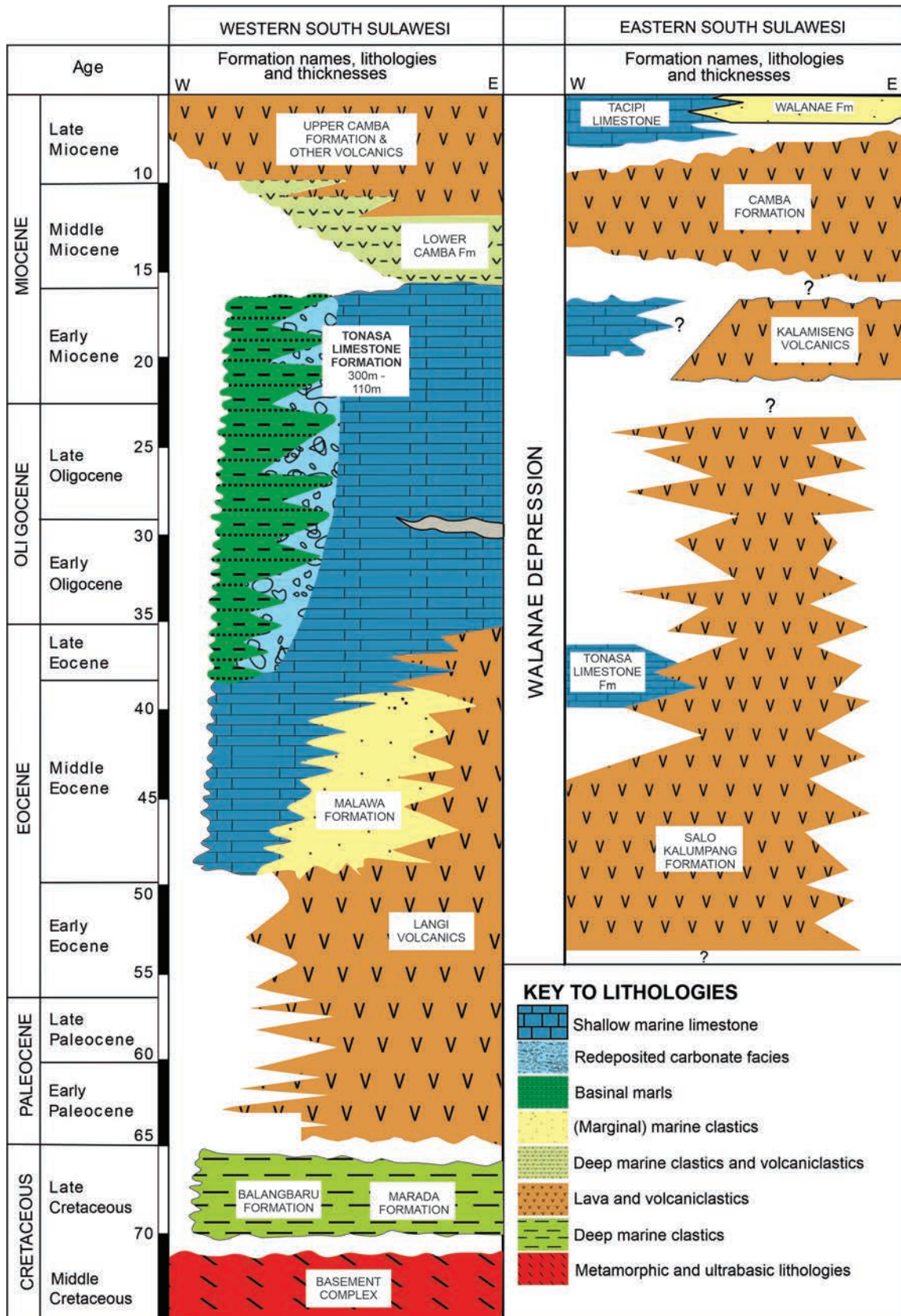


Figure 2. Geological map of the south arm of Sulawesi (modified from Wilson and Bosence 1996).

Formation with respect to the younger rock formations (Sukamto 1982; Sukamto and Supriatna 1982; Wilson and Bosence 1996) (Fig. 3). The study area is situated

in the southernmost part of the Tonasa Formation and is included in western of South Sulawesi, where spot-like outcrops are found in the Jeneponto area.



**Figure 3.** Stratigraphic comparison between western South Sulawesi and eastern South Sulawesi. The Tonasa Formation was deposited from the Middle Eocene to Early Miocene in western South Sulawesi. Modified from Wilson and Bosence (1996).

## Samples and methods

A systematic calcareous nannofossil analysis was conducted starting from field data collection, sample preparation, and determination of the different species composing the assemblage. Samples were collected at each layer of the Karama A section by using measured stratigraphy methods at interbedded limestone and marl. A total of 23 layers were sampled and prepared using the smear slide method with a cover glass of 24 mm × 24 mm in size. Observation under a polarized microscope with 1000× magnification was carried out to recognize the species present in the assemblage (Bown 1999; Farida et al. 2019). The age was determined based on the First Occurrence (FO) and the Last Occurrence (LO) of marker species, following the standard zonation by Martini (1971), Okada and Bukry (1980), and also datum by Perch-Nielsen (1985). The paleotemperature could be analyzed based on the presence of species known to flourish under a specific climate. The semi-quantitative method was used to obtain the nannofossil abundance

based on Kapid and Suprijanto (1996), using the four categories scheme: Abundant (> 15%), Common (10% <n<15%), Few (1%<n<10%), and Rare (<1%).

## Result

As a result of investigating the calcareous nannofossil content of the Tonasa Formation, 20 species were identified. These are *Braarudosphaera bigelowii*, *Coccolithus pelagicus*, *Coccolithus* sp., *Cyclicargolithus abisectus*, *Cyclicargolithus floridanus*, *Dyctiococcites bisecta*, *Dyctiococcites scrippsae*, *Cyclicargolithus luminis*, *Reticulofenestra* sp., *Reticulofenestra hillae*, *Reticulofenestra* spp., *Discoaster deflandrei*, *Discoaster tanii*, *Discoaster* sp., *Sphenolithus moriformis*, *Sphenolithus distentus*, *Sphenolithus predistentus*, *Sphenolithus pseudoradians*, *Sphenolithus tribulosus*, *Zygrhablithus bijugatus*. Fig. 4 shows the photomicrograph of nannofossils, and Fig. 5A, B show the distribution through the section, respectively. The

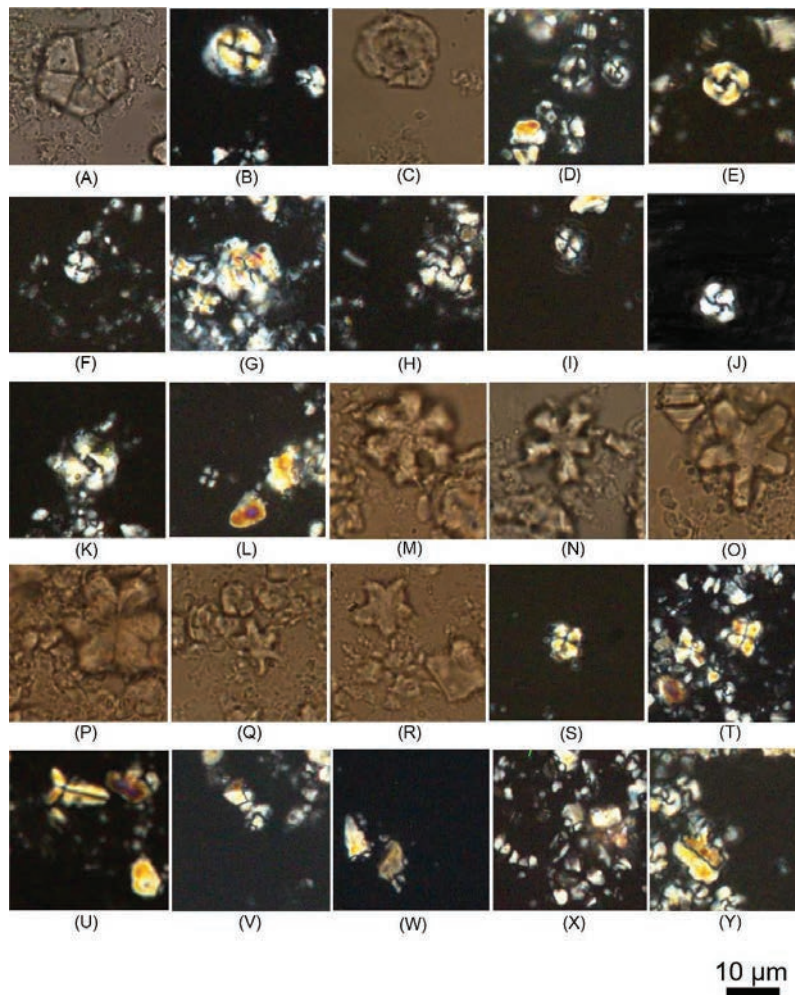


**Figure 4.** Photomicrograph of nannofossils of the Karama A section with 1000× magnification: **A.** *Braarudosphaera bigelowii*. **B, C.** *Coccolithus pelagicus*. **D.** *Coccolithus* sp. **E.** *Cyclicargolithus abisectus*. **F.** *Cyclicargolithus floridanus*. **G.** *Reticulofenestra bisecta*. **H.** *Dyctiococcites scrippsae*. **I.** *Cyclicargolithus luminis*. **J.** *Reticulofenestra* sp. **K.** *Reticulofenestra hillae*. **L.** *Reticulofenestra* spp. **M.** *Discoaster deflandrei*. **N, O.** *Discoaster tanii*. **P–R.** *Discoaster* sp. **S, T.** *Sphenolithus moriformis*. **U.** *Sphenolithus pseudoradians*. **V.** *Sphenolithus distentus*. **W.** *Sphenolithus predistentus*. **X.** *Sphenolithus tribulosus*. **Y.** *Zygrhablithus bijugatus*.

biostratigraphy based on analysis of FO and LO and paleotemperature identification is discussed in the following paragraph.

## Biostratigraphy

Biozonation schemes were used to determine biostratigraphy of the Tonasa Formation in the Karama A section on the basis of calcareous nannofossils from the NP zonation of Martini (1971), the CP Zonation of Okada-Bukry (1980), and the age correlation of Perch-Nielsen (1985) to examine the age of calcareous nannofossils (datums). The results of the biostratigraphy of the study area are (Fig. 6) as follows:

### Zonal boundary NP.19/NP.20

This zone is characterized by the FO of *Sphenolithus pseudoradians* (Martini 1971), which is present for the first appearance in layer 3. The nannofossil assemblages from layer 1 to 3 consist of 16 species: *Braarudosphaera bigelowii*, *Coccolithus pelagicus*, *Coccolithus* sp., *Cyclicargolithus floridanus*, *C. luminis*, *Dictyococcites scrippsae*, *Reticulofenestra bisecta*, *Reticulofenestra* sp., *Reticulofenestra* spp., *Discoaster deflandrei*, *D. tanii*, *Discoaster* sp., *Sphenolithus moriformis*, *S. predistentus*, *S. pseudoradians*, *Zygrhablithus bijugatus*. The dominant species of these layers are *Cyclicargolithus floridanus*, and *Sphenolithus moriformis* (appearing from layers 1–3), and *Discoaster* (present in almost all these layers).

### Zonal boundary CP.16/CP.17

The next zonal boundary is CP16/CP17, which is marked by the FO of *Sphenolithus distentus* (Okada and Bukry 1980) or equivalent to NP22/NP23 by Martini (1971). This boundary is traceable in layer 12. A total of 19 species from layer 4 to layer 12 are present. These are *Braarudosphaera bigelowii*, *Coccolithus pelagicus*, *Coccolithus* sp., *Cyclicargolithus floridanus*, *C. luminis*, *Reticulofenestra bisecta*, *R. hillae*, *Reticulofenestra* sp., *Reticulofenestra* spp., *Dictyococcites scrippsae*, *Discoaster deflandrei*, *D. tanii*, *Discoaster* sp., *Sphenolithus moriformis*, *S. distentus*, *S. predistentus*, *S. pseudoradians*, *S. tribulosus*, and *Zygrhablithus bijugatus*. As explained in the previous zonal boundary, from layers 4 to 12, the species diversity and the number of specimens *Discoaster* and *Sphenolithus* decreased.

### Zonal boundary NP23/NP24

This zonal boundary is based on the LO of *Sphenolithus predistentus* (Perch-Nielsen 1985). This species was the top appearance in layer 18, and the first appearance of *C. abisectus* also occurred in this layer. The following calcareous nannofossils were identified from layers 13 to 18 (18 species): *Braarudosphaera bigelowii*, *Coccolithus*

*pelagicus*, *Coccolithus* sp., *Cyclicargolithus abisectus*, *C. floridanus*, *Dictyococcites scrippsae*, *Discoaster deflandrei*, *D. tanii*, *Discoaster* sp., *Reticulofenestra bisecta*, *R. hillae*, *Reticulofenestra* sp., *Reticulofenestra* spp., *Sphenolithus moriformis*, *S. predistentus*, *S. pseudoradians*, *S. tribulosus*, and *Zygrhablithus bijugatus*. Some species such as *Cyclicargolithus floridanus* and *Reticulofenestra bisecta* are still abundant (> 15%) and increasing at the end of the section. However, *Discoaster tanii* was decreasing and disappearing until layer 18, while the number of *Discoaster deflandrei* and *Discoaster* sp. were increased.

## Paleoclimatic Indication

Calcareous nannofossils are known as a good tool to reconstruct paleoclimate, paleoenvironment, paleoceanography, or paleoecology. The presence of calcareous nannofossils that live in a typical climate indicates the climatic conditions when these rocks were deposited. For instance, *Discoaster*, *Sphenolithus*, and *Zygrhablithus bijugatus*, typically lived in warm water conditions. These species are present and almost abundant from the bottom to the top of the Karama A section, although their diversity declined and some species decreased in abundance.

As mentioned above, *Discoaster* is one of the typical species that lived in warm water. In the study area, *Discoaster* is observed almost all throughout the Karama A section, even though they are not abundant, and the numbers tended to decrease and finally disappeared (Fig. 5A). However, the presence of these species indicates that the basin was under warm water conditions and associated with the lower photic zone. Besides that, a few to rare *Coccolithus pelagicus* are also present throughout this section, and the low abundance of this species indicated warm water conditions.

## Discussion

A previous study investigated the biostratigraphy of the Tonasa Formation in the Karama area using planktonic foraminifera and identified a Late Eocene (Supardi and Bariato 2017). The determination of the calcareous nannofossil datum may use different approaches. The present study refers to the zonation proposed by Martini (1971) and Okada and Bukry (1980) and also refers to the age correlation proposed by Perch-Nielsen (1985). Therefore, the age of the Tonasa Formation in the Karama area (section A) from the calcareous nannofossils is Late Eocene - Middle Oligocene.

Wilson and Bosence (1997) reported that Oligocene strata of the Tonasa Formation in the Jenepono area were not known. Beside that, the age determination of the Tonasa Formation using nannofossils has already been conducted in Barru area, and yielded a Middle Eocene to Early Miocene age (Farida et al. 2022a). From the

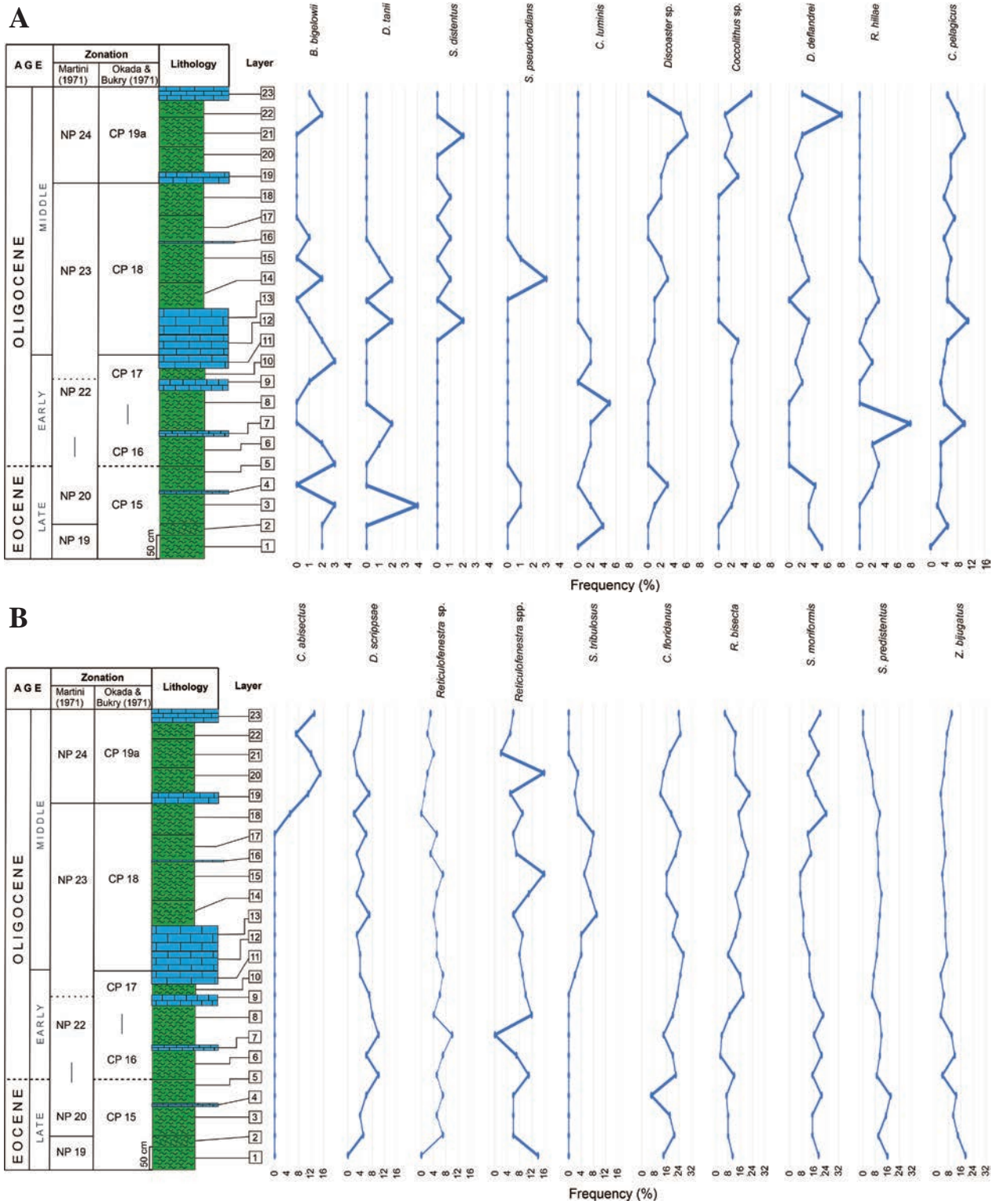


**Figure 5. A.** Distribution of nanofossils from bottom to the top of the section, some species became extinct and others appeared. **B.** Distribution of calcareous nanofossils from bottom to top of the section, some species disappearing and others appearing during the Oligocene.

results of this study, we will develop our understanding, knowledge, and research experience, especially in placing bioevent datums into the framework of the stratigraphic sequence in this area. Therefore, the Tonasa Formation in this area is located approximately in the middle part of the Tonasa Formation in the regional stratigraphic framework.

The calcareous nanoplankton shows a clear latitudinal distribution, related to the specified tolerance at different temperatures (Malfino and McIntyre 1990; Melinte 2004). As previously mentioned, previous researchers found that global climate cooling occurred through the Eocene and Oligocene. These events

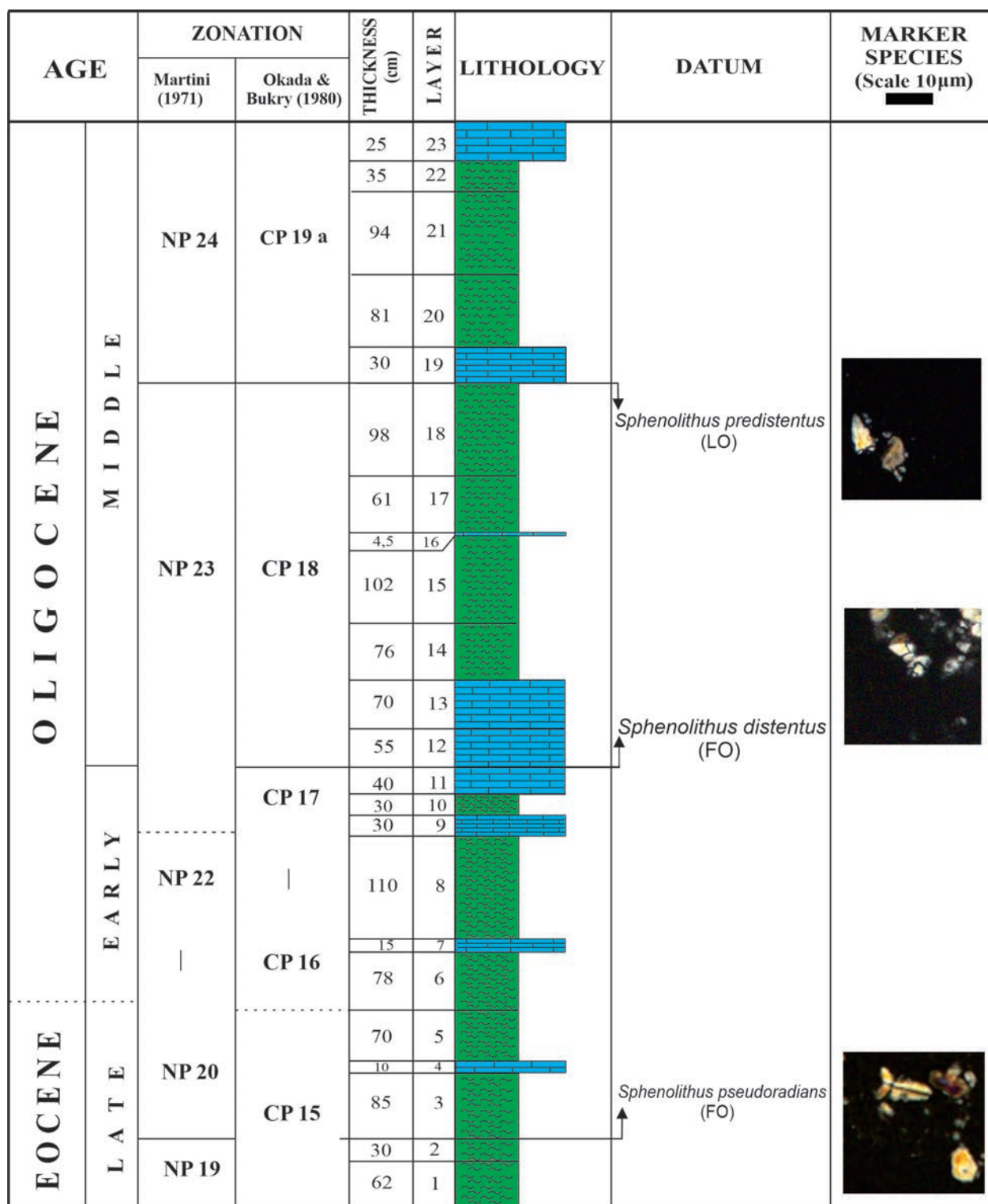


**Figure 6.** Biostratigraphic column of the Karama A section showing calcareous nannofossil datums from the Late Eocene to the Middle Oligocene. Scale bar: 10 µm.

occurred globally and affected marine organisms' life when the Tonasa Formation was deposited. Although the changes of nannofossil assemblages in the study area did not show a sharp collapse, the trend of assemblages shown in the number of species and specimens tended to decrease in Oligocene compared to the Eocene (Fig. 5A, B).

Some *Discoaster* and *Sphenolithus* are poorly preserved, which is why determining the species is difficult. Therefore, preservation has an effect on species quantification. Additionally, diagenetic processes such as overgrowth also make the identification of species impossible. The existence of *Discoaster* as a typical warm water species is important for the reconstruction

of seawater temperature. However, it is not found in all layers and is not abundant. Therefore, we assume that the conditions of the studied area experienced a decrease in temperature, thus reducing the number of *Discoaster* individuals. *Coccolithus pelagicus* as typical cold-water species (Flores et al. 2005) became rare to absent in low-latitude regions (Sato et al. 2004), the distribution of this species shown in Fig. 5A. *Sphenolithus* are generally found common to abundant in low to middle latitudes (Fornaciari et al. 2010). *Sphenolithus* and *Zygrhablithus* are Oligotrophic taxa, present under warm-water conditions (Aubry 1998; Agnini et al. 2007; Villa et al. 2008). In addition, *Zygrhablithus bijugatus*, *Sphenolithus*, and *Discoaster* show warm water affinity, and they became less abundant during the Oligocene. However, they increased again in the upper part of the Middle Oligocene (Fig. 5A, B). This event shows that despite the warm carbonate environment, the temperature decreased, which caused a decrease in the number of species, both in the diversity and in the number of specimens. Therefore, we concluded that water cooling occurred.

## Conclusion

In this study, we identify three calcareous nannofossil datums, which are the FO of *Sphenolithus pseudoradians* (NP.19/NP.20), FO of *Sphenolithus distentus* (CP.16/CP.17), and LO *Sphenolithus predistentus* (NP.23/NP.24). The age of the Tonasa Formation in the Karama area (section A) is Late Eocene to Middle Oligocene. The diversity and number of specimens tend to decrease from the Eocene to the Oligocene but some increased again in the upper part of the Middle Oligocene, i.e. *Discoaster*, *Sphenolithus*, and *Zygrhablithus*, and the presence of these species indicate that the climate was under warm water to water cooling conditions through the Late Eocene to the Middle Oligocene.

## Author contributions

M. F. initiated the research, conceptualized this study, and wrote the original manuscript. A.J., A.A., and J.N., are contributed to the discussion. All authors contributed to the writing of this paper.

## Acknowledgements

We express our gratitude to the many parties who have helped conduct this study, the Research and Community Service Institution of Hasanuddin University for Penelitian Dasar UNHAS grant of Hasanuddin University in 2022, and to Akita University for the supporting equipment. We also thank the students who have participated in this study, either in the field or in the laboratory. Their hard work is highly appreciated. The authors also express their deepest gratitude to the Jeneponto Government

for the research permit. Finally, we especially thank the anonymous reviewers for their comments to improve the quality of the manuscript.

## References

- Ali MY (2009) High-resolution calcareous nannofossil biostratigraphy and paleoecology across the Lates Danian Event (LDE) in central Eastern Desert, Egypt. *Marine Micropaleontology* 72: 111–128. <https://doi.org/10.1016/j.marmicro.2009.03.007>
- Agnini C, Fornaciari E, Rio D, Tateo F, Backman J, Giusberti L (2007) Responses of calcareous nannofossil assemblages, mineralogy and geochemistry to environmental perturbations across the Paleocene/Eocene boundary in the Venetian Pre-Alps. *Marine Micropaleontology* 63: 19–38. <https://doi.org/10.1016/j.marmicro.2006.10.002>
- Agnini C, Monechi S, Raffi I (2017) Calcareous nannofossil biostratigraphy: historical background and application in Cenozoic chronostratigraphy. *Lethaia* 50: 447–463. <https://doi.org/10.1111/let.12218>
- Aubry MP (1992) Late Paleogene calcareous nannoplankton evolution: A tale of climatic deterioration, In: Prothero DR, Berggren WA (Eds) Eocene – Oligocene climatic and biotic evolution. Princeton University Press, Princeton, 272–309. <https://doi.org/10.1515/9781400862924.272>
- Aubry MP (1998) Early Paleogene calcareous nannoplankton evolution: a tale of climatic amelioration. In: Aubry MP, Lucas S, Berggren WA (Eds) Late Paleocene and Early Eocene Climatic and Biotic Evolution. Columbia University Press, New York, 158–203.
- Bakosurtanal (1991) Peta rupa bumi Indonesia skala 1:50.000, Lembar 2010 - 33, Cibinong, Bogor.
- Berggren WA, Prothero DR (1992) Eocene – Oligocene climatic and biotic evolution: an overview, In: Prothero DR, Berggren WA (Eds) Eocene–Oligocene climatic and biotic evolution. Princeton University Press, Princeton, 1–28. <https://doi.org/10.1515/9781400862924.1>
- Bukry D (1971) *Discoaster* Evolutionary Trends. *Micropaleontology* 17(1): 43–52. <https://doi.org/10.2307/1485036>
- Bukry D (1973) Coccolith and silicoflagellate stratigraphy, Tasman Sea and Southwestern Pacific Ocean, Deep Sea Drilling Project Leg 21. In: Burns RE, Andrew JE, et al. (Eds) Initial Reports of the Deep Sea Drilling Project 21. US. Government Printing Office, Washington, 885–893. <https://doi.org/10.2973/dsdp.proc.21.127.1973>
- De Vargas C, Aubry MP, Probert I, Young J (2007) Origin and evolution of coccolithophores: From coastal hunter to oceanic farmers. Falkowski PG, Knoll AH (Eds) Evolution of primary producers in the sea. Elsevier. Amsterdam, 251–285. <https://doi.org/10.1016/B978-012370518-1/50013-8>
- Farida M, Imai R, Sato T (2012) Miocene to Pliocene paleoceanography of the western equatorial Pacific Ocean based on calcareous nannofossils. ODP Hole 805B. *Open Journal of Geology* 2: 72–79. <https://doi.org/10.4236/ojg.2012.22008>
- Farida M, Jaya A, Nugraha J (2022a) Calcareous nannofossil biostratigraphy of Tonasa Formation at Barru River Traverse, South Sulawesi, Indonesia. *Indonesian Journal on Geoscience* 9(3): 371–381. <https://doi.org/10.17014/ijog.9.3.371-381>
- Farida M, Alimuddin I, Fauzielly L, Nugraha J (2022b) Identifying the calcareous nannofossils from the Tonasa Limestone of the Karama Traverse, Jeneponto area, South Sulawesi, Indonesia. AIP Conference Proceedings 2543: 050011. <https://doi.org/10.1063/5.0094841>

- Flores JA, Sierro FJ, Filippelli GM, Bárcena MÁ, Pérez-Folgado M, Vázquez A, Utrilla R (2005) Surface water dynamics and phytoplankton communities during deposition of cyclic Late Messinian sapropel sequences in the western Mediterranean. *Marine Micropaleontology* 56: 50–79. <https://doi.org/10.1016/j.marmicro.2005.04.002>
- Fornaciari E, Agnini C, Catanzariti R, Rio D, Bolla EM, Valvasoni E (2010) Mid-latitude calcareous nannofossil biostratigraphy and biochronology across the Middle to Late Eocene transition. *Stratigraphy* 7(4): 229–264. <https://doi.org/10.29041/strat.07.4.01>
- Imai R, Farida M, Sato T, Iryu Y (2015) Evidence for eutrophication in the northwestern Pacific and eastern Indian oceans during the Miocene to Pleistocene based on the nannofossil accumulation rate, *Discoaster* abundance, and coccolith size distribution of *Reticulofenestra*. *Marine Micropleontology* 116: 15–27. <https://doi.org/10.1016/j.marmicro.2015.01.001>
- Kanungo S, Young J, Skowron G (2017) Microfossils: Calcareous Nannoplankton (Nannofossils). In Sorkhabi R (Ed.) *Encyclopedia of Petroleum Geoscience*. *Encyclopedia of Earth Sciences Series*. Springer, Cham, 1–18. [https://doi.org/10.1007/978-3-319-02330-4\\_4-2](https://doi.org/10.1007/978-3-319-02330-4_4-2)
- Kapid R, Suprijanto SE (1996) Batas Miosen-Pliosen berdasarkan nannoplankton pada Formasi Ledok dan Mundu di daerah Bukit Kapuan, Jawa Timur. *Bulletin Geologi* 26(1): 55–64.
- Malfino B, McIntyre A (1990) Processional forcing of nutricline dynamic in the Equatorial Atlantic. *Science* 249(4970): 766–769. <https://doi.org/10.1126/science.249.4970.766>
- Martini E (1971) Standard Tertiary and Quaternary calcareous nannoplankton zonation. In: Farinacci A (Ed.) *Proceedings of the 2<sup>nd</sup> Planktonic Conference, Roma 1970* Technoscienza, 739–785.
- Melinte MC (2004) Calcareous nannoplankton, a tool to assign environmental changes. *Proceedings of Euro-EcoGeoCentre-Romania* 9–10: 1–8.
- Okada H, Bukry D (1980) Supplementary modification and introduction of code numbers to the low-latitude coccolith biostratigraphic zonation (Bukry, 1973; 1975). *Marine Micropaleontology* 5(3): 321–325. [https://doi.org/10.1016/0377-8398\(80\)90016-X](https://doi.org/10.1016/0377-8398(80)90016-X)
- Perch-Nielsen K (1985) Cenozoic calcareous nannofossil. In: Bolli HM, Saunders JB, Perch-Nielsen K (Eds) *Plankton stratigraphy: Volume 1, Planktic Foraminifera, Calcareous Nannofossils and Calpionellids*. Cambridge University Press, Cambridge, 427–554.
- Persico D, Villa G (2004) Eocene – Oligocene calcareous nannofossils from Maud Rise and Kerguelen Plateau (Antartica): Paleocological and paleoceanographic implications. *Marine Micropaleontology* 52: 153–179. <https://doi.org/10.1016/j.marmicro.2004.05.002>
- Sato T, Yuguchi S, Takayama T, Kameo K (2004) Drastic change in the geographical distribution of the cold-water nannofossil *Coccolithus pelagicus* (Wallich) Schiller at 2.74 Ma in the Late Pliocene, with special reference to glaciation in the Arctic Ocean. *Marine Micropaleontology* 52: 181–193. <https://doi.org/10.1016/j.marmicro.2004.05.003>
- Sato T, Chiyonobu S (2009) Cenozoic paleoceanography indicated by size change of calcareous nannofossil and *Discoaster* abundance. *Fossils (The Palaeontological Society of Japan)* 86: 12–19.
- Sukanto R (1982) *Geologi Lembar Pangkajene dan Watampone bagian barat, Sulawesi*. Geological Research and Development Centre, Bandung.
- Sukanto R, Supriatna S (1982) *Geologi Lembar Ujung Pandang, Benteng dan Sinjai quadrangles, Sulawesi*, Geological Research and Development Centre, Bandung.
- Supardi N, Barianto DH (2017) *Fasies dan Porositas Batuan Karbonat Formasi Tonasa pada Daerah Barru dan Jeneponto, Sulawesi Selatan*. Proceeding, Seminar Nasional Kebumihan Ke-10, Yogyakarta.
- Van Leeuwen TM (1981) The geology of Southwest Sulawesi with special reference to the Biru area. In: Barber A, Wiryosujono S (Eds) *The geology and tectonics of eastern Indonesia*, Geological research and Development Centre Special Publication 2, 277–304.
- Villa G, Fioroni C, Pea I, Bohaty S, Persico D (2008) Middle Eocene – Late Oligocene climate variability: calcareous nannofossil response at Kerguelen Plateau, Site 748. *Marine Micropaleontology* 69: 173–192. <https://doi.org/10.1016/j.marmicro.2008.07.006>
- Wilson MEJ, Bosence WJ (1996) The Tertiary evolution of South Sulawesi, Indonesia: A record in redeposited carbonate facies on the Tonasa Limestone Formation, near Barru. In: Hall R, Blundell DJ (Eds) *Tectonic Evolution of Southeast Asia*. Geological Society of London, Special Publications 106: 365–389. <https://doi.org/10.1144/GSL.SP.1996.106.01.24>
- Wilson MEJ, Bosence DWJ (1997) Platform-top and ramp deposits of the Tonasa carbonate platform, Sulawesi, Indonesia. In: Fraser A, Matthews SJ, Murphy RW (Eds) *Petroleum Geology of SE Asia*. Geological Society of London, Special Publication, 126: 247–279. <https://doi.org/10.1144/GSL.SP.1997.126.01.16>
- Zachos JC, Pagani M, Sloan L, Thomas E, Billups K (2001) Trends, rhythms, and aberrations in global climate 65 Ma to Present. *Science* 292: 686–693. <https://doi.org/10.1126/science.1059412>

## Appendix 1

### Taxonomy of the nannofossil from The Tonasa Formation

- Order COCCOSPHAERALES Haeckel, 1894  
 Family BRAARUDOSPHAERACEAE Deflandre, 1947  
 Genus *Brarudospheara* Deflandre, 1947  
*Braarudospheara bigelowii*, Deflandre, 1947  
 Layer: 1, 2, 3, 5, 6, 9, 10, 11, 12, 14, 16, 22, 23.
- Order COCCOLITHALES Schwarz, 1932  
 Family COCCOLITHACEAE Poche, 1913  
 Genus *Coccolithus* Schwarz, 1954

*Coccolithus pelagicus* (Wallich) Schiller, 1930,  
 Layer: 2, 3, 4, 5, 6, 7, 8, 9, 10, 11, 12, 13, 14,  
 15, 16, 17, 18, 19, 20, 21, 22, 23.

*Coccolithus* sp., Layer 3, 4, 5, 6, 7, 8, 9, 10, 11,  
 19, 20, 21, 22.

- Order DISCOASTERALES Hay, 1977  
 Family DISCOASTERACEAE Tan, 1927  
 Genus *Discoaster* Tan, 1927  
*Discoaster deflandrei* Bramlette & Riedel, 1954,  
 Layer: 1, 2, 3, 4, 9, 10, 11, 12, 14, 15, 16, 18,  
 19, 20, 21, 22, 23.

*Discoaster* sp. Layer: 3, 4, 9, 11, 12, 13, 14, 15, 18, 19, 20, 21, 22.

*Discoaster tanii* Bramlette & Riedel, 1954, Layer: 3, 6, 7, 12, 14, 15.

Family SPHENOLITHACEAE Deflandre, 1952

Genus *Sphenolithus* Deflandre, 1952

*Sphenolithus moriformis* Bramlette & Wilcoxon, Layer: 1, 2, 3, 4, 5, 6, 7, 8, 9, 10, 11, 12, 13, 14, 15, 16, 17, 18, 19, 20, 21, 22, 23.

*Sphenolithus distentus* (Martini, 1965) Bramlette & Wilcoxon, 1967, Layer: 12, 14, 16, 18, 21.

*Sphenolithus predistentus* Bramlette & Wilcoxon, 1967, Layer: 1, 2, 3, 4, 5, 6, 7, 8, 9, 10, 11, 12, 13, 14, 15, 16, 17, 18, 19, 20.

*Sphenolithus pseudoradians* Bramlette & Wilcoxon, 1967, Layer: 3, 4, 14, 15.

*Sphenolithus tribulosus* Roth, 1970, Layer: 10, 11, 12, 13, 14, 15, 16, 17, 18, 19, 20.

Order ISOCHRYSIDALES Pascher, 1910

Family NOELAERHABDACEAE Jerkovic, 1970 emend. Young & Bown, 1997

Genus *Reticulofenestra* Hay, Mohler & Wade, 1966

*Cyclicargolithus abisectus* Wise, 1973, Layer: 18, 19, 20, 21, 22, 23.

*Cyclicargolithus floridanus* Bukry, Layer: 1, 2, 3, 4, 5, 6, 7, 8, 9, 10, 11, 12, 13, 14, 15, 16, 17, 18, 19, 20, 21, 22, 23.

*Cyclicargolithus luminis* Bukry, Layer: 2, 3, 5, 6, 7, 8, 10, 11.

*Reticulofenestra hillae* Bukry & Percival, 1971, Layer: 4, 5, 6, 7, 10, 12, 13, 14,

*Reticulofenestra* sp. Layer: 2, 3, 4, 5, 6, 7, 8, 9, 10, 11, 13, 14, 15, 16, 17, 19, 20, 21, 22, 23.

*Reticulofenestra* spp. Layer: 1, 2, 3, 4, 5, 6, 8, 9, 10, 11, 13, 14, 15, 16, 17, 19, 20, 21, 22, 23.

*Reticulofenestra bisecta* (Hay, Mohler & Wade, 1966) Roth, 1970, Layer: 1, 2, 3, 4, 5, 6, 8, 9, 10, 11, 12, 13, 14, 15, 16, 17, 18, 19, 20, 21, 22, 23.

Order COCCOLITHOPHYCEAE *ORDO INCERTAE SEDIS* Baky, 1988.

Genus *Dictyococcites* Black, 1967

*Dictyococcites scrippsae* Bukry & Percival, 1971, Layer: 2, 3, 4, 5, 6, 8, 9, 10, 11, 12, 13, 14, 15, 16, 17, 18, 19, 20, 21, 22, 23.

*Holococcoliths sensu* Young et al., 2003

Genus *Zygrhablithus* Deflandre, 1959

*Zygrhablithus bijugatus* Deflandre, 1959, Layer: 1, 2, 3, 4, 5, 6, 7, 8, 9, 10, 11, 12, 13, 14, 15, 16, 17, 18, 19, 20, 21, 22, 23



# A large brachyopoid from the Middle Triassic of northern Arizona and the diversity of brachyopoid temnospondyls from the Moenkopi Formation

Calvin So<sup>1</sup>, Arjan Mann<sup>2</sup>

<sup>1</sup> Department of Biological Sciences, George Washington University, Washington, DC, 20011, USA

<sup>2</sup> Department of Geology, Negaunee Integrated Research Center, Field Museum of Natural History, 1400 S Dusable Lake Shore Dr, Chicago, IL, 60605, USA

<https://zoobank.org/C084A289-5E44-4FD0-8FBB-AEEB61A83DD1>

Corresponding author: Calvin So ([calvinso@gwmail.gwu.edu](mailto:calvinso@gwmail.gwu.edu))

Academic editor: Florian Witzmann ♦ Received 19 December 2023 ♦ Accepted 7 June 2024 ♦ Published 25 June 2024

## Abstract

Brachyopoids represent a diverse and late surviving temnospondyl group, lasting until the Early Cretaceous. Here, we report on brachyopoid material previously assigned to *Hadrokkosaurus bradyi* that represents a distinct brachyopoid taxon, characterised by a smaller number of large, robust mandibular teeth, a feature rarely observed in other temnospondyls. We also revisit an angular previously referred to *Hadrokkosaurus* potentially belonging to other temnospondyl taxa present in the Middle Triassic of North America. In light of the abundance of material of possible taxa distinct from *Hadrokkosaurus*, we express the need to re-examine previously collected specimens as new information changes the landscape of palaeontology. Parsimony analyses using exclusively mandibular characters recover the new brachyopoid taxon from the locality in a polytomy with *Hadrokkosaurus* and *Vanastega* at the base of Brachyopoidea, adding to a diversity of mandibular morphology of temnospondyls in the Middle Triassic of North America.

## Key Words

Amphibian, fossil, paleontology, phylogeny, temnospondyl

## Introduction

The Triassic Period (ca. 252 to 201 Ma) is a critical stage of vertebrate recovery, evolution and survival for several major clades between two mass extinctions (Dal Corso et al. 2020). This period records the first occurrences of several major temnospondyl amphibian clades, including Brachyopidae, Chigutisauridae and lissamphibians (Piveteau 1936; Rage and Roček 1989; Ruta and Benton 2008). The general consensus considers lissamphibians to be modern day surviving temnospondyls (Bolt 1969; Pardo et al. 2017; Schoch et al. 2020; Kligman et al. 2023; but see Marjanović and Laurin (2007); Ruta and Coates (2007); Anderson et al. (2008) for other hypotheses for lissamphibian origins), which emphasises the importance

of temnospondyl research in contextualising the evolution and origin of modern amphibians.

Following the Permo-Triassic extinction, brachyopid and chigutisaurid temnospondyls appeared and diversified across the globe, spreading across both Northern and Southern Hemispheres. Their presence would last until the Early Cretaceous, represented by *Koolasuchus cleelandi* (Warren et al. 1997). The brachyopoids of what would become North America in northern Pangea during the Triassic are *Hadrokkosaurus bradyi* and *Vigilius wellesi*. Originally, *Hadrokkosaurus bradyi* was assigned the generic name *Taphrognathus* (a name occupied by a conodont; Welles (1947); Welles (1957)). *Hadrokkosaurus* once referred to a large set of specimens from two different quarries (V3922 and V4207)

approximately 160 kilometres apart in Arizona from the Holbrook Member of the Moenkopi Formation (Welles and Estes 1969; Warren and Marsicano 2000). V3922 produced the holotype mandible of *Hadrokkosaurus* (UCMP 36199) and several disarticulated skeletal elements referred to *Hadrokkosaurus*. In V4207, a brachyopoid skull (UCMP 38165) was excavated and referred to *Hadrokkosaurus* by Welles (1957) and Welles and Estes (1969), but eventually placed in its own genus, *Vigilius wellesi*, by Warren and Marsicano (2000). However, in establishing *Vigilius*, they also assigned several mandibular, cranial and post-cranial elements from V3922 to *Vigilius* (Warren and Marsicano 2000).

Here, we present a detailed description of the material from V3922 and uncover new temnospondyl diversity. Some of the material outside of the holotype cursorily addressed in previous publications suggests the presence of a third brachyopoid taxon in the Holbrook member of the Moenkopi Formation. The previously unknown brachyopoid taxon is recognised from several mandibular elements, including an incomplete right mandible that is preserved from the symphysis to the suture between the first and second coronoid. It is characterised by noticeably wider and rounder teeth that are fewer in number compared to *Hadrokkosaurus*. Phylogenetic analyses place this new taxon within Brachyopoidea.

## Methods

The specimens were studied in person at the University of California Museum of Paleontology and the Field Museum of Natural History. Images of the specimens were photographed using a Canon EOS 7D with a Canon Zoom Lens EF 24-105 mm F/4L IS USM.

## Terminology

The definition of Brachyopoidea and its relationship with Plagiosauridae is relevant to this study. Warren and Hutchinson (1983) found a monophyletic Brachyopoidea consisting of Brachyopidae and Chigutisauridae. Yates and Warren (2000) recovered Brachyopoidea as a paraphyletic grade towards Plagiosauridae and *Laidleria* (Plagiosauroidea). The majority of studies that included temnospondyl systematics in the past decade used the dataset of Schoch (2013) as the base, which also recovered Brachyopoidea forming a grade towards Plagiosauridae and *Laidleria*. Most recently, Witzmann and Schoch (2024) recovered a monophyletic Brachyopoidea sister to a monophyletic Plagiosauroidea, though they used Plagiosauroidea both including and excluding *Laidleria*. In this study, we follow the most recent results Witzmann and Schoch (2024) and operate on the definition of Brachyopoidea as the clade formed by Brachyopidae and Chigutisauridae.

## Institutional abbreviations

**UCMP**, University of California Museum of Paleontology, Berkeley, California, USA; **MCNAM-PV**, Museo de Ciencias Naturales y Antropológicas Juan Cornelio Moyano paleovertebrados collection, Mendoza, Argentina; **QM F**, Queensland Museum, Brisbane, Queensland, Australia

## Anatomical abbreviations

**a**, angular; **af**, adductor fossa; **aMf**, anterior Meckelian fenestra; **cd**, coronoid dentition; **c1**, first coronoid; **c2**, second coronoid; **c3**, third coronoid; **d**, dentary; **dt**, marginal dentition; **pMf**, posterior Meckelian fenestra; **psy**, postsymphyseal foramen; **pra**, pre-articular; **pos**, postsplenial; **prs**, presplenial; **sa**, surangular; **sf**, symphyseal fang; **sym**, mandibular symphysis.

## Results

### Systematic Paleontology

**Temnospondyli Zittel, 1888**

**Stereospondyli Zittel, 1888**

**Brachyopoidea Lydekker, 1885**

***Hadrokkosaurus* Welles, 1957**

***Hadrokkosaurus bradyi* Welles & Estes, 1969**

**Holotype.** UCMP 31699 (right mandible lacking only the articular).

**Horizon and locality.** Uppermost channel sandstone of Holbrook Member, Moenkopi Formation; early Anisian, lowermost Middle Triassic. V3922, Geronimo (Holbrook) fossil vertebrate quarry near Holbrook, Coconino County, north-eastern Arizona.

**Referred material.** UCMP 36200, anterior right dentary; UCMP 36201, partial right dentary; UCMP 36203, partial left dentary; UCMP 36205, partial left pre-articular; UCMP 36836, left pre-articular; UCMP 36837, left pre-articular; UCMP 36838, right surangular.

**Revised diagnosis (modified from Ruta and Bolt (2008)).** A brachyopid temnospondyl with the following unique combination of features: total length of angular ventrolateral margin greater than or equal to half of total lateral mandible length; angular posteriormost margin straight in lateral aspect; greatest depth of angular lateral surface less than or equal to greatest depth of dentary lateral surface; ventral margin of posterior Meckelian fenestra formed only by angular; anterior Meckelian fenestra in middle third of postsplenial mesial lamina.

**Description.** The holotype right mandible possesses several features that maintain its status as a brachyopoid, such as the long postglenoid area and the curvature of the mandible that can be extrapolated to fit a broad and

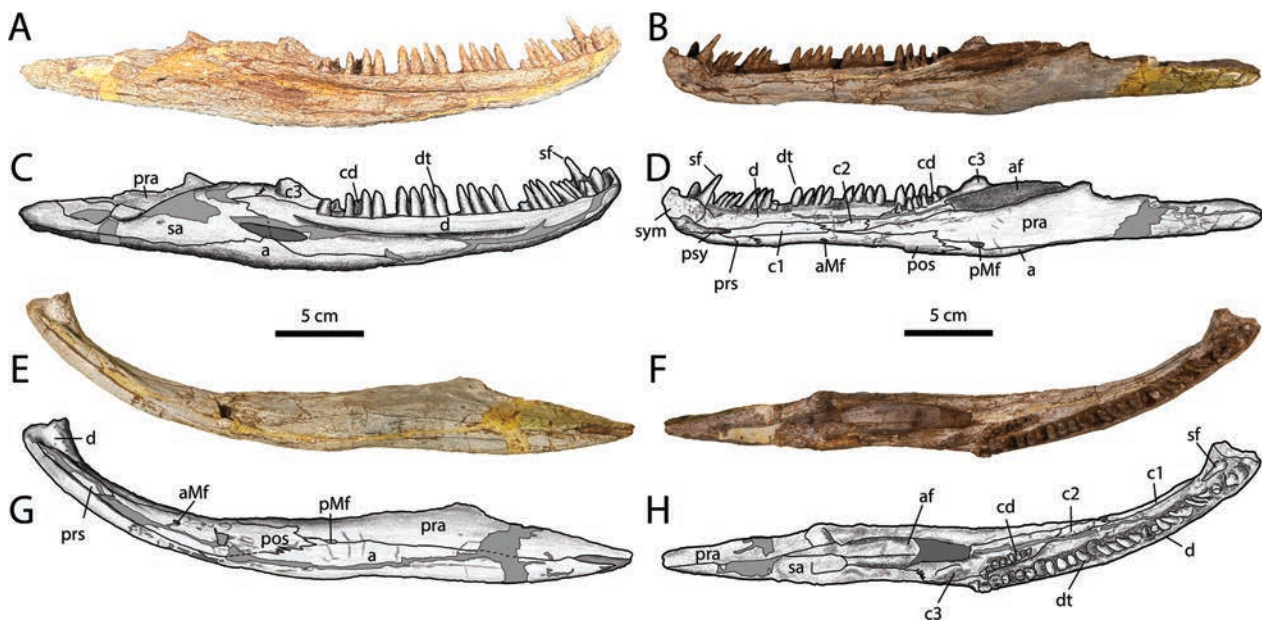


**Figure 1.** UCMP 36199 holotype right mandible of *Hadrokkosaurus bradyi* photographed and illustrated in: labial view (A, C); lingual view (B, D); ventral view (E, G); and dorsal view (F, H).

short-snouted temnospondyl (Fig. 1). It maintains the full plesiomorphic complement of ten bones found with most temnospondyls. The postglenoid area is substantially long, as present in other brachyopoid mandibles (Warren and Marsicano 2000). Several partial and fragmentary dentaries besides the holotype have been referred to *Hadrokkosaurus*.

The dentary of *Hadrokkosaurus* is thin (Fig. 1). The dorsal surface of the dentary (i.e. the dental shelf) is narrow, contributing to the gracile and narrow appearance of the mandible, but towards the symphysis, the shelf broadens to accommodate the larger symphyseal tusk. The dentition of the dentary is represented by small, lingually recurving teeth, with wider than long bases. There is a count of 32 tooth positions. Towards the tips, the dentary teeth are labiolingually compressed and carinated. UCMP 36200, UCMP 36201, UCMP 36203, UCMP 75434 and UCMP 152391 (Suppl. material 1: fig. S1) are partially preserved dentaries; they are likely also *Hadrokkosaurus*, based on the narrowness of the dental shelf and tooth sockets that would be implanted with small teeth.

The dentary forms a wide parabolic shape that curves towards the symphysis (Fig. 1). The straight linear measurement from the anteriormost tip of the symphysis to the posteriormost extent of the dentary measures approximately 21 cm. From the anteriormost tip of the mandibular symphysis to the anteriormost sutural contact between the first and second coronoid, it measures 9.5 cm. At the mandibular symphysis, the dentary is vertically short, but, as it continues posteriorly, it deepens considerably. The dentary sutures to the presplenial and postsplenial ventrally. The symphysis is formed entirely by the dentary. Lingually, the large postsymphyseal foramen is bounded by the dentary dorsally, the first coronoid posteriorly and the presplenial ventrally. The

foramen exits into an open Meckelian canal that opens on the dentary beginning on the lingual surface and ends on the ventral surface as it continues towards the symphysis (Fig. 1B, D, E, G). The size of the postsymphyseal foramen is large and comparable to the condition in *Bathignathus poikilops* (Damiani and Jeannot 2002). The symphyseal tusk is angled posterodorsally on the symphyseal plate (Fig. 1). The dental row is framed lingually and labially by ridges. In the transverse aspect of the dentary, the ridges are formed by the dental shelf on the lingual side, while the labial ridge is formed by a thin lamina running along the length of the dentary. The dentary teeth are implanted within individual sockets.

While the dental shelf is narrow, the teeth are even narrower, resulting in the dorsal exposure of the dental shelf along the length of the dentary (Fig. 1F, H). The labial lamina of the dentary is shortest at the symphysis, but becomes taller towards the posterior. The lingual side of the dental shelf possesses a lamina that projects ventrally, contributing to the lingual surface of the mandible. The lingual lamina primarily projects ventrally for most of the dentary, but, towards the posterior extent of the element, the lamina possesses a 90-degree torsion before suturing to the third coronoid. It overlies and sutures to the first and second coronoids dorsally. The lamina ends where the dentary sutures to the third coronoid posteriorly, leaving the dental shelf occupied by the last few teeth on the dentary without a lingual lamina. The surface of the dentary lingual lamina is smooth until the portion just before the suture to the third coronoid, where the texture of the surface changes drastically. It is marked with antero-posteriorly orientated striations. This roughness may have been the attachment site for musculature. The labial side of the dentary is deep and forms the majority of the anterior labial surface of the mandible (Fig. 1A, C).

A deep trench runs along the labial side of the dentary (Fig. 1A, C). Ruta and Bolt (2008) discuss this trench; they note that this groove is present and homologous in the dentaries from V3922 and in other brachyopoids (Damiani and Kitching 2003), but they do not consider it to be the oral sulcus. They suggest that an external mandibular artery may have been set within the lateral groove (Morales and Shishkin 2002) and question its identity as an oral sulcus. Lydekkerinids have been described to have an oral sulcus that extends from the posterior mandible on to the dentary and towards the mandibular symphysis (Jupp and Warren 1986; Jeannot et al. 2006), which is the case in *Hadrokkosaurus*. The mandible of *Brachyops allos* (Warren 1981) possesses a “groove” in the same topological position, but it is identified as an oral sulcus. Similar grooves can be observed across other trematosaurians (e.g. Sulej (2007); Schoch (2019)) and capitosaurians (e.g. Morales and Shishkin (2002); Eltink et al. (2016)), suggesting the feature to be broadly distributed across stereospondyls. The groove on the labial surface of the dentary has been widely discussed amongst other descriptions of stereospondyls. Given the aquatic nature of stereospondyls, it is likely that the groove is a lateral line sulcus.

Three coronoid bones are present as in other temnospondyls (Fig. 1B, D, F, H). The first coronoid is a long, splint-like element on the lingual surface of the mandible, wedged between the dentary dorsally and the presplenial ventrally. Posteriorly, the first coronoid is sutured to the second coronoid. The first coronoid frames the posteriormost tip of the Meckelian canal forming the postsymphyseal foramen. The second coronoid forms an interdigitating suture with the first coronoid anteriorly. It is foreshortened as it compensates for a lengthened first coronoid. Ventrally, the second coronoid is sutured to the postsplenial. Posteriorly, it is sutured to the third coronoid.

The third coronoid is tooth-bearing (Fig. 1B, D, F, H). It is positioned more dorsally compared to the other coronoids, almost reaching the tips of the crowns of the marginal dentition. The third coronoid sutures to the second coronoid anteriorly. Ventrally, it is sutured to the pre-articular. The body of the third coronoid is lingually expanded to form the anterior margin of the adductor chamber (Fig. 1F, H). A process of the third coronoid extends posteriorly, lingual to the posterior process of the dentary to form the anterior half of the labial margin of the adductor chamber. The posterior process is well exposed in labial view and forms an interdigitating suture with the surangular. The third coronoid also possesses a lamina that descends from its body and contributes to the lingual surface of the mandible. The third coronoid teeth are smaller than the marginal teeth, but they are similar in shape. There are eight tooth positions forming a row on the third coronoid. The coronoid process is formed by the third coronoid without contribution by the dentary.

The presplenial is short and trough-shaped, positioned near the symphysis on the ventral surface of the mandible (Fig. 1B, D, E, G). The presplenial forms the ventral margin of the canal into which the postsymphyseal

foramen exits. It sutures to the dentary dorsally within the canal and to the postsplenial posteriorly. The suture between the presplenial and postsplenial is interdigitating. The presplenial also forms a suture with the first coronoid lingually towards its posterior. The suture between the presplenial and the postsplenial is interdigitating and visible on the lingual surface of the mandible. The suture continues around the ventral mandibular mandible, where it is obscured by plaster. In labial view, the presplenial is barely visible as a narrow splint, where it also sutures to the labial component of the dentary. It does not participate in the mandibular symphysis.

The postsplenial is longer than the presplenial (Fig. 1B, D, E, G). Anteriorly, it is similarly trough-shaped, but towards the posterior, it twists and becomes flat and primarily exposed lingually. It forms interdigitating sutures with the presplenial anteriorly, with the angular posteroventrally and with the pre-articular posteriorly. On the lingual surface, the postsplenial sutures to the first, second and third coronoid dorsally. On the labial surface, the postsplenial sutures to the dentary dorsally.

The angular is poorly ornamented and forms the majority of the floor of the adductor chamber (Fig. 1). It is trough-shaped, contributing to the ventral labial and lingual surfaces of the mandible. The angular has a low exposure on the labial surface of the mandible, reaching only the mid-point of the height of the dentary (Fig. 1A, C). As the angular curves lingually around the ventral mandible to form the adductor chamber floor, it contributes to a narrow ventral portion of the lingual surface. The angular extends posteriorly to contribute to the ventral surface of the postglenoid area, along the length of which it sutures to the surangular dorsally on the labial surface. The anterior angular on the labial surface sutures to the dentary dorsally. It forms a straight suture with the pre-articular on the lingual surface. Anteriorly, the angular forms an interdigitating suture to the postsplenial.

The surangular of *Hadrokkosaurus* is a large element on the labial surface of the mandible (Fig. 1A, C). It forms the posterior labial margin of the adductor chamber (Fig. 1F, H), where it forms an interdigitating suture with the third coronoid anteriorly and stepped suture to the angular ventrally on the labial side. The surangular forms a straight simple suture with the angular on the ventral postglenoid area. The surangular would underlie the articular, which is not preserved. It forms the labial half of the postglenoid area, where it forms a simple straight suture with the retro-articular process of the pre-articular on the dorsal surface of the postglenoid area. The surangular forms a low preglenoid process, only slightly taller than the prearticular wall of the adductor chamber (Fig. 1A, C).

The pre-articular is tall and forms the majority of the posterior lingual surface of the mandible (Fig. 1B, D). It forms the lingual wall of the adductor chamber (Fig. 1F, H). UCMP 36836, UCMP 36837 and UCMP 36838 are referred to as partial pre-articulars that share with the holotype a dorsal process that curls

lingually (Suppl. material 1: fig. S1E, F). UCMP 36839 could be the postglenoid process of the pre-articular or the surangular, but there is not enough information preserved to discern its identity (Suppl. material 1: fig. S1H). The pre-articular forms a simple suture with the third coronoid anterodorsally and to the angular ventrally. It shares with the angular an interdigitating suture with the postsplenial. The pre-articular forms the lingual half of the postglenoid area, where it forms a simple suture with the surangular labially on the dorsal postglenoid area.

The articular is not preserved in the mandible. It may have been poorly ossified or it could have been disarticulated during the preservation of the mandible. However, the surangular and pre-articular preserve the facet upon which the articular would sit.

**Temnospondyli Zittel, 1888**  
**Stereospondyli Zittel, 1888**  
**Brachyopoidea Lydekker, 1885**

**Brachyopoidea indet.**

**Horizon and locality.** Uppermost channel sandstone of Holbrook Member, Moenkopi Formation; early Anisian, lowermost Middle Triassic. V3922, Geronimo (Holbrook) fossil vertebrate quarry near Holbrook, Coconino County, north-eastern Arizona.

**Referred material.** UCMP 36202, partial posterior left dentary; UCMP 36833, partial anterior right mandible; UCMP 36834, near complete right dentary; UCMP 36385, partial right dentary; UCMP 152390, right dentary fragment.

**Description.** UCMP 36833 is a well-preserved anterior right mandible that demonstrates different morphology from *Hadrokkosaurus* (Figs 2, 3). Welles (1947) previously noted that some of the dentaries referred to *Hadrokkosaurus* had different tooth morphology than the type. These additional specimens share the same features as UCMP 36833. While these specimens provide significant morphological detail, they exhibit the same preservation quality as *Hadrokkosaurus*. UCMP 36202 is a disarticulated posterior left dentary, with partial dentition preserved (Suppl. material 1: fig. S2). It is noticeably laterally compressed in preservation. The teeth are large and robust, as in UCMP 36833 and unlike in *Hadrokkosaurus*. UCMP 36834 is a well-preserved right dentary, retaining most if not all of the morphology (Fig. 3). It preserves the same tooth morphology as in UCMP 36833. UCMP 152390 is a mid-section fragment of a right dentary; it also exhibits the same tooth morphology as in UCMP 36833.

UCMP 36833 preserves the dentary, the first coronoid, the presplenial, the anterior second coronoid and the anterior postsplenial (Fig. 2). The mandibular symphysis of UCMP 36833 is partially reconstructed in plaster. Based

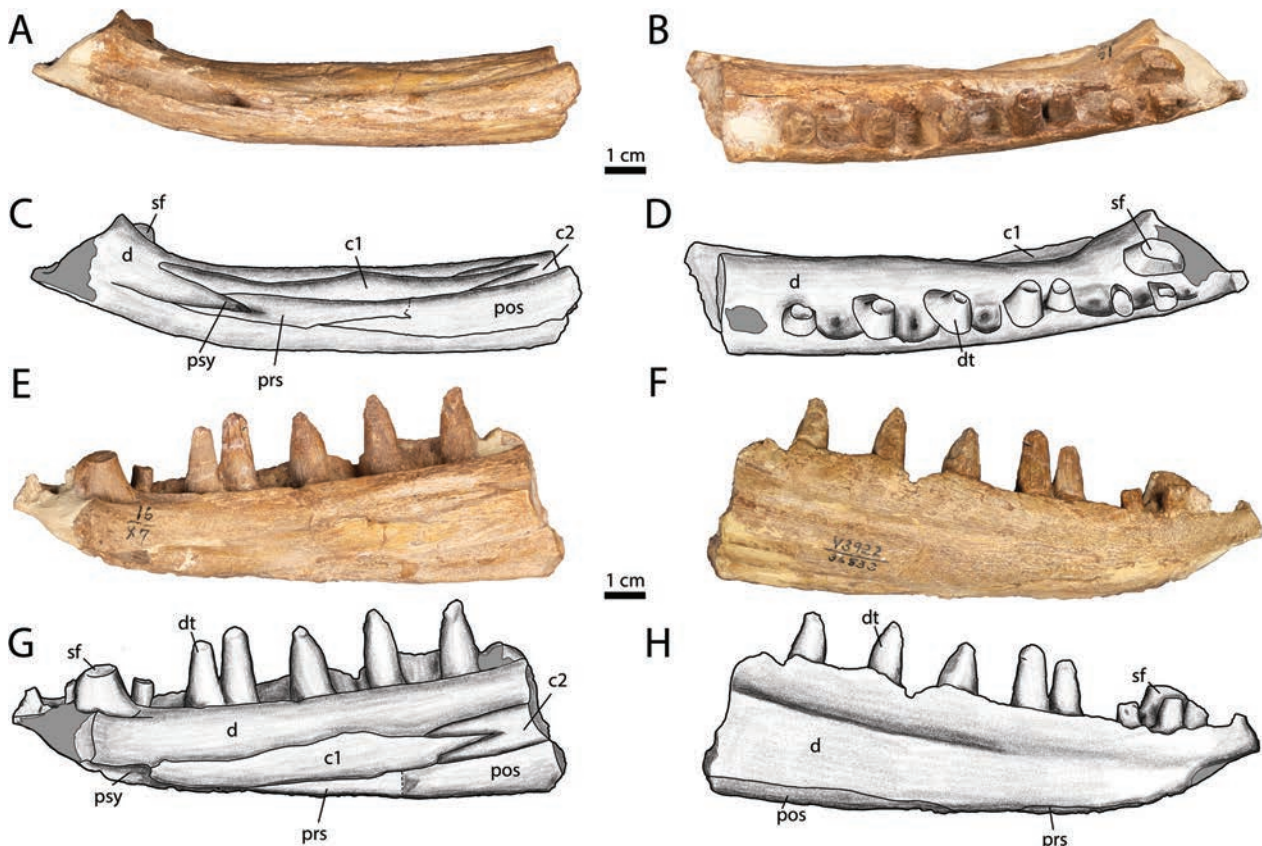


**Figure 2.** UCMP 36833, an incompletely preserved right mandible of the novel brachyopoid photographed and illustrated in: ventral view (A, C), dorsal view (B, D), lingual view (E, G) and labial view (F, H).



**Figure 3.** UCMP 36834, a complete right dentary of the novel brachyopoid photographed in: lingual view (A), ventral view (B) and dorsal view (C).

on UCMP 36834, consisting of a nearly complete dentary, the curvature of the mandible suggests it would have accompanied a very wide and parabolic skull (Figs 2, 3). The ornamentation that is typically present on the temnospondyl mandible is significantly eroded, though there are hints of its distribution present. It appears the ornamentation may have been more polygonal on UCMP 36833 in the symphyseal area and more represented by elongate grooves and ridges towards the posterior. Otherwise, the other specimens belonging to this new brachyopoid taxon do not preserve ornamentation. The dentition consists of tooth bases that are anteroposteriorly compressed ovals in the cross section of the base. The teeth are slightly lingually recurved. They also possess a slight labiolingual narrowing at the crown, but are far less labiolingually compressed than the teeth in *Hadrokkosaurus*. Although slightly eroded, the consistent shape across all teeth in all specimens of the unidentified brachyopoid shows that the lack of carinae is not a result of taphonomic processes. Generally, the tooth morphology can be broadly extrapolated to be larger at the base, rounder overall and fewer in number to accommodate the limited space of the dentary. Amongst brachyopoids, this tooth morphology is found only in *Koolasuchus cleelandi* from the Early Cretaceous of Australia (Warren et al. 1997) and an

incomplete mandible from the Late Triassic of Argentina (Marsicano 2005). The straight linear measurement from the anteriormost tip of the mandibular symphysis to the anteriormost sutural contact between the first and second coronoid of UCMP 36833 measures 10.7 cm. Measured from the anteriormost tip of the symphysis to the posteriormost extent of the mandible, UCMP 36834 measures approximately 14 cm. In total, there are approximately 21 tooth positions present on UCMP 36834, far fewer than the count of 32 on the *Hadrokkosaurus* mandible and the count of 40 on the *Koolasuchus* mandible.

The dentary is more robust compared to the dentary of *Hadrokkosaurus* (Figs 2, 3). The dental shelf is notably wider. The dentary forms most of the labial surface of the anterior mandible, similar to the condition of the anterior mandible of *Koolasuchus* (Warren et al. 1997). It is low anteriorly towards the symphysis and deepens to become a tall and robust element towards the posterior. The width of the dentition is wide enough to span the width of dorsal facing surface of the dentary on which the dentition sits. This differs from *Hadrokkosaurus*, in which the teeth are smaller, leaving a partially exposed dorsal-facing surface of the dentary. The entire width of the dental shelf is occupied entirely by the width of the dentition, resulting in a dorsally unexposed dental

shelf unlike in *Hadrokkosaurus*. The dentary is markedly exposed on the lingual surface of the mandible, extending ventrally from the dentary shelf. The lingual lamina of the dentary curves horizontally and then posteriorly from the shelf. It forms straight sutures ventrally with the first and second coronoid. It sutures to the presplenial and postsplenial labially and ventrally. On the labial surface, there is a shallow groove that is likely homologous with the “horizontal groove” noted by Welles (1947) in *Hadrokkosaurus* and by Damiani and Kitching (2003) in *Vanastega* (Fig. 2F, H). As mentioned before, this feature is found broadly across temnospondyls.

The mandibular symphysis is poorly preserved in UCMP 36833 and reconstructed in plaster; however, based on the anterior extent of the presplenial, the symphysis is formed by the dentary alone (Fig. 2B, D, E, G). Although the symphysis is not preserved in its entirety in UCMP 36833, it is well-preserved in UCMP 36834, where the reduction in the height of the dentary can be seen at the mandibular symphysis. The symphysis widens posteriorly and accommodates a pair of symphyseal fangs in both UCMP 36833 and 36834. The first coronoid is a long element that begins at the posterior extent of the symphyseal shelf. The first coronoid composes the lingual wall and margin of the postsymphyseal foramen. It extends posteriorly, where it forms a double scarf suture with the second coronoid. The first coronoid forms a straight suture to the dentary dorsally and to the presplenial ventrally. It is a relatively shorter element compared to the first coronoid in *Hadrokkosaurus*.

A postsymphyseal foramen is present in UCMP 36833 (Fig. 2A, C, E, G). The foramen exits into a distally widening Meckelian canal positioned on the ventral aspect of the mandible. The foramen and canal are entirely exposed on the mandible ventrally, compared to UCMP 36199, in which the postsymphyseal foramen and canal initially appear on the lingual surface of the mandible before the canal curves ventrally. When viewed at the symphyseal surface, the canal forms a ventrally opening concavity. The presplenial contributes to the ventral margin and the first coronoid forms the lingual margin. Other temnospondyl taxa possess a postsymphyseal groove that lies lingually or sometimes ventrally on

the mandible and participate in the mandibular symphysis (Damiani 2001; Jeannot et al. 2006).

### Temnospondyli Jaekel, 1909

#### Temnospondyli indet.

**Horizon and locality.** Uppermost channel sandstone of Holbrook Member, Moenkopi Formation; early Anisian, lowermost Middle Triassic. V3922, Geronimo (Holbrook) fossil vertebrate quarry near Holbrook, Coconino County, north-eastern Arizona.

**Referred material.** UCMP 36210, partial ventral angular.

**Description.** UCMP 36210 is a partial right angular that would have floored the adductor chamber of the right mandible (Fig. 4). It was noted by Ruta and Bolt (2008) to belong to a different temnospondyl than *Hadrokkosaurus* due to a “boss-like process” upon the floor that is absent in *Hadrokkosaurus* (Fig. 1F, H; Fig. 4). The pit-and-ridge ornamentation is slightly worn, but noticeable on the ventral side, unlike in *Hadrokkosaurus*. In light of the presence of another temnospondyl taxon in this locality, the process may have belonged to a temnospondyl with a strong adductor muscle inserted to produce a stronger bite or hold the prey of the animal. A similar process has been reported in the contemporaries *Plagiosternum* and *Gerrothorax* (Schoch and Witzmann 2011), but noted by Ruta and Bolt (2008) to also be present in *Aphaneramma* (Nilsson 1943), *Dvinosaurus* (Shishkin 1973), *Archegosaurus* (Gubin 1997), *Acroplous* and *Trimerorhachis*.

### Phylogenetic analysis

The matrix is derived from the dataset of Ruta and Bolt (2008) (Suppl. material 1: data S3). We made additions to the taxon sampling in the dataset. Our additions include UCMP 36833 as an operational taxonomic unit (OTU), *Keratobrachyops australis* (Warren, 1981b) and *Plagiosuchus pustuliferus* (Damiani et al. 2009). The



**Figure 4.** UCMP 36210, a right angular in dorsal view (A) and oblique view (B). The arrow points to the boss-like process.

matrix is available for download under project 5265 on Morphobank.org (<http://morphobank.org/permalink/?P5265>). Three additional characters were added regarding the postsymphyseal foramen, as follows:

126. Postsymphyseal foramen: absent (0) or present (1).  
 127. Postsymphyseal foramen position: the foramen is on the lingual surface of the mandible (0) or the foramen is on the ventral surface of the mandible (1).  
 128. Postsymphyseal foramen and the Meckelian canal: the foramen opens to a flat surface of the mandible (0) or the foramen opens into an exposed Meckelian canal (1).

We ran the analyses using TNT 1.6 (Goloboff and Morales 2023) under the New Technology search method. Parallel searches were run under equal weights (EW) and implied weights (IW; Goloboff (1993)). The modified dataset consists of 59 taxa and 128 unordered characters. The EW analysis was conducted for 3,000 additional sequences. The subsequent equally most-parsimonious trees (MPTs) were subjected to an additional round of tree bisection reconnection (TBR). We recovered 328 MPTs with a length of 757 steps (CI = 0.210; RI = 0.571). We explored different values of the concavity constant ( $k$ ) for IW to better explore the data. We specifically used a concavity constant of  $k = 3$  as a generally accepted

default value (Goloboff 1993). We also employed  $k = 12$ , which has been shown to be more effective at identifying topologies (Goloboff et al. 2018). We conducted an IW analysis with  $k = 3$  for 3,000 additional sequences. The resultant MPTs were subjected to an additional round of TBR. This analysis recovered three MPTs of fit 64.29 (CI = 0.204; RI = 0.555). The IW analysis with  $k = 12$  was conducted and subjected to an additional round of TBR. It recovered one MPT of fit 31.82 (CI = 0.209; RI = 0.567).

The strict consensus topology from the EW analysis resulted in poor resolution (Fig. 5A). A large polytomy of temnospondyls, tetrapodomorphs and other early tetrapods was recovered. Higher-nested stereospondyls grouped together in a monophyly, but the internal relationships were not reconcilable with previously-published topologies. Nominal brachyopoids are found to group together, but their monophyly includes *Mastodonsaurus*, *Kupferzellia* and *Plagiosuchus*. The IW analysis under  $k = 3$  produced a more resolved topology (Fig. 5B). Nominal Temnospondyli was recovered, but it includes several amniote-line tetrapods. The analysis also recovered a monophyletic Brachyopoidea (Brachyopidae + Chigutisauridae) to the exclusion of *Keratobrachyops*. The IW analysis under  $k = 12$  produced a clade that included all nominal temnospondyls, except for *Edops*, which diverges before a clade including

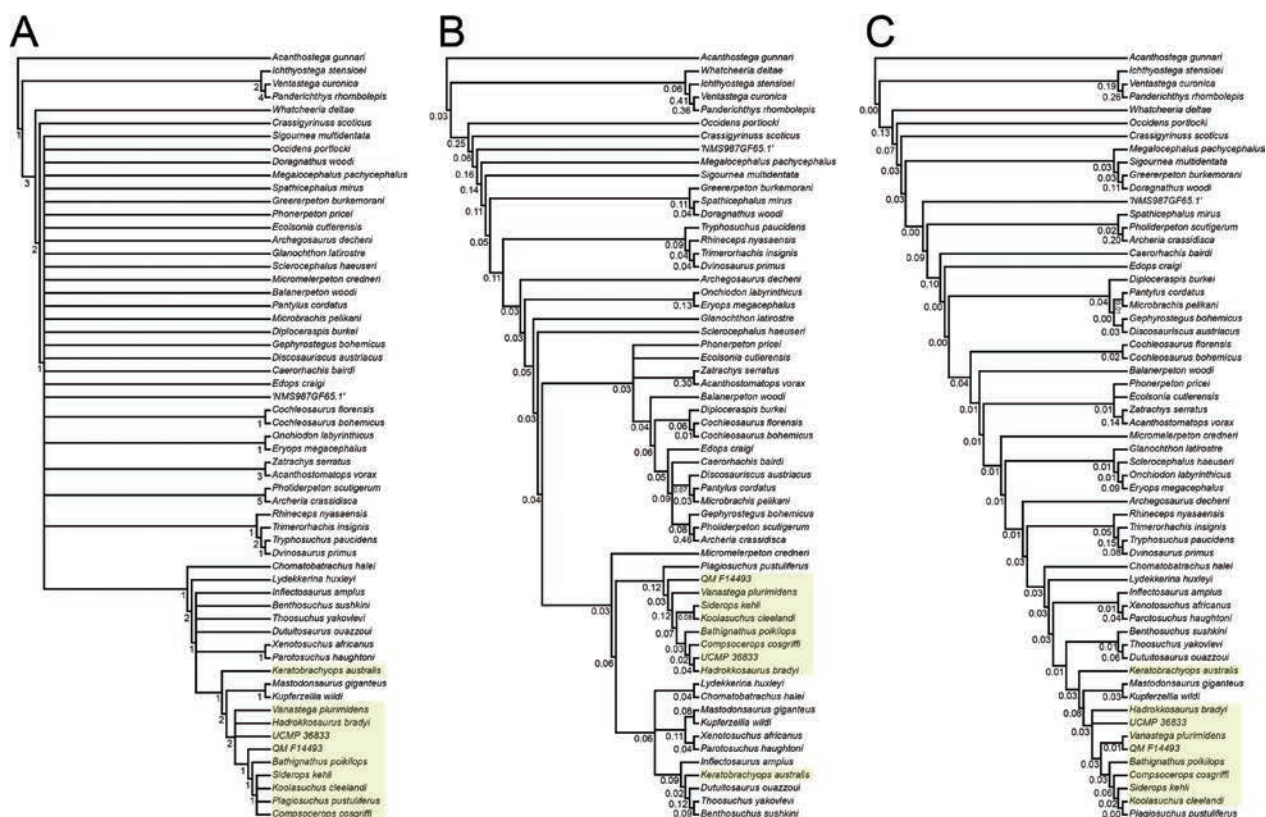


**Figure 5.** Results of the phylogenetic analyses. Strict consensus and Bremer supports for EW analysis (A); strict consensus and relative fit difference (RFD) for IW ( $k = 3$ ) analysis (B); strict consensus for IW ( $k = 12$ ) analysis (C). The green box highlights nominal brachyopoids (Brachyopidae + Chigutisauridae). RFD shows the ratio of the amount of favourable evidence relative to the amount of contradictory evidence (Goloboff and Farris 2001). In the case of an RFD of 0.12, the amount of contradictory evidence is 88% of the amount of favourable evidence, equivalent to a conflict of 25 characters versus 22 characters.

nominal “lepospondyls” and “reptiliomorphs (Fig. 5C). The nominal brachyopoid relationships recovered in this analysis mirror the results of the EW analysis, but both include *Mastodonsaurus* and *Kupferzellia* and resolves *Plagiosuchus* as a highly-nested brachyopoid.

## Discussion

### Taxonomic identifications

UCMP 36833 and UCMP 36834 both exhibit a strong curvature from the symphysis to the rest of the mandible, suggesting that a complete set of left and right mandibles would correspond to a widely parabolic skull of a temnospondyl. During the Middle Triassic of North America, temnospondyls were broadly represented by the capitosauroids, trematosauroids, plagiosaurids and brachyopoids. Given that most capitosauroids and trematosauroids, except for the capitosauroid *Sclerorhax* (Schoch et al. 2007), possessed longirostrine skulls, the unidentified temnospondyl is unlikely to belong to these taxa. Brachyopoids are stereospondyls that possess brevirostrine skull morphology that would match the widely curving contour of UCMP 36833 and UCMP 36834. Plagiosaurids also possess similar brevirostrine skulls, but in North America, they are limited to Greenland. Additionally, the diagnostic feature of pustular dermal ornamentation of plagiosaurine plagiosaurids is not present on any of the specimens (Damiani et al. 2009; Schoch and Witzmann 2012), although the surfaces are too eroded to confidently exclude pustular ornamentation. *Sclerorhax* was an early-diverging Early Triassic capitosauroid with a short and broad skull morphology (Schoch 2007) and could be considered here as a possible candidate; however, the preserved mandibles are sharply curved, aligning the posterior half of the mandible parallel to the mid-line. Coronoid teeth are not present on at least the first and second coronoid in UCMP 36833, unlike the continuous row of coronoid teeth of *Gerorhax* (Schoch and Witzmann 2012). In plagiosaurids, symphyseal fangs are either absent or present as small, rudimentary fangs (Warren and Davey 1992), which is in stark contrast to the large symphyseal fangs observed in UCMP 36834 (Fig. 3). Based on these observations, we provisionally assign the unidentified temnospondyl to Brachyopoidea, which is supported by our phylogenetic results.

Angulars with a boss-like process as in UCMP 36210 are observed in several other taxa as previously noted. In this context, plagiosaurids and trematosauroids are relevant as temnospondyls present in the Middle Triassic with the process. Pustular ornamentation is diagnostic for plagiosaurine plagiosaurids, which are not present on UCMP 36210. Instead, the ventral surface of UCMP 36210 exhibits typical temnospondyl pit and ridge ornamentation. UCMP 36210 has no overlap of anatomy with the unidentified brachyopoid, which does not preserve an angular. Furthermore, with the process present on

non-stereospondyl temnospondyls as well, the process may be the result of ecology rather than phylogeny. At this stage, we are unable to establish any further identification of UCMP 36210 to a more specific level than Temnospondyli.

### Phylogenetic results

The results of the TNT phylogenetic analysis using only mandibular characters differ from the topology recovered in Ruta and Bolt (2008) in several areas of the tree. We recover relationships far from currently accepted temnospondyl phylogenies, though there is recovery of nominal brachyopoid relationships (Fig. 5). UCMP 36833 is consistently recovered as a brachyopoid. In analyses under EW and IW when  $k = 12$ , UCMP 36833 is recovered as part of a grade of “brachyopids” leading to Chigutisauridae. However, under IW when  $k = 3$ , UCMP 36833 is recovered as sister to *Hadrokkosaurus*, highly nested within chigutisaurids.

A consistent pattern emerges from the analyses, in which *Keratobrachyops* does not fall within a traditional brachyopoid monophyly. *Mastodonsaurus* and *Kupferzellia* are found to be more closely related to brachyopoids than *Keratobrachyops* in the analyses under EW and IW when  $k = 12$  (Fig. 5A, C), while in the IW analysis when  $k = 3$ , *Keratobrachyops* is recovered as a trematosauroid (*sensu* Schoch (2013)). In the context of these analyses, it is possible that the proposed brachyopoid features of *Keratobrachyops* may be homoplasies, but the exclusion of skull roof characters should cause some scepticism regarding these results. The results of the phylogenetic analyses highlight a need to revisit and refine mandibular characters to better test relationships and homology.

### Palaeoecological and palaeogeographic interpretations

The Moenkopi Formation spreads widely across the southwest United States and, given its coverage, we expect to capture a broad sampling of Middle Triassic temnospondyls. The Moenkopi Formation exhibits a co-occurrence of Brachyopoidea, Capitosauria and Trematosauria, but lacks representation of plagiosaurids, despite their rich record in Greenland and western Europe. Brachyopoids would eventually become the latest surviving stereospondyl clade (Warren et al. 1997) and one of two surviving temnospondyl clades past the end-Triassic mass extinction, the other being trematosauroids (Maisch et al. 2004), making brachyopoids an important taxon for understanding temnospondyl faunal turnover.

The unidentified brachyopoid has a novel dental ecomorphotype observed in the temnospondyls in this ecosystem. The tooth morphology of tetrapods is widely considered to correlate with diet (Hotton 1995; Evans et al. 2007),

including amphibians (Gregory et al. 2016). Following this, the robust dentition in the unidentified brachyopoid may have enabled a different diet and lifestyle than *Hadrokkosaurus*, *Vigilius* and other temnospondyls of the Middle Triassic Moenkopi Formation (Fig. 6). Few temnospondyl fossils preserve teeth like the unidentified brachyopoid. A likely brachyopoid, MCNACM-PV-3195, was also described to possess relatively large teeth from the Late Triassic of Brazil (Marsicano 2005). Marsicano (2005) also noted that the only other brachyopoid taxon possessing proportionately large teeth is *Koolasuchus*. The size of the dentition in the unidentified brachyopoid is comparable to the dentition in *Koolasuchus* (Warren et al. 1997), a chigutisaurid with few, but large teeth. However, this tooth condition does not appear to be a synapomorphy of chigutisaurids as *Siderops* and *Compsocerops* do not have as large dentition of the dentaries (Warren and Hutchinson 1983; Sengupta 1988) and our phylogeny recovers the unidentified brachyopoid on the grade of brachyopoids outside of chigutisaurids. Additionally, the tooth count of the unidentified brachyopoid is far fewer compared to coeval Moenkopi Formation stereospondyls, such as *Eocyclotosaurus* (98–100 teeth; Rinehart et al. (2015)), further supporting ecological differentiation of the unidentified brachyopoid. The variation seen between *Hadrokkosaurus* and the unidentified Moenkopi brachyopoid may reflect differentiation into different ecological niches. This would be in line with the novel dental ecomorphotype of the unidentified brachyopoid. Differentiation into a more diverse feeding regime spanning broader ecological niches could have contributed to the post-Triassic success of the brachyopoids, enabling brachyopids in the Northern

Hemisphere to co-exist with phytosaurs and sphenosuchian crocodiles (Warren et al. 1997).

The presence of multiple large-bodied stereospondyls at this locality strongly suggests that they diversified into niches occupied by other local aquatic tetrapods. This is contrary to the expectation that diversity decreases progressively towards higher trophic levels (Evans et al. 2005), assuming shared resources in lower trophic levels. In this case, it appears that the Moenkopi Formation brachyopoids were able to exploit resources that did not overlap with other large aquatic tetrapods and between the brachyopoids. The horizon of V3922 is a channel sandstone deposit, which would have been established by a meandering river in a floodplain. Seasonal floods may have provided the necessary nutrients to this locality, supporting multiple temnospondyl taxa. The expansion into novel niches may be what allowed brachyopoids to survive past the End Triassic extinction, as niches previously occupied by other large-bodied stereospondyls disappeared.

At the formation level, the ecosystem supported brachyopids, trematosauroids and capitosauroids. However, if this locality was able to support diverse stereospondyl taxa without necessarily competing for resources, then it begs the question as to why some Triassic stereospondyl clades are not represented, such as the plagiosaurids. Plagiosaurids are a diverse and common component at the higher latitudes of northern Pangean assemblages (e.g. Schoch et al. (2014); Damiani et al. (2009); Witzmann and Schoch (2024)). They are also observed in southern Pangea at higher latitudes (Dias-Da-Silva and Milner 2010; Gee and Sidor 2022), which leaves a conspicuous geographic

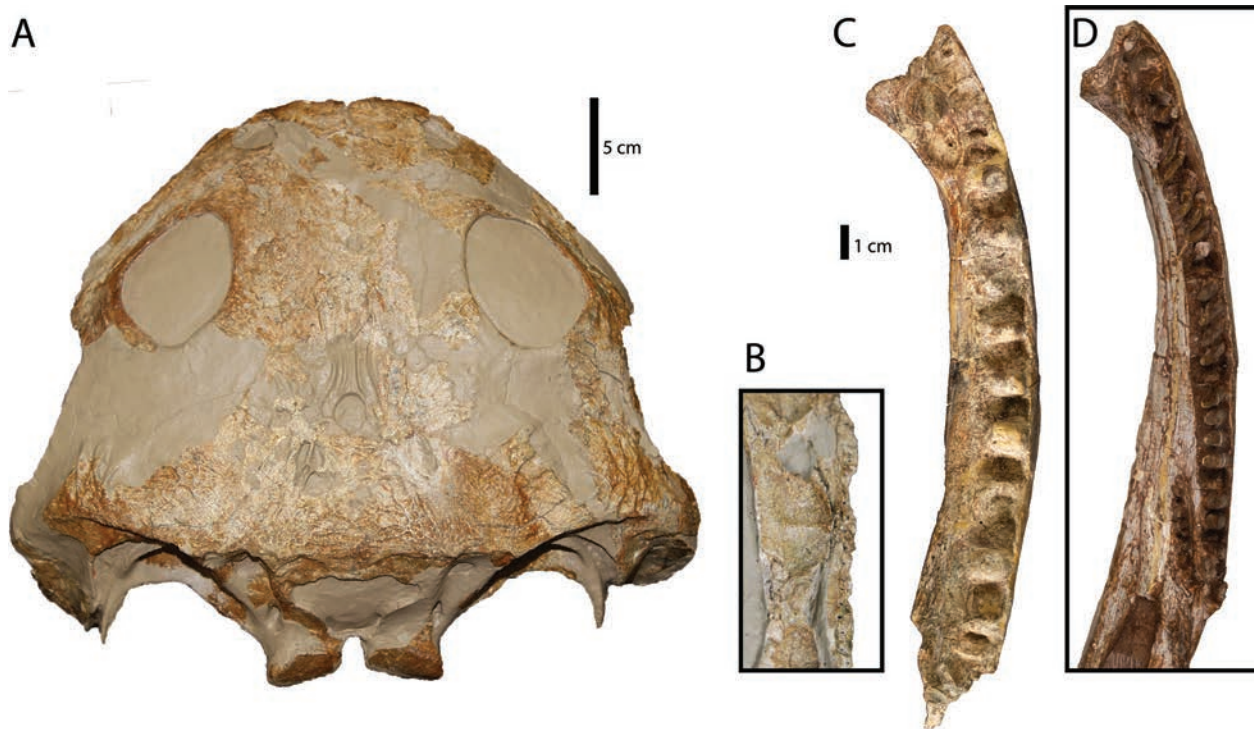


**Figure 6.** UCMP 31865, the holotype skull of *Vigilius welllesi* (A). The maxilla of the holotype does not preserve any dentition, but the marginal tooth sockets are small (B), especially when compared to the sockets and dentition of the dentary teeth in UCMP 36834 (C). *Hadrokkosaurus* dentition and sockets also appear to be larger than the sockets of *Vigilius* (D).

gap near the palaeo-equator. It has been demonstrated that plagiosaurids have the capacity to endure habitats with salinity fluctuations and low level of nutrients (Witzmann and Soler-Gijón 2010; Sanchez and Schoch 2013), which would have been advantageous in the severe seasonality at the palaeo-equator, allowing for possible co-occurrence with other stereospondyl clades. Indeed, plagiosaurids are also present alongside other large stereospondyls in northern Pangea (Milner et al. 1996; Nonsrirach et al. 2021), where there have been less environmental fluctuations in salinity. Overlapping brevirostrine morphology between brachyopoids and plagiosaurids may be a factor in limiting their co-occurrence, but there is evidence of their co-occurrence in some localities (Warren 1985; Nonsrirach et al. 2021). The absence of plagiosaurids in some communities have previously been explored, pointing to a possible preference for marginal habitats which are potentially present in these systems, but not preserved (Gee and Sidor 2021).

## Conclusions

The Moenkopi Formation has been shown to be an ecosystem with a diverse assemblage of stereospondyls. The novel identification of another brachyopoid in the Moenkopi Formation highlights the need to critically re-examine closely-collected material; unobserved diversity may be hiding amongst them. Further exploring the historical collections and localities from the Holbrook Member of the Moenkopi Formation allows us to contribute to a bigger picture of ancient local systems in the Middle Triassic of south-western North America. The diversity of brachyopoid mandibles may be a clue to their specialised morphology enabling exploration of different roles in the ecosystem, which may have allowed the clade to survive the end-Triassic extinction.

## Acknowledgements

The authors would like to thank James Clark for his patience and advice. The authors are significantly grateful to Pat Holroyd for allowing a collection visit and aid in tracking down fossil specimens. The authors would like to thank Ken Angielczyk, Bill Simpson and Adrienne Stroup for organising and accommodating rapid collections visit to the Field Museum of Natural History. Further, the authors would like to thank Jason Pardo for his guidance and support of this research. Finally, the authors would like to thank the Museum für Naturkunde Berlin, Bryan Gee and reviewer 2 for their publication support.

## References

- Bolt JR (1969) Lissamphibian origins: possible protolissamphibian from the Lower Permian of Oklahoma. *Science* 166(3907): 888–891. <https://doi.org/10.1126/science.166.3907.888>
- Broom R (1903) V.—On a new Stegocephalian (*Batrachosuchus Browni*) from the Karroo Beds of Ariwal North, South Africa. *Geological Magazine* 10(11): 499–501. <https://doi.org/10.1017/S0016756800179609>
- Brown B (1933) A new genus of Stegocephalia from the Triassic of Arizona. *American Museum Novitates* 640: 1–4.
- Cabrera Á (1944) Sobre un estegocéfalo de la Provincia de Mendoza. *Notas Mus. La Plata* 9: 421–429.
- Dal Corso J, Bernardi M, Sun Y, Song H, Seyfullah LJ, Preto N, Gianolla P, Ruffell A, Kustatcher E, Roghi G, Merico A, Hohn S, Schmidt AR, Marzoli A, Newton RJ, Wignall PB, Benton MJ (2020) Extinction and dawn of the modern world in the Carnian (Late Triassic). *Science Advances* 6(38): eaba0099. <https://doi.org/10.1126/sciadv.aba0099>
- Damiani RJ (2001) *Parotosuchus* (Amphibia, Temnospondyli) from the Cynognathus Assemblage Zone (Early Triassic) of South Africa: cranial morphology and relationships. *Alcheringa* 25(4): 351–379. <https://doi.org/10.1080/03115510108619226>
- Damiani RJ, Jeannot AM (2002) A brachyopid temnospondyl from the lower Cynognathus Assemblage Zone in the northern Karoo Basin, South Africa. *Palaeontologia Africana* 38: 57–69.
- Damiani RJ, Kitching JW (2003) A new brachyopid temnospondyl from the Cynognathus Assemblage Zone, upper Beaufort Group, South Africa. *Journal of Vertebrate Paleontology* 23(1): 67–78. [https://doi.org/10.1671/0272-4634\(2003\)23\[67:ANBFTF\]2.0.CO;2](https://doi.org/10.1671/0272-4634(2003)23[67:ANBFTF]2.0.CO;2)
- Damiani RJ, Warren A (1996) A new look at members of the Superfamily Brachyopoidea (Amphibia, Temnospondyli) from the Early Triassic of Queensland and a preliminary analysis of brachyopoid relationships. *Alcheringa* 20(4): 277–300. <https://doi.org/10.1080/03115519608619472>
- Damiani RJ, Schoch RR, Hellrung H, Werneburg R, Gastou S (2009) The plagiosaurid temnospondyl *Plagiosuchus pustuliferus* (Amphibia: Temnospondyli) from the Middle Triassic of Germany: anatomy and functional morphology of the skull. *Zoological Journal of the Linnean Society* 155(2): 348–373. <https://doi.org/10.1111/j.1096-3642.2008.00444.x>
- Dias-Da-Silva S, Milner AR (2010) The pustulated temnospondyl revisited—a plagiosternine plagiosaurid from the Lower Triassic of Brazil. *Acta Palaeontologica Polonica* 55(3): 561–563. <https://doi.org/10.4202/app.2009.0131>
- Dong ZM (1985) A Middle Jurassic labyrinthodont (*Sinobrachyops placenticephalus* gen et sp. nov) from Dashanpu, Zigong, Sichuan Province. *Vertebrata Palasiatica* 23(4): 301.
- Eltink E, Da-Rosa ÁAS, Dias-da-Silva S (2017) A capitosauroid from the Lower Triassic of South America (Sanga do Cabral Supersequence: Paraná Basin), its phylogenetic relationships and biostratigraphic implications. *Historical Biology* 29(7): 863–874. <https://doi.org/10.1080/08912963.2016.1255736>
- Evans KL, Warren PH, Gaston KJ (2005) Species–energy relationships at the macroecological scale: a review of the mechanisms. *Biological Reviews* 80(1): 1–25. <https://doi.org/10.1017/S1464793104006517>
- Evans AR, Wilson GP, Fortelius M, Jernvall J (2007) High-level similarity of dentitions in carnivorans and rodents. *Nature* 445(7123): 78–81. <https://doi.org/10.1038/nature05433>
- Fortuny J, Gastou S, Escuillié F, Ranivoharimanana L, Steyer JS (2018) A new extreme longirostrine temnospondyl from the Triassic of Madagascar: phylogenetic and palaeobiogeographical implications for trematosaurids. *Journal of Systematic Palaeontology* 16(8): 675–688. <https://doi.org/10.1080/14772019.2017.1335805>

- Goloboff PA (1993) Estimating character weights during tree search. *Cladistics* 9(1): 83–91. <https://doi.org/10.1111/j.1096-0031.1993.tb00209.x>
- Goloboff PA, Farris JS (2001) Methods for quick consensus estimation. *Cladistics* 17(1): S26–S34. <https://doi.org/10.1006/clad.2000.0156>
- Goloboff PA, Morales ME (2023) TNT version 1.6, with a graphical interface for MacOS and Linux, including new routines in parallel. *Cladistics* 39: 144–153. <https://doi.org/10.1111/cla.12524>
- Goloboff PA, Torres A, Arias JS (2018) Weighted parsimony outperforms other methods of phylogenetic inference under models appropriate for morphology. *Cladistics* 34(4): 407–437. <https://doi.org/10.1111/cla.12205>
- Gregory AL, Sears BR, Wooten JA, Camp CD, Falk A, O'Quin, K, Pauley TK (2016) Evolution of dentition in salamanders: relative roles of phylogeny and diet. *Biological Journal of the Linnean Society* 119(4): 960–973. <https://doi.org/10.1111/bij.12831>
- Gubin YM (1997) Skull morphology of *Archegosaurus decheni* Goldfuss (Amphibia, Temnospondyli) from the early Permian of Germany. *Alcheringa* 20: 277–300. <https://doi.org/10.1080/03115519708619178>
- Hellrung H (2003) *Gerrothorax pustuloglomeratus*, ein Temnospondyle (Amphibia) mit knöcherner Branchialkammer aus dem Unteren Keuper von Kupferzell (Süddeutschland): *Gerrothorax pustuloglomeratus*, a temnospondyle (Amphibia) with a bony branchial chamber from the Lower Keuper of Kupferzell (South Germany). *Staatliches Museum für Naturkunde*.
- Hotton III N (1955) A survey of adaptive relationships of dentition to diet in the North American Iguanidae. *American Midland Naturalist* 88–114. <https://doi.org/10.2307/2422301>
- Howie A (1972) A brachyopid labyrinthodont from the Lower Trias of Queensland. *Proceedings of the Linnean Society of New South Wales* 96: 268–277.
- Huxley TH (1859) On some amphibian and reptilian remains from South Africa and Australia. *Quarterly Journal of the Geological Society* 15(1–2): 642–658. <https://doi.org/10.1144/GSL.JGS.1859.015.01-02.71>
- Jeannot AM, Damiani R, Rubidge BS (2006) Cranial anatomy of the Early Triassic stereospondyl *Lydekkerina huxleyi* (Tetrapoda: Temnospondyli) and the taxonomy of South African lydekkerinids. *Journal of Vertebrate Paleontology* 26(4): 822–838. [https://doi.org/10.1671/0272-4634\(2006\)26\[822:CAOTET\]2.0.CO;2](https://doi.org/10.1671/0272-4634(2006)26[822:CAOTET]2.0.CO;2)
- Jenkins FA (1994) Late Triassic continental vertebrates and depositional environments of the Fleming Fjord Formation, Jameson Land, east Greenland. Vol. 32. Commission for Scientific Research in Greenland. <https://doi.org/10.7146/moggeosci.v32i.140904>
- Jupp R, Warren AA (1986) The mandibles of the Triassic temnospondyl amphibians. *Alcheringa* 10(2): 99–124. <https://doi.org/10.1080/03115518608619164>
- Kligman BT, Gee BM, Marsh AD, Nesbitt SJ, Smith ME, Parker WG, Stocker MR (2023) Triassic stem caecilian supports dissorophoid origin of living amphibians. *Nature* 614(7946): 102–107. <https://doi.org/10.1038/s41586-022-05646-5>
- Maisch MW, Matzke AT (2004) Temnospondyl amphibians from the Jurassic of the southern Junggar Basin (NW China). *Paläontologische Zeitschrift* 79: 285–301. <https://doi.org/10.1007/BF02990189>
- Milner AR, Duffin C, Delsate D (1996) Plagiosaurid and capitosaurid amphibian material from the Late Triassic of Medernach, Grand-Duchy of Luxembourg: preliminary note. *Bulletin de la Société belge de Géologie* 104: 42–53.
- Morales M, Shishkin MA (2001) A re-assessment of *Parotosuchus africanus* (Broom), a capitosaurid temnospondyl amphibian from the Triassic of South Africa. *Journal of Vertebrate Paleontology* 22(1): 1–11. [https://doi.org/10.1671/0272-4634\(2002\)022\[0001:ARAOP-A\]2.0.CO;2](https://doi.org/10.1671/0272-4634(2002)022[0001:ARAOP-A]2.0.CO;2)
- Nonsrirach T, Manikoon S, Lauprasert K (2021) First occurrence of brachyopid temnospondyls in Southeast Asia and review of the Mesozoic amphibians from Thailand. *Fossil Record* 24: 33–47. <https://doi.org/10.5194/fr-24-33-2021>
- Nilsson T (1943) Über einige postkraniale Skelettreste der triassischen Stegocephalen Spitzbergens. *Bulletin of the Geological Institute, University of Uppsala* 30: 227–272.
- Pardo JD, Small BJ, Huttenlocker AK (2017) Stem caecilian from the Triassic of Colorado sheds light on the origins of Lissamphibia. *Proceedings of the National Academy of Sciences* 114(27): E5389–E5395. <https://doi.org/10.1073/pnas.1706752114>
- Piveteau J (1936) Une forme ancestrale des Amphibiens Anoures dans le Trias inférieur de Madagascar. *Comptes Rendus de l'Académie des Sciences* 102: 1607–1608.
- Rage JC, Roček Z (1989) Redescription of *Triadobatrachus massinoti* (Piveteau, 1936) an anuran amphibian from the early Triassic. *Palaeontographica A* 206(1–3): 1–16.
- Rinehart LF, Lucas SG, Schoch RR (2015) *Eocyclotosaurus appetolatus*, a new cyclotosaurid amphibian from the Middle Triassic (Perovkan) Moenkopi Formation of New Mexico, USA. *Journal of Vertebrate Paleontology* 35(3): e929140. <https://doi.org/10.1080/02724634.2014.929140>
- Ruta M, Bolt JR (2008) The brachyopoid *Hadrokkosaurus bradyi* from the early Middle Triassic of Arizona, and a phylogenetic analysis of lower jaw characters in temnospondyl amphibians. *Acta Palaeontologica Polonica* 53(4): 579–592. <https://doi.org/10.4202/app.2008.0403>
- Sanchez S, Schoch RR (2013) Bone histology reveals a high environmental and metabolic plasticity as a successful evolutionary strategy in a long-lived homeostatic Triassic temnospondyl. *Evolutionary Biology* 40: 627–647. <https://doi.org/10.1007/s11692-013-9238-3>
- Schoch RR (2013) The evolution of major temnospondyl clades: an inclusive phylogenetic analysis. *Journal of Systematic Palaeontology* 11(6): 673–705. <https://doi.org/10.1080/14772019.2012.699006>
- Schoch RR (2019) Osteology of the temnospondyl *Trematosaurus brauni* Burmeister, 1849 from the Middle Buntsandstein of Bernburg, Germany. *Palaeodiversity* 12(1): 41–63. <https://doi.org/10.18476/pale.v12.a4>
- Schoch RR, Fastnacht M, Fichter J, Keller T (2007) Anatomy and relationships of the Triassic temnospondyl *Sclerothorax*. *Acta Palaeontologica Polonica* 52(1): 117–136.
- Schoch RR, Milner AR, Witzmann F (2014) Skull morphology and phylogenetic relationships of a new Middle Triassic plagiosaurid temnospondyl from Germany, and the evolution of plagiosaurid eyes. *Palaeontology* 57(5): 1045–1058. <https://doi.org/10.1111/pala.12101>
- Schoch RR, Werneburg R, Voigt S (2020) A Triassic stem-salamander from Kyrgyzstan and the origin of salamanders. *Proceedings of the National Academy of Sciences* 117(21): 11584–11588. <https://doi.org/10.1073/pnas.2001424117>
- Schoch RR, Witzmann F (2012) Cranial morphology of the plagiosaurid *Gerrothorax pulcherrimus* as an extreme example of evolutionary stasis. *Lethaia* 45(3): 371–385. <https://doi.org/10.1111/j.1502-3931.2011.00290.x>

- Sengupta DP (1988) Chigutisaurid temnospondyls from the Late Triassic of India and review of the family Chigutisauridae. *Palaeontology* 38: 313–339.
- Shishkin MA (1967) A brachyopid labyrinthodont from the Triassic of the Russian Platform. *International Geology Review* 9(3): 310–322. <https://doi.org/10.1080/00206816709474470>
- Shishkin MA (1973) The morphology of the early Amphibia and some problems of lower tetrapod evolution. *Trudy Paleontologiceskogo Instituta Akademia Nauk SSR* 137: 1–257.
- Sulej T (2007) Osteology, variability, and evolution of *Metoposaurus*, a temnospondyl from the Late Triassic of Poland. *Palaeontologia Polonica* 64: 29–139.
- Warren AA (1981a) The lower jaw of the labyrinthodont family Brachyopidae. *Memoirs of the Queensland Museum* 20(2): 285–289.
- Warren AA (1981b) A horned member of the labyrinthodont super-family Brachyopoidea from the Early Triassic of Queensland. *Alcheringa* 5(4): 273–288. <https://doi.org/10.1080/03115518108566995>
- Warren AA (1985) Triassic Australian plagiosauroid. *Journal of Paleontology* 59: 236–241.
- Warren AA, Hutchinson MN (1983) The last labyrinthodont? A new brachyopoid (Amphibia, Temnospondyli) from the early Jurassic Evergreen Formation of Queensland, Australia. *Philosophical Transactions of the Royal Society of London, B, Biological Sciences* 303(1113): 1–62. <https://doi.org/10.1098/rstb.1983.0080>
- Warren AA, Marsicano C (2000) A phylogeny of the Brachyopoidea (Temnospondyli, Stereospondyli). *Journal of Vertebrate Paleontology* 20(3): 462–483. [https://doi.org/10.1671/0272-4634\(2000\)020\[0462:APOTBT\]2.0.CO;2](https://doi.org/10.1671/0272-4634(2000)020[0462:APOTBT]2.0.CO;2)
- Warren AA, Rich TH, Vickers-Rich P (1997) The last last labyrinthodonts. *Palaeontographica A* 247: 1–24. <https://doi.org/10.1127/pala/247/1997/1>
- Welles SP (1947) Vertebrates from the upper Moenkopi Formation of northern Arizona. University of California Publications, Bulletin of the Department of Geological Sciences 27(7): 241–294.
- Welles SP (1993) A review of lonchorhynchine trematosauroids (Labyrinthodontia), and a description of a new genus and species from the lower Moenkopi Formation of Arizona. *PaleoBios* 14: 1–24.
- Welles SP, Estes R (1969) *Hadrokkosaurus bradyi* from the Upper Moenkopi Formation of Arizona: with a review of the brachyopid labyrinthodonts. University of California Publications in Geological Sciences 84: 1–61.
- Witzmann F, Schoch RR (2024) Osteology and phylogenetic position of *Plagiosaurus depressus* (Temnospondyli: Plagiosauridae) from the Late Triassic of Germany and the repeated loss of dermal bones in plagiosaurids. *Zoological Journal of the Linnean Society: zlae014*. <https://doi.org/10.1093/zoolinnean/zlae014>
- Witzmann F, Soler-Gijón R (2010) The bone histology of osteoderms in temnospondyl amphibians and in the chroniosuchian *Bystrowiella*. *Acta Zoologica* 91(1): 96–114. <https://doi.org/10.1111/j.1463-6395.2008.00385.x>
- Woodward AS (1904) 11. On Two New Labyrinthodont Skulls of the Genera *Capitosaurus* and *Aphaneramma*. *Proceedings of the Zoological Society of London* 74(3): 170–176. <https://doi.org/10.1111/j.1469-7998.1904.tb08328.x>

## Supplementary material 1

### Supporting information

Authors: Calvin So, Arjan Mann

Data type: docx

Explanation note: fig. S1: Referred *Hadrokkosaurus* specimens; fig. S2: Specimens of the novel brachyopoid taxon; S3: Character changes.

Copyright notice: This dataset is made available under the Open Database License (<http://opendatacommons.org/licenses/odbl/1.0>). The Open Database License (ODbL) is a license agreement intended to allow users to freely share, modify, and use this Dataset while maintaining this same freedom for others, provided that the original source and author(s) are credited.

Link: <https://doi.org/10.3897/fr.27.117611.suppl1>

